FLUORESCENČNÍ SPEKTROSKOPIE VE VÝZKUMU KOLOIDNÍCH SYSTÉMŮ

Habilitační práce

BRNO 2018

Filip Mravec

Můj dík patří v prvé řadě mé rodině, manželce Lídě a mým dětem Bětušce a Ondráškovi, kterým je tato práce věnována.

Mé velké díky patří všem, kteří mě v životě podporovali, svými otázkami stimulovali, kladli mi překážky a pomáhali mi přes ně přejít.

Můj obrovský dík patří mým rodičům, že mě nechali si vybrat svou cestu, mým sestrám Míše a Gabče za to, že mě svými úspěchy inspirovaly k mému vlastnímu rozvoji. Můj dík patří mému vedoucímu a mentorovi prof. Pekařovi, že mi umožnil se věnovat bez omezení tomu, co mě baví.

Můj dík patří i všem mým studentům a mým kolegům, kteří mě svými otázkami posouvali dál za hranice mých vědomostí a pozitivně mě nutili se zlepšovat a prohlubovat znalosti o rozsáhlém tématu fluorescence.

V Brně, 2018

Filip Mravec

OBSAH

1 ÚVOD

Vážená čtenářko, vážený čtenáři.

Tato habilitační práce si dala za cíl popsat využití jevu fluorescence v různě složitých koloidních systémech, které zahrnují jak micely, tak různé části živých systémů na buněčné úrovni. Autor habilitační práce k těmto oběma tématům přistupuje s respektem k jejich šíři, a proto se v této práci objeví některé vybrané a zobecněné principy, jak kvantově mechanický jev pomáhá v odhalování vlastností a zákonitostí v živých i neživých systémech.

Různé druhy luminiscence provázejí a fascinují lidstvo od nepaměti. Pozorování „horkého" žhnutím uhlíků[1], obdiv nad „chladným" světélkováním nočních živočichů[2] nebo obavy z „kouzelného" modrého záření zahřátých kamenů okolo ohniště[3]. Tato fascinace později přecházela ve zvědavost a v touhu vysvětlit a osvětlit původ tohoto světla. Tyto aktivity dosáhly vrcholu v intervalu od poloviny 19. do poloviny 20. století, kdy byly publikovány průlomové teorie a provedeny první katalogizace těchto jevů.

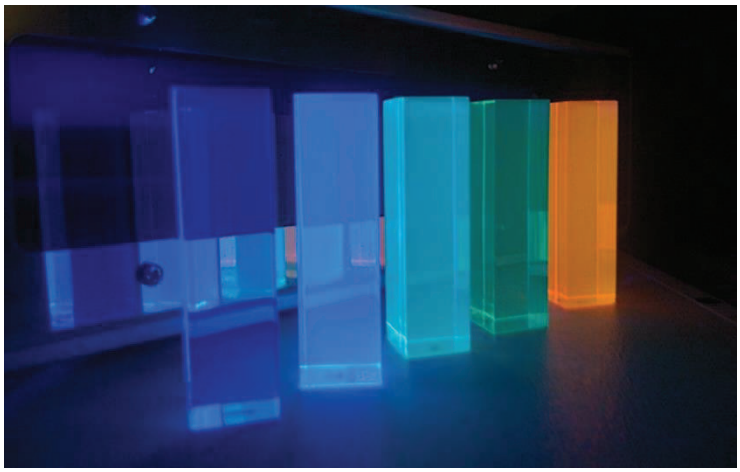

Obrázek 1 Fluorescenční standardy excitované 365 nm. Zleva doprava: anthracen, ovalen, tetrafenylbutadien, sloučenina 610, Rhodamin 6G. Ze sady 6BF (Starna Ltd.).

V současnosti se setkáváme s rozdělením na tepelnou a elektronovou radiaci, ke kterým můžeme přidat vysoce energetické fotony z anihilačních reakcí (elektron-pozitron), které mají příčinu v jaderných procesech, a Čerenkovovo záření[4]. Toto dělení, jistě ne ideální, pak může mezi luminiscence (světélkování způsobené změnou elektronového stavu) zahrnout například i mechanoluminiscenci, která je založená na

[1] Žhnutí – inkadescence, speciální poddruh tepelného záření. Plamen ohně je sám o sobě kombinací různých jevů od tepelného záření po různé typy ionizace.
[2] Bioluminiscence.
[3] Termoluminiscence, tepelné „uvolnění" zakonzervovaného excitovaného stavu.
[4] Částice s fázovou rychlostí větší než je rychlost světla způsobuje polarizaci částic prostředí, jejichž energie se při depolarizaci vhodně sčítá a vytvoří tak elektromagnetickou rázovou vlnu.

mechanickém přerušení chemických vazeb[5]. K luminiscencím pak řadíme dle způsobu excitace elektroluminiscenci (LED), fotoluminiscenci (fluorescence a fosforescence), chemiluminiscenci s poddruhem bioluminiscence, sonoluminiscenci[6] a již zmiňovanou mechano- a termoluminiscenci. Na následujících stránkách budou shrnuty a vysvětleny některé techniky fotoluminiscence, a to zejména fluorescence pro „vlastní oko", pro standardní a vysoce specializované spektrofotometry a velmi pokročilé mikroskopy.

Postupem času se luminiscence stala z kuriozity vědecky studovaným jevem, který i na počátku 21. století je stále živý a stále aktivně rozvíjený v nepřeberné variantě různých výzkumných technik. Podle současného vývoje v publikacích a na vědeckých sympoziích jsou stále zmiňovány dva hlavní zájmové směry ve fluorescenční spektroskopii – *multiparametrická analýza* (zahrnuje i různé hybridní techniky zapojením dalších „nesvětelných" technik) a *vysoce rozlišená mikroskopie* (ta se snaží pomocí různých technik překonat difrakční limity v zobrazování). Myšlenka klasické multiparametrické analýzy, kdy ke správné interpretaci je zapotřebí znát všechny emisní charakteristiky, bude dále rozvíjena v následujícím textu.

Vývoj chemie koloidních systémů nebo lépe koloidní vědy[7] jako chemie a fyziky částic od 1 do 500 nm je spjat s mnoha velkými jmény světové vědy jako Albert Einstein, George Gabriel Stokes, Marian Smoluchowski, Wilhelm Ostwald, Wolfgang Ostwald, Aladár Buzágh a mnoho dalších[8], jejichž jména nesou jevy nebo matematické postuláty, které vysvětlují zákonitosti v této oblasti bádání. Samotné začátky tohoto vědního odvětví, a především pojmenování, jsou spojeny se jménem Thomase Grahama, kterému připomněl zákal po chemické reakci roztok klihu.

Koloidní soustavy, nebo také koloidně disperzní soustavy, mají z definice spojitou a nespojitou část, kdy nespojitá část má alespoň jeden rozměr ve výše zmíněném rozsahu od 1 do 500 nm. Touto definicí zahrnuje koloidní věda systémy od disperzí supramolekul a krystalů po membrány – biologické membrány, pěny atp.

Definice hranic koloidních disperzí souvisí s praktickým pohledem na problematiku. Horní hranice bývá udávána jako nejlepší rozlišení optického mikroskopu, který se udával ve své době jako hodnota 1000 nm – hodnota 500 nm se udává jako střední hodnota vlnové délky viditelného světla. V dnešní době s rozvojem objektivů s vysokou hodnotou numerické apertury (N.A. > 1,0) a rozvojem konfokální (fluorescenční) optické mikroskopie a vysoce rozlišené mikroskopie se rozlišení pohybuje, dle použité vlnové

---

5 Nejlépe lze tento jev pozorovat v tmavé místnosti při rozlepování obálek případně „izolepy" nebo při drcení (kleštěmi) tvrdých bonbónů.

6 Sonoluminiscence vzniká implozí bublinek plynů v kapalinách a v současnosti nemá svou konzistentní teorii vzniku. V současnosti se řadí stále mezi luminiscence, čili se předpokládá, že za emisi fotonu je zodpovědná excitace elektronu.

7 Aladár Buzágh (1895-1962) a Wolfgang Ostwald (1883-1943) byli od začátku proti, aby bylo téma koloidů přiřazeno jako větev fyzikální chemie, ale aby byl přítomný vždy pohled jak chemický, tak i fyzikální a „koloidní věda" byla vnímána jako samostatná disciplína.

8 Hauser, E. A. *J Chem Educ* (1955), 1

délky, okolo 180 nm[9] u konfokálních mikroskopů a až 15 nm v případě vysoce rozlišených mikroskopií (STED mikroskopie). Technika současnosti tedy posunula měřítko pro horní hranici a tato definice již není použitelná. Spodní rozměr souvisí pak s fyzikálně-chemickou definicí povrchu, kdy se předpokládá, že aby bylo možno rozlišit vnitřní a vnější atomy je nejmenším útvarem kulovitý agregát poskládaný z 13 atomů a rozměrem cca 1 nm. Správněji bývá však spodní hranice koloidního „světa" udávána mezi 1 a 5 nm.

Tabulka 1 Přehled koloidních systémů

		Disperzní podíl		
		plyn	**kapalina**	**pevná látka**
Disperzní prostředí	**plyn**	X	aerosol (mlha)	aerosol (dým)
	kapalina	pěna	emulze	sol
	pevná látka	tuhá pěna	gel	tuhý sol

Podrobný výzkum koloidních soustav lze spojit s výzkumem živých systémů, neboť základní funkční složky živých organismů (biopolymery, membrány, organely, buňky) patří svými vlastnostmi do oboru koloidní vědy. Současný rozvoj „nanotechnologie" (technologie systémů velikosti nanometrů) je jen pokračováním výzkumu započatého v 19. století a využívá takřka století půl získaných vlastností a technik vyvinutých pro studium roztoků polymerů, suspenzí, emulzí, pěn a solů. Koloidy jsou všudypřítomné[10], jak již napsal zakladatel fyzikálně chemického výzkumu na „C.k. vysoké škole technické Františka Josefa v Brně" (předtím Česká vysoká škola technická, nyní Vysoké učení technické v Brně), a proto existuje nepřeberné množství variant a typů koloidů, které lze studovat a prohloubit tak pochopení zákonitostí přírody.

[9] Pro rozlišení optického mikroskopu platí spojení Rayleighova kritéria s difrakcí na kruhovém otvoru (cloně) a udává se jako minimální vzdálenost dvou bodů, které je ještě možné rozlišit $x_{\min} = 0{,}61 \cdot \lambda/\mathrm{N.A.}$, kde při hodnotách λ = 400 nm a N.A.(olejová imerze) = 1,4 je $x_{\min}$ = 174 nm.

[10] Baborovský, J. Všudypřítomné koloidy – úvod chemie a fysiky koloidního stavu, *Čin* (1944), 1-207

2 OBECNĚ I PRAKTICKY O FLUORESCENCI VE VÝZKUMU KOLOIDŮ

Tato kapitola bude věnována obecným principům, jak lze využít fluorescenční spektroskopii ke studiu koloidních systémů. Pro pochopení konkrétních případů budou na začátku shrnuty fluorescenční charakteristiky, na jejichž základě pak definujeme vlastnosti studovaných systémů. Dále bude představen návrh obecného schématu pro studium agregujících systémů a budou zmíněny limity, omezení této techniky.

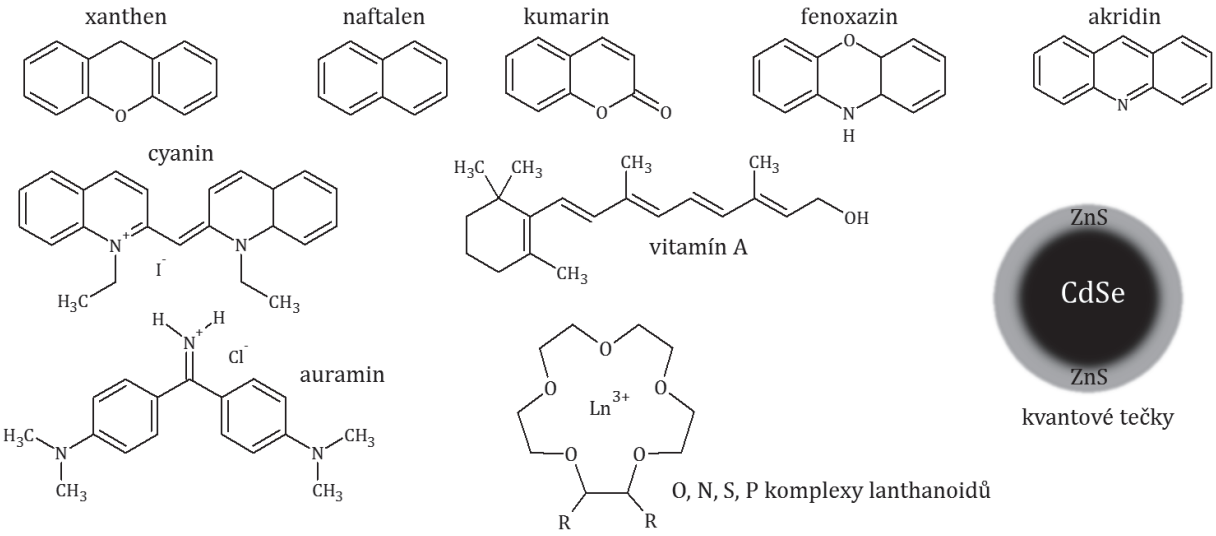

Obrázek 2 Vybrané struktury fluoroforů

Fluorescence je jev, který je spjatý s konkrétními částicemi zvanými fluorofory. V předchozí větě je záměrně užito slova „částice“, protože fluorofory mohou být celé organické molekuly, části organických supramolekul nebo např. různé druhy krystalů. Tyto částice jsou obklopeny svým okolím, které je více či méně ovlivňuje. Pokud je toto ovlivnění známo a je kvantifikovatelné pomocí dané fluorescenční charakteristiky, stává se z daného fluoroforu silný nástroj ke zkoumání vlastností právě tohoto okolí. Je potřeba mít však stále na mysli, že fluorofory jsou ovlivňovány lokálním prostředím a že během standardních experimentů dostáváme výsledné charakteristiky jako kombinaci signálu ze všech prostředí, typů okolí, ve kterých se daný fluorofor nachází. Naštěstí v tomto i jiných případech si fluorescenční spektroskopie dokáže poradit, a dokonce tato spektra od sebe oddělit (technika časově rozlišená emisní spektroskopie). Lokálnost fluoroforu lze vymezit oběma směry, a to pomocí jevů, kdy se excitovaná energie z fluoroforu ztratí. První z nich je tvorba excitovaných dimerů (obecně excitovaných komplexů), kdy například u látky pyren byla stanovena vzdálenost 0,353 nm[11]. Obecně tak nejmenší vzdálenost pro ovlivnění fluoroforu lze definovat jako rovnovážný bod, kdy ještě nedochází k repulzi elektronových obalů. Největší vzdálenost, kdy se ovlivňuje konkrétní fluorofor, pak může být vzata z dosahu jevu rezonanční přenos energie, kdy může být

[11] Mezirovinná vzdálenost dimeru dle Birks, J. B. *Rep Prog Phys* 38 (1975), 903-974

fluoroforu odebrána excitovaná energie až na vzdálenost 10 nm (100 Å). Samostatnou kapitolou pak budou jevy, které ovlivňují fluorofor vázaný na supramolekulární komplex větší než 10 nm a zabraňují například rotaci toho komplexu.

Fluorofory tedy mohou být od velikosti od cca 0,5 nm (naftalen) po krystaly v řádu stovek nanometrů (kvantové tečky, nanodiamanty)[12]. Rozměry společně s chemicky modifikovatelnou afinitou z nich dělají výborné nástroje pro výzkum lokálních vlastností systémů od jednotek do stovek nanometrů – tzv. koloidních systémů (Obrázek 2).

2.1 FLUORESCENČNÍ CHARAKTERISTIKY

Jako fluorescenční charakteristiky míníme vlastnosti světla emitovaného příslušným fluoroforem nebo fluorescenční částicí. Jednotlivý foton má dvě základní charakteristiky – energii (vlnovou délku) a rovinu polarizace vůči námi stanovenému vztažnému systému. Soubor fotonů ze skupiny fluoroforů pak má pak širší distribuci energií i rovin polarizace. Ty odpovídají energetické a časové náročnosti nezářivých procesů v excitovaném stavu (různé druhy relaxace, přenosu náboje) a pravděpodobnosti zářivých přechodů z nejnižšího vibračního stavu prvního excitovaného stavu (i relaxovaného) na různé vibrační hladiny základního stavu – Kashovo pravidlo. Rozložení pravděpodobnosti (četnosti) přechodu pro jednotlivé energie emitovaných fotonů označujeme jako emisní spektrum a distribuci rovin polarizace pak zjednodušujeme promítnutím jednotlivých rovin do dvou základních rovin – horizontální (x-y rovina) a vertikální (y-z rovina).

2.1.1 Stokesův posun

Výše uvedené charakteristiky budou platné pro všechny druhy luminiscence i radiace bez ohledu na excitační mechanismus. Pokud je zdrojem excitace elektromagnetické záření, pak můžeme porovnat energetickou ztrátu emitovaného světla neboli energetickou náročnost nezářivých procesů, porovnáním se světlem excitačním. Tento posun k nižším energiím a tím k vyšším vlnovým délkám je obecným Kashovým pravidlem[13] a posun mezi elektronově ekvivalentními přechody $S_0^0 \rightarrow S_1^0$ pro excitaci a $S_1^0 \rightarrow S_0^0$ pro emisi Stokesovým posunem. Na tomto posunu jsou založeny například technologie optických zjasňovacích prostředků, které absorbují v blízké UV a viditelné fialové oblasti (350-410 nm) a emitují světlo v modré části spektra (400-480 nm). Tedy

[12] Kvantové tečky, up-konverzní částice apod. bývají často označovány za fluorescentní „částice“ a vymezují se tak od fluoroforů, kde lze vysledovat, který z elektronů je zodpovědný za absorpci a emisi.

[13] Jako klasická výjimka bývá uváděn izomer naftalenu **azulen**, který, na rozdíl od naftalenu, má poměrně vysoký dipólový moment, protože je ve skutečnosti tvořený tropyliovým kationtem a cyklopentadienylovým aniontem. V tomto případě pak i takto malá organická molekula emituje záření ve viditelném spektru s nenulovým kvantovým výtěžkem z hladiny S_2^0.

k emisnímu spektru a distribuci polarizace přibyl obecně posun emisního spektra od excitačního (absorpčního)[14].

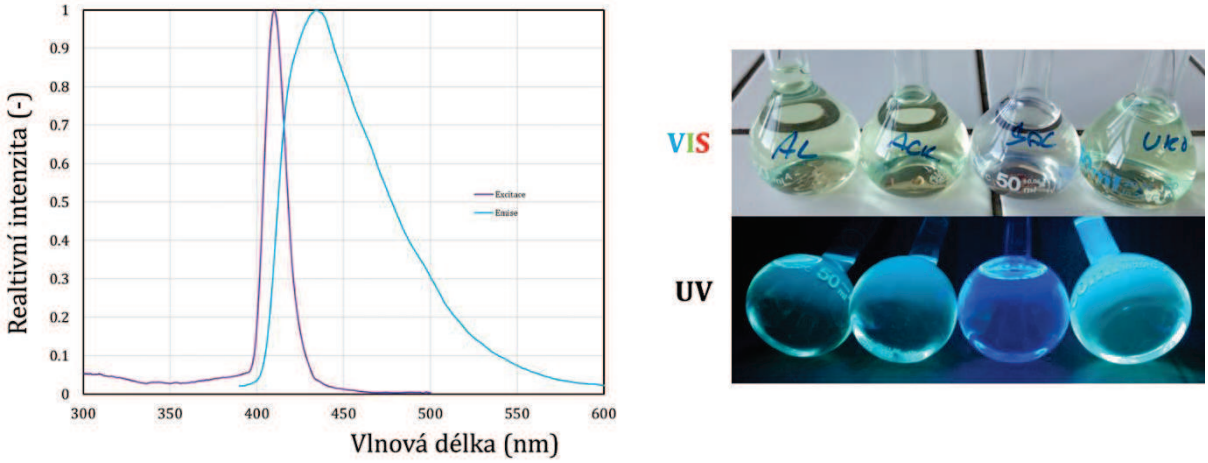

Obrázek 3 Absorpční a emisní spektrum komerčního optického zjasňovacího prostředku Leucophor SAC (Archroma). Vpravo fotky roztoků komerčních OZP Leucophor.

2.1.2 Anisotropie

Pokud máme zdroj excitačního záření s definovanou rovinou polarizace, můžeme projekce rovin polarizace jednotlivých fotonů vztáhnout právě k této rovině a obdržet tak stejnojmennou charakteristiku „polarizace" nebo při zahrnutí všech potenciálních rovin polarizace častěji používanou veličinu anisotropie. Pokud tedy stanovíme intenzitu fluorescence v rovině polarizace shodné s excitační rovinou $I_{\parallel}$ a v rovině k ní kolmé $I_{\perp}$, můžeme polarizaci vyjádřit jako $p = \frac{I_{\parallel}-I_{\perp}}{I_{\parallel}+I_{\perp}}$ a anisotropii jako $r = \frac{I_{\parallel}-I_{\perp}}{I_{\parallel}+2I_{\perp}}$.

2.1.3 Doba života

Další velmi důležitou charakteristikou je střední doba, po kterou trvá záření, pokud excitační záření vyhasne. Jeden elektron se vrátí na základní hladinu v daném konkrétním čase, elektrony skupiny fluoroforů vykazují v čase návratu distribuční charakter, který popisuje adekvátně kinetika prvního řádu. Střední dobou trvání v tomto případě je doba, kdy počet excitovaných elektronů klesne na hodnotu 1/2,71828… (reciproká hodnota Eulerova čísla). V takovém případě pak v daném čase je 67 % elektronů již v základním stavu a 33 % zůstává v excitovaném stavu. Charakteristický čas je tak rychlostní konstantou této reakce a je označován jako doba života excitovaného stavu. Pokud nehrají roli žádné nezářivé procesy, pak tato doba je označovaná jako zářivá (radiační) doba života. Nezářivé procesy, které reálnou dobu života excitovaného stavu ovlivní, jsou většinou výsledkem interakce reálného fluoroforu s reálným prostředím a stanovená

[14] Další výjimka z pravidel se týká důsledku Kashova zákona, který postuluje, že emisní spektrum je nezávislé na použité excitační vlnové délce. V jistých případech (polární molekula ve viskózním polárním prostředí) v důsledku časové shody relaxace okolí a doby života excitovaného stavu dochází k posunu maxima emise s posunem excitační vlnové délky – anglicky Red Edge Excitation Shift. Tento posun může být zajímavý z hlediska prokázání slabé interakce fluoroforu např. s polymery, nebo naopak nese informace o struktuře okolního prostředí.

doba života je tedy charakteristická pro danou kombinaci fluorofor–prostředí. Pokud srovnáme zářivou dobu fluorescence s dobou ovlivněnou všemi dalšími procesy excitovaného stavu, dostáváme efektivitu zářivého procesu, která se nazývá kvantový výtěžek (ϕ).

2.1.4 Intenzita fluorescence

Nezanedbatelnou vlastností je samozřejmě i celkový počet fotonů v daném spektrálním rozmezí za jednotku času – intenzita fluorescence. Z definice intenzity fluorescence vyplývá omezení této charakteristiky[15] – je závislá na třech na sobě nezávislých veličinách: a) molárním extinkčním koeficientu; b) koncentraci; c) kvantovém výtěžku. Tyto tři veličiny mohou výrazně ovlivnit stanovenou hodnotu, a proto tato hodnota nemusí být spolehlivou charakteristikou ohledně informací vlastnosti okolí. Například při vybarvování buněk není reálně ovlivnitelný konečný počet molekul fluoroforu, který daná buňka absorbuje. Dále, při vysoké koncentraci fluoroforů může docházet interakcí v excitovaném stavu ke snižování kvantového výtěžku bez ovlivnění extinkčního koeficientu (pyren a jeho deriváty) nebo dojde k různým typům agregace, které mění jak extinkční koeficient, tak kvantový výtěžek (H a J typy agregace – akridinová oranž, hemicyaninová barviva, atd.). Z toho plyne, že intenzita fluorescence, mimo přísně definované podmínky, není vhodnou fluorescenční charakteristikou a není vhodné ji tak například používat do rovnic vyjadřující Stern-Volmerovu kinetiku nebo Försterův rezonanční přenos energie.

Výjimkou pro praktické použití intenzity fluorescence je ovšem využití dvou nebo více hodnot z emisního nebo excitačního spektra, pokud příslušejí například různým elektronovým stavům (lokálně excitované; stavy s přenosem náboje/elektronu/protonu) nebo různým formám (protonovaná-deprotonovaná). Prosté poměry intenzity jsou intenzivně využívány v automatizovaných analýzách, jako jsou průtokové cytometry, čtečky mikrodestiček apod. V koloidní vědě nenajdeme asi využívanější poměr, než je poměr intenzit pro přechody $S_1^0 \rightarrow S_0^0$ a $S_1^0 \rightarrow S_0^2$ v molekule pyrenu. Tento poměr má mnoho názvů, ale vyjadřuje to samé – jaká je polarita nejbližšího okolí molekul pyrenu. O využití a omezení toho parametru bude pojednávat kapitola 2.4. Je důležité zmínit, že využití poměru intenzit může být užitečné i pro situace, kdy chceme kvantifikovat jemný posun emisního/excitačního spektra, například o 2-5 nm.

2.1.5 Fluktuace fluorescence

Další využití intenzity spočívá v zaznamenávání její časové změny. Pokud tato časová změna má periodický charakter, fluktuuje, můžeme pomocí vhodné matematické metody tuto periodicitu odhalit a přiřadit jí amplitudu a charakteristický čas. Tento čas

---

[15] Intenzita fluorescence F je definována vztahem $F = k \cdot I_0 \cdot \Phi \cdot (1 - 10^{-\varepsilon_\lambda \cdot c \cdot l})$, kde k je přístrojová konstanta, I_0 je intenzita dopadajícího záření, Φ je kvantový výtěžek, ε_λ je molární extinkční koeficient, c je molární koncentrace fluoroforu/částice a l je optická dráha v centimetrech. Pokud je pohlceno méně než 2 % dopadajícího záření, rovnice přechází na tvar: $F = k \cdot I_0 \cdot \Phi \cdot \varepsilon_\lambda \cdot c \cdot l$.

může být dále interpretován podle zdroje fluktuací jako translační nebo rotační difúzní koeficient, rychlostní konstanta chemické reakce apod. Amplituda je přiřazena střednímu počtu částic v daném místě pozorování. Pokud intenzita fluorescence nefluktuuje, ale klesá nebo stoupá, jedná se o další techniky, které se využívají na odhalení mobility jednotlivých fluoroforů nebo částic tyto fluorofory nesoucích.

Pro analýzu koloidních systémů jsou tedy k dispozici:

- tvar a pozice emisního spektra,
- doba života její distribuce pro různé vlnové délky,
- anisotropie – střední hodnota, rozložení během doby života, distribuce pro různé vlnové délky,
- intenzita fluorescence a její fluktuace.

Ke všem výše zmíněným charakteristikám lze přiřadit ještě prostorovou distribuci při použití např. konfokálního mikroskopu s možností skenování nebo jeho ekvivalentní varianty.

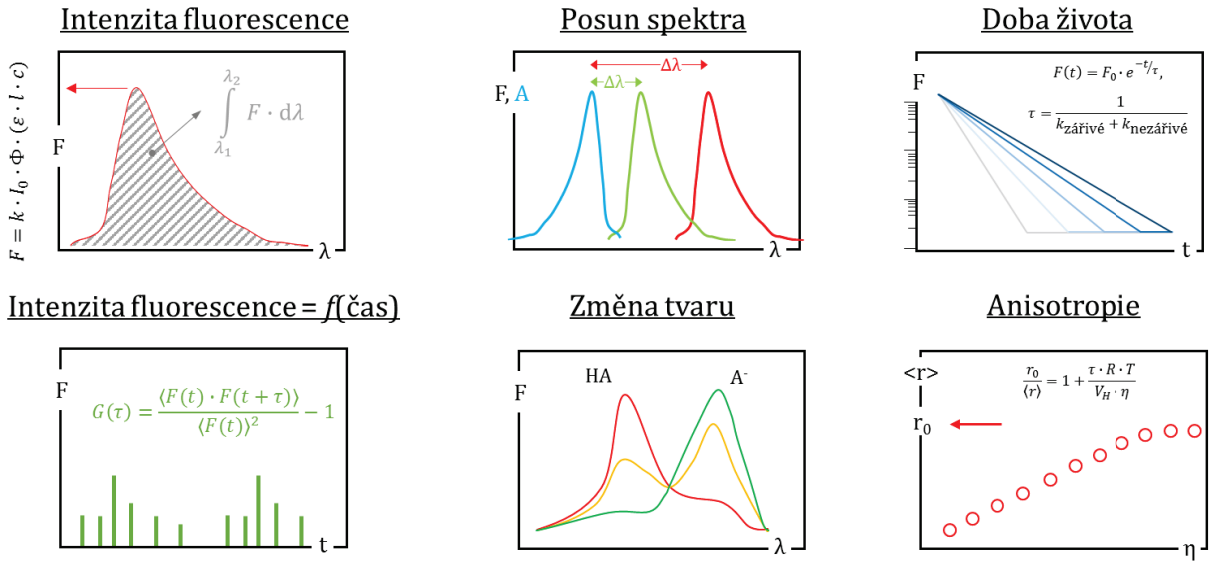

Obrázek 4 Přehled fluorescenčních charakteristik a jejich vybraných závislostí.

2.2 NÁVRH OBECNÉHO STUDIA AGREGAČNÍCH PROCESŮ

V rámci spolupráce s komerčními výrobci hydrofobně modifikovaných derivátů polymerů vznikla potřeba stanovit konečným počtem kroků, zda výsledný derivát splňuje kvalitativní vlastnosti požadované pro nosičový systém. Další požadavek byl, aby se nepoužívalo příliš sofistikované vybavení. Vytvořením tohoto návrhu byl pověřen autor této habilitace.

Níže uvedené schéma (Obrázek 5) ukazuje takovýto návrh. Sleduje cestu možných jednoduchých testů a navrhuje i další možnosti využití derivátů, které nesplní očekávané

hodnoty. Schéma není vyčerpávající z hlediska finalizace nosičového systému, nicméně může tvořit dobrý základ jako první série testů a pomoct tak v první fázi vyřadit nevhodné nebo neagregující systémy.

Základní testování spočívá ve využití tří typově odlišných fluorescenčních sond. Perylen je velmi omezeně rozpustný ve vodě ($1{,}58 \cdot 10^{-9}$ mol·L^{-1} při 25 °C)[16] a preferuje nejnepolárnější části agregátů (logaritmická hodnota rozdělovacího koeficientu log K_{OW} = 6,30)[17]. Pyren je nejpoužívanější sonda pro studium průběhu agregace díky citlivější reakci na změnu polarity, což mu právě umožňuje jeho vyšší rozpustnost ve vodě ($6{,}68 \cdot 10^{-7}$ mol·L^{-1} při 25 °C)[18] a nižší rozdělovací koeficient olej/voda (log K_{OW} = 4,88)[19]. 1-anilinonaftalen-8-sulfonát amonný (ANSA) je nejrozpustnější z uvažovaných sond (dle produktového listu dodavatele 0,16 mol·L^{-1})[20], nicméně i tato vykazuje fluorescenci pouze po navázání do hydrofobních domén bílkovin, micelární palisádové vrstvy apod.

Úvaha je následující: pokud daný systém rozpustný ve vodě je schopný solubilizovat perylen, znamená to, že i přes hydrofilní charakter obsahuje velmi nepolární jádro. Pomocí pyrenu je pak možno popsat agregační proces daného systému a rozhodnout, jestli systém agreguje v rámci jedné molekuly (roubované kopolymery formující polymerní micely jako intramolekulární agregáty), nebo je to vícemolekulový proces (intermolekulární agregáty amfifilních látek nebo blokových kopolymerů).

V případě intramolekulárních agregátů odpadají potíže se zředěním daného systému, ovšem nastává otázka rozměru nepolární domény a její schopnosti nejen nést, ale zároveň chránit nepolární aktivní látku. Velké bioaktivní molekuly nemají většinou jednotný charakter polární/nepolární, ale obsahují často skupiny nebo oblasti s různou afinitou k prostředí. Takovéto molekuly se pak mohou částečně solubilizovat, částečně adsorbovat na nosič. V tomto případě je taková látka vystavena prostředí, které může ovlivnit její funkci nebo může být uvolněna na nevhodném místě, případně adsorbována nepolárními doménami přítomných supramolekulárních agregátů. U tohoto typu agregátů je pak potřeba solubilizačními nebo lokalizačními testy prokázat rozměr a kvalitu hydrofobní domény a lokalizaci aktivní látky.

Intermolekulární agregáty jsou tvořeny obvykle desítkami až stovkami nízkomolekulárních amfifilních látek případně jednotkami až desítkami molekul blokových kopolymerů (di-blok, tri-blok). Takovéto systémy jsou dle velikostí svých monomerů a předpokládanému typu agregátů – micely nebo vezikuly – predikovatelné co do solubilizačních schopností vůči různě velkým solubilizátům. U těchto látek nastává

[16] Yalkowsky, S.H., He, Yan, Jain, P. *Handbook of Aqueous Solubility Data* Second Edition. CRC Press, Boca Raton, FL 2010, p. 1216
[17] Andersson, J.T., Schrader, W. *Anal Chem* 71 (1999), 3610-3614
[18] Miller, M.M. et al. *Environ Sci Technol* 19 (1985) 522-529
[19] Hansch, C., Leo, A., Hoekman, D. *American Chemical Society*. (1995), 137
[20] https://www.sigmaaldrich.com/content/dam/sigma-aldrich/docs/Sigma/Product_Information_Sheet/a3125pis.pdf (2.5.2018)

problém s jejich praktickým použitím, kdy se např. při intravenózním podání naředí daná směs až 1 000krát[21]. V tomto případě je vhodné volit pro tyto aplikace agregáty na bázi liposomů, které se po formování při ředění nerozpadají. Dalším pomocným měřítkem bude hydrofilně-lipofilní rovnováha (hydrophilic-lipophilic balance), která například pomocí sumy příspěvků jednotlivých skupin pomůže určit afinitu amififilní látky k polárnímu nebo nepolárnímu prostředí.

Varianta, kdy ze systému svítí jen ANSA, znamená, že hydrofobní domény jsou malé a pouze na povrchu, respektive že jsou dostupné právě jen ty na povrchu. V tomto případě, pokud má systém nějakou přidanou hodnotu, je přípravu potřeba rozšířit o fyzikálně-chemické postupy zahrnující například dialýzu z roztoku látek ve směsi rozpouštědel vhodných pro obě složky oproti vodě, lyofilizaci roztoku látek ze směsi rozpouštědel apod. Případné solubilizáty ve formě fluorescenčních sond nebo aktivních látek je potřeba přidávat ve většině případů do výchozí směsi před např. dialýzou.

Posledním měřítkem bude rozměr samotného agregátu společně s charakterem jeho povrchu. V případě stanovení rozměru agregátu (hydrodynamického poloměru), lze s úspěchem využít metodu fluorescenční korelační spektroskopie, která je vhodná i pro studium stability nebo případné sorpce ostatních látek na systém v daném prostředí. Obecně se uvádí, že pro úspěšnou dlouhodobou cirkulaci v těle (enhanced permeability and retention effect, EPR effect), je potřeba držet rozměry agregátu mezi 5 až 200 nm (někde uváděno užší rozmezí 10-100 nm)[22], což jsou rozměry, se kterými ideálně pracuje metoda FCS[23]. Pro úplnost zmíněný charakter povrchu, ideálně bez sorpce bílkovin, hydrofilní a nenabitý, je charakterizovatelný pomocí fluorescenční spektroskopie, nicméně je zde jednodušeji využitelná metoda stanovení zeta-potenciálu.

Metoda fluorescenční sondy má jednu výhodu, která spočívá v tom, že netestuje „prázdné“ agregáty, ale podává přehled o těch, které obsahují fluorescenční sondu. Měřením vlastností takovýchto agregátů pak pokládá základ pro solubilizační testování případných nosičových systémů. Lze tedy říci, že pokud se nepodaří „vybarvit“ agregát fluorescenční sondou, pak pravděpodobně nebude možné tento systém „naplnit“ aktivní látkou stejného charakteru. Existují aktivní látky, které fluoreskují (vitamíny A, E, B_2; cytostatikum doxorubicin apod.) a lze je použít pro výzkum i kvantifikaci solubilizace danými systémy. Díky velkému množství fluoreskujících látek lze takřka pro každou nefluoreskující a obtížně stanovitelnou aktivní látku najít fluorescenční analog, který poslouží pro testování nosičového systému. Jako dva základní parametry shodnosti aktivní látky a fluoroforu můžeme navrhnout solvodynamický poloměr a rozdělovací koeficient.

[21] Číslo založeno na administraci 5 mL roztoku do cca 5 L krve.
[22] Petros, R.A., DeSimone, J.M. *Nat Rev Drug Discov* 9 (2010), 615-627
[23] Velmi cenné review **Koynov, K., Butt, H.-J., Curr Opin Colloid In 17 (2012) 377–387**

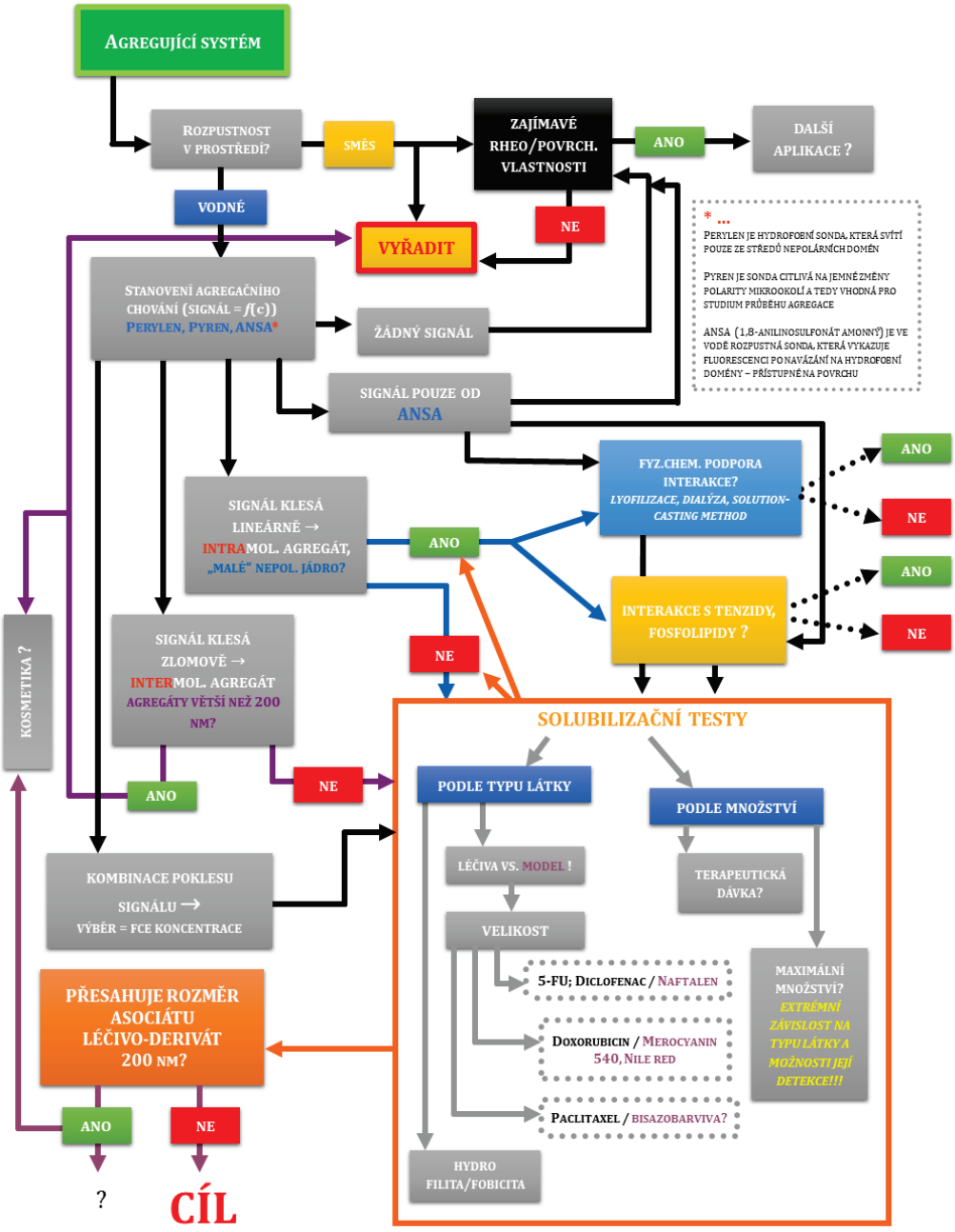

Obrázek 5 Workflow schéma využití fluorescenční spektroskopie pro studium agregujících systémů s uvažovaným využitím v nosičových systémech.

Pokud tedy se systém ukáže jako vhodný pro přenos dané látky a výsledný komplex opět bude v přijatelném rozsahu velikostí, může následovat pokročilejší testování systémů, které mohou být založeny na pokročilejších fluorescenčních technikách.

Jako první můžeme uvést lokalizaci dané látky nebo fluoreskujícího analogu v rámci agregátu pomocí místně selektivních zhášečů fluorescence. Nejúčinnějším zhášečem je atom jódu, který může být použitý jako součást organického nebo anorganického komplexu. Pro exponované fluorofory umístěné ve vnějších vrstvách agregátů je účinným zhášečem anion iodu, nejčastěji ve formě KI. Hlouběji zanořené fluorofory, které se

pohybují v palisádové vrstvě, se používá 3-iodpropanová kyselina nebo cetyltrimethylamonium chlorid. Fluoreskující látky zanořené do hydrofobního jádra zháší fenyliodid[24].

Druhou technikou, kterou lze úspěšně využít, je fluorescenční korelační spektroskopie, využitelná pro stanovení nízkých koncentrací látek a je tak použitelná ve studiu uvolňování aktivních látek. Z měření zároveň vyplývá, jestli fluoreskující látka je rozpuštěná v molekulární formě, nebo je součástí většího agregátu – tyto informace poskytuje difúzní koeficient.

Závěrem této části lze shrnout, že uvedené schéma i přes svou složitost nakonec odpovídá logickým krokům pro studium podobných systémů. V případě malého množství vzorku lze jednotlivé členy agregační řady využít k dalším experimentům např. pro stanovení vlivu iontové síly nebo stanovení hydrodynamické poloměru apod.

2.3 OMEZENÍ, PROBLÉMY… A JEJICH MOŽNÉ ŘEŠENÍ

Technika fluorescenční spektroskopie bude citlivá na podobné problémy jako jakákoliv spektroskopie využívající spektrální oblast 200 až 800 nm, respektive až 1 500 nm. Problémy se mohou týkat jak samotné instrumentace, tak i charakteru vzorku. Opomenutí těchto omezení pak vede ke špatné interpretaci naměřených dat.

2.3.1 Excitace a detekce

Standardní spektrofluorimetry nebo luminiscenční spektrometry mají rozsah excitačních vlnových délek daný rozsahem excitačního zdroje, kterým bývá nejčastěji xenonová výbojka. Tyto výbojky jsou pro praktické použití vybaveny vrstvou, která absorbuje vlnové délky do cca 250 nm z důvodu omezení tvorby ozonu, nicméně toto zmenšuje dostupný excitační rozsah. Kromě zdrojů s více či méně kontinuálním spektrem emitovaných vlnových délek lze použít ještě diskrétní laserové zdroje, které mají velmi úzkou distribuci vlnových délek a je tak omezena jejich univerzálnost. V současnosti jsou na trhu dostupné takzvané „bílé lasery“ nebo „superkontinuální lasery“, které kombinací krystalů nebo laserových barviv pokrývají aktuálně spektrální rozsah 400-900 nm, což opět není příliš praktické z důvodu chybějících vlnových délek pod 400 nm. Z hlediska koloidních systémů je výhodné mít co nejširší excitační možnosti, především z hlediska rozptylu excitačního paprsku, který bývá často přítomný v koloidních systémech.

2.3.2 Kompenzace rozptylu a vysoké koncentrace fluoroforů

Rozptyl je nepřímo úměrný mocnině vlnové délky a je tedy výhodnější použít vlnovou délku 800 nm spíše než 400 nm. Nutnou podmínkou ovšem je získat shodné informace při použití různé vlnové délky. To lze řešit použitím sond s výrazně posunutou absorpcí k blízké infračervené části, které mají obdobnou reakci na studovanou veličinu.

[24] Deumié, M., El Baraka, M., Quinones, E. *J Photoch Photobio A* 87 (1995), 105-113

V tomto případě je ale nutné mít i příslušný detektor, citlivý na příslušnou oblast, což v současnosti není jednoduché[25].

Pokud není možné změnit fluorofor, je potřeba co nejvíce potlačit rozptyl světla v takovýchto systémech. V tomto případě se rozptyl týká i emitovaných vlnových délek, protože o ty jde především. V zásadě lze použít tři různé přístupy: 1) změnit trajektorii excitace a emise; 2) použít polarizátory a 3) kompenzovat spektrální prostupnost pro různé vlnové délky pomocí absorpční spektrofotometrie - potlačení vnitřních filtračních efektů I. a II. druhu.

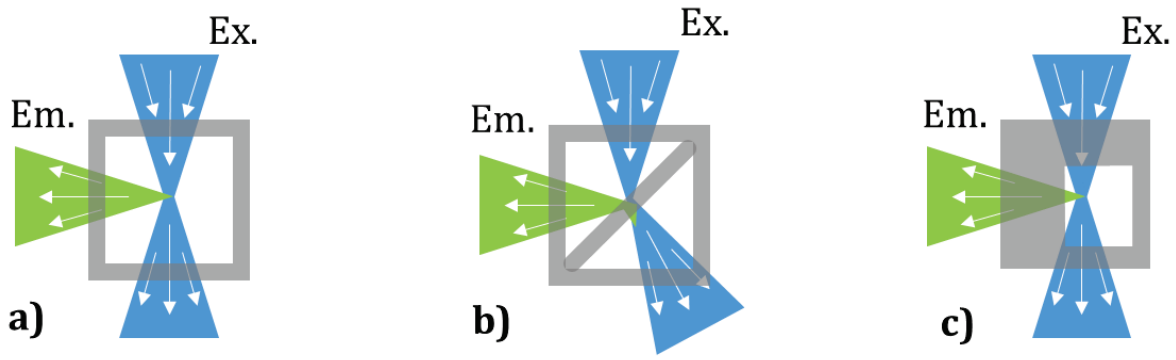

Obrázek 6 Různé způsoby excitace za použití speciálních kyvet. Obrázek schematicky ukazuje, jak lze za použití speciálních kyvet dosáhnout různých způsobů excitace. a) pravoúhlá excitace (RA); b) excitace povrchové vrstvy (FF); c) mimostředová excitace (OC).

1) Změna trajektorie souvisí s různým úhlem mezi excitačním emisním paprskem. Ve většině případů „klasických" stolních spektrofluorimetrů se užívá pravoúhlé uspořádání, které bývá nazýváno anglicky „right-angle" (Obrázek 6). Dalšími možnostmi jak excitovat a posléze snímat jsou například tzv. „front-face" (snímání z přední povrchové vrstvy) případně „off-center"(mimostředová excitace). Tyto typy geometrií jsou využívány přednostně v případech, kdy jsou vzorky příliš koncentrované (z hlediska fluoroforu), zakalené nebo pevné. Ve většině případů se pro tato měření vyrábějí speciální kyvety, které jsou kompatibilní se standardním kyvetovým prostorem. Speciální variantou je i použití integrační sféry (integrating sphere). Tato sférická dutina je pokrytá takřka 100% odrazivým materiálem (například slinutý PTFE tzv. Spectralon), který zvyšuje vícenásobným odrazem od stěn směrem ke vzorku pravděpodobnost absorpce, pokud fotony

[25] Z hlediska současné dostupné instrumentace je nejpalčivější problém detekce právě v přechodové oblasti VIS-NIR tj. v oblasti mezi 800 a 900 nm. U standardních fluorimetrů se předpokládá větší pravděpodobnost práce v UV-VIS než v VIS-NIR oblasti, proto je většina fluorimetrů vybavena fotonásobiči, které efektivně pokrývají spektrální rozsah mezi 220-800 nm. Pro oblast blízké NIR je pak používán další detektor, nejčastěji kapalným dusíkem chlazený InGaAs detektor s deklarovanou citlivostí 800–1500 nm. V každém případě je dle dostupných charakteristik kvantová účinnost detektorů v dané oblasti okolo 10 %. Jsou dostupné i excelentně citlivé detektory s kvantovou účinností ~10-15 % při 900 nm (např. křemíkové Excelitas® detektory).

první průchodem nebyly absorbovány. Zároveň sbírá i rozptýlené emitované fotony, kterým umožnuje průchod na detektor jen jedním výstupem.

2) Použití polarizátorů značně zeslabuje excitační a detekovaný proud fotonů, nicméně může pomoci, zvláště pokud je potřeba vykreslit spektrum látky s velmi malým Stokesovým posuvem v zakalené disperzi. Polarizátory se používají v kolmé konfiguraci (horizontálně umístěný emisní polarizátor odfiltruje většinu rozptýleného vertikálně polarizovaného excitačního záření, protože rozptýlené světlo udržuje původní směr polarizace) nebo je ponechán excitační polarizátor vertikálně a emisní je nastaven na hodnotu magického úhlu 54,7°. Toto samozřejmě neplatí vždy ideálně a podle typu materiálu (přítomnosti různých chirálních center) dochází různě ke stáčení roviny polarizace rozptýleného světla.

3) Poslední přístup je nejzásadnější a pro vykreslování spekter a následné používání intenzity fluorescence, ať jako integrál pod spektrem nebo při jedné vlnové délce, je absolutně nezbytný. Pomocí absorpčního spektrofotometru lze otestovat vzorek pro spektrální propustnost na všech excitačních i emisních vlnových délkách a pro danou optickou dráhu (různá při různých geometriích). Standardně se vztahuje pozorovaná intenzita fluorescence na transmitanci při dané excitační a emisní vlnové délce. Prakticky se provádí měření v kyvetě s optickou dráhou 1 cm tak, aby absorpční spektrum zahrnulo všechny excitační a emisní vlnové délky. Obdržené hodnoty absorbance se vztáhnou k hodnotě optické dráhy a dostáváme univerzální veličinu optická hustota (optical density, OD), která vyjadřuje zeslabení vzorku absorpcí a rozptylem. Tato veličina se pak násobí danou optickou dráhou *l* pro excitaci a emisi (v pravoúhlé konfiguraci obě 0,5 cm) a její negativní hodnota jako mocnina čísla deset pak putuje do jmenovatele pro korekci pozorované intenzity fluorescence. Korekční vztah pak je:

$$F_{korigovaná} = F_{pozorovaná} \cdot 10^{l_{ex} \cdot OD_{ex}} \cdot 10^{l_{em} \cdot OD_{em}}.$$

Omezení tohoto přístupu bude omezením rozsahu absorpčního spektrofotometru, kdy současný střízlivý limit pro měření absorbance je do hodnoty 3. Od této hodnoty výše pak přístroje vykazují značný, převážně náhodný, šum hodnot.

Nezbytnost korekce zvláště pomocí posledně zmíněného přístupu lze jen těžko pominout, nicméně v mnoha vědeckých článcích tato korekce není zmíněna. Zvláště patrné je to při měření koncentrovanějších roztoků, než je například 10^{-7} mol·L^{-1} pro fluorofory s extinkčním koeficientem 60 000-100 000 L·mol^{-1}·cm^{-1} (viz Tabulka 2) nebo pokud vzorek obsahuje jiné chromofory případně fluorofory, které mohou absorbovat různě pravděpodobně na různých vlnových délkách (např. půdní výluhy). Zároveň je toto korigování nezbytné i v případě měření rezonančního přenosu energie se zvyšujícím se množství akceptoru, který z principu metody má absorbovat při emisních vlnových délkách donoru.

Tabulka 2 *Tabulka pro modelový příklad nutnosti použití korekce vnitřních filtračních efektů pro různě koncentrované roztoky fluoroforů bez zahrnutí rozptylu nebo koabsorbce dalšími fluorofory. První sloupec představuje koncentraci fluoroforu, druhý hodnotu extinkčního koeficientu při excitační vlnové délce, třetí sloupec zahrnuje vlnové délky, kdy je 25% pravděpodobnost reabsorpce emitovaného fotonu druhým fluoroforem stejného druhu. Čtvrtý sloupec pak ukazuje hodnoty korigované hodnoty fluorescence při naměřené hodnotě fluorescence* ***100,0*** *pro vlnové délky s 25% šancí reabsorpce, Fkor 25 %, a pátý sloupec pro nulovou pravděpodobnost reabsorpce, Fkor 0 %.*

koncentrace	extinkční koeficient při excitační vlnové délce	extinkční koeficient při emisní vlnové délce	Fkor 25 %	Fkor 0 %
mol L^{-1}	L mol^{-1} cm^{-1}	L mol^{-1} cm^{-1}	a.u.	a.u.
10^{-8}	**100 000**	**25 000**	100,1	100,1
	80 000	**20 000**	100,1	100,1
	60 000	**15 000**	100,1	100,1
10^{-7}	**100 000**	**25 000**	101,4	101,2
	80 000	**20 000**	101,2	100,9
	60 000	**15 000**	100,9	100,7
10^{-6}	**100 000**	**25 000**	115,5	112,2
	80 000	**20 000**	112,2	109,6
	60 000	**15 000**	109,0	107,2
10^{-5}	**100 000**	**25 000**	421,7	316,2
	80 000	**20 000**	316,2	251,2
	60 000	**15 000**	237,1	199,5

2.3.3 Příprava vzorků pro spektroskopii

Většina koloidních systémů nevykazuje fluorescenci sama o sobě, tzv. autofluorescenci, ale je potřeba je fluorescenčně vybarvit. Fluorescenční barvení je obecně dvou typů: a) metoda fluorescenční značky (angl. Fluorescence labeling); b) metoda fluorescenční sondy (angl. Fluorescence probing).

V prvním případě dochází k chemickému navázání fluoroforu na danou koloidní částici, což může samozřejmě změnit její chování v roztoku. Chemická vazba fluoroforu je tak přijatelná povětšinou pro velké a rigidní polymery (polysacharidy, bílkoviny). Nevýhody tohoto přístupu jsou již zmíněné ovlivnění vlastností koloidu a případná nestabilita vazby, protože fluorofor nemá většinou sám o sobě afinitu k místu, ke kterému je fyzikálně vázán. Z měření spekter, intenzity fluorescence nebo doby života nelze určit, jestli je měřen komplex koloid-značka nebo směs koloid + fluorofor. To lze odhalit pokročilejšími měřeními jako je fluorescenční korelační spektroskopie nebo anisotropie[26].

[26] Příkladem mylného vyhodnocení může být situace, kdy je využito rezonančního přenosu energie pro studium změny konformace proteinu. Vymizení efektu přenosu energie může být způsobeno oddálením segmentů nesoucích donor a akceptor, stejně tak ovšem může být způsobena hydrolýzou vazby donoru nebo akceptoru. Existuje však způsob ověření, jestli jsou stále oba fluorofory součástí jedné koloidní částice, a to dvoubarevná FCS, kdy dostáváme nenulový signál při kroskorelaci donorového a akceptorového kanálu jen v případě, že jsou oba lokalizovány na stejné částici, která difunduje pozorovaným objemem.

Metoda fluorescenční sondy přináší jiná úskalí. Jedno z největších je konkrétní lokalizace v heterogenních systémech, protože fluorofory se v tomto případě rozdělují v systému dle své afinity k danému prostředí. Rozdělování v mnoha případech podléhá rovnováze a je tedy obtížné najít jednu fluorescenční sondu jen na jednom místě. Příkladem můžou být dvě velmi často používané fluorescenční sondy – perylen a *N*,*N*-dimethyl-6-propionyl-2-naftylamin (prodan). V micelárním systému je perylen, silně hydrofobní polyaromatický uhlovodík, z 99,9 % lokalizovaný v nejhydrofobnější části koloidního systému - micelárním jádře (dle 16 a 17). Substituovaný naftalen prodan je naopak zastoupen různou měrou ve všech prostředích micelárního systému – volné prostředí, palisádová vrstva a micelární jádro[27]. Jednotlivá prostředí v heterogenních systémech se liší polaritou, relaxačním časem okolního prostředí, lokální hustotou náboje v případě např. ionogenních tenzidů. Toto všechno se projevuje ve spektrech například posunem nebo rozdvojením emisních pásů, protože iluminovaný a detekovaný objem je o několik řádů větší, než jsou struktury ve studovaném systému a přístroj detekuje signál ze všech domén. Velkou pomocí v tomto případě je stanovení doby života, která bude v různých částech odlišná a umožní při znalosti rozložení dob života při emisních vlnových délkách dekonvoluci takového signálu (časově rozlišená emisní spektroskopie, time-resolved emission spectroscopy, TRES).

Další problém může představovat vnášení fluorescenční sondy do systému. V předchozím oddíle jsme ukázali, že optimální koncentrace fluoroforu pro měření na klasickém spektrofluorimetru je řádově 10^{-7} mol·L^{-1}. Minimální objem vzorku pro měření ve standardní kyvetě s optickou dráhou 1 cm je 3 mL resp. naplnění kyvety o základně 1 x 1 cm do výšky 3 cm[28]. Pokud tedy zvolíme základní objem vzorku třeba 5 mL, je celkové látkové množství fluoroforu ve vzorku $5 \cdot 10^{-10}$ mol. Při střední molekulové hmotnosti 500 g·mol^{-1} je pak celková navážka pro jeden vzorek $2{,}5 \cdot 10^{-7}$ g, což je mimo možnosti přímého vážení. Toto se řeší dvěma různými způsoby s ohledem na rozpustnost sondy ve vodě:

a) Fluorofory rozpustné ve vodě je možno připravit ve formě o tři řády koncentrovanějšího zásobního roztoku, než je požadovaná finální koncentrace. V případě vzorku o konečném objemu 5 mL je možné k danému systému přidat například 5 µL zásobního roztoku a započítat ředění, nebo ředění zanést již do přípravy daného sytému. V případě měření koncentračních závislostí koloidních systémů lze říci, že oba přístupy jsou ekvivalentní a záleží na složitosti přípravy samotného koloidního systému.
b) Elegantnější varianta je využívána u vzorků nerozpustných ve vodě. Obdobně se připraví o tři řády koncentrovanější roztok fluoroforu v těkavém rozpouštědle – ideálně acetonu, případně chloroformu nebo

[27] Např. Karukstis, K., McDonough, J. *Langmuir*, 2005, vol. 21, pp. 5716-5721.
[28] Skutečný profil paprsku, který dopadá na kyvetu je daný konečnou velikostí výstupní štěrbiny a případným dalším fokusačním prvkem, čočkou, a tedy může se měnit dle daného typu spektrofluorimetru.

methanolu. Do prázdné vialky se napipetuje příslušné množství zásobního roztoku a rozpouštědlo se nechá vytěkat, nebo se mu pomůže zahřátím, snížením tlaku nebo prouděním vzduchu či inertu (N_2, Ar, He) okolo ústí vialky. Fluorofor na dně vialky rekrystalizuje do formy velmi malých krystalků (Obrázek 7), které pak mohou být snadněji solubilizovány koloidním systémem.

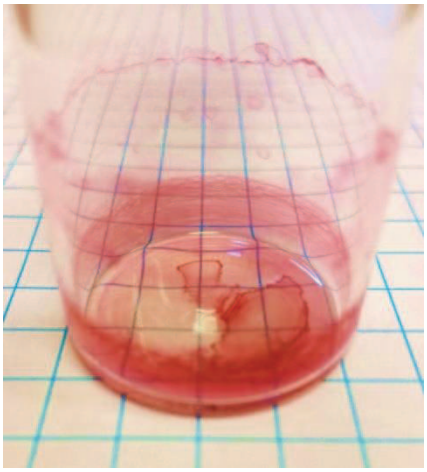

Obrázek 7 Rekrystalizované barvivo Nilská červeň z acetonového roztoku ve vialce. Množství barviva je řádově větší pro lepší vizualizaci.

2.3.4 Příprava vzorků pro mikroskopii

Příprava mikroskopických vzorků je velmi rozmanitá a záleží na druhu vzorku a požadované analýze – jiné podmínky budou platit pro měření fluktuace fluorescence v koloidech jiné pro mapování pH v živých buňkách. Popsat komplexní přípravu mikroskopických vzorků překračuje rámec této práce, nicméně některé specifické metody fixace a přípravy vzorků budou popsány v kapitolách s konkrétními praktickými příklady.

Pokud se zaměříme pouze na vybarvování vzorků, pak máme před sebou tři možné situace: 1) vzorek je fluorescentní; 2) vzorek je nefluorescentní; 3) vzorek nevykazuje požadovanou fluorescenci, a navíc je živý.

V prvním případě je problém, pokud je vzorek „dobrým“ (vysoká absorpce, vysoký kvantový výtěžek) fluoroforem nebo fluorescentní částicí. Pro měření parametrů pomocí fluorescenční korelační spektroskopie platí omezení počtu částic v pozorovaném objemu. Pokud je tedy studována koncentrační závislost, musí se rozmezí držet v daném, v absolutních hodnotách nízkém, koncentračním rozsahu. Další variantou je tento experiment provést s nefluorescentními částicemi stejného druhu – fluorescentní částice by pak měly charakter fluorescenční sondy. Toto je například nezbytné, pokud studujeme agregace pozorováním změny difúzního koeficientu například pomocí fluorescenčně

značených polymerů[29]. Pokud toto není možné, tak je zde možnost použití jiného dalšího, bathochromně posunutého, fluoroforu nebo jiná varianta difúzního studia (alternativa pro FCS by mohl FRAP – sledování obnovení fluorescence po fotovybělení).

Pokud pracujeme s nefluorescentním vzorkem, pak postup vybarvení bude záviset na charakteru vzorku a příslušné formy fluoroforu. Pro aplikace využívající fluktuaci intenzity je opět nutné držet koncentraci fluoroforu v nanomolární koncentraci. Vzorky o definované koncentraci se velmi obtížně připravují a finální vzorek není takřka možné zkontrolovat jiným analytickým postupem. Jako nejoptimálnější se jeví postup, kdy pomocí známého extinkčního koeficientu nebo připravené kalibrační závislosti stanovíme koncentraci vzorku s absorbancí v rozmezí 0,1-0,5. Tento vzorek se pak rozředí pomocí analytických vah na požadovanou koncentraci. Při přípravě je potřeba uvažovat i způsob jeho vnesení do vzorku, jestli nese kladný náboj nebo je například hydrolyzovatelný. Pokud si připravujeme zředěný zásobní roztok, který hodláme dále ředit o 2 až 3 řády, je vhodné jej připravit například jako roztok v DMSO, který zabrání hydrolýze (v ledničce tuhne), má nízkou tenzi par, vysoký bod varu a je ředitelný vodou.

Třetí varianta je nejkomplikovanější a paradoxně zároveň nejjednodušší. Jednoduchost spočívá v existenci spousty předpřipravených postupů a kitů, které celou věc značně ulehčují. Živé buňky je potřeba s barvivem a pomocnými látkami kultivovat v optimálním prostředí, které umožní průnik látky přes membrány. Komplikovanost souvisí s úrovní vybarvení jednotlivých buněk, resp. organel. Pro analýzy založené na monitorování doby života nebo intenzity fluorescence na různých kanálech toto není velkým problémem, ovšem pro koncentračně citlivou metodu jako je FCS to naopak problémem je. U živých systémů navíc hraje roli i silná autofluorescence v UV i VIS oblasti, která bude fluktuační analýzy rušit. Je potřeba samozřejmě počítat, že tak komplexní koloidní systémy jako jsou živé buňky, se chovají autonomně.

2.4 PYREN JAKO FLUORESCENČNÍ SONDA

Pyren, systematicky benzo[d,e,f]fenanthren, je bezesporu nejpoužívanější fluorescenční sondou pro studium agregačních procesů v koloidních systémech. Je rovněž hojně využíván pro stanovení agregačního čísla pomocí zhášení. Je to sudý alternující uhlovodík s D2h symetrií.

Využití pyrenu jako fluorescenční sondy je spojeno s jeho vcelku unikátní reakcí na polaritu svého mikrookolí. Obecně se dá říci, že intenzita prvního vibračního přechodu ($S_1^0 \rightarrow S_0^0$, lokalizovaného okolo 373 nm) a společně s ním i druhý ($S_1^0 \rightarrow S_0^1$, lokalizovaný

[29] Pokud byl studovaným polymerem například nativní hyaluronan, předpokládá se, že přechod ze zředěného do polozředěného režimu nastává u jednotek gramů na litr. Při průměrné molekulové hmotnosti nativního hyaluronanu 1 000 kg mol^{-1} je koncentrace řetězců v řádech mikromolů na litr. Takto dlouhý řetězec není reálné vybarvit pouze jedním fluoroforem – komerčně dostupné jsou deriváty se stupněm substituce v jednotkách procent. Při průměrném počtu monomerů cca 2500 znamená i 1% stupeň vybarvení 25 molů barviva na jeden mol řetězce.

okolo 378 nm) zvyšují svou hodnotu při přechodu z nepolárního do polárního prostředí. Ostatní přechody jsou ovlivněny pouze minimálně, a tak třetí vibrační přechod ($S_1^0 \rightarrow S_0^2$, lokalizovaný okolo 383 nm) je používaný jako referenční. Poměr intenzit těchto přechodů I_1/I_3 (Py 1:3 apod.) je pak úměrný polaritě daného mikrookolí. Tento poměr bude nadále označovaný v práci jako emisní polaritní index se zkratkou EmPI.

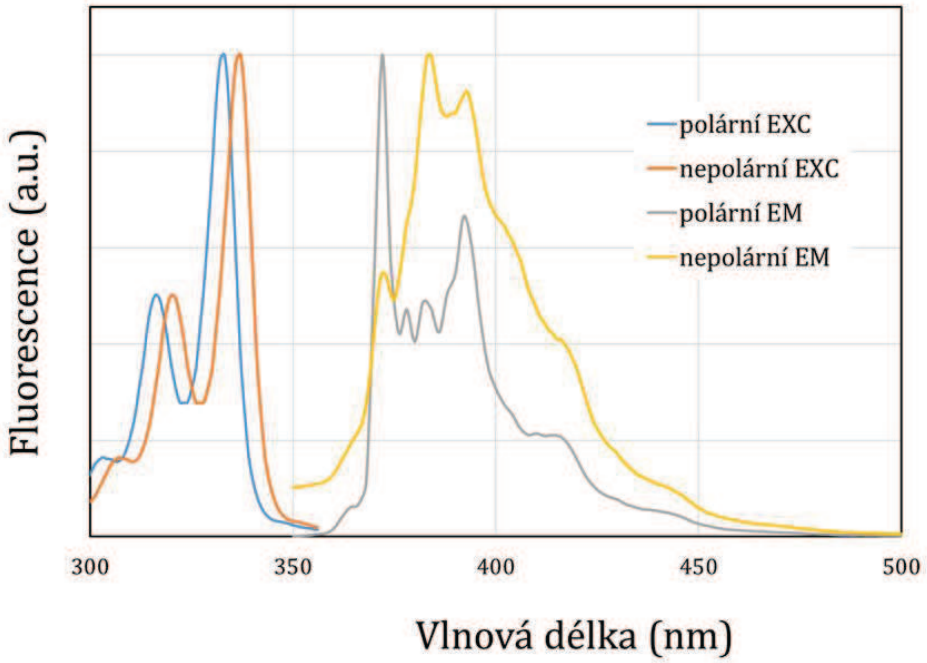

Obrázek 8 Excitační a emisní spektra pyrenu v polárním a nepolárním prostředí.

Mezi nejstarší a nejcitovanější[30] práce v této oblasti patří slavná publikace autorů Dao Cong Donga a Mitchella Winnika vydaná v roce 1984 v časopise *Canadian Journal of Chemistry*[31], která navazuje na starší práci obou autorů[32] v této oblasti. V této a zmíněné starší práci je shrnutí první dekády využití pyrenu, sumarizace raných prací ohledně reakce pyrenu na polaritu, a především ustavení pyrenové polaritní škály (ang. Py scale) a její korelaci v rámci protických a aprotických rozpouštědel s Kamlet-Taftovým modelem a Dimroth-Reichardtovým rozpouštědlovým parametrem **E_T30**. Autoři této práce srovnávali 94 rozpouštědel a pyrenové páry a vznikl tak poměrně široký přehled hodnot EmPI pro různá rozpouštědla. Navrhli navíc vztahy EmPI pro stanovení polaritních parametrů všech v té době využívaných popisů interakce solut-solvent. Je potřeba ovšem zmínit nejpůvodnější práci Akiry Nakajimy[33] z roku 1971 s 322 citacemi (WoS, květen 2018), která jako první popisuje vliv rozpouštědla na absorpční a emisní vlastnosti pyrenu.

[30] 677 citací (květen 2018, *Web of Science Core Collection*)
[31] Dong, D.C., Winnik, M.A. *Can J Chem* 62 (1984), 2560-2565
[32] Dong, D.C., Winnik, M.A. *Photochem and Photobio* 35 (1982), 17-21
[33] Nakajima, A. *Bull Chem Soc Jpn* 44 (1971) 3272-3277

Dalším používaným parametrem je tzv. excitační polaritní index, označovaný jako v literatuře[34] jako I_{333}:I_{338} nebo I_{338}:I_{333}, dále označovaný jako ExPI. Tento poměr vychází z rozdílné absorpce pyrenu v polárním (~333 nm) a nepolárním (~338 nm) prostředí. Tento pás patří přechodu označovanému jako La ($S_0 \longrightarrow S_2$)[35]. Protože není vždy jednoduché přesně určit pozici maxima absorpce, využívá se faktu, že pík přechodu nemění při změně polarity svůj tvar (při zachování stejné šířky štěrbiny), ale jen se hypsochromně/bathochromně posunuje. V tomto případě je rozsah ExPI širší než u EmPI. Skutečnou hodnotu poměru můžou ovlivnit všechny efekty rozšiřující obecně spektrální pásy.

Třetím parametrem, pocházejícím z emisního spektra, je zastoupení excimeru. Excimer je tvořený sandwichovou strukturou skládající se z excitované molekuly a molekuly v základním stavu. Vzdálenost mezi molekulami je 3,53 Å [11]. Proces formování je bimolekulový proces, který je závislý na koncentraci a difúzním koeficientu. Tento proces zháší monomerní emisi a sám emituje záření, které je posunuté k nižším energiím (maximum 450-470 nm) a je posunutý i v čase.

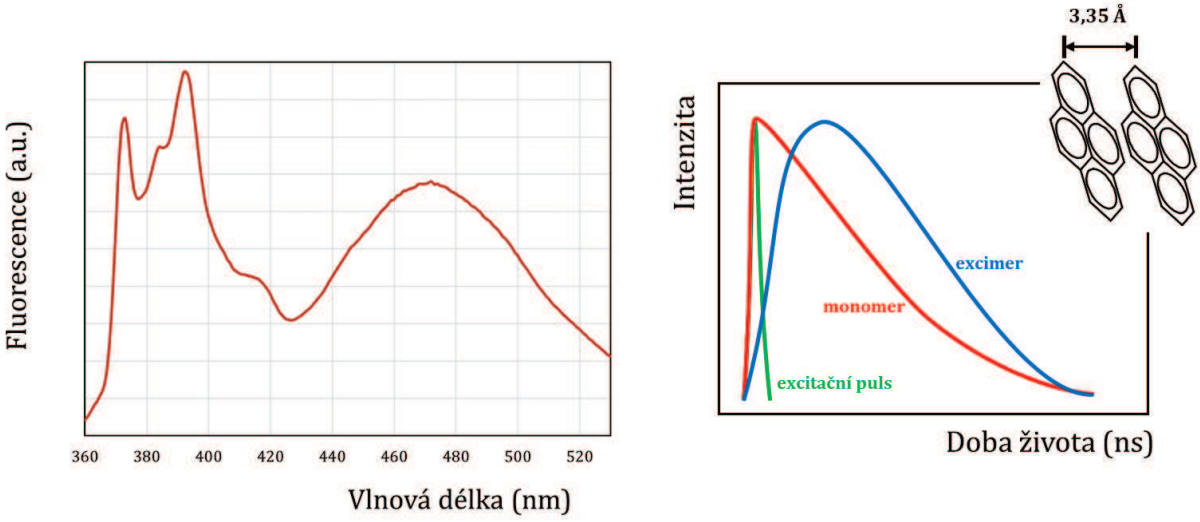

Obrázek 9 Emisní spektrum monomeru a excimeru pyrenu (vlevo). Časový profil intenzity fluorescence po krátkém excitačním pulzu (zeleně) z pohledu monomeru (červeně) a excimeru (modrá).

Čtvrtým parametrem je intenzita fluorescence, která je ovšem ovlivněna extinkčním koeficientem, koncentrací a kvantovým výtěžkem. Spojeným parametrem je doba života, která je ovšem v případě pyrenu extrémně dlouhá ve stovkách nanosekund[36]. To umožňuje využití časového rozlišení od dalších fluoroforů, nicméně její délka je zároveň komplikací, protože typické doby života jsou v jednotkách nanosekud. Je ještě důležité zmínit, že pokud v oblastech tvorby excimeru je potřeba zúžit (vhodným emisním filtrem, monochromátorem a šířkou štěrbiny) oblast detekce mimo emisi excimeru. Vzhledem

[34] např. Mohanty, A. K. et al. *Prog Biomater* 4 (2015), 89–100
Shen, Y. et al. *Carbohyd Polym* 77 (2009), 95-104
Zhang, J.X. et al. *J Biomed Mater Res A* 76A (2006), 773-780
[35] Wilhelm, M. et al. *Macromolecules* 24 (1991), 1033-1040
[36] Nakajima, A. *Bull Chem Soc Jpn* 46 (1973), 2602-2604

k tomu, že je časově posunutý vůči emisi monomeru, nebude vyhasínací křivka odpovídat váženému součtu jednotlivých exponenciálních křivek, ale projeví se jako proces, který je nutné odečíst a má zápornou hodnotu amplitudy.

Všechny čtyři parametry lze využít ke studiu koloidních systémů a některé příklady jsou v následující kapitole. Vybrané aplikace. V použití pyrenu ve výzkumu asociativních koloidů je potřeba zmínit důležitou publikaci skupiny z Málagy[37]. V roztoku roste koncentrace tenzidu přes hodnotu kritické micelární koncentrace za přítomnosti pyrenu a pozorované emisní parametry EmPI a ExPI vykazují typickou sigmoidní závislost, kterou popisuje Boltzmannova funkce (Obrázek 10). Tato čtyřparametrická funkce má tři charakteristické hodnoty – první zlom, poloha inflexního bodu a druhý zlom. V této práci byl porovnáním např. s vodivostním měřením navrhnut parametr poměru hodnoty *x*-ové souřadnice inflexního bodu a gradientu změny. Tento parametr pak ukazuje, jestli jako hodnotu kritické agregační (micelární) koncentrace využít inflexní bod nebo druhý zlom. Jestli je vyšší než hodnota „10“, je vhodné jako agregační koncentraci brát druhý zlom, pokud je nižší, tak inflexní bod.

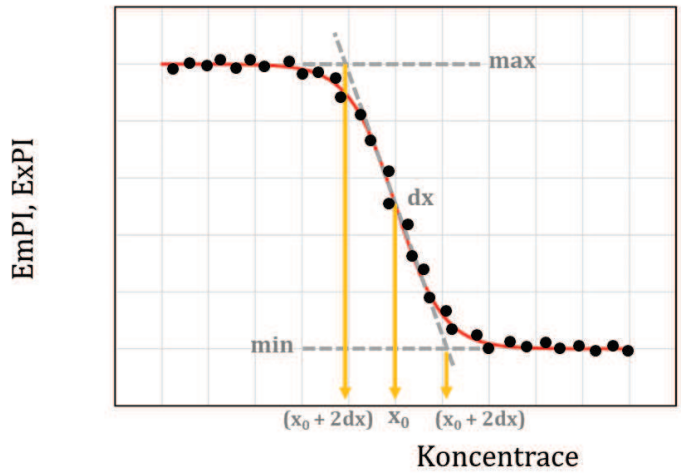

$$\text{EmPI, ExPI} = \frac{max - min}{1 + e^{\frac{koncentrace - x_0}{dx}}}$$

Obrázek 10 Boltzmannova křivka jako model průběhu změny polaritních indexů na koncentraci agregujících systémů okolo kritické agregační koncentrace.

[37] Aguiar, J., Carpena, P., Molina-Bolívar, J.A., Ruiz, C.C. *J Colloid Interface Sci* 258 (2003), 116-122

3 VYBRANÉ APLIKACE FLUORESCENCE VE VÝZKUMU KOLOIDŮ

Tato kapitola si dává za cíl na praktických příkladech ukázat, jak platná je fluorescenční spektroskopie ve výzkumu různých koloidních systémů. Jednotlivé shrnutí aplikací, které jsou součástí publikací, na nichž se autor této spolupodílel, bude doplněno i rozšířeným komentářem k jednotlivým technikám, které byly použity pro získání výsledků.

Pro lepší přehlednost budou práce děleny do jednotlivých kapitol dle svého zaměření na daný koloidní systém. Jednotlivé citované práce pak budou přiloženy.

3.1 Nativní hyaluronan

Studium nativního hyaluronanu, sodné soli kyseliny hyaluronové, pomocí fluorescenční spektroskopie je velmi obtížné. Samotná kyselina hyaluronová nefluoreskuje a je ji tak třeba modifikovat. Chemická modifikace (viz poznámka 29), navázání fluorescenční značky, pak může změnit charakter a interakční vlastnosti takto modifikovaného polymeru. Takto značené polymery jsou finančně nákladné nebo náročné z hlediska přípravy - především purifikace. Další variantou je použití fyzikálního afinitního značení, které v případě hyaluronanu zahrnuje nejvhodněji s karboxylovým aniontem D-glukoronové podjednotky.

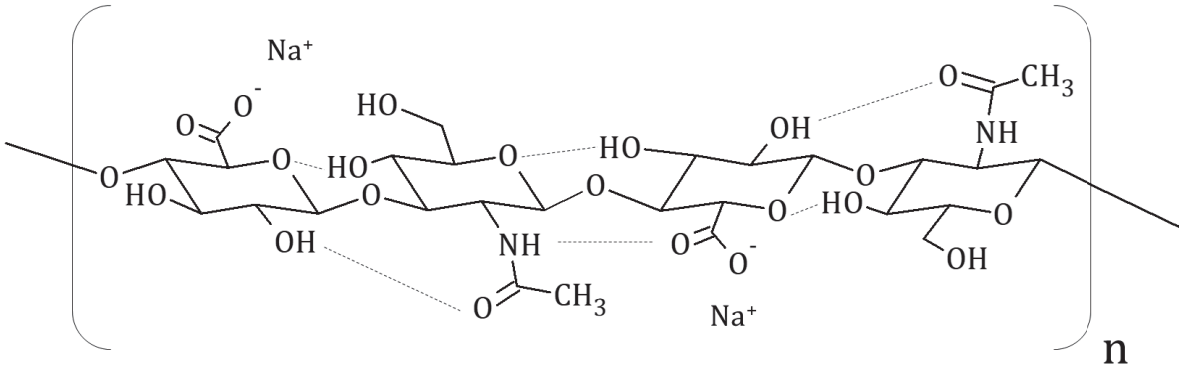

Obrázek 11 Sekundární struktura hyaluronanu, sodné soli kyseliny hyaluronové

Pro fyzikální interakci tak bude nejvhodnější použít malé fluoreskující kladně nabité molekuly, jako je například akridinová oranž (AO). Hydrochlorid této fluorescenční sondy (AO+) nese kladný náboj, který se může vázat na karboxylové skupiny D-glukuronové podjednotky hyaluronanu. Akridinová oranž je zároveň typem barviva, které od koncentrace cca $5 \cdot 10^{-5}$ mol·L^{-1} ve vodném prostředí tvoří v základním stavu komplexy, tzv. H-typ agregátů (sandwichový typ agregace)[38]. Tyto komplexy, dimery a oligomery,

[38] dalším typem je J-typ agregace, označovaný jako „head-to-tail“

jsou spojeny přenosem elektronu a vznikem excitonu (Obrázek 12)[39]. Výsledkem zformování dimerů je hypsochromní posun absorpce (465 nm, β-pás)[40] oproti absorpci monomeru (492 nm, α-pás), potlačení fluorescence monomeru a vznik bathochromně

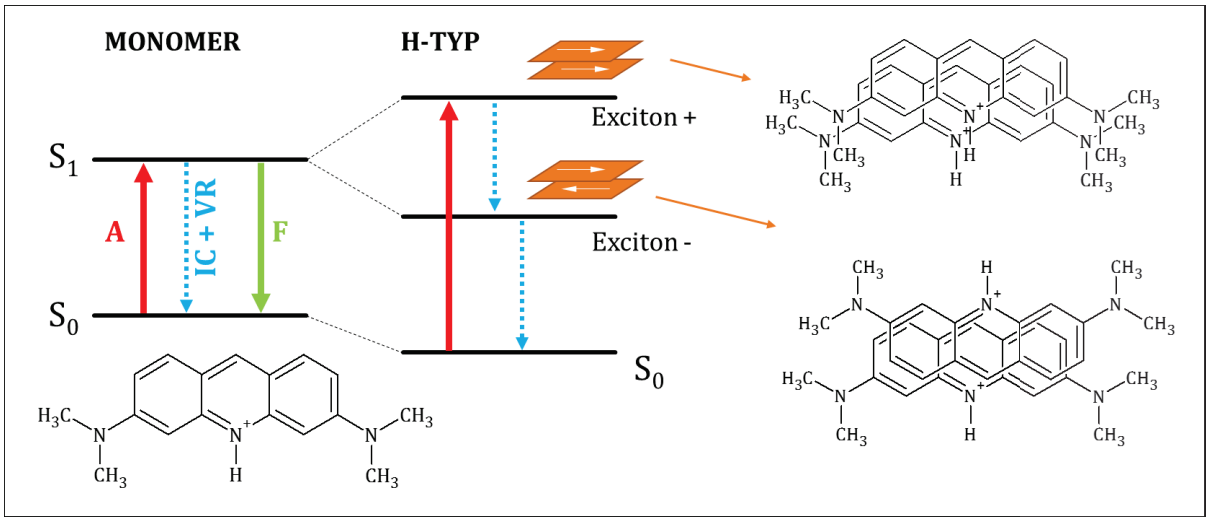

Obrázek 12 Zjednodušený Perrin-Jabłońskiho diagram pro tvorbu excitonových pásů při H-typu agregace Akridinové oranže. Zkratka „A" značí proces absorpce, „F" fluorescenci a „IC + VR" nezářivou deaktivaci procesem vnitřní konverze a vibrační relaxace.

posunutého emisního pásu dimeru, který je kvantově mechanicky zakázaný, a proto velmi slabý[41]. Pokud je přítomné vhodné vazné místo pro molekulu AO+ (karboxylový aniont), je možno pozorovat formování agregátů už při řádově nižších koncentracích. Změnou koncentrace vazných míst nebo AO+ pak můžeme studovat interakci a rozložení dostupných vazných míst polymeru pro interakci s molekulou AO+. Pokud chceme studovat změny ve větším rozsahu, může být překážkou koncentrace, kdy se tvoří dimery AO+ samostatně v roztoku. V případě hyaluronanu nás zajímají vyšší koncentrace, proto není vhodné postupné přidávání AO+, protože by nebylo možné rozhodnout, jestli je tvorba dimerů podmíněna přítomným volným vazným místem, nebo vysokou koncentrací AO+ v roztoku.

Pro popis koncentračních změn je používán místo přímých hodnot koncentrace poměr počtu vazných míst a molekul AO+, který se označuje jako poměr P/D. Předpokládáme-li, že je pokles fluorescence spojen s formováním agregátů, pak teoreticky nejnižší hodnota signálu by měla nastat při hodnotě P/D = 0,5. Při nižších hodnotách poměru bude v systému přebytek AO+, který bude fluoreskovat, při vyšších poměrech pak dojde k redistribuci AO+ na nadbytek vazných míst a fluorescence opět vzroste. Místu s nejnižší hodnotou fluorescence se říká bod ekvivalence, který bývá v literatuře označován $(P/D)_e$.

[39] dle Bayda, M. et al. *Dalton Trans* 46 (2016), 1914-1926
[40] oligomer absorbuje při 450 nm a je označován jako γ-pás
[41] např. Costantino, L. et al. *J Chem Eng Data* 29 (1984), 62-66
nebo Peyratout, C., Donath, E., Daehne, L. *J Photoch Photobio A* 142 (2001), 51-57

Velmi vhodným doplněním těchto experimentů je stanovení poměru absorbance dimeru vůči monomeru (poměr β a α pásu). Jak již bylo diskutováno v kapitole 2.1.4, změna intenzity může být ovlivněna i způsobem přípravy vzorku. Porovnáním fluorescence a absorpce se lze vyhnout špatné interpretaci získaných dat. Modelové průběhy fluorescence a poměru absorbancí shrnuje Obrázek 13.

Pomocí agregující sondy AO+ byla studována pomocí intenzity fluorescence koncentrační řada nativního hyaluronanu a vliv iontové síly na interakci sonda-polymer při konstantní koncentraci AO+. Byly obdrženy atypické výsledky, které byly publikovány jako část rozsáhlejšího článku zahrnující i později intenzivně studované interakce hyaluronanu a kladně nabitého tenzidu[42]. Tyto výsledky, které navazují a rozšiřují dříve zpracovávané bakalářské a diplomové práce a projekty komerčního výzkumu[43], však stojí za to podrobněji diskutovat.

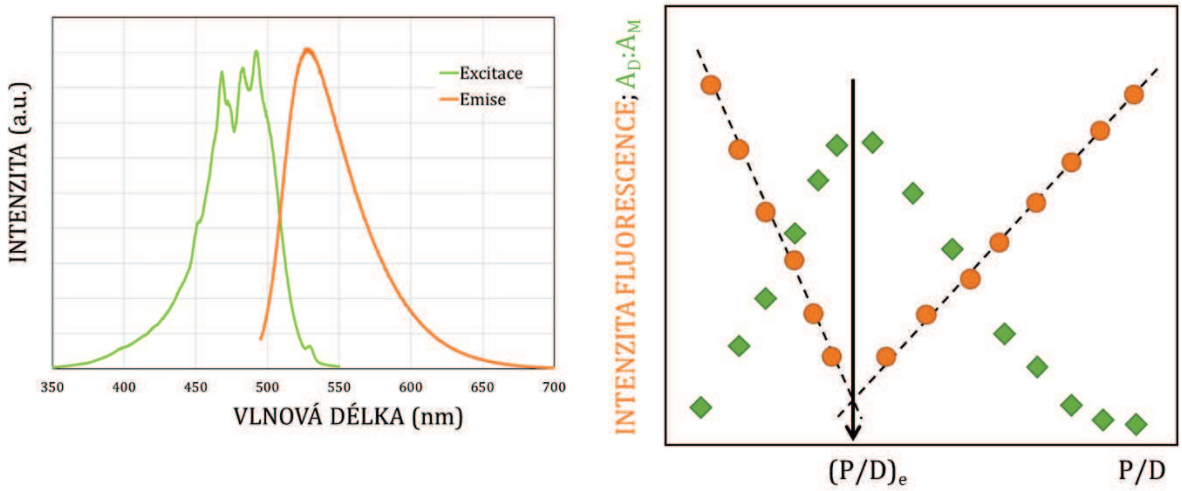

Obrázek 13 Excitační a emisní spektrum AO+ v nízké koncentraci (bez výrazných pásů dimerů a oligomerů) a naznačená závislost intenzity fluorescence se stanovením bodu ekvivalence. Doplněno o průběh závislosti poměru absorbance dimerů vůči absorbanci monomerů.

Za první atypický výsledek lze považovat, že minimum závislosti bylo nalezeno při hodnotě $(P/D)_e = 3$. Tato hodnota je 6x větší než teoretická hodnota bodu ekvivalence. To může mít několik důvodů. Jedno z vysvětlení by mohlo být, že ne všechny karboxylové skupiny jsou stericky dostupné a že tuto dostupnost ovlivňuje konformace polymeru v roztoku a samotná nenulová velikost iontu AO+. To by ovšem znamenalo, že pro interakci je dostupných necelých 17 % přítomných vazných míst. Pokud vezmeme v úvahu, že skutečná koncentrace v bodě ekvivalence je 20 $mg \cdot L^{-1}$, potom víme, že se pohybujeme ve velmi zředěném režimu a můžeme vyloučit intermolekulární interakce. Ze sekundární struktury hyaluronanu plyne, že každý další monomer je otočen vůči předchozímu o 180°. Pokud by tedy struktura řetězce v roztoku kopírovala povrch koule,

[42] Mondek J., **Mravec, F.** et al *Langmuir* 30 (2014), 8726-8734
[43] **např.** LONDINOVÁ, M. Fluorescence ve výzkumu hydrofilních oblastí asociativních koloidů. Brno: Vysoké učení technické v Brně, Fakulta chemická, 2008. 68s. Vedoucí diplomové práce doc. Ing. Miloslav Pekař, CSc. **nebo** Mondek, J. Kationaktivní fluorescenční sondy v systému polyanion-tenzid. Brno: Vysoké učení technické v Brně, Fakulta chemická, 2010. 38 s. Vedoucí bakalářské práce prof. Ing. Miloslav Pekař, CSc.

který není proniknutelný pro AO+, byla by, v nejhorším možném případě orientace karboxylové skupiny kolmo ke kulové ploše, dostupná jen polovina karboxylových skupin. Další pokles by pak mohl připsán sterickým faktorům. Alternativní vysvětlení by pak znamenalo, že vazná místa jsou stericky dostupná, ovšem nejsou ionizovaná. Toto alternativní vysvětlení ovšem stojí proti předpokladu, že hyaluronan je 100% sodnou solí kyseliny hyaluronové a faktu, že i zbývající karboxylové skupiny mají své pKa[44] mezi hodnotami 3-4, což při pH roztoku hyaluronanu 6-7 znamená plnou disociaci. Zde je na místě ovšem poznamenat, že i podle Specifikačních listů výrobců může pH nabývat kyselého charakteru, což by v případě soli slabé kyseliny a silné zásady nemělo být možné.

Dalším atypickým výsledkem je chování intenzity fluorescence a poměru A_D:A_M při zvyšující se koncentraci polymeru. V tomto případě za bodem ekvivalence nastává očekávaný nárůst intenzity fluorescence a pokles poměru absorbancí. U poměru absorbancí pak dochází ke dvojité změně trendu, kdy nárůst intenzity fluorescence je doprovázen nárůstem a následným poklesem poměru A_D:A_M. Toto chaotické chování poměru lze snad dát do souvislosti i s faktem, že celkový nárůst fluorescence není prudký a jsou zde oblasti se silně se překrývajícími chybovými úsečkami. Tyto změny v chování pak lze teoreticky připsat změně rozložení oligomerů vůči dimerům při narůstajícím obsahu potencionálních vazných míst v systému. Podporu pro tuto teorii přináší Obrázek 14, který obsahuje dosud nepublikovaná data závislostí oligomeru. Z těchto dat vyplývá, že když roste zastoupení dimeru, tak narůstá i zastoupení oligomerů, což je zvláště v nižších P/D (nižší koncentrace polymeru) očekávatelné díky přebytku barviva. Zajímavým faktem je, že zastoupení dimeru ve srovnání s oligomerem klesá, i když celkově oproti monomeru roste. Závislost A_D:A_O tak kopíruje průběh intenzity fluorescence.

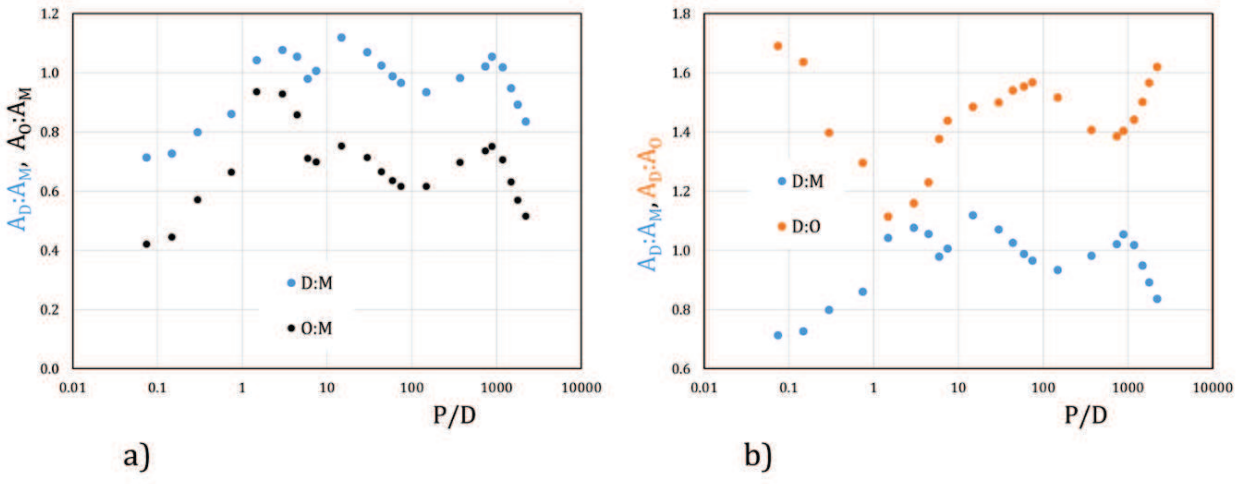

Obrázek 14 Srovnání nepublikovaných závislostí poměru absorpce oligomeru k monomeru (a, černá) a závislost absorpce dimeru k monomeru (b, oranžová). Doplněno o publikovanou závislost dimeru k monomeru (modrá).

[44] Mero, A., Campisi, M. *Polymers* 6 (2014), 346-369

Nejpřekvapivější výsledek ovšem nastává při překročení hodnoty P/D = 100. V této oblasti, kdy má počet vazných míst o dva řády převyšovat počet molekul barviva dochází k opětovnému poklesu fluorescence spojené s nárůstem obsahu dimeru. Pokles dosahuje minima při hodnotě P/D = 1 000, což odpovídá koncentraci hyaluronanu cca 7 $g \cdot L^{-1}$ (!). V následující oblasti P/D od 1000 do 3000 pak následuje strmý nárůst intenzity fluorescence spolu s poklesem obsahu dimeru. Pro toto podivné chování připadá v úvahu teorie, která zahrnuje fakt, že při hodnotě P/D = 142 je koncentrace hyaluronanu 1 $g \cdot L^{-1}$, což znamená přechod ze zředěné do polozředěné oblasti[45]. V této fázi pak řetězce mohou preferovat vzájemné interakce a tvořit vnitřní, pro AO+ nedosažitelné, domény. Zároveň může hrát roli i fakt, že nabitá AO+ bude zachytávána na povrchu takovýchto agregátů a nebude penetrovat do vnitřní části k volným vazným místům. Tato teorie ovšem dobře nevysvětluje náhlý nárůst fluorescence se zvyšující se koncentrací, pokud ovšem při koncentraci odpovídající P/D = 1 000 nedojde k další změně systému, která by znamenala uvolnění domén pro snadnější penetraci AO+ a roztok hyaluronanu by tak nepřešel do „gelu podobné“ fáze.

Výše zmíněné úvahy částečně podporují v článku zmíněné mikroreologické experimenty[46]. Data v polozředěném režimu vykazují postupný nárůst, který se změní v prudký po překročení koncentrace zhruba 5 $g \cdot L^{-1}$. Mikroreologická data vypadají posunutá k nižším hodnotám koncentrace oproti hodnotám fluorescence, což lze připsat teoreticky řádovým rozdílům ve velikosti AO+ a mikroreologické částice, která tak bude reagovat dříve na formování sítě.

SHRNUTÍ: Podrobnou analýzou absorpčních/excitačních spekter a emisních můžeme podpořit nebo vyvrátit domněnky o chování koloidních systémů. Na základě tohoto „třídění“ hypotéz pak zůstanou konkrétní otázky, ze kterých vyplývá, jaké instrumentální techniky použít k jejich zodpovězení. Výhoda fluorescenční spektroskopie je v její relativní rychlosti, kdy lze proměřit během jedné hodiny přibližně 40 vzorků. Vždy je vhodné doplnit fluorescenční měření absorpční spektrofotometrií, pokud nejsou použity příliš nízké koncentrace fluoroforů. Správně provedené spektrofotometrické pomůže potvrdit nebo vyvrátit změny v koncentraci a interakce v základním stavu.

[45] Polozředěná oblast, oblast kde dochází k propletení řetězců (chain entanglement), byla stanovena (Fouissac, E.; Milas, M.; Rinaudo, M. *Macromolecules* 26(1993), 6945–6951.) pomocí součinu koncentrace a relativní molární hmotnosti na hodnotu 280 000 g L^{-1}. To znamená, že v rozsahu relativních molárních hmotností 300 000-1 400 000 jsou přechodové koncentrace 0,93-0,2 g L^{-1}.

[46] Byla použita varianta pasivní mikroreologie tzv. video particle tracking.

3.2 Deriváty hyaluronanu

Studium derivátů hyaluronanu, mj. hlavního polymeru extracelulární matrix, bylo součástí obhájené disertační práce autora[47]. Na základě tohoto výzkumu pak byly sepsány tři publikační výstupy[48, 49, 50], přičemž nejdůležitějším byl výstup v *Colloid and Polymer Science* [50], a poznatky byly prezentovány také v rámci různých konferenčních příspěvků.

Alkyl deriváty hyaluronanu[51] jsou roubovanými kopolymery hyaluronanu u kterých lze měnit typ alkylového řetězce, stupeň substituce a molekulovou hmotnost výchozího polymeru. U takovéhoto typu derivátu lze očekávat koncentračně závislé agregační chování, které může mít typově dva hlavní mechanismy a jeden přechodný. První mechanismus je založen na předpokladu, že daný modifikovaný polymer není schopen vytvořit intramolekulární agregát (např. kvůli nízkému stupni substituce nebo nedostatečné ohebnosti polysacharidové kostry) a bude tedy mít svou hodnotu agregační koncentrace. Druhý mechanismus je založen na vzniku intramolekulárních derivátů. Kombinovaný agregát si lze představit jako intramolekulární agregát, který od jisté koncentrace váže další řetězce tak, že nevytváří nové hydrofobní domény.

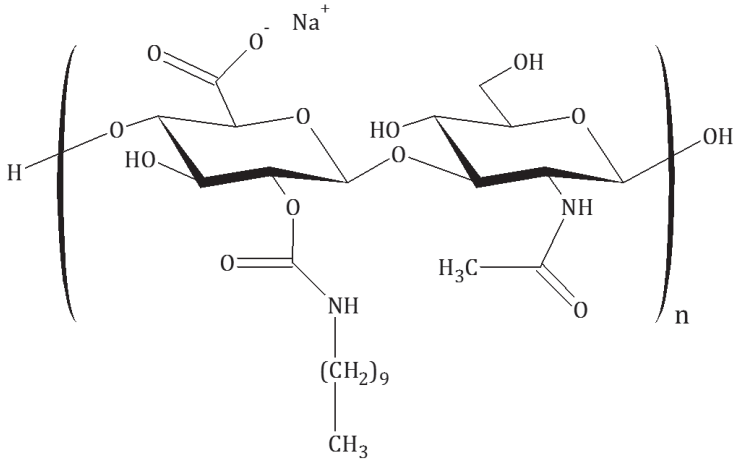

Obrázek 15 Struktura hydrofobně modifikovaného hyaluronanu.

Vliv stupně substituce a výchozí molekulové hmotnosti na hodnotu agregační koncentrace popisuje publikace v *Colloid Polym Sci* [50] a podrobně se jí věnuje disertační práce [47]. Širší diskusi si zaslouží ovšem studium mechanismu agregace. Právě při rozvahách, jak popsat nejlépe daný systém pomocí fluorescenční spektroskopie, vzniklo schéma uvedené v kapitole 2.2 (Obrázek 5).

---

[47] **Mravec, F.** *Aggregation behavior of polysaccharides in aqueous solutions.* Brno, 2008. 119 s. Disertační práce na Fakultě chemické Vysokého učení technického v Brně, Ústavu fyzikální a spotřební chemie. Vedoucí disertační práce doc. Ing. Miloslav Pekař, CSc.
[48] **Mravec, F.**, Pekař, M. *Chemické listy*, 99 (2005), 594-595
[49] **Mravec, F.** et al. *Chemické listy*, 2008, 102 (2008), 1096-1096
[50] **Mravec F.**, Pekař, M., Velebný, V. *Colloid Polym Sci*, 286 (2008), 1681-1685
[51] Mlčochová P. et al. *Biopolymers* 82 (2006), 74-79

Základní myšlenka rozdělení intra- a intermolekulárních agregátů ve vodných roztocích spočívá ve sledování koncentrační změny vybraného parametru, například polarity okolí sondy. Mějme sondu s afinitou k nepolárnímu prostředí, u které pozorovatelná emisní charakteristika eviduje polaritu jejího nejbližšího okolí. Dále je potřeba uvést, že sonda ve vodném prostředí neemituje nebo emise z vodného prostředí je zanedbatelná a neruší emisi ze zformovaných agregátů (těmto podmínkám částečně vyhovuje sonda Nilská červeň nebo amonná sůl 1-anilinonaftalen-8-sulfonové kyseliny). V případě, že systém tvoří intramolekulární agregáty, pak budeme už od nejmenšího přídavku evidovat konstantní hodnotu daného polaritního parametru. U intermolekulárních agregátů pak tuto hodnotu budeme evidovat až od jisté koncentrace. U reálných systémů dochází ovšem k fluktuacím ať už díky citlivosti systému nebo různým sorpčním efektům na hydrofobních částech neagregovaných polymerů. Výhodou fluorescenční spektroskopie jako metody je, že málokdy měříme pouze jednu jedinou charakteristiku. Měření polaritního parametru lze doplnit takřka vždy intenzitou fluorescence, ideálně vyjádřené jako integrál pod emisním spektrem. V případě intramolekulárních agregátů pak konstantní hodnotu polaritního indexu doplní lineárně rostoucí závislost fluorescence (do bodu, kdy bude veškerá sonda solubilizována jádry agregátů), u intermolekulárních agregátů najdeme obdobnou křivku ovšem posunutou k agregační koncentraci.

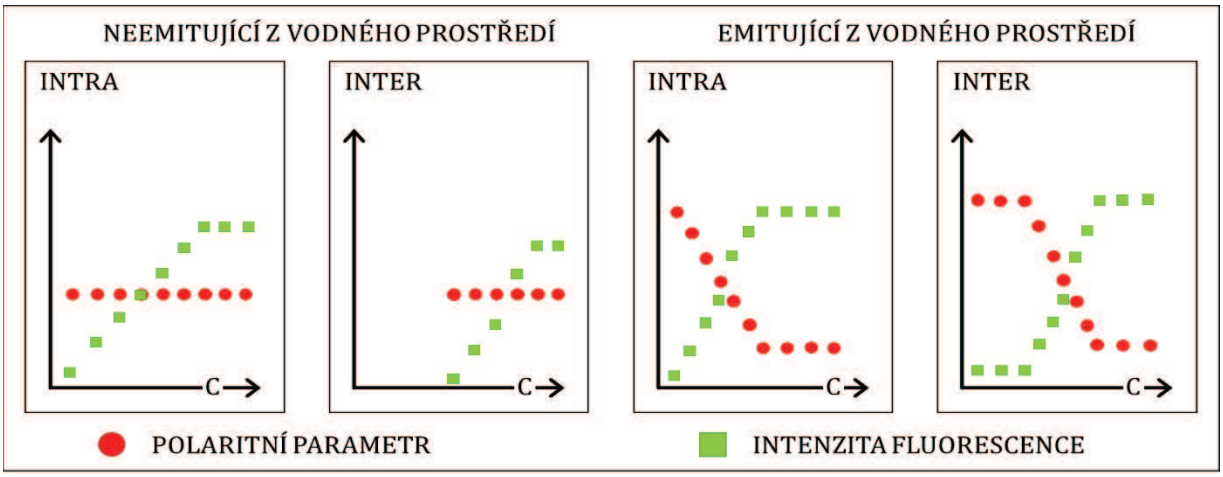

Obrázek 16 Schématické znázornění možných koncentračních závislostí fluorescenčních parametrů z vodných roztoků roubovaných kopolymerů.

Pokud budeme systém sledovat pomocí polaritní sondy, která ovšem nemá nulovou emisi z vodného prostředí (např. pyren nebo prodan), bude situace složitější. U intramolekulových agregátů bude postupně klesat hodnota polaritního parametru a růst intenzita do konstantní hodnoty. Závislosti parametru a intenzity fluorescence budou u intermolekulárních agregátů mít tvar klesající resp. u intenzity fluorescence rostoucí S-křivky. Je potřeba ovšem upozornit na významné odchylky u fluorescenčních sond,

které tvoří excitované dimery, jako je právě pyren[52]. Výše popsané jednodušší případy shrnuje graficky Obrázek 16.

Samostatnou diskusi si zaslouží i přechodný typ agregátu, kdy ke vznikajícím agregátům např. intramolekulárním se od jisté koncentrace naváží další řetězce. Takovéto agregáty mají praktický dopad na využití nosičových systémů[53]. Po navázání dalšího řetězce se zvětší agregát, ale není vytvořena nová hydrofobní doména. Toto lze prokázat například tak, že se ke studovaným fluorescenčním charakteristikám přidá i sledování fluktuace intenzity (fluorescenční korelační spektroskopie), ze které se přes stanovení difuzního koeficientu přidá informace o velikosti agregátu. V takovém případě bude sledovaná velikost s koncentrací narůstat, aniž by se měnila intenzita fluorescence – polarita hydrofobní domény se nebude měnit nebo bude jen velmi málo klesat v souvislosti se zapojením dalších hydrofobních řetězců do již vzniklé domény[54]. Představu o agregátech vzniklých z roubovaných kopolymerů shrnuje Obrázek 17.

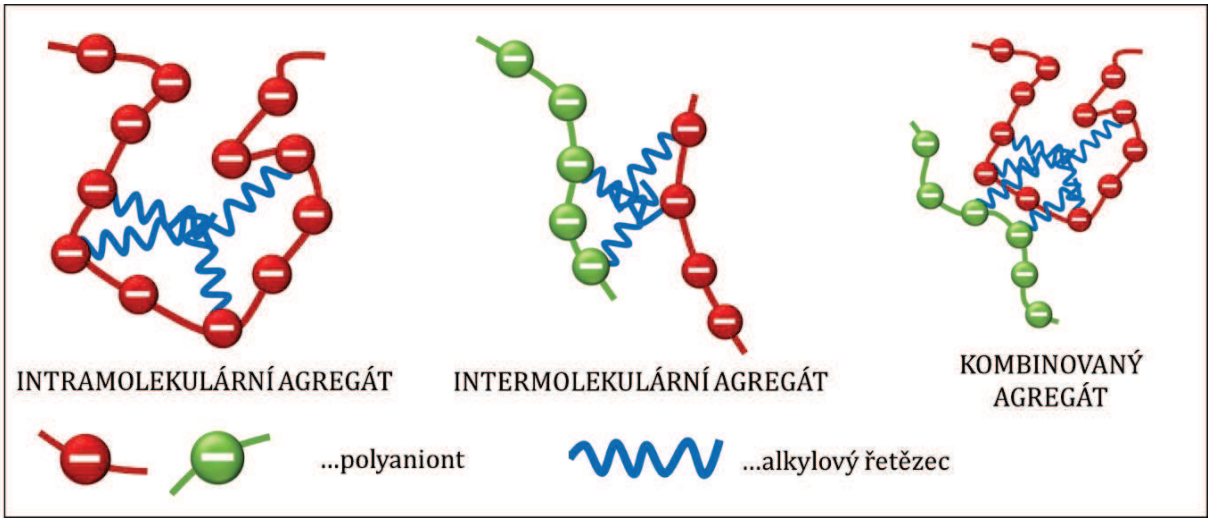

Obrázek 17 Schématické znázornění typů agregátů tvořených roubovaným polymerem

Z publikovaných dat vyplývá, že průběh závislostí pro daný typ agregátu odpovídá formování intermolekulárního agregátu. Závislosti emisních parametrů tvoří S-křivku, která znamená, že v jistém nízkém koncentračním rozmezí přídavek derivátu nevytváří hydrofobní domény schopné solubilizovat fluorescenční sondy. Polaritní parametry, jako

[52] V nízkých koncentracích agregátů, obecně nízké koncentrace intramolekulových agregátů a za agregační koncentrací intermolekulových agregátů, dochází k zakoncentrování molekul pyrenu v jádrech a ke zhášení fluorescence monomeru. Takovýto systém pak nevykazuje u monomeru intenzitu fluorescence a jeho spektrum se nesčítá s emisním spektrem ostatních molekul. To způsobuje například lokální pokles intenzity fluorescence v okolí agregační koncentrace. Ovšem u pyrenu je výhoda, že excimer je emitující komplex a jeho koncentrační závislost lze využít k popisu agregačního chování systému.

[53] Pozitivní dopad může mít interakce v případě, že obalí nebiokompatibilní nebo nestabilní částici a propůjčí jí tak část své biokompatibility. Negativní dopad bude spojen s dogmatem o velikosti agregátů, kdy velikost takovéhoto kombinovaného agregátu překročí hranici 200 nm[22].

[54] Rozeznávání jednotlivých typů agregátů je možno provést i dalšími technikami mimo fluorescenčních technik (FCS, FRAP apod.), jako je například stanovení molekulové hmotnosti agregátu pomocí statického rozptylu světla při znalosti molární hmotnosti jednoho řetězce. Další alternativou je stanovení difúzního koeficientu, například difúzní varianta NMR (DOSY NMR, diffusion ordered spectroscopy), nebo pomocí difúzních cel.

je EmPI od pyrenu nebo poloha maxima u Nilské červeně, zůstávají na hodnotách odpovídajících vodnému prostředí. Za povšimnutí stojí ovšem celkový průběh S-křivky. Při podrobnější analýze derivátu s nejnižší molekulovou hmotností 30 kg·mol^{-1} a stupněm substituce 30 % je závislost výrazně komplikovanější, než nabízí model Boltzmannovy S-křivky. Pro stanovení agregační koncentrace, jako inflexního bodu závislosti, je potřeba využít fyzikálních limitací hodnot parametrů, kterých může dosáhnout daná fluorescenční sonda. Ty se pak zadají jako omezení (constraints) pro fitovací program. Obdržená hodnota je pak samozřejmě zatížena větší chybou z hlediska statistiky, nicméně menší chybou z hlediska skutečnosti. Je potřeba i uvážit, že derivát s tak nízkou molekulovou hmotností obsahuje jen cca 80 monomerních jednotek, které se mohou chovat rozdílně ve srovnání s takřka o dva řády většími molekulami.

Rozdíl v průběhu agregace lze alternativně popsat pomocí gradientu poklesu dalších sledovaných parametrů. Samotná hodnota gradientu, označovaná jako „Δ*x*“ nebo „d*x*“, je závislá na koncentračním rozsahu. Poměr inflexního bodu a gradientu, navržený v práci Aguiara [37], lépe reflektuje strmost změny polaritního indexu (Obrázek 18). Dle tabulky v obrázku pak můžeme porovnat strmost jednotlivých závislostí.

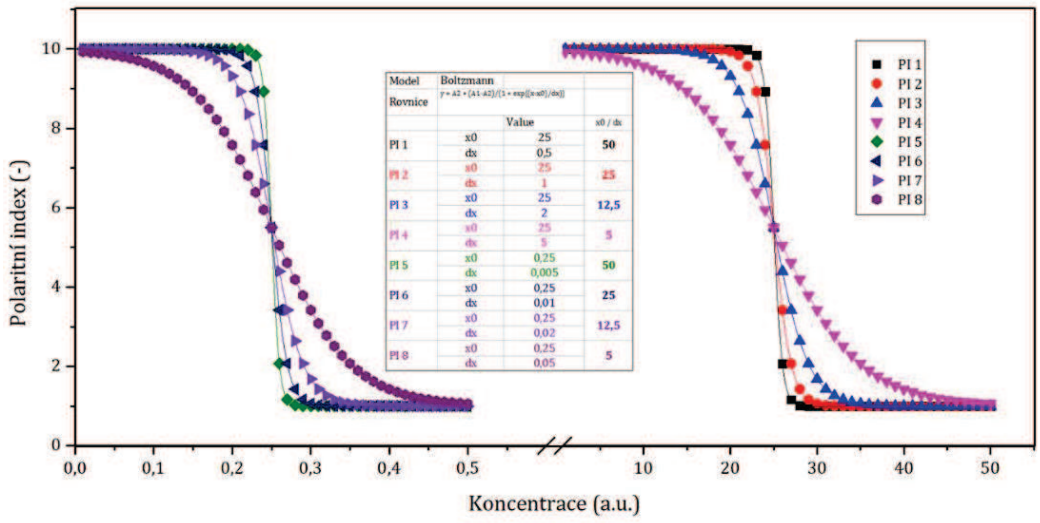

Obrázek 18 Modelové závislosti polaritního indexu na koncentraci pro různé koncentrační rozsahy a hodnoty inflexního bodu. Vložená tabulka shrnuje hodnoty gradientu, pozice inflexního bodu a hodnoty poměru.

Obrázek 19 ukazuje vybraná data se shodným stupněm substituce, z vložených hodnot vyplývá, že poměr je nízký a nevykazuje významný trend v rámci změny molekulové hmotnosti. S ohledem na výše zmíněnou práci pak můžeme konstatovat, že agregace v tomto typu agregátů odpovídá agregaci ionogenních tenzidů, a tak tvorbě intermolekulárních agregátů.

SHRNUTÍ: Při současné úrovni znalostí a dostupností technik by bylo vhodné zvolit při studiu těchto systémů pokročilejší metody, jako je především fluorescenční korelační spektroskopie. Při zpracování disertační práce a publikací byla většina technik jen obtížně dostupná, proto byl hledán alternativní přístup ke studiu průběhu agregace. Na základě experimentů s nativní formou hyaluronanu byla do experimentů zapojena například

hydrofilní sonda akridinová oranž podrobně popsaná v předchozí kapitole. Zároveň bylo v rámci disertace, i když ne vyloženě explicitně, použito schéma studia navržené v úvodu této práce.

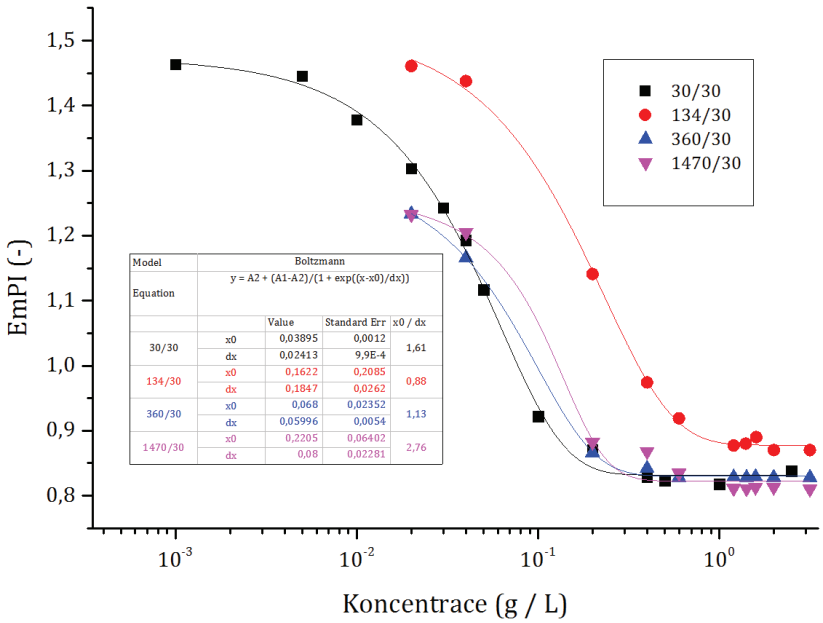

Obrázek 19 Reinterpretované závislosti dle [47] s vloženou analýzou poměru pozice inflexního bodu a gradientu závislosti. Popis v legendě je molekulová hmotnost v kg·mol^{-1}/stupeň substituce v %.

3.3 Interakce polymerů a amfifilních molekul

Výzkum v této oblasti je více než vhodný pro studium pomocí fluorescenční spektroskopie. Obecně lze od interakce mezi polymerem a amfifilní látkou očekávat dřívější vznik hydrofobních domén a/nebo stabilizaci agregátů amfifilních molekul. Speciálním případem pak je tvorba fázově separovaných systémů, když přes destabilizaci koloidního roztoku dostáváme velmi stabilní hydrogelovou matrici.

Studium interakce mezi polymery, specifičtěji mezi polyelektrolyty a opačně nabitými tenzidy, probíhá v rámci Fakulty chemické VUT od roku 2008. Prvotní motivací pro studium těchto interakcí byla tvorba stabilizovaných koloidních částic, která by v sobě kombinovala výhody hydrofilních, biokompatibilních polyelektrolytů a zároveň umožňovala solubilizaci nepolárním a amfifilním látkám. Takovéto systémy by byly formovány na základě fyzikálních sil, dominantně na základě nábojových interakcí. Fyzikálně vázané agregáty by pak také nebránily biodegradaci jednotlivých složek systému.

Nejčastěji se ve studiích objevuje biopolymer hyaluronan, u kterého je hlavním důvodem využití jeho biokompatibilita a zároveň biodegradabilita. Jak se podle získaných výsledků jeví, tak jeho největší slabinou je potřeba interakce se silně kladným tenzidem, kvartérním amoniovým iontem. Diskuse popisu interakce pomocí technik fluorescenční spektroskopie bude předmětem následující podkapitoly, která navazuje na studium

pomocí akridinové oranže (kapitola 3.1) a prakticky pokračuje až do současnosti. Souběžně se studiem struktury agregátů mezi hyaluronanen a amoniovými tenzidy probíhaly i testy biokompatibility na vybraných buněčných kmenech na spolupracujícím pracovišti, které byly publikovány v zahraničních časopisech[55, 56]. Součástí těchto výzkumů nebyla fluorescenční spektroskopie, pouze návrh a příprava komplexů, proto nebudou dále podrobně rozebírány.

Další kapitolu představuje tvorba komplexů tak, aby byly všechny složky co nejvíce biokompatibilní a zároveň byla zachována interakce mezi polymerem a látkou formující hydrofobní doménu. V tomto případě bylo využito směsných amfifilních systémů.

3.3.1 Interakce polyelektrolytů a opačně nabitých tenzidů

Základním předpokladem je, že malé ionogenní amfifilní molekuly budou v přítomnosti opačně nabitého řetězce tvořit hydrofobní domény dříve než v roztoku bez polymeru za stejných termodynamických podmínek. Pokud sledujeme rostoucí koncentraci tenzidu v přítomnosti polymeru ve vodném prostředí, můžeme na základě citlivosti metody sledovat vázání tenzidu na polymer spojenou s indukcí a po vysycení všech potenciálních vazných míst pak tvorbu volných agregátů v roztoku. Obecný vývoj z pohledu fluorescenční sondy pyren, emisní polaritní index s intenzitou fluorescence a zastoupením excimeru, shrnuje Obrázek 20. Ve vývoji parametrů můžeme najít pět oblastí, označených římskými číslicemi I-V, a které jsou graficky prezentovány.

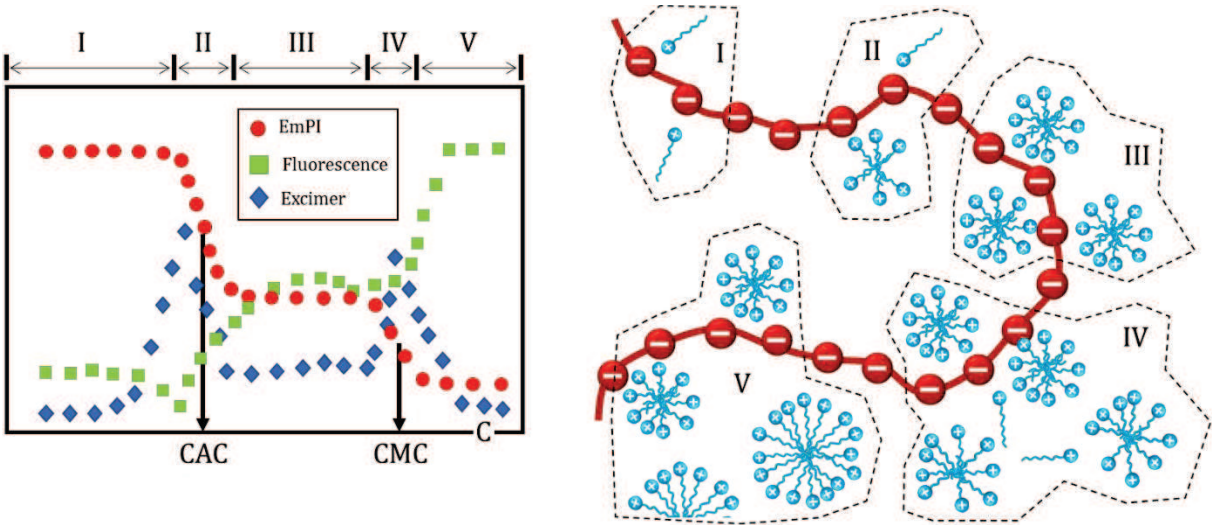

Obrázek 20 Model závislosti pyrenových parametrů emisního polaritního indexu (●), intenzity fluorescence (■) a zastoupení excimeru (◆) v případě konstantního obsahu polyaniontu hyaluronanu (⌒) a rostoucí koncentrace kationaktivního tenzidu (○〰) ve vodném prostředí. Šipky označují začátek indukované agregace (kritickou agregační koncentraci, CAC) a při nasycení řetězce pak kritickou micelární agregaci (CMC). Protionty nejsou zobrazeny.

[55] Kalbáčová, M.; Verdánová, M.; **Mravec, F.**; Halasová, T.; Pekař, M. *Colloid Surface A* 460 (2014), 204-208
[56] Sauerová, P., Verdánová, M.; Pilgrová, T.; Venerová, T.; **Mravec, F.**; Kalbáčová, M.; Pekař, M. *Colloid Surface A* 483 (2015),155-161

Výše uvedený model se snaží zachytit všechny podstatné fáze agregace:

- **Oblast I** je typická pro z vody emitující fluorescenční sondu. Pyren neinteraguje s hyaluronanem tak, aby měnil své emisní nebo excitační spektrum [47]. V přítomnosti polymeru a při nízké koncentraci tenzidu nebudou tvořeny hydrofobní domény, i když se část tenzidu bude vázat na přítomný řetězec. Tuto domněnku lze doložit experimentem publikovaným v časopise *Langmuir* [42] v roce 2014. Pomocí adsorbované akridinové oranže ve formě dimerů bylo možno pozorovat vázání tenzidu hluboko pod jeho kritickou micelární koncentrací (od $2 \cdot 10^{-7}$ mol·L^{-1}, CMC ~ 1 mM[57]) tak, že byl pozorován rozpad dimeru a nárůst fluorescence. Oblasti I končí poklesem fluorescence, což znamená, že molekuly pyrenu se lokálně zakoncentrovávají ve formujících se nepolárních doménách, které tak obsahují více molekul pyrenu a roste pravděpodobnost tvorby excimeru, jehož signál tím narůstá.
- **Oblast II** odpovídá poklesu polaritního indexu, buď na základě mixování signálu z polárních a nepolárních částí koloidního roztoku nebo na základě postupného formování indukovaných micel, poklesu zastoupení excimeru a nárůstu fluorescence. Inflexní bod v této oblasti ze závislosti EmPI = $f(c_{tenzidu})$ je pak brán jako bod kritické agregační koncentrace.
- **Oblast III** je nejkomplikovanější oblastí, protože zde může dojít k velkému množství jevů. Popsaná závislost předpokládá, že dalším přídavkem tenzidu budou obsazena další vazná místa polymeru, kde se budou indukovat micely. Micely budou postupně plnit řetězec, nicméně se předpokládá, že vznikne stabilní struktura popisovaná jako „struktura perlového náhrdelníku" (pearl-necklace structure). Micely sice vykompenzují záporný náboj polymeru, ale samy jako makroionty budou obsahovat přebytek kladného náboje, který bude stabilizovat strukturu v roztoku. Protože narůstá pouze množství micel v roztoku, polaritní index zůstává stejný a narůstá intenzita fluorescence, která je ovšem kompenzována tvorbou excimerů. Tato oblast bude tedy silně citlivá na poměr molekul pyrenu vůči indukovaným micelám a také na celkový obsah dostupných vazných míst na polymeru (problematika viz kapitola 3.1). Oblast končí po nasycení všech polymerních vazných míst.
- **Oblast IV** odpovídá formování přebytku tenzidu do volných micel v roztoku. Dochází k vázání zbylých molekul pyrenu a poklesu polaritního indexu, opět narůstá zastoupení excimeru. Nejobtížnější je modelovat vývoj intenzity fluorescence, která by měla narůstat inkorporací dalších molekul pyrenu a klesat formováním excimerů. V tomto modelu byla zvolena jako výsledný stav dynamická rovnováha.

[57] různí autoři uvádějí CMC_{CTAB} od 0,9 do 1 mM v závislosti na metodě, např. Sánchez, G. F. et al. *J Lumin* 69 (2009), 2127

- **Oblast V** je finální oblastí, přídavek tenzidu navyšuje počet micel, polaritní index se nemění, excimer se vytrácí a intenzita fluorescence by měla dosáhnout maximální hodnoty.

Navržené schéma však předpokládá jisté chování polymeru a tenzidu. U tenzidu se předpokládá, že tvoří sférické micely a nedochází u něho nad kritickou micelární koncentrací k fázovým přechodům v daném koncentračním rozsahu. U polymeru se předpokládá vysoká stabilita a hydrofilita. Zároveň se předpokládá, že iontová síla roztoku není navyšována přídavkem nízkomolekulárního elektrolytu. Zvýšená iontová síla potlačuje interakci nabitých komponent, snižuje repulzi mezi shodnými náboji a vede tak ke snížení kritické micelární koncentrace tenzidu a může negovat vliv přítomnosti polymeru. Podrobným studiem interakce mezi cetyltrimethylamonium bromidem (CTAB) nebo carbethopendecinium bromidem (Septonex)a hyaluronanem se zabývá práce publikovaná v International *Journal of Biological Macromolecules*[58] a interakci ve vodném prostředí se zvýšenou iontovou silou společná publikace v *Colloid Surface A* z roku 2011[59].

Na základě těchto dat pak je nutné upravit tento model pro konkrétní případ interakce ve vodných roztocích hyaluronanu a CTAB, jak shrnuje Obrázek 21. V tomto obrázku přibyla mezi oblastí III a IV oblast označená písmenem „S“, kde dochází k fázové separaci, tvorbě sraženiny, která přechází na gel. Tento gel lze pozorovat, pokud systém obsahuje hydrofobní barvivo. To samo o sobě je důkazem, že tento gel zachovává hydrofobní domény, které mohou solubilizovat nepolární látky. O zachování nepolárních domén svědčí i pozorovatelná emise Nilské červeně, která je ve vodném prostředí zhášena.

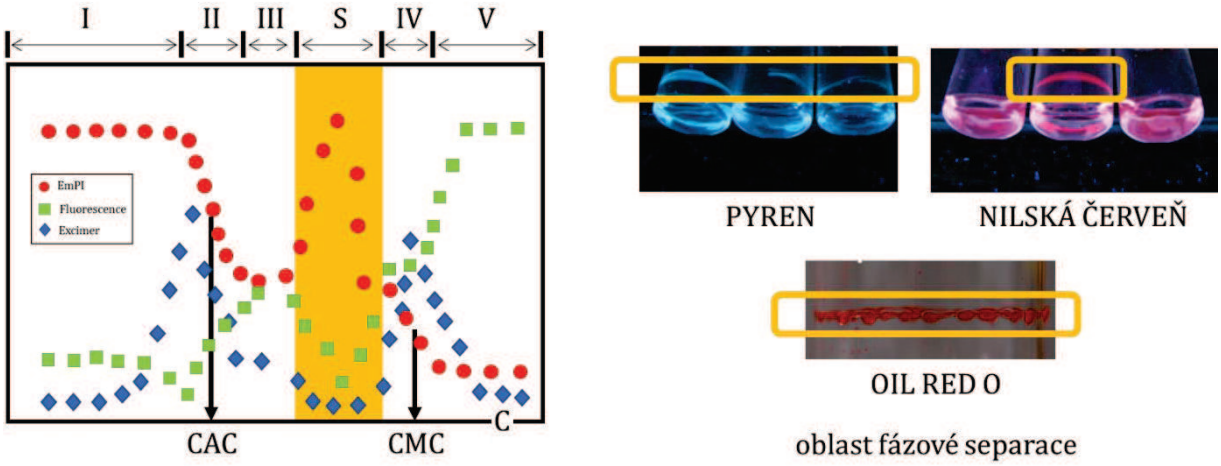

Obrázek 21 Grafická interpretace případu, kdy dochází k fázové separaci. Oblast označená písmenem „S“ koresponduje se žlutě označenou oblastí na fotce, kde lze vidět pod UV-lampou vzorky s pyrenem a Nilskou červení, u nichž došlo k fázové separaci a následné depozici gelové fáze na okraje vialek. Vzorky doplňuje shodná fotka s Olejovou červení.

[58] Pilgrová, T., Venerová, T., **Mravec, F.**, Pekař, M. International *Int J Biol Macromol* 112(2018), 241-249
[59] Halasová, T., Krouská, J., **Mravec, F.**, Pekař, M. *Colloid Surface A* 391 (2011), 25-31

Množství vznikajícího hydrogelu je proměnné a v pracovních koncentracích fluoroforu velmi těžko odhalitelné (barevně) i přes depozici do relativně tenké vrstvy. Interpretace pouze jednoho parametru, nejpoužívanějšího emisního polaritního indexu, by vedla k chybné interpretaci záměny vzorku v koncentrační řadě nebo špatně připraveného vzorku. Při použití dalšího parametru, intenzity fluorescence se ukazuje, že zatímco v oblasti fázové separace EmPI roste k původním hodnotám, fluorescence klesá pod hodnotu pyrenu ve vodném roztoku. Poslední parametr, který vyloučí, že pokles fluorescence je způsoben zakoncentrováním pyrenu, je analýza zastoupení excimeru. V tomto případě je hodnota velmi nízká a znamená to, že se sonda nedostala se vzorkem z vialky do měřící kyvety.

Metoda fluorescenční sondy je tedy velmi elegantní metodou studia interakce, zvláště pokud je k dispozici víceparametrový systém, jako pyren. V každém případě je měření vhodné doplnit i typem sondy, která neemituje z vodného prostředí a je tak schopna přinést informace ohledně formované hydrofobní domény.

Pokud upravíme iontovou sílu roztoku na fyziologickou hodnotu 0,15 mol·L^{-1}, vymizí dvojzlomový průběh i průběh s fázovou separací, agregace odpovídá jednoduché Boltzmannově křivce a zlomová část je posunuta k nižším koncentracím (viz [59]). Jako zajímavý můžeme označit vliv přídavku hyaluronanu, který naopak posouvá agregační hodnoty k vyšším hodnotám (Obrázek 22). Pokud porovnáme parametr $x_0/\Delta x$ pak pro CTAB dostáváme hodnotu 0,048, pro nízkomolekulární hyaluronan 0,095 a vysokomolekulární 0,060. Jak lze pozorovat, poměr v přítomnosti hyaluronanu se zvýšil, nicméně zůstává velmi nízký, a tak jako agregační koncentrace je brán inflexní bod proložené závislosti. Posun agregační koncentrace dobře ilustruje i závislost obsahu excimeru.

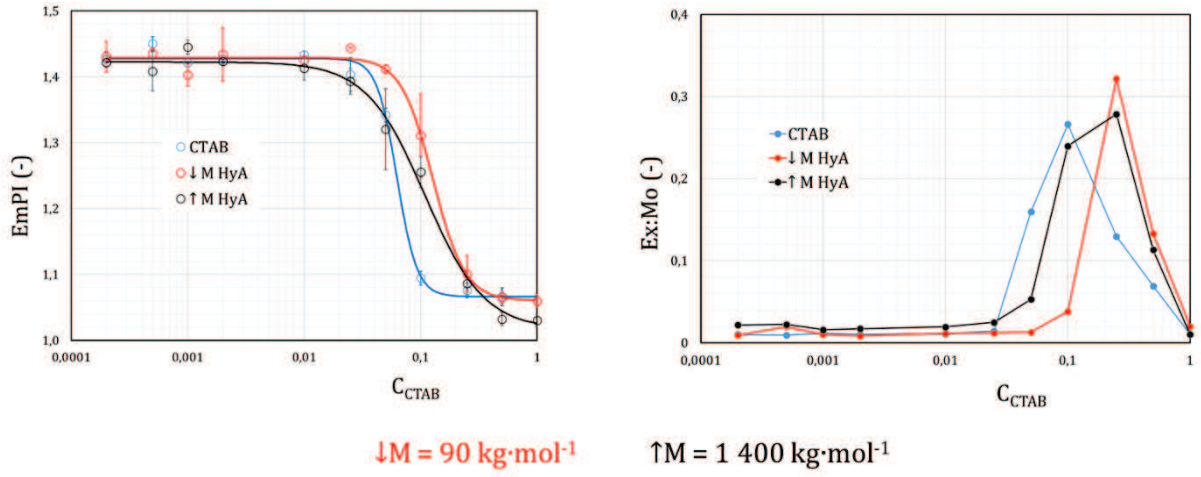

Obrázek 22 Závislost emisního polaritního indexu (adaptováno z [59]) a poměru excimer:monomer (nepublikovaná data) na koncentraci kationaktivního tenzidu ve vodě v přítomnosti hyaluronanu o koncentraci 1 g·L^{-1} a iontové síle 0,15 M upravené NaCl.

3.3.2 Fázová separace v systému polymer-tenzid za vysokých koncentrací

Z předchozí kapitoly vyplynulo, že při specifické kombinaci podmínek dochází u systémů k fázové separaci a tvorbě hydrogelové fáze. Toto by se dalo využít ke tvorbě nové třídy hydrogelů, protože, jak je patrné z fotek (Obrázek 21), jsou i v prostředí hydrogelu zachované nepolární domény.

Takovýto systém by pak mohl kombinovat výhody obou složek např. při mokrém hojení, kdy hydrofilní složka zajistí vlhčení, chlazení a distribuci ve vodě rozpustných látek a nepolární pak solubilizaci nebo uvolňování hydrofobních složek.

Pro praktické využití je ovšem tvorbu hydrogelu potřeba výrazně navýšit. Z praxe plyne, že toto nelze udělat ve vodném roztoku, protože opačně nabité tenzidy vytváří s hyaluronanem sraženinu v procesu purifikace a izolace opačně nabitých polymerů. Jak bylo zjištěno[60], pokud je v systému přítomné zvýšené množství nízkomolekulárního elektrolytu, přechází systém ve vysokých koncentracích na hydrogel, obdobně jako v nízkých koncentracích bez zvýšené iontové síly.

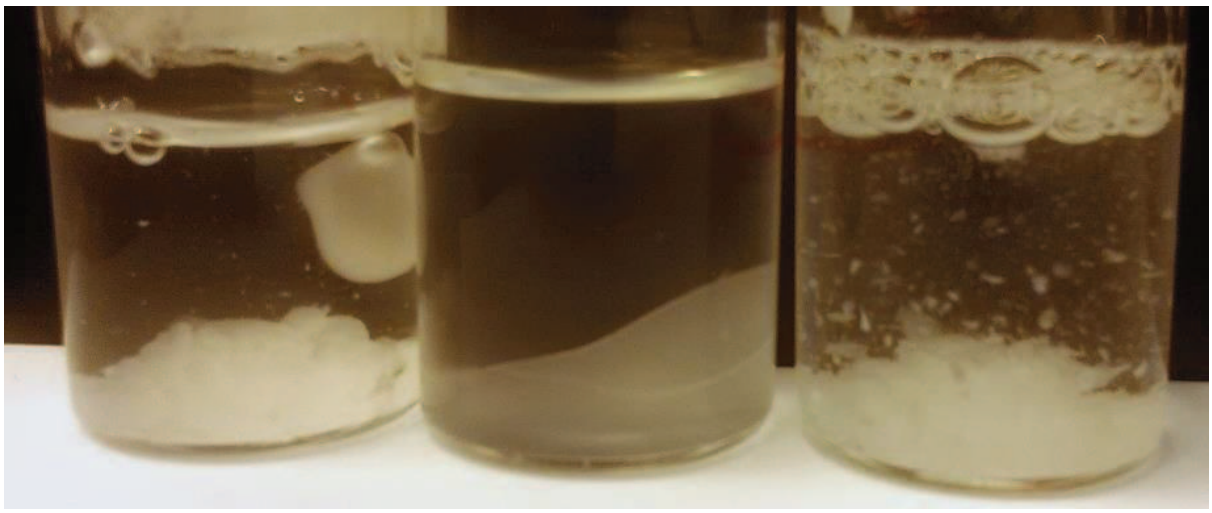

Obrázek 23 Fázově separovaný hydrogel z tenzidu CTAB a hyaluronanu. Mléčné zakalení je způsobeno intenzivním protřepáním na vortexu před odstředěním. Tato opalizace vymizí do 48 h při nerušením stání za laboratorních podmínek. Různé formy hydrogelu před ustálením ukazují vliv molekulové hmotnosti – zleva doprava vysoká (~1 500 kDa), střední (~500 kDa) a nízká (~80 kDa).

Obrázek 23 ukazuje výsledek fázové separace v systému, který byl připraven smícháním 3 mL 2% hm. vodného roztoku hyaluronanu a 3 mL 200 mM roztoku CTAB v prostředí iontové síly 0,15 M upravené NaCl. Vzorky se liší použitou molekulovou hmotností hyaluronanu a jsou zachyceny cca 4 hodiny od smíchání, tedy před ustálením.

[60] např. Kratochvílová, O. *Nový způsob přípravy hydrogelů.* Brno: Vysoké učení technické v Brně, Fakulta chemická, 2016. 45 s. Vedoucí bakalářské práce Ing. Filip Mravec, Ph.D. **nebo** HEGER, R. *Vliv podmínek na tvorbu hydrogelů.* Brno: Vysoké učení technické v Brně, Fakulta chemická, 2016. 44 s. Vedoucí bakalářské práce Ing. Filip Mravec, Ph.D.

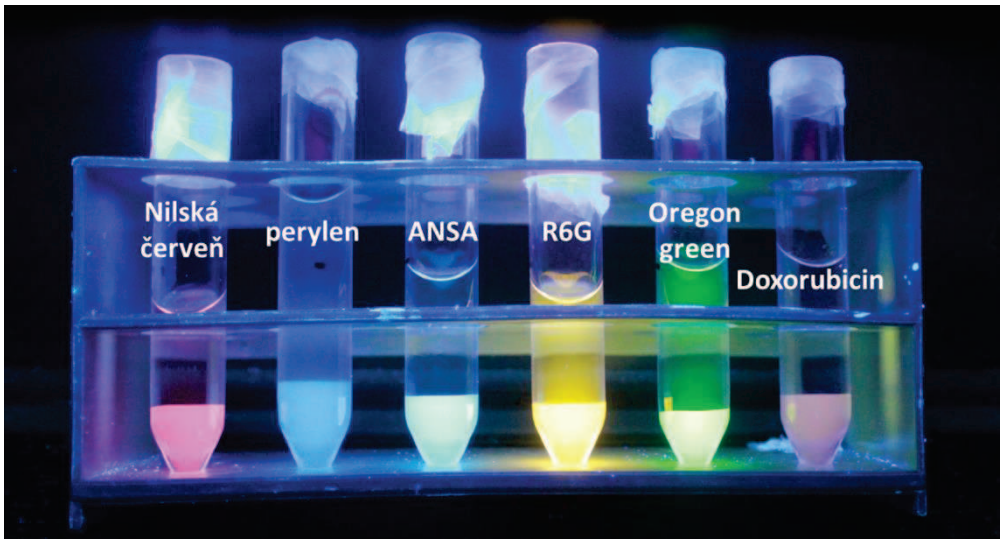

Obrázek 25 Hydrogely na bázi CTAB a hyaluronanu s inkorporovanými látkami s různými vlastnostmi. ANSA 8 anilinonaftalensulfonát amonný; R6G Rhodamin 6G.

Vzniklý systém obsahuje jak vodnou fázi, tak i fázi micelární, která se může od standardní micely lišit. Díky této struktuře mohou být v gelu inkorporovány jak hydrofilní, tak hydrofobní složky, případně i supramolekulární částice, které budou zadrženy stericky. Příklady některých látek pod UV-lampou ukazuje Obrázek 25. Na obrázku jsou zachyceny látky emitující z nepolárních částí jako Nilská červeň, perylen a ANSA a látky emitují i z vodného prostředí – Rhodamin 6G a Oregon green. U posledně zmíněných látek lze pozorovat, že jejich emise je výraznější z hydrogelové fáze. Posledním vzorkem na obrázku je fluoreskující cytostatikum Doxorubicin, fluoreskující pouze z hydrogelové fáze.

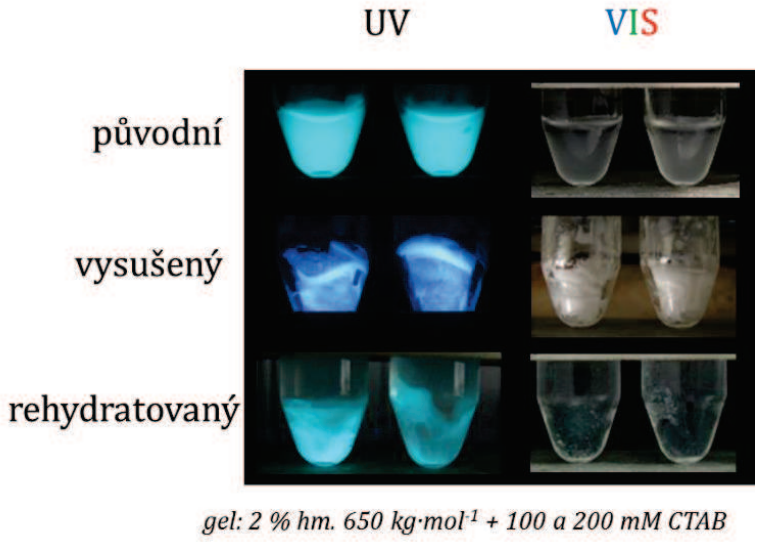

Obrázek 24 Vizualizace vysychání a rehydratace hydrogelu pomocí sondy prodan.

Pokud do hydrogelu inkorporujeme vhodnou sondu, můžeme pozorovat například jeho přechod na xerogelovou formu. Vhodnou fluorescenční sondou je prodan, vykazující modrou emisi v nepolárním prostředí a zelenou emisi v prostředí vodném. Ve fázově separovaném hydrogelu pak díky přítomnosti polárních i nepolárních domén vykazuje

smíšenou emisi, která se jeví při pozorování jako tyrkysová. Při postupném sušení se pak emise posouvá s úbytkem vody postupně do modré oblasti, která odpovídá emisi pouze nepolárních domén. Při přídavku vody se struktura s postupující rehydratací obnovuje a emise hydrogelu pod UV-lampou je opět tyrkysová (Obrázek 24).

Dalším zajímavým pokusem je bližší výzkum fluidity hydrofobních domén ve fázově separovaném hydrogelu. K tomuto pokusu lze využít speciální sondu P3P (1,3-bis(pyren-1-yl)propan), která vykazuje ve fluidním prostředí tyrkysovou excimerovou fluorescenci a v prostředí o vysoké viskozitě pak modrofialovou fluorescenci monomeru. Jak bylo pozorováno, z micelárního prostředí vykazuje P3P tyrkysovou fluorescenci. To odpovídá předpokladu vysoké fluidity micely. Zajímavějším faktem je, že shodnou fluorescenci pak vykazuje i hydrogel (Obrázek 26 vlevo nahoře), který je jinak mechanicky velmi pevný. To lze interpretovat tak, že:

a) micely jsou interakcí s polymerem nezměněné,

b) micely fúzují do větších agregátů, micelárních kanálů nebo supermicel,

c) pozorovaná excimerní fluorescence nepochází z formování vnitřního excimeru, který vyžaduje vysokou fluiditu, ale z překryvu jednotlivých pyrenylových skupin díky blízkému kontaktu a zakoncentrování.

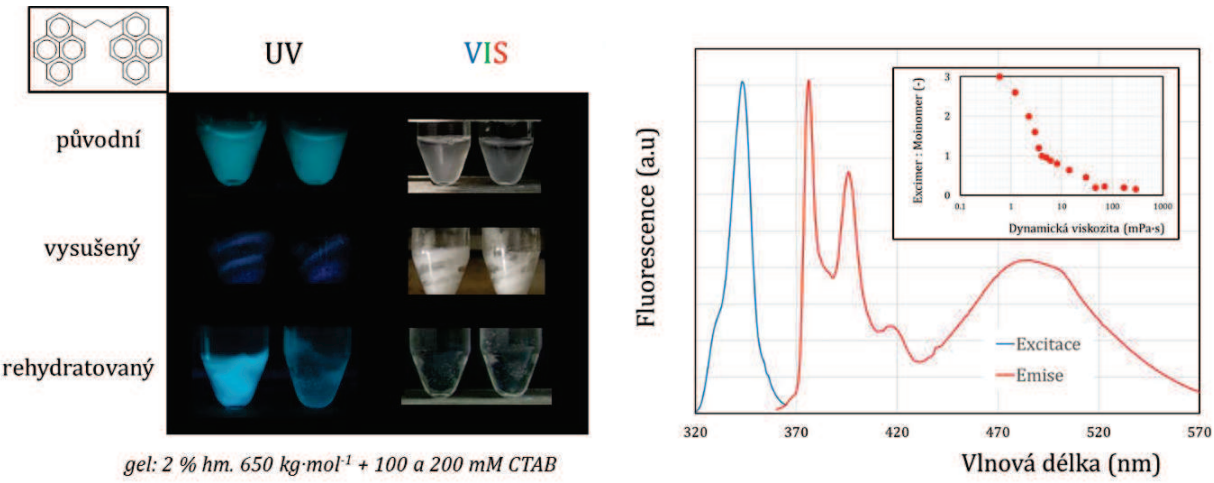

Obrázek 26 Vizualizace vysychání a rehydratace hydrogelu pomocí viskozitní sondy P3P. Na grafu vpravo je excitační a emisní spektrum P3P a ve vloženém grafu nepublikovaná data závislosti poměru intenzity excimeru k intenzitě monomeru na viskozitě. Viskozitní řada byla připravena kombinací methanolu a glycerolu v různých objemových poměrech.

Pokud zvážíme možnost c), ta byla testována monomerním pyrenem. Do gelu bylo inkorporováno molárně dvojnásobné množství pyrenu než sondy P3P. Hydrofobní sondy jsou předsolubilizovány do roztoku tenzidu, který je následně smísen s roztokem polymeru. Po excitaci 365 nm vzorek gelu s P3P vykazuje tyrkysovou fluorescenci a vzorek s pyrenem fialovou fluorescenci monomeru. V tomto případě vylučujeme možnost c).

Možnost a) není příliš pravděpodobná na základě předchozích kapitol. I v případě zvýšené iontové síly pomocí nízkomolekulárního elektrolytu dochází k interakci mezi řetězci v nízkých koncentracích obou složek a k fázové separaci ve vysokých koncentracích. Tato varianta může i mít i svou speciální verzi, kdy budeme uvažovat, že k vázání řetězců je využita jen velmi malá část tenzidu a zbylé micely se pohybují volně v disperzním prostředí bez interakce s řetězcem.

Jako nejpravděpodobnější možnost se pak jeví varianta b). K této variantě lze přidat měření pomocí sledování fluktuace fluorescence hydrofobní sondy Nilská červeň. V tomto případě pak nejsou zajímavé přímo stanovené hodnoty, ale samotný fakt, že fluktuaci lze naměřit. Vysvětlení pomocí micelární fúze je pak velmi pravděpodobné, i když nelze vyloučit i výše zmíněnou speciální variantu, kdy systém obsahuje volné micely.

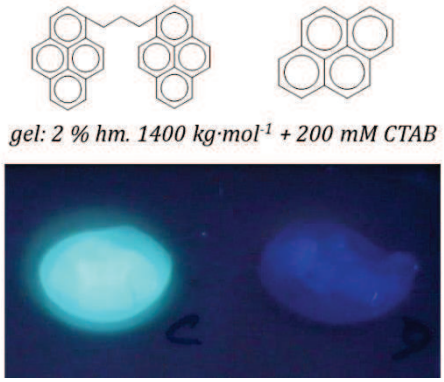

Obrázek 27 Porovnání emise P3P a pyrenu ve shodných molárních množstvích fluoroforů v prostředí fázově separovaného hydrogelu.

V současné době stále probíhá intenzivní výzkum těchto systémů, který kromě fluorescenční spektroskopie využívá i reologii a při správné interpretaci naměřených dat může přinést odpovědi ohledně vnitřního uspořádání těchto fázově separovaných systémů.

3.3.3 Interakce v systému polymer-lipid

V předchozích kapitolách jsme ukázali využití fluorescenční spektroskopie při studiu interakce mezi standardními jednořetězcovými kationaktivními tenzidy a hyaluronanem s diskutabilním stupněm neutralizace/disociace. Rozšířenějšímu využití těchto systémů v medicíně brání převážně tenzidová složka.

Fluorescenční spektroskopie byla použita při studiu náhrady standardních tenzidů biologicky akceptovatelnými variantami. Různé přístupy shrnují publikované práce[61,62,63]. Metody mají společný základ v použití směsných systémů. Navrhovaná základní úvaha

[61] **Mravec, F.**; Klučáková, M.; Pekař, M. Fluorescence Spectroscopy Study of Hyaluronan-Phospholipid Interactions. In *Advances in Planar Lipid Bilayers and Liposomes*. Burlington: Academic Press, 2011. p. 235-255. ISBN: 978-0-12-387720-8.
[62] Burdíková, J., **Mravec, F.**, Pekař, M. *Colloid Polymer Sci* 294 (2016) 823-831
[63] Burdíková, J.; Solná, I.; Doskočil, L.; **Mravec, F.**; Pekař, M. *Colloid Polymer Sci* 295 (2017), 1131-1140

stojí na myšlence využití amfoterních nebo neionogenních systémů dopovaných amfifilními látkami nesoucími kladný náboj.

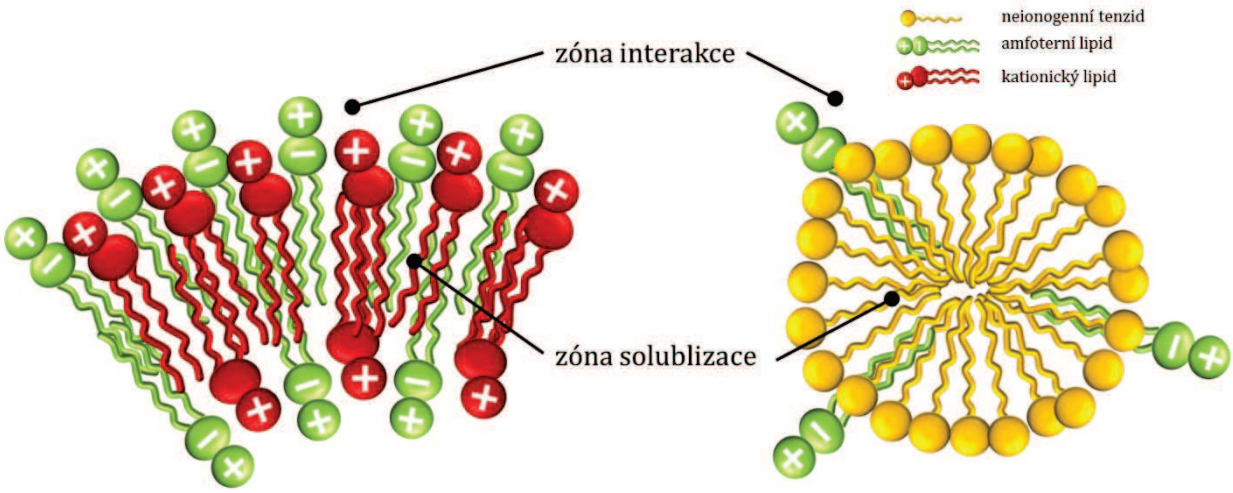

Obrázek 28 Grafická reprezentace uvažovaných směsných agregačních systémů.

Fluorescence byla využita ve studiu pro potvrzení nebo vyvrácení nábojové interakce mezi fosfolipidem DPPC (dipalmitoylfosfatidylcholin) a hyaluronanem obdobně, jak bylo popsáno v kapitole 3.1. K danému množství hyaluronanu bylo přidáno takové množství akridinové oranže, aby poměr P/D dosáhl hodnoty 3. Dále byl do systému přidán DPPC v konečné koncentraci 5, 20 a 50 $mg \cdot L^{-1}$, což jsou hodnoty nad stanovenou agregační (vesikulární) koncentrací pomocí pyrenových charakteristik, která je přibližně 1 $mg \cdot L^{-1}$ (dle [61]). Jak již bylo zmíněno výše, pro potvrzení interakce je vhodné sledovat nejen intenzitu fluorescence, ale zároveň poměr zastoupení dimeru k monomeru z absorpčního/excitačního spektra, jak shrnuje Obrázek 29.

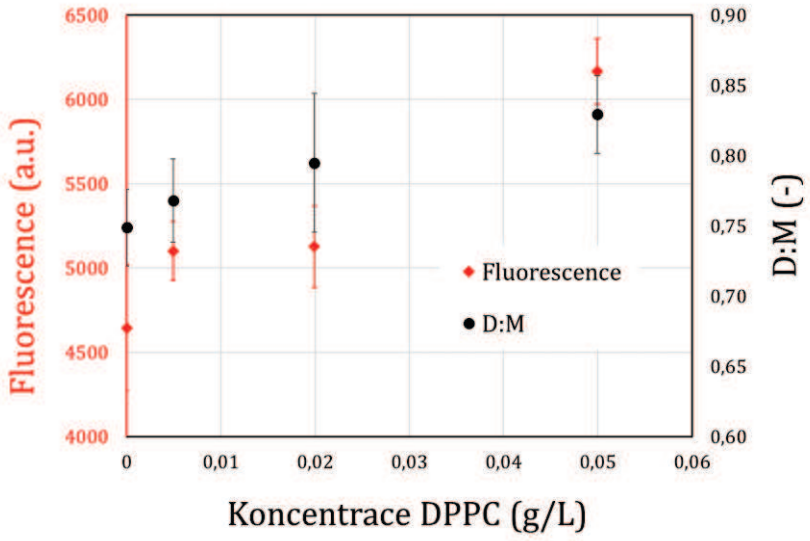

Obrázek 29 Závislost intenzity fluorescence a poměru dimer:monomer z emisního, respektive absorpčního spektra akridinové oranže v přítomnosti hyaluronanu (P/D = 3) za rostoucí koncentrace fosfolipidu DPPC. Data dle [61], doplněna.

Zobrazená data ukazují, že v rámci chyby lze pozorovat nárůst intenzity fluorescence až při padesátinásobku stanovené agregační koncentrace. Důležitým ukazatelem je fakt, že tento nárůst nelze připsat rozpadu dimerů, ale naopak dochází spíše k nárůstu poměru D:M. V tomto případě můžeme tedy takřka vyloučit, že by mezi DPPC a hyaluronanem šlo o nábojovou interakci. Jedno z možných vysvětlení je, že interakce mezi fosfolipidovým agregátem (liposomem) pro řetězec hyaluronanu nedostupná ze sterických důvodů, případně že liposomy z DPPC vykazují velmi nízký negativní zeta-potenciál mezi -1 až -2 mV[64].

Velmi zajímavé výsledky dostaneme, pokud necháme interagovat neionogenní micelární systém dopovaný DPPC. Zvolíme-li například jako neionogenní systém dodecylmaltosid, potřebujeme znát, kolik molekul tenzidu tvoří jednu micelu. K tomu lze opět využít fluorescenční spektroskopii, když stanovíme závislost zhášení pyrenu cetylpyridinium chloridem, ze které lze určit agregační číslo micely dodecylmaltosidu [62]. K takovéto micele bylo přidáno takové množství DPPC, aby molární poměr n_{DPPC}/n_{micel} byl mezi 1 a 1,5[65]. Takto připravený systém přidáváme opět k hyaluronanu s nasorbovanou akridinovou oranží a výsledek shrnuje Obrázek 30.

Data z experimentu s komplexem ukazují, že „rozředění“ amfoterního fosfolipidu v neionogenní micele přineslo z pohledu fluorescence úspěch ve formě nárůstu fluorescence doprovázená poklesem zastoupení dimeru. V tomto případě lze považovat interakci mezi hyaluronanem a komplexem jako elektrostatickou.

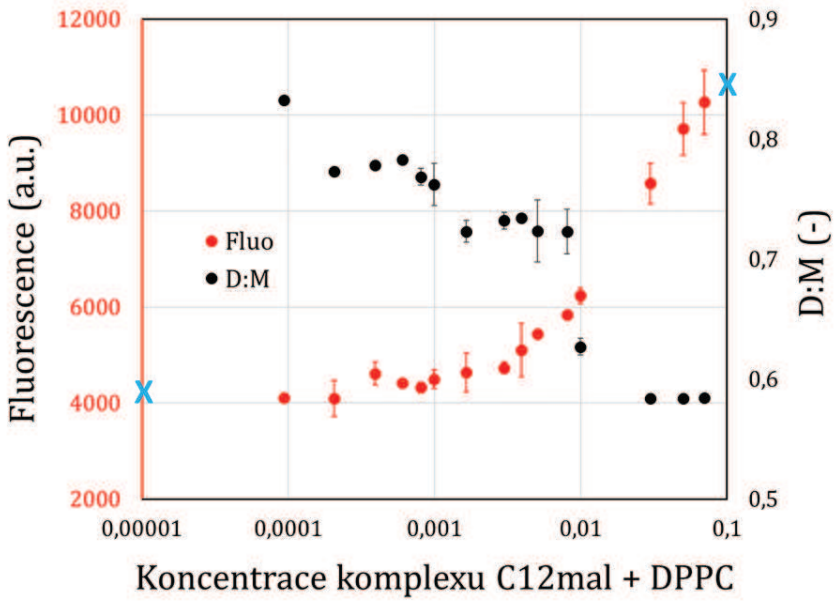

Obrázek 30 Závislost intenzity fluorescence a poměru dimer:monomer z emisního, respektive absorpčního spektra akridinové oranže v přítomnosti hyaluronanu (P/D = 3) za rostoucí koncentrace komplexu dodecyl maltosidu a DPPC v molárním poměru 98:1. Modré křížky indikují výchozí hodnoty fluorescence a D:M pro systém bez přídavku komplexu.

[64] Různí autoři, například Henriksen, I. et al. *Int J Pharma* 101 (1994), 227-236
[65] Tento rozsah je dán širokým rozsahem agregačního čísla. Dle dodavatele (Sigma-Aldrich) bylo agregační číslo 98 [61], námi stanovené pak 67 ± 9 [62]

Chování směsných systémů lze popsat velmi komplexně pomocí dalších fluorescenčních technik a sond. Směs amfoterního fosfolipidu DPPC a kationaktivního lipidu DPTAP (1,2-dipalmitoyl-3-trimetylamonium-propan) byla popsána nejen pomocí pyrenu z hlediska agregace, ale byly využity i anizotropní difenylhexatrien pro studium stupně organizace lipidové vrstvy (Lipid Order Parameter) a polaritní Laurdan, pro stanovení fázového přechodu lipidů ze změny přítomnosti vody v nejbližším okolí [63].

3.4 Fluorescentní částice

Pokročilé mikroskopické techniky byly využity ve studiu dvou odlišných koloidních systémů – nanodiamantů s dusíkovými vakancemi[66] a kvantových teček[67].

3.4.1 Nanodiamanty

Velmi rozsáhlá, teoretická i experimentální, studie pracoval s modelováním, přípravou a stanovením magnetických a optických vlastností nanodiamantů s N-vakancemi a různým způsobem terminace. Fluorescenční spektroskopie, ve formě časově rozlišené fluorescenční mikroskopie (FLIM), byla využita pro stanovení dob života excitovaného stavu těchto systémů v pevném stavu. Pro rozsáhlost této studie se v publikaci objevily pouze shrnuté výsledky popisující jednotlivé experimenty.

Z předchozích spektroskopických měření byly vybrány tři emisní oblasti při dvou různých excitacích. Jako první byla při excitaci 375 nm vzata oblast od 405 nm výše a porovnána s oblastí od 519 nm dále. Pro srovnání byl pak vzorek excitován laserem o vlnové délce 510 nm a emise byla sbírána od 519 nm dále. Pokud se podíváme na naměřená data, je zřejmé, že systém nevykazuje monoexponenciální vyhasínací křivku. Doby života byly měřené při 20 ± 0,5 °C. Pro zelenou excitaci se frakce s dobou života nad 15 ns zvyšuje s přítomností kyslíku. Pro ultrafialovou excitaci se zlomek nejdelší doby života zvyšuje v povrchové modifikaci řady hydrogenované-oxidované-oxidované po žíhání 750 °C. Pro všechny terminace nanodiamantů při excitaci vyšší vlnovou délkou (510 nm) je relativní množství delších dob života vyšší než pro kratší vlnové délky excitace (375 nm). Při vysokoenergetické excitaci je větší množství elektronů excitováno z hlubokých defektů. Potom jsou tripletové elektrony v NV^- defektech silně ovlivněny nejen fonony a materiálními defekty, ale i obrovským množstvím dalších excitovaných elektronů - tyto interakce zkracují dobu života luminiscence.

[66] Kratochvílová, I.; Šebera, J.; Ashcheulov, P.; Golan, M.; Ledvina, M.; Míčová, J.; **Mravec, F.**; Kovalenko, A.; Zverev, D.; Yavkin, B.; Orlinskii, S.; Záliš, S.; Fišerová, A.; Richter, J.; Šefc, L.; Turánek, J. *J Phys Chem C* 118 (2014), 25245-25252

[67] Nejdl, L.; Zítka, J.; **Mravec, F.**; Milosavljević, V.; Zítka, O.; Kopel, P.; Adam, V.; Vaculovičová, M. *Microchim Acta* 184 (2017), 1489-1497.

Obrázek 31 zachycuje emisi agregátu nanodiamantu (oxidovaný a žíhaný) při excitaci 375 nm fluorescence byla zaznamenávána spektrálně od 405 nm. Jak lze vidět, v tuhém stavu jsou nanodiamanty agregované v různě velkých útvarech, což stěžuje jejich praktickou aplikovatelnost a zahrnuje pro značení buněk další, dezintegrační, krok.

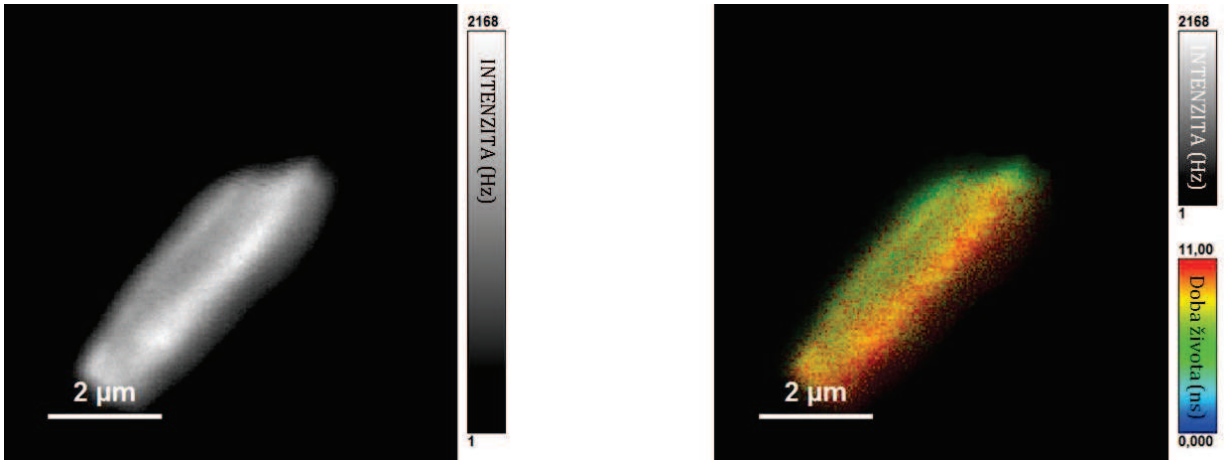

Obrázek 31 Obrázky agregátu nanodiamantů získané pomocí FLIM. Vlevo je obrázek interpretován pouze v intenzitním rozsahu, vpravo pak v kombinaci s rozsahem dob života.

3.4.2 Kvantové tečky

Kvantové tečky patří již dlouhou dobu k oblíbeným fluoroforům. Lze je připravit z různých prekurzorů například pomocí UV záření za stabilizačního efektu 2-sulfanylbutandiové kyseliny.

Pomocí Fluorescenční korelační spektroskopie byl studován vznik a změna emisních a difúzních vlastností u systému Cd:Se. Jako první bylo potřeba systém nastavit pomocí měření již vytvořených kvantových teček pro správné určení doby života, difúzního koeficientu a koncentrace vznikajících QD. Je tedy nutné stanovit parametry konfokálního objemu, nastavit počet fotonů dopadající na detektor[68] a stanovit frekvenci excitačního pulzu laserové hlavice pro správné stanovení doby života. K nastavení tohoto systému se tak přistupuje iterativně.

Obdobně obtížným úkolem je pak i fyzická příprava experimentu, neboť pro správnou genezi kvantových teček je potřeba vlnové délky ~250 nm. Protože jádrem systému je epifluorescenční inverzní mikroskop, bylo přistoupeno k iluminaci seshora. Malé množství roztoků prekurzorů bylo umístěno na krycí sklíčko a nad něj byla umístěna iluminační dioda. Celková vzdálenost nepřesáhla 1 cm. Situace je schematicky zobrazena na následujícím obrázku (Obrázek 32).

[68] Použité detektory mají své omezení, kdy při celkové intenzitě $2 \cdot 10^6$ fotonů·s^{-1} se vypínají. Celkovou intenzitu ovlivňuje mimo jiné i frekvence laserové hlavice, která úzce souvisí se stanovitelným rozsahem dob života.

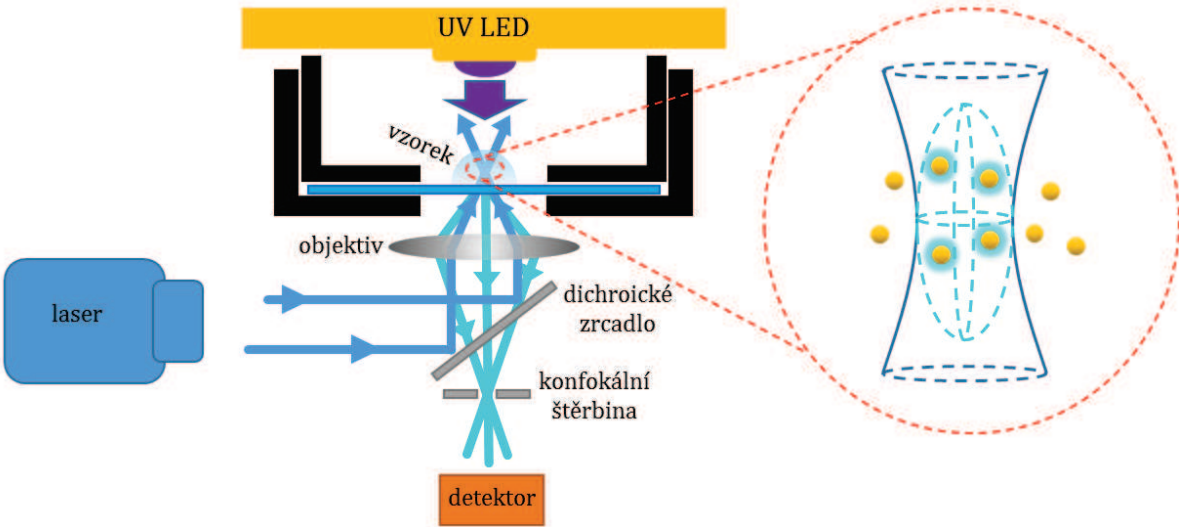

Obrázek 32 Schématická reprezentace uspořádání experimentu pro stanovení temporálních a difúzních parametrů při fotogeneraci kvantových teček. V červeném výřezu je pak tmavě modře naznačený iluminační profil, světle modře konfokální objem a žlutě fluorofory.

Při měření a celkovém nastavení je pak důležitý i vliv iluminační LED. Pokud by dioda generovala nějaké pozadí, muselo by toto být pak odečteno od získaných charakteristik. LED svítí kontinuálně, proto se neočekává výrazný vliv na temporální charakteristiky, nicméně například celkový intenzitní profil by ovlivněný být mohl. Dalším ovlivněním by mohla být luminiscence skleněných součástí experimentu. Proto při měření charakteristik, jako stanovení doby excitačního profilu (Instrument response function) a parametrů konfokálního objemu, byl vliv iluminační diody vždy zahrnut.

Obrázek 33 shrnuje obdržená data při monitorování geneze kvantových teček a ukazuje i široké možnosti multiparametrické analýzy. V datech byly nalezeny oblasti, kde stanovené parametry jsou zatížené nejnižší chybou, které rozdělují průběh na pět oblastí. Díky použití časově rozlišených detektorů, lze takto surová data interpretovat buď jen jako intenzitní záznam, nebo je lze vztáhnout k časové značce excitačního pulzu a obdržet TCSPC histogram pro analýzu dob života anebo korelovat časové rozložení intenzity fluorescence od desetin mikrosekund do jednotek sekund a obdržet tak autokorelační křivku pro analýzu difúzního koeficientu a koncentrace fluoroforu v konfokálním objemu. Výsledky jednotlivých analýz jsou součástí publikace [67] a Obrázek 33 obsahuje i nepublikované analýzy difúzních koeficientů.

Obdržená data odpovídají předpokládanému chování kvantových teček. Čím delší doba iluminace, tím více kvantových teček. Kvantové tečky se poté zvětšují (nárůst difúzního koeficientu) a se zvětšující se velikostí prodlužují dobu života.

Tento experiment tak ukazuje, že i přes složitější a časově náročnější adaptaci měřic soustavy pro daný experiment, je fluorescence velmi elegantním a silným nástrojem pro stanovení koloidních i luminiscenčních vlastností.

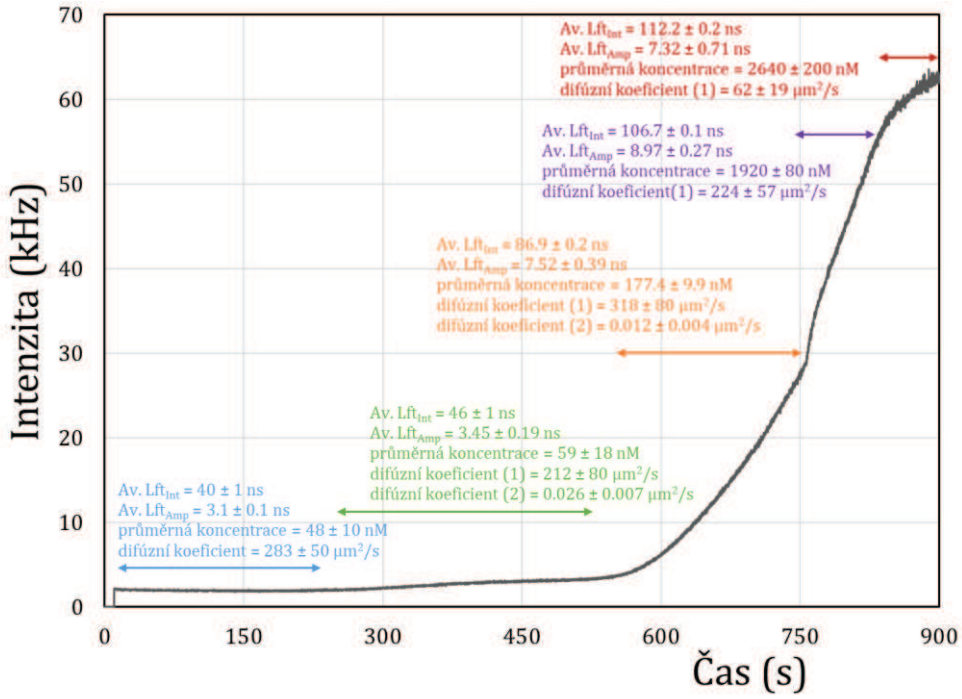

Obrázek 33 Průběh nárůstu intenzity fluorescence v čase při iluminaci prekurzorů Cd:Se. Šipky naznačují oblasti s obdobným chováním (posuzováno podle chyb stanovení jednotlivých parametrů). U jednotlivých oblastí jsou zaznamenány parametry doby života zprůměrované přes intenzitu (Av. Lft$_{Int}$), doby života zprůměrované přes amplitudu (Av. Lft$_{Amp}$), průměrnou koncentraci a difúzní koeficient(y).

3.5 Biokoloidní systémy

Poslední kapitolou pro ilustraci širokého využití fluorescenční spektroskopie jsou koloidní systémy v živých organismech. Jako biokoloidní jsou zde myšleny plazmatické membrány, cytoplazma nebo inkluze zásobních polymerů v koloidních rozměrech.

Fluorescence ve formě fluorescenční mikroskopie je zásadním vědeckým nástrojem ve studiu buněk. Celou kapitolu by zabral asi jen výčet technik, které se používají pro zobrazování, detekci nebo studium těchto živých systémů (sekvenace DNA, DNA čipy, průtoková cytometrie, microscale thermophoresis, imunologie,...). Ve výzkumu se používá buď fluorescence přirozeně se vyskytujících látek, nebo cílené vybarvování. Obrázek 34 ukazuje kompozitní RGB obrázek získaný z analýzy FLIM kvasinky *Cystofilobasidium capitatum* a jednotlivé barevné kanály, které přísluší typickým časům získaným z globální fitovací analýzy. Ta sečte časové informace ze všech bodů obrázku do jedné vyhasínací křivky. Při excitaci 467 nm v rozsahu emisních vlnových délek 520 ± 35 nm jsou nalezeny tři časy, z nichž dva delší odpovídají různým formám flavinů (riboflavin, flavinmononukleotid, flavinadenindinukleotid) a poslední, velmi krátký, pak karotenoidům.

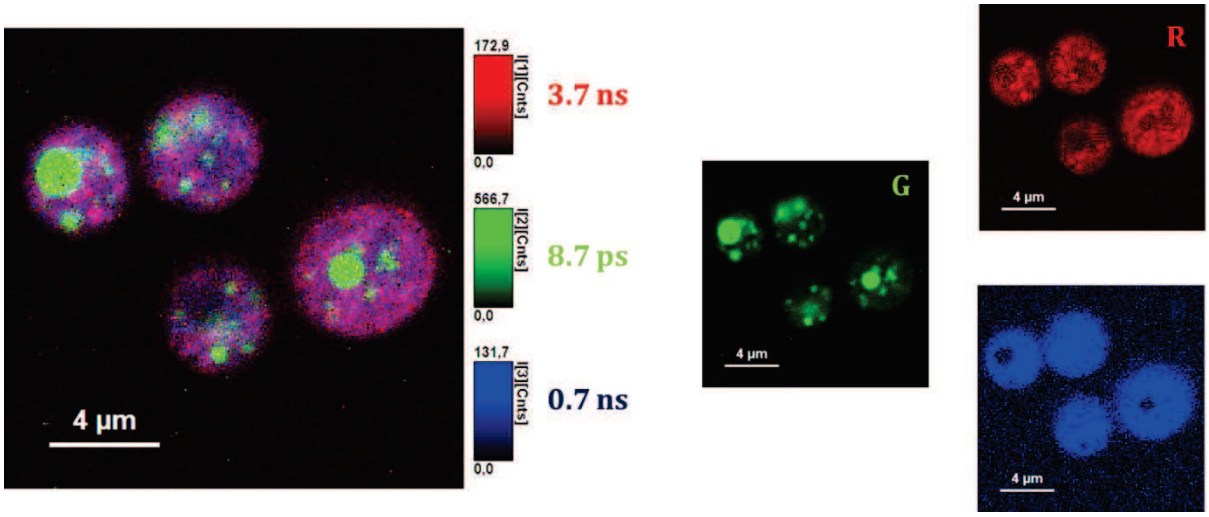

Obrázek 34 Kompozitní RGB obrázek autofluorescence C. capitatum z FLIM analýzy. Zelený kanál zobrazuje fluorescenci karotenoidů.

Při studiu živých systémů je obecně nutné použit složitější přístup. Je nutné získat z jednoho skenu tvarové a funkční informace. Tato nutnost vyplývá například z fotovybělování nebo obtížného způsobu fixace, kdy je malé množství bakteriální suspenze, typicky 50 uL, převrstveno a promícháno s horkým 2-3%roztokem agarózy na krycím skle. Čím vyšší je teplota agarózového solu, tím nižší viskozita a lépe se promíchá s buněčnou suspenzí. Vysoká teplota může ovšem vzorek „rozvařit", vyextrahovat fluorofory z cytoplazmy, což se projeví vysoce fluorescentním pozadím. Při nízké teplotě se špatně agaróza dávkuje a rychleji tuhne při styku s krycím sklem. Vytvoří se oblasti gelovité agarózy mezi nimiž je v mezi prostoru umístěna bakteriální suspenze. Při měření je nezářivými procesy disipována část laserové energie, která při dlouhém měření může lokálně snížit viskozitu fixačního gelu a umožnit posun měřeného objektu.

Z tohoto důvodu je vhodné využití multiparametrického měření ideálně se spektrálně rozlišenými informacemi, pokud je k dispozici více detektorů. V opačném případě je nutné použít vícenásobnou excitaci a/nebo časové rozlišení.

3.5.1 Strukturní studie

Metoda fluorescenční sondy v kombinaci s FLIM byla využita při studiu akumulace zásobního polymeru polyhydroxyalkanoátu (PHA) v bakteriích *Cupriavidus necator H16* při kultivaci s porovnáním s neprodukčním mutantem *C. necator* PHB-4[69].

Z výše uvedených důvodů bylo použito dvojnásobné barvení pro granule i pro membránu pro stanovení obrysového rozměru. To samo o sobě není dostačující, protože lipofilní barvivo Nilská červeň spektrálně zasahuje do žluté (lipofilní emise) i do červené oblasti (emise z hydrofilních oblastí). Pro vizualizaci vnějších vrstev bylo přistoupeno

[69] **Mravec, F.;** Obruča, S. et al. *FEMS Microbiol Lett* 363 (2016), 1-6.

k využití modrého (červená excitace, červená emise) amfifilního barviva DiD®[70], které neprochází přes vnější vrstvy. DiD® lze ovšem excitovat i vlnovou délkou pro excitaci Nilské červeně. Proto bylo přistoupeno ke kombinaci spektrálního časového rozlišení se střídající se excitací (PIE, pulsed-interleaved excitation). Při excitaci se střídaly zelený a červený laser s frekvencí 20 MHz, signál byl rozdělený na dva detektory ve spektrálních oblastech žlutá 550 ± 49 nm a červená 690 ± 70 nm. Žlutý signál byl detekován mezi 0-25 ns, červený mezi 25-50 ns. Tak bylo docíleno, že jeden z kanálů zobrazoval pouze emisi z granulí a druhý obrys bakterie. Situaci shrnuje Obrázek 35.

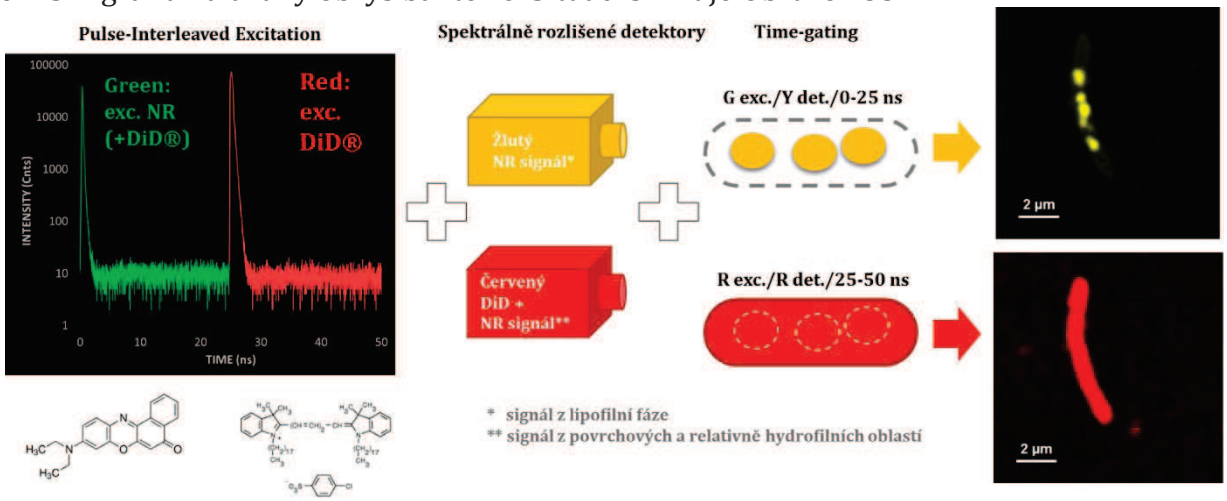

Obrázek 35 Přehled nastavení experimentu pro stanovení zastoupení granulí PHA v bakteriích. Adaptováno dle [69].

Dalším zajímavým výsledkem je intenzitní profil vybarvené granule, který lze proložit Gaussovou křivkou (Obrázek 36). Takové rozložení znamená, že lipofilní barvivo probarvilo celou granuli a není zachyceno jen na povrchu[71].

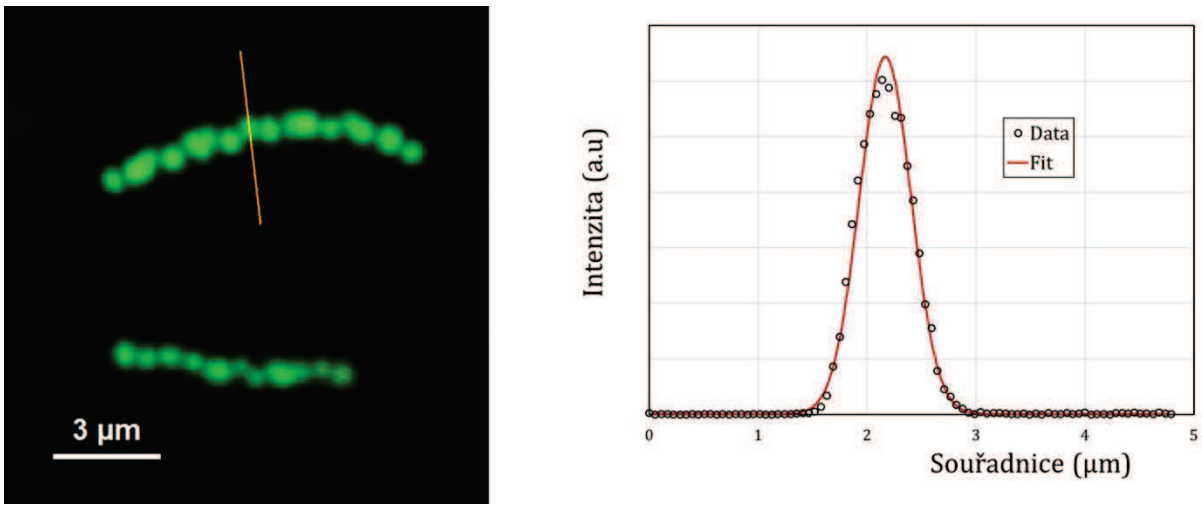

Obrázek 36 Intenzitní profil granule PHA v C. necator H16 s proložením Gaussovou křivkou.

[70] 1,1'-Dioktadecyl-3,3,3',3'-tetramethylindodikarbocyanine, 4-chlorobenzenesulfonát
[71] Úvaha je založena na projekci elipsoidu, pozorovaného konfokálního objemu s výškou 1 µm a šířkou 200 nm na vybarvenou granuli.

Výsledky získané pomocí fluorescenční mikroskopie jsou v dobré shodě se zjištěnými výsledky pomocí elektronové mikroskopie a pomohly zjistit, že maximální objemové procento granulí je okolo 40 %.

3.5.2 Studie cytoplazmy

Pokud jsou buňky vystaveny stresu jako teplota/chlad nebo hypertonickému/hypotonickému prostředí, můžou být ovlivněny vlastnosti cytoplazmy. Z důležitých vlastností cytoplazmy mohou být ovlivněny viskozita nebo pH případně i koncentrace nízkomolekulárních elektrolytů. Tímto mohou být ovlivněny transportní vlastnosti cytoplazmy nebo elektrostatické interakce látek v cytoplazmě interagující.

Pro studium fyzikálně-chemických vlastností cytoplazmy se využívají např. příslušné sondy reagující na pH, chelatační činidla pro ionty či „trackery" pro sledování dělení. Je zároveň mnoho technik, jak dostat fluoreskující činidlo do buněk[72]. Nenabité látky mohou procházet pasivní difúzí přes buněčnou membránu. Takový mechanismus rozdělení ale nepreferuje buňku před vnějším prostředím a při měření by fluoreskující látky tvořily vysoký šum. Jedním ze způsobů, jak toto překonat je blokovat fluorescenci např. esterifikací. V biologickém prostředí buňky pak hydrolýza za účasti nespecifických hydrolytických enzymů bude probíhat výrazně rychleji než ve vnějším vodném prostředí (Obrázek 37). Tím roste kontrast mezi vnitrobuněčným prostorem a vnějším prostředím.

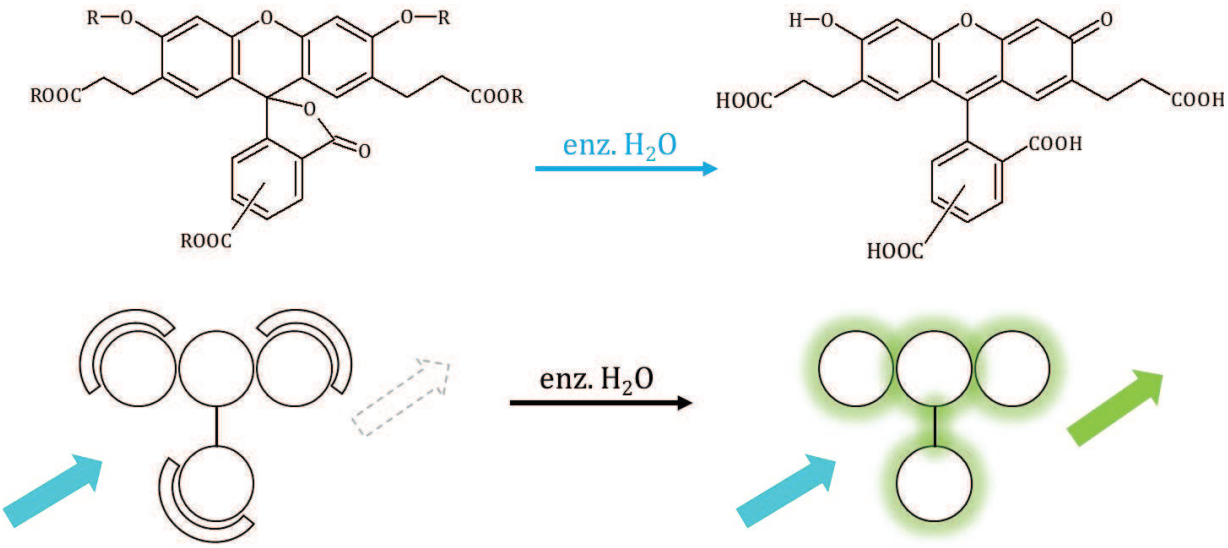

Obrázek 37 Schematické znázornění hydrolýzy izomeru esteru fluorescenční pH sondy BCECF (2',7'-bis-(2-karboxyethyl)-5-karboxyfluorescein).

Pokud je k dispozici měřící systém, který má více detektorů, je možné použít tyto sondy na stanovení fluidních vlastností cytoplazmy pomocí měření anizotropie. V kombinaci se skenerem je tak možné vytvořit anizotropní obrázek, který mapuje rozložení anizotropie a tím i viskozitu cytoplazmy. V ideálním případě pak lze signál

[72] ATP, pinocytóza, elektroporace, fúze s kationickými lipidy, fúze s červenými krvinkami, mikroinjekce, bombardování mikroprojektily, skleněné kuličky, ultrasonifikace, … viz. Molecular Probes Handbook, A Guide to Fluorescent Probes and Labeling Technologies, 11th Edition, ISBN: 0982927916

rozdělit podle roviny polarizace na dva časově rozlišené detektory a získat tak doby života zároveň s anisotropií.

Tento přístup byl použit ve studii dopadu hypertonického prostředí na bakterie produkující granule (*C. necator* H16) a mutantní kmen (*C. necator* PHB-4)[73]. Fluorescenční mikroskopie byla jedna z technik zahrnující elektronové mikroskopie, Ramanova spektroskopie, plynová chromatografie a thermogravimetrie. Výsledky z fluorescenční části výzkumu ukázaly rozdíly mezi H16 a PHB-4 v reakci na hypertonické prostředí. Zatímco průměrné pH u obou kmenů je bez větších rozdílů ve standardním prostředí (7,4-7,5), v hypertonickém prostředí je pokles pH výraznější u neprodukčního kmene PHB-4. To by mohlo ukazovat na protržení buněčné membrány a rychlejší rozvrat neprodukujícího PHB-4. FLIM obrázky také ukazují jednotlivé PHB-4 bakterie velmi neostře s difúzními okraji v hypertonickém prostředí ve srovnání s prostředím standardním.

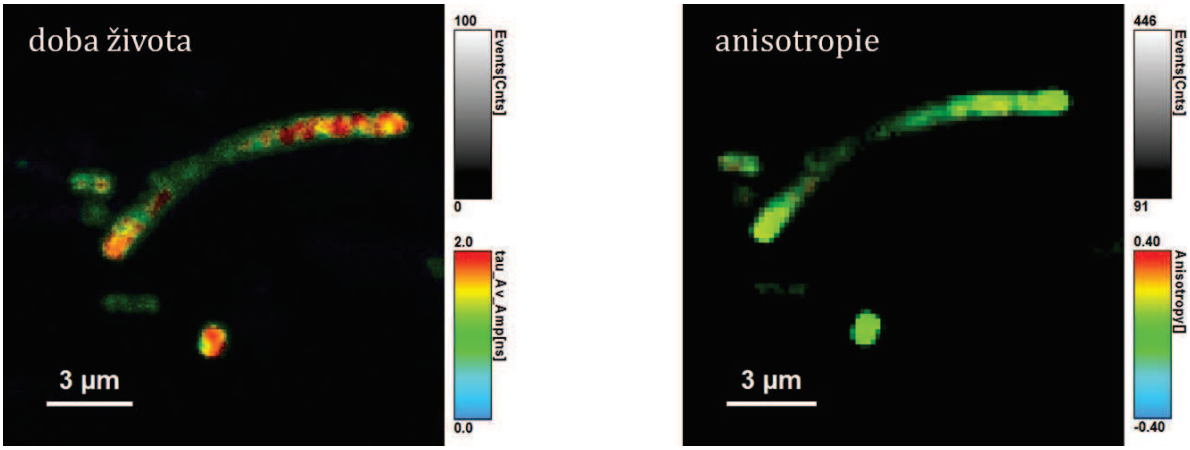

Obrázek 38 FLIM a anizotropní obrázek bakterie Cuprividus necator H16. V levém obrázku jsou data škálována podle doby života průměrované přes amplitudy, vpravo je pak škálování na základě anizotropie. Rozsah byl zvolen tak, že vlevo červené oblasti odpovídají převážně deprotonované formě a vlevo jsou plně fluidní oblasti, uprostřed škály s <r> = 0, zelené.

Mapování viskozity přineslo v chování obou kmenů rozdílné výsledky a podpořilo interpretaci změny pH. Vliv hypertonického prostředí znamenal zvýšení hodnoty anisotropie u H16 a pokles u PHB-4, což by šlo vysvětlit tak, že u H16 došlo k zahuštění vnitřního prostředí v důsledku osmózy a u PHB-4 k protržení membrány a rozředění vnějším prostředím. Pozoruhodný fakt je, že ve standardním prostředí vykazuje anisotropie sondy BCECF vyšší hodnotu u PHB-4 než H16. Toto může souviset s myšlenkou lokalizace sondy nebo hydrolytického aparátu, který umožňuje vyšší rotační pohyb sondy u H16 než u PHB-4.

Obdobně lze pohlížet i na rozložení intenzity fluorescence u FLIM obrázků. Zatímco je u PHB-4 intenzita rozložena víceméně rovnoměrně v celé bakterii, u H16 jsou vidět místa s vyšší a nižší intenzitou. Jedním z možných vysvětlení je rozdílné místo, kde probíhá hydrolýza esteru fluorescenční sondy. U PHB-4 by to pak znamenalo, že

[73] Obruča, S., Sedláček, P., **Mravec, F**. et al. *New Biotechnol* 39 (2017), 68-80

hydrolýza probíhá u buněčné membrány, u H16 v mezigranulárním prostoru nebo na povrchu granule.

3.5.3 UV protektivita

Fluorimetr lze použít i jiným způsobem než jen k měření emisních/excitačních vlastností. Geometrie fluorimetru, kdy je excitační a detekční systém vůči sobě v úhlu 90°, umožňuje sledovat například rozptýlené světlo. Tuto techniku je možno brát jako variantu nefelometrie, kdy je pozorován Tyndallův jev[74].

Tato technika byla použita při studiu rozptylujících vlastností PHB granulích[75]. Jeden z myšlených důsledků přítomnosti granulí je ochrana buněčných systémů proti UV záření. Tato myšlenka byla testována kultivačními testy, průtokovou cytometrií pro stanovení Reaktivních forem kyslíku a rozptylovými technikami.

Pro měření rozptylových charakteristik je potřeba nastavit fluorimetr tak, aby nebyl poškozen detektor. V tomto případě je potřeba suspenzi ručním nastavením otestovat pro různé vlnové délky. Charakteristika je pak měřena metodou Synchronního skenu, kdy se nastaví nulová diference mezi excitační a emisní vlnovou délkou. Dalším důležitým nastavením je detektorová algebra, kdy je potřeba emisní kanál vztáhnout k referenčnímu pro potlačení intenzitního profilu lampy.

Pokud porovnáme při shodném nastavení přístroje a shodné absorbanci vzorku kmen H16 a PHB-4, zjistíme, že rozptyl H16 je výraznější než u PHB-4 a to nejvíce právě v UV oblasti. To by potvrzovalo zjištěné výsledky, kdy kmen H16 vykazoval v dalších testech vyšší odolnost proti UV záření než bez granulí kmen PHB-4.

[74] Rozptyl světla na koloidních (a větších) částicích.
[75] Slaninova, E., Sedlacek, P., **Mravec, F**. et al. *Appl Microbiol Biotechnol* 102 (2018), 1923–1931

4 ZÁVĚR

Tato habilitační práce se zabývá využitím vybraných fluorescenčních technik ve studiu různě komplexních koloidních systémů – od roztoků polymerů po mikroorganismy. Na praktických příkladech bylo ukázáno, že fluorescenční techniky od spektroskopických po mikroskopické jsou velmi silným nástrojem pro výzkum živé i neživé přírody. Množství technik se neustále rozvíjí, zvláště pak v oboru vysoce rozlišené mikroskopie, a množství fluorescenčních sond a značek pro různé aplikace je obrovské.

Uvedené praktické příklady neměly ukázat jen šíři fluorescenčních technik dostupných v rámci Fakulty chemické, ale zabývaly se i hlubší interpretací již publikovaných výsledků. Správná interpretace získaných dat se dá totiž považovat za nejsložitější část použití fluorescenčních technik a to především v případě, kdy pozorované struktury nevykazují vlastní fluorescenci. Obtížnost interpretace naměřených dat lze snížit, pokud je dostupných více technik. Jako vhodným, ne-li rovnou nezbytným, doplňkem stacionární fluorescenční spektroskopie je dynamická časově rozlišená spektroskopie nebo obdobně dynamická technika měření fluorescenční anisotropie (byť je většinou pořizována ve stacionárním módu). Pokud je k dispozici i mikroskopická technika fluktuační spektroskopie (např. FCS), jsou pak dostupné veškeré charakteristiky daného fluoroforu – interakce v excitovaném stavu a mobilita v daném prostředí.

Tento souhrnný přehled pak také ukazuje, že je zde velmi široké pole pro rozvoj dalších technik na FCH VUT, které nebyly v práci zmíněné, ale ve kterých pokračuje výzkum s připravovanými publikačními výstupy. Za všechny lze zmínit například techniku Rezonančního přenosu energie. Zároveň se počítá s rozšířením mikroskopického systému o mikroskop atomárních sil a do budoucna i o systém laserové skenovací mikroskopie, který umožní použití stochastických superrozlišovacích metod. Před technikami fluktuační spektroskopie také stojí velký úkol převodu autokorelačních křivek na frekvenční závislosti elastického a ztrátového modulu pro stanovení mechanických vlastností na mikroskopické úrovni. Techniky využívající fluorescenci se tak budou nadále rozvíjet a bude je možno využívat v nových oblastech výzkumu a aplikacích.

5 SEZNAM PŘÍLOH

Přílohou jsou odborné publikace v plném znění podle toho, jak jsou zmiňovány v textu habilitační práce.

1) MONDEK, J.; **MRAVEC, F.**; VENEROVÁ, T.; HNYLUCHOVÁ, Z.; PEKAŘ, M. Formation and Dissociation of the Acridine Orange Dimer as a Tool Formation and Dissociation of the Acridine Orange Dimer as a Tool for Studying Polyelectrolyte-Surfactant Interactions. *Langmuir,* 2014, vol. 30, no. 29, p. 8726-8734. ISSN: 0743-7463.
2) **MRAVEC, F.**; PEKAŘ, M.; VELEBNÝ, V. Aggregation behavior of novel hyaluronan derivatives-a fluorescence probe study. *Colloid and Polymer Science,* 2008, vol. 286, no. 14-15, p. 1681-1685. ISSN: 0303-402X
3) KALBÁČOVÁ, M.; VERDÁNOVÁ, M.; **MRAVEC, F.**; HALASOVÁ, T.; PEKAŘ, M. Effect of CTAB and CTAB in the presence of hyaluronan on selected human cell types. *Colloids and Surfaces A: Physicochemical and Engineering Aspects,* 2014, vol. 460, no. 1, p. 204-208. ISSN: 0927-7757
4) SAUEROVÁ, P.; VERDÁNOVÁ, M.; PILGROVÁ, T.; VENEROVÁ, T.; **MRAVEC, F.**; KALBÁČOVÁ, M.; PEKAŘ, M. Hyaluronic acid as a modulator of the cytotoxic effects of cationic surfactants. *Colloids and Surfaces A: Physicochemical and Engineering Aspects,* 2015, vol. 483, no. 1, p. 155-161. ISSN: 0927-7757.
5) PILGROVÁ, T.; VENEROVÁ, T.; **MRAVEC, F.**; PEKAŘ, M. Interactions of hyaluronan with oppositely charged surfactants in very diluted solutions in water. *INTERNATIONAL JOURNAL OF BIOLOGICAL MACROMOLECULES,* 2018, vol. 112, no. 1, p. 241-249. ISSN: 0141-8130.
6) HALASOVÁ, T.; KROUSKÁ, J.; **MRAVEC, F.**; PEKAŘ, M. Hyaluronan-surfactant interactions in physiological solution studied by tensiometry and fluorescence probe techniques. *Colloids and Surfaces A: Physicochemical and Engineering Aspects,* 2011, vol. 391, no. 1-3, p. 25-31. ISSN: 0927-7757.
7) **MRAVEC, F.**; KLUČÁKOVÁ, M.; PEKAŘ, M. Fluorescence Spectroscopy Study of Hyaluronan-Phospholipid Interactions. In *Advances in Planar Lipid Bilayers and Liposomes.* Burlington: Academic Press, 2011. p. 235-255. ISBN: 978-0-12-387720-8.
8) BURDÍKOVÁ, J.; **MRAVEC, F.**; PEKAŘ, M. The formation of mixed micelles of sugar surfactants and phospholipids and their interactions with hyaluronan. *Colloid and Polymer Science,* 2016, vol. 294, no. 5, p. 823-831. ISSN: 0303-402X.
9) BURDÍKOVÁ, J.; TÜRKEOVÁ, I.; DOSKOČIL, L.; **MRAVEC, F.**; PEKAŘ, M. A study of zwitterionic/cationic vesicle formation and the influence of hyaluronan on this formation. *Colloid and Polymer Science,* 2017, vol. 295, no. 7, p. 1131-1140. ISSN: 0303-402X.
10) KRATOCHVÍLOVÁ, I.; ŠEBERA, J.; ASHCHEULOV, P.; GOLAN, M.; LEDVINA, M.; MÍČOVÁ, J.; **MRAVEC, F.**; KOVALENKO, A.; ZVEREV, D.; YAVKIN, B.; ORLINSKII, S.; ZÁLIŠ, S.; FIŠEROVÁ, A.; RICHTER, J.; ŠEFC, L.; TURÁNEK, J. Magnetical and Optical Properties of Nanodiamonds Can Be Tuned by Particles Surface Chemistry: Theoretical and Experimental Study. *Journal of Physical Chemistry C (print),* 2014, vol. 118, no. 43, p. 25245-25252. ISSN: 1932-7447.
11) NEJDL, L.; ZÍTKA, J.; **MRAVEC, F.**; MILOSAVLJEVIĆ, V.; ZÍTKA, O.; KOPEL, P.; ADAM, V.; VACULOVIČOVÁ, M. Real-time monitoring of the UV-induced formation of quantum dots on a milliliter, microliter, and nanoliter scale. *Microchimica Acta,* 2017, vol. 184, no. 5, p. 1489-1497. ISSN: 0026-3672
12) **MRAVEC, F.**; OBRUČA, S.; KRZYŽÁNEK, V.; SEDLÁČEK, P.; HRUBANOVÁ, K.; SAMEK, O.; KUČERA, D.; BENEŠOVÁ, P.; NEBESÁŘOVÁ, J. Accumulation of PHA granules in Cupriavidus necator as seen by confocal fluorescence microscopy. *FEMS Microbiology Letters,* 2016, vol. 363, no. 10, p. 1-6. ISSN: 0378-1097
13) OBRUČA, S.; SEDLÁČEK, P.; **MRAVEC, F.**; KRZYZANEK, V.; NEBESAROVA, J.; SAMEK, O.; KUČERA, D.; BENEŠOVÁ, P.; HRUBANOVA, K.; MILÉŘOVÁ, M.; MÁROVÁ, I. The presence of PHB granules in cytoplasm protects non-halophilic bacterial cells against the harmful impact of hypertonic environments. *New Biotechnology,* 2017, vol. 39, no. A, p. 68-80. ISSN: 1871-6784.
14) SLANINOVÁ, E.; SEDLÁČEK, P.; **MRAVEC, F.**; MÜLLEROVÁ, L.; SAMEK, O.; KOLLER, M.; HESKO, O.; KUČERA, D.; MÁROVÁ, I.; OBRUČA, S. Light scattering on PHA granules protects bacterial cells against the harmful effects of UV radiation. *Applied Microbiology and Biotechnology,* 2018, vol. 102, no. 4, p. 1923-1931. ISSN: 1432-0614.

Langmuir

Article

pubs.acs.org/Langmuir

Formation and Dissociation of the Acridine Orange Dimer as a Tool for Studying Polyelectrolyte−Surfactant Interactions

Jakub Mondek,* Filip Mravec, Tereza Halasová, Zuzana Hnyluchová, and Miloslav Pekař

Brno University of Technology, Faculty of Chemistry, Institute of Physical and Applied Chemistry and Materials Research Centre, Purkyňova 464/118, 612 00 Brno, Czech Republic

Supporting Information

ABSTRACT: Steady-state and time-resolved fluorescence and UV−vis techniques were used to study the formation and dissociation of acridine orange dimer in order to investigate hyaluronan−acridine orange, hyaluronan−CTAB (cetyltrimethylammonium bromide), polystyrenesulfonate−acridine orange, and polystyrenesulfonate−CTAB interactions in aqueous solution. Steady-state and time-resolved fluorescence and the dimer:monomer absorbance ratio of acridine orange (AO) were used to determine dimer formation on polymer chains of polyelectrolytes. Acridine orange clearly formed dimers on polystyrensulfonate chains as well as on hyaluronan, but we show that the electrostatic interaction is much weaker in the case of hyaluronan. After the addition of surfactant, we observed an enhancement of fluorescence intensity, indicating the dissociation of AO dimers into monomers and the replacement of acridine orange on polymer chains by surfactant molecules. Importantly, we show that surfactant molecules bind to polymer chains before the critical micelle concentration is reached and form the so-called "bottle-brush" structure.

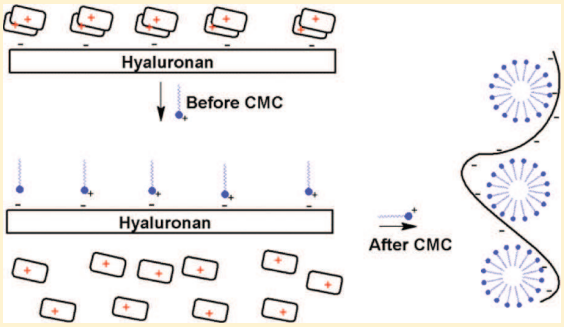

1. INTRODUCTION

The solubilization of hydrophobic molecules in water−micellar environments is a very well known phenomenon[1−3] which enables further investigation of micelle microenvironments or interfaces by fluorescence techniques. For example, critical micelle concentrations (CMC)[4−7] and micellar aggregation numbers[8−10] are widely studied by steady-state or time-resolved fluorescence spectroscopy. The aggregation of acridine dyes is also a well-described phenomenon.[11−14] Negative charge, represented for example by a polyelectrolyte or surfactant, added to a solution of acridine dye causes the aggregation of these molecules into dimers due to van der Waals forces and the strong coupling of molecular transition dipole moments. Coupling causes a wavelength shift in the absorption spectrum. When a red or blue shift occurs, aggregates are called J-aggregates or H-aggregates, respectively.[12] The H-type aggregates have forbidden radiative decay from the excited state, and their absorption band is blue-shifted. From a spectroscopic point of view, the fluorescence of the sample at nearly 530 nm decreases with an increasing amount of dye aggregate; the probability of absorption at 492 nm (monomer band, the α-band) decreases with a concomitant increase in absorption at 465 nm (dimer band, β-band) and at 450 nm (oligomer band, the γ-band). The formation of dye aggregates is, of course, concentration-dependent, and in the case of acridine orange (AO) the aggregates appear at and above its concentration of 5×10^{-5} mol·L^{-1} in aqueous solution.[11] In the presence of a negative binding site, for example, the negative charge of a surfactant or a polyanion, monomers of AO condense on these sites and the dimer form of AO is preferred, which changes its fluorescence intensity and a dimer fluorescent peak appears in the fluorescence spectrum at around 657 nm.[12] This depends on the concentration of both AO and binding sites, and above a critical concentration, AO starts to form nonfluorescent condensate dimers or even oligomers.[11−16] Acridine orange aggregates were used to study negatively charged polyelectrolytes,[12] probe−DNA interactions,[15−17] and probe−protein or protein−surfactant interactions.[18,19]

In this study, acridine orange was used as a fluorescent label which is physically attached to the oppositely charged polyelectrolyte. Physical (electrostatic) binding is supposed to provide an advantage over traditional chemical (covalent) fluorescence labeling in the study of interactions between (labeled) polyelectrolytes and oppositely charged surfactants. The label is attached directly to the interaction site, but its weak physical bond should not prevent interactions with the surfactant, which can be detected by changes in the aggregation behavior of the acridine orange label. Systems comprising oppositely charged polyelectrolytes and surfactants are of growing interest not only as a subject of pure research but also due to their various practical applications. For an overview of this area see several excellent reviews.[20−23]

Received: May 23, 2014
Revised: July 7, 2014
Published: July 8, 2014

Hyaluronan (more precisely, the sodium salt of hyaluronic acid), one of the most important polysaccharides originating from the mammalian body, was selected as the anionic polyelectrolyte for this study due to our long-term interest in its behavior and its potential applications in delivery systems. The understanding of its importance has increased dramatically over the last two decades. Many studies have focused on its physical−chemical behavior, its role in tissues, and its cell proliferation capacity, and methods have been developed to use this polysaccharide in the healing of injuries, drug delivery systems, antiaging applications, and so on. Hyaluronan is a biocompatible and biodegradable polysaccharide consisting of disaccharide units D-glucuronic acid and *N*-acetyl-D-glucosamine[24] (Figure 1). Hyaluronan−surfactant or hyaluronan−

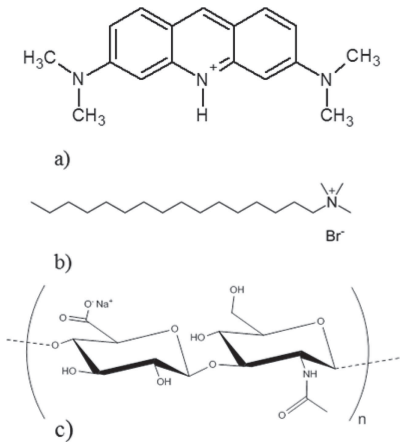

Figure 1. Structure of (a) acridine orange, (b) CTAB, and (c) hyaluronic acid.

liposome interactions provide a useful model for anticancer drug delivery systems based on hyaluronan sensitivity to the CD44 receptor.[25−27] Delivery systems based on hyaluronan should be quite selective for tumor cells because CD44 is overexpressed in cancer cells.[28] Micelles provide, in this model, a good environment for drug solubilization and controlled release, and hyaluronan provides controlled targeting of the drug.

The paper is organized as follows. In the first part, we present a study of the interaction between hyaluronan and acridine orange in the absence of surfactant; in the following part, the interaction between cationic surfactant and a hyaluronan−AO system is presented. Then, a comparative study of the interaction between polystyrenesulfonate (PSS) and acridine orange in the presence of cationic surfactant is added to compare a synthetic polymer with a higher charge density (a "stronger polyelectrolyte") and hyaluronan biopolymer. PSS was selected because it is a well-known and defined polymer and a strong polyelectrolyte and because interactions between PSS and cationic surfactants have been proven and investigated in other studies.[12,29] On the other hand, hyaluronan is known to have a low charge density and to interact relatively weakly with cationic surfactants.[30]

2. MATERIALS AND METHODS

2.1. Materials. All reagents and solvents were used as received, and their purity was higher than 97%. Hyaluronan (molecular weight of 300 kDa) was purchased from CPN spol. s.r.o. (Czech Republic). Polystyrenesulfonate (molecular weight 70 kDa), CTAB, and acridine orange hydrochloride hydrate were purchased from Sigma-Aldrich. Stock solutions of hyaluronan, polystyrenesulfonate, surfactant, and acridine orange were prepared in deionized water. For experiments in the presence of NaCl, 0.15 or 0.5 M NaCl solution was used. Samples for acridine orange and polyelectrolyte interaction were prepared as follows: 25 μL of acridine orange stock solution were added to plastic vials and a fluorescent probe was diluted with an appropriate volume of hyaluronan and solvent to achieve a concentration range for hylauronan from 5×10^{-4} to 15 g·L^{-1} and that for polystyrenesulfonate from 1.25×10^{-5} to 3.6 g·L^{-1}. Samples for polymer−surfactant interaction were prepared with a constant concentration of acridine orange and polymer (respective equivalence point for each polymer determined by the formation of acridine orange dimer) and with an increasing concentration of surfactant ranging from 3×10^{-7} to 4×10^{-3} mol·L^{-1}. All samples were stirred overnight to ensure equilibration. The concentration of the fluorescent probe (AO) in all samples was 1.7×10^{-5} mol·L^{-1} to avoid the presence of the dimer absorption band in the bulk solution.[11] The determined pH of all hyaluronan samples varied between 6.6 and 5.6 (see examples in Supporting Information, Table S1), which is well above the hyaluronan intrinsic pK_a (3.2[31]). It can therefore be reasonably expected that hyaluronan was fully dissociated. PSS is fully ionized in the 6.2−8.9 pH range.[32] The determined pH of all PSS samples varied between 6.7 and 4.6, but pH was, in most cases, below 6.2 (see Supporting Information, Table S1). It can be expected that PSS was not fully dissociated. All measurements were made at 22 °C.

2.2. UV−Vis and Fluorescence Spectroscopy. Absorption spectra were recorded on a Varian Cary 50 UV−vis spectrophotometer with a wavelength range from 200 to 700 nm, and fluorescence spectra were recorded on a FluoroLog Horiba Jobin Yvon spectrofluorimeter. Fluorescence spectra were recorded with the excitation monochromator at 492 nm and in the emission wavelength range of 500 to 650 nm. Because of the inner filter effect, the correction of emission spectra was made according to the equation[33]

$$F_{corr} = F_{obs} \times 10^{1/2(A_{ex}+A_{em})} \quad (1)$$

where F_{corr} and F_{obs} are the corrected and observed fluorescence intensities, respectively, and A_{ex} and A_{em} represent absorbance at the excitation and emission wavelengths, respectively. Time-resolved measurements were performed with a Fluorocube Horiba Jobin Yvon spectrometer by means of a time-correlated single photon counting technique. A 469 nm LED was used as the excitation source. Fluorescence decays were collected with a 495 nm cut-off filter. A time-to-amplitude (TAC) converter was set to the 50 ns window for the measurement of acridine orange and the acridine orange−hyaluronan system. During measurements of polystyrensulfonate−acridine orange, the TAC range was changed from the 50 ns to the 200 ns window because of the increase in the fluorescence lifetime. The repetition rate was set to 1 MHz, and the delay of the signal caused by the cable path was always set 15 ns higher than the respective TAC range.

Time-resolved fluorescence decays were analyzed by the iterative reconvolution procedure of fitting the model function to experimental data, and the fit was judged by nonlinear least-squares analysis.[34,35] Time-resolved data analyses were performed with DAS6 software from Horiba Jobin Yvon using models for multiexponential decay with n components using the equation

$$I(t) = \sum_{i=1}^{n} \alpha_i \exp(-t/\tau_i) \quad (2)$$

where α_i is a preexponential factor which relates to the amount of each fluorescent component present in the system and τ_i is the fluorescence lifetime of the ith component. The goodness of fit was judged by reduced χ_R^2, which evaluates a mismatch between the data and the fitted function and is independent of the number of degrees of freedom.[33]

2.3. Microrheology. For microrheology experiments, a concentration series of hyaluronan solutions in water was prepared by diluting a stock solution. Ten microliters of a 1 μm polystyrene particle 2.5%

dx.doi.org/10.1021/la502011s | *Langmuir* 2014, 30, 8726−8734

suspension obtained from Sigma-Aldrich was added to 5 mL of sample. Samples were stirred using a vortex stirrer for 10 s and then were left to stand for 1 h.

Hardware for the microrheology experiments consisted of a Nikon Eclipse e200 microscope and a Canon digital camera. Particle movement in samples was recorded for 10 s at 50 fps and at a resolution of 1280 × 720 in a dark field. Open source program ImageJ with the ParticleTracking plugin was used for image analysis and the determination of particle trajectories. This program yielded the x and y coordinates of particle position as a function of time, which are used to determine the dependency of the mean square displacement (MSD) on time. The MSD is given by

$$\mathrm{MSD} = \langle [x(t+\tau) - x(t)]^2 + [y(t+\tau) - y(t)]^2 \rangle = 2dDt \quad (3)$$

where d is the dimensionality or spatial extent[36] (in our case two dimensions), D is the diffusion coefficient, $x(t)$ and $y(t)$ are the positions of particle i at time t, and $\langle\ \rangle$ represents an average over time. For the determination of the microviscosity of the medium in the vicinity of tracer particles, the Stokes−Einstein equation was used.[37,38]

$$D = \frac{k_B T}{6\pi\eta r} \quad (4)$$

As the hydrodynamic radius (r), the radius of tracer particles reported by the manufacturer was used (0.5 μm). The final viscosity is the mean value of the viscosities obtained from the MSD of at least 30 particles.

3. RESULTS AND DISCUSSION

Results are displayed as the dependency of the studied physical quantity on the polymer/dye ratio (P/D). The P/D ratio represents moles of binding sites (carboxylic groups of hyaluronan or sulfonate groups of polystyrenesulfonate) per moles of dye. For hyaluronan, the molecular weight of its basic dimer unit bearing one carboxyl group is 401.299 g/mol.

3.1. Interaction of Hyaluronan with Acridine Orange.

The spectral properties of AO are shown in Figure 2. At a concentration of around 5×10^{-5} mol·L^{-1}, it is clearly shown that the monomer absorption band is joined by the dimer absorption band. The absorption band of the dye oligomers appears as a shoulder at 450 nm. These results also determined the experimental setup of measurements with AO. To avoid the formation of AO dimers in solution, we used a lower concentration of acridine orange in samples (1.7×10^{-5} mol·L^{-1}); the absorption spectrum is shown in Figure 2. To cover a wide range of P/D, our experiments were carried out with a constant amount of dye and with changing polyelectrolyte concentration.

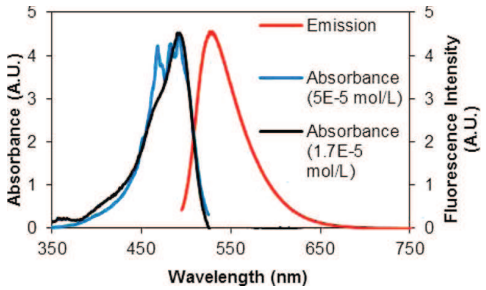

Figure 2. Spectral properties of acridine orange in aqueous solution at a concentration of 5×10^{-5} mol·L^{-1} of the dye and the absorption spectrum for the aqueous solution at a concentration of 1.7×10^{-5} mol·L^{-1}.

Figure 3a shows the dependency of the relative fluorescence intensity measured at 527 nm (the emission maximum shown in Figure 2) on the P/D. (A table of P/D values and the respective hyaluronan concentrations is shown in the Supporting Information.) Relative fluorescence was relative to the fluorescence of the sample without hyaluronan. It is necessary to take into account the fact that the displayed data are not obtained as titration curves. Rather, all points from this dependency were prepared as separate samples, measured at least three times and averaged.

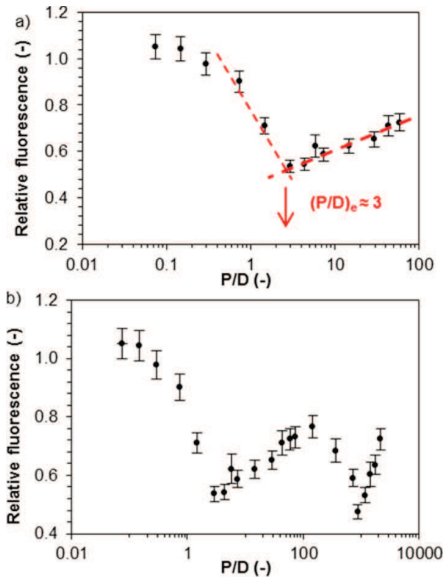

Figure 3. Dependency of the relative fluorescence intensity on the P/D of the system with a constant concentration of acridine orange of 1.7×10^{-5} mol·L^{-1}. Fluorescence is relative to the sample in which hyaluronan is not present. The concentration of hyaluronan in (a) covers the range from 0.5 to 400 mg L^{-1}. In (b), we expanded the concentration range up to 15 g L^{-1}.

The minimum in the relative fluorescence intensity can be found in the dependency in Figure 3a. This minimum is considered to be a point of equivalence, the point where all probe molecules condense as dimers on the accessible binding sites of the polymer. If all carboxylic groups are taken into account as possible binding sites and the acridine orange molecules condense to form dimers, then a value of 0.5 for the point of equivalence can easily be predicted (for each carboxylic anion, two probe molecules are necessary). As is obvious from Figure 3a, the fluorescence intensity starts to decrease only at a P/D of 0.5, and the experimental value of the equivalence point is found at around P/D = 3 and is denoted as $(P/D)_e$.

The high value of the equivalence point can be explained in three different ways. First, hyaluronan is not fully dissociated under these experimental conditions, but the pH of samples suggests the full dissociation of hyaluronan. Second, some carboxylic groups are not accessible for AO molecules, or AO dimer formation is prevented probably because of interchain interactions. Third, interactions between AO and hyaluronan are weak, which contributes to the high value of the equivalence point. It is possible that AO dimers are formed via interchain interactions which could cause the inaccessibility of other carboxylic groups. The value P/D = 3 means that only (100/6)% of polymer binding sites (carboxylic groups) are accessible

dx.doi.org/10.1021/la502011s | Langmuir 2014, 30, 8726−8734

for the formation of acridine orange dimers. The calculation of the accessibility of polymer binding sites is based on the assumption that, for fully dissociated polymer, each carboxylic group possesses two molecules of acridine orange to form dimers and to obtain the minimum in fluorescence intensity. In other words, P/D = 3 represents a 6-fold less efficient degree of AO dimer formation when compared to the ideal case. It should be noted that the real concentration of hyaluronan in the sample at this equivalence point is 20 mg L^{-1}. At this concentration we are dealing with a highly diluted polymer regime; therefore, the polyelectrolyte hyaluronan should be stretched and fully dissociated.[39] However, in the presence of oppositely charged acridine orange, a similar phenomenon of a partial collapse may occur, as observed in polyelectrolyte−surfactant systems[22] in which the chain extension is decreased, which may also result in the hiding of hyaluronan carboxylic groups. If this is the case, then the hyaluronan concentration for such collapse in the presence of AO should be around 0.02 g/L. The relatively high $(P/D)_e$ value is also consistent with the observation of no phase separation in hyaluronan−AO systems, which again indicates some similarity with polyelectrolyte−surfactant systems in which the formation of electrostatically stabilized colloidal dispersions was observed at high polyelectrolyte-to-surfactant ratios.[22]

Above the $(P/D)_e$, the number of available polymer binding sites increases with a concomitant increase in the fluorescence intensity because of the dissociation of acridine orange dimers. It is remarkable that when the concentration of binding sites, in fact, of sodium hyaluronate, increases nearly 30 times (from P/D ≈ 3−90), the fluorescence intensity measured for P/D ≈ 90 is lower than the values at low P/D. This suppressed fluorescence intensity may be caused by conformational changes in hyaluronan.

If we expand the P/D range to the higher concentrations of hyaluronan, then unexpected results are obtained. As can be seen in Figure 3b, above a P/D of 147 (when the hyaluronan concentration is exactly 1 g L^{-1}) another decrease in fluorescence intensity is observed; a second minimum can be found at P/D = 882 (when the concentration of hyaluronan is around 6 g L^{-1}).

At first sight it seems that this decrease cannot be easily explained by dimer condensation because the theoretical number of polymer binding sites is too high. On the other hand, the decrease and subsequent increase in fluorescence is statistically relevant. Because of the sensitivity of the excited state with respect to many conditions (e.g., viscosity, polarity, the presence of ions,...) another method to confirm the obtained results would be useful. In the case of AO, absorption spectroscopy can yield important information.

The absorption maximum of the monomeric form of AO is located at 492 nm and is often called the α-band. In absorption spectra, another two peaks can be found. The first, the β-band, is located at 465 nm and is related to the dimer peak. Between the α- and β-bands, an isosbestic point can be found at around 470 nm. At a high concentration of AO in the system, the β-band is replaced by the γ-band at ∼450 nm. This band is related to the absorption band for AO oligomers.[11]

In our study we compared fluorescence and absorption data (Figure 4). For the absorption spectra we used the ratio of dimer to monomer absorbance determined at 465 and 492 nm, respectively (in Figure 4 depicted as dimer:monomer, which directly reflects changes in dimer presence in the sample). Despite the fact that the fluorescence and absorption data were collected according to different photophysical processes, they exhibit correlation behavior. In the region where fluorescence decreases, an increasing dimer:monomer ratio can be found and vice versa.

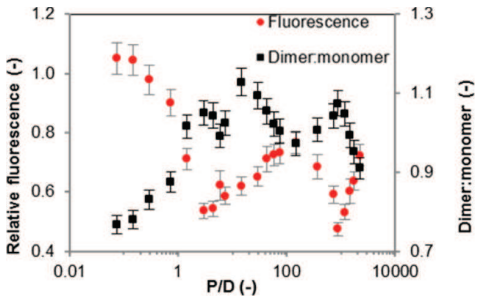

Figure 4. Comparison of dependencies of the relative fluorescence intensity and dimer:monomer ratio on the P/D. The concentration of hyaluronan covers the range from 0.5 mg L^{-1} to 15 g L^{-1}. Fluorescence is relative to the sample in which hyaluronan is not present.

It can also be shown that interactions between acridine orange and hyaluronan have an electrostatic origin. In this case, the addition of low-molecular-weight salt can directly suppress the interaction via the shielding of charges. Figure 5 summarizes the results from these experiments. At first sight, the addition of sodium chloride to the environment leads to suppression of the interaction between probe and polymer. This is manifested in higher values of relative fluorescence around $(P/D)_e$ with increasing ionic strength. The value of $(P/D)_e$ remains roughly the same for 0.15 M and decreases slightly from 3 to 2 for 0.5 M NaCl. Also, for the region between $(P/D)_e$ and a P/D of around 147, values of relative fluorescence follow changes in ionic strength.

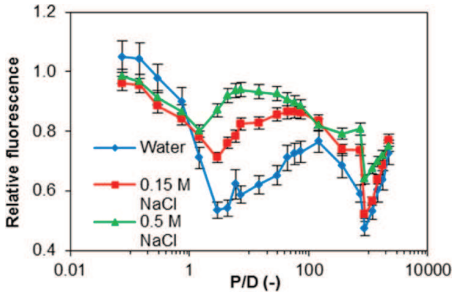

Figure 5. Dependencies of relative fluorescence intensity on P/D at different ionic strengths of the solution. The ionic strength was influenced by sodium chloride. Fluorescence is relative to the sample in which hyaluronan is not present.

A remarkable phenomenon occurs in the second-decrease region. This decrease is still present, and for 0.15 M NaCl, it seems not to be suppressed as much as the decrease around $(P/D)_e$. This phenomenon is interesting because hyaluronan occurs in mammalian tissue in units of grams per liter, and 0.15 M is the ionic strength of the human physiological environment. However, the mechanism behind it is open to discussion.

Thus, it can be concluded that the obtained results from the fluorescence measurements are a relevant reflection of dimer:monomer proportions in solution and that changes in fluorescence intensities are not caused by probe concentration fluctuations. AO labels at least a portion of hyaluronan

dx.doi.org/10.1021/la502011s | Langmuir 2014, 30, 8726−8734

carboxylic groups with the equivalence point of $(P/D)_e = 3$, which corresponds to some saturation of the label on the labeled groups. However, these results do not directly explain the second decrease or rather the second region where the amount of AO dimer significantly increases.

One of the possible explanations of this phenomenon could be found in conformational changes in hyaluronan chains in solution or intrachain interactions. In units of grams per liter, hyaluronan should take a conformation that makes most binding sites inaccessible for electrostatic interaction with acridine orange. We showed changes in conformation using microrheology. This method allows the determination of the mean viscosity of the microstructure of a sample because small sensors used for microrheology determine the microviscosity of the microenvironment in contrast to macroscopic rheology or viscosity measurements. These small sensors better reflect small conformational changes in a sample. Of course, hyaluronan solutions, especially at concentrations above tens of milligrams per liter, are non-Newtonian fluids, so the obtained microviscosity values from microrheology are relevant only for comparison between them. The microrheology method was calibrated to the viscosity of water.

Figure 6 compares the obtained fluorescence and viscosity data. Both types of data were obtained for hyaluronan with a molecular weight of 300 kg mol^{-1} in aqueous solution. The dependency of viscosity on concentration increases steeply at first and then shows a leveling off with a weak maximum within the range of roughly 3−5 g of hyaluronan per liter. It then exhibits an abrupt increase, which corresponds to the reincrease in relative fluorescence (after the second minimum in Figure 4).

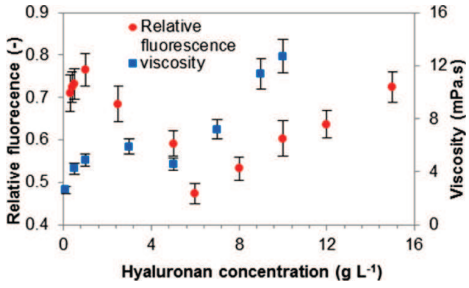

Figure 6. Dependencies of the fluorescence intensity and viscosity obtained from microrheology experiments on the hyaluronan concentration. Fluorescence is relative to the sample in which hyaluronan is not present.

More accurately, after $(P/D)_e = 3$ (hyaluronan concentration of 0.02 g L^{-1}, cf. Table S1), there is a region where the viscosity as well as fluorescence intensity (or dimer:monomer ratio) increases. This can be explained by the increasing concentration of polymer in solution, with more polymer chains meaning more binding sites and more barriers. An increase in viscosity is hindered in the region around 1 g L^{-1} hyaluronan, and at this point, the fluorescence starts to decrease significantly with increasing hyaluronan concentration. Thus, in the concentration region of 1 to 5 or 6 g L^{-1}, it appears that more chains in solution mean fewer binding sites and a smaller effect on the viscosity of the solution. In the region between 5 and 6 g L^{-1} both dependencies have their minimum, and above this region the viscosity as well as fluorescence intensity increases linearly. This increase can be explained by interchain interactions of hyaluronan because at this concentration the chain domains start to overlap.

Here it can be concluded that changes in the occupation of polymer binding sites by cationic probes are commensurate with changes in viscosity. Especially in the region from 1 to 5 or 6 g L^{-1} it seems that polymer chains added to the solution form some kind of aggregate which does not affect the microviscosity and shields charged binding sites against interactions with cationic probes.

3.2. Interaction of CTAB with the Acridine Orange−Hyaluronan System. In this part of our study we were interested in whether the cationic surfactant CTAB is able to replace acridine orange dimers attached to the hyaluronan chain. We used a constant concentration of hyaluronan and acridine orange corresponding to the equivalence point determined in the previous section.

The absorption spectra showed a significant increase in absorbance when even 10^{-7} mol·L^{-1} CTAB was added to the acridine orange−hyaluronan system (spectra are shown in Supporting Information; they are represented also by the dimer:monomer ratio in Figure 7, see further in the text). In the absence of hyaluronan, there was no change in absorption spectra when CTAB was added to the AO solution; thus, the changes in absorption spectra in the presence of hyaluronan and with increasing CTAB concentration were caused by the electrostatic interaction of CTAB with hyaluronan. CTAB started to replace the acridine orange dimers, the dimers dissociated, and the dimer:monomer ratio decreased (i.e., the absorbance increased), especially around the CTAB concentration of 10^{-5} M. An interesting phenomenon occurred around the critical micelle concentration (in the literature, the CMC of CTAB is 0.92−1 mM[6]) as the dimer:monomer ratio increased again (i.e., the absorbance decreased). CTAB probably started to form free micelles, which led to electrostatic attraction between acridine orange monomers in bulk solution and dissociated carboxylic groups. Acridine orange dimers were formed again, which was the reason for the increase in the dimer:monomer ratio. The reaggregation of acridine orange dimers caused both an increase in absorbance and a change in the dimer:monomer ratio.

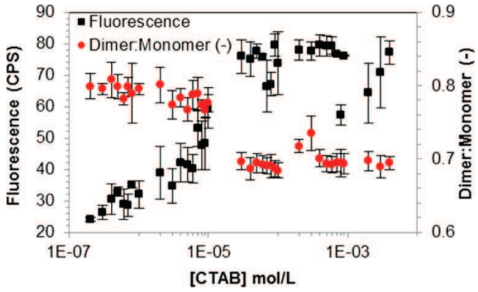

Figure 7. Dependencies of the fluorescence intensity and dimer:monomer ratio as a function of CTAB concentration in the AO−hyaluronan−CTAB system (concentrations of AO and hyaluronan correspond to the equivalence point $(P/D)_e = 3$).

The interaction of CTAB with the AO−hyaluronan system was further studied by steady-state fluorescence (Figure 7). The fluorescence intensity of acridine orange in a sample at the equivalence point $(P/D)_e$ without the addition of CTAB was significantly smaller than the fluorescence intensity in the presence of CTAB at the lowest concentration used, which

dx.doi.org/10.1021/la502011s | Langmuir 2014, 30, 8726−8734

indicates that, at the equivalence point, there should be significant occupation of carboxylic groups of hyaluronan by AO dimers. The AO dimer has a reported emission band at around 650 nm.[16,12,40] In our case, no such peak appeared around this region in any sample, which would suggest either no or very weak aggregation of AO on carboxylic groups of hyaluronan. However, the dependency of both relative fluorescence and the dimer:monomer ratio on P/D depicted in Figure 4 shows changes in the fluorescence intensity and dimer:monomer ratio, respectively, and confirms the formation of AO dimers.

After the addition of surfactant at a concentration lower than its CMC, the fluorescence intensity increased rapidly (Figure 7). This increase in fluorescence intensity (as well as the decrease in absorbance described above in the text) could be ascribed to the electrostatic interaction between hyaluronan and CTAB and to the dissociation of AO dimers. When the surfactant concentration was close to its CMC, the fluorescence intensity decreased (Figure 7). Such a phenomenon may be caused by the aggregation of some AO monomers into dimers again. Before the critical micelle concentration was reached, the electrostatic interaction caused the molecules of the surfactant not to remain at the air−water interface but to bind to carboxylic groups of hyaluronan.[20−23] When the CMC of CTAB was reached, the surfactant molecules formed micelles not only on the hyaluronan chain but also in bulk water, which may again have led to the reavailability of some binding sites for AO. We believe that after the formation of micelles there are again some free binding sites on the hyaluronan chain where acridine orange forms dimers and that this is the reason that the fluorescence intensity decreased. This situation was seen also in absorption spectra, where the ratio of acridine orange dimer and monomer absorption increased when the CMC of CTAB was reached. In our study, the polyelectrolyte caused the single surfactant molecules to be pulled electrostatically into the water environment and to bind to the polymer chain before the critical micelle concentration was reached. Therefore, in general, electrostatic interactions must be stronger than repulsion between the surfactant chain and bulk water. Molecular dynamics simulations performed by Liu et al.[41] showed the formation of the so-called "bottle-brush" structure caused by the adsorption of surfactants on the polyelectrolyte chain. We believe that this structure can also explain our results with AO. This hypothesis is supported by (unpublished) data from our other fluorescence study, which used traditional fluorescent probe pyrene to investigate the polarity of the microenvironment of the probe. The pyrene excitation polarity index (ExPI) as a function of surfactant concentration was used to evaluate this measurement. The ExPI is based on the fact that in the ground state the pyrene absorption band is shifted bathochromically in a nonpolar environment. The ExPI is obtained when the fluorescence intensities at two positions of the excitation monochromator (333 and 338 nm) are measured while the position of the emission monochromator (392 nm) remains constant.[42] An example of data collected for hyaluronan is shown in Figure S3 in the Supporting Information, together with the data from this work. At low surfactant concentrations (before the critical aggregation concentration) we can see no change in ExPI when compared to water, while the fluorescence intensity of AO increases (cf. Figure 7). This means that surfactants bind to the polyelectrolyte chain but do not form any micellelike aggregates (i.e., they probably form the bottle-brush structure). The formation of aggregates is detected at higher concentrations by decreasing ExPI (and by the leveling-off of the AO fluorescence intensity).

Fluorescence lifetimes were determined in the pure AO solution and in hyaluronan−AO and hyaluronan−AO−surfactant systems. In a diluted solution of acridine orange, we assumed monoexponential decay; in the AO−hyaluronan system, we assumed bi- or triexponential decay according to the formation of the AO dimer and/or oligomer with longer lifetimes than that of the monomer because fluorescence from the AO dimer excited state is a forbidden process.[12] Then, we assumed that after the addition of surfactant there should be an increase in the relative amplitude of the acridine orange monomer lifetime and that the decay should be monoexponential after the dissociation of all of the dimers. We obtained a monoexponential decay for diluted pure acridine orange solution with a lifetime of 1.75 ns as expected. The lifetime calculated from the decay curve of the equivalence point in hyaluronan−AO was 1.78 ns (i.e., very close to the value determined for pure AO). The equivalence point was determined by steady-state fluorescence as described in the previous section, where we also showed that the decrease in fluorescence intensity suggests the formation of AO aggregates. Lifetime measurements do not confirm the formation of AO dimers, but fluorescence from acridine orange aggregates is a forbidden process, which means that the lifetimes of acridine orange aggregates may not appear in the fluorescence decay. We assume that in steady-state measurements of samples around the equivalence point all we can see is the weak fluorescence of remaining nonaggregated acridine orange monomers. This was also assumed from the fluorescence spectra, where no dimer fluorescence peak appeared. The interaction between acridine orange and hyaluronan is probably not as strong as we assumed (also we have to consider that only 16% of binding sites appear to be available); however, there is still a weak electrostatic interaction and the dimers are still formed, which could be the reason that the fluorescence intensity decreased so rapidly before the equivalence point (Figure 4). Yet, the probability of fluorescence in these aggregates is low; thus, we do not see any other (dimer or oligomer) fluorescence peak in addition to the monomer lifetime. But if we had observed no increase in fluorescence intensity, it would have meant that the surfactant had not replaced acridine orange. It is also possible that the hydrophilic head of CTAB is too large to bond electrostatically to carboxylic groups of hyaluronan because of the hydration of the hyaluronan chain; however, we believe that this is not the case because we see changes in fluorescence intensities as a function of surfactant concentration. The hyaluronan hydration shell was probably the reason that acridine orange formed dimers with no significant fluorescence and why we saw only decreasing (or increasing in the case of interaction with the surfactant) fluorescence from acridine orange monomers.

3.3. Interaction of CTAB with an Acridine Orange−Polystyrenesulfonate System. According to the fluorescence and absorption spectra of acridine orange in the presence of polystyrenesulfonate (PSS), we assume that acridine orange forms dimers in the presence of polystyrenesulfonate (Figure 8). As in the case of hyaluronan, the fluorescence intensity of AO decreased with a concomitant increase in PSS concentration; the minimum was very shallow (Figure 8a) and it was not easy to determine the equivalence point. Apparently, the break point is at a P/D close to 1, in agreement with Peyratout

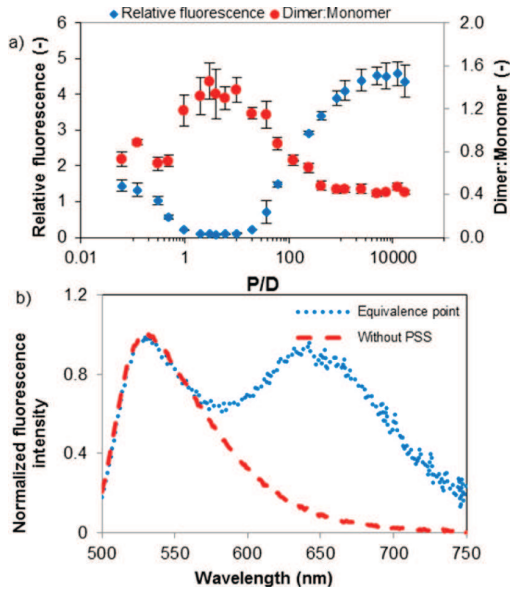

Figure 8. (a) Ratio of relative fluorescence and absorbance (D:M) of acridine orange monomer and dimer in the PSS–AO system. Fluorescence is relative to the sample in which PSS is not present. (b) Emission spectrum of acridine orange from a sample without PSS and with PSS (at the equivalence point determined in this section, P/D = 4).

et al.[12] in which, however, a very narrow range of P/D was used. Taking into account the numerical values of fluorescence intensities at P/D above 1 (and up to 20–30), their error bars, the corresponding D:M absorbance, and the relative representation of dimer fluorescence lifetimes (see further in the text), the equivalence point for $(P/D)_e$ was determined to be around 4 (0.825 mg/L). We assume that this value and the shallow minimum are a result of stronger AO interactions with PSS because of the formation of AO oligomers, which were determined using time-resolved fluorescence as described further in the text. Fluorescence spectra also showed the formation of a new (dimer) peak at around 650 nm (see the example of the system at the equivalence point in Figure 8b) when the PSS concentration was increased.[12,19] This result suggests that AO dimer formation is much stronger in the presence of polystyrenesulfonate than in the presence of hyaluronan. At a P/D of around 10, there was an increase in fluorescence intensity accompanied by a decrease in the dimer:monomer absorbance ratio, which was obviously caused by the dissociation of acridine orange dimers due to the existence of too many binding sites to occupy. At this moment, acridine orange binds to the PSS chain, preferably in monomeric form.

After the addition of a premicellar concentration of surfactant (10^{-5} mol/L) to the PSS–AO system, the absorbance of the dimer:monomer ratio rapidly decreased, which suggests the dissociation of acridine orange dimers. Most importantly, however, the dimer peak at around 650 nm disappeared and the fluorescence intensity increased rapidly (results not shown). This means that the surfactant replaced the acridine orange dimers on the polystyrenesulfonate chain. The acridine orange dimers dissociated, which caused an increase in fluorescence intensity and the disappearance of the emission band of the AO dimer. Fluorescence lifetime measurements confirmed steady-state data. The fluorescence decay of acridine orange at the determined equivalence point of $(P/D)_e = 4$ exhibited a lifetime of 1.66 ns for monomer, 15.94 ns for dimer, and 6.15 ns probably for other AO aggregates or the formation of an acridine orange–PSS complex, as reported for acridine orange–DNA complexes.[43] We assumed that the lifetime of 15.94 ns was the dimer lifetime because iterative reconvolution recovered the majority of long-lived components when we set the emission monochromator to 650 nm, where the emission maximum of the AO dimer is located. According to Ito et al., the lifetime of the AO dimer in the PVA film was around 10 ns.[16] The relative representation of AO dimers increased with increasing P/D, and the maximum was recovered at around P/D = 4. Then, the relative representation of AO dimers decreased with the increasing representation of AO oligomers. A triexponential function to fit data around the equivalence point was used because the correlation between the measured data and fitting parameters was poor for a biexponential function (Figure S2 in Supporting Information). When a triexponential function was used, standard deviation values were randomly distributed around zero (Figure S2) and the χ_R^2 value decreased from 2.3 to 1.2 when compared to the biexponential function. After the addition of the above-mentioned concentration of surfactant (10^{-5} mol/L), fluorescence decay became monoexponential with a lifetime of 1.8 ns.

On the basis of the above results, the titration of acridine orange and PSS solution with CTAB was performed with an automatic titrator, and the emission spectrum of acridine orange was measured after every addition of surfactant. We managed to obtain a micro- to millimolar concentration range with minimized human error during the preparation of such small concentrations and the pipetting of such small volumes. From the plot of fluorescence intensity as a function of CTAB concentration, it is obvious that after the addition of a micromolar concentration the fluorescence intensity increased (Figure 9a). The increase in fluorescence intensity means that monomeric surfactant molecules replaced acridine orange dimers. These assumptions are confirmed in a plot of the monomer:dimer fluorescence intensity ratio as a function of CTAB concentration (Figure 9b). The monomer/dimer fluorescence intensity ratio increased after the first addition of surfactant until this ratio stabilized. The stabilization suggests the replacement of most of the AO dimers with surfactant molecules. Figure 9b suggests that the monomer:dimer ratio was stable after the addition of more than 1×10^{-5} M concentration of surfactant. This means that, as suggested in Figure 9a, the decrease in fluorescence intensity was caused by the dilution of the sample while the system was titrated by the surfactant.

3.4. Comparison of the Two Polyelectrolytes. A comparison of Figures 4 and 8a shows that labeling the two polyelectrolytes with acridine orange initially followed the same pattern (at low values of P/D) except for the first two or three points where the polymer concentration was very low, when the fluorescence intensity decreased with increasing P/D, and the absorbance ratio of dimer:monomer decreased in the same time. After the equivalence (saturation) point was reached, the fluorescence intensity in the case of PSS (the polyelectrolyte with higher charge density) started to increase and the dimer:monomer ratio decreased, which corresponded to the increasing number of AO bound in monomeric form to the increased number of available sulfonate groups. In the case of hyaluronan, the polyelectrolyte with low charge density, the

dx.doi.org/10.1021/la502011s | Langmuir 2014, 30, 8726–8734

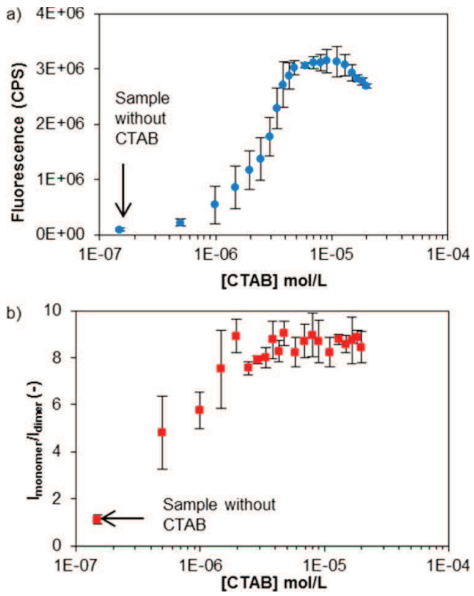

Figure 9. (a) Plot of the acridine orange fluorescence intensity as a function of increasing CTAB concentration. (b) Plot of the AO monomer/dimer fluorescence intensity ratio as a function of surfactant concentration. The concentrations of AO and PSS were held constant in all samples.

situation above the equivalence point was more complex. The fluorescence intensity showed a second minimum accompanied by a maximum in the dimer:monomer ratio dependence. This was probably caused by overlapping hydrated biopolymer chains and related microrheological effects at high hyaluronan concentrations. In the hyaluronan-containing systems, no fluorescence characteristics (either stationary or time-resolved) corresponding to the AO dimer were detected. In these systems, AO dimer fluorescence was quenched by effects of the dimer microenvironment, and dimer existence could be followed by absorption spectroscopy only. Both hyaluronan- and PSS-based systems prepared at the equivalence point composition responded to the addition of CTAB already at very low concentrations. The fluorescence intensity increased in comparison to both the surfactant-free system and with increasing surfactant concentration, and at the same time, the proportion of AO dimer decreased (which was more pronounced for the PSS-based systems). This demonstrated interactions between (AO-labeled) polyelectrolyte and surfactant. The changes in spectroscopic characteristics with surfactant concentration leveled off at a CTAB concentration of about 3×10^{-5} M for hyaluronan and 4×10^{-6} M for PSS, which are believed to correspond to the replacement of AO by the surfactant. These concentrations can be viewed as kinds of critical aggregation concentrations determined by the fluorescence method; as expected on the basis of charge density, the value for the PSS-based system was significantly lower than that for the hyaluronan-based system. These conclusions are also supported by the experiments with pyrene mentioned above and are illustrated for hyaluronan in Figure S3 and for PSS in Figure S4 in the Supporting Information. At the stated concentrations, the pyrene excitation polarity index started to decrease, indicating the formation of aggregates with hydrophobic domains. The value for PSS was significantly lower than characteristic values reported in the literature on the basis of surface tension measurements,[21] but the value for hyaluronan was in excellent agreement with the critical binding concentration determined from NMR self-diffusion measurements.[30] The fluorescence method presented in this work, like the NMR measurements, is more sensitive to interactions on the molecular level than methods such as surface tension.

4. CONCLUSIONS

Acridine orange was used as a fluorescent label attached to oppositely charged functional groups of biopolymer or synthetic polyelectrolyte—hyaluronan and polystyrenesulfonate, respectively. The labeling changed the fluorescence and absorption properties of dye molecules due to the formation of AO dimers. The ratio of the number of polymer binding sites to the number of dye molecules (P/D) at the equivalence point was determined at the point of the fluorescence intensity minimum. In the case of hyaluronan, a second minimum was detected at a much higher P/D value, probably caused by hyaluronan conformational changes at high concentrations. The dissociation of the AO dimer upon the addition of surfactant to the system corresponding to the equivalent P/D value was then used to study polymer—surfactant interactions. The interactions between hyaluronan and AO or surfactant were found to be weaker than the interactions with polystyrenesulfonate, probably due to the high hydration of hyaluronan chains. Critical aggregation concentrations of CTAB determined by the fluorescence method were 3×10^{-5} M for hyaluronan and 4×10^{-6} M for PSS. In the presence of both polyelectrolytes, surfactant molecules were pulled into the solution before the critical micelle concentration was reached. The formation and dissociation of acridine orange dimer exhibited the formation of the bottle-brush structure caused by the adsorption of surfactants on the polyelectrolyte chain.

■ ASSOCIATED CONTENT

Ⓢ Supporting Information

Hyaluronan and PSS concentrations and respective P/D and pH values. UV—vis spectra of acridine orange in the presence of hyaluronan with increasing concentration of CTAB. This material is available free of charge via the Internet at http://pubs.acs.org.

■ AUTHOR INFORMATION

Corresponding Author

*E-mail: xcmondek@fch.vutbr.cz.

Notes

The authors declare no competing financial interest.

■ ACKNOWLEDGMENTS

This work was supported by project no. LO1211 (Ministry of Education, Czech Republic).

■ REFERENCES

(1) Hiemenz, P. C.; Rajagopalan, R. *Principles of Colloid and Surface Chemistry*, 3rd ed.; Marcel Dekker: New York, 1997; p 650.

(2) Kabanov, A. V.; Nazarova, I. R.; Astafieva, I. V.; Batrakova, E. V.; Alakhov, V. Y.; Yaroslavov, A. A.; Kabanov, V. A. Micelle Formation and Solubilization of Fluorescent Probes in Poly(oxyethylene-b-oxypropylene-b-oxyethylene) Solutions. *Macromolecules* **1995**, *28*, 2303—2314.

(3) Weiss, J.; Coupland, J. N.; McClements, D. J. Solubilization of Hydrocarbon Emulsion Droplets Suspended in Nonionic Surfactant Micelle Solutions. *J. Phys. Chem.* **1996**, *100*, 1066—1071.

(4) Goddard, E. D.; Turro, N. J.; Kuo, P. L.; Ananthapadmanabhan, K. P. Fluorescence probes for critical micelle concentration determination. *Langmuir* **1985**, *1*, 352−355.
(5) Dominguez, A.; Fernandez, A.; Gonzalez, N.; Iglesias, E.; Montenegro, L. Determination of Critical Micelle Concentration of Some Surfactants by Three Techniques. *J. Chem. Educ.* **1997**, *74*, 1227.
(6) Aguiar, J.; Carpena, P.; Molina-Bolívar, J. A.; Carnero Ruiz, C. On the determination of the critical micelle concentration by the pyrene 1:3 ratio method. *J. Colloid Interface Sci.* **2003**, *258*, 116−122.
(7) Yu, L.; Tan, M.; Ho, B.; Ding, J. L.; Wohland, T. Determination of critical micelle concentrations and aggregation numbers by fluorescence correlation spectroscopy: Aggregation of a lipopolysaccharide. *Anal. Chim. Acta* **2006**, *556*, 216−225.
(8) Gehlen, M. H.; De Schryver, F. C. Time-resolved fluorescence quenching in micellar assemblies. *Chem. Rev.* **1993**, *93*, 199−221.
(9) Alargova, R. G.; Kochijashky, I. I.; Sierra, M. L.; Zana, R. Micelle Aggregation Numbers of Surfactants in Aqueous Solutions: A Comparison between the Results from Steady-State and Time-Resolved Fluorescence Quenching. *Langmuir* **1998**, *14*, 5412−5418.
(10) Wattebled, L.; Laschewsky, A.; Moussa, A.; Habib-Jiwan, J.-L. Aggregation Numbers of Cationic Oligomeric Surfactants: A Time-Resolved Fluorescence Quenching Study. *Langmuir* **2006**, *22*, 2551−2557.
(11) Costantino, L.; Guarino, G.; Ortona, O.; Vitagliano, V. Acridine orange association equilibrium in aqueous solution. *J. Chem. Eng. Data* **1984**, *29*, 62−66.
(12) Peyratout, C.; Donath, E.; Daehne, L. Electrostatic interactions of cationic dyes with negatively charged polyelectrolytes in aqueous solution. *J. Photochem. Photobiol., A* **2001**, *142*, 51−57.
(13) Lamm, M. E.; Neville, D. M. The Dimer Spectrum of Acridine Orange Hydrochloride. *J. Phys. Chem.* **1965**, *69*, 3872−3877.
(14) Antonov, L.; Gergov, G.; Petrov, V.; Kubista, M.; Nygren, J. UV-Vis spectroscopic and chemometric study on the aggregation of ionic dyes in water. *Talanta* **1999**, *49*, 99−106.
(15) Lauretti, F.; Lucas de Melo, F.; Benati, F.; amp, x; cio, J.; de Mello Volotão, E.; Santos, N.; Linhares, R. E. C.; Nozawa, C. Use of acridine orange staining for the detection of rotavirus RNA in polyacrylamide gels. *J. Virol. Methods* **2003**, *114*, 29−35.
(16) Ito, F.; Kakiuchi, T.; Nagamura, T., Excitation Energy Migration of Acridine Orange Intercalated into Deoxyribonucleic Acid Thin Films. *J. Phys. Chem. C* **2007**, *111*, 6983−6988.
(17) Sarkar, D.; Misra, T. N. Electrical conduction in some nucleic acid base complexes with acridine orange dye: study of localized levels. *Biomaterials* **1989**, *10*, 202−205.
(18) Smal, J.; Kathuria, S.; De Meyts, P. Acridine orange, an inhibitor of protein kinase C, abolishes insulin and growth hormone stimulation of lipogenesis in rat adipocytes. *FEBS Lett.* **1989**, *244*, 465−468.
(19) Wang, F.; Yang, J.; Wu, X.; Wang, X.; Feng, L.; Jia, Z.; Guo, C. Study on the formation and depolymerization of acridine orange dimer in acridine orange−sodium dodecyl benzene sulfonate−protein system. *J. Colloid Interface Sci.* **2006**, *298*, 757−764.
(20) Goddard, E. D. Polymer/Surfactant Interaction: Interfacial Aspects. *J. Colloid Interface Sci.* **2002**, *256*, 228−235.
(21) Taylor, D. J. F.; Thomas, R. K.; Penfold, J. Polymer/surfactant interactions at the air/water interface. *Adv. Colloid Interface Sci.* **2007**, *132*, 69−110.
(22) Bain, C. D.; Claesson, P. M.; Langevin, D.; Meszaros, R.; Nylander, T.; Stubenrauch, C.; Titmuss, S.; von Klitzing, R. Complexes of surfactants with oppositely charged polymers at surfaces and in bulk. *Adv. Colloid Interface Sci.* **2010**, *155*, 32−49.
(23) Goddard, E. D.; Ananthapadmanabhan, K. P. Applications of Polymer-Surfactant Systems. In *Polymer-Surfactant Systems*; Kwak, J. C. T., Ed.; Marcel Dekker: New York, 1998; Vol. *77*, pp 21−65.
(24) Lapčík, L.; De Smedt, S.; Demeester, J.; Chabreček, P. Hyaluronan: Preparation, Structure, Properties, and Applications. *Chem. Rev.* **1998**, *98*, 2663−2684.
(25) Di Meo, C.; Panza, L.; Capitani, D.; Mannina, L.; Banzato, A.; Rondina, M.; Renier, D.; Rosato, A.; Crescenzi, V. Hyaluronan as Carrier of Carboranes for Tumor Targeting in Boron Neutron Capture Therapy. *Biomacromolecules* **2007**, *8*, 552−559.
(26) Qhattal, H. S. S.; Liu, X. Characterization of CD44-Mediated Cancer Cell Uptake and Intracellular Distribution of Hyaluronan-Grafted Liposomes. *Mol. Pharmaceutics* **2011**, *8*, 1233−1246.
(27) Oh, E. J.; Park, K.; Kim, K. S.; Kim, J.; Yang, J.-A.; Kong, J.-H.; Lee, M. Y.; Hoffman, A. S.; Hahn, S. K. Target specific and long-acting delivery of protein, peptide, and nucleotide therapeutics using hyaluronic acid derivatives. *J. Controlled Release* **2010**, *141*, 2−12.
(28) Platt, V. M.; Szoka, F. C. Anticancer Therapeutics: Targeting Macromolecules and Nanocarriers to Hyaluronan or CD44, a Hyaluronan Receptor. *Mol. Pharmaceutics* **2008**, *5*, 474−486.
(29) Vitagliano, V.; Costantino, L.; Zagari, A. Interaction between Acridine Orange and poly(styrenesulfonic acid). *J. Phys. Chem.* **1973**, *77*, 204−210.
(30) Thalberg, K.; Lindman, B. Interaction between hyaluronan and cationic surfactants. *J. Phys. Chem.* **1989**, *93*, 1478−1483.
(31) Cowman, M. K.; Matsuoka, S. Experimental approaches to hyaluronan structure. *Carbohydr. Res.* **2005**, *340*, 791−809.
(32) Francius, G.; Hemmerlé, J.; Voegel, J. C.; Schaaf, P.; Senger, B.; Ball, V. Anomalous Thickness Evolution of Multilayer Films Made from Poly-l-lysine and Mixtures of Hyaluronic Acid and Polystyrene Sulfonate. *Langmuir* **2006**, *23*, 2602−2607.
(33) Lakowicz, J. R. *Principles of Fluorescence Spectroscopy*, 3rd ed.; Springer: New York, 2006; p 954.
(34) Periasamy, N. Analysis of Fluorescence Decay by the Nonlinear Least Squares Method. *Biophys. J.* **1988**, *54*, 961−967.
(35) Grinvald, A.; Steinberg, I. Z. On the analysis of fluorescence decay kinetics by the method of least-squares. *Anal. Biochem.* **1974**, *59*, 583−598.
(36) Gardel, M. L., Valentine, M. T., Weitz, D. A. Microrheology. In *Microscale Diagnostic Techniques*; Springer: Berlin, 2005; pp 1−50.
(37) Mason, T. G.; Weitz, D. A. Optical Measurements of Frequency-Dependent Linear Viscoelastic Moduli of Complex Fluids. *Phys. Rev. Lett.* **1995**, *74*, 1250−1253.
(38) Wirtz, D. Particle-Tracking Microrheology of Living Cells: Principles and Applications. *Annu. Rev. Biophys.* **2009**, *38*, 301−326.
(39) Matteini, P.; Dei, L.; Carretti, E.; Volpi, N.; Goti, A.; Pini, R. Structural Behavior of Highly Concentrated Hyaluronan. *Biomacromolecules* **2009**, *10*, 1516−1522.
(40) Byrne, C. D.; de Mello, A. J.; Barnes, W. L. Variable-Angle Time-Resolved Evanescent Wave-Induced Fluorescence Spectroscopy (VATR-EWIFS): A Technique for Concentration Profiling Fluorophores at Dielectric Interfaces. *J. Phys. Chem. B* **1998**, *102*, 10326−10333.
(41) Liu, Z.; Shang, Y.; Feng, J.; Peng, C.; Liu, H.; Hu, Y. Effect of Hydrophilicity or Hydrophobicity of Polyelectrolyte on the Interaction between Polyelectrolyte and Surfactants: Molecular Dynamics Simulations. *J. Phys. Chem. B* **2012**, *116*, 5516−5526.
(42) Astafieva, I.; Zhong, X. F.; Eisenberg, A. Critical micellization phenomena in block polyelectrolyte solutions. *Macromolecules* **1993**, *26*, 7339−7352.
(43) Kononov, A. I.; Moroshkina, E. B.; Tkachenko, N. V.; Lemmetyinen, H. Photophysical Processes in the Complexes of DNA with Ethidium Bromide and Acridine Orange: A Femtosecond Study. *J. Phys. Chem. B* **2000**, *105*, 535−541.

Colloid Polym Sci (2008) 286:1681–1685
DOI 10.1007/s00396-008-1941-8

SHORT COMMUNICATION

Aggregation behavior of novel hyaluronan derivatives—a fluorescence probe study

Filip Mravec · Miloslav Pekař · Vladimír Velebný

Received: 17 June 2008 / Revised: 15 September 2008 / Accepted: 30 September 2008 / Published online: 22 October 2008

Abstract Aggregation properties of hydrophobized hyaluronan with different molecular weights and degrees of substitution were studied using pyrene and perylene as fluorescence probes. Both probes in contrast to native biopolymer confirmed aggregation of modified hyaluronan. The critical aggregation concentration (cac) was determined by the pyrene I_1/I_3 and perylene fluorescence intensity method. The cac value varied both with the molecular weight and the degree of substitution and was between 0.610 and 0.003 $g \cdot L^{-1}$. Pyrene polarity scale confirmed formation of hydrophobic domains.

Keywords Hyaluronate derivatives · Fluorescence probes · Critical aggregation concentration · Core hydrophobicity

Introduction

Polysaccharides and their derivatives have become major components in the development of biocompatible and biodegradable materials with many areas of applications (e.g., tissue engineering, drug delivery). Chemical modification, which does not affect the biodegradability and does not suppress biological activity, can lead to further expansion of medicine and engineering applications [1, 2].

Hyaluronan (HA) is a major component of pericellular and extracellular matrices [3]. It is a linear polymer formed by repeating disaccharide units composed of the disaccharide unit formed by D-glucuronic acid-1-β-3-*N*-acetylglukosamine. It plays an important role in stabilizing the extracellular matrix in many tissues by binding to specific proteins called hyaladherines. The main hyaluronan fraction is localized in the skin tissue [4].

Synthesis of hyaluronan derivatives is generally based on the esterification on the D-glucuronic subunit [5]. Recently, preparation of new type derivatives that are subject of this study was reported [6]. Modification was made on the secondary hydroxyls of the glucuronic subunit. This way of modification leaves all carboxylic groups free in contrast to common derivatives prepared via esterification on the COOH group and enables to achieve high substitution degrees while maintaining polyelectrolytic character. Amphiphilic hyaluronan polyelectrolyte is thus obtained (hydrophobized hyaluronan, hHA), which is supposed to be still water-soluble and to aggregate in aqueous solution forming micelle-like structures with a non-polar core that will be able to entrap hydrophobic species, e.g., drugs.

In this work, first results on studying their aggregation capabilities are reported. Aggregation behavior of amphiphiles can be studied by non-polar fluorescence probes, which can be solubilized into this core. Fluorescence probe techniques have been used successfully in the study of a wide range of surfactants [7–9]. They are able to determine not only the critical micellar or aggregation concentration (cac) but also the polarity index of probe's microenvironment [10–12] and effective viscosity of the micellar core [13, 14].

F. Mravec (✉) · M. Pekař
Institute of Physical and Applied Chemistry,
Faculty of Chemistry, Brno University of Technology,
Purkyňova 118,
612 00 Brno, Czech Republic
e-mail: filip.mravec@centrum.cz
URL: www.hyaluronan.cz

F. Mravec · V. Velebný
CPN spol. s.r.o.,
Dolní Dobrouč 401,
561 02 Dolní Dobrouč, Czech Republic

Pyrene I_1/I_3 ratio method is a widely used method to determine the cac value for many surfactant-based systems. Its unique response to the microenvironment polarity is well known and described [15]. In this method, the ratio of the fluorescence intensity at 373 nm (I_1) and at 383 nm (I_3) is plotted against the logarithm of the aggregating molecule concentration. Below the cac, the pyrene I_1/I_3 ratio does not change in a wide range of concentration. Near the cac value, this ratio sharply decreases with increasing concentration up to a final, nearly constant, value.

To confirm the results obtained with pyrene, we used also the perylene fluorescence method [16]. Using different probes in aggregation studies is not common. Perylene is non-fluorescent in aqueous environment. Fluorescence intensity of the perylene increases with the number of non-polar domains formed in the solution. No fluorescence is observed until these domains are present in solution. When the domains are formed, a sharp increase in the fluorescence is observed. Straight lines can fit these two trends and the concentration-coordinate of their point of intersection define the cac value directly.

Materials and methods

Sodium hyaluronate and its alkyl derivatives (Fig. 1) were obtained from CPN (Dolní Dobrouč, Czech Republic). Details on the synthesis of derivatives and their molecular characteristics have been published elsewhere [6]. Hyaluronans were of the following weight-average molecular weights: 97, 560, and 1,630 kg·mol^{-1}.

Derivatives were of the weight-average molecular weights of 44, 134, 183, 360, and 1,470 kg·mol^{-1}, and their substitution degrees were in the range of 10–70%. Substitution degree is defined as the ratio of the mole of substituents per mole of the disaccharide unit [6], e.g., SD 100% means one alkyl chain per each disaccharide unit in the hyaluronate chain. Molecular weights were determined by size-exclusion chromatography/multi-angle laser light scattering and the substitution degree is defined from the ^{1}H NMR spectra (for details, see [6]). All the molecular parameters were determined and provided by the producer. The hyaluronate samples were dissolved in doubly distilled water to the concentration 2 g·L^{-1}. This stock solution was stabilized by addition of sodium azide (p.a., Lachema) in final concentration 10^{-3} mol·L^{-1}. The alkyl-type abbreviation comes as the first followed by the original molecular weight (before the derivatization) and the substitution degree. For example, D 134/10 means C_{10}-derivate of the molecular weight 134 kg·mol^{-1} and with the substitution degree 10%.

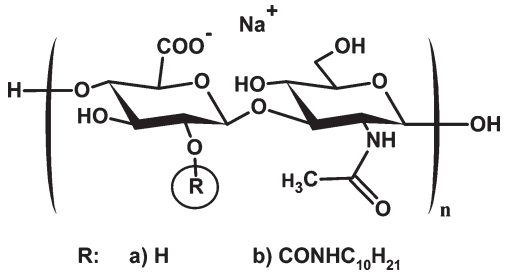

Fig. 1 Schematic structure of the sodium hyaluronate (**a**) and its C_{10} alkyl derivative

Sodium dodecylsulfate (p.a., Lachema) was dissolved in water to obtain concentration of 2×10^{-2} mol·L^{-1}.

Pyrene and perylene (fluorescence grade) were obtained from Fluka, acetone p.a. from Lachema.

The hyaluronate samples were listed in correspondence to their characteristics. Stock solutions of pyrene and perylene were prepared in acetone in final concentration 10^{-4} mol·L^{-1}. Probe stock solution was introduced into a vial and acetone was evaporated. The concentration of both probes in final samples was set to 5×10^{-6} mol·L^{-1}. The stock solution of HA or hHA was introduced into the vial with the probe, diluted to the desired concentration, and the resulting solution was sonicated for 4 h and stored during next 20 h. The fluorescence emission spectra were monitored with a luminescence spectrophotometer (AMINCO-Bowman, Series 2) at 293.15±0.1 K. The excitation and emission slit widths were set to 4 nm, and the excitation wavelength was 335 and 408 nm for pyrene and perylene, respectively.

The experimental data, i.e., the pyrene I_1/I_3 ratio (y) dependency on concentration (x), were evaluated using nonlinear fitting with Boltzman's curve containing four parameters—the maximum (a), the minimum (b), the inflex point (x_0), and the width of the step change (Δx; Eq. 1).

$$y = \frac{a-b}{1+e^{\frac{(x-x_0)}{\Delta x}}} + b. \quad (1)$$

The data were fitted using the nonlinear curve fitting with Origin 75. The cac was obtained from the inflex point of the nonlinear fitting. This is denoted as the cac_1 point. Alternatively, we determined also the cac_2 point defined as (cf. Fig. 2)

$$cac_2 = x_0 + 2\Delta x. \quad (2)$$

Figure 2 shows the typical dependency of the I_1/I_3 on the logarithm of the concentration in a model surfactant system, sodium dodecyl sulfate, with two possible points, cac_1 and cac_2, which can determine the critical aggregation concentration. Its critical aggregation concentration, 8.2×10^{-3} mol·L^{-1} in aqueous solution at 293.15 K, via surface tension experiments was reported elsewhere [17]. Obtained

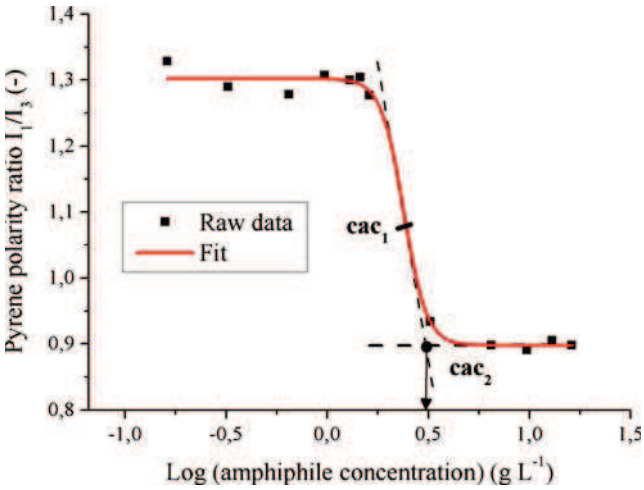

Fig. 2 Typical dependency of the pyrene polarity ratio on the concentration of an amphiphile (sodium dodecyl sulfate)

cac values from the fit are 8.3 and 10.2×10^{-3} mol·L^{-1} for cac_1 and cac_2, respectively. It is obvious that the cac_1 value is closer to surface tension value and it seems to be more relevant as cac point.

Perylene data evaluation was based on a fit of two linear trends. From equations of these straight lines, "*x*-coordinate" of the point of intersection was evaluated as the cac.

Results and discussion

Aggregation properties

First measurements were focused on possible aggregation behavior of native hyaluronan in aqueous solution. Three molecular weights (97, 560, and 1,630 kg·mol^{-1}) were selected to investigate possible aggregation of native hyaluronan using the pyrene fluorescence method. Figure 3 shows that the I_1/I_3 ratio, also called the polarity index, ranges from 1.37 to 1.45 through a wide concentration range. Value of the polarity index in this concentration range can be taken as constant and invariant. Therefore, from the hydrophobic polarity probe point of view, no aggregation behavior was observed in these solutions. Hydrophobic patches supposed to exist along HA chain [18] do not form domains able to solubilize non-polar substances like pyrene.

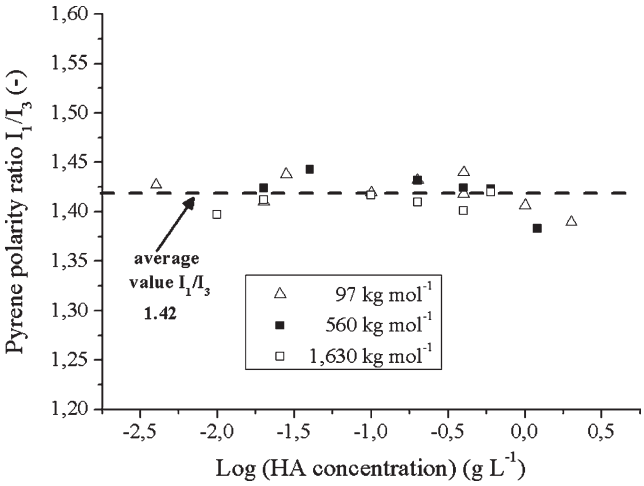

Fig. 3 Plot of the I_1/I_3 vs. log C_{HA} for native hyaluronan in aqueous solution of different molecular weights

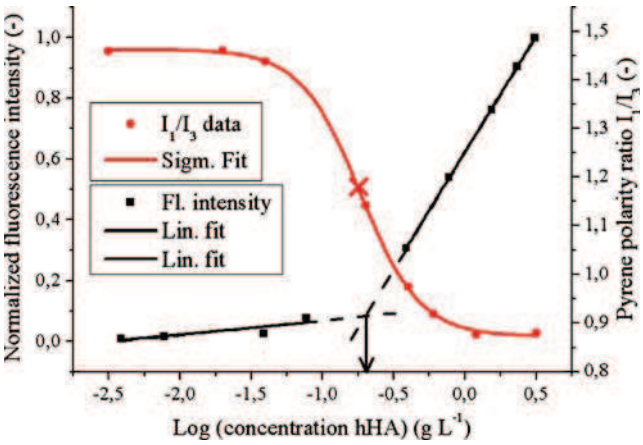

Fig. 4 Plot of the normalized integral fluorescence (I_F) and the I_1/I_3 vs. the log C_{HA} for the D134/30 sample. The perylene data are fitted with two lines. The pyrene data are fitted by sigmoid curve with marked cac_1 (*X*). The point of intersection (*down arrow*) from perylene dependence (*x*-coordinate value=−0.747, which is equal to 0.179 g·L^{-1}) is identical with the pyrene cac_1 point (*x*-coordinate value=−0.750, which is equal to 0.178 g·L^{-1})

On the contrary, hyaluronate derivatives manifested clear aggregation behavior. Example of results obtained for D134/10 is presented in Fig. 4. As explained above, there are two possible cac points on the concentration dependency of the pyrene I_1/I_3 ratio. Aguiar et al. [15] suggested a condition to select the cac value from the pyrene I_1/I_3 ratio. If the $x_0/\Delta x$ (cf. Eq. 1) is less than 10, the cac point is determined by the *x*-coordinate of the inflex point x_0—cac_1 in our case. Table 1 examples determined values of the $x_0/\Delta x$ ratio of hyaluronate derivatives. All of them passed the "less than 10 condition".

Table 1 The representative samples of hydrophobized hyaluronan with the x_0, Δx, and criterion value obtained from curve fitting

Samples	x_0 (g·L^{-1})	Δx (g·L^{-1})	$x_0/\Delta x$	R^2
D44/10	0.54	1.42	0.38	0.99
D134/10	0.61	1.51	0.40	0.99
D183/30	0.15	1.55	0.10	0.98
D360/50	0.08	1.48	0.05	0.98
D1470/70	0.20	1.03	0.19	0.97

Table 2 Overview of the cac values for hHA samples from pyrene and perylene, in brackets, experiments

	M_W (kg·mol^{-1})	SD (%)			
		10	30	50	70
cac (g·L^{-1})	44	0.540 (0.520)	0.045 (0.050)	0.003 (0.003)	ND (ND)
	134	0.610 (0.600)	0.179 (0.180)	0.130 (0.140)	0.030 (0.025)
	183	0.190 (0.210)	0.150 (0.170)	0.110 (ND)	ND (ND)
	360	0.190 (0.200)	0.080 (ND)	0.110 (0.140)	ND (ND)
	1,470	ND (ND)	0.260 (0.280)	0.110 (0.130)	0.200 (0.160)

ND not determined

Perylene results confirmed the selection of cac_1 as the proper critical concentration. In Fig. 4, the integral perylene fluorescence intensity is plotted against the logarithm of hyaluronate concentration. The perylene data, resolved by two straight lines, lead to the cac value 0.179 g·L^{-1}, which corresponds to the cac_1 value determined by the pyrene method (0.178 g·L^{-1}). Accordingly, we used cac_1 for the evaluation of the pyrene data.

The cac values of various derivatives decrease when the substitution degree increases, with a small exception for samples D 1470 (Table 2). At constant substitution degree, there is no clear trend of cac change with molecular weight (Table 2). The greatest decrease of cac values with increasing substitution degree was observed for samples D 44. These samples have the shortest biopolymer chain. Aggregation is driven by hydrophobic interactions introduced by the alkylation of native hyaluronan backbone. Formation of aggregates is accompanied by reorientation of hyaluronan chains and also by changing its conformation. Short chains can be reoriented and deformed more easily than long ones; therefore, their cac values are more sensitive to the degree of substitution. But not only cac values are decisive for the final selection of the derivative, which can be used in future for an application in drug delivery system.

In comparison of cac values with another alkyl-derivative of HA [19], pyrene as the cac probe was used and the cac value was realized as the first decreasing of the pyrene polarity index dependency on the derivative concentration, our derivatives with high SD or MW have the same or lower cac values. Similarly, in the same orders of magnitude, range cac values of the alkyl-chitosan [20, 21], cholesteryl-chitosan derivatives [22], or heparin-deoxycholic acid derivative [23], where decreasing tendency of the cac on increasing SD, were observed.

Domain hydrophobicity

As the base for determination of the hydrophobicity of the non-polar core, the pyrene polarity scale (PPS) was selected [24]. The limiting values of the I_1/I_3 ratio from the concentration dependencies are shown in Table 3. Data indicate a general trend of increasing hydrophobicity (decreasing pyrene polarity parameter) with increase in the substitution degree, which is easily understandable and expectable. Closer inspection of data obtained for samples of the same molecular weight of the native hyaluronan does not always reveal simple trend (Table 3). This can indicate different distribution of alkyl substituents along the polysaccharide backbone of varying substitution degree, non-uniform alkyl distribution on highly substituted hyaluronan, and also different changes in conformational behavior of chains of various molecular weights modified by alkyls to different degrees.

Conclusion

The novel hyaluronan derivatives show surfactant-like aggregation behavior in aqueous solutions. Their critical aggregation concentrations can be modified by the molecular weight and substitution degree and ranges between 0.610 and 0.003 g·L^{-1}. Hydrophobic domains are formed with the relative hydrophobic index (PPS) nearby 0.85. This value is comparable to that of simple surfactants. Novel hyaluronate hydrophobized derivatives with preserved free carboxyl groups are thus potential candidates for preparing systems for targeted delivery of hydrophobic active substances.

Table 3 Overview of the hydrophobicity indexes for hHA samples

	M_W (kg·mol^{-1})	SD (%)			
		10	30	50	70
Pyrene polarity parameter	44	0.96	0.83	0.89	–
	134	0.88	0.86	0.79	0.82
	183	0.89	0.80	0.82	–
	360	0.96	0.83	0.8	–
	1,470	–	0.84	0.81	0.81

Acknowledgment We thank CPN Ltd Dolní Dobrouč (Czech Republic) for material and financial support. The research was supported also by the Ministry of Education of the Czech Republic, project. no. MSM 00216305001.

References

1. Luo Y, Prestwich GD (2001) Hyaluronic acid-*N*-hydroxysuccinimide: a useful intermediate for bioconjugation. Bioconjugate Chem 12:1085–1088
2. Ghosh K, Shu XZ, Mou R, Lombardi J et al (2005) Rheological characterization of in situ cross-linkable hyaluronan hydrogels. Biomacromolecules 6:2857–2865
3. Lapčík L Jr, Lapčík L, De Smedt S, Demeester K (1998) Hyaluronan: preparation, structure, properties, and applications. Chem Rev 98:2663–2684
4. Tammi R, Tammi M (1998) Hyaluronan in the epidermis. Available via DIALOG. http://glycoforum.gr.jp/science/hyaluronan/HA04/HA04E.html. Accessed 10 Apr 2008
5. Bulpitt P, Aeschlimann DJ (1999) New strategy for chemical modification of hyaluronic acid: preparation of functionalized derivatives and their use in the formation of novel biocompatible hydrogels. Biomed Mater Res 47:152–169
6. Mlčochová P, Bystrický S, Steiner B et al (2006) Synthesis and characterization of new biodegradable hyaluronan alkyl derivatives. Biopolymers 82:74–79
7. Kalyanasundaram K, Thomas JK (1977) Environmental effects on vibronic band intensities in pyrene monomer fluorescence and their application in studies of micellar systems. J Am Chem Soc 99:2039–2044
8. Glushko V, Thaler MSR, Karp DC (1981) Pyrene fluorescence fine structure as a polarity probe of hydrophobic regions: behavior in model solvents. Arch Biochem Biophys 210:33–42
9. Lianos P, Zana RJ (1981) Fluorescence probe studies of the effect of concentration on the state of aggregation of surfactants in aqueous solution. Colloid Interface Sci 84:100–107
10. Offen HW, Turley WD (1982) Pyrene fluorescence spectra in micelles at high pressures. J Phys Chem 86:3501–3503
11. Ruiz CC, Sánchez FG (1994) Effect of urea on aggregation behavior of triton X-100 micellar solutions: a photophysical study. J Colloid Interface Sci 165:110–115
12. Molina-Bolívar JA, Aguiar J, Peula-García JM, Ruiz CC (2004) Surface activity, micelle formation, and growth of *n*-octyl-*β*-D-thioglucopyranoside in aqueous solutions at different temperatures. J Phys Chem B 108:12813–12820
13. Ruiz CC (2000) Fluorescence anisotropy of probes solubilized in micelles of tetradecyltrymethylammonium bromide: effect of ethylene glycol added. J Colloid Interface Sci 221:262–267
14. Crosas E, Egea MA, Reig FJ (2006) Spectroscopic techniques applied to the study of laminin fragments inserted into model membranes. Colloid Interface Sci 295:264–269
15. Aguiar J, Carpena P, Molina-Bolívar JA, Ruiz CC (2003) On the determination of the critical micelle concentration by the pyrene 1:3 ratio method. J Colloid Interface Sci 258:116–122
16. Mast RC, Haynes LV (1975) The use of the fluorescent probes perylene and magnesium 8-anilinonaphthalene-1-sulfonate to determine the critical micelle concentration of surfactants in aqueous solution. J Colloid Interface Sci 53:35–41
17. Elworthy PH, Mysels KJ (1966) The surface tension of sodium dodecylsulfate solutions and the phase separation model of micelle formation. J Colloid Sci 21:331–347
18. Scott JE, Heatley F (2002) Biological properties of hyaluronan in aqueous solution are controlled and sequestered by reversible tertiary structures, defined by NMR spectroscopy. Biomacromolecules 3:547–553
19. Creuzet C, Kadi S, Rinaudo M, Auzély-Velty R (2006) New associative systems based on alkylated hyaluronic acid. Synthesis and aqueous solution properties. Polymer 47:2706–2713
20. Liu W, Sun SJ, Zhang X, De Yao K (2003) Self-aggregation bahavior of alkylated chitosans and its effect on the release of a hydrophobic drug. J Biomater Sci Polym Edn 14:851–859
21. Philippova OE, Volkov EV, Sitnikova NL, Khokhlov AR, Desbrieres J, Rinaudo M (2001) Two types of hydrophobic aggregates in aqueous solution of chitosan and its hydrophobic derivative. Biomacromolecules 2:483–490
22. Yingsong W, Lingrong L, Jian W, Zhang Q (2007) Preparation and characterization of self-aggregated nanoparticles of cholesterol-modified *O*-carboxylmethyl chitosan conjugates. Carbohydr Polym 69:597–606
23. Park K, Kim K, Kwon IC, Kim SK, Lee S, Lee DY, Byun Y (2004) Preparation and characterization of self-assembled nanoparticles of heparin-deoxycholic acid conjugates. Langmuir 20:11726–11731
24. Dong DC, Winnik F (1985) The Py scale of solvent polarities. Can J Chem 62:2560–2566

Colloids and Surfaces A: Physicochem. Eng. Aspects 460 (2014) 204–208

Contents lists available at ScienceDirect

Colloids and Surfaces A: Physicochemical and Engineering Aspects

journal homepage: www.elsevier.com/locate/colsurfa

Effect of CTAB and CTAB in the presence of hyaluronan on selected human cell types

Marie Kalbáčová[a,b], Martina Verdánová[a,c], Filip Mravec[d], Tereza Halasová[d], Miloslav Pekař[d,*]

[a] Institute of Metabolic Disorders, 1st Faculty of Medicine, Charles University in Prague, Ke Karlovu 2, Prague 2, 128 08, Czech Republic
[b] Biomedical Centre, Faculty of Medicine in Plzen, Charles University in Prague, Husova 3, Plzen, 306 05, Czech Republic
[c] Department of Genetics and Microbiology, Faculty of Science, Charles University in Prague, Albertov 6, Prague 2, 128 43, Czech Republic
[d] Materials Research Centre, Faculty of Chemistry, Brno University of Technology, Purkyňova 118, Brno, 612 00, Czech Republic

HIGHLIGHTS

- CTAB is toxic for osteoblasts and keratinocytes.
- Hyaluronan can suppress the negative effect of the surfactant.
- The protective effect was observed only at low surfactant concentration.
- Fetal bovine serum participated in the hyaluronan protective effect.

GRAPHICAL ABSTRACT

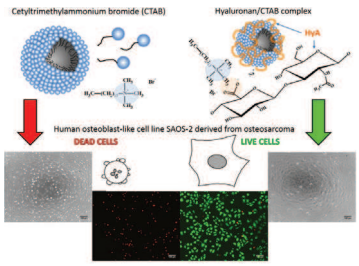

ARTICLE INFO

Article history:
Received 25 October 2013
Received in revised form
13 December 2013
Accepted 22 December 2013
Available online 3 January 2014

Keywords:
Cetyltrimethylammonium bromide
Cytoprotection
Cytotoxicity
Hyaluronan
Keratinocyte
Osteoblast

ABSTRACT

The effect of different concentrations of CTAB (in the range of 0.2 mM^{-2} mM, i.e., including its critical micelle concentration) on viability of selected human cells (osteoblasts and keratinocytes) was studied by a variety of methods (immunocytochemical and biochemical), testing the cell viability and the metabolism, to get a complex overview. All of the used methods confirmed the cytotoxic effect of CTAB, which could, however, be suppressed by the presence of hyaluronan (molecular weight 806 kDa, in the concentration of 1 g/l) in the case of the lowest CTAB concentration used (0.2 mM) when the fetal bovine serum was also present in the cultivation medium. Thus, it could be concluded that hyaluronan can be used as successful protector of specific cell types against cytotoxic CTAB at low concentrations.

1. Introduction

Surfactants are indispensable components of many traditional products in almost every chemical industry, e.g., cosmetics, paints, dyestuffs, pharmaceuticals, agrochemicals, fibres, or plastics. Nowadays they also play a role in modern systems designed within the area of nanotechnology, particularly in the development of delivery systems for various biologically active compounds like drugs, antioxidants, nutrients, or agents for gene therapy [1,2]. Biological aspects of surfactants are vital issues in all their applications. Often a biocidal effect of surfactant is faced which is the result of the surfactant action on the cell membrane or on the microorganism surface. This effect is favored by high surface activity and high surfactant unimer concentration [3]. The biological effects of surfactants can be roughly classified with respect to their

* Corresponding author. Tel.: +420 541149330; fax: +420 541149398.
E-mail address: pekar@fch.vutbr.cz (M. Pekař).

0927-7757/$ – see front matter © 2014 Elsevier B.V. All rights reserved.
http://dx.doi.org/10.1016/j.colsurfa.2013.12.048

basic types. For example, the zwitterionic or non-ionic surfactants are usually less skin irritant than the anionic types [3,4]. Many surfaces, including the cell membranes, are negatively charged. The cationic surfactants thus have a high tendency to adsorb on these surfaces. The cell membrane can be subsequently damaged by the surface activity and the solubilization ability of attached surfactants. Most studies on the biological effects of surfactants were related to environmental (biodegradation and biodegradability, aquatic toxicity) or dermatological aspects [3,4]. This work is focused on cetyl trimethyl ammonium bromide (CTAB) which was also the subject of several studies on the surfactant effects on microorganisms or cells. CTAB was included in the study on effects of detergents on the proliferation and metabolism of human keratinocytes [5]. Both tested surfactants (CTAB and anionic sodium lauryl sulphate or SDS) showed the toxic effects on keratinocytes at the concentrations as low as 3 mg/g. However, both surfactants were found to activate keratinocytes at very low concentrations. Serum partially protected keratinocytes against the toxic and stimulatory activities of both surfactants. Inacio et al. [6] published an in vitro study on the effects of various surfactants on the viability of mammalian cell types typically encountered in vagina. All cationic surfactants (including CTAB) were toxic at the concentrations far below their critical micellar concentrations and showed significant differences in their toxicity toward polarized cells compared to non-polarized ones. Their toxicity was also dependent on the chemical nature of the polar head group. The authors concluded that cationic surfactants demonstrated an intracellular locus of action and that their structure-activity relationships could be profitably exploited for the prophylaxis in vaginal gel formulations. Hrenovic and Jankovic [7] reported high acute toxicity of both CTAB and SDS against Acinetobacter junii, a phosphate-accumulating bacterium. Liu et al. [8] studied the toxicosis of surfactants targeted to albumin isolated from bovine serum and the mechanism of detoxification. They found that whereas sodium dodecyl benzene sulphate (SDBS) induces the denaturalization of albumin, CTAB facilitates the refolding of this protein. Small quantity of CTAB was found to combine with preformed SDBS–BSA complex to form a three-component complex and with the cumulation of quantity, CTAB captured SDBS from the SDBS–BSA complex by the electrostatic attraction and the CTMAB-SDBS complex was formed, while liberating BSA.

CTAB could be used for the preparation of nano- or microcarriers, for example, after the complexation with oppositely charged polyelectrolyte, preferably selected from a family of biopolymers. Hyaluronic acid (usually in the sodium form; hyaluronan) is an excellent example of such bio-polyelectrolyte which is produced also in human body. Hyaluronan is naturally occurring polysaccharide with a very simple structure but unusual properties and a variety of functions [9]. It is a negatively charged monotonic co-polymer with repeating disaccharide unit composed of D-glucuronate and *N*-acetyl-D-glucosamine residues linked by β(1–4) and β(1–3) bonds, which are connected to unbranched chains. The biological or physiological functions of hyaluronan are mostly determined either by its physical and physico-chemical properties or by the interactions with hyaluronan-binding proteins. At physiological pH, the hyaluronan carboxyl groups are predominantly ionized, and hyaluronan behaves like a polyanion, which can interact or associate with cationic counterions to maintain the charge neutrality. Because it is an ubiquitous polysaccharidic component of tissues and body fluids, it does not confer immunological reactions and is metabolized in lysosomes of certain cells. Via the interaction with a variety of receptors, such as CD44, RHAMM (receptor for hyaluronan–mediated motility expressed protein), LYVE-1 (lymphatic vessel endothelial hyaluronan receptor-1, and HARE (hyaluronan receptor for endocytosis, stabillin-2), hyaluronan is capable of acting as a signalling molecule [10], triggering diverse signalling pathways, such as Ras, mitogen-activated protein (MAP) kinases, c-Src, PI3kinase/Akt, and is involved in the regulation of cell growth, differentiation, adhesion, and motility, thereby influencing the embryonic development, tumorigenesis, atherosclerosis, and lung and kidney injury [10–12].

The interactions between hyaluronan and cationic surfactants are well documented and the formation of complexes in different colloidal forms ranging from sols to gels was found [13–16]. Binding of surfactant to polymer may suppress its solubility, i.e., the presence in the solution either in monomeric or micellar form, which could result in suppressed availability for undesired interactions with cell membranes. Here we report on the results of a pilot study testing this hypothesis.

2. Materials and methods

2.1. Surfactant and biopolymer

Cetyl trimethyl ammonium bromide (CTAB; Sigma–Aldrich, USA) was used as cationic surfactant. Sodium hyaluronate (HyA; Contipro Group, Czech Republic) of the molecular weight of 806 kDa was used as anionic polyelectrolyte.

2.2. Cells and culture conditions

Human osteoblast-like cell line SAOS-2 derived from osteosarcoma was obtained from DSMZ, Germany (Deutsche Sammlung von Mikroorganismen und Zellkulturen, GmbH). SAOS-2 cells were cultured in McCoy's 5A medium without phenol red (PromoCell, Germany) supplemented with 15% heat inactivated fetal bovine serum (FBS; PAA, Austria), penicillin (20 U/ml, Sigma–Aldrich, USA) and streptomycin (20 μg/ml, Sigma–Aldrich, USA).

Spontaneously immortalized human keratinocyte cell line HaCaT was obtained as kind gift from Prof. Dr. N. Fusenig, Deutsches Krebsforschungszentrum, Heidelberg, Germany. HaCaT cells were grown in DMEM medium (Sigma–Aldrich, USA) supplemented with 10% heat inactivated FBS, 1% L-glutamine (Sigma–Aldrich, USA) and 0.1% gentamicin (Sigma–Aldrich, USA).

Both cell types were cultivated at 37 °C and in 5% CO_2 atmosphere.

2.3. Cell treatment with CTAB and HyA

Cells were collected in an exponential growth phase and counted using the Bürker chamber. These cells were plated (20,000 or 40,000 cells/cm^2) onto the 96-well plate in appropriate culture medium with FBS and incubated for 24 h under the tissue culture conditions.

After 24 h, cells were washed by PBS and different concentrations of CTAB and/or HyA were added to cells. CTAB and HyA were diluted in the culture medium with or without FBS.

2.4. Determination of metabolic activity

Metabolic activity test (Cell Titer 96 AQueous One Solution Cell Proliferation Assay, MTS, Promega, USA) was performed according to the standard protocol: the absorbance (490 and 655 nm as reference) of soluble formazan accomplished by metabolically active cellular dehydrogenases was determined in 96-well plate 24 h after the incubation of cells with CTAB and HyA. The results were normalized (in percentage) with respect to the control cells without the treatment.

2.5. Determination of live and dead cells

Viability/cytotoxicity test (LIVE/DEAD Viability/Cytotoxicity kit for mammalian cells, Life Technologies, USA) was performed

according to the standard protocol: stained cells (green - live cells with calcein and red - dead cells with Ehidium homodimer-1) were observed by the fluorescence microscope (Nikon Eclipse Ti-E). Subsequent image analysis (cell number of live and dead cells from five images from each sample) was performed using ImageJ, Cell Profiler (Broad Ins.) and NIS-Elements (Nikon) software. Live/Dead test was performed after 5 and 24 h of incubation of cells with CTAB and HyA.

2.6. Determination of cell index

SAOS-2 cells were plated (20,000 cells/cm^2) onto the 16-well E-plates with gold electrodes on the bottom (Roche, Switzerland) and incubated in xCELLigence RTCA DP device (Roche, Switzerland) at 37 °C and in 5% CO_2 atmosphere for 24 h. After that, cells were washed once with PBS and different concentrations of CTAB and HyA were added to cells. The cell indexes were measured during whole cultivation based on the change of impedance.

2.7. Statistical analysis

The results from MTS test and LIVE/DEAD kit were obtained from two independent experiments performed in 3 parallels. One way ANOVA was applied to analyze the data and the values were tested for statistically significant differences at $p < 0.01$. Extreme values were excluded from the analysis. The results from xCELLigence device were then obtained from one experiment performed in 2 parallels. The same ANOVA procedure was applied to obtained data. The statistical evaluation was performed using Microsoft Excel software.

3. Results and discussion

The experiments were realized in three series and in control: with the addition of surfactant, with the addition of hyaluronan and with the addition of both the surfactant and hyaluronan to cells; in the control experiments no such treatment was applied. CTAB was used at several concentrations–0.2, 0.4, 0.5, 1, and 2 mM. The concentration range was selected to cover the interval from below to above the CTAB aqueous critical micellar concentration (about 0.9 mM [17]) taking into account also the charge ratio–electrostatic interactions are expected between cationic CTAB and anionic hyaluronan and the charge ratio CTAB:hyaluronan should not exceed (preferably was lower than) one. Due to the ionic character of the cell media the micellization during the cell cultivation can be expected because the critical micellar concentration is decreased in about an order of magnitude at the physiological salt concentration [16]. Hyaluronan was applied at single concentration of 1 mg/ml which is a standard in the studies of hyaluronan-surfactant interactions [13–16] and corresponds to the concentration in tissues or synovial fluid [18,19].

The metabolic activity of human osteoblasts was measured after 24 h at different conditions (see Fig. 1). First, 20,000 and 40,000 cells/cm^2 were seeded for 24 h in fully supplemented medium and then CTAB of specific concentration or/and hyaluronan was added. After 24 h of incubation the metabolic activity was determined by MTS assay. Fig. 1 shows that the metabolic activity was reduced with increased concentration of surfactant and that starting from the surfactant concentration of 1 mM the metabolic activity was reduced completely in both samples with different cell concentrations. In case of the lowest concentration of surfactant (0.2 mM), more concentrated cells in the sample (40,000 cells/cm^2) can better overcome the negative effect of surfactant. Higher number of cells and their tighter connection positively affect their fight with toxic agents.

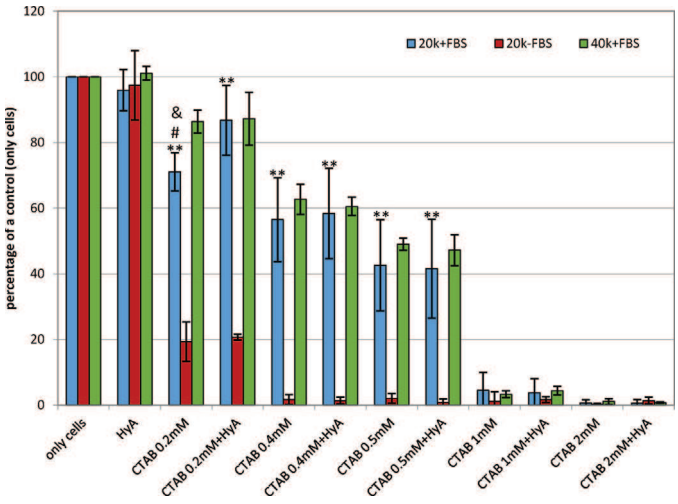

Fig. 1. Metabolic activity of human osteoblasts cultivated with CTAB and/or hyaluronan (HyA) for 24 h. Effect of different seeding concentrations, 20,000 (20k) and 40,000 (40k) cells/cm^2, and the presence (+) or absence (−) of FBS. Significant differences at $p < 0.01$ for 20k + FBS vs. 20k − FBS (**), for CTAB vs. CTAB and HyA (#), for 20k vs. 40k (&).

The fetal bovine serum is a mixture of different not well described proteins of multiple functions in the cultivation medium (mediation of cell adhesion, binding, and sequestration of ions, chaperones, growth factors, etc.). Its main component is a bovine serum albumin (50% of all proteins in FBS) which can bind different molecules (proteins, lipids, ions) and mediate their interactions. The treatment with the surfactant and HyA could be highly affected by the presence of FBS, thus the experiments were performed in the presence of FBS but also in the medium without FBS (at the concentration 20,000 cells/cm^2). Fig. 1 shows that even the lowest concentration of surfactant used (0.2 mM) has negative effect on the cell metabolism when FBS is not present and that from 0.4 mM surfactant cells do not respond at all. The addition of hyaluronic acid to the samples treated with surfactant had positive effect on the cell metabolic activity but only when the lowest concentration (0.2 mM) of surfactant was applied and in case when cells were in optimal conditions, i.e. FBS was present in the cultivation medium. This is in accordance with a certain protective effect of serum found in previous study on keratinocytes [5] which used the surfactants without the addition of hyaluronan. Cells in the cultivation medium without FBS were already stressed and the addition of surfactant abolished their metabolic activity dramatically. As expected, hyaluronan itself had no adverse effect.

Not only the cell metabolic activity but also the cell number shows that there is a positive effect of hyaluronan present in the sample with the lowest surfactant concentration (Fig. 2).

Since the surfactant together with hyaluronic acid could be applied on the skin, keratinocytes were also tested for their response to CTAB and its combination with hyaluronan. Human keratinocytes were incubated at the same concentrations of surfactant and HyA as osteoblasts for 24 h. Fig. 3 shows that as in previous experiments the surfactant causes the decrease in metabolic activity of cells and in case of keratinocytes it has even stronger negative effect. Just as in osteoblasts, HyA can suppress the negative effect of surfactant but again only in case of the lowest surfactant concentration (0.2 mM).

The proliferative activity of cells was determined using the xCELLigence system. Cells were plated on the 16-well plate and the same concentrations of surfactant and HyA as in previous experiments determining the metabolic activity were studied. Fig. 4 shows that cells treated with surfactant do not proliferate but stay intact. This inhibitory effect was most probably caused by the

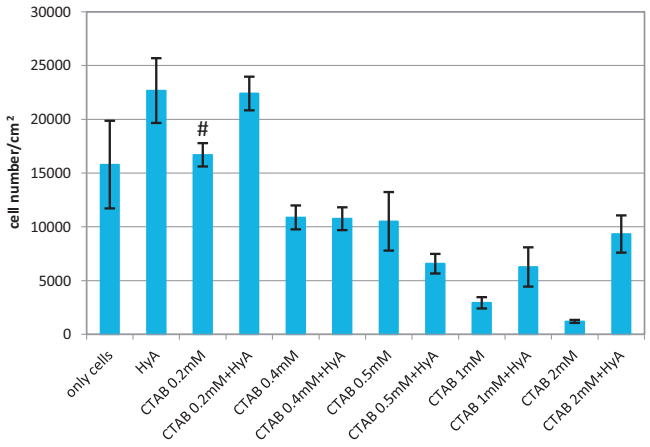

Fig. 2. Cell number of osteoblasts cultivated with CTAB and/or hyaluronan (HyA) in the presence of FBS for 24 h. Significant differences at $p < 0.01$ for CTAB vs. CTAB and HyA (#).

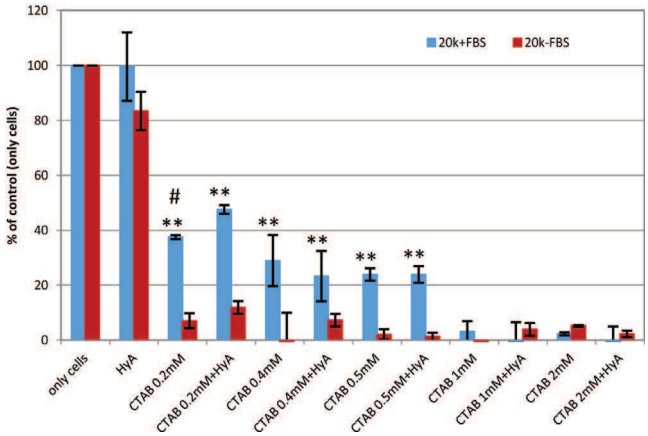

Fig. 3. Metabolic activity of human keratinocytes (20,000 cells/cm^2) cultivated with CTAB and/or hyaluronan (HyA) for 24 h. Effect of the presence (+) or absence (−) of FBS. Significant differences at $p < 0.01$ for 20k + FBS vs. 20k − FBS (**) and for CTAB vs. CTAB and HyA (#).

experimental setup; cells were monitored every 5 min during the first hour, which has a negative effect on cells at even the lowest surfactant concentration. However, the rescuing effect of HyA on the lowest concentration of surfactant is apparent even in this method.

The cell viability was determined by the fluorescent staining of intracellular active esterases and the cell death by the staining of cell DNA by intercalating fluorescent probe which enters the cells with interrupted membrane (live/dead assay). Fig. 5 shows that cells without surfactant treatment as well as cells treated with the lowest surfactant concentration did not die. Higher surfactant concentrations caused significant reduction in the cells viability and in case of the highest surfactant concentration (2 mM) all cells are apparently dead. This robust method did not discriminate between cells protected and not protected by hyaluronan as it was possible with more gentle and specialized methods for the metabolic activity determination.

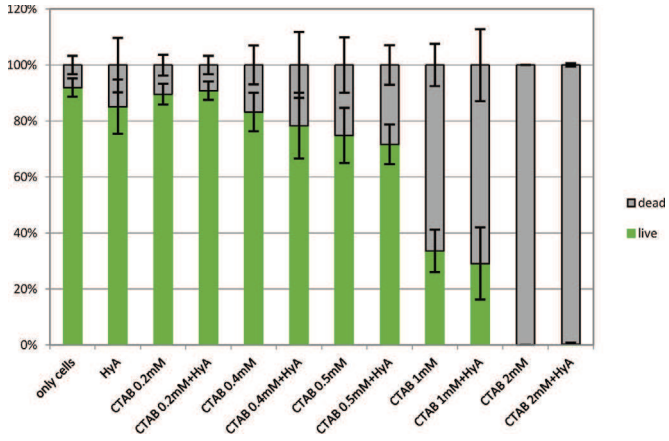

Fig. 5. Effect of CTAB and/or hyaluronan (HyA) on osteoblasts viability determined by live/dead assay after 24 h cultivation.

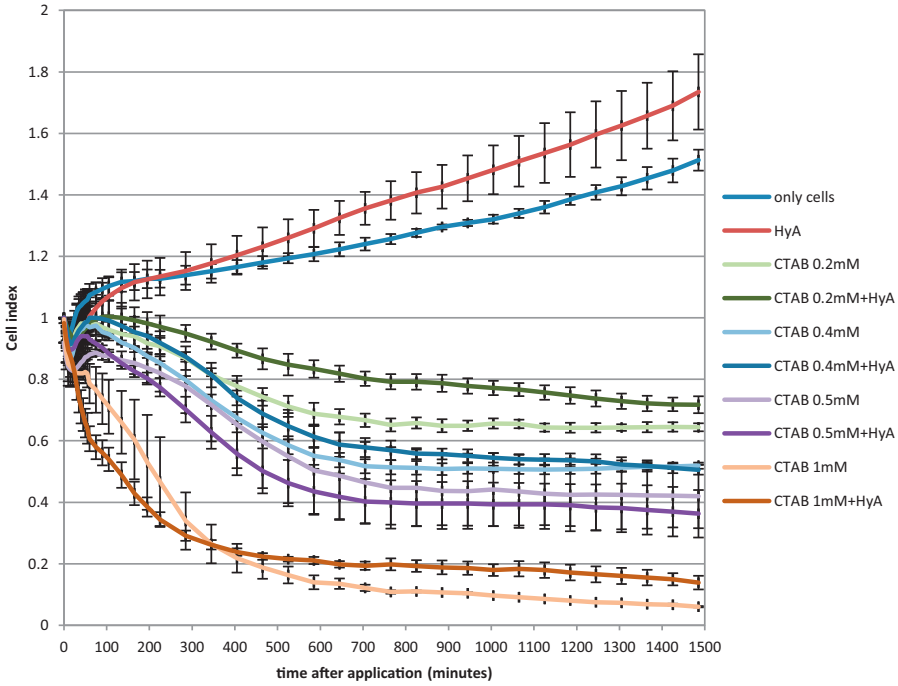

Fig. 4. Effect of CTAB and/or hyaluronan (HyA) on osteoblasts proliferation measured by xCELLigence system (16-well chamber).

The protective effect of hyaluronan described above was found for in about an order of magnitude lower surfactant concentration (0.2 mM) than that of the protecting hyaluronan unit (2.5 mM of hyaluronan basic dimer unit). This indicates that the surfactant molecules or micelles should be sufficiently wrapped within the hyaluronan chain to prevent cells from damage. On average, a chain of about 12 or 13 hyaluronan dimer units per one CTAB monomer is necessary to suppress the harmful surfactant effect. Because the protective effect was observed in the presence of the fetal bovine serum it is probable that also the serum proteins are included in the protection mechanism. Probably, a similar complex including the surfactant, hyaluronan, and proteins as that described by Liu et al. [8] was formed and responsible for the protection. The presence of hyaluronan can not only wrap the surfactant micelles and thus protect cells but can also stimulate them positively via the receptor-mediated pathway [10–12].

4. Conclusion

The adverse effect of CTAB on metabolic activity, proliferation, and viability of selected human cells (osteoblasts and keratinocytes) was found at all tested surfactant concentrations. The addition of hyaluronan suppressed the effect and protected cells only in the case of the lowest surfactant concentration used (0.2 mM) and under optimal culture conditions, i.e., when the fetal bovine serum was also present in the cultivation medium. This is indicative of the formation of some complexes among the surfactant, hyaluronan, and probably proteinaceous components of serum, similar to those reported in ref. [8].

Acknowledgements

This work was supported by the COST action CM1101, the project No. LD12068 (Ministry of Education, Czech Republic), Charles University in Prague, 1st Faculty of Medicine - project PRVOUK-P24/LF1/3and Faculty of Science - project GAUK no. 501212, grant (SVV-2013-267205 and by the project ED2.1.00/03.0076 from European Regional Development Fund (ERDF). Materials Research Centre at the Faculty of Chemistry, BUT is supported by the project No. CZ.1.05/2.1.00/01.0012 from ERDF.

References

[1] A.P.R. Johnston, G.K. Such, S.L. Ng, F. Caruso, Challenges facing colloidal delivery systems: from synthesis to the clinic, Curr. Opin. Colloid Interface Sci. 16 (2011) 171–181.
[2] B. Mishra, B.B. Patel, S. Tiwari, Colloidal nanocarriers: a review on formulation technology, types and applications toward targeted drug delivery, Nanomedicine: NBM 6 (2010) 9–24.
[3] K. Holmberg, B. Jönsson, B. Kronberg, B. Lindman, Surfactants and polymers in aqueous solution, Wiley, Chichester, 2007.
[4] T.F. Tadros, Applied Surfactants, Wiley-VCH, Weinheim, 2005.
[5] P.L. Bigliardi, M.J. Herron, R.D. Nelson, M.V. Dahl, Effects of detergents on proliferation and metabolism of human keratinocytes, Exp. Dermatol. 3 (1994) 89–94.
[6] A.S. Inacio, K.A. Mesquita, M. Baptista, J. Ramalho-Santos, W.L.C. Vaz, O.V. Vieira, In vitro surfactant structure-toxicity relationships: implications for surfactant use in sexually transmitted infection prophylaxis and contraception, PLoS One 6 (2011) e19850.
[7] J. Hrenovic, T. Ivankovic, Toxicity of anionic and cationic surfactant to Acinetobacter junii in pure culture, Cent. Eur. J. Biol. 2 (2007) 405–414.
[8] R. Liu, W. Zong, K. Jin, X. Lu, J. Zhu, L. Zhang, C. Gao, The toxicosis and detoxification of anionic/cationic surfactants targeted to bovine serum albumin, Spectrochim. Acta Part A 70 (1) (2008) 198–200.
[9] P. Prehm, Hyaluronan, in: A. Steinbüchel, R.H. Marchessault (Eds.), Biopolymers for Medical and Pharmaceutical Applications, 2, Wiley-VCH, Weinheim, 2005, pp. 617–644.
[10] D. Jiang, J. Liang, P.W. Noble, Hyaluronan in tissue injury and repair, Annu. Rev. Cell Dev. Biol. 23 (2007) 435–461.
[11] N. Itano, Simple primary structure, complex turnover regulation and multiple roles of hyaluronan, J. Biochem. 144 (2008) 131–137.
[12] T.N. Wight, Arterial remodeling in vascular disease: a key role for hyaluronan and versican, Front Biosci. 13 (2008) 4933–4937.
[13] K. Thalberg, B. Lindman, Interaction between hyaluronan and cationic surfactants, J. Phys. Chem. 93 (1989) 1478–1483.
[14] K. Thalberg, B. Lindman, G. Karlström, Phase behavior of systems of cationic surfactant and anionic polyelectrolyte: influence of surfactant chain length and polyelectrolyte molecular weight, J. Phys. Chem. 95 (1991) 3370–3376.
[15] A. Herslöf, L.O. Sundelöf, K. Edsman, Interaction between polyelectrolyte and surfactant of opposite charge. Hydrodynamic effects in the sodium hyaluronate/tetradecyltrimethylammonium bromide/sodium chloride/water system, J. Phys. Chem. 96 (1992) 2345–2348.
[16] T. Halasová, J. Krouská, F. Mravec, M. Pekař, Hyaluronan-surfactant interactions in physiological solution studied by tensiometry and fluorescence probe techniques, Colloids Surf., A 391 (2011) 25–31.
[17] P. Mukerjee, K.J. Mysels, Critical Micelle Concentrations of Aqueous Surfactant Systems, NBS, Washington, 1971.
[18] W.D. Comper, T.C. Laurent, Physiological function of connective tissue polysaccharides, Physiol. Rev. 58 (1978) 255–303.
[19] E.J. Oh, K. Park, K.S. Kim, J. Kim, J.A. Yang, J.H. Kong, M.Y. Lee, A.S. Hoffman, S.K. Hahn, Target specific and long-acting delivery of protein, peptide, and nucleotide therapeutics using hyaluronic acid derivatives, J. Controlled Release 141 (2010) 2–12.

Colloids and Surfaces A: Physicochem. Eng. Aspects 483 (2015) 155–161

Contents lists available at ScienceDirect

Colloids and Surfaces A: Physicochemical and Engineering Aspects

journal homepage: www.elsevier.com/locate/colsurfa

Hyaluronic acid as a modulator of the cytotoxic effects of cationic surfactants

Pavla Sauerová[a], Martina Verdánová[b,c], Filip Mravec[d], Tereza Pilgrová[d], Tereza Venerová[d], Marie Hubálek Kalbáčová[a,c,e], Miloslav Pekař[d,*]

[a] Biomedical Centre, Faculty of Medicine in Pilsen, Charles University in Prague, alej Svobody 1655/76, Pilsen 323 00, Czech Republic
[b] Department of Genetics and Microbiology, Faculty of Science, Charles University in Prague, Albertov 6, Prague 2 128 43, Czech Republic
[c] Institute of Inherited Metabolic Disorders, 1st Faculty of Medicine, Charles University in Prague, Ke Karlovu 2, Prague 2 128 08, Czech Republic
[d] Materials Research Centre, Faculty of Chemistry, Brno University of Technology, Purkyňova 464/118, Brno 612 00, Czech Republic
[e] Department of Histology and Embryology, Faculty of Medicine in Pilsen, Charles University in Prague, Karlovarská 48, Pilsen 301 66, Czech Republic

HIGHLIGHTS

- Surfactants (CTAB and Septonex) are toxic for osteoblasts.
- When complexed with hyaluronan their cytotoxicity is suppressed.
- Fetal bovine serum plays a positive role in the cytotoxicity suppression.

GRAPHICAL ABSTRACT

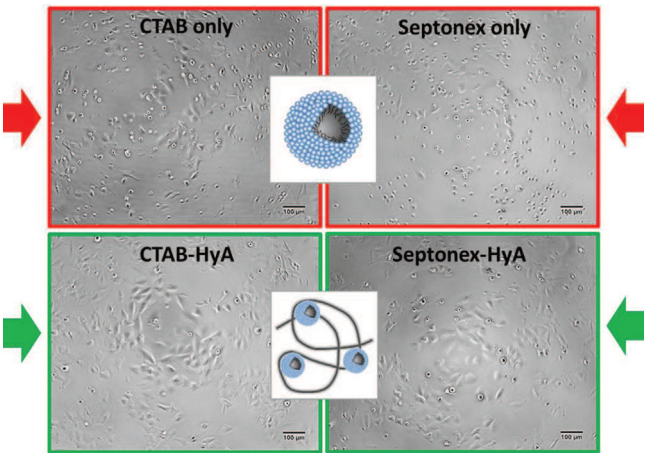

ARTICLE INFO

Article history:
Received 18 May 2015
Accepted 29 June 2015
Available online 17 July 2015

Keywords:
Cytotoxicity
Cell metabolic activity
Human osteoblasts
Hyaluronan
Surfactant
CTAB
Septonex

ABSTRACT

CTAB (cetyltrimethylammonium bromide) and Septonex (carbethoxypendecinium bromide) are cationic surfactants known for harmful effects on different cell types (bacteria, fungi, mammal cells, etc.). Colloidal complexes of CTAB or Septonex with oppositely charged hyaluronic acid (HyA), based primarily on electrostatic interactions, were prepared with the aim to test potential modulation of surfactants cytotoxic effects. Complexes were tested for their cytotoxicity on human osteoblasts—the cell metabolic activity was determined after 24 h of treatment. Our data show that CTAB–HyA or Septonex–HyA complexes reduce (in different rate according to the used surfactant and HyA concentrations) cytotoxicity of both surfactants in all tested concentrations. In addition, a significant role of fetal bovine serum (important supplement of cell culture medium) in cell recovery under the stress conditions like CTAB or Septonex presence was observed. Taken together, HyA could be a useful modulator of CTAB or Septonex effects on cells at diverse levels. Drug or nucleic acid delivery system, diagnostic dye carriers or cosmetic industry are the possible applications of prepared complexes.

* Corresponding author.
E-mail address: pekar@fch.vutbr.cz (M. Pekař).

http://dx.doi.org/10.1016/j.colsurfa.2015.06.058
0927-7757/

1. Introduction

Cationic surfactants are known for their cytotoxic properties [1–4] but due to their interactions with negatively charged substances – some kinds of drugs, nucleic acids, cellular surfaces, etc. – they can serve as an interesting tool in drug or gene cell delivery, for the study of cell trafficking processes, or in other cell structure visualisation techniques. The ability to form micelles is another positive property of surfactants and a benefit which is used in drug carriers [5]. Cetyltrimethylammonium bromide (CTAB), in particular, is commonly used as a compound in drug delivery systems; for example, it is an ideal "shape-inducing" agent [6]. In general, it is known that cationic surfactants exhibit the highest cytotoxicity in comparison to anionic and non-ionic ones [7]. In spite of this, several studies have shown the anticancer effect of CTAB or other molecules containing the quaternary ammonium group [8–11]. Additionally, it was showed that these surfactants can behave as cytotoxic agents in dependence on the target cell type – surfactants were substantially cytotoxic to non-polarized cells in contrast to polarized cells [12]. Interestingly, it was shown that CTAB cytotoxicity can be depressed by polymers: Alkilany et al. reduced the CTAB-induced cytotoxicity of a CTAB-capped nanorods solution by PAA (polyacrylic acid) polymer over-coating [13].

The ideal polymer for our study, aimed at surfactant cytotoxicity modulation by forming complexes with oppositely charged biopolymer, appeared to be hyaluronan (HyA), because in our previous study, the reduction of the cytotoxic effects of CTAB on specific cell types in the presence of free sodium hyaluronate (HyA) was described [14]. Hyaluronan is a naturally occurring glycosaminoglycan composed of repeating β-1,4-D-glucuronic acid and β-1,3-*N*-acetyl-D-glucosamine disaccharide subunits [15]. HyA exhibits a wide spectrum of functions at various organism levels [16] and due to its favourable properties – biocompatibility, biodegradability, unique biomechanical features, and modifiability (functional groups) – HyA is called a biomaterial of the near future. Many HyA functions are conditioned by interactions with HyA-binding proteins, which are specific to the place of concrete HyA action [17–20].

As mentioned above, surfactants cytotoxicity could be regulated when complexed with hyaluronan. However, HyA in these complexes can play more roles, not only cell protecting but also it can also help the complex to bind onto the cell surface (via its receptors) and subsequently to move within the cell. Thus, the surfactant-HyA complex can serve as a carrier of non-polar drugs solubilized within the cores of surfactant micelles. HyA is degraded by hyaluronidases (Hyals), especially Hyal1 and Hyal2. Extracellular HyA is attached to Hyal2 anchored in the cell membrane and then cleaved [21]. It seems that this process is in cooperation with the HyA receptor CD44. HyA is then transferred into the cell by endocytosis. In lysosomal vesicles, HyA is cleaved again, but by HyAl1 and then by exoglycosidases into monomers [16,22,23]. This pathway alone could be a way for the delivery of complexes to cells. The effects of HyA on cells have been well described, mostly thanks to its wide medical applications and the needs of regenerative medicine [24–31].

In this work, CTAB–HyA and Septonex–HyA complexes were prepared and their cytotoxicity was determined in comparison to native surfactants. In contrast to the previous study [14], in which the surfactant and hyaluronan were added to cells separately one at a time, the pre-prepared surfactant–HyA complexes were applied on cells. Further, Septonex, a structural analogue of CTAB, was also investigated. In addition, we were interested in the role of fetal bovine serum (FBS) in the ability of cells to overcome stress conditions (i.e. the presence of native surfactants or surfactants–HyA complexes). FBS (the blood fraction after clotting, free of blood cell elements) is a crucial component of the cell growth medium because it provides supplements important for cell cultivation in vitro (for adhesion, division, survival etc.). However, the major compound of FBS, bovine serum albumin, is known to interact with various molecules (it provides a variety of binding sites for both hydrophobic and negatively charged hydrophilic moieties), and the behaviour of surfactants in complexes could be affected by this protein [33,34]. Moreover, it has already been demonstrated that cell behaviour and morphology can be substantially influenced by the presence or absence of FBS in general [14,35].

Surfactants with regulated cytotoxicity might play a role in drug, gene, or diagnostic dye carriers (thanks to the use of the natural HyA-transport system) and could exhibit only a moderate and controllable antiseptic activity (thanks to HyA's protective activity). The results could help to raise the profile of surfactant–HyA complexes with respect to their use in practical cell biology and clinical applications.

Table 1
Composition of hyaluronan–surfactant complexes and their zeta potential (values in parentheses represent the standard deviation).

CTAB (mM)	HyA (mg/l)	Zeta potential (mV)
0.04	5	−14(2)
0.05	5	−8(2)
0.05	30	−15(2)
0.05	50	−34(5)
0.08	30	−29(1)
0.08	50	−19(5)
0.10	30	−26(1)
0.10	50	−28(4)
Septonex (mM)	**HyA (g/l)**	**Zeta potential (mV)**
0.03	1	−70(1)
0.06	1	−72(2)
0.08	1	−68(3)

2. Materials and methods

2.1. Surfactants and hyaluronan

Cetyltrimethylammonium bromide (CTAB) was purchased from Sigma–Aldrich (Czech Republic) and carbethoxypendecinium bromide (Septonex) from GNB chem (Czech Republic), both used as received. Hyaluronan was purchased from Contipro Biotech (Czech Republic); two batches were acquired—one with a weight-average molecular weight of 1000 kDa was used in the preparation of complexes with CTAB, while the other with a weight-average molecular weight of 936 kDa was used in complexes with Septonex.

Solutions of complexes were prepared by mixing hyaluronan and surfactant stock solutions, prepared in deionized water, to obtain the desired final concentration. The surfactant solution was always added dropwise to the hyaluronan solution. In the case of CTAB–hyaluronan complexes, the hyaluronan concentration had to be sufficiently low in order to prevent precipitation and prepare homogeneous solutions of complexes. The concentrations of CTAB in complex solutions were 40, 50, 80 and 100 μM; three hyaluronan concentrations were tested: 5, 30 and 50 mg/l. In the case of Septonex–hyaluronan complexes, only one hyaluronan concentration was used (1 g/l) at three different surfactant concentrations: 30, 60 and 80 μM. Eleven different samples of complexes were thus prepared and used in experiments; their exact composition is given in Table 1.

The prepared complexes were characterized by their particle size distribution (measured by dynamic light scattering) and their zeta potential (measured by laser Doppler micro-electrophoresis) using a Zetasizer Nano ZS (Malvern Instruments, UK).

2.2. Cell culture

Human osteoblasts were used because they are a well-established and reproducible cell line suitable for this type of primary testing. The cells were incubated under different conditions for 24 h, when the treated cells were observed using light microscopy. This time period was found to be reasonable to obtain reproducible data and before all cells were destroyed in the presence of surfactants only. SAOS-2 cells (a human osteoblast-like cell line derived from osteosarcoma, obtained from Deutsche Sammlung von Mikroorganismen und Zellkulturen (GmbH) in Germany) were cultured at 37 °C in a 5% CO_2 atmosphere and in McCoy's 5A medium without phenol red (PromoCell, Germany) supplemented with 15% heat inactivated FBS (PAA, Austria), penicillin (20 U/ml, Sigma–Aldrich, USA) and streptomycin (20 μg/ml Sigma–Aldrich, USA).

2.3. Cell treatment with surfactant–HyA complexes

SAOS-2 cells were suspended using trypsin/EDTA and plated at a concentration of 20,000 cells/cm^2 onto a 96-well plate in the above mentioned culture medium and under the abovementioned conditions for 24 h. After 24 h, the cells were treated with complexes diluted 1:9 in fresh medium, with "only HyA", or with "only surfactant" with or without FBS. In the latter, after 4 h of incubation without FBS, FBS was added to a final concentration of 15% (non-standard conditions).

2.4. Light microscopy

Phase contrast images of the cells were obtained using an Eclipse Ti-S microscope (Nikon, Japan) and a DS-Qi1Mc DigitalCamera (Nikon). Images were acquired with a 10× lens and adjusted by ImageJ (Rasband, W.S., ImageJ, US National Institutes of Health, Bethesda, Maryland, USA, http://imagej.nih.gov/ij/, 1997–2015) and Cell Profiler (Broad Institute, USA) software. Fig. 1 shows typical examples of obtained images.

2.5. Measurement of cell metabolic activity

A metabolic activity test (Cell Titer 96 AQueous One Solution Cell Proliferation Assay, MTS, Promega, USA) was performed according to the standard protocol (the reduction of MTS reagent to a coloured formazan product was induced by viable cells). 24 h after the addition of surfactant, the absorbance was measured in a 96-well plate using a multi-detection micro-plate reader (Synergy™ 2, BioTek, USA). The measured results were expressed relative to the control ("only cells").

2.6. Statistical analysis

Results from MTS tests were obtained from two independent experiments performed in four parallels. Data were statistically analysed by the Wilcoxon rang test; the obtained values were tested for statistically significant differences at an alpha level of 0.05. The statistical evaluation was performed using Statistica (StatSoft CR, s.r.o.) and Microsoft Excel software.

3. Results and discussion

Our previous study [14] revealed that osteoblasts treated with low CTAB concentrations did not show significantly reduced cell viability; however, their metabolic activity decreased with increasing CTAB concentrations. A 1 mM or higher CTAB concentration caused a dramatic reduction in cell metabolic activity. Adding HyA to the medium CTAB cytotoxicity was moderated, but only at the low CTAB concentration (not exceeding 0.2 mM). Consequently, low surfactant concentrations were used in the present work. These low concentrations were also dictated by the effort to avoid the precipitation of hyaluronan–surfactant aggregates which occurs at elevated surfactant concentrations [36,37] and to obtain clear colloidal solutions of hyaluronan–surfactant complexes.

In contrast to the previous study [14], the surfactant and hyaluronan were added to cells just in the form of the pre-prepared complexes. The formation of complexes between oppositely charged surfactants and polyelectrolytes, mainly on the basis of their electrostatic interactions, is a well-known fact [32,36,37]. The complexes were characterized by the two parameters relevant for their supposed interactions with cells—the size and charge. Measurements of particle sizes showed no clear dependence on concentration; all complexes were polydisperse with a main peak around 30 nm and a minor peak around 250 nm. A typical example of the measured size distribution is given in Fig. S1 in Supplementary material. Because the surfactant concentrations were well below their standard critical micellar concentrations, the polydispersity is believed to have been caused essentially by the presence of hyaluronan chains containing different numbers of attached induced micelles or even by the presence of structures formed by several biopolymer chains attached to the same induced micellar structure. The induced micelles are the micellar structures which are formed in solutions containing a polyelectrolyte and an oppositely charged surfactant at a concentration lower than their critical micellar concentration [32]. Zeta potential values are given in Table 1. They had negative values in all cases, indicating the prevailing negative charge of the complexes. This is an indication of the "elimination" of the surfactant's positive charges by interactions with hyaluronan. Complexes prepared from Septonex had significantly lower values due to the higher concentration of anionic hyaluronan. In the case of CTAB-based complexes, a lower hyaluronan concentration usually resulted in increased values of zeta potential. A typical example of the measured zeta potential distribution is shown in Fig. S2 in Supplementary material.

Fig. 2 shows that under standard conditions, the metabolic activity of cells treated with all of the used "only CTAB" concentrations was significantly decreased in comparison to the "only cells" control. Levels of cell metabolic activity after 4 μM or 5 μM CTAB treatments reached 75% or 80%, respectively. This is on the edge of cytotoxicity. Cytotoxicity is often defined by a drop in cell metabolic activity to under 75% [38], thus 8 μM or 10 μM CTAB concentrations (cf. Fig. 2) were already determined to be cytotoxic (inducing cell viabilities of 72% or 59%, respectively). The lowest HyA concentration (0.5 mg/l) was able to reduce the negative effect of "only CTAB" at its lowest concentration (4 μM). Higher HyA concentrations (3 mg/l and 5 mg/l) were able to significantly reduce the negative effects of all higher CTAB concentrations (5 μM, 8 μM and 10 μM). The contrast between the protective effects of the lowest and higher HyA concentrations is clearly apparent at the 5 μM concentration of CTAB and its complexes (see Fig. 2). As shown in the graph, the regenerative ability of HyA increased proportionally with the increase in CTAB concentration. All "only HyA" concentrations exhibited a positive effect on cell viability. Taken together, statistically significant differences between "only CTAB" and their complex analogues with higher HyA concentrations (3 mg/l and 5 mg/l) were observed in all cases. Thus, HyA in CTAB complexes is able to moderate the cytotoxicity induced by CTAB in general. Our results are more or less analogous to a reduction in CTAB cytotoxicity achieved by coating particles with polymers (specifically PAA) [13]. The moderation of cytotoxicity by HyA could be used for CTAB applications in which this surfactant plays the role of an effective disinfectant [4]. Thus, HyA could be used to regulate surfactant antiseptic effects.

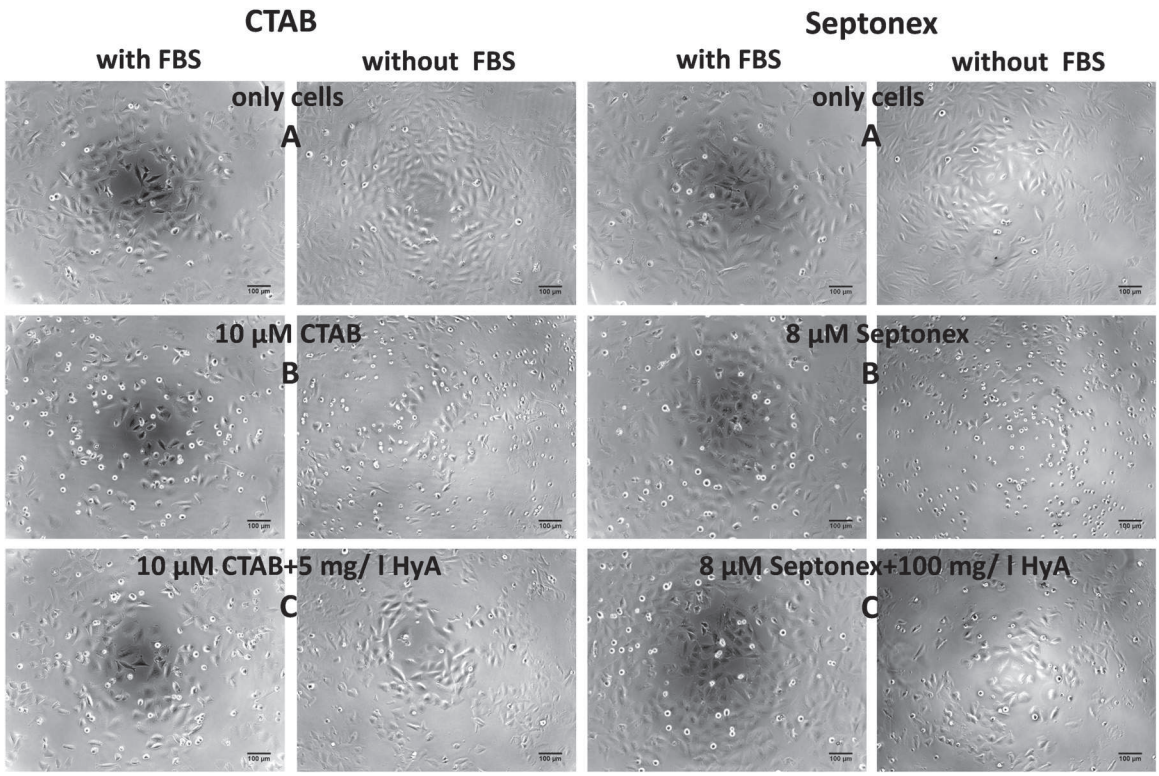

Fig. 1. Phase contrast images (10× magnification) of human osteoblasts (SAOS-2) after 24 h treatment with surfactants (CTAB or Septonex (B)) or with complexes of surfactants and HyA (C) in the presence of FBS (with FBS) or in the absence of FBS (without FBS) during first 4 h of cultivation. (A)—untreated cells (only cells).

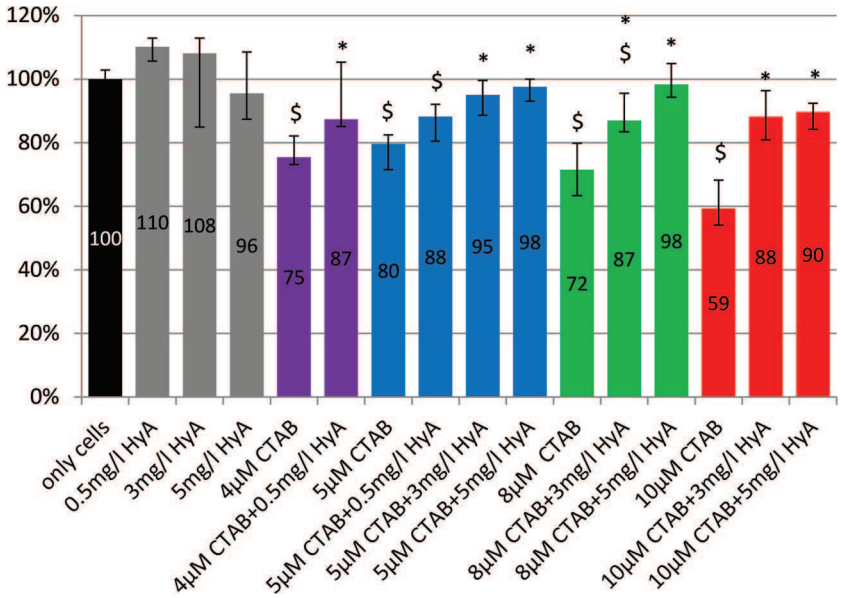

Fig. 2. Human osteoblast metabolic activity after 24 h treatment with CTAB or CTAB–HyA complexes. FBS was present during the whole period of treatment (standard conditions). $—significance at alpha level 0.05 compared to control (only cells); *—significance at alpha level 0.05 compared to surfactant alone at the corresponding concentration based on the Wilcoxon rang test.

Results obtained under non-standard conditions with CTAB are shown in Fig. 3. A significant decrease in cell viability in most of the "only CTAB" samples (but not at the 4 μM CTAB concentration) compared to the "only cells" control was observed. Surprisingly, cells under non-standard conditions withstood the presence of 4 μM CTAB better than those under standard conditions, which could be explained by mild stress inducing higher mitochondrial activity (and, hence, the detection of higher metabolic activity). On the other hand, higher CTAB concentrations (5 μM and above) were tolerated by cells under non-standard conditions substantially worse than under standard conditions. This indicates higher cell sensitivity to higher CTAB concentrations under non-standard conditions compared to standard conditions. The differences between "only CTAB" and its complex analogues were statistically significant in all cases. Moreover, the differences were more marked when compared to standard conditions. In contrast to standard

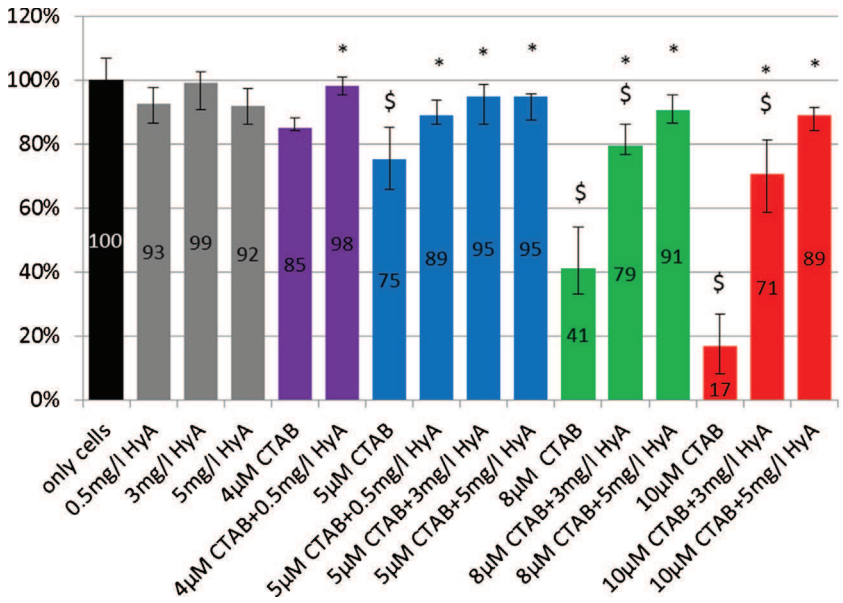

Fig. 3. Human osteoblast metabolic activity after 24 h treatment with CTAB or CTAB–HyA complexes. FBS was added after the first 4 h of treatment (non-standard conditions). $—significance at alpha level 0.05 compared to control (only cells); *—significance at alpha level 0.05 compared to surfactant alone at the corresponding concentration based on the Wilcoxon rang test.

conditions, even the lowest HyA concentration (0.5 mg/l) statistically significantly reduced the negative effects caused by the 5 μM CTAB concentration. Higher HyA concentrations (3 mg/l and 5 mg/l) in complexes with CTAB exhibited a highly positive effect on cell metabolic activity—this effect again rose proportionally with increasing CTAB concentration.

Generally, our results obtained with CTAB suggest that (i) cells are more sensitive to CTAB cytotoxicity (at concentrations above 5 μM) in the absence of FBS (non-standard conditions) compared to the setup with FBS present (standard conditions), (ii) FBS plays a positive role under the stress conditions induced by the presence of surfactant, and (iii) the cell protection offered by HyA is greater in the temporary absence of FBS (non-standard conditions). These results are in agreement with those from our previous study [14], in which free HyA was added to CTAB treated cells under standard and non-standard conditions. Furthermore, the protective effect of serum was also previously observed on keratinocytes [39]. FBS positive role could be ascribed to its binding on the cell surface and/or formation of aggregates between the Hya–surfactant complexes and proteinaceous components of serum [14].

Cells under standard conditions treated by Septonex showed a significant decrease in metabolic activity when treated with “only Septonex” and also with all of the Septonex complexes with HyA in comparison to the “only cells” control (see Fig. 4). However, cytotoxicity was observed only at higher concentrations (6 μM and 8 μM). Statistically significantly higher levels of cell viability were observed in all Septonex complexes with HyA compared to “only Septonex”. Although these differences were not as apparent as in the case of CTAB, the positive effect of HyA rose proportionally with increasing Septonex concentration. Thus, HyA in complexes was again able to reduce cytotoxicity—in this case, the cytotoxicity induced by Septonex. In addition, the use of a comparable concentration of Septonex and CTAB (8 μM) indicated that Septonex was more cytotoxic. This could point to differences in CTAB and Septonex binding to cell membrane due to their structural differences.

Fig. 5 shows that under non-standard conditions, the data revealed a significant drop in cell metabolic activity under the “only Septonex” treatment and also under all of the Septonex/complex treatments in comparison to the “only cells” control (similarly to standard conditions). Cytotoxicity was observed when Septonex at concentrations of 6 μM and above was used (see Fig. 5). This cytotoxicity was higher under non-standard conditions compared to standard conditions. Nevertheless, significantly higher cell metabolic activities were detected when Septonex complexes were added to cells in comparison to “only Septonex”, the one exception being Septonex at a concentration of 3 μM. Interestingly, the cell metabolic activities corresponding to 3 μM Septonex and the 3 μM Septonex–HyA complex were comparable. It seems that 3 μM Septonex under non-standard conditions acted as a mitochondrial activator. It is possible that very low Septonex concentrations could provoke cells to increase their metabolic activity. A similar effect was also observed in a previous study, when low concentrations of detergents caused increases in proliferative activity and mitochondrial metabolism in keratinocytes [39]. The cytotoxicity induced by higher Septonex concentrations (6 μM and 8 μM) was substantially reduced by the presence of HyA—this effect again rose proportionally with increasing Septonex concentration. The trend of metabolic activity in the presence and absence of FBS was similar, but cell viability under non-standard conditions was reduced overall. Thus, similarly to the results obtained for CTAB, a positive effect of FBS on cells treated by Septonex was observed. More significant HyA protection under non-standard conditions compared to standard conditions was also detected. In general, surfactant cytotoxicity reduction induced by HyA under higher surfactant concentrations could be due to the formation of stable micellar structures anchored on the biopolymer chain under these concentration conditions, preventing surfactant molecules from interactions with cell membranes.

Direct comparison with previous results, in which HyA and surfactants were not in the form of complexes, is very difficult due to the differences in concentrations which can be used in the preparation of complexes. The differences in cytotoxicity between plain surfactant and surfactant combined with hyaluronan were found to be more profound if hyualuronan was present in the form of a complex with surfactant. Therefore, it can be generally concluded that the protective effect of hyaluronan is greater when complexed with surfactant.

Taken together, all the presented results indicate the potential of HyA as a useful modulator of CTAB or Septonex induced cytotoxicity.

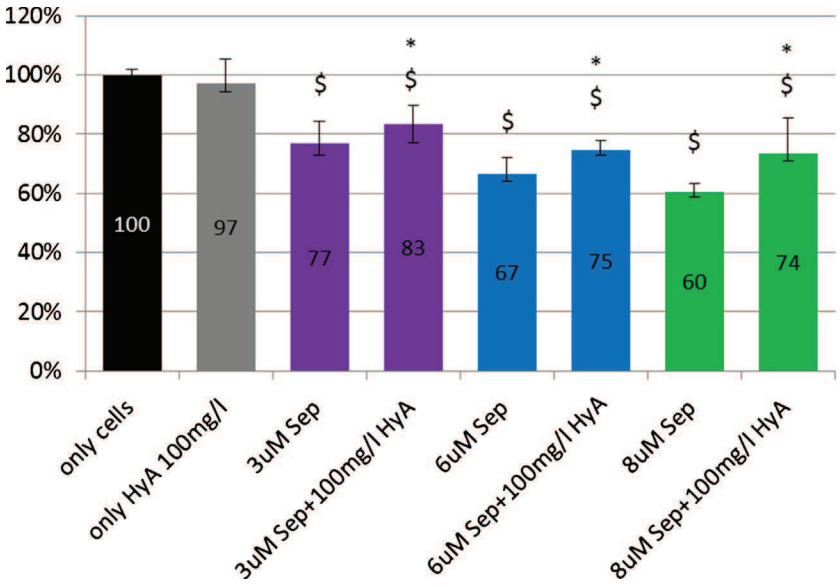

Fig. 4. Human osteoblast metabolic activity after 24 h treatment with Septonex or Septonex–HyA complexes. FBS was present during the whole period of treatment (standard conditions). $—significance at alpha level 0.05 compared to control (only cells); *—significance at alpha level 0.05 compared to surfactant alone at the corresponding concentration based on the Wilcoxon rang test.

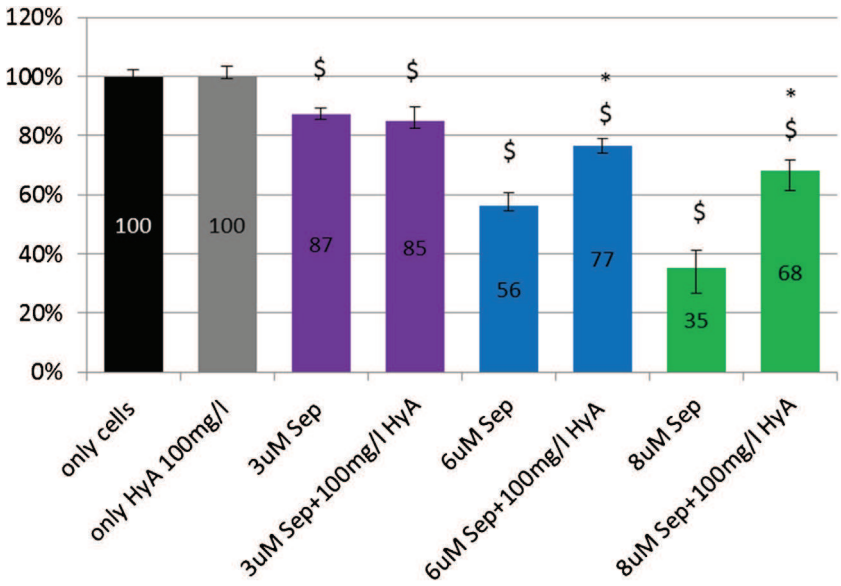

Fig. 5. Human osteoblast metabolic activity after 24 h treatment with Septonex or Septonex–HyA complexes. FBS was added after the first 4 h of treatment (non-standard conditions). $—significance at alpha level 0.05 compared to control (only cells); *—significance at alpha level 0.05 compared to surfactant alone at the corresponding concentration based on the Wilcoxon rang test.

4. Conclusion

In our study, HyA demonstrated the ability to protect cells against toxic cationic surfactants (CTAB and Septonex) when present in the form of a pre-prepared surfactant–HyA complex. The results also confirm and emphasize the role of FBS in cell response to stress conditions. Cells were more sensitive to surfactant toxicity in the absence of FBS. At the same time, cell protection by HyA was more efficient during the temporary absence of FBS. The combination of HyA and FBS thus provides the most efficient form of cell protection.

Acknowledgements

This work was supported by COST action CM1101 and projects No. LO1211 funded by the National Sustainability Programme I and LD12068 (Ministry of Education, Czech Republic). The Faculty of Medicine in Pilsen was supported by projects CZ.1.05/2.1.00/03.0076 (European Regional Development Fund) and grant SVV-2015 No. 260170, the 1st Faculty of Medicine by the project PRVOUK-P24/LF1/3, and the Faculty of Science by the project SVV-2015-260209. Special thanks go to Blanka Bílková for technical assistance.

Appendix A. Supplementary data

Supplementary data associated with this article can be found, in the online version, at http://dx.doi.org/10.1016/j.colsurfa.2015.06.058

References

[1] Â.S. Inácio, G.N. Costa, N.S. Domingues, M.S. Santos, A.J.M. Moreno, W.L.C. Vaz, O.V. Vieira, Mitochondrial dysfunction is the focus of quaternary ammonium surfactant toxicity to mammalian epithelial cells, Antimicrob. Agents Chemother. 57 (2013) 2631–2639, http://dx.doi.org/10.1128/AAC.02437-12

[2] L. Strakova, Z. Strosova, E. Sevcikova, Septonex color spray—a new disinfectant for the treatment of umbilical stubs (in Czech), Veterinarstvi 34 (1984) 69–70.

[3] K. Nakata, T. Tsuchido, Y. Matsumura, Antimicrobial cationic surfactant, cetyltrimethylammonium bromide, induces superoxide stress in *Escherichiacoli* cells, J. Appl. Microbiol. 110 (2011) 568–579, http://dx.doi.org/10.1111/j.1365-2672.2010.04912.x

[4] O.V. Vieira, D.O. Hartmann, C.M.P. Cardoso, D. Oberdoerfer, M. Baptista, M.A.S. Santos, L. Almeida, J. Ramalho-Santos, W.L.C. Vaz, Y.-S. Bahn, Surfactants as microbicides and contraceptive agents: a systematic in vitro study, PLoS One 3 (2008) e2913, http://dx.doi.org/10.1371/journal.pone.0002913

[5] V.P. Torchilin, Structure and design of polymeric surfactant-based drug delivery systems, J. Control. Release 73 (2001) 137–172, http://dx.doi.org/10.1016/S0168-3659(01)00299-1

[6] I. Pastoriza-Santos, J. Pérez-Juste, L.M. Liz-Marzán, Silica-coating and hydrophobation of CTAB-stabilized gold nanorods, Chem. Mater. 18 (2006) 2465–2467, http://dx.doi.org/10.1021/cm060293g

[7] R.L. Grant, C. Yao, D. Gabaldon, D. Acosta, Evaluation of surfactant cytotoxicity potential by primary cultures of ocular tissues: I. Characterization of rabbit corneal epithelial cells and initial injury and delayed toxicity studies, Toxicology 76 (1992) 153–176, http://dx.doi.org/10.1016/0300-483X(92)90162-8

[8] Q. He, J. Shi, F. Chen, M. Zhu, L. Zhang, An anticancer drug delivery system based on surfactant-templated mesoporous silica nanoparticles, Biomaterials 31 (2010) 3335–3346, http://dx.doi.org/10.1016/j.biomaterials.2010.01.015

[9] I. Giraud, M. Rapp, J.-C. Maurizis, J.-C. Madelmont, Synthesis and in vitro evaluation of quaternary ammonium derivatives of chlorambucil and melphalan, anticancer drugs designed for the chemotherapy of chondrosarcoma, J. Med. Chem. 45 (2002) 2116–2119, http://dx.doi.org/10.1021/jm010926x

[10] E. Ito, K.W. Yip, D. Katz, S.B. Fonseca, D.W. Hedley, S. Chow, G.W. Xu, T.E. Wood, C. Bastianutto, A.D. Schimmer, S.O. Kelley, F.-F. Liu, Potential use of cetrimonium bromide as an apoptosis-promoting anticancer agent for head and neck cancer, Mol. Pharmacol. 76 (2009) 969–983, http://dx.doi.org/10.1124/mol.109.055277

[11] M.J. Weiss, J.R. Wong, C.S. Ha, R. Bleday, R.R. Salem, G.D. Steele, L.B. Chen, Dequalinium, a topical antimicrobial agent, displays anticarcinoma activity based on selective mitochondrial accumulation, Proc. Natl. Acad. Sci. U. S. A. 84 (1987) 5444–5448.

[12] Â.S. Inácio, K.A. Mesquita, M. Baptista, W.L.C. Ramalho-Santos, O.V. Vieira, D.T. Covas, In vitro surfactant structure–toxicity relationships: implications for surfactant use in sexually transmitted infection prophylaxis and contraception, PLoS One 6 (2011) e19850, http://dx.doi.org/10.1371/journal.pone.0019850

[13] A.M. Alkilany, P.K. Nagaria, C.R. Hexel, T.J. Shaw, C.J. Murphy, M.D. Wyatt, Cellular uptake and cytotoxicity of gold nanorods: molecular origin of cytotoxicity and surface effects, Small 5 (2009) 701–708, http://dx.doi.org/10.1002/smll.200801546

[14] M. Kalbáčová, M. Verdánová, F. Mravec, T. Halasová, M. Pekař, Effect of CTAB and CTAB in the presence of hyaluronan on selected human cell types, Colloids Surf. A: Physicochem. Eng. Aspects 460 (2014) 204–208, http://dx.doi.org/10.1016/j.colsurfa.2013.12.048

[15] K. Meyer, Chemical structure of hyaluronic acid, Fed. Proc. 17 (1958) 1075–1077.

[16] K.T. Dicker, L.A. Gurski, S. Pradhan-Bhatt, R.L. Witt, M.C. Farach-Carson, X. Jia, Hyaluronan: a simple polysaccharide with diverse biological functions, Acta Biomater. 10 (2014) 1558–1570, http://dx.doi.org/10.1016/j.actbio.2013.12.019

[17] A. Aruffo, I. Stamenkovic, M. Melnick, C.B. Underhill, B. Seed, CD44 is the principal cell surface receptor for hyaluronate, Cell 61 (1990) 1303–1313, http://dx.doi.org/10.1016/0092-8674(90)90694-A

[18] C.B. Knudson, Hyaluronan and CD44: strategic players for cell–matrix interactions during chondrogenesis and matrix assembly, Birth Defects Res. Part C: Embryo Today: Rev. 69 (2003) 174–196, http://dx.doi.org/10.1002/bdrc.10013

[19] H. Ponta, L. Sherman, P.A. Herrlich, CD4: from adhesion molecules to signalling regulators, Nat. Rev. Mol. Cell Biol. 4 (2003) 33–45, http://dx.doi.org/10.1038/nrm1004

[20] W.F. Cheung, T.F. Cruz, E.A. Turley, Receptor for hyaluronan-mediated motility (RHAMM), a hyaladherin that regulates cell responses to growth factors, Biochem. Soc. Trans. 27 (1999) 8.

[21] G. Lepperdinger, J. Müllegger, G. Kreil, Hyal2—less active, but more versatile? Matrix Biol. 20 (2001) 509–514, http://dx.doi.org/10.1016/S0945-053X(01)00170-6

[22] H. Harada, M. Takahashi, CD44-dependent intracellular and extracellular catabolism of hyaluronic acid by hyaluronidase-1 and -2, J. Biol. Chem. 282 (2007) 5597–5607, http://dx.doi.org/10.1074/jbc.M608358200

[23] E.S.A. Hofinger, J. Hoechstetter, M. Oettl, G. Bernhardt, A. Buschauer, Isoenzyme-specific differences in the degradation of hyaluronic acid by mammalian-type hyaluronidases, Glycoconj. J. 25 (2008) 101–109, http://dx.doi.org/10.1007/s10719-007-9058-8

[24] G.D. Prestwich, Hyaluronic acid-based clinical biomaterials derived for cell and molecule delivery in regenerative medicine, J. Control. Release 155 (2011) 193–199, http://dx.doi.org/10.1016/j.jconrel.2011.04.007

[25] B.P. Toole, Hyaluronan: from extracellular glue to pericellular cue, Nat. Rev. Cancer 4 (2004) 528–539, http://dx.doi.org/10.1038/nrc1391

[26] B.P. Toole, T.N. Wight, M.I. Tammi, Hyaluronan–cell interactions in cancer and vascular disease, J. Biol. Chem. 277 (2002) 4593–4596, http://dx.doi.org/10.1074/jbc.R100039200

[27] J. Lam, W.E. Lowry, S.T. Carmichael, T. Segura, Delivery of iPS-NPCs to the stroke cavity within a hyaluronic acid matrix promotes the differentiation of transplanted cells, Adv. Funct. Mater. 24 (2014) 7053–7062, http://dx.doi.org/10.1002/adfm.201401483

[28] S.K. Seidlits, Z.Z. Khaing, R.R. Petersen, J.D. Nickels, J.E. Vanscoy, J.B. Shear, C.E. Schmidt, The effects of hyaluronic acid hydrogels with tunable mechanical properties on neural progenitor cell differentiation, Biomaterials 31 (2010) 3930–3940, http://dx.doi.org/10.1016/j.biomaterials.2010.01.125

[29] J. Lam, N.F. Truong, T. Segura, Design of cell–matrix interactions in hyaluronic acid hydrogel scaffolds, Acta Biomater. 10 (2014) 1571–1580, http://dx.doi.org/10.1016/j.actbio.2013.07.025

[30] M.J. Wilson, S.J. Liliensiek, C.J. Murphy, W.L. Murphy, P.F. Nealey, Hydrogels with well-defined peptide-hydrogel spacing and concentration: impact on epithelial cell behavior, Soft Matter 8 (2012) 390–398, http://dx.doi.org/10.1039/C1SM06589K

[31] Y. Lee, H. Lee, Y.B. Kim, J. Kim, T. Hyeon, H. Park, P.B. Messersmith, T.G. Park, Bioinspired surface immobilization of hyaluronic acid on monodisperse magnetite nanocrystals for targeted cancer imaging, Adv. Mater. 20 (2008) 4154–4157, http://dx.doi.org/10.1002/adma.200800756

[32] K. Holmberg, B. Jönsson, B. Kronberg, B. Lindman, Surfactants and Polymers in Aqueous Solution, Wiley, Chichester, 2007.

[33] M. Fasano, S. Curry, E. Terreno, M. Galliano, G. Fanali, P. Narciso, S. Notari, P. Ascenzi, The extraordinary ligand binding properties of human serum albumin, IUBMB Life 57 (2005) 787–796, http://dx.doi.org/10.1080/15216540500404093

[34] W.C. Little, R. Schwartlander, M.L. Smith, D. Gourdon, V. Vogel, Stretched extracellular matrix proteins turn fouling and are functionally rescued by the chaperones albumin and casein, Nano Lett. 9 (2009) 4158–4167, http://dx.doi.org/10.1021/nl902365z

[35] M. Verdanova, A. Broz, M. Kalbac, M. Kalbacova, Influence of oxygen and hydrogen treated graphene on cell adhesion in the presence or absence of fetal bovine serum, Phys. Status Solidi (b) 249 (2012) 2503–2506, http://dx.doi.org/10.1002/pssb.201200099

[36] K. Thalberg, B. Lindman, Interaction between hyaluronan and cationic surfactants, J. Phys. Chem. 93 (1989) 1478–1483.

[37] A. Kargerová, M. Pekař, High-resolution ultrasonic spectroscopy study of interactions between hyaluronan and cationic surfactants, Langmuir 30 (2014) 11866–11872.

[38] E. Flahaut, M.C. Durrieu, M. Remy-Zolghadri, R. Bareille, C. Baquey, Investigation of the cytotoxicity of CCVD carbon nanotubes towards human umbilical vein endothelial cells, Carbon 44 (2006) 1093–1099, http://dx.doi.org/10.1016/j.carbon.2005.11.007

[39] P.L. Bigliardi, M.J. Herron, R.D. Nelson, M.V. Dahl, Effects of detergents on proliferation and metabolism of human keratinocytes, Exp. Dermatol. 3 (1994) 89–94, http://dx.doi.org/10.1111/j.1600-0625.1994.tb00053.x.

International Journal of Biological Macromolecules 112 (2018) 241–249

Contents lists available at ScienceDirect

International Journal of Biological Macromolecules

journal homepage: https://www.journals.elsevier.com/ijbiomac

Interactions of hyaluronan with oppositely charged surfactants in very diluted solutions in water

Tereza Pilgrová, Tereza Venerová, Filip Mravec, Miloslav Pekař *

Faculty of Chemistry, Brno University of Technology, Purkyňova 464/118, 612 00 Brno, Czech Republic

ARTICLE INFO

Article history:
Received 14 November 2017
Received in revised form 11 January 2018
Accepted 26 January 2018
Available online 31 January 2018

Keywords:
Hyaluronan
Interactions
Surfactants

ABSTRACT

The phase behavior of aqueous systems containing hyaluronan, at concentrations between 2 and 100 mg/L, and oppositely charged surfactants was investigated. A fluorescence probe technique revealed the formation of micellar structures on the hyaluronan in homogeneous systems well below the surfactant standard, critical, micellar concentration. Moreover, regions of gel-phase separation were revealed. A detailed phase diagram was, thus, constructed in the very diluted region and the hyaluronan concentration was found to be the main parameter controlling the phase behavior, in contrast to the charge ratio. The stability of hyaluronan-surfactant aggregates in the homogeneous systems while in storage at 4 °C (up to three months), against dilution, salt addition and on heating-cooling (between 10 and 50 °C) was also investigated. The aggregates were stable while in storage or upon increasing and decreasing the temperature. The dilution of hyaluronan-surfactant complexes or the addition of 0.15 M NaCl led to their disintegration. Finally, systems prepared in a 0.15 M NaCl solution showed that interactions are suppressed and no aggregation below the standard critical micellar concentration was observed.

1. Introduction

Hyaluronan is a naturally occurring polysaccharide formed by repeating disaccharide units composed of D-glucuronate and *N*-acetyl-D-glucosamine residues linked by $\beta(1\rightarrow4)$ and $\beta(1\rightarrow3)$ bonds, which are connected to unbranched chains. The name hyaluronan commonly denotes a sodium salt of hyaluronic acid which is the form that occurs in various living organisms, including human bodies. Hyaluronan is a principal component of the extracellular matrix and plays important roles in lubrication, water sorption, water retention, and a number of cellular functions, such as attachment, migration, and proliferation. In the human body, hyaluronan is found mainly in connective tissues, such as the vitreous, the umbilical cord, joint fluid, etc. [1]. Hyaluronan is, therefore, an attractive building block for preparing new biocompatible and biodegradable materials that could find applications in drug delivery, tissue engineering, viscosupplementation or cosmetics [2–5].

In an aqueous solution, the carboxyl group on hyaluronan is in a dissociated form giving, theoretically, each repeating unit a negative charge, consequently, hyaluronan can be generally described as a negatively charged polyelectrolyte. Interactions between polyelectrolytes and an oppositely charged surfactant are an area of vital scientific research. This is due to the theoretical significance of the understanding electrostatic and other (e.g., hydrophobic or excluded volume) interactions between charged polymers and low molecular counterpartners and also due to practical applications of polyelectrolyte-surfactant colloidal systems [6–9]. For instance, when prepared from biocompatible polymers, they can find applications in pharmaceutical and medical industries. They can stabilize encapsulated proteins or may be prepared as materials responsive to external stimuli [10]. Other application fields include detergency, the modification of rheological properties, or paints [11]. Also, their surface (interfacial) effects are important [12].

Hyaluronan-surfactant interactions were the subject of several previous studies. Perhaps the most detailed study was published in a series of papers by Swedish researchers [13–16] who investigated the phase behavior of systems containing water, hyaluronan, alkyl trimethylammonium bromides (a tetradecyl derivative was the most studied type) and salt (mostly NaBr). The binding of the surfactant to the hyaluronan was detected for surfactants with an alkyl chain consisting of at least ten carbon atoms. A ternary phase diagram of tetradecyltrimethylammonium bromide (TTAB)-hyaluronan (300 or 240 kDa)-water was constructed in the ref. [14]. It consisted of a droplet-shaped two-phase region emerging from the water apex of the triangular diagram and entirely enclosed by a one-phase area. The diagram shape demonstrated marked dissymmetry – for example, concentrated surfactant solutions almost immediately phase-separated upon the addition of hyaluronan in contrast to systems with high hyaluronan concentrations in which a rather large amount of surfactant could be added without phase separation. The effect of the surfactant alkyl chain length and the hyaluronan molecular weight was

* Corresponding author at: Materials Research Centre, Faculty of Chemistry, Brno University of Technology, Purkyňova 464/118, 612 00 Brno, Czech Republic.
E-mail address: pekar@fch.vut.cz (M. Pekař).

https://doi.org/10.1016/j.ijbiomac.2018.01.176
0141-8130/

investigated in the ref. [17]. Hyaluronans of molecular weights of 250, 90, 60, and 23 kDa (weight average) were used. A decrease in the molecular weight resulted in a slight shift in position of the two-phase region while its size remained almost unaffected. This size was much more sensitive to the alkyl chain length of the surfactant – the longer the chain, the larger the size. Due to the prevailing electrostatic nature of the hyaluronan-cationic surfactant interactions, the phase behavior is affected by the presence of salt also. The effect of sodium bromide on the TTAB-hyaluronan system was described in the paper by Thalberg et al. [18]. The addition of low concentrations of NaBr reduced the size of the two-phase region of the phase diagram and this region disappeared at 250 mM NaBr. Another type of phase separation was observed with high NaBr concentrations (at and above 500 mM). Generally, oppositely charged polyelectrolyte-surfactant systems are characterized by association without added electrolyte, miscibility at intermediate electrolyte concentration and segregative phase separation at high ionic strength [7].

Fukada et al. [19] investigated the interaction between hyaluronan and decyltrimethylammonium bromide by rheological methods. Also, they presented a part of the phase diagram in a hyaluronan concentration region below 10 g/L and a surfactant concentration below 1 mol/L. The phase separation region was indicated when the surfactant concentration was between 0.03 and 0.35 mol/L and the hyaluronan concentration was above ca 0.05 g/L. Eventually, the authors focused their study on the isotropic region with a large surfactant excess.

In the referred experiments, concentrated solutions of hyaluronan and surfactants were usually investigated. Our preliminary fluorescence probe study of similar systems prepared in water did not reveal dependencies of fluorescence indices on the surfactant concentration, which are typical for the formation of micellar aggregates on polyelectrolyte chains, prior to the phase separation. In other words, the fluorescence data did not indicate the formation of hyaluronan-micelle aggregates in isotropic, clear solutions, which would occur well below the critical micellar concentration of a pure surfactant. From the previous studies, only ref. [20] reports on the solubilization of the fluorescence probe (pyrene), but in a single system of a high surfactant excess. Actually, our work in this area was initiated by an attempt of a hyaluronan producer to get hyaluronan-decorated micelles and test their applicability as delivery systems for hydrophobic substances. Therefore, we focused on interactions in a dilute (with respect to hyaluronan), and clear solutions that have not been directly investigated thus far. Some diluted solutions were mentioned by Fukada et al. [19] but they eventually studied rheological properties of concentrated systems only. Our main purpose was not to prepare delivery systems, but to investigate the diluted region for hyaluronan-surfactant interactions and for stability properties of the hyaluronan-micelle aggregates. In this study, we revealed that the phase behavior in diluted systems is not as simple as could be expected from previous studies.

2. Materials and method

2.1. Materials

Hyaluronan (a sodium salt of hyaluronic acid; HyA) of several chain lengths were purchased from Contipro, Ltd., Czech Republic. Here they are denoted as low (LMW, 75–100 kDa), medium (MMW, 650–750 kDa) and high (HMW, 1400–2000 kDa) molecular weight hyaluronan (the values in parentheses give the range of the weight of the averaged molecular weights of the used batches, determined by the producer using the SEC-MALLS technique). Cationic surfactant cetyltrimethylammonium bromide (CTAB) was purchased from Sigma-Aldrich, Czech Republic and carbethopendecinium bromide (Septonex) was purchased from GBNchem, Czech Republic. The surfactants were of the best available quality and used as received without further purification.

Stock solutions of hyaluronan and surfactants were prepared in deionized water, in a phosphate buffer solution or in a model physiological solution (0.15 M NaCl).

The fluorescence probe pyrene (Fluka, purity ≥99.0%; Sigma Aldrich, Czech Republic) was used for the fluorescence measurements. The stock solution of the fluorescence probe was prepared in a volatile solvent (acetone). An appropriate amount of the stock solution was added to a glass vial and acetone was evaporated under reduced pressure to obtain the final concentration of pyrene in the samples equal to 10^{-7} M. Subsequently, samples of the required composition and solvent were prepared in these vials by mixing corresponding volumes of hyaluronan and surfactant solutions. All samples were stirred for 24 h, at least, at laboratory temperature before the acquisition of their fluorescence spectra. In this way, series of samples were prepared with constant hyaluronan and increasing surfactant concentrations.

Samples with varying surfactant concentration and no hyaluronan were prepared by simple dilution of the surfactant stock solution of the concentration about ten times higher than the critical micelle concentration.

2.2. Methods

The aggregation and solubilization properties were studied by means of pyrene as the fluorescence probe. The fluorescence emission spectra were recorded on a FLUOROLOG (Horiba Scientific, France) fluorescence spectrometer. For the emission spectra, recording the excitation wavelength was set at 336 nm and the emission scan was acquired in the range from 360 to 530 nm. In the excitation measurements, the emission wavelength was set at 392 nm and the excitation scan was acquired in the range from 310 to 340 nm.

Pyrene experiments were evaluated by plotting the fluorescence intensity ratio of the first and third vibronic peaks from the emission scan at 373 and 383 nm, respectively (EmPI – the pyrene emission polarity index), against the surfactant concentration. The pyrene polarity index is the reflection of the polarity in the vicinity of the pyrene environment and it is used to detect the localization of pyrene in the system. A typical sigmoidal curve was obtained indicating the formation of nonpolar domains (micelles with hydrophobic cores) solubilizing pyrene molecules. Ideally, a sharp decrease would be observed at the critical aggregation or micellar concentration. Curves were fitted by the Boltzmann model and the concentration at the inflex point can be considered as the critical micelle (or critical aggregation) concentration.

The Boltzmann model equation is given by:

$$y = \frac{A_1 - A_2}{1 + e^{\frac{x - x_0}{\Delta x}}} + A_2,$$

where the variable y corresponds to the EmPI value, the independent variable (x) is the total concentration of the surfactant, A_1 and A_2 are the upper and lower limits of the sigmoid, respectively, x_0 is the center of the sigmoid, and Δx is directly related to the independent variable range, where the abrupt change of the dependent variable occurs.

Thus, from the Boltzmann equation, the width of the concentration interval in which the sharp intensity decrease occurred can be obtained. This interval spreads from the onset up to the offset of the aggregates (micelles) formation, i.e., to the concentration range in which aggregates capable of pyrene solubilization are progressively formed.

The pyrene experiments were also evaluated by the ratio of fluorescence intensities at 470 nm, which corresponds to the excimer emission maximum, and the first vibronic peak (at 373 nm). This ratio is referred to as the Ex:Mo. It is an indicator of the probability of the excimer formation in the system and reflects the accumulation of pyrene molecules in hydrophobic domains.

In addition, the pyrene experiments were evaluated by the ratio of fluorescence intensities at 333 and 338 nm of the excitation spectra also. This ratio is called the pyrene excitation polarity index (ExPI) and

it is the reflection of the polarity in the vicinity of the pyrene environment. The dependency of the ExPI on the surfactant concentration typically has a sigmoidal shape and can be fitted to the Boltzmann model also. The lines in the figures showing the concentration dependences of EmPI or ExPI represent examples of data fitting by the Boltzmann equation.

The stability of the hyaluronan-surfactant systems under various conditions like storage stability, response to temperature changes, addition of electrolyte and dilution effects were investigated using fluorescence spectroscopy and dynamic light scattering (Zetasizer Nano ZS, Malvern Instruments, standard measurement procedure). The hyaluronan-surfactant systems for the stability studies contained the final hyaluronan concentration of 15 mg/L and the final concentration of the surfactant of 0.05 or 0.07 mM, which correspond to the area of the formation of clear systems containing hyaluronan-micelle aggregates. The hyaluronan of two molecular weights (LMW and HMW) was used in this study. In the case of storage stability experiments, the tested system was measured every week over one month. All samples were stored at 4–6 °C and equilibrated to the laboratory temperature before the measurement. In the case of the study of the effect of increased ionic strength, 121 μL of the saturated solution of sodium chloride (6.2 mol/L) was added to the sample, so that the final concentration of sodium chloride was 0.15 mol/L and the sample volume remained almost unchanged (the dilution factor about 0.98). Temperature stability was studied in the temperature range of 10–50 °C. The dilution stability was realized by adding hyaluronan solution (15 mg/L) to the clear hyaluronan-surfactant system to obtain ten times lower surfactant concentration.

All measurements were performed in triplicate at least. The error bars in the figures represent the standard deviations.

3. Results and discussion

3.1. CMC of CTAB and Septonex

The critical micelle concentrations of CTAB and Septonex were first determined using the pyrene fluorescence spectroscopy method. The concentration dependency of the EmPI was fitted to the Boltzmann model and the concentration at the inflex point was considered as the critical micelle concentration (CMC). The effect of ionic environments on the CMC was studied using a phosphate buffer (pH = 7.0) and an NaCl solution (0.15 M). The results are shown in Table 1, which also shows good agreement with published data.

3.2. Interactions with CTAB in water – concentration effect of hyaluronan

Preliminary experiments were performed to find the reasonable (dilute) concentration region of hyaluronan, where the formation of surfactant aggregates could be detected at no phase separation (no formation of cloudiness or precipitates) upon its mixing with CTAB. The experiments showed that the suitable region lies in the range of micrograms or tens of micrograms per liter. For the first time in hyaluronan-containing systems, "double" S-curves (see below) could be measured with the pyrene method at the hyaluronan concentration above about 2 mg/L, in contrast to previous studies with higher hyaluronan concentrations. More detailed experiments in the selected concentration region (2–100 mg/L) followed and revealed a more complex behavior; their results are reported below.

The presence of hyaluronan at the constant concentration of 2 mg/L had an insignificant effect on the "aggregation curve" of CTAB, i.e., the dependence of ExPI or EmPI on the surfactant concentration. Only a very minor effect on the standard critical micellar concentration was observed – in the presence of hyaluronan, it was about 0.8 mM as detected from the inflex point of the ExPI-concentration dependence and the maximum on the Ex:Mo-concentration curve. Thus, only a similar effect to that of the salt addition was observed. In this case, the pyrene probe method did not reveal the formation of the CTAB micelles, below its standard critical micellar concentration, induced by the presence of hyaluronan. This can be caused by the long-range electrostatic interactions between the hyaluronan polyions and by the related hydrolysis of the hyaluronan carboxyl groups – these effects become important in dilute polyelectrolyte solutions with no added salt [30,31] and lead to decreased charge density on the hyaluronan chain.

Increasing the hyaluronan concentration to 5 mg/L, the "double" S-curve, mentioned above, was observed, clearly indicating a surfactant aggregation well below its standard critical micellar concentration (Fig. 1). At surfactant concentrations lower than about 0.005 mM and 0.05 mM, the curves measured for pure CTAB and for CTAB in the presence of hyaluronan, respectively, coincide, indicating the presence of no aggregates which could solubilize a hydrophobic fluorescence probe in their interior, in both cases. The first sharp decrease of ExPI in the presence of the hyaluronan and CTAB concentration of about 0.005–0.02 mM characterizes the polymer-induced aggregation of the surfactant and it is this interval where the critical aggregation concentration should be located (this is taken as the inflex point within this interval).

When the surfactant concentration in the system increases, surfactant molecules are bound on the polymer chain. The local concentration of the surfactant on the polymer chains increases because of the electrostatic binding of the positively charged surfactant head on the negatively charged dissociated carboxylic group of hyaluronan. Hyaluronan reduces the mobility of the surfactant molecules in a solution, the surfactant molecules aggregate at a lower concentration than in a pure solution and induced micelle-like aggregates are created on the polymer chain. Pyrene molecules are solubilized in these aggregates and ExPI decreases.

The decrease of ExPI observed both in the pure surfactant solution and in the presence of hyaluronan around the CTAB concentration of 0.9 mM corresponds to the standard micellization of the free surfactant molecules at normal critical micellar concentration.

It should be noted that the pyrene fluorescence intensity (and the corresponding values of ExPI) measured in the aggregation regions is generally composed of signals coming from different environments, basically from the pyrene molecules dissolved in water and from those solubilized in the aggregates.

Fig. 1 also shows an unexpected finding – a rather strange increase of ExPI up to the values measured in pre-micellar regions, in a concentration interval centered around 0.1 mM. This means a sudden loss of solubilization abilities of the system. The cause was revealed only after a change from brown to clear vials and a careful inspection of their content. In the reported concentration region, a thin rim of gelled material

Table 1
Critical micelle concentrations determined from the pyrene emission polarity index (25 °C).

	CMC (mM)			
	CTAB		Septonex	
	This work	Published value	This work	Published value
Water	0.98 ± 0.01	0.89 [21]; 0.91 [22]; 0.92 [23]; 0.96 [24]	0.75 ± 0.02	0.81 [27]; 0.78 [28]; 0.77 [29]
Phosphate buffer	0.086 ± 0.004	–	–	–
0.15 M NaCl	0.062 ± 0.002	0.062 [25]; 0.07 [26]	0.078 ± 0.002	0.11 [29][a]

[a] 0.1 M NaCl.

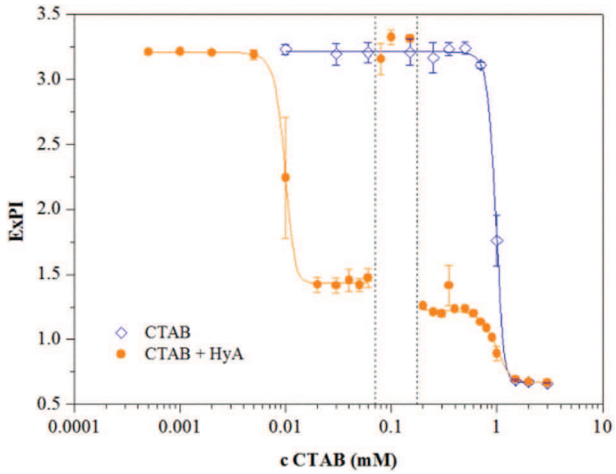

Fig. 1. Effect of hyaluronan addition (MMW, 5 mg/L) on the aggregation behavior of CTAB in water; the region between the dashed lines represents the gel phase separation.

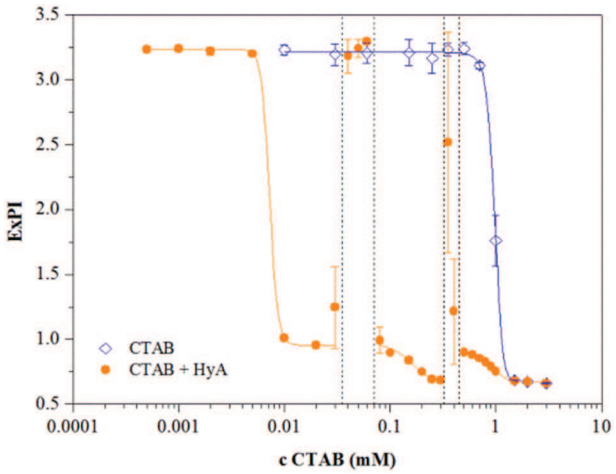

Fig. 2. Effect of hyaluronan addition (MMW, 15 mg/L) on the aggregation behavior of CTAB in water; the regions between the dashed lines represent the gel phase separation.

was observed on the walls of the vials along the liquid surface. Using a UV lamp, intensive pyrene fluorescence was observed from the gel phase (see Fig. SF1 in the Supplementary material). Thus, most of the pyrene molecules were collected in micelles participating in the formation of a tiny amount of the gel phase. Only the free pyrene molecules remained in the liquid phase which was actually transferred into fluorescence cuvettes and only their fluorescence from the aqueous environment was measured in that concentration interval. The gel-like phase separation can be viewed as a specific example of complex coacervation known for systems containing two oppositely charged macroions [9]. Complex coacervation should occur subsequent to the binding of macromolecular ions on micellar colloids which is consistent with our findings. The separated hyaluronan-surfactant complexes were not formed when an excess of the surfactant was present which also accords with previous findings [7,9,14,18].

The conclusions made on the basis of the polarity index were further confirmed by the dependence of Ex:Mo ratio on the surfactant concentration (Fig. SF2 in the Supplementary material). The ratio starts to increase as micelles are formed and the probability of the formation of the excited dimer between the pyrene molecules solubilized inside the micelles increases. Induced micelles, i.e., micelles bound on the polyelectrolyte chain, are reported to be smaller than free micelles [32], which contributes to the increased probability of excimer formation. In the region of gel-phase separation, a sharp decrease of Ex:Mo indicates the presence of (only) free pyrene monomers in the measured solution – pyrene molecules remaining in the supernatant are not solubilized in the hydrophobic environment and the probability of excimer formation is very low there. When the gel phase disappears, the Ex:Mo ratio increases due to the presence of the induced micellar structures in the homogeneous colloidal solution. Another decrease of this ratio above the standard critical micellar concentration is attributed to the progressive distribution of pyrene molecules in the increasing number of (free) micelles, which decreases the probability of finding more than one pyrene molecule in a micelle.

Similar behavior was observed for systems with an increased hyaluronan concentration also, i.e., 15, 30, 50, and 100 mg/L, except that two concentration intervals of gel-phase separation were found. The second interval was found at surfactant concentrations higher than those of the first interval, but still lower than the standard critical micellar concentration of the pure surfactant; an example can be seen in Fig. 2. The second interval is narrower and its existence was, in fact, indicated in the system with hyaluronan concentration of 5 mg/L also, cf. the point of ExPI corresponding to the CTAB concentration of 0.35 mM in Fig. 1. The values of both the ExPI and Ex:Mo ratio (Fig. SF3 in the Supplementary material) in the second interval are more scattered upon replicated measurements than in any other part of measured dependencies. This probably indicates the formation of some metastable structures in the second interval in which the distribution of pyrene between the aqueous and hydrophobic environments is not easily exactly reproducible in the replicated measurements.

The ExPI gradually decreases behind the second region of the gel-phase separation – here, the surfactant concentration becomes closer and closer to the normal critical micellar concentration and free micelles are supposed to be formed. The comparison of the two curves is shown in Fig. 2, it is shown that in this region, in the presence of hyaluronan, the formation of free micelles proceeds in a broader interval of surfactant concentration than in the case of the pure surfactant. A similar broadening was observed in a previous study on hyaluronan interactions with surfactants of a different ionic type in the presence of NaCl at a physiological concentration [25].

Table 2 collects charge ratios of hyaluronan:surfactant and their changes for all studied CTAB+MMW hyaluronan systems where the gel-phase separation was observed. The charge ratio was calculated taking the determined hyaluronan molecular weight into account and supposing the existence of one charge on each surfactant molecule and one charge per hyaluronan basic dimeric unit (sodium form) with a molecular weight of 401.299 g/mol. It is clearly seen that the charge ratio need not be the controlling parameter, either for the critical aggregation concentration or for the phase separation in contrast to the situation found in more concentrated systems [6,7]. The critical aggregation concentration is located between the charge ratio values from 1.3 to 50 depending on the hyaluronan concentration; the value of the charge ratio corresponding to the critical aggregation concentration seems to increase with the increasing hyaluronan concentration. On the other hand, regardless of the hyaluronan concentration, the value of the critical aggregation concentration is located approximately around the same surfactant concentration value of 0.01 mM (specific values of the critical aggregation concentration are shown in Table 3). Thus, the hyaluronan concentration seems to be a much more important parameter for the induced micellar aggregation in (very) diluted hyaluronan solutions.

Except for the lowest and highest hyaluronan concentrations, the first gel-phase separation occurs when the charge ratio decreased somewhat below 1 (viz. 0.4–0.9), i.e., when the surfactant concentration slightly exceeded the point of the charge equilibration. In the case of the lowest hyaluronan concentration, this occurs at a higher surfactant concentration still (i.e., lower charge ratio), whereas at the highest hyaluronan concentration, this occurs at a lower surfactant concentration (higher charge ratio) already. The gel-phase evidently contains micelles, which should be considered as crosslinking points of the formed gel. The destabilization caused by the charge equilibration around the

Table 2
Charge ratios of investigated samples; the blue lines indicate the location of the critical aggregation concentrations; the values in italics indicate the phase separated samples. System with CTAB and MMW hyaluronan.

c_{CTAB} (mM)	Hyaluronan concentration (mg/L)				
	5	15	30	50	100
	Charge ratio				
0.0005	25	75	150	249	498
0.001	12	37	75	125	249
0.002	6	19	37	62	125
0.005	2	7.5	15	25	50
0.01	1.25	3.7	7.5	12	25
0.02	0.62	1.9	3.7	6	12
0.03	0.42	1.2	2.5	4	8
0.04	0.31	*0.9*	1.9	3	6
0.05	0.25	*0.7*	1.5	2.5	5
0.06	0.21	*0.6*	1.2	2.1	4
0.08	*0.16*	0.47	0.9	1.6	*3*
0.1	*0.12*	0.37	0.7	1.2	*2.5*
0.15	*0.08*	0.25	*0.5*	*0.8*	1.7
0.2	0.06	0.19	*0.4*	*0.6*	1.2
0.25	0.05	0.15	0.3	*0.5*	1.0
0.3	0.042	0.12	0.25	0.42	0.8
0.35	*0.036*	*0.11*	*0.21*	*0.36*	*0.7*
0.4	0.031	*0.09*	*0.19*	*0.31*	*0.6*
0.5	0.025	0.07	0.15	*0.25*	*0.5*
0.6	0.021	0.06	0.12	0.21	*0.42*
0.7	0.018	0.05	0.11	0.18	0.36
0.8	0.016	0.047	0.09	0.16	0.31
0.9	0.014	0.042	0.08	0.14	0.28
1	0.012	0.037	0.07	0.12	0.25
1.5	0.008	0.025	0.05	0.08	0.17
2	0.006	0.019	0.04	0.06	0.12
3	0.004	0.012	0.02	0.04	0.08

charge ratio of one proceeds via attaching, on average, one micelle to at least two hyaluronan chains, thus forming a crosslink. When the hyaluronan concentration is too low, this type of "bridging" is more difficult due to the increased distance between the encountered chains and needs a higher concentration of surfactant (micelles). On the other hand, at a sufficiently high polymer concentration, such "bridging" is more likely to occur even at a lower surfactant concentration.

The second gel-phase separation is found for a relatively broad interval of charge ratio ranging from 0.036 to 0.7. The corresponding surfactant concentration region is much narrower – from 0.35 to 0.6 mM – and particularly, the concentration of the starting point of the second gel-phase separation was always the same (0.35 mM). Thus, as in the case of critical aggregation concentration, it seems that a specific surfactant concentration is more substantial for the occurrence of the second gel-phase separation. Upon an increased hyaluronan concentration, an increased amount of the gel phase was observed – more biopolymer chains are available for the gel formation.

The values of ExPI provide some information about the hydrophobicity-hydrophilicity of the environment of the fluorescing pyrene molecules. The two parameters of the Boltzmann model equation giving the (limiting) ExPI values at the maximum and minimum of the corresponding S-curve are shown in Table ST1 in the Supplementary material. The parameter A_1 and A_2 reflect the situation before aggregation (micellization) and after its completion, respectively. Regardless of the hyaluronan concentration, A_1 is around 3.2–3.3 in the region of the induced aggregation. This ExPI value corresponds to the pyrene fluorescence from the aqueous environment and its independence from the hyaluronan concentration indicates that pyrene does not interact with it or with surfactant monomers before the onset of the aggregation and that there are no aggregates with a hydrophobic core in the system. The lowered value of A_2 in the region of the induced aggregation is due to the pyrene solubilization in the hydrophobic core of the formed micellar structures. Its value decreases somewhat with the increasing hyaluronan concentration which is probably the result of the formation

Table 3
Critical aggregation (CAC) and micelle (CMC) concentration summary.

M_w HyA (kDa)	c HyA (mg/L)	CAC (mM)		CMC (mM)	
		CTAB	Septonex	CTAB	Septonex
MMW	5	0.009 ± 0.001	–	0.92 ± 0.70	–
LMW	15	0.007 ± 0.001	0.022 ± 0.001	0.79 ± 0.02	0.90 ± 0.03
MMW	15	0.007 ± 0.001	–	0.77 ± 0.16	–
HMW	15	0.008 ± 0.001	0.024 ± 0.001	0.74 ± 0.13	0.88 ± 0.02
MMW	30	0.014 ± 0.001	–	0.74 ± 0.08	–
MMW	50	0.014 ± 0.001	–	0.81 ± 0.15	–
MMW	100	0.009 ± 0.001	–	0.97 ± 0.01	–
Water		–	–	0.98 ± 0.01	0.75 ± 0.02

of a higher number of solubilizing aggregates on the higher number of hyaluronan chains in the system.

A similar dependence on hyaluronan concentration is observed for the values of the parameter A_1 in the micellization region which brings information on the system before the free micelle formation. Its values are comparable to those of A_2 in the aggregation region as expected. The value of A_2 evaluated for the micellization region is independent to the hyaluronan concentration and corresponds to the values found for free micelles of the pure surfactant solution in water. This is in agreement with the supposed formation of free micelles in this region.

The effect of the molecular weight of hyaluronan on the aggregation of CTAB in water was studied. The concentration series of the surfactant with hyaluronan at a concentration of 15 mg/L and different molecular weights were prepared. When hyaluronan of different molecular weights was used, no significant changes were observed during the aggregation process and the curves of all the measured parameters had very similar shapes. This was confirmed by the fact that Boltzmann fits to these curves also, which resulted in very similar parameter values for all investigated hyaluronan molecular weights.

Finally, Table 3 summarizes the critical aggregation and micelle concentration values for the different hyaluronan concentrations as well as for the different hyaluronan molecular weights. These values were calculated as averages of the values obtained from the Boltzmann model equations for EmPI and ExPI dependencies. It can be seen that the critical aggregation concentration values are about two orders of magnitude lower than the critical micelle concentration values. The hyaluronan molecular weight had no significant effect on the interactions in these systems.

Based on our results, the phase diagram of this system could be specified in the (very) diluted area. The diagrams published in refs. [14,17] are very crude in this domain and indicate a broad, single, two-phase region with a notice on the "larger uncertainty in this region". Although the diagram published by Fukada et al. [19] gives more details (for decyltrimethylammonium bromide), it is still rather crude and does not report on the gel separation. The phase diagram constructed on the basis of our florescence measurements for the MMW hyaluronan system is shown in Fig. 3 and includes, not only areas of macroscopic phase separations, but different states of aggregates formation also. The surfactant concentration is given in a logarithmic scale due to the broad range of the tested concentrations; a cut-out containing the low surfactant concentrations in a linear scale can be seen in the Supplementary material (Fig. SF4 in the Supplementary material).

3.3. Salt effect on CTAB-hyaluronan interactions

The effect of ionic environment was studied with hyaluronan at all three different molecular weights and at the concentration of 5 mg/L. A phosphate buffer at pH = 7.0 was used instead of water. In all cases, the dependencies of the ExPI or EmPI parameters on the surfactant concentration had a simple sigmoidal shape with the inflex point at around the same surfactant concentration. In other words, no formation of the induced micelles at concentrations below the critical micellar concentration of the pure surfactant was detected. Furthermore, no gel-phase separation was observed. An example of the experimental data is shown in Fig. 4. The critical aggregation concentrations and the fitted parameters of the Boltzmann equation can be found in the Supplementary material (Table ST2). Again, no significant effect of the hyaluronan molecular weight was found. The value of the A_2 parameter of the fit with the Boltzmann equation was about 1.08 for all studied samples which indicates a similar polarity of the pyrene environment in all systems. A slightly more abrupt EmPI (or ExPI) decrease was observed in the presence of hyaluronan (see the inset in Fig. 4) giving somewhat smaller values of the parameter Δx.

These observations can be explained in accordance with the published experience as a result of screening the electrostatic interactions between the surfactant and hyaluronan which are the main cause of the sub-micellar aggregation and the formation of the induced micelles, as well as the formation of the gel-phase. Increased ionic strength is known to lead to dissolution of complexes made by polyelectrolytes and oppositely charged colloids [9,18].

3.4. Septonex

In addition, the aggregation of hyaluronan with the Septonex surfactant was investigated. The purpose was to check the effect of small variations in the surfactant structure. Septonex differs from CTAB in the presence of an ethoxycarbonyl-group close to the trimethylammonium group and has a hydrophobic chain of fifteen carbon atoms. The principal difference is, thus, in the structure of the polar head. Hyaluronan of two molecular weights (LMW and HMW) at the concentration of 15 mg/L was selected for this study. Generally, no principal differences were found – "double" S-curves were also observed indicating the formation of the induced and free micelles. However, in contrast to CTAB, only one separation region of the gel-phase was observed, see Fig. SF5 in the Supplementary material. This separation was observed in the surfactant concentration range from 0.07 to 0.6 mM, which is in a broader interval compared to CTAB. It seems that Septonex has a broader region in contrast to CTAB which had two narrower regions of the gel-phase

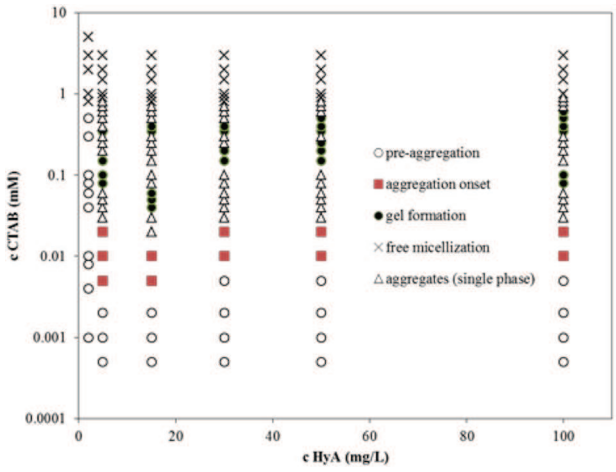

Fig. 3. Phase diagram of the CTAB-hyaluronan (MMW) system in the diluted region estimated on the basis of the fluorescence measurements.

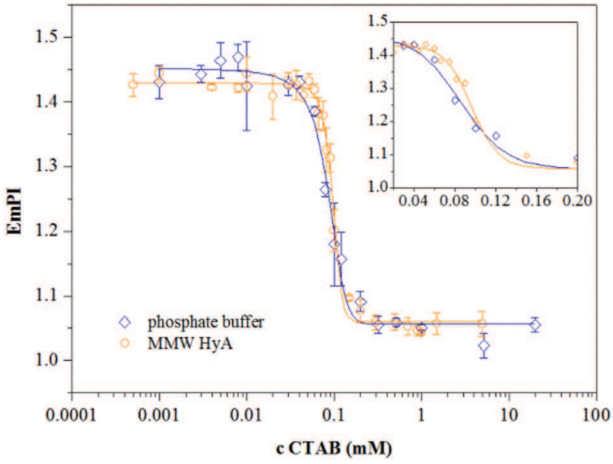

Fig. 4. EmPI dependence on the surfactant (CTAB) concentration in the phosphate buffer without the addition of hyaluronan and with the addition of MMW hyaluronan at a concentration of 5 mg/L. The inset shows the aggregation region only, in a linear scale.

separation in the approximate same concentration interval. At the same time, the region of the (induced) aggregation is broader and the first decrease of ExPI is less steep than in the case of CTAB (see also the Boltzmann model parameters in Table ST3 in the Supplementary material). As a results of the width of the aggregation region and of the corresponding steepness of ExPI decrease, the critical aggregation and micelle concentration are higher for Septonex compared to CTAB (Table 3): This is probably result of the more bulkier structure of the ethoxycarbonyl-substituted charged group of Septonex which sterically complicates the formation of Septonex aggregates on the hyaluronan chain. The critical micelle concentration of pure Septonex in water is somewhat lower than that of CTAB (Table 1) which can be also due to the effects of the bulky Septonex polar head – the liquid surface is filled at a lower concentration of the more spacious Septonex monomers and then the micellar aggregation in the bulk begins at the lower concentration.

3.5. Stability of CTAB/Septonex–hyaluronan system

Due to the potential applications of hyaluronan-surfactant aggregates as delivery systems, a basic stability study was performed testing their storage stability and resistance to temperature changes, with the addition of an electrolyte and against dilution. The stability was checked by detecting changes in fluorescence probe characteristics and in particle sizes measured by dynamic light scattering.

The stability experiments were realized with a single hyaluronan concentration of 15 mg/L and two surfactant concentrations located behind the critical aggregation concentration in the homogeneous region, just before the gel-phase separation (0.02 and 0.03 mM in the case of CTAB, 0.05 and 0.07 mM in the case of Septonex). Hyaluronans of two molecular weights (LMW and HMW) were tested.

Generally, no significant differences in the stability between the CTAB and Septonex systems were found. The size distributions of both types of the systems before any temperature changes or composition modifications, were almost the same or very similar. Shifts of maximum of size distribution showed no significant trends which would depend on the surfactant. The fluorescence indices EmPI and ExPI indicated a similar polarity in both systems under the given conditions, whereas the Ex:Mo parameters were slightly lower for systems containing Septonex compared to the system with CTAB, probably due to various critical aggregation and critical micelle concentrations in the systems with CTAB and Septonex. Only the results obtained for the Septonex systems are discussed.

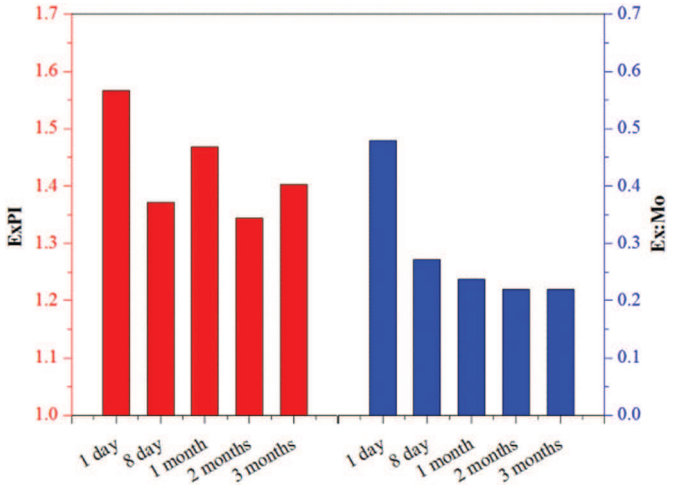

Fig. 5. Dependency of the ExPI and Ex:Mo parameters on the storage time for systems containing 0.05 mM of Septonex and 15 mg/L of HMW hyaluronan.

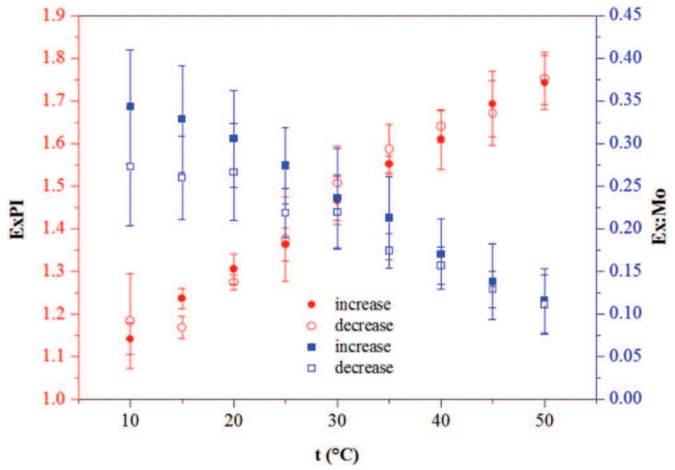

Fig. 6. Dependency of the ExPI and Ex:Mo parameters on an increasing (full symbols) or decreasing (empty symbols) temperature for systems containing 0.05 mM of Septonex and 15 mg/L of LMW hyaluronan.

3.5.1. Time stability

The pyrene polarity indices did not show changes pointing to disaggregation during the three months of storage at 4 °C; for example, see Fig. 5. ExPI values of about 1.3 correspond to the occurrence of the induced micelles in the systems after the critical aggregation concentration. This indicates the stability of the formed hydrophobic domains and their solubilization abilities. The excimer to monomer ratio decreased in time, especially after about one month of storage. This points to an uneven distribution of the solubilized pyrene molecules just after the preparation of the samples. During storage, pyrene is redistributed more evenly and, thereby, the probability of excimer formation is reduced. This can be viewed like some "ripening" of the system containing solubilized hydrophobes. All of the studied systems showed similar trends in the fluorescence parameters.

From the point of view of the particle size distribution, it was found that distributions changed only negligibly and systems remained monodisperse. Particle sizes were mostly in the range of 100–400 nm (see Fig. SF6 in the Supplementary material).

3.5.2. Temperature stability

The polarity indices EmPI and ExPI slightly increased or were around constant values with the increasing temperature in the investigated

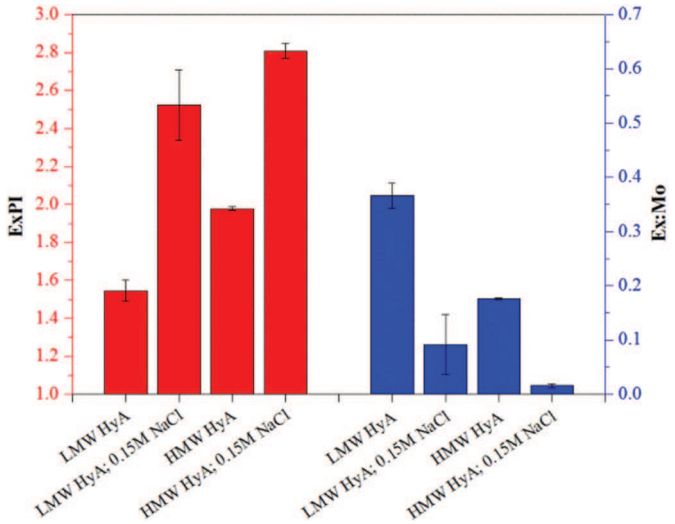

Fig. 7. Polarity index of the ExPI and Ex:Mo ratio changes after the NaCl addition to the Septonex (0.05 mM)-hyaluronan (15 mg/L) system.

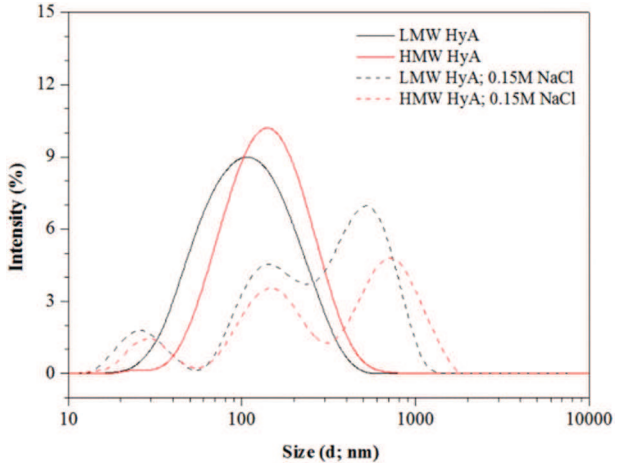

Fig. 8. Particle size distribution of the Septonex (0.05 mM)-hyaluronan (15 mg/L) system in water (solid line) and after the NaCl addition (dashed line).

range of 10–50 °C. The most significant change of polarity indices showed the system with the surfactant concentration of 0.05 mM in combination with LMW hyaluronan (Fig. 6). The recorded polarity changes showed that the aggregate shell becomes less compact at a higher temperature, probably due to the increased mobility of the surfactant molecules, and enables water penetration closer to the hydrophobic inner core. The polarity indices values at high temperatures were not far from the situation where micelle aggregates are disintegrated and pyrene molecules emit from the aqueous environment. The Ex:Mo ratio decreased with the increased temperature corresponding to the decreased probability of excimer formation. This is, again, a result of pyrene redistribution also connected to the loosened aggregates structure. It should be noted that structural changes in the system are reversible, the fluorescence parameters approximately return to the original values after returning the temperature from 50 °C to 10 °C. The aggregates can be viewed as stable in a heating-cooling cycle.

3.5.3. Effect of ionic strength

As stated in Section 3.3 above, the presence of a low molecular weight electrolyte in the system during the mixing of the hyaluronan and surfactant solutions had a profound effect on their mutual interactions. Here, the stability of the hyaluronan-surfactant aggregates prepared in pure water against the addition of NaCl at a physiological concentration was tested. The polarity indices showed significant increases after the addition of NaCl (remember the negligible volume change, i.e. dilution) indicating the disintegration of the aggregates in the system which corresponds to the EmPI and ExPI values of about 1.5 and 2.6, respectively. The Ex:Mo parameter decreased which corresponds to the structural changes in the system, which occurs as a result of the screening of the electrostatic attraction in the system after the NaCl addition (Fig. 7). Structural changes showed up in the size distribution of the system too. In the case of an aqueous solution, the system was monodisperse and the particle sizes were in the range of 100–150 nm. After the NaCl addition (in the physiological solution), the system became polydisperse and the particle sizes were in the range from 30 nm to 2200 nm with three maxima (Fig. 8).

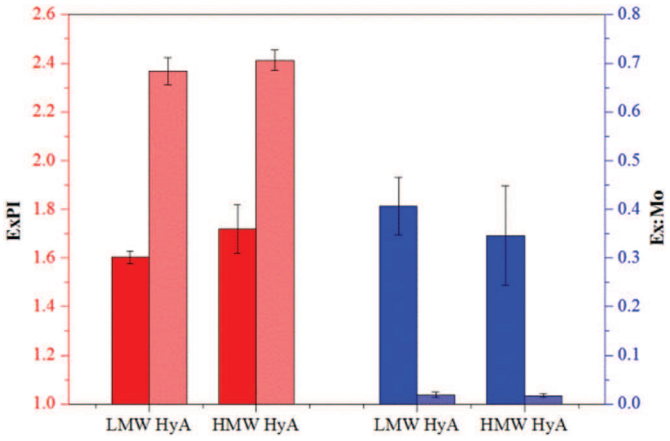

Fig. 9. The polarity index ExPI and the Ex:Mo ratio in the Septonex (0.05 mM)-hyaluronan (15 mg/L; two different molecular weights) system before (darker columns) and after dilution (lighter columns).

3.5.4. Effect of dilution

After dilution by hyaluronan solution, the polarity indices increased and the probability of excimer formation (the Ex:Mo ratio) decreased significantly (Fig. 9); the values of all fluorescence ratios roughly corresponded to the values found before the induced aggregates formation during the experiments discussed in Section 3.4 above. These changes should be attributed to the disintegration of the aggregates in the system and demonstrate the reversibility of the aggregates formation. Consequently, the aggregates are not sufficiently stable to maintain a hydrophobic solute in their interior upon dilution. In comparison to the gel phase, which could not be dissolved in pure water, the electrostatic and hydrophobic [26] interactions holding the aggregates in non-separated, clear systems are weaker.

4. Conclusions

The phase behavior of aqueous systems containing hyaluronan and oppositely charged surfactants was investigated in a very diluted region, i.e., at hyaluronan concentrations between 2 and 100 mg/L. The fluorescence probe technique with pyrene showed a typical double-S dependency of pyrene polarity indices on the surfactant concentrations in non-phase separating systems for the first time in hyaluronan-containing systems, no previous worked reported this. This confirmed the formation of micellar structures induced by the presence of the oppositely charged hyaluronan well below the standard critic al micellar concentration. Moreover, regions of the gel-phase separation were also revealed. The gels incorporated the majority of the micellar structures, which are supposed to form the crosslinks in the gel network. The phase diagram could be specified in the very diluted region. The hyaluronan concentration, not the polyelectrolyte:surfactant charge ratio was found to be the main parameter controlling the phase behavior.

Aggregates formed in the homogeneous systems, represented by hyaluronan chains with induced micelles attached, were stable during storage for three months, but were sensitive to various disturbances. The smallest effect was found for the heating and cooling cycle, which caused reversible changes in the aggregates structure. Significant changes, the destabilization of the aggregates and the release of a solubilized hydrophobic substance, were observed upon dilution (by hyaluronan solution) or the increase of the ionic strength. Their potential application as delivery systems of hydrophobes is, thus, questionable.

Acknowledgement

This work was supported by the Czech Science Foundation (project No. 16-12477S); the Materials Research Centre is supported by the Ministry of Education, Czech Republic (project No. LO1211).

Appendix A. Supplementary data

Supplementary data to this article can be found online at https://doi.org/10.1016/j.ijbiomac.2018.01.176.

References

[1] P. Prehm, Hyaluronan, in: A. Steinbüchel, R.H. Marchessault (Eds.), Biopolymers for Medical and Pharmaceutical Applications, vol. 1, Wiley-VCH, Weinheim 2005, pp. 617–644.
[2] A. Fakhari, C. Berkland, Applications and emerging trends of hyaluronic acid in tissue engineering, as a dermal filler and in osteoarthritis treatment, Acta Biomater. 9 (2013) 7081–7092.
[3] G. Kogan, L. Šoltés, R. Stern, P. Gemeiner, Hyaluronic acid: a natural biopolymer with a broad range of biomedical and industrial applications, Biotechnol. Lett. 29 (2006) 17–25.
[4] K. Dicker, L. Gurski, S. Pradhan-Bhatt, R. Witt, M. Farach-Carson, X. Jia, Hyaluronan: a simple polysaccharide with diverse biological functions, Acta Biomater. 10 (2014) 1558–1570.
[5] M. Hemshekhar, R. Thushara, S. Chandranayaka, L. Sherman, K. Kemparaju, K. Girish, Emerging roles of hyaluronic acid bioscaffolds in tissue engineering and regenerative medicine, Int. J. Biol. Macromol. 86 (2016) 917–928.
[6] I. Hoffmann, P. Heunemann, S. Prévost, R. Schweins, N. Wagner, M. Gradzielski, Self-aggregation of mixtures of oppositely charged polyelectrolytes and surfactants studied by rheology, dynamic light scattering and small-angle neutron scattering, Langmuir 27 (2011) 4386–4396.
[7] K. Holmberg, B. Jönsson, B. Kronberg, B. Lindman, Surfactants and Polymers in Aqueous Solution, second ed. John Wiley, Hoboken, 2003.
[8] H. Bao, L. Li, L. Gan, H. Zhang, Interactions between ionic surfactants and polysaccharides in aqueous solutions, Macromolecules 41 (2008) 9406–9412.
[9] E. Kizilay, A.B. Kayitmazer, P.L. Dubin, Complexation and coacervation of polyelectrolytes with oppositely charged colloids, Adv. Colloid Interf. Sci. 167 (2011) 24–37.
[10] Y. Lapitsky, Ionically crosslinked polyelectrolyte nanocarriers: recent advances and open problems, Curr. Opin. Colloid Interface Sci. 19 (2014) 122–130.
[11] L. Chiappisi, I. Hoffmann, M. Gradzielski, Complexes of oppositely charged polyelectrolytes and surfactants – recent developments in the field of biologically derived polyelectrolytes, Soft Matter 9 (2013) 3896–3909.
[12] S. Aidarova, A. Sharipova, J. Krägel, R. Miller, Polyelectrolyte/surfactant mixtures in the bulk and at water/oil interfaces, Adv. Colloid Interf. Sci. 205 (2014) 87–93.
[13] K. Thalberg, B. Lindman, Interaction between hyaluronan and cationic surfactants, J. Phys. Chem. 93 (1989) 1478–1483.
[14] K. Thalberg, B. Lindman, G. Karlstroem, Phase diagram of a system of cationic surfactant and anionic polyelectrolyte: tetradecyltrimethylammonium bromide-hyaluronan-water, J. Phys. Chem. 94 (1990) 4289–4295.
[15] A. Hersloef, L. Sundeloef, K. Edsman, Interaction between polyelectrolyte and surfactant of opposite charge: hydrodynamic effects in the sodium hyaluronate/tetradecyltrimethylammonium bromide/sodium chloride/water system, J. Phys. Chem. 96 (1992) 2345–2348.
[16] M. Bjoerling, A. Hersloef-Bjoerling, P. Stilbs, An NMR self-diffusion study of the interaction between sodium hyaluronate and tetradecyltrimethylammonium bromide, Macromolecules 28 (1995) 6970–6975.
[17] K. Thalberg, B. Lindman, G. Karlstroem, Phase behavior of systems of cationic surfactant and anionic polyelectrolyte: influence of surfactant chain length and polyelectrolyte molecular weight, J. Phys. Chem. 95 (1991) 3370–3376.
[18] K. Thalberg, B. Lindman, G. Karlstroem, Phase behavior of a system of cationic surfactant and anionic polyelectrolyte: the effect of salt, J. Phys. Chem. 95 (1991) 6004–6011.
[19] K. Fukada, E. Suzuki, T. Seimiya, Rheological properties of sodium hyaluronate in decyltrimethylammonium bromide aqueous solutions, Langmuir 15 (1999) 4217–4221.
[20] K. Thalberg, J. Stam, C. Lindblad, M. Almgren, B. Lindman, Time-resolved fluorescence and self-diffusion studies in systems of a cationic surfactant and an anionic polyelectrolyte, J. Phys. Chem. 95 (1991) 8975–8982.
[21] N. Li, S. Liu, H. Luo, A new method for the determination of the first and second CMC in CTAB solution by resonance Rayleigh scattering technology, Anal. Lett. 35 (2002) 1229–1238.
[22] E. Fuguet, C. Ràfols, M. Rosés, E. Bosch, Critical micelle concentration of surfactants in aqueous buffered and unbuffered systems, Anal. Chim. Acta 548 (2005) 95–100.
[23] G. González-Gaitano, A. Crespo, G. Tardajos, Thermodynamic investigation (volume and compressibility) of the systems β-cyclodextrin n-alkyltrimethylammonium bromides water, J. Phys. Chem. B 104 (2000) 1869–1879.
[24] V. Mosquera, J. del Río, D. Attwood, M. García, M. Jones, G. Prieto, M. Suarez, F. Sarmiento, A study of the aggregation behavior of hexyltrimethylammonium bromide in aqueous solution, J. Colloid Interface Sci. 206 (1998) 66–76.
[25] T. Halasová, J. Krouská, F. Mravec, M. Pekař, Hyaluronan-surfactant interactions in physiological solution studied by tensiometry and fluorescence probe techniques, Colloids Surf. A Physicochem. Eng. Asp. 391 (2011) 25–31.
[26] A. Kargerová, M. Pekař, High-resolution ultrasonic spectroscopy study of interactions between hyaluronan and cationic surfactants, Langmuir 30 (2014) 11866–11872.
[27] J. Oremusová, Z. Vitková, P. Herdová, Influence of alcohols on micellar and release balances of cationic surfactant – carbethopendecinium bromide (Septonex), Tenside Surfactant Deterg. 51 (2014) 339–347.
[28] O. Greksáková, J. Oremusová, M. Vojteková, F. Kopecký, Spectrophotometric study of the effect of univalent electrolytes on critical micelle concentrations of [1-(ethoxycarbonyl)pentadecyl]trimethylammonium, 1-hexadecylpyridinium, and dimethylbenzyldodecylammonium bromides, Chem. Pap. 48 (1994) 300–305.
[29] L. Čermáková, J. Rosendorfová, M. Malát, Determination of critical micelle concentration of 1-carbethoxypentadecyltrimethylammonium bromide, ChemPlusChem 45 (1980) 210–213.
[30] H. Vink, Rheology of dilute polyelectrolyte solutions, Polymer 33 (1992) 3711–3716.
[31] M. Rinaudo, M. Milas, N. Jouon, R. Borsali, On some original properties of dilute polyelectrolyte solutions at low salt content: sodium hyaluronate example, Polymer 34 (1993) 3710–3715.
[32] K. Kogej, J. Škerjanc, Surfactant binding to polyelectrolytes, in: T. Radeva (Ed.), Physical Chemistry of Polyelectrolytes, Surfactant Science Series, vol. 99, Marcel Dekker, New York 2001, pp. 794–796.

Colloids and Surfaces A: Physicochem. Eng. Aspects 391 (2011) 25–31

Contents lists available at ScienceDirect

Colloids and Surfaces A: Physicochemical and Engineering Aspects

journal homepage: www.elsevier.com/locate/colsurfa

Hyaluronan-surfactant interactions in physiological solution studied by tensiometry and fluorescence probe techniques

T. Halasová, J. Krouská, F. Mravec, M. Pekař*

Brno University of Technology, Faculty of Chemistry, Centre for Materials Research CZ.1.05/2.1.00/01.0012, Purkyňova 118, Brno CZ-61200, Czech Republic

ARTICLE INFO

Article history:
Received 24 February 2011
Received in revised form 16 May 2011
Accepted 18 May 2011
Available online 27 May 2011

Keywords:
Fluorescence probes
Hyaluronan
Polyelectrolyte-surfactant interactions
Surfactants

ABSTRACT

Interactions of hyaluronan of two molecular weights with surfactants of different types were studied in NaCl solution. Results showed that although the presence of NaCl may suppress interactions between oppositely charged polyelectrolyte and surfactant, the interactions are still present in some hyaluronan-surfactant systems regardless the surfactant ionic nature. These interactions were demonstrated mainly by fluorescence probe techniques whereas tensiometry detected only minor effects. Fluorescence data showed that formation of aggregates (micelles) occurs rather in a certain interval of surfactant concentrations than in a single point, especially in the presence of hyaluronan. The greatest influence of hyaluronan was observed on nonionic Tween 20 and cationic cetyl trimethylammonium bromide.

1. Introduction

Hyaluronan is a naturally occurring polysaccharide, commonly found in connective tissues in the body such as vitreous, umbilical cord and joint fluid [1]. As a component of the extracellular matrix, hyaluronan plays an important role in lubrication, water sorption, water retention, and a number of cellular functions such as attachment, migration, and proliferation [2–6]. Hyaluronan is therefore an attractive building block for new biocompatible and biodegradable polymers that have applications in drug delivery, tissue engineering, and viscosupplementation [7–9]. It is a negatively charged monotonic co-polymer with repeating disaccharide unit composed of D-glucuronate and N-acetyl-D-glucosamine residues linked by β(1–4) and β(1–3) bonds, which are connected to unbranched chains [10].

Hyaluronan is a unique molecule not only from the view of physical properties but also from the view of its biological properties. It is of great interest that such a simple molecule that hyaluronan can exercise so many biological functions. In tissues, hyaluronan is mostly found as a high-molecular compound. In addition to these macromolecules there are also products of hyaluronan degradation in tissues, fragments with much lower molecular weight. Just in different molecular weights of hyaluronan lies the diversity of its biological functions [4,5].

Cells posses several specific receptors recognizing hyaluronan, among them CD44 is probably the most important, which further enhances its potential for application in targeted drug delivery systems. Hyaluronan is highly hydrophilic biopolymer with massive hydration shell and cannot be directly used to carry nonpolar substances. Because many efficient drugs, e.g. for fighting cancer, are hydrophobic, hyaluronan has been chemically modified, hydrophobized, to induce micelle-like properties or directly conjugated with hydrophobic biologically active molecules (drugs). Besides chemical modifications which could change also biological activity or compatibility of hyaluronan, physical interactions with suitable molecular partner may be another way to solubilize hydrophobes in the presence of hyaluronan. For example, combination of hyaluronan with surfactant may lead to formation of associates in which the surfactant hydrophobic domains solubilize hydrophobes and hyaluronan plays a role of biocompatible carrier and targeting agent.

Hyaluronan-surfactant interactions were subject of several previous studies. Because of negative hyaluronan charge almost all of them used cationic surfactants. Only Yin et al. [11] reported some results obtained with anionic and nonionic surfactants. Hyaluronan interactions with cationic surfactants were studied as a specific case of general polyelectrolyte-surfactant interactions to elucidate their phase behavior and physical causes of their interactions including the effect of electrolytes. Little is still known about solubilization in hyaluronan-surfactant associates, especially at physiological ionic conditions.

Detailed study on phase behavior of systems containing water, hyaluronan, alkyl trimethylammonium bromides (tetradecyl derivative was the most studied type) and salt (mostly NaBr)

* Corresponding author. Tel.: +420 541149330; fax: +420 541149398.
E-mail addresses: xchalasova@fch.vutbr.cz (T. Halasová), xckrouska@fch.vutbr.cz (J. Krouská), mravec@fch.vutbr.cz (F. Mravec), pekar@fch.vutbr.cz (M. Pekař).

0927-7757/$ – see front matter © 2011 Elsevier B.V. All rights reserved.
doi:10.1016/j.colsurfa.2011.05.035

was published in a series of papers by Swedish researchers [12–18]. They found that there is a certain cationic surfactant concentration below which only general electrostatic interactions take place and only above it marked formation of hyaluronan-surfactant complexes can be observed. Their results indicated strong cooperativity of surfactant binding on hyaluronan macromolecule resulting in binding in the form of micelle-like clusters in which both hyaluronan carboxylates and background electrolyte anions participate as counterions. Increasing electrolyte (salt) concentration disfavored formation of hyaluronan-bound micelles in comparison to free micelles. The authors constructed phase diagrams for studied systems which essentially contain an area of homogeneous single phase surrounding two-phase region. Phase separation was observed as formation of precipitate or gel-like phase upon increasing surfactant concentration. Increasing concentration of added salt reduced the two-phase area unless the salt concentration was very high when phase separation occurred again. Binding of surfactant to hyaluronan was detected for surfactants with alkyl chain consisting from at least ten carbon atoms. The longer the surfactant alkyl chain the larger two-phase region was observed.

Yin et al. [11] used pyrene fluorescence to investigate interactions of (high molecular weight) hyaluronan with anionic sodium dodecyl sulfate (SDS) and nonionic Cremophor EL and Tween 80 in water. Practically no interactions between hyaluronan and nonionics were detected whereas certain decrease of SDS critical micellar concentration was observed. Hyaluronan in SDS solutions thus acts similarly as low molecular weight electrolyte as demonstrated by similar experiments with surfactant solutions free of hyaluronan but containing sodium chloride. This was explained by interactions of SDS polar heads with domains formed by hyaluronan hydroxyls.

The aim of this work was to obtain additional information on hyaluronan-surfactant interactions in solutions with physiological salt concentration by tensiometry and fluorescence probe techniques. Tensiometry gives information primarily on the solution surface layers and interactions therein and indirectly information on the bulk solution, especially on micellization (aggregation). Fluorescence probe informs on its local environment in solution, on domains where it can be dissolved or solubilized in solution. From this information deductions on aggregation in solution can be also made and on solubilizing properties of domains formed by aggregates. All this information is a base for design of hyaluronan-surfactant systems for targeted delivery of nonpolar biologically active substances (e.g., drugs). Fluorescence technique is not limited here to pyrene, perhaps the most popular probe for aggregation studies and determining critical micellar concentrations. Nile red was used as an additional, comparative probe that can also provide additional information on solubilizing hydrophobic domains [19–21]. Though pyrene is considered to be nonpolar its limited solubility in water is still high enough to produce remarkable fluorescence signal. Nile red fluorescence is quenched by water [22,23] therefore only those molecules give sufficient fluorescence intensity that is in the water-free domains. Pyrene as well as nile red can interact with charged parts of ionic surfactants. This means that both probes are located in the micellar palisade layer which still contains some water molecules. Whereas pyrene fluorescence occurs also from aqueous environment the nile red fluorescence from the water-rich palisade layer should be quenched. In the case of non-ionic surfactant also hydrogen bond interactions can be expected between nile red and surfactant. Direct interaction of this probe with surfactant can decrease its fluorescence intensity.

2. Materials and methods

Hyaluronan of two molecular weights (90 kDa and 1.4 MDa, i.e. the low and high molecular weight, respectively) was purchased from CPN, Ltd., Czech Republic. Surfactants tetradecyl trimethylammonium bromide (TTAB, cationic), cetyl trimethylammonium bromide (CTAB, cationic), cetyl trimethylammonium p-toluene sulfonate (CTAT, cationic), sucrose monolaurate (nonionic), octyl-β-D-glucopyranoside, and Tween 20 (nonionic) were from Sigma–Aldrich (Czech Republic); sodium dodecyl sulfate (SDS, anionic) and n-dodecyl-β-D-maltoside (nonionic) were purchased from Fluka (Czech Republic). Zwitterionic betaine surfactants Betadet THC 2 and cetyl betaine were purchased from Chemos (Czech Republic). All surfactants were of the best available quality and used as received without further purification.

Stock solutions of hyaluronan in physiological solution (0.15 mol/l NaCl) were prepared in concentration of 0.5% (w/v) by slowly adding solid hyaluronan to the salt solution under stirring, followed by 24 h stirring in closed vessel to ensure complete dissolution. Hyaluronan stock solution was then used to prepare samples for tensiometry and fluorescence measurements with final constant hyaluronan concentration of 0.1% (w/v).

Samples with varying surfactant concentration and no hyaluronan were prepared by simple diluting surfactant stock solution prepared in 0.15 mol/l NaCl at concentration about ten times higher than its critical micellar concentration in this salt solution. Samples with varying surfactant concentration and containing hyaluronan (0.1%, w/v) were prepared by mixing hyaluronan (10 ml) and surfactant stock solutions and diluting with the physiological solution to the final volume of 15 ml (no phase separation was observed). The samples with hyaluronan were stabilized with NaN_3 (0.05%, w/v) and stirred overnight.

Surface tension measurement was performed with a platinum/iridium Du Noüy ring (diameter 9.545 mm) on tensiometer KSV Sigma 701 at room temperature.

Aggregation and solubilization properties were studied by means of two fluorescence probes – pyrene and nile red. Stock solutions of both fluorescence probes were prepared in volatile solvent – acetone (10^{-4} mol/l). An amount of stock solution to obtain final concentration of pyrene or nile red in samples equal to 10^{-6} mol/l was added to glass vial and acetone was evaporated under reduced pressure. Then 3 ml of hyaluronan or hyaluronan-surfactant solution was added to vial with fluorescent probe and incubated for 24 h at laboratory temperature.

Fluorescence emission spectra were recorded on AMINCO Bowman Series 2 fluorescence spectrometer. In the case of pyrene the excitation wavelength was 336 nm and emission scan was acquired in the range from 360 to 540 nm. Nile red was excited at 550 nm and emission spectra were recorded from 610 to 700 nm.

All measurements were done in duplicates, at least. Confidence intervals in table and error bars (shown when not smaller than the symbols) in figures represent the standard deviation.

Pyrene experiments were evaluated by plotting the intensity ratio I_1/I_3 (the pyrene polarity index or the ratio of fluorescence intensities at 373 and 383 nm) against surfactant concentration [24]. Typical sigmoidal curve was obtained indicating formation of nonpolar domains (micelles with hydrophobic cores) solubilizing pyrene molecules. Ideally, a sharp step change would be observed at the critical micellar concentration. However, the change was usually more or less broadened indicating micellization (aggregation) region (concentration range within which the polarity index decreases) rather than single point. Curves were fitted by Boltzmann equation and inflex point in the micellization region was considered as an estimate of critical micellar concentration. From the Boltzmann equation also points (concentrations) of beginning and end of the micellization region, i.e. the width of this region, can be obtained.

Nile red fluorescence spectra were evaluated by two methods. The first one was plotting normalized values of the total integral of fluorescence intensity (in the wavelength range 610–700 nm)

Table 1
Effect of low (LMW) and high (HMW) molecular weight hyaluronan (HyA) on the critical micellar concentration (CMC) as determined by pyrene (upper) and surface tension (bottom) methods.

Surfactant	CMC (mmol/l)		
	no HyA	LMW HyA	HMW HyA
Sucrose monolaurate	0.288 ± 0.006	0.26 ± 0.05	0.25 ± 0.03
	0.25 ± 0.02	0.26 ± 0.03	0.3 ± 0.1
n-Dodecyl-β-D-maltoside	0.160 ± 0.001	0.150 ± 0.003	0.160 ± 0.002
	0.149 ± 0.007	0.136 ± 0.006	0.19 ± 0.08
Octyl-β-D-glucopyranoside	20.2 ± 0.1	19.9 ± 0.3	19.9 ± 0.3
	20.6 ± 0.4	19 ± 1	21 ± 2
Tween 20	0.048 ± 0.001	0.014 ± 0.001	0.014 ± 0.002
	0.072 ± 0.003	0.053 ± 0.004	0.05 ± 0.02
SDS	1.04 ± 0.01	0.740 ± 0.001	0.80 ± 0.03
	0.87 ± 0.05	0.7 ± 0.1	0.7 ± 0.2
TTAB	0.52 ± 0.03	0.51 ± 0.03	0.61 ± 0.01
	0.49 ± 0.02	0.58 ± 0.01	0.5 ± 0.2
CTAB	0.062 ± 0.002	0.12 ± 0.02	0.11 ± 0.02
	0.030 ± 0.004	0.025 ± 0.006	0.040 ± 0.001
CTAT	0.056 ± 0.001	0.072 ± 0.001	0.15 ± 0.05
	0.036 ± 0.004	0.099 ± 0.007	0.058 ± 0.008
Cetyl betaine	0.016 ± 0.001	0.009 ± 0.001	0.021 ± 0.005
	0.009 ± 0.001	0.010 ± 0.001	0.051 ± 0.003
Betadet THC2	0.14 ± 0.01	0.10 ± 0.01	0.100 ± 0.001
	0.13 ± 0.03	0.10 ± 0.03	0.27 ± 0.03

against surfactant concentration. The integrals (I_r) were normalized with respect to maximum value which was usually measured for the highest surfactant concentration, i.e. the normalized values ranged from 0 to 1 within each measured system. At low surfactant concentrations the integral intensity is zero or very low and not changing with concentration. At a certain concentration the intensity starts to increase, usually linearly. This is the point of the critical micellar concentration (the intersection of two linear branches). In the second method dependence of the maximum emission wavelength on surfactant concentration was plotted giving similar sigmoidal curve as the pyrene polarity index – mathematical treatment was then similar as for this index.

3. Results and discussion

3.1. Surface tension

Measurement of surface tension detects, in fact, surfactant accumulation on the liquid surface (adsorption). Indirectly it provides information on surfactant behavior in solution, specifically on its micellization which is supposed to start when the sharp drop of surface tension with increasing surfactant concentration stops. Measurements with hyaluronan solutions confirmed no hyaluronan surface activity [25] up to the concentration of about 2 g/l which is consistent with findings of Riberio et al. [26]. All measured data for the dependence of the surface tension on surfactant concentration in physiological solution showed no or small effect of hyaluronan (of any molecular weight) on surface activity and particularly on micellization, i.e. the value of the critical micellar concentration as determined by tensiometry was practically not affected by the addition of hyaluronan, see Table 1. Examples of tensiometry results are given in Fig. 1 for sucrose monolaurate and CTAB. In the case of sucrose monolaurate all three data curves are practically identical and are typical examples of most measured surface tension data. Thus from the point of view of tensiometry there are no specific interactions between hyaluronan and sucrose monolaurate (and most of the other surfactants) and the surface and micellization behavior of this surfactant is not influenced by the presence of hyaluronan chains. CTAB is oppositely charged than hyaluronan therefore some electrostatic interactions could be expected. Fig. 1b shows that hyaluronan of both molecular weights seems to slightly decrease the surface tension of CTAB physiological solutions in the premicellar region. However, the value of the critical micellar concentration (CMC), as determined by tensiometry, is not affected. Tensiometry thus indicates that hyaluronan influences only the interactions within the CTAB surface layer and does not intervene in the micellization process. No effect on micellization is a result of screening the electrostatic interactions between hyaluronan and CTAB by the presence of NaCl in physiological solution which seems to be more effective in the bulk solution than in

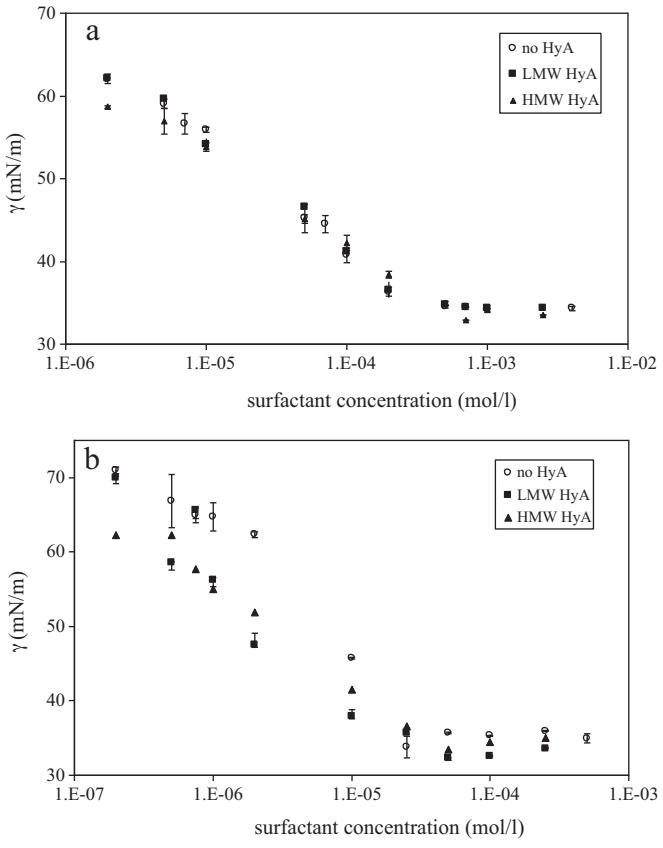

Fig. 1. Effect of low (LMW) and high (HMW) molecular weight hyaluronan (HyA) on surface tension of sucrose monolaurate (a) and CTAB (b) solutions.

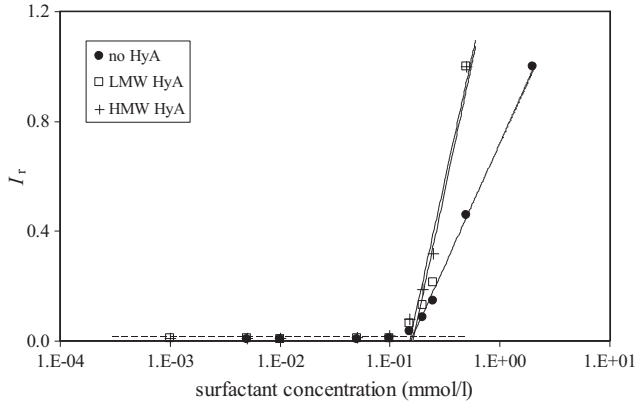

Fig. 2. Effect of low (LMW) and high (HMW) molecular weight hyaluronan (HyA) on nile red integral intensity dependence on dodecyl maltoside concentration.

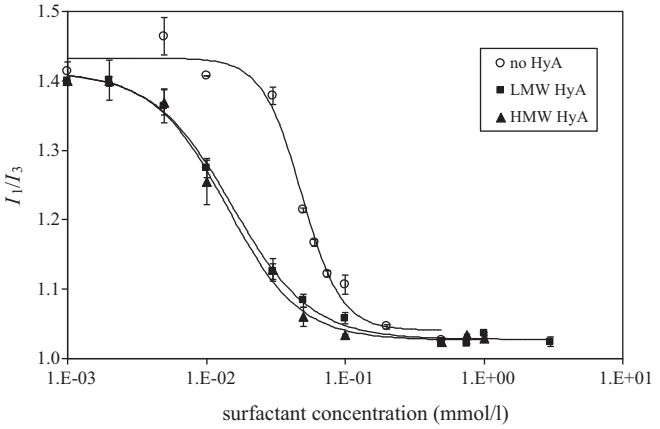

Fig. 3. Effect of low (LMW) and high (HMW) molecular weight hyaluronan (HyA) on pyrene polarity index dependence on Tween 20 concentration. Solid lines show fits by Boltzmann curve.

its surface layers. Because the CMC value, as determined by tensiometry, was not influenced by hyaluronan, it probably does not change the amount of CTAB on the solution surface in the premicellar region but changes only interactions in this layer which are the cause of (lowered) surface tension. The lower surface tension may be also caused by larger binding of sodium from the added salt to hyaluronan as counterions. Similar decrease of surface tension in premicellar region was observed also for SDS and for TTAB in the presence of high molecular weight hyaluronan. Specific results obtained for Tween 20 are discussed below.

3.2. Fluorescence probes – nonionic surfactants

Fluorescence probes, in contrast to tensiometry, provide information directly from the bulk solution or even directly from the formed micelles or from their close vicinity. Pyrene is considered to be insoluble in water. However, it has some though limited solubility in water and its location in water is detected by the high value of the pyrene polarity index. Fluorescence of nile red is quenched in water and its emission maximum wavelength decreases with decreasing polarity.

Critical micellar concentrations determined by the pyrene probe method are summarized in Table 1 and data obtained by all three different fluorescence approaches can be seen in Table S1 (Supplementary material) but the whole measured curves (concentration dependences) are more convenient for discussion of results.

First, the results for nonionic surfactants will be discussed. Data for dodecyl maltoside measured with pyrene and for the nile red emission maximum showed no effect of hyaluronans. Nile red integral intensity detected no change in critical micellar concentration but revealed increased slope of intensity dependence on concentration after formation of micelles (see Fig. 2). Increased fluorescence intensity is supposed to be caused by increased number of solubilized nile red molecules. Hyaluronan thus influences the solubilization capacity of dodecyl maltoside probably through the influence on shape, size or number of its micelles.

Pyrene and nile red curves measured for sucrose monolaurate showed no differences when hyaluronans were added.

Pyrene data for octyl glucopyranoside showed slight broadening of micellization region and slight increase of CMC upon addition of hyaluronan with no specific effect of its molecular weight. The CMC increase was observed also on the nile red emission maximum curve but here the effect of the high molecular weight hyaluronan was more distinct. Nile red intensity data showed increasing CMC value in the order of solutions with: no hyaluronan < low < high molecular weight hyaluronan. Hyaluronan also slightly increased slope of intensity dependence on concentration in post micellar region. Octyl glucopyranoside is relatively small molecule (monosaccharide with relatively short alkyl) what probably facilitates interactions of single surfactant molecules with hyaluronan through their hydroxyl groups disturbing thus the micellization process.

Pyrene data for Tween 20 revealed significant effects of hyaluronan of both molecular weights on the behavior of this surfactant in physiological solution (see Fig. 3). In the presence of hylauronans, the CMC was substantially decreased and the concentration interval where micellization occurs was significantly broadened. Very similar results were obtained also for the nile red emission maximum measurements (the curves are not shown – their shapes are very similar to those for pyrene in Fig. 3). On contrary, the nile red integral intensity showed increased CMC upon addition of hyaluronans; this increase was a little bit higher for the low molecular weight hyaluronan. The latter also gave somewhat smaller slope of intensity dependence on concentration in post micellar region, i.e. decreased solubilization. The apparently contradictory results can be explained by different photophysical basis of detection by the two different fluorescence probes quoted in introduction. Pyrene polarity index in the region of its decrease from the value corresponding to aqueous medium to the value corresponding to low polarity environment is composed from signals coming from pyrene molecules located in the formed micelles, from free pyrene molecules in water, and probably also from ("premicellar") aggregates formed by hyaluronan-surfactant interactions which consist of domains of higher polarity (higher water contents) than regular Tween micelles. Similarly, the nile red emission maximum measures the polarity of environment within which the nile red molecules are located or solubilized; the shift of this maximum is detectable even when the fluorescence intensity is very low, i.e. when most nile red molecules are surrounded by water that quenches their fluorescence. On contrary, the nile red fluorescence intensity is principally determined by the number of nile red molecules located in non-aqueous environment, i.e. solubilized within the nonpolar aggregates or micelles. Sufficient number of solubilized molecules, i.e. of micelles with the true non-aqueous interior, is formed in the presence of hyaluronan only at sufficiently high surfactant concentration. This probably occurs when interactions between Tween 20 and hyaluronan are "saturated", formation of hyaluronan-surfactant premicellar aggregates (of higher polarity than standard Tween micelles) is essentially completed and free Tween micelles start to be formed.

In contrast to the other used sugar-based surfactants, Tween 20 has relatively bulky polar head with several end hydroxyl groups on oligoethylene glycol chains, projecting from the head like

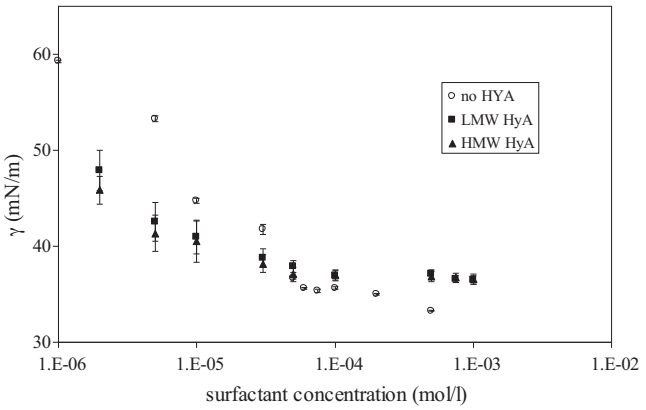

Fig. 4. Effect of low (LMW) and high (HMW) molecular weight hyaluronan (HyA) on surface tension of Tween 20 solutions.

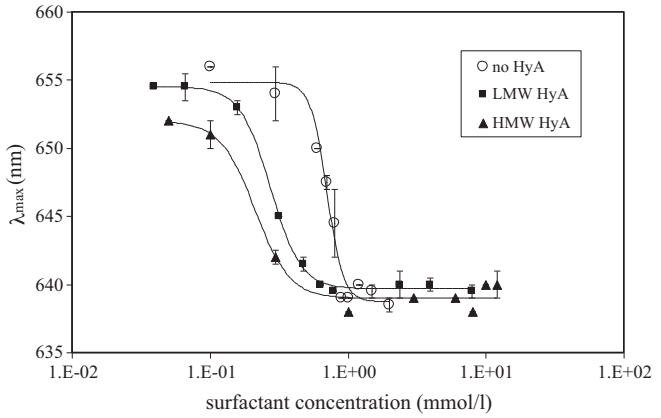

Fig. 5. Effect of low (LMW) and high (HMW) molecular weight hyaluronan (HyA) on dependence of nile red emission maximum wavelength on SDS concentration. Solid lines show fits by Boltzmann curve.

"antennas". One cause for formation of aggregates in the presence of hyaluronan may thus be steric exclusion by voluminous hyaluronan coils. Further, Tween "antenna" hydroxyl groups may participate in hydrogen bonding with hyaluronan hydroxyls or even carboxyls. Molecular modeling of hyaluronan hydration demonstrated numerous hydrogen bonds between hyaluronan disaccharide units and water molecules – some of them even form water bridges between adjacent hydroxyls of monosaccharide subunits [27,28]. Water thus can participate in the premicellar aggregate formation or can be entrapped within their structure. Formation of premicellar aggregates is not reflected in the value of critical micellar concentration as determined by surface tension but some effect of hyaluronan on the surface tension of Tween 20 physiological solutions can be seen (Fig. 4). Below the regular CMC value the solution surface tension is lower in the presence of hyaluronans which could confirm the hypothesis on hydrogen bonding between hyaluronan and surfactant which occurs also in the surface layers and decreases the surface energy. Constant and higher surface tension behind the regular CMC in the presence of hyaluronans could point to steric exclusion by hyaluronan of additional surfactant molecules to enter the surface layer and forcing them to form free micelles only.

Yin et al. [11] reported no interactions of hyaluronan with similar nonionic surfactant, Tween 80. However, this refers to experiments carried out in water. Sensitivity of hyaluronan conformation to ionic strength is well documented, e.g., by rheological properties of its solutions [29,30]. Also the hydration of hyaluronan chain and hydrogen bonds formed between hyaluronan functional groups and water molecules are influenced by the presence of added electrolyte ions [28]. Even Yin et al. [11] present influence of NaCl on the pyrene I_1/I_3 ratio in the presence of hyaluronan but give it only for five selected surfactant concentrations and do not show the whole curve. Nevertheless, the trends observed by Yin et al. upon addition of NaCl correspond to those seen in Fig. 3. Presence of NaCl thus influences interactions between hyaluronan and Tween surfactants despite of their nonionic nature.

3.3. Fluorescence probes – anionic surfactants

Representative data of pyrene polarity index measured for ionic surfactants can be seen in Figs. S1–S3 (Supplementary material). SDS was the only one anionic surfactant tested. Pyrene curves measured for SDS showed slight broadening of micellization region and slight decrease of CMC in the presence of hyaluronan. Yet more expressive broadening and CMC decrease was indicated by nile red emission maximum (Fig. 5). Nile red integral intensity showed almost no change of CMC but a change of the shape of its dependency on surfactant concentration in post micellar region. Solutions without hyaluronan had usual linear shape while in the presence of hyaluronans S-shape appeared indicating some saturation of nile red solubilization. Decreased CMC is consistent with findings of Yin et al. [11] where aqueous solutions (no added salt) were studied; because there was the added salt in our case the results seem to confirm hypothesis on hydrogen bonding nature of the CMC decrease [11]. The saturation of nile red solubilization probably points to formation of smaller micelles in the presence of hyaluronan with limited space to dissolve relatively large nile red molecule.

3.4. Fluorescence probes – cationic surfactants

Three cationic surfactants were included in this study. Pyrene polarity index curves measured for TTAB in the presence of hyaluronan were close to that obtained when no hyaluronan was present. Similar results were obtained from the nile red emission maximum curves, except somewhat broadened micellization region found especially when the high molecular weight hyaluronan was present. Nile red integral intensity data were also close for all three systems except slightly increased slope in the postmicellar region in the presence of the low molecular weight hyaluronan. Hyaluronan is known to induce aggregation in aqueous TTAB solutions at lower surfactant concentrations than is the CMC which is explained by surfactant cooperative binding on the biopolymer backbone and forming micelle-like aggregates. Salts are known to depress these interactions. Pyrene data thus show that the added salt probably completely screened interactions and the formed aggregates are free micelles of (non-bound) TTAB in saline solution. In other words, no solubilization was detected at surfactant concentrations below the CMC in physiological solution. Similar conclusions can be drawn from the nile red intensity data. Broadening of dependencies measured for the nile red emission maxima show that the probe molecules may be located in environments of different polarity. Whereas pyrene is a "pure" hydrocarbon of limited solubility in water, nile red is a heterocyclic compound containing also nitrogen atoms and in the solution can interact with heteroatoms of the other components also when it is not solubilized in nonpolar domains.

In the case of CTAB, hyaluronan of both molecular weights increased the critical micellar concentration detected by the inflex point on the pyrene polarity index curve. Also the micellization region was broadened especially in the case of the high molecular weight preparation (Fig. 6). Similar results were obtained from the nile red emission maximum. Increased CMC was also demonstrated by the nile red integral intensity data but here no differences were detected between the two hyaluronans. Interactions between

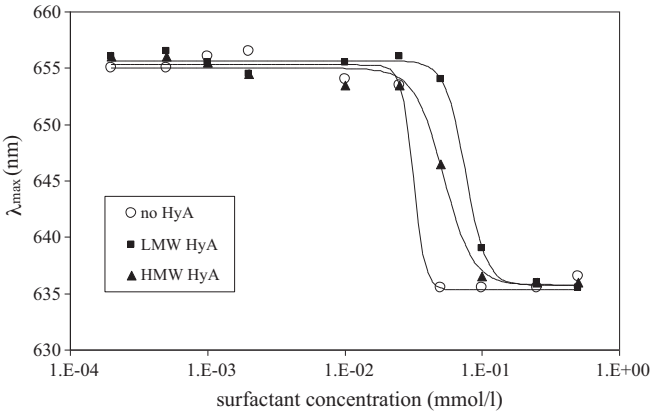

Fig. 6. Effect of low (LMW) and high (HMW) molecular weight hyaluronan (HyA) on dependence of nile red emission maximum wavelength on CTAB concentration. Solid lines show fits by Boltzmann curve.

hyaluronan and CTAB are demonstrated by increased CMC and broadening of micellization regions as detected by the pyrene and nile red sigmoidal curves. Aggregation of CTAB, in comparison with TTAB, is much more affected by the presence of hyaluronan which could be attributed to the longer surfactant alkyl chain. Increased CMC of CTAB in the presence of hyaluronan can be caused by stronger hydrophobic interactions between longer cetyl chain and hydrophobic patches on hyaluronan backbone [31,32]. Hydrophobic interactions are supposed not to be screened by the added salt as much as is the case of electrostatic interactions. Hydrophobically bound surfactant molecules are then not able to participate in micelles formation.

Pyrene polarity index curves measured for CTAT only and for CTAT with the low molecular weight hyaluronan are similar except slightly higher value of this index for the former in the premicellar region. Presence of the high molecular weight hyaluronan again shifted the inflex point to higher surfactant concentrations and broadened the micellization region. Nile red emission maximum showed increased CMC values for both hyaluronans, higher for the low molecular weight preparation; the high molecular weight type gave very narrow micellization region. The nile red integral intensity showed the same and increased CMC in the presence of both hyaluronans. CTAT results are thus somewhere between the results for TTAB and CTAB. Introducing different types of polar head (aromatic, with sulfate counterion) into cationic surfactant did not substantially change its interactions with hyaluronan and solubilization properties of formed aggregates.

3.5. *Fluorescence probes – zwitterionic surfactants*

Finally, two amphoteric surfactants were tested. Nile red data obtained for cetyl betaine were similar regardless the presence of hyaluronan. Only pyrene polarity index showed a minor decrease of CMC in the presence of the low molecular weight hyaluronan. Thus no significant hyaluronan-cetyl betaine interactions were observed in physiological solution. In the case of Betadet THC 2 nile red intensity showed certain difference – increased CMC in the presence of both hyaluronan samples. Betadet is a commercial cosmetic product based on disodium cocoamphodiacetate with unspecified additional ingredients. Hyaluronans added to this composition thus did not intervene its interactions too much except changing the number or size of aggregates capable to solubilize nile red.

4. Conclusions

Although the presence of NaCl may suppress interactions between oppositely charged polyelectrolyte and surfactant results of this work showed that they are still present in some hyaluronan-surfactant systems regardless the surfactant ionic nature. These interactions were demonstrated mainly by fluorescence probe techniques whereas tensiometry detected only minor effects. Fluorescence data demonstrated that formation of aggregates (micelles) occurs rather in a certain interval of surfactant concentrations than in a single point. It is thus more appropriate to speak about micellization (aggregation) region than single critical micellar (aggregation) concentration, especially in the presence of hyaluronan because its main effect on fluorescence data was broadening of concentration interval in which the fluorescence probe starts to be and is solubilized in nonpolar domains. Broadening of this interval usually changes the value of its mid-point which can be considered as a point estimate of the critical micellar (aggregation) concentration. Tensiometry did not detected changes in the critical micellar concentration, only in several systems slight decrease of surface tension in the premicellar region was observed in the presence of hyaluronan.

The greatest differences between surfactant physiological solution and surfactant + hyaluronan physiological solution were found for nonionic Tween 20 and cationic CTAB. This was rather surprising for the former, first because of its nonionic nature and second because of no such differences were observed for the other nonionic surfactants. Specificity of Tween 20 was attributed to its structural features – relatively bulky and sugar-based polar head capable of weak physical interactions, preferably hydrogen bonding, with hyaluronan chain. Interactions of hyaluronan with CTAB, an oppositely charged molecule, were expected, however, in contrast to aqueous solution, in physiological solution used here they manifested in increased CMC or, more precisely, they shifted solubilization capability to higher surfactant concentrations. This is probably a result of hydrophobic interactions of sufficiently long surfactant alkyl chain with low-polarity parts of hyaluronan backbone which are promoted in physiological solution where the electrostatic interactions are screened.

Fluorescence data also demonstrated that there can be differences in results obtained with different fluorescence probes which are caused by their different location and solubility in studied system and by differences in the nature of their photophysical behavior. Pyrene seems to be a useful probe to detect the onset of micellization process and the width of concentration interval where this process occurs. Wavelength of the nile red fluorescence emission maximum can provide similar information whereas its intensity determines when a sufficient number of really hydrophobic domains is formed in studied system.

From the point of view of targeted delivery it is important to note that fluorescence probes demonstrated that solubilization properties of all tested surfactants were retained in the presence of hyaluronan, i.e. eventual hyaluronan-surfactant interactions do not destroy aggregates containing non-polar domains (micelles).

Acknowledgements

This work was supported by the COST action D43 and corresponding Czech project No. OC08004. The Centre for Materials Research at FC BUT is supported by the project No. CZ.1.05/2.1.00/01.0012 from ERDF.

Appendix A. Supplementary data

Supplementary data associated with this article can be found, in the online version, at doi:10.1016/j.colsurfa.2011.05.035.

References

[1] H.G. Garg, C.A. Hales (Eds.), Chemistry and Biology of Hyaluronan, Elsevier, Amsterdam, 2004.
[2] L. Robert, A.M. Robert, G. Renard, Biological effects of hyaluronan in connective tissues, eye, skin, venous wall. Role in aging, Pathol. Biol. 58 (2010) 187–198.
[3] N. Volpi, J. Schiller, R. Stern, L. Šoltés, Role, metabolism, chemical modifications and applications of hyaluronan, Curr. Med. Chem. 16 (2009) 1718–1745.
[4] N. Itano, Simple primary structure, complex turnover regulation and multiple roles of hyaluronan, J. Biochem. 144 (2008) 131–137.
[5] A. Almond, Hyaluronan, Cell. Mol. Life Sci. 64 (2007) 1591–1596.
[6] K.S. Girish, K. Kemparaju, The magic glue hyaluronan and its eraser hyaluronidase: a biological overview, Life Sci. 80 (2007) 1921–1943.
[7] D.A. Ossipov, Nanostructured hyaluronic acid-based materials for active delivery to cancer, Expert Opin. Drug Deliv. 7 (2010) 681–703.
[8] K. Beer, N. Solish, Hyaluronics for soft-tissue augmentation: practical considerations and technical recommendations, J. Drugs Dermatol. 8 (2009) 1086–1091.
[9] E.A. Balazs, Therapeutic use of hyaluronan, Struct. Chem. 20 (2009) 341–349.
[10] I. Hargittai, M. Hargittai, Molecular structure of hyaluronan: an introduction, Struct. Chem. 19 (2008) 697–717.
[11] D. Yin, W. Yang, Z. Ge, Y. Yuan, A fluorescence study of sodium hyaluronate/surfactant interactions in aqueous media, Carbohydr. Res. 340 (2005) 1201–1206.
[12] K. Thalberg, B. Lindman, Interaction between hyaluronan and cationic surfactants, J. Phys. Chem. 93 (1989) 1478–1483.
[13] K. Thalberg, B. Lindman, G. Karlström, Phase diagram of a system of cationic surfactant and anionic polyelectrolyte: tetradecyltrimethylammonium bromide-hyaluronan-water, J. Phys. Chem. 94 (1990) 4289–4295.
[14] K. Thalberg, B. Lindman, G. Karlström, Phase behavior of systems of cationic surfactant and anionic polyelectrolyte: influence of surfactant chain length and polyelectrolyte molecular weight, J. Phys. Chem. 95 (1991) 3370–3376.
[15] K. Thalberg, B. Lindman, G. Karlström, Phase behavior of systems of cationic surfactant and anionic polyelectrolyte: the effect of salt, J. Phys. Chem. 95 (1991) 6004–6011.
[16] K. Thalberg, B. Lindman, Gel formation in aqueous systems of a polyanion and an oppositely charged surfactant, Langmuir 7 (1991) 277–283.
[17] A. Herslöf, L.O. Sundelöf, K. Edsman, Interaction between polyelectrolyte and surfactant of opposite charge. hydrodynamic effects in the sodium hyaluronate/tetradecyltrimethylammonium bromide/sodium chloride/water system, J. Phys. Chem. 96 (1992) 2345–2348.
[18] M. Björling, A. Herslöf-Björling, P. Stilbs, An NMR self-diffusion study of the interaction between sodium hyaluronate and tetradecyltrimethylammonium Bromide, Macromolecules 28 (1995) 6970–6975.
[19] V.J.P. Srivatsavoy, Enhancement of excited state nonradiative deactivation of Nile Red in β-cyclodextrin: evidence for multiple inclusion complexes, J. Lumin. 82 (1999) 17–23.
[20] M.E.C.D.R. Oliveira, G. Hungerford, M. da, G. Miguel, H.D. Burrows, Solvatochromic fluorescent probes in bicontinuous microemulsions, J. Mol. Struct. 563–564 (2001) 443–447.
[21] S. Mukherjee, H. Raghuraman, A. Chattopadhyay, Membrane localization and dynamics of nile red: effect of cholesterol, Biochim. Biophys. Acta 1768 (2007) 59–66.
[22] P. Greenspan, S.D. Fowler, Spectrofluorometric studies of the lipid probe, nile red, J. Lipid Res. 26 (1985) 781–789.
[23] G. Nagwa, Photophysics of Nile red in solution: steady state spectroscopy, Spectrochim. Acta Part A 56 (2000) 1003–1010.
[24] J. Aguiar, P. Carpena, J.A. Molina-Bolívar, C.C. Ruiz, On the determination of the critical micelle concentration by the pyrene 1: 3 ratio method, J. Colloid Interface Sci. 258 (2003) 116–122.
[25] M. Chytil, J. Krouská, P. Kulilová, M. Pekař, Maximum bubble pressure and the du Noüy platinum ring method of surface tension measurements of sodium dodecyl sulfate and sodium hyaluronate, Chem. Listy 102 (2008) s1139–s1141.
[26] W. Riberio, J.L. Mata, B. Saramago, Effect of concentration and temperature on surface tension of sodium hyaluronate saline solutions, Langmuir 23 (2007) 7014–7017.
[27] F. Heatley, J.E. Scott, A water molecule participates in the secondary structure of hyaluronan, Biochem. J. 254 (1988) 489–493.
[28] A. Almond, Towards understanding the interaction between oligosaccharides and water molecules, Carbohydr. Res. 340 (2005) 907–920.
[29] E. Fouissac, M. Milas, M. Rinaudo, R. Borsali, Influence of the ionic strength on the dimensions of sodium hyaluronate, Macromolecules 25 (1992) 5613–5617.
[30] W.E. Krause, E.G. Bellomo, R.H. Colby, Rheology of sodium hyaluronate under physiological conditions, Biomacromolecules 2 (2001) 65–69.
[31] C.S. Sundari, D. Balasubramanian, Hydrophobic surfaces in saccharide chains, Prog. Biophys. Mol. Biol. 67 (1997) 183–216.
[32] J.E. Scott, F. Heatley, Biological properties of hyaluronan in aqueous solution are controlled and sequestered by reversible tertiary structures, defined by NMR spectroscopy, Biomacromolecules 3 (2002) 547–553.

CHAPTER EIGHT

Fluorescence Spectroscopy Study of Hyaluronan–Phospholipid Interactions

Filip Mravec,[1] Martina Klučáková,[1] *and* Miloslav Pekař[1,*]

Contents

Abstract

Capability of phospholipids with positive charge to form complexes with hyaluronan in aqueous solutions, in a similar way as traditional cationic surfactants, was investigated by fluorescence probes. DPPC and lecithin aggregate in aqueous solution to form micelle-like structures capable to solubilize hydrophobic molecules. Changes in aggregation behavior after adding hyaluronan were observed only in the case of lecithin. Further, nonionic biocompatible surfactant was used as additional dispersion environment in phospholipid–hyaluronan system with phospholipid molecules acting as a physical linker bonding micelles and biopolymer.

* Corresponding author. Tel.: +420-541149330; Fax: +420-541149398.
E-mail address: pekar@fch.vutbr.cz

[1] Centre for Materials Research, Faculty of Chemistry, Brno University of Technology, Brno, Czech Republic

Advances in Planar Lipid Bilayers and Liposomes, Volume 14
ISSN 1554-4516, DOI: 10.1016/B978-0-12-387720-8.00008-X

1. Introduction

Polysaccharides and their derivatives have become major components in the development of biocompatible and biodegradable materials with many areas of applications especially in beauty and health care (e.g., cosmetics, tissue engineering, or drug delivery). Phospholipids are another class of biomolecules with specific function particularly in forming cellular structures. Also, phospholipids have found practical applications in cosmetic and medical products, mainly in the form of liposomes.

Among polysaccharides, hyaluronan (HA) can be viewed as a rather unique macromolecule which has very simple chemical structure (repeating unit) but several and different physiological functions. Hyaluronan is a common name for hyaluronic acid or, more precisely, its sodium salt. Hyaluronan is a naturally occurring linear high molecular polysaccharide composed of repeating β-(1→4)-D-glucuronic acid β-(1→3)-*N*-acetyl-D-glucosamine disaccharide units [1–3] (see Fig. 1).

Hyaluronan is a polymer with a wide range of naturally occurring molecular masses from several hundred to 10 million g mol^{-1} [1,3] possessing one carboxylate group per disaccharide repeating unit, and is therefore a polyelectrolyte bearing a negative charge. Hyaluronan can be found primarily in the extracellular matrix [1–3] of all higher organisms, especially in connective tissues, synovial fluid, and eye vitreous and is produced by certain strains of bacteria. The biological functions of hyaluronan include maintenance of elastoviscosity of liquid connective tissues such as joint synovial fluid and eye vitreous, control of tissues hydration and water transport due to its immense ability to retain water [4,5]. Hyaluronan participates in supramolecular assembly of proteoglycans in the extracellular matrix and in numerous receptor-mediated roles in cell detachment, mitosis, migration, tumor development, metastasis, and inflammation [2,4,6].

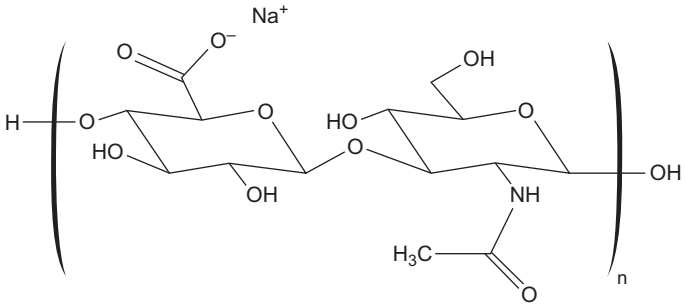

Figure 1 Structural unit of hyaluronan.

For these functions, multivalent interactions of HA with specific cell surface receptors such as CD44 and RHAMM are important [1,3,4,6]. Various tumors overexpress hyaluronan-binding receptors and consequently these tumor cells show enhanced binding and internalization of HA. Thus, HA coupled with, for instance, cytotoxic agents represents a nontoxic prodrug [6] and such conjugate is internalized into tumor cells through receptor-mediated endocytosis, followed by a release of active drugs, thus restoring their original toxicity.

Hyaluronan has, therefore, found important applications in drug delivery and surgery, and has been found to enhance absorption of drugs and proteins through mucus tissues [1,3,7]. It is used as an adjuvant for ophthalmic drug delivery [1,3] as a viscosity enhancing polymer for eye drops [1,8]. Hyaluronan has found important applications in the field of visco-surgery, visco-supplementation, and wound healing, furthermore as a supplementation of the synovial fluid in patients with osteoarthritis [3,7]. Hyaluronan is increasingly used in cosmetics, mainly as a moisturizing, epidermal renewal, and antiaging agent.

Phospholipids and phosphatidylcholine, in particular, are found as the most important constituents of many biological membranes. In cells, they work not only as a semipermeable barrier separating and protecting the cell from its environment and enabling transfer of ions but participate also in various cellular events. When used in cosmetic products, phospholipids show conditioning, softening, nourishing, and refattening effects. Conveniently, they are applied in liposomal form which is perhaps the most natural form of these molecules. However, just this form is not really substantial for turning out the desirable functions of phospholipids and their effectiveness is more a matter of the chemical composition of the cosmetic product than of the liposomal structure. Liposomes also have limited bearing capacity especially for lipophilic cosmetic ingredients and are not very suitable for lipid-rich cosmetic products. Different colloids or even nanosystems like nanoemulsions are, therefore, sought to extend applicability of phospholipids [8].

From the colloid chemistry point of view, phospholipids can be considered as a special type of surfactants. Hyaluronan, because of its negative charge, is known to interact with cationic surfactants, in particular, forming hyaluronan-surfactant complexes at concentrations well below the critical micellar concentration of pure surfactant. In this work, positively charged phospholipids were viewed and used as "common surfactants" and tested for their interactions with hyaluronan.

Study of hyaluronan–surfactant interactions is not a completely new field but the interest has been focused preferably on interactions between hyaluronan and liposomes.

The interactions of high molecular weight hyaluronan with di-palmitoyl phosphatidylcholine (DPPC) liposomes in aqueous buffer were investigated by Crescenzi *et al.* [9]. The superstructures resulting from co-incubation *in vitro*

were observed by means of negative staining and rotary shadowing electron microscopy. The existence of supramolecular complex between hyaluronan and DPPC was demonstrated. The complex would exist *in vivo* in the synovial fluid and should be responsible for the unique physiological properties.

Gómez-Gaete *et al.* [10] described the supramolecular organization of hybrid microparticles encapsulating dexamethasone (DXM) prepared by spray drying DPPC and hyaluronic acid. The effect of DXM concentration on size distribution and encapsulation efficacy was evaluated as a function of concentration of hyaluronic acid. *In vitro* release studies showed that hyaluronic acid does not influence DXM release kinetics. In the dry microparticles, DXM is probably mostly in amorphous domains within the DPPC–hyaluronic matrix. Upon hydration, the majority of the drug is released and only a small amount of DXM interacts with DPPC.

The chain flexibility of solutions of hyaluronan of different molecular weights in the absence and presence of the DPPC by ^{1}H-NMR spectroscopy, gel permeation chromatography, and multi-angle laser-light-scattering photometry were studied in [11] and [12]. Authors demonstrated that the sonication of high or low molecular weight hyaluronan with DPPC for periods markedly increased the chain flexibility of hyaluronan. They proposed that DPPC competes for the hydrophobic centers along the hyaluronan chain which are normally responsible for the inter and intra chain interactions and which confer stiffness to the molecule of hyaluronan.

Japan authors in [13] examined the effects of DPPC on the flexor tendon and its protective effect against postoperative adhesion. The friction coefficient was significantly lower with the mixture of DPCC and hyaluronan than with saline solution of hyaluronan. They concluded that the decreased friction coefficient indicates that DPPC could complement the boundary-lubricating ability of the tendon.

The lubrication systems in many sites in the body were reviewed in [14]. The systems consist of fluid adjacent to surfaces coated with an oligolamellar lining of surface-active phospholipid (SAPL) acting as a back-up boundary lubricant wherever the fluid film fails to support the load—a likely event at physiological velocities. It was explained how proteoglycans and hyaluronic acid could have carrier functions for the highly insoluble SAPL, while hyaluronic acid has good wetting properties needed to promote hydrodynamic lubrication of a very hydrophobic articular surface by an aqueous fluid wherever the load permits.

A standard (four-ball) test were used to study the anti-wear capabilities of ovine synovial fluid, the phospholipid extracted from it, a synthetic synovial fluid, and the phospholipid removed from the articular surface by a lipid solvent. The results were discussed as consistent with the hypothesis that the joints are lubricated by oligolamellar phospholipid as a lamellated solid (graphite-like) lubricant adsorbed onto the articular surface or otherwise deposited from synovial fluid [15].

Kawano *et al.* [16] examined *in vivo* the effects of a mixture of high molecular weight hyaluronic acid plus L-δ-dipalmitoyl phosphatidylcholine liposomes on joint lubrication and articular cartilage degeneration. Experimental osteoarthritis of the right knee was induced by anterior cruciate and medial collateral ligament in rabbits. The injected knees had a tendency to demonstrate less damage to the articular cartilage compared with control group.

The lubricating abilities of hyaluronic acid and the DPPC and mixture of both hyaluronic acid and DPPC were assessed in an *in vitro* model. Lubrication was found not to be concentration dependant for hyaluronic acid, but concentration was key for DPPC lubrication. Penetration of hyaluronic acid into bovine cartilage by up to 300 μm from the surface was observed over a 48-h period. It was observed that hyaluronic acid specifically targeted the chondrocytes as it was primarily found within the lacunae surrounding the cells [17].

Pasquali-Ronchetti *et al.* [18] studied *in vitro* interactions between hyaluronan of different molecular weights and phospholipids (DPPC and egg lecithin) in the form of either unilamellar particles or multilamellar vesicles. Both phospholipids changed their organization in the presence of hyaluronan, giving rise to the formation of huge perforated membrane-like structures lying on the substrate or thick cylinders with a tendency to aggregate and to form sheets. These structures were seen only in the presence of high-molecular weight hyaluronan, whereas low-molecular-weight one induced fragmentation of liposomes and formation of a few short rollers. They proposed that such interactions may not be as efficient in arthritic joints, where hyaluronan is degraded to low-molecular-weight fragments.

Steffan *et al.* [19] studied interactions of various polyanionic polysaccharides, including hyaluronic acid, with multilamellar dimyristoyl phosphatidylcholine liposomes. They concluded that the interactions of anionic polysaccharides with phospholipid membranes is due to the presence of divalent cations which require a certain electron configuration and ionic radius. They depend (among others) on chain length and on the kind of involved phospholipid. The observed temperature shift of the lipid phase transition is caused by a strong dehydration of the membrane surface, which can be inhibited by high concentrations of NaCl.

Taglienti *et al.* [20] utilized diffusional NMR techniques for investigation of the interactions between hyaluronan and phospholipids (DPPC and 1,2-Dipalmitoyl-*sn*-glycero-3-phospho-*rac*-(1-glycerol) sodium salt). They showed that they are dependent both on charge and hydrophobicity factors.

The complex of hyaluronic acid and egg lecithin (named Haplex) was prepared by film dispersion and sonication in [21]. The physico-chemical properties, studied by IR spectrometry and differential scanning calorimetry, of Haplex were different from hyaluronic acid or lecithin or their

mixture. After Haplex was administered to rats orally, the serum concentration of hyaluronic acid increased when compared with the mixture or control groups.

The role of hyaluronic acid in protecting SAPLs from lysis by exogenous phospholipase A_2 (PLA_2) was studied in [22]. It was found that hyaluronic acid adhered to the phospholipid membrane (liposomes), inhibited their lysis by PLA_2. However, in its degraded form, hyaluronic acid not only failed to inhibit PLA_2-lysing activity, but accelerated it. They concluded that when the rate of degradation of hyaluronic acid exceeds that of synthesis, there will be insufficient replacement of hyaluronic acid and/or SAPLs, resulting in denudation of the articular surfaces. These are then exposed to increasing friction, and hence increased danger of degenerative joint changes.

An active cosmetic solution based on hyaluronic acid and phospholipids in combination with other active substance (e.g., ceramide-6, chitosan derivative, vitamin C) was tested in order to improve health of very dry skin (xerosis). The obtained results were compared with simultaneously used placebo consisting phospholipids as vehicle for the active components. It was found that the improvement starts to be evident after 4 weeks of daily treatment, even if remarkable differences between the skin surface treated with vehicle and the active cream were not so strong. Probably that is due to the specific activity of the phospholipids which surely improve the skin appearance for their hydrating and restructuring properties [23].

Here, we investigate capability of phospholipids with positive charge to form complexes with hyaluronan in aqueous solutions in a similar simple way as traditional single- or double-alkyl chain cationic surfactants do. In particular, we were interested in solubilization properties of formed colloids towards hydrophobic molecules. For this purpose, fluorescence probe method is a suitable technique giving information both on complexation (aggregation) and solubilization behavior.

2. Fluorescence Probe Techniques

Determination of aggregation properties of phospholipid systems was based on fluorescence spectroscopy, a fluorescence probe method. Pyrene is a hydrophobic polyaromatic hydrocarbon with low solubility in water ($\sim 10^{-7}$ mol L^{-1}). Excitation and emission spectra of pyrene can be used to determine aggregation behavior of colloids. From these spectra, two polarity indexes are obtained—the emission polarity index (EmPI) and the excitation polarity index (ExPI). Photophysical origin of these two indexes is slightly different. The ExPI is based on the fact that in ground state the maximum absorption band is shifted bathochromically in nonpolar

environment. Because of extremely narrow interval of wavelengths, from ~333 nm to ~338 nm, it is difficult to precisely determine a maximum of excitation, consequently, the ExPI as a ratio of fluorescence intensity at two wavelengths is used.

The emission spectrum of pyrene presents a fine vibrational structure (Fig. 2) where the relative peak intensities are highly influenced by the polarity of the solvent molecules by which this probe is surrounded. The ratio of the fluorescence intensity of the highest energy vibrational band to that of the third highest energy band correlates with the solvent polarity and is denoted as EmPI. This unique property is based on the fact that the dipole moment of pyrene (3.24 ± 0.1 D) predicts in situations when some apolar domain exists in an aqueous solution that the pyrene is situated in less polar area and indicates local environment by changes in the value of EmPI. Both of these indexes, ExPI and EmPI, brought fully comparable results in our case.

In a system where the aggregation occurs, both indexes show the sigmoid decrease with increasing concentration of the aggregating molecules which form apolar domains within the aggregates (e.g., surfactants aggregating into micelles). The sigmoidal plots can adequately described by a decreasing Boltzmann curve, which is given by

$$\mathrm{EmPI},\ \mathrm{ExPI} = \frac{\max - \min}{1 + e^{(x - x_0/\Delta x)}} + \min,$$

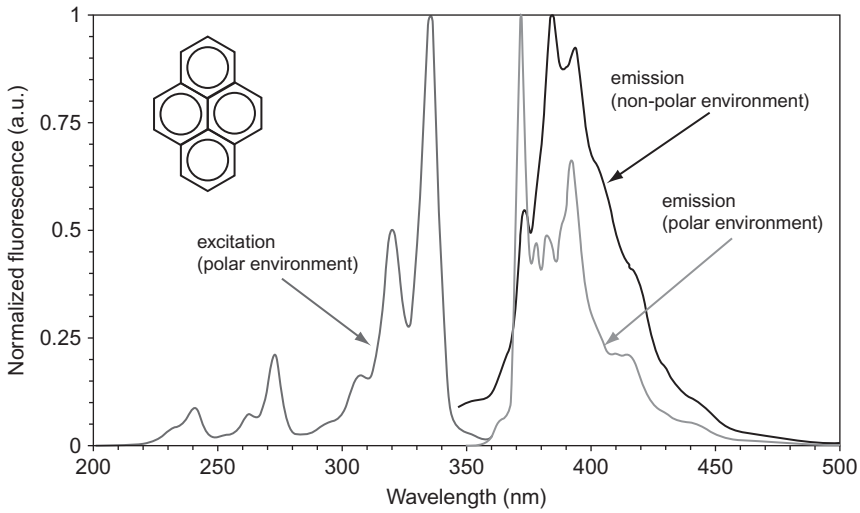

Figure 2 Fluorescence properties of pyrene in environments of different polarity.

where the independent variable x is the total surfactant concentration, max and min are the upper and lower limits of the sigmoid curve, x_0 is the center of the sigmoid (inflection point), and Δx is directly related to the independent variable range where abrupt change of dependent variable occurs. In this case, as aggregation concentration the x_0 point was taken.

In case of determination of surfactant binding on hyaluronan, a different type of fluorescence probe is appropriate. Acridine orange (AO), as a hydrochloride, has a positive charge located at the central nitrogen atom. Structure and fluorescence spectra and of AO are shown in Fig. 3. This type of dye forms in solution at high concentration the H-type of dye aggregate, an AO dimer. The AO dimers have the blue-shifted absorption band, from 492 nm to 465 nm and the fluorescence is forbidden (weak emission band at 650 nm). The monomer emission band has its maximum localized around 530 nm. In DNA, structure of AO dimer is sterically stabilized and probability of radiative transition in dimer strongly increases—e.g., DNA–AO associates show the red fluorescence instead of RNA–AO aggregates, which exhibits the green fluorescence.

The formation of nonfluorescent AO dimers in solution of polyanions is dependent on the number of dye molecules (D) and of polymer binding sites (P)—in our case, the number of negatively charged groups. This is described by the P/D ratio. In an ideal situation, when all negative groups are associated to AO dimers, the P/D value is 0.5.

Forming or breaking up of AO dimer can be observed in two different ways. Because of forbidden radiative transition from excited state of dimer, fluorescence intensity is inversely proportional to the dimer formation.

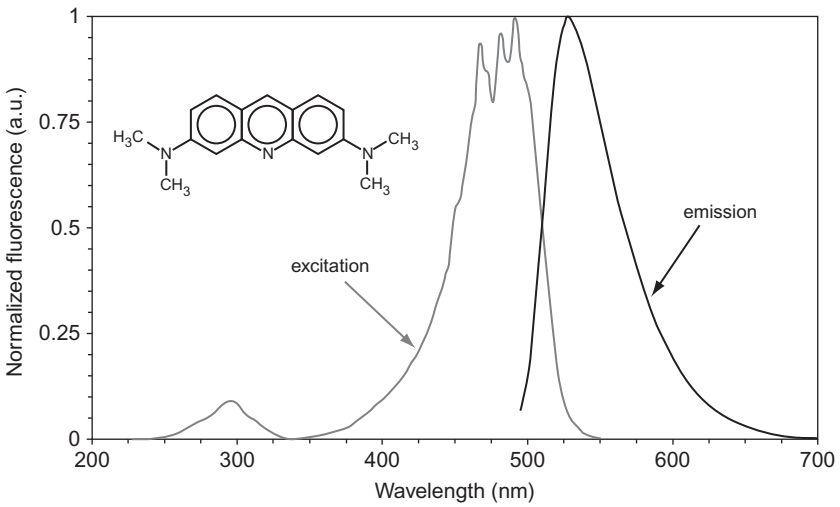

Figure 3 Fluorescence properties of acridine orange in aqueous environment.

As second parameter, a relative absorbance of dimer is used, expressed as ratio of absorbance at 465 nm (AO dimer) to absorbance at 492 nm (AO monomer) and denoted as "D:M."

As stated in introduction, our goal was an investigation of interactions between phospholipids and sodium salt of hyaluronic acid when the phospholipids play role of common surfactants.

The interaction between quaternary nitrogen and negatively charged carboxylic group can lead to the formation of electrostatically stabilized complex. This complex may result in the physically grafted copolymer, hydrophobically modified hyaluronan. The partially water-insoluble polymer can form aggregates with hydrophobic core and hydrophilic shell. This aggregate can solubilize amphiphilic and hydrophobic matters, for example, biologically active substances.

As was reported in introduction, phospholipids are mainly used in vesicular form. Phospholipid vesicles, liposomes, are initial colloidal particles in aqueous mixtures above the specific concentration, critical aggregation concentration. This fact is due to their packing parameter.

3. Materials and Methods

Selected phospholipids, DPPC (1,2-Dipalmitoyl-sn-glycero-3-phosphocholine, CAS # 63-89-8) and lecithin (1,2-diacyl-*sn*-glycero-3-fosfocholin, type XVI-E, CAS 8002 43 5) were purchased from Sigma-Aldrich. n-Dodecyl β-D-maltoside (C_{12}maltoside, CAS # 69227-93-6) was also purchased from Sigma-Aldrich company. Hyaluronan in different molecular weights were purchased from CPN Ltd., Czech Republic. All fluorescence probes, pyrene, and AO were of fluorescence grade and were purchased from Sigma-Aldrich. Solvents in this study were in spectrophotometric grade, and water was triple distilled.

Fluorescence spectra were recorded on AMINCO-Bowman Series 2 luminiscence spectrometer (ThermoSpectronics, Inc.) and absorption spectra were collected on Cary 50 (Varian, Inc.).

Stock solution of hyaluronan was prepared in triple distilled water and was stirred during 48 h at room temperature. Stock solutions of the phospholipids were prepared in chloroform. Pyrene's stock solution was prepared in acetone; on the other hand, stock solution of AO was prepared in triple distilled water.

In samples with lecithin or DPPC, phospholipid stock solution in chloroform was introduced into a vial and chloroform was evaporated. After evaporation stock solution of hyaluronan and/or dodecyl-maltoside was added.

Samples containing pyrene. Pyrene stock solution was introduced into a vial and acetone was evaporated. Final concentration of the pyrene in samples was $\sim 10^{-6}$ mol L^{-1}.The stock solution of the studied system was introduced into a flask with evaporating probe, was diluted to the desirable concentration, and the resulting solution was sonicated during 4 h and stored during next 20 h.

Samples containing acridine orange. AO stock solution was introduced into a vial. Final concentration of AO in samples was held to 5×10^{-6} mol L^{-1}. The stock solution of the studied system was introduced into a flask with probe solution.

4. Phospholipid Aggregation

As reported elsewhere [24], even phospholipids have their critical micelle concentrations. Above this concentration, only micelles or micelle-like aggregates are present in solution.

Concentration dependency of the aggregates formation process in solutions looks to be smooth. In a wide region of concentration, vesicles and micelles are coexisting in equilibrium. This can be one of the explanations of dependency of the ExPI on concentration of the phospholipid DPPC (see Fig. 4). From the Boltzman S-type curve the values of three independent variables, concentrations, which determine start and end of

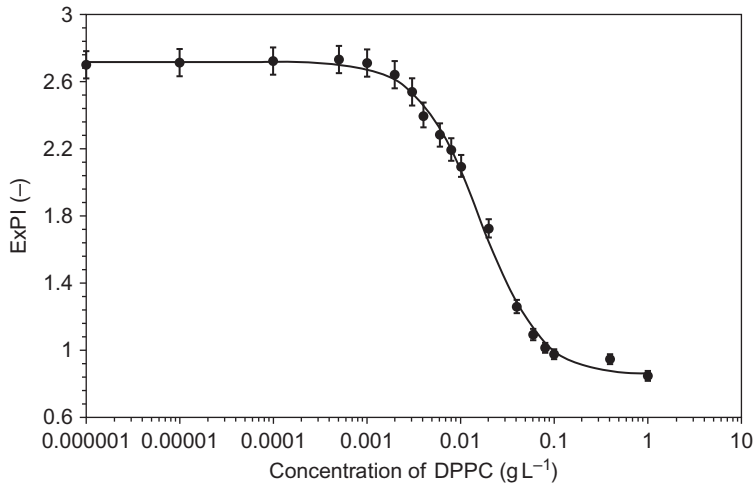

Figure 4 Dependency of the excitation polarity index (ExPI) on concentration of DPPC. Data were fitted by Boltzman sigmoidal curve and fitted parameters were used to characterize aggregation process, see Table 1.

the aggregation and the inflex point, were directly evaluated as the fit parameters.

The obtained fitted values of data from Fig. 4 are listed in Table 1 including fit parameters and goodness-of-fit statistics. As the data show, there is a wide range of concentrations between "start" and "end" point. The difference between these two points is nearby two orders of magnitude. As follows from the Boltzman equation, the parameter Δx is directly connected to the intensity of function decreasing.

This very slow decrease of polarity parameter can be explained in two different ways. At first, the resulting spectrum of fluorescence probes from each sample is a superposition of different signals coming from different probe's localizations. The solubility of pyrene probe in aqueous environment is sufficient to interfere with the signal of probe from nonpolar cores, especially in case when the system contains a small amount of these cores. Due to a low quantum yield of pyrene in aqueous environment, this effect takes a place only at extremely low micellar concentrations, or when a high amount of fluorescence probe is present in the sample. At second, when the concentration of phospholipid is increasing, the whole amount of added molecules is not used to form aggregates with nonpolar cores, or to form domains that are able to solubilize this type of probe. It is possible that added molecules are incorporated in existing aggregates and they are increasing the aggregation number of these aggregates. The enlargement of these aggregates leads to the phase transition of formed colloidal particles from micellar to vesicular type.

The other studied phospholipid, lecithin, showed similar aggregation behavior in aqueous solution like DPPC (see Fig. 5). Lecithin is 1,2-diacyl-*sn*-glycero-3-fosfocholin (type XVI-E, Sigma Aldrich, ~ 99%, CAS 8002-43-5). Lecithin is composed of different types of fatty acids—approx. 33% 16:0 (palmitic acid), 13% 18:0 (stearic acid), 31% 18:1(oleic acid), 15% 18:2 (linoleic acid), and minor residues. Compared to DPPC, the lecithin samples were transparent even at high phospholipid concentrations. Measurements performed with lecithin did not need to be corrected for the

Table 1 Fitted values from the Boltzmann fit of the dependency of ExPI on DPPC concentration (error given as the standard deviation)

Value	Concentration ($g\ L^{-1}$)	Error ($g\ L^{-1}$)				
start	0.004	0.002	*R*-Sq	0.9998	χ^2/DoF[a]	10^{-4}
inflex	0.016	0.005				
end	0.072	0.004				

[a] Goodness-of-fit—reduced chi-square is obtained by dividing the residual sum of squares by the degrees of freedom.

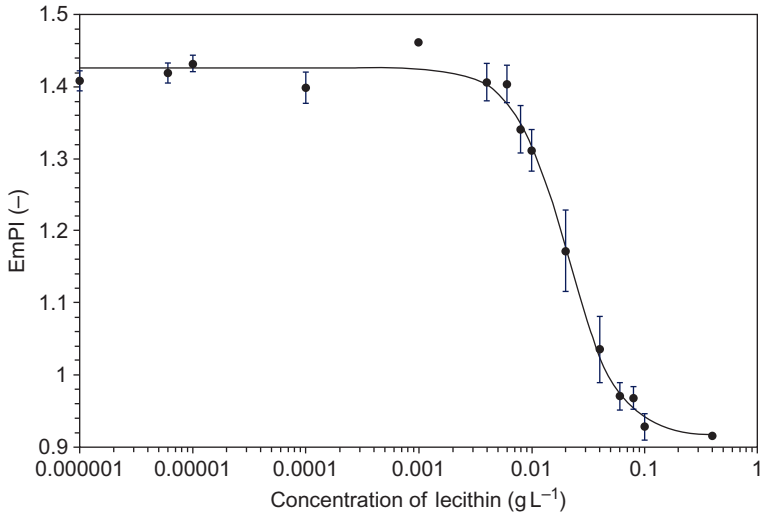

Figure 5 Dependency of the emission polarity index (EmPI) on concentration of lecithin. Data were fitted by Boltzman sigmoidal curve and fitted parameters were used to characterize aggregation process of lecithin, see Table 2.

Table 2 Fitted values from the Boltzmann fit of the dependency of EmPI on lecithin concentration (error given as the standard deviation)

Value	Concentration ($g\ L^{-1}$)	Error ($g\ L^{-1}$)				
start	0.007	0.001	*R*-Sq	0.9925	χ^2/DoF[a]	10^{-4}
inflex	0.021	0.003				
end	0.059	0.003				

[a] Goodness-of-fit—reduced chi-square is obtained by dividing the residual sum of squares by the degrees of freedom.

inner filter effect. Aggregation concentration of lecithin was determined from the dependency of the EmPI on PL concentration and obtained data are summarized in Table 2.

5. Presence of Hyaluronan

If we focus on aggregation behavior, expressed as a concentration dependency of some proper physical quantity, we should be able to prove interaction between phospholipid and hyaluronan. The phospholipid aggregation can be influenced by condensation of monomeric form of PL in solution on hyaluronan's chain. This condensation leads to formation of

some kind of different aggregates directly connected to the polymeric chain. This type of aggregate can form nonpolar cores, which are able to solubilize nonpolar species, one, two, or even more orders of magnitude below the critical aggregation concentration of phospholipid in pure aqueous solution. Formation of these aggregates is manifested as an "earlier" decrease of polarity index on the concentration axis. This decrease does not need to be intensive, but always should be marked. The intensity of this decrease is related to the fraction of pyrene molecule solubilized in these aggregates relatively to the amount of pyrene remaining in water. This fact must be taken into account especially in cases, when values of the polarity indexes are assigning to the polarity (relative permittivity, Δf function, etc.) of environment.

The aggregation behavior of lecithin, in the presence of native hyaluronan, is shown in Fig. 6. It is obvious that dependencies of the EmPI in the presence of hyaluronan are slightly shifted to the lower values comparing to the case when no hyaluronan is present in the solution. Numerical evaluation of this shift based on inflection points shows that aggregation in the presence of hyaluronan occurs at $\sim$3.8 mg L^{-1} compared with 5.6 mg L^{-1} in solution without biopolymer.

One can take into account that the added biopolymer is in fact a salt. With the biopolymer chain an equivalent amount of counter ions are added. These lead to increasing ionic strength, which can be responsible for slight shift of the aggregation dependencies. On the other hand, in case of absolute dissociation of sodium cation from hyaluronan backbone, the ionic strength

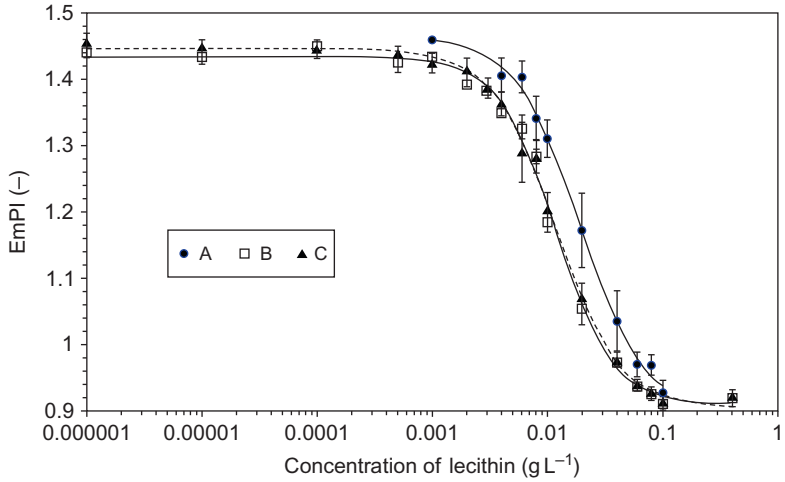

Figure 6 Aggregation behavior of lecithin in the presence of native hyaluronan (MW 73,000 g mol^{-1}) shown as dependency of the EmPI on the concentration of lecithin. (A) without HA; (B) with HA, $c = 1$ g L^{-1}; (C) with HA, $c = 15$ mg L^{-1}.

increases only for 0.0025 mol L^{-1}. In addition, showed dependencies for significantly different hyaluronan concentrations (1 g L^{-1} and 15 mg L^{-1}) seem to be independent on hyaluronan concentration.

The slight decrease of aggregation concentration can be directly connected to the interaction with hyaluronan chain (Fig. 7). This interaction is not strong but is present. This resulted in slightly "earlier" formation of the phospholipid aggregates. In this place, it can be noted that fluorescence spectroscopy refers only to cores which are able to solubilize hydrophobic species. These cores are in the center of interest, because they are potentially binding sites for drugs. This also means that in solution the phospholipid/biopolymer aggregates exist without a stable hydrophobic core.

Further experiments brought interesting information. Lecithin molecules were mixed with hyaluronans with higher molecular weight, viz. 300 kg mol^{-1} and 1460 kg mol^{-1}. Individual dependencies, together with the obtained aggregation concentration, clearly show that aggregation and the value of aggregation concentration are completely independent not only on the hyaluronan concentration but also on its molecular weight (see Table 3). Note that hyaluronan concentration spanned a broad region from 15 mg to 1 g per liter, which means that the concentration of biopolymer chains rapidly decreased in comparison with the first experiments described above but the number of monomers remained the same.

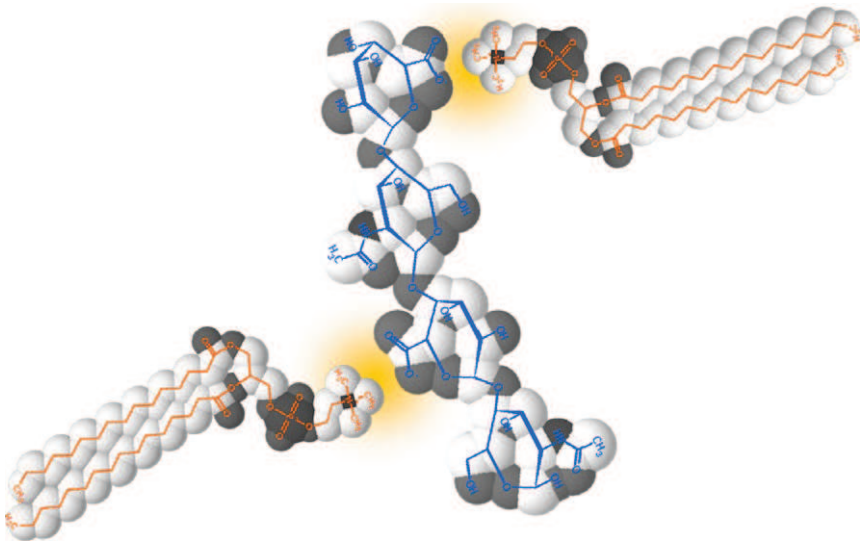

Figure 7 Illustration of supposed interaction between phospholipid and hyaluronan anion.

Table 3 Summary of hyaluronan effect on phospholipids aggregation concentration

HA MW (kg mol^{-1})	HA conc. (g L^{-1})	Aggregation concentration (mg L^{-1})	
		Lecithin	DPPC
Without HA		5.6 ± 0.1	0.8 ± 0.1
73	1	3.8 ± 0.3	0.9 ± 0.1
	0.015	3.3 ± 0.5	1.0 ± 0.1
300	1	3.8 ± 0.1	0.8 ± 0.1
	0.015	3.5 ± 0.3	1.4 ± 0.1
1460	1	3.9 ± 0.1	0.8 ± 0.1
	0.015	3.8 ± 0.1	0.9 ± 0.1

Another information extractable from the fluorescence experiments can be described as a "core quality." The final value of polarity index can be taken as its descriptor. From this point of view, formed aggregates are equal and there is no difference between free-formed aggregates and hyaluronan-complexed ones. Values of polarity indexes can be hardly assigned to a proper value of polarity, but can act as a good criterion for comparison of samples.

On the other hand, our experiments with DPPC in the presence of hyaluronan gave different results. Aggregation of free DPPC and in solution with biopolymer showed no difference. The obtained aggregation concentration values and other parameters of fit remained unchanged on the specified level of confidence.

Obtained results are summarized in Table 3. As can be seen, results for the DPPC only fluctuate around the mean value of 1 g L^{-1}. There is no obvious trend for this phospholipid.

Differences between aggregation behavior of lecithin and DPPC are quite interesting. This fact can be explained if we take into account what the name "lecithin" exactly covers. Lecithin used in this study consisted of 33% of DPPC the rest being various saturated and unsaturated analogues. The heterogeneity of this mixture allows the system to aggregate easily and to form smaller particles, which resulted in a clear solution even at higher concentrations in comparison with opalescent DPPC samples. This fact is inspiring for next work, which include combination of phospholipid and suitable surfactant. Another attempt was realized to prove interactions between DPPC and HA. Possible polymer binding sites were marked by AO dimers. These dimers showed no fluorescence when condensed on hyaluronan chain. If there is a stronger interaction between phospholipid and hyaluronan, than between AO and HA, AO dimers break-down and free monomers increase the fluorescence intensity from the sample. Of course, changes in absorption spectra, related to the absorbance of dimer, were also expected.

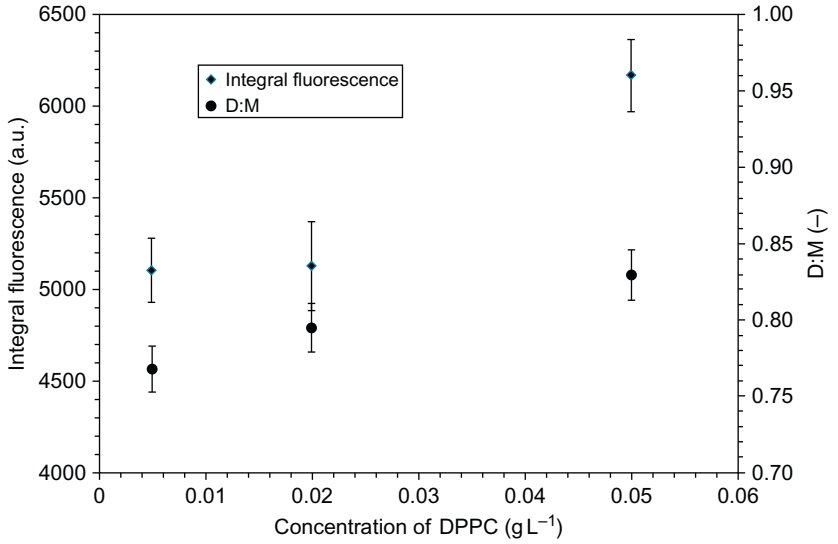

Figure 8 Dependency of the fluorescence intensity of acridine orange (as total integral) and D:M ratio on concentration of DPPC in the presence of hyaluronan (MW 73,000 g mol^{-1}; 15 mg L^{-1}).

From Fig. 8, it is obvious that increasing concentration of DDPC caused slightly increasing fluorescence intensity. The increasing intensity is accompanied by small increase of D:M ratio. These two opposite dependencies mean that there are no notable changes in this system and from the fluorescence-point-of-view there is no interaction between DPPC and native hyaluronan in aqueous solution.

6. Mixed System

Results obtained for DPPC failed to prove interactions of this phospholipid with hyaluronan but in the same time inspired additional experimentation. DPPC was further used only as an "interaction mediator." Main solubilization responsibility was transferred to suitable nonionic biocompatible surfactant and phospholipid should act as a linker to the hyaluronan macromolecule. In fact, formation of mixed surfactant-phospholipid micelles was supposed.

As surfactant for the experiments with mixed micelles, n-dodecyl β-D-maltoside (C_{12}maltoside, CAS #69227-93-6), a nonionic sugar-based amphiphile, was selected. The main idea was to use the nonionic surfactant as a medium for phospholipid dispergation and also as a solubilizing

environment. Phospholipid can act as a linking agent that bonds micelles and biopolymer together and also can act as an active nutritive component.

First, aggregation of nonionic surfactant in the presence of DPPC was investigated. Aggregation behavior as demonstrated by the dependency of the EmPI on surfactant concentration in the presence and absence of DPPC is shown on Fig. 8. Concentration of DPPC was set to 5 mg L^{-1}. From Fig. 9, it is evident that aggregation of C_{12}maltoside is quite simple, represented as simple sigmoidal curve, on contrary to the case when DPPC is present. Dependency of C_{12}maltoside aggregation in the presence of phospholipid showed local minimum nearby 0.05 mM. This concentration belongs to the induced aggregates of DPPC and maltoside. This fact is taken as a confirmation of interaction between DDPC and C_{12}maltoside surfactant. DPPC is directly solubilized into the sugar micelles and act as cosurfactant (Fig. 10).

These aggregates were used to interact with the AO labeled hyaluronan. From the previous measurements with DDPC, it was found out that the proper value of the dye amount on hyaluronan chain is nearby 0.3 mol of dye per mol of theoretical carboxylic groups. Complex of phospholipid and maltoside surfactant was prepared in the ratio of components PL:C12Mal 1:98. Value 98 came from aggregation number of maltoside surfactant in aqueous solution in region above its CMC, as were reported by producer [25]. In other words 1 mol of PL was present in the solution per 1 mol of theoretical C_{12}maltoside micelle.

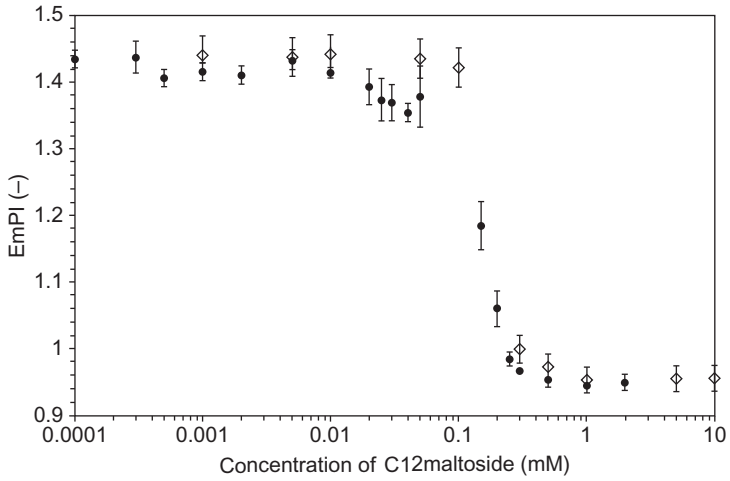

Figure 9 Dependency of the emission polarity index (EmPI) on C_{12}maltoside concentration in the presence (●) and absence (◇) of DPPC.

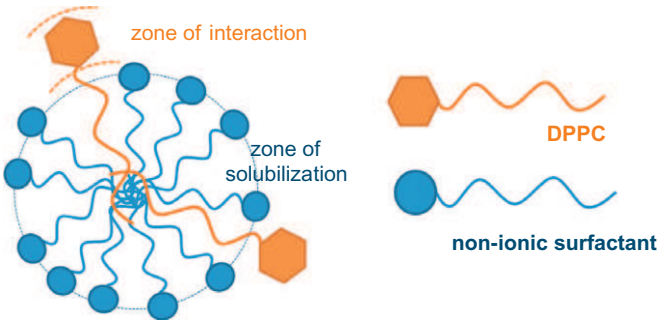

Figure 10 Illustration of supposed phospholipid–C_{12}maltoside complex.

The presence of the third component changes initial condition (besides the changed environment). Phospholipid was now only a minor part of the system from the "mass-point-of-view," but still remained the most important component. Phospholipid was used below its aggregation concentration and its presence could induce formation of nonionic surfactant micelles at lower concentration. All this made the experimental design a little bit problematic. A lot of parameters should be covered, for example, the ratio between PL and surfactant. Another problem was how to prove interactions between the amphiphiles complex and the biopolymer. One possible way was to mark the binding sites by the AO dimer, as reported above in the case of interaction of DPPC with hyaluronan.

Figure 11 displays dependencies of the fluorescence intensity of AO and D:M ratio on the concentration of the PL-surfactant complex. Addition of the complex increased fluorescence intensity that is related to the AO dimer breakdown. This was confirmed by the D:M dependency which showed that the amount of dimer in the system decreased. D:M ratio, as observable parameter, looked to be more sensitive to the changes in this complex solution. With respect to the error bars, there are three plateaus in this dependency. The plateaus indicate that complex should interact with nonlabeled parts of biopolymer. These parts can be primarily nonlabeled, due to interaction with complex these part are coming accessible for interaction, or they are firstly bonded aggregates and coming complexes only increase their aggregation number.

Fluorescence intensity slightly increased up to concentration around 5 mg L^{-1}. After this concentration, the fluorescence intensity increased rapidly. With respect to the D:M dependency, this increase can be explained as dimer breaking.

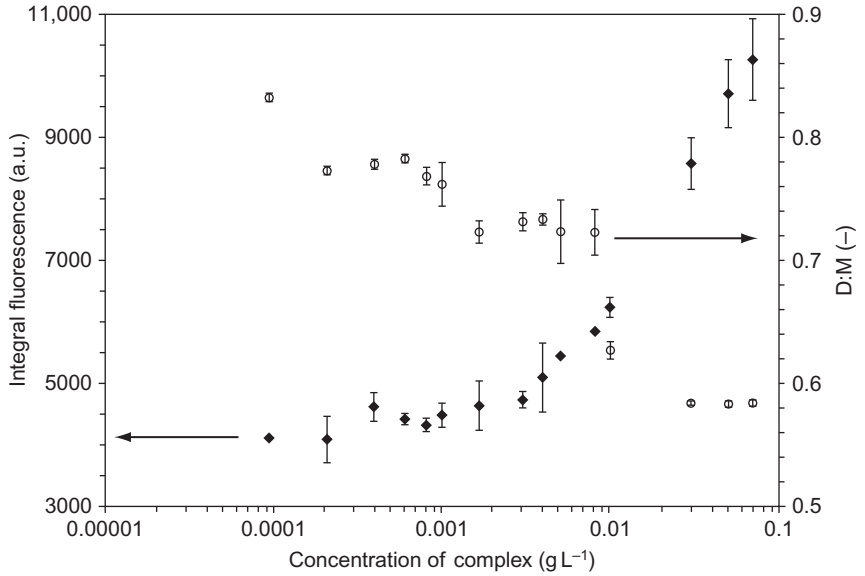

Figure 11 Dependency of the fluorescence intensity of acridine orange (as total integral; ◆) and D:M (○) ratio on concentration of DPPC–C_{12}maltoside complex.

7. Conclusion

Fluorescence probes showed that phospholipids, DPPC and lecithin, aggregate in aqueous solution to form micelle-like structures capable to solubilize hydrophobic molecules. Only in the case of lecithin, changes in its aggregation behavior were observable after adding hyaluronan. Presence of hyaluronan shifted aggregation concentration of the lecithin to the lower values. On the other hand, experiments with DPPC did not bring any evidence of interaction.

As a novel approach of this work in forming hyaluronan–phospholipid complexes, nonionic biocompatible surfactant was used as a dispersion environment for phospholipid molecules. Phospholipid than could act as a physical linker which bonds micelles and biopolymer together by physical forces and could also serve as an active nourishing agent. This new type complex can be used as a part of cosmetic formulation combining hydrating and nourishing effects or in pharmaceutics for the delivery of water insoluble active molecules.

ACKNOWLEDGMENTS

This work was supported by the Czech Ministry of Education, project No. OC08004 and COST action D43. The Centre for Materials Research at FC BUT is supported by project No. CZ.1.05/2.1.00/01.0012 from ERDF. Assistance of Tereza Halasová, Iva Maivaldová, and Jana Szewieczková in experimental work is gratefully acknowledged.

REFERENCES

[1] L. Lapčík, L. Lapčík, S. De Smedt, J. Demeester, P. Chabreček, Hyaluronan: preparation, structure, properties, and applications, Chem. Rev. 98 (1998) 2663–2684.
[2] M.K. Cowman, S. Matsuoka, Experimental approaches to hyaluronan structure, Carbohyd. Res. 340 (2005) 791–809.
[3] K.P. Vercruysse, G.D. Prestwich, Hyaluronate derivatives in drug delivery, Crit. Rev. Ther. Drug 15 (1998) 513–555.
[4] H.G. Garg, C.A. Hales (Eds.), Chemistry and Biology of Hyaluronan, Elsevier, Amsterdam, 2004.
[5] C.B. Knudson, W. Knudson, Hyaluronan-binding proteins in development, tissue homeostasis, and disease, FASEB J. 7 (1993) 1233–1241.
[6] S. Jaracz, J. Chen, L.V. Kuznetsova, I. Ojima, Recent advances in tumor-targeting anticancer drug conjugates, Bioorgan. Med. Chem. 13 (2005) 5043–5054.
[7] P. Prehm, Hyaluronan, in: E.J. Vandomme, S. De Baets, A. Steinbückel (Eds.), Biopolymers, Polysaccharides I: Polysaccharides from Prokaryotes, vol. 5, Wiley, Weinheim, 2002, pp. 379–406.
[8] M. Paye, A.O. Barel, H.I. Maibach (Eds.), Handbook of Cosmetic Science and Technology, Taylor & Francis, New York, 2006.
[9] V. Crescenzi, A. Taglienti, I. Pasquali-Ronchetti, Supramolecular structures prevailing in aqueous hyaluronic acid and phospholipid vesicles mixtures: an electron microscopy and rheometric study, Colloid. Surf. A 245 (2004) 133–135.
[10] C. Gomez-Gaete, N. Tsapis, L. Silva, C. Bourgaux, M. Besnard, A. Bochot, E. Fattal, Supramolecular organization and release properties of phospholipid-hyaluronan microparticles encapsulating dexamethasone, Eur. J. Pharm. Biopharm. 70 (2008) 116–126.
[11] P. Ghosh, N. Hutadilok, N. Adam, A. Lentini, Interactions of hyaluronan (hyaluronic-acid) with phospholipids as determined by gel-permeation chromatography, multi-angle laser-light-scattering photometry and H-1-NMR spectroscopy, Int. J. Biol. Macromol. 16 (1994) 237–244.
[12] P. Ghosh, N. Hutadilok, A. Lentini, Nuclear-magnetic-resonance studies of hyaluronan (HA): evidence of competitive-inhibition of interchain associations by phospholipids which may result in decreased antiinflammatory and cartilage protecting properties of HA, Heterocycles 38 (1994) 1757–1774.
[13] T. Moro-oka, H. Miura, T. Mawatari, T. Kawano, Y. Nakanishi, H. Higaki, Y. Iwamoto, Mixture of hyaluronic acid and phospholipid prevents adhesion formation on the injured flexor tendon in rabbits, J. Orthop. Res. 18 (2000) 835–840.
[14] B.A. Hills, Boundary lubrication *in vivo*, Proc. Inst. Mech. Eng. H J. Eng. Med. 214 (2000) 83–94.
[15] B.A. Hills, Remarkable antiwear properties of joint surfactant, Ann. Biomed. Eng. 23 (1995) 112–115.
[16] T. Kawano, H. Miura, T. Mawatari, T. Moro-Oka, Y. Nakanishi, H. Higaki, Y. Iwamoto, Mechanical effects of the intraarticular administration of high molecular weight phospholipid on synovial joint articular cartilage degeneration hyaluronic acid

plus lubrication and prevention of in experimental osteoarthritis, Arthritis Rheum-us 48 (2003) 1923–1929.
[17] R.W. Forsey, J. Fisher, J. Thompson, M.H. Stone, C. Bell, E. Ingham, The effect of hyaluronic acid and phospholipid based lubricants on friction within a human cartilage damage model, Biomaterials 27 (2006) 4581–4590.
[18] I. Pasquali-Ronchetti, D. Quaglino, G. Mori, B. Bacchelli, P. Ghosh, Hyaluronan–phospholipid interactions, J. Struct. Biol. 120 (1997) 1–10.
[19] G. Steffan, S. Wulff, H.J. Galla, Divalent cation-dependent interaction of sulfated polysaccharides with phosphatidylcholine and mixed phosphatidylcholine phosphatidylglycerol liposomes, Chem. Phys. Lipids 74 (1994) 141–150.
[20] A. Taglienti, F. Cellesi, V. Crescenzi, P. Sequi, M. Valentini, N. Tirelli, Investigating the interactions of hyaluronan derivatives with biomolecules. The use of diffusional NMR techniques, Macromol. Biosci. 6 (2006) 611–622.
[21] S.L. Huang, P.X. Ling, T.M. Zhang, Oral absorption of hyaluronic acid and phospholipids complexes in rats, World J. Gastroentero. 13 (2007) 945–949.
[22] D.W. Nitzan, U. Nitzan, P. Dan, S. Yedgar, The role of hyaluronic acid in protecting surface-active phospholipids from lysis by exogenous phospholipase A(2), Rheumatology 40 (2001) 336–340.
[23] P. Morganti, G. Fabrizi, B. James, A new cosmetic solution for a mild to moderate xerosis, J. Appl. Cosmetol. 17 (1999) 86–93.
[24] D. Marsh, Handbook of Lipid Bilayers, first ed., CRC Press, Boca Raton, 1990.
[25] http://www.sigmaaldrich.com, (accessed on February 24, 2011).

Colloid Polym Sci (2016) 294:823–831
DOI 10.1007/s00396-016-3840-8

ORIGINAL CONTRIBUTION

The formation of mixed micelles of sugar surfactants and phospholipids and their interactions with hyaluronan

Jana Burdíková [1,2] · **Filip Mravec** [1,2] · **Miloslav Pekař** [1,2]

Received: 2 November 2015 / Revised: 7 January 2016 / Accepted: 18 January 2016 / Published online: 12 February 2016

Abstract The aggregation of sugar surfactants and the incorporation of phospholipids into sugar surfactant micelles were investigated by means of fluorescence spectroscopy. Two representatives from the family of alkyl glucosides were studied: dodecyl-β-D-maltoside and octyl-β-D-glucopyranoside. The presence of 1,2-dipalmitoyl-*sn*-glycero-3-phosphatidylcholine (DPPC) in the sugar surfactant system promoted the formation of new structures at sugar surfactant concentration below its critical micelle concentrations. According to the aggregation number measurements studied by a fluorescence quenching of hexadecylpyridinium chloride measurements, the premicellar aggregates formed from octyl-β-D-glucopyranoside and DPPC were composed of the third of molecules compared to the octyl-β-D-glucopyranoside micelles. Interactions of the formed mixed micelle systems composed of sugar surfactant and DPPC with hyaluronan were explored. The addition of hyaluronan had different effects on the dodecyl-β-D-maltoside/DPPC and octyl-β-D-glucopyranoside/DPPC mixed systems. In addition, the mixed system of dodecyl-β-D-maltoside and lecithin was studied, but possibly, only a coexistence of lipid aggregates and sugar surfactant micelles was observed.

Keywords Sugar-based surfactants · Hyaluronan · 1,2-Dipalmitoyl-*sn*-glycero-3-phosphatidylcholine · Premicellar aggregate · Fluorescence spectroscopy · Pyrene

Abbreviations

DM	Dodecyl-β-D-maltoside
OG	Octyl-β-D-glucopyranoside
EmPI	Emission polarity index
ExPI	Excitation polarity index
CMC	Critical micelle concentrations
CPC	Hexadecylpyridinium chloride monohydrate
DPPC	1,2-Dipalmitoyl-*sn*-glycero-3-phosphatidylcholine
Hya	Hyaluronan
CBA	Concentration at the beginning of an aggregation
R^2	Reliability

Introduction

Hyaluronan, an important and multifunctional polysaccharide, is known to form aggregates with oppositely charged (cationic) surfactants [1, 2]. These aggregates could be considered as potential candidates for the delivery of non-polar drugs—hyaluronan forms biocompatible and targeting envelope whereas micelle-like structures formed by surfactant molecules on the biopolymeric chain provide solubilization ability. However, cationic surfactants are also known for their cytotoxic effects which are only moderately suppressed in the presence of hyaluronan [3]. In our previous study [4], we tried to replace cationic surfactants by phospholipids bearing positive charge, but their interactions with hyaluronan were weak. In this work, we elaborate on the idea of combining phospholipids with sugar-based non-ionic surfactant formulated in ref. [4].

Electronic supplementary material The online version of this article (doi:10.1007/s00396-016-3840-8) contains supplementary material, which is available to authorized users.

✉ Filip Mravec
mravec@fch.vutbr.cz

[1] Institute of Physical and Applied Chemistry, Faculty of Chemistry, Brno University of Technology, Purkyňova 118/464, 612 00 Brno, Czech Republic

[2] Materials Research Centre, Faculty of Chemistry, Brno University of Technology, Purkyňova 118/464, 612 00 Brno, Czech Republic

Non-ionic surfactants, a category of non-ionic amphiphiles, are generally considered to be mild and relatively non-denaturing, as they break lipid–lipid interactions and lipid–protein interactions rather than protein–protein interactions [5]. Sugar-based surfactants are widely (or predominantly) used for membrane protein extraction in the study of protein–lipid interactions [6–10] and membrane protein structure and function [11, 12]. The combination of sugar-based surfactants and the principal component of cell membranes, with phospholipids can result in interesting aggregates which can find potential applications in the area of biocompatible drug carrier systems generally.

Because of the combination of a relatively large amphoteric double-tail phospholipid with a small non-ionic single-tail one, the resulting structure of the aggregates will be strongly dependent on their molar ratio [13–16]. There are two main types of expected aggregates—liposome-based with a dominant fraction of phospholipids and micelle-based with a dominant fraction of single-tail surfactant. The phase transition of a lipid from a membranous to a micellar state is assumed to run through three stages. First, the non-micellar surfactant incorporates into the phospholipid bilayer, the surfactant micelles serving as a reservoir to continually replenish the amount of non-micellar surfactant which is removed by the interaction with the membrane. In the second stage, phospholipid membranes saturated with incorporated surfactant coexist in thermodynamic equilibrium with mixed phospholipid/surfactant micelles saturated with phospholipid, whereas in the last stage, the phospholipid is fully solubilized by its uptake into surfactant micelles and mixed micelles are formed [14, 16]. This second aggregate type is subject of this work.

It has been reported that both dodecyl-β-D-maltoside (DM) and octyl-β-D-glucopyranoside (OG) have high ability to solubilize liposomes [17] and that below the critical micelle concentration (CMC), the unbound surfactant incorporates into the membranes and a strongly cooperative binding process occurs [16]. The dependence of mixed micelle stoichiometry on the concentration of aqueous OG is consistent with the assumptions that ideal mixing of the two amphiphiles in the mixed micelles takes place and that mixed micelles can be treated as a distinct phase [18].

These two surfactants were used in this work which is organized as follows. First, results of study on 1,2-dipalmitoyl-*sn*-glycero-3-phosphatidylcholine (DPPC) aggregation are described. In the second part, the formation of mixed micelles of sugar surfactants and DPPC is studied. Following parts report on surfactant aggregation numbers and (very weak) interactions of DM with lecithin. In the last part, interactions of mixed surfactant-DPPC micelles with hyaluronan are investigated. Fluorescence techniques were used throughout the whole study.

Materials and methods

Materials

Hyaluronic acid, sodium salt (0.31 MDa) was purchased from Contipro (Czech Republic); dodecyl-β-D-maltoside from Fluka (99.0 %); octyl-β-D-glucopyranoside (98.0 %), DPPC (99.0 %), hexadecylpyridinium chloride monohydrate (CPC, 99.0 %), lecithin (type XVI-E), and chloroform from Sigma-Aldrich. These structures are shown in the Supplementary Material, Fig. S1. Pyrene (p. a. for fluorescence), perylene (for fluorescence), Nile Red (for fluorescence), and sudan red (96.0 %) were purchased from Fluka. All experiments were performed in ultrapure water.

Fluorescence probe technique

All systems were studied by fluorescence spectroscopy using a Fluorolog HORIBA Jobin Yvon instrument; CMC values were obtained using fluorescence spectroscopy with pyrene as a fluorescence probe. Pyrene emission spectra were measured in the range of 360–540 nm with an excitation wavelength of 335 nm. From these spectra, the emission polarity index (EmPI) was obtained from the ratio of the fluorescence intensities of the first (373 nm) and third (383 nm) bands [19–24]. Fluorescence intensities of the excimer band (470 nm) and monomer band (373 nm) were used to calculate the excimer/monomer ratio (Ex/Mo).

Excitation spectra of pyrene were recorded in the range of 330–340 nm with an emission wavelength of 392 nm. The excitation polarity index (ExPI) was calculated as the ratio of fluorescence intensities at 333 and 338 nm [25–27]. The dependence EmPI or ExPI on the surfactant concentration was then fitted by means of a Boltzmann sigmoid curve (Eq. 1), where y corresponds to EmPI (ExPI), the independent variable x to the surfactant concentration with the point of inflection x_0, parameter Δx is connected to the slope of the curve, and A_1 and A_2 are y-coordinates of the first and second breaks. The CMC was obtained as its point of inflection.

$$y = \frac{A_1 - A_2}{1 + e^{\frac{x - x_0}{\Delta x}}} + A_2 \quad (1)$$

The DPPC aggregation was also studied using Nile Red as fluorophore. Nile Red is suitable for this application. Since this hydrophobic dye is poorly soluble in water, its fluorescence is sensitive to polarity of local environment [28, 29]. Emission spectra of Nile Red were recorded in the range of 500–750 nm with an emission wavelength of 490 nm, and the total integral of Nile Red emission spectra was monitored.

Aggregation of sugar surfactants

The required amount of sugar surfactant was dissolved in water. Then, pyrene dissolved in acetone was pipetted into vials to achieve final pyrene concentrations in the order of magnitude 10^{-7} or 10^{-6} M. After the evaporation of acetone under reduced pressure, an increasing amount of surfactant stock solution was pipetted into the vials and water was added to achieve a series of sugar surfactant concentrations in the range of 0.001–2 mM (in some cases, 0.0001–10 mM). Then, after 24 h of agitation, their critical micelle concentrations were measured by fluorescence spectroscopy as described in Fluorescence probe technique section. Results of this basic study are given in Supporting Information.

Aggregation of DPPC

With usage of Nile Red

DPPC was dissolved in chloroform in a vial. After evaporation of the chloroform, water was added to achieve a DPPC concentration of 1 g dm^{-3} and the solution was sonicated for 30 min at 45 °C. Then, Nile Red dissolved in acetone was pipetted into the series of vials to achieve a final Nile Red concentration in DPPC samples in the order of magnitude 10^{-7} M. After evaporation of the acetone, different amount of stock solution of DPPC was added to these vials to obtain a concentration series of DPPC. Samples were refilled with water to total volume of 4 ml. Samples were measured by fluorescence spectroscopy after 24 h of agitation. In the case of phospholipids, micelles are formed at very low concentrations (nM); thus, the concentration at which the nature of aggregates changes from micelles to liposomes was measured and called the critical aggregation concentration (CAC_{PL}) of phospholipids.

With usage of saturated pyrene solution

A stock solution of DPPC was prepared as described above (With usage of Nile red section), but, instead of water, a saturated aqueous solution of pyrene was added to DPPC film after evaporation of chloroform. The stock solution was diluted by the saturated aqueous solution of pyrene to prepare solutions with lower concentrations of DPPC.

Formation of mixed micelles

DPPC (or lecithin) was dissolved in chloroform. The required amount of this solution was pipetted into vials (to achieve a final DPPC concentration of 0.005 or 0.07 g dm^{-3} or a final lecithin concentration of 0.5 or 5 g dm^{-3}). The chloroform was evaporated, an increasing amount of surfactant stock solution was pipetted into the vials containing DPPC (or lecithin), and water was added to achieve the required volume. The solutions were then sonicated for 30 min and, after 24 h of agitation, pipetted into vials preprepared with pyrene as described above (from an acetone solution). Then, after 24 h of agitation, the critical aggregation concentration of mixed sugar-based surfactant/lipid system (CAC_M) and critical micelle concentration of sugar-based surfactants (DM and OG) were determined as the first and second point of inflection on the EmPI or ExPI dependence on sugar-based surfactant concentration. To distinguish aggregation in mixed system from that of pure phospholipids, subscript "M" was used in the former.

Interaction of mixed micelles with hyaluronan

A stock solution of hyaluronan was prepared by dissolving the required amount of hyaluronan in water. Then, the procedure was the same as described above in Formation of mixed micelles section. The same amount of hyaluronan stock solution was pipetted into each vial already containing the sugar-based surfactant solution and pyrene, then, after 24 h of agitation, the critical aggregation concentration of mixed sugar-based (CAC_M) surfactant/DPPC/hyaluronan system.

Determination of aggregation number of sugar surfactants

A series of solutions with the same concentration of sugar surfactant and pyrene and increasing concentrations of CPC were prepared as mentioned above in Aggregation of sugar surfactants section. An increasing amount of bulk solution of CPC was pipetted into pyrene-containing vials immediately after the sugar surfactant was added. Then, fluorescence spectra of pyrene were measured, and the aggregation number of the sugar surfactants was calculated. The concentration of sugar surfactant was above its CMC, and, in the case of the sugar surfactant and DPPC mixture, the concentration of sugar surfactant was above the CAC_M and below the CMC of the mixture.

The aggregation number depends on the surfactant concentration according to Eq. 2, where c_s is the surfactant concentration, CMC is the critical micelle concentration of this surfactant, I_0 is the fluorescence intensity in the absence of a quencher, I is intensity of fluorescence in the presence of a quencher, and [Q] is the quencher concentration [30].

$$N_{agg} = \frac{c_s - \mathrm{CMC}}{\ln\left({}^{I_0}/_{I}\right)\ [Q]} \tag{2}$$

Table 1 Concentration of the beginning of an aggregation (CBA) and CAC_{PL} of DPPC

Fluorescence probe	Dependence	CBA (g dm^{-3})	CAC (g dm^{-3})
Pyrene	EmPI	0.0043	0.0138
	ExPI	0.0026	0.0110
Nile Red	Tot. integral	0.0045	0.0147
Average		0.0038	0.0132
Deviation		0.0011	0.0019

Results and discussion

Aggregation of DPPC

The aggregation behavior of DPPC was examined by two methods to compare results. First, the CAC_{PL} in saturated pyrene solution was measured. Figure 1 shows the dependence of pyrene EmPI and ExPI on DPPC concentration; the obtained CAC_{PL} values are listed in Table 1.

In the second method, the CAC_{PL} of DPPC was measured with Nile Red as the fluorescence probe. Figure 2 shows the dependence of the total integral of Nile Red emission spectra in the range of 525–750 nm on DPPC concentration. Two breaks are evident—the dependence was fitted by three straight lines, and two breaks were obtained. The first break corresponds well to the first break of the Boltzmann curve from the measurement mentioned above. We can assume that a two-break dependence indicates a rather gradual transformation from micelles to vesicles, rather than a fast one. Thus, the concentration at the first break was called the concentration at the beginning of an aggregation (CBA), while the second was labeled as the CAC_{PL} of DPPC. In solution, the transformation from micelle-like structures to other aggregates (liposomes, vesicles) probably begins at CBA and ends at CAC_{PL}, when these new aggregates (new type of aggregates) are formed. All measured concentrations are listed in Table 1. The data

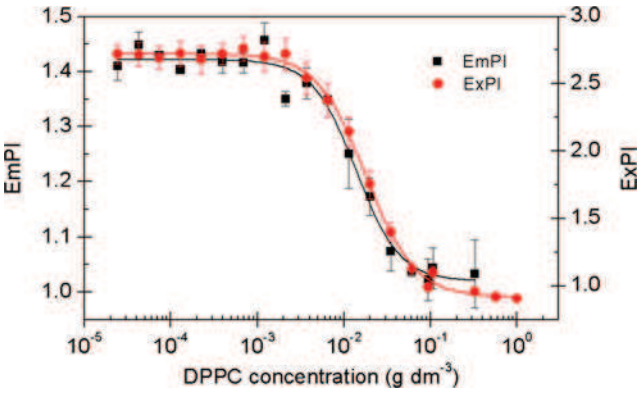

Fig. 1 Dependence of pyrene EmPI and ExPI on DPPC concentration. The first break in the Boltzmann curve corresponds to the concentration at the beginning of an aggregation (CBA), while the point of inflection corresponds to the CAC_{PL} of DPPC

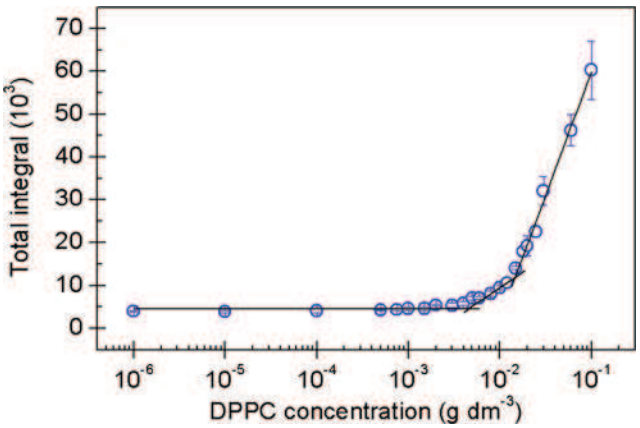

Fig. 2 Dependence of total integral of Nile Red emission spectra on DPPC concentration, fitted by three straight lines. The first point of intersection corresponds to CBA, while the second corresponds to CAC_{PL} of DPPC

obtained from measurements of pyrene EmPI and the Nile Red total integral are in good agreement with each other. On the other hand, the CBA and CAC_{PL} obtained from measurements of pyrene ExPI are slightly lower.

For further measurements of mixed micelle formation, a DPPC concentration of 5 mg dm^{-3} (close to CBA) was chosen. Next, samples with higher concentrations of DPPC were tested to choose a higher concentration of DPPC for further study (higher than its CAC_{PL}). Figure S2 shows samples with different DPPC concentrations; only in the case of the sample with the lowest DPPC concentration (0.07 g dm^{-3}) was complete dissolution achieved, leaving the sample transparent. Thus, this concentration of DPPC was also chosen for subsequent experiments.

Mixed micelle formation

Results of preliminary study on the aggregation of pure surfactants are given in Supporting Material. At the beginning of the mixed micelle formation study, it was necessary to choose an optimal concentration of pyrene. In Fig. S5 in the Supplementary Material, the dependences of pyrene EmPI on DM concentration for different concentrations of pyrene are shown. The pyrene concentration of 5×10^{-7} M was chosen as the best, because, at lower pyrene concentrations, data did not show sigmoidal dependence and standard deviations were too large, while at higher pyrene concentrations, there was no smooth dependence on DM concentration just before CMC appeared.

Then, a series of mixtures of sugar surfactant (DM or OG) with DPPC (0.005 and 0.07 g dm^{-3}) was prepared, with increasing sugar surfactant concentrations. In the case of the mixtures of sugar surfactant with the higher DPPC concentration (0.07 g dm^{-3}), incomplete dissolution was achieved at concentrations of sugar surfactant lower than their CMC, the measured data showing large deviations (Fig. S6). At higher

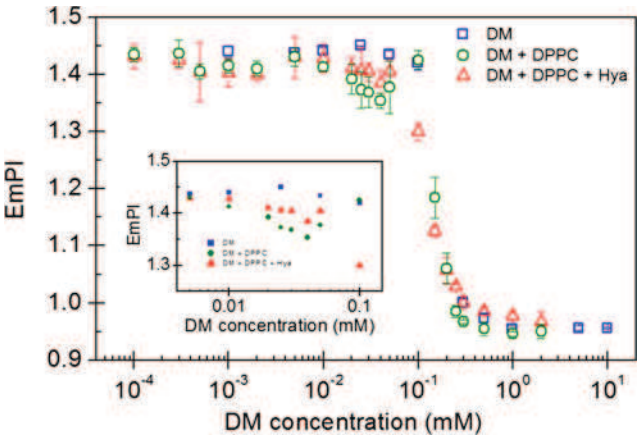

Fig. 3 Dependences of pyrene EmPI on DM concentration of DM and its mixture with DPPC and DPPC with Hya

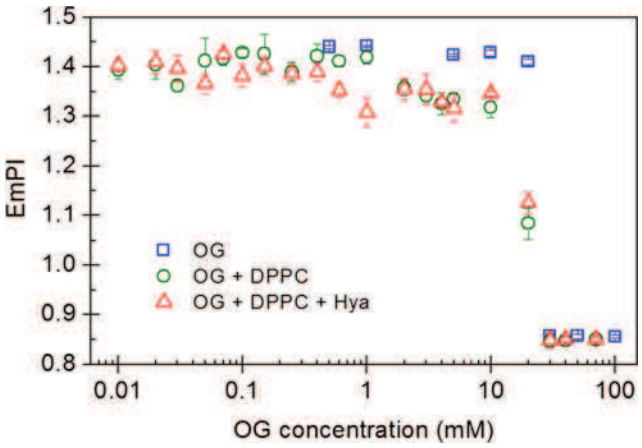

Fig. 4 Dependences of pyrene EmPI on the OG concentration of OG and its mixture with DPPC and DPPC with Hya

concentrations of sugar surfactant, samples were entirely clear and standard deviations in the data were narrow. At a DPPC concentration of 0.07 g dm^{-3}, the system is in a biphasic micellar region up to a DM concentration of 0.15 mM (DM/DPPC molar ratio 1.5). Above this concentration, only one micellar phase is present in the solution [14]. The presence of two micellar phases may be the cause of system instability.

Figure 3 shows the dependences of EmPI on DM concentration for DM and its mixtures with DPPC. In the dependence for the mixture of DM and DPPC, the decrease in EmPI at a DM concentration of about 0.01 mM and the following increase in the range of DM concentrations of 0.04–0.1 mM are obvious. This variation in EmPI could indicate the formation of premicellar aggregates and their disintegration just before CMC and micelle formation. This dependence was analyzed in two different ways—by fitting it according to one or two Boltzmann curves. In the case of two Boltzmann curves, the first point of inflection was labeled CAC_M (the formation of the first aggregates with a hydrophobic core), while the second was labeled CMC. If the dependence was fitted by only one Boltzmann curve, the only point of inflection was labeled CMC. Table 2 presents the parameters of the Boltzmann curves. For the mixture of DM and DPPC, it is evident that fitting by two Boltzmann curves is better (the reliability is greater (values shown in Table S2, Supplementary Material), and lower chi^2 are calculated from the difference between the measured values and the fitting curve).

From the obtained CMCs listed in Table 2, it is apparent that CMC decreases with the addition of DPPC to DM. In the case of the mixture of DM and DPPC, CAC_M is localized approximately at a ten times lower concentration than CMC.

Figure 4 shows the dependences of EmPI on OG concentration for OG and its mixtures with DPPC. The mixture containing OG and DPPC exhibits a first decrease in EmPI at an OG concentration of about 2 mM. This can indicate, as with the mixture of DM and DPPC, the formation of premicellar aggregates before micelle formation. However, in contrast to the DM and DPPC mixture, there is no increase in EmPI—probably, the formed premicellar aggregates do not disintegrate but instead transform into micelles. This difference of DM and OG behavior in the presence of DPPC could be hidden in their different molecular shapes. Probably due to dimeric head group of DM molecule, DM micelles have larger shell thickness compared to OG and phosphocholines [31, 32], which could cause the DPPC/DM aggregates' nestability. Then, the dependence shows a sharp decrease in EmPI, and its point of inflection corresponds to the CMC of the system. Table 3 lists the obtained values of CAC_M and CMC and clearly shows that the addition of DPPC to OG slightly lowers

Table 2 Parameters of Boltzmann curves for DM and its mixtures with DPPC and Hya—CMC, CAC_M, and chi^2, according to the number of Boltzmann curves (N_B) used for fitting

Added constituents	N_B	CAC_M				CMC			
		EmPI (mM)	Chi^2 (10^{-5})	ExPI (mM)	Chi^2 (10^{-5})	EmPI (mM)	Chi^2 (10^{-5})	ExPI (mM)	Chi^2 (10^{-5})
–	1	–	–	–	–	0.2126	4.05	0.1917	44.8
DPPC	1	–	–	–	–	0.1589	85.9	0.1497	1200
	2	0.0162	1.02	0.0149	6.81	0.1557	53.5	0.1432	144
DPPC; Hya	1	–	–	–	–	0.1286	23.8	0.1215	180

Table 3 Parameters of Boltzmann curves for OG and its mixtures with DPPC and Hya—CMC, CAC_M, and chi^2, according to number of Boltzmann curves (N_B) used for fitting

Added constituents	N_B	CAC_M				CMC			
		EmPI (mM)	Chi^2 (10^{-5})	ExPI (mM)	Chi^2 (10^{-5})	EmPI (mM)	Chi^2 (10^{-5})	ExPI (mM)	Chi^2 (10^{-5})
–	1	–	–	–	–	21.2	8.76	19.7	204
DPPC	1	–	–	–	–	17.3	87.2	18.0	932
	2	1.80	9.37	1.60	91.5	19.9	6.39	19.3	3.88
DPPC; Hya	1	–	–	–	–	20.4	155	14.5	1180
	2	0.44	18.7	0.45	242	20.11	23.6	19.94	114

the CMC of the system. Note that the CAC_M of the OG and DPPC mixture is approximately ten times lower than its CMC.

It has been reported [15] that the solubilization of PC vesicles by OG begins with the transformation to vesicles with a lower radius of curvature, which then open with narrow and wide pores before collapsing to long cylindrical micelles that coexist with small spheroidal micelles, which are the dominant structure at high surfactant concentrations. In spite of the different approach in this work, where the DPPC concentration was fixed in the region where vesicles are not formed, it can be assumed that at concentrations where CAC_M was found, cylindrical micelles are formed, which are transformed into mixed micelles at CMC.

Aggregation number of sugar surfactant determination

The aggregation numbers of DM and OG were determined to find the number of sugar surfactant molecules needed to form a micelle for comparison with mixtures of sugar surfactant and DPPC at the sugar surfactant concentration at which premicellar aggregates are present (the concentration of sugar surfactant above its CAC_M but below its CMC). The DPPC concentration was 0.005 g dm^{-3} as in previous measurements. Critical micellar concentration of CPC, which was used as a quencher in the determination of aggregation numbers, was also measured—for method and results, see Supporting Information.

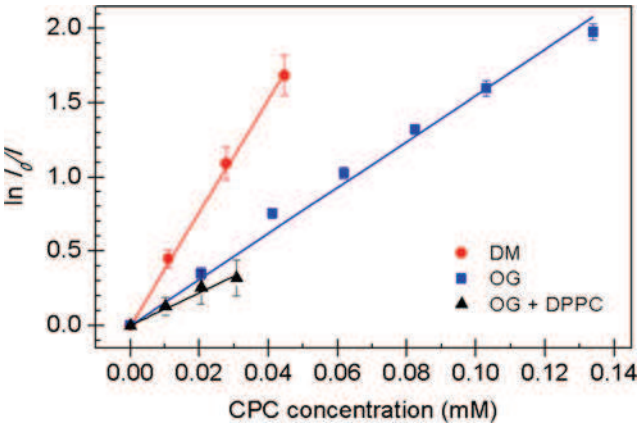

Fig. 5 Dependences of ln I_0/I on CPC concentration for determination of the aggregation numbers of DM, OG, and the mixture of OG and DPPC

Figure 5 shows the obtained dependences. I_0 is the fluorescence intensity in the absence of a quencher (CPC), and I is the fluorescence intensity in the presence of a quencher. In the case of the DM and DPPC mixture, the obtained data did not show any dependence and an aggregation number for this mixture was not determined. This was probably because of the disintegration of the formed premicellar aggregates just before CMC as described in Mixed micelle formation section. Elsewhere, aggregation numbers were calculated from the slopes of straight lines; they are listed in Table 4. The measured values for the DM and OG aggregation numbers (N_{agg}) are in good agreement with those from literature. The wide range of reference values results from the wide variety of shapes that surfactants can form. It can be seen that N_{agg} of the OG and DPPC mixture is approximately three times lower than N_{agg} of OG alone. From this, we can conclude that premicellar aggregates are slightly smaller than OG micelles.

DM and lecithin mixed systems

Finally, the aggregation of DM in the presence of lecithin was investigated (in the same way as in the case with DPPC present). The first concentration of lecithin was approximately 5 mg dm^{-3} [36], its concentration at the beginning of aggregation, and second concentration was ten times lower (0.5 mg dm^{-3}).

Figure 6 shows the dependence of Ex/Mo on DM concentration for the DM mixture with lecithin, which is compared with that for DM. Table 5 lists the CMCs obtained from these measurements by fitting the dependences of pyrene EmPI

Table 4 Measured and reference values for aggregation numbers of DM, OG, and the mixture of OG and DPPC

System	Measured value	Reference value
DM	69 ± 7	132 [33]; 70–140 [34]
OG	105 ± 3	27–100 [35]
OG + DPPC	36 ± 1	–

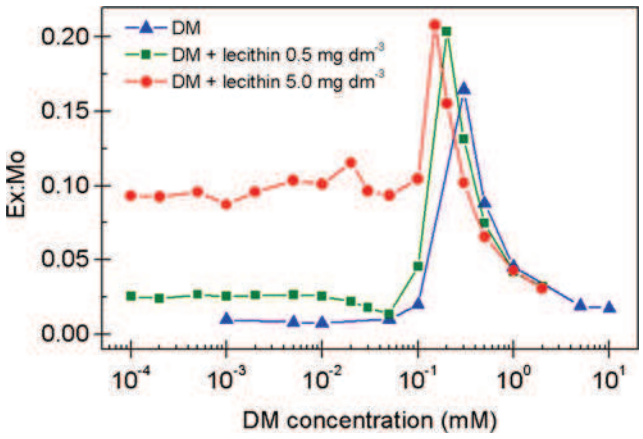

Fig. 6 Dependences of pyrene Ex/Mo on the DM concentration of DM and on the DM concentration of DM mixtures with lecithin at a concentration 0.5 g dm^{-3} and with lecithin at a concentration of 5.0 g dm^{-3}

(Fig. S8) and ExPI to the DM concentration. It is evident that the CMC is slightly reduced with the addition of lecithin. The presence of lecithin at a low concentration (0.5 mg dm^{-3}) probably supports micelle formation, but the CMC is reduced only slightly; therefore, this may be caused by the presence of another amphiphilic substance in the system. This assumption was confirmed by the following measurement of the DM mixture with lecithin at a concentration of 5 mg dm^{-3}. Figure 6 shows the dependence of Ex/Mo on DM concentration for this measurement. Note that, in the case of the DM mixture with lecithin of a higher concentration at the region with a low concentration of DM, the Ex/Mo ratio is higher than in the case of the other mixtures. The explanation may be the formation of aggregates in the system regardless of the addition of DM.

Interactions of mixed micelles with hyaluronan

Based on previous experiments, mixed micelles of DM or OG with DPPC were investigated for their interactions with Hya. Figure 3 shows the dependences of EmPI on surfactant concentration for DM-based mixed micelles. Just one Boltzmann curve was necessary to fit the data which showed a decrease of CMC in the presence of Hya (see also Table 2).

The OG-based micelles showed different behavior in the presence of Hya—two decreases on the dependence of polarity indices on surfactant concentration were detected. The first decrease in the dependence of pyrene EmPI on the OG concentration occurred at an OG concentration of about 0.4 mM, and then, no increase in EmPI was observed, but it decreased sharply at about an OG concentration of 20 mM, the point of inflection corresponding to the CMC of system (Fig. 4). In the case of ExPI, the dependence was quite similar.

The dependence of pyrene EmPI (and also ExPI—data not shown) on the OG concentration in the mixture of the OG-DPPC mixed micelles and Hya was fitted both by one and by two Boltzmann curves (in contrast to the analogous system based on DM), and CAC_Ms and CMCs were obtained. In the case of both mixtures (OG with DPPC and OG, DPPC with Hya), fitting by two Boltzmann curves was again better than fitting by only one (in most cases, fitting by two curves exhibited higher reliability, see Table S3 in the Supplementary Material, and lower chi^2). All obtained data are listed in Table 3.

The addition of Hya to OG and DPPC mixtures decreases the CAC_M to values lower by an order of magnitude, but the CMC does not change. Thus, the CAC_M of the OG, DPPC, and Hya mixture is nearly 50 times lower than its CMC.

Table 5 CMCs of DM and lecithin mixed systems

c_{Lec} (mg dm^{-3})	EmPI	ExPI	Average
0	0.213	0.192	0.202 ± 0.015
0.5	0.169	0.177	0.173 ± 0.006
5.0	0.139	0.141	0.140 ± 0.001

Conclusion

In this work, we demonstrated that the interaction of DPPC with non-ionic surfactants (sugar-based surfactants) is possible, but lecithin does not interact with these surfactants.

After the addition of DPPC (at a concentration of 5 mg dm^{-3}) to both sugar surfactants DM and OG, their CMCs were reduced, premicellar aggregates were probably formed, and the CAC_M of the systems could be detected at approximately ten times lower concentration than CMCs were found. The aggregation number of OG was found to decrease from 105 (OG micelles) to 36 (DPPC/OG premicellar aggregates). After the addition of Hya to the DM/DPPC mixed system, no change was observed; however, after the addition of Hya to the OG/DPPC mixed system, the CAC_M of the system was reduced. Thus, preferably, the OG/DPPC/Hya system can be recommended for potential applications in drug delivery.

Acknowledgments This work was supported by Project Nr. LO1211, Materials Research Centre at FCH BUT-Sustainability and Development (National Program for Sustainability I, Ministry of Education, Youth and Sports of the Czech Republic).

Compliance with ethical standards

Conflicts of interest The authors declare that they have no conflict of interest.

Funding This study was funded by Project Nr. LO1211, Materials Research Centre at FCH BUT-Sustainability and Development (National Program for Sustainability I, Ministry of Education, Youth and Sports of the Czech Republic).

References

1. Thalberg K, Lindman B (1989) Interaction between hyaluronan and cationic surfactants. J Phys Chem 93:1478–1483. doi:10.1021/j100341a058
2. Halasová T, Krouská J, Mravec F, Pekař M (2011) Hyaluronan-surfactant interactions in physiological solution studies by tensiometry and fluorescence probe techniques. Colloids Surf A 391:25–31. doi:10.1016/j.colsurfa.2011.05.035
3. Kalbáčová M, Verdánová M, Mravec F, Halasová T, Pekař M (2014) Effect of CTAB in the presence of hyaluronan on selected human cell types. Colloids Surf A 460:204–208. doi:10.1016/j.colsurfa.2013.12.048
4. Mravec F, Klučáková M, Pekař M (2011) Fluorescence spectroscopy study of hyaluronan-phospholipid interactions. In: Iglič A (ed) Advances in planar lipid bilayers and liposomes, 1st edn. Academic Press, Burlington, pp. 235–255
5. Seddon AM, Curnow P, Booth PJ (2004) Membrane proteins, lipids and detergents: not just a soap opera. Biochim Biophys Acta 1666:105–117. doi:10.1016/j.bbamem.2004.04.011
6. Sasaki T, Demura M, Kato N, Mukai Y (2011) Sensitive detection of protein-lipid interaction change on bacteriorhodopsin using dodecyl β-d-maltoside. Biochemistry 50:2283–2290. doi:10.1021/bi101993s
7. Aivaliotis M, Karas M, Tsiotis G (2007) An alternative strategy for the membrane proteome analysis of the green sulfur bacterium Chlorobium tepidum using blue native PAGE and 2-D PAGE on purified membranes. J Proteome Res 6:1048–1058. doi:10.1021/pr060553u
8. Pham MD, Yu SSF, Han CC, Chan SI (2013) Improved mass spectrometric analysis of membrane proteins based on rapid and versatile sample preparation on nanodiamond particles. Anal Chem 85:6748–6755. doi:10.1021/ac400713g
9. Angelov B, Ollivon M, Angelova A (1999) X-ray diffraction study of the effect of the detergent octyl glucoside on the structure of lamellar and nonlamellar lipid/water phases of use for membrane protein reconstitution. Langmuir 15:8225–8234. doi:10.1021/la9902338
10. Does C, Manting EH, Kaufmann A, Lutz M, Driessen AJM (1998) Interaction between SecA and SecYEG in micellar solution and formation of the membrane-inserted state. Biochemistry 37:201–210. doi:10.1021/bi972105t
11. Rouse SL, Sansom MSP (2015) Interactions of lipids and detergents with a viral ion channel protein: molecular dynamics simulation studies. J Phys Chem B 119:764–772. doi:10.1021/jp505127y
12. Yokogawa M, Takeuchi K, Shimada I (2005) Bead-linked proteoliposomes: a reconstitution method for NMR analyses of membrane protein-ligand interactions. J Am Chem Soc 127:12021–12027. doi:10.1021/ja0511772
13. Oku N, Tsudera J, Kurohane K, Okada S (1996) Effect of freeze-thawing on phospholipid/surfactant mixed bilayers. Chem Pharm Bull 44:1928–1930. doi:10.1248/cpb.44.1928
14. Almgren M (2000) Mixed micelles and other structures in the solubilization of bilayer lipid membranes by surfactants. Biochim Biophys Acta 1508:146–163. doi:10.1016/S0005-2736(00)00309-6
15. Vinson PK, Talmon Y, Walter A (1989) Vesicle-micelle transition of phosphatidylcholine and octyl glucoside elucidated by cryo-transmission electron microscopy. Biophys J 56:669–681. doi:10.1016/S0006-3495(89)82714-6
16. Maire M, Champeil P, Møller JV (2000) Interaction of membrane proteins and lipids with solubilizing detergents. Biochim Biophys Acta 1508:86–111. doi:10.1016/S0304-4157(00)00010-1
17. de la Maza A, Lopez O, Baucells J, Gonzalez P, Parra JL (1998) Solubilization of phosphatidylcholine unilamellar liposomes caused by alkyl glucosides. J Surfactant Deterg 1:381–386. doi:10.1007/s11743-998-0039-x
18. Eidelman O, Blumenthal R, Walter A (1988) Composition of octyl glucoside-phosphatidylcholine mixed micelles. Biochemistry 27:2839–2846. doi:10.1021/bi00408a027
19. Ghosh S, Burman AD, De GC, Das AR (2011) Interfacial and self-organization of binary mixtures of anionic amphiphiles in aqueous medium. J Phys Chem B 115:11098–11112. doi:10.1021/jp204223t
20. Mitra D, Chakraborty I, Bhattacharya SC, Moulik SP, Roy S, Das D, Das PK (2006) Physicochemical studies on cetylammonium bromide and its modified (mono-, di-, and trihydroxyethylated) head group analogues. Their Micellization Characteristics in Water and Thermodynamic and Structural Aspects of Water-in-Oil Microemulsions Formed with Them along with n-Hexanol and Isooctane. J Phys Chem B 110:11314–11326. doi:10.1021/jp055720c
21. Aguiar J, Carpena P, Molina-Bolívar JA, Ruiz CC (2003) On the determination of the critical micelle concentration by the pyrene 1:3 ratio method. J Colloid Interface Sci 258:116–122. doi:10.1016/S0021-9797(02)00082-6
22. Behera K, Pandey S (2007) Concentration-dependent dual behavior of hydrophilic ionic liquid in changing properties of aqueous sodium dodecyl sulfate. J Phys Chem B 111:13307–13315. doi:10.1021/jp076430u
23. Hierrezuelo JM, Aguiar J, Carnero Ruiz C (2004) Stability, interaction, size, and microenvironmental properties of mixed micelles of decanoyl-N-methylglucamide and sodium dodecyl sulfate. Langmuir 20:10419–10426. doi:10.1021/la048278i
24. Céu Rei M, Coutinho P, Castanheira EMS, Real Oliveira MECD (2004) $C_{12}E_7$-DPPC mixed systems studied by pyrene fluorescence emision. Progr Colloid Polym Sci 123:83–87. doi:10.1007/978-3-540-36462-7_20
25. Li M, Jiang M (1997) Fluorescence studies of hydrophobic association of fluorocarbon-modified poly(N-isopropylacrylamide). Macromolecules 30:470–478. doi:10.1021/ma960966o
26. Li X, Ji J, Shen J (2006) Synthesis of hydroxyl-capped comb-like poly(ethylene glycol) to develop shell cross-linkable micelles. Polymer 47:1987–1994. doi:10.1016/j.polymer.2006.01.011
27. Urbano B, Silva P, Olea AF, Fuentes I, Martinez F (2008) Self-assembly of triblock copolymers in aqueous solution. J Chil Chem Soc 53:1507–1510. doi:10.4067/S0717-97072008000200013
28. Sackett DL, Wolf J (1987) Nile Red as a polarity-sensitive fluorescent probe of hydrophobic protein surfaces. Anal Biochem 167:228–234. doi:10.1016/0003-2697(87)90157-6
29. Ghoneim N (2000) Photophysics of Nile Red in solution: steady state spectroscopy. Spectrochim Acta A 56:1003–1010. doi:10.1016/S1386-1425(99)00199-7
30. Dar AA, Garai A, Das AR, Ghosh S (2010) Rheological and fluorescence investigation of interaction between hexadecyltrimethylammonium bromide and methylcellulose in the presence of hydrophobic salts. J Phys Chem A 114:5083–5091. doi:10.1021/jp911545j
31. Lipfert J, Columbus L, Chu VB, Lesley SA, Doniach S (2007) Size and shape of detergent micelles by small-angle scattering. J Phys Chem B 111:12427–12438. doi:10.1021/jp0730161
32. Oliver RC, Lipfert J, Fox DA, Lo RH, Doniach S, Columbus L (2013) Dependence of micelle size and shape on detergent alkyl chain length and head group. PLoS One 8(5):e62488. doi:10.1371/journal.pone.0062488

33. Dupuy C, Auvray X, Petipas C, Rico-Lattes I, Lattes A (1997) Anomeric effects on the structure of micelles of alkyl maltosides in water. Langmuir 13:3965–3967. doi:10.1021/la9604285
34. Thermo Fisher Scientific Inc.: *n-Dodecyl-beta-D-Matoside*: https://www.lifetechnologies.com/order/catalog/product/89902. Accessed 30 July 2015
35. Lorber B, Bishop JB, DeLucas LJ (1990) Purification of octyl [beta]-d-glucopyranoside and re-estimation of its micellar size. Biochim Biophys Acta 1023:254–265. doi:10.1016/0005-2736(90)90421-J
36. Maivaldová (2010) Interaction of phospholipids with polyelectrolytes in aqueous medium. Diploma thesis, Brno University of Technology

Colloid Polym Sci (2017) 295:1131–1140
DOI 10.1007/s00396-017-4103-z

ORIGINAL CONTRIBUTION

A study of zwitterionic/cationic vesicle formation and the influence of hyaluronan on this formation

Jana Burdíková[1] · **Irena Solná**[1,2] · **Leoš Doskočil**[2] · **Filip Mravec**[1,2] · **Miloslav Pekař**[1,2]

Received: 17 November 2016 / Revised: 15 February 2017 / Accepted: 16 April 2017 / Published online: 15 May 2017

Abstract The aggregation behavior of the biocompatible and naturally occurring zwiterionic phospholipid 1,2-dipalmitoyl-sn-glycero-3-phosphatidylcholine (DPPC) combined with its synthetic cationic analogue 1,2-dipalmitoyl-3-trimetylammonium-propan (DPTAP) was studied. Further, the physical properties of the formed DPPC/DPTAP liposomes were determined. The phase transition temperature of DPPC/DPTAP mixtures was studied using the steady-state fluorescence of laurdan, and the results were compared with those obtained from microcalorimetry measurements. The phase transition temperature was higher for all DPPC/DPTAP mixtures compared to that for pure DPPC and DPTAP, this increase being particularly pronounced for equimolar mixtures of DPPC and DPTAP. Membrane fluidity was determined by means of 1,6-diphenyl-1,3,5-hexatriene fluorescence anisotropy measurements. While the ratio of DPPC in DPPC/DPTAP liposomes was increased, the results suggest the formation of more tightly packed membranes. The interaction of DPPC/DPTAP liposomes with hyaluronan (Hya) was also studied. The formation of complexes was observed at a specific DPTAP/Hya concentration ratio independently of DPPC concentration or the molecular weight of Hya.

Electronic supplementary material The online version of this article (doi:10.1007/s00396-017-4103-z) contains supplementary material, which is available to authorized users.

✉ Jana Burdíková
xcszewieczkovaj@fch.vutbr.cz

[1] Institute of Physical and Applied Chemistry, Faculty of Chemistry, Brno University of Technology, Purkynova 118/464, 612 00 Brno, Czech Republic

[2] Materials Research Centre, Faculty of Chemistry, Brno University of Technology, Purkynova 118/464, 612 00 Brno, Czech Republic

Keywords Liposome · Lipid · Phase transition temperature · Lipid order parameter · Fluidity · Hyaluronan

Introduction

Liposomes are important delivery systems composed of lipid bilayers, which have considerable potential for application in medicine and cosmetics. Liposomes can undergo aggregation, fusion, and flocculation due to interactions with serum proteins under physiological conditions [1]. They have the capability to solubilize various forms of bioactives, regardless of hydrophilicity. Bioactives soluble in water can be loaded into hydrophilic regions while hydrophobic therapeutics can be captured in lipid regions at high densities. Lipid encapsulation can provide protection of the loaded bioactive from harsh environmental conditions and limits systemic exposure, which is advantageous in the case of therapeutics having undesired cytotoxic side effects [2]. Cationic liposomes have been shown to be absorbed by immature vascular endothelial cells due to the negative electric charge of their outer cell membrane. The antitumor efficacy of paclitaxel encapsulated in cationic liposomes was demonstrated as a promising new method for the treatment of prostate cancer reducing the primary tumor mass [3].

The instability of membrane conformation, which is essential to the delivery function of liposomes, could be improved by inclusion of a helper lipid. Stable and relatively small unilamellar vesicles were obtained by the insertion of lipid with cationic head groups such as 1,2-dioleyl-3-trimetylamonium-propan (DOTAP) in zwitterionic phosphatidylcholine (PC) membranes [4]. The mixture of 1,2-dipalmitoyl-sn-glycero-3-phosphatidylcholine (DPPC) and 1,2-dipalmitoyl-3-trimetylammonium-propan (DPTAP) is widely used in a variety of applications, e.g., for the formation of lipoparticles [5, 6] or the coating of superparamagnetic iron oxide nanoparticles

[7]. The proportion of each one in the formulation controls the cationic charge of the vesicle surface [8]. Independently of DPPC/DPTAP molar ratios, DPPC and DPTAP spontaneously assemble into vesicles in water media. Significant electrostatic interactions between lipids can be demonstrated by a higher phase transition temperature compared to that of pure lipids. The strongest interactions were found in the case of equimolar mixtures of DPPC and DPTAP revealing the tightest packing density of lipids [9].

Phospholipids are in the gel or liquid crystalline phase at physiological temperature. The DPPC phase transition temperature is around 41.5 °C and can be modified by the incorporation of other lipids. This change in phase transition temperature depends both on the length and saturation of the acyl chain and the type of polar residues [10]. For example, the incorporation of DOTAP into DPPC membranes causes a decrease in its phase transition temperature [4], while DPTAP has the opposite effect [9]. For steady-state fluorescence research into phase transition temperature, the prodan derivative laurdan can be utilized, this containing the lauric acid tail; this compound is thus tightly anchored within the hydrophobic core by cooperative van der Waals interactions between the lauric acid tail and the lipid hydrocarbon chains [11]. Due to the presence of naphthalene moiety, it is sensitive to both the polarity of the local environment and the membrane phase state [12, 13]. The essence of this sensitivity to polarity is subsumed in the partial charge separation between the 2-dimethylamino and 6-carbonyl residues forming a dipole moment, which increases upon excitation and may cause reorientation of the surrounding solvent dipoles. This solvent reorientation consumes energy and decreases the probe's excited state energy resulting in a continuous red shift of the probe's emission spectrum [12, 14]. Thus, the red shift in laurdan emission spectra indicates the increased concentration of water in the bilayer and its increased mobility [12].

Fluorescence anisotropy can be utilized for the investigation of lipid order. For this purpose, the fluorescent probe 1,6-diphenyl-1,3,5-hexatriene (DPH) allows information about the degree of membrane fluidity or physical changes in membranes to be obtained on the basis of the determination of the molecular orientational order and reorientational dynamics of the fluorescent probe in the core of the membrane bilayer [15, 16]. DPH is a rather rigid, linear, rod-like fluorophore characterized by an absence of polar groups; therefore, it is distributed spontaneously into the hydrophobic acyl chain region of the membrane [17], oriented such that the long axis of DPH along its rod-like shape is approximately aligned normal to the bilayer, thus reflecting the ordering of lipid acyl chains [17, 18]. The fluorescence anisotropy of DPH works well for studies of membrane fluidity in systems that are in the liquid-disordered phase. In the liquid-ordered phase, the fluorescence anisotropy of DPH serves well as a qualitative tool, while the quantitative accuracy is limited [19].

Hyaluronan (Hya) is a carbohydrate polymer occurring naturally in all living organisms. Hya is a linear, unbranched polymer, which is composed of a repeating disaccharide structure [20]. It can be several thousands of disaccharide units long [21] but can also exist as small fragments or oligosaccharides. At physiological pH, Hya exists mostly as a sodium salt and is therefore highly charged. This highly charged nature of Hya provides its solubility and ability to bind water extensively [22]. Hya plays a critical role in the physiology of joint function, including lubrication of the synovial surfaces. Interactions between Hya and phospholipids were studied as a simplified model of synovial fluid. Phospholipids could facilitate Hya binding to cells due to its strong affinity to cell surfaces. A complex of Hya and phospholipids (Haplex) was prepared using the film dispersion and sonication method, resulting in the enhancement of the oral absorption of Hya [23]. After the addition of Hya to monolamellar or multilamellar phospholipid suspensions, phospholipid organization was significantly affected by the presence of Hya in dependence on its molecular weight, not by the initial organization of the phospholipid or its nature (DPPC or egg lecithin) [24]. The presence of liposomes (DPPC) leads to an abrupt decrease in the viscosity of Hya because DPPC membranes bound to Hya cause the collapse of Hya chains. The possible explanation is that DPPC membranes bind to hydrophobic "patches" situated along the Hya polymer resulting in the collapse of the Hya chain [25, 26].

This work is aimed at preparation and characterization of DPPC/DPTAP vesicles with positive charge and study of their interactions with negatively charged Hya.

Experimental section

Materials

Sodium hyaluronate (137, 458, 1697 kDa) was purchased from Contipro (Czech Republic); 1,2-dipalmitoyl-3-trimetylammonium-propan, chloride salt (DPTAP) was purchased from Avanti Polar Lipids. 1,2-Dipalmitoyl-sn-glycero-3-phosphatidylcholine (DPPC), 1,6-diphenyl-1,3,5-hexatriene (DPH), pyrene, and chloroform were purchased from Fluka. All experiments were performed in water purified by an ELGA lab system (PURELAB flex).

Vesicle formation

The required amount of DPTAP or DPPC and DPTAP (with molar ratios 0:100, 50:50, 75:25, 80:20, 90:10) was dissolved in chloroform. After the removal of chloroform by evaporation, the required amount of water was added and the solution was sonicated at a temperature above the phase transition temperature until opalescent.

Microcalorimetry measurements

Microcalorimetry studies were conducted using a TAM III thermal activity monitor (TA Instruments, New Castle, DE, USA). Two-and-a-half-gram lipid or lipid mixture samples prepared as described previously in vesicle formation (with a total lipid concentration of 2.7 mM) were placed into disposable crimp seal ampoules. Samples were equilibrated for 15 min at 25 °C. The scanning rate was set to 2 °C/h. Any heat generated or absorbed by the sample was measured continuously over time. Measurements were carried out in the temperature range 25–65 °C. The baseline was subtracted.

Samples for fluorescence measurements

A fluorescence probe (laurdan, DPH, pyrene) dissolved in acetone was added to vials. After the evaporation of acetone under reduced pressure, an increasing amount of DPTAP or DPPC/DPTAP bulk solution and water was added into the vials to achieve a DPTAP or DPPC/DPTAP concentration series (in the range of 10^{-4}–1 mM) or to achieve a specific lipid concentration (in the case of samples containing laurdan or DPH). Eventually, a given amount of Hya bulk solution was added. Samples were measured after 24 h of agitation.

Laurdan generalized polarization

The characteristics of the laurdan emission spectrum describing the presence/absence of water molecules in the vicinity of laurdan naphthalene moiety may be expressed by the generalized emission polarization (GP) value [10, 27] given by the following:

$$GP = \frac{I_{440} - I_{490}}{I_{440} + I_{490}}$$

where I_{440} and I_{490} are the fluorescence intensities measured at 440 and 490 nm [10, 12], the wavelengths at which laurdan emission maxima occur in the gel phase and in the liquid crystalline phase, respectively [12, 14]. The phase transition temperature was determined from the first intersection of straight-line segments fitting plots of the laurdan GP value versus temperature.

All steady-state fluorescence measurements were performed using a Fluorolog Horiba Jobin Yvon spectrofluorimeter. Laurdan emission spectra were collected in the range 380–550 nm using an excitation wavelength of 329 nm. All samples were measured as a function of temperature in the range 35–65 °C or wider when necessary. Temperature was controlled by a circulating water bath. Sample temperature homogeneity was maintained by magnetic stirring.

Phospholipid CAC determination

For samples containing pyrene as a fluorescence probe, excitation spectra (in the range 330–340 nm with an emission wavelength of 392 nm) and emission spectra (in the range 360–540 nm with an excitation wavelength of 335 nm) were measured. The emission polarity index (EmPI) was obtained from the emission spectrum by dividing the fluorescence intensity of the first emission band (373 nm) by that of the third emission band (383 nm). The excimer to monomer (Ex/Mo) ratio was determined by dividing the fluorescence intensity of the excimer band (470 nm) by that of the monomer (383 nm) band. The excitation polarity index (ExPI) was calculated from excitation spectra as the ratio of fluorescence intensities at 333 and 338 nm. The dependences of EmPI (or ExPI) on lipid concentration were analyzed using the OriginLab software by fitting a Boltzmann sigmoid with the following form:

$$y = \frac{A_1 - A_2}{1 + e^{\frac{x - x_0}{\Delta x}}} + A_2$$

where y corresponds to EmPI or ExPI, A_1 and A_2 are the upper and lower limits of the sigmoidal curve, the independent variable x represents the total concentration of surfactant, x_0 represents the point of inflection, and Δx is the gradient at which the step change takes place. Critical concentrations of aggregation (CACs) were obtained as the point of inflection (x_0).

Anisotropy of DPH determination

Samples were prepared as described earlier in "Samples for fluorescence measurements" section. The concentration of the DPPC/DPTAP mixture was above the concentration corresponding to the second break in the sigmoidal curve. DPH anisotropy was measured using a time-resolved fluorescence spectrometer (FluoroCube Horiba). Samples were excited at 372 nm using a laser diode with an appropriate filter, and the DPH emission was measured at 426 nm with the slit adjusted to 8 nm.

For each vesicle composition with different DPPC/DPTAP ratios, fluorescence intensities were measured under four separate polarizer conditions: I_{vh} (vertically polarized excitation and horizontally polarized emission), I_{vv} (vertically polarized excitation and emission), I_{hh} (horizontally polarized excitation and emission), and I_{hh} (horizontally polarized excitation and emission).

These intensities were then fitted by impulse reconvolution using the general equation:

$$F(t) = R(inf) + B_i \exp\left(\frac{-t}{\tau_i}\right)$$

where R(inf) corresponds to the intrinsic anisotropy, t is the fluorescence lifetime, τ_i is the rotational correlation time, and

B_i a pre-exponential factor. The actual DPH fluorescence decay ($I(t)$) is assumed to follow a double exponential model:

$$I(t) = R(inf) + B_1 \exp\left(\frac{-t}{\tau_1}\right) + B_2 \exp\left(\frac{-t}{\tau_2}\right)$$

Then, the G-factor was calculated as the average value of the intensity ratio to minimize the consequences of the fact that monochromators do not transmit polarized components of light equally.

$$G = \left(\frac{I_{hv}(t)}{I_{hh}(t)}\right)$$

Using the G-factor and intensity values, the anisotropy $r(t)$ was then calculated according to the relationship:

$$r(t) = \frac{I_{vv}(t) - GI_{vh}(t)}{I_{vv}(t) + 2GI_{vh}(t)}$$

Lipid order parameter calculation

The lipid order parameter (S) and effective lipid order parameter (S_{eff}) were calculated using values of fluorescence anisotropy as follows [28, 29]:

$$S = \left(\frac{r}{r_0}\right)^{1/2}, S_{eff} = \left(\frac{r}{0.4}\right)^{1/2}$$

where r is the observed anisotropy and r_0 is the intrinsic anisotropy of the molecule. The term r_0 is used to refer to the anisotropy observed in the absence of other depolarizing processes such as rotational diffusion or energy transfer. For DPH, r_0 values as high as 0.39 have been measured. The anisotropy of 0.39 corresponds to an angle of 7.4° between the dipoles, whereas an r_0 value of 0.4 corresponds to an angle of 0° [30].

Results and discussion

The phase transition temperature was studied by means of fluorescence spectroscopy and microcalorimetry. The results of microcalorimetry measurements are shown in Fig. 1. A sharp phase transition is clearly observable in the case of pure lipids (DPPC, DPTAP) and mixtures with a DPPC/DPTAP ratio of 50:50. The phase transition temperatures for DPPC and DPTAP are localized at 42 and 43 °C, respectively, while it moves to higher temperatures in the case of mixed vesicles prepared from these two lipids. The highest phase transition temperature was found for a mixture with a DPPC/DPTAP ratio of 50:50 and was localized approximately at 57 °C. The reason for the shift of the phase transition temperature

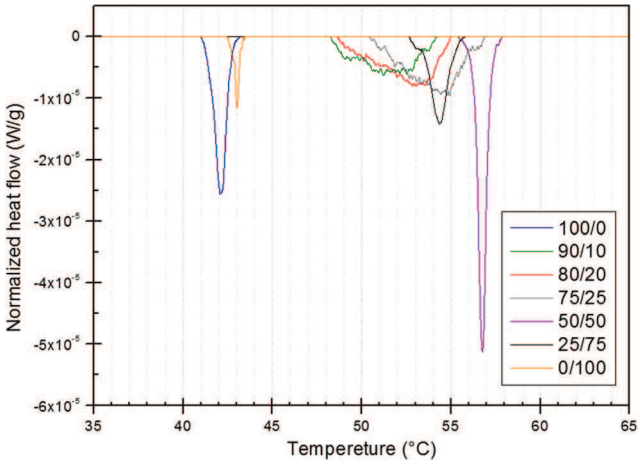

Fig. 1 Normalized heat flow in DPPC/DPTAP vesicles

to higher values in the case of all DPPC/DPTAP mixtures probably lies in the DPPC headgroup dipole orientation resulting from the presence of DPTAP. Charge repulsion between DPTAP and the terminal $N^+(CH_3)_3$ group in DPPC hinders the dipole reorientation that accompanies melting (from perpendicular to the interface to parallel to the interface) and prolongs the gel phase [7].

The dependences of normalized heat flow on temperature corresponding to DPPC/DPTAP mixtures with an excess of DPPC (90:10, 80:20, and 75:25) are noticeably broader than the others. Vesicles of these compositions are probably not homogenous through the entire sample volume; thus, they do not exhibit a sharp phase transition, but rather a continuous one.

The spectral shifts with increasing temperature in laurdan emission spectra were quantified using generalized polarization (GP) values. GPs as a function of temperature are shown in Fig. 2 and have a sigmoid character for all studied mixtures. We observed the same character in all dependencies—a slight

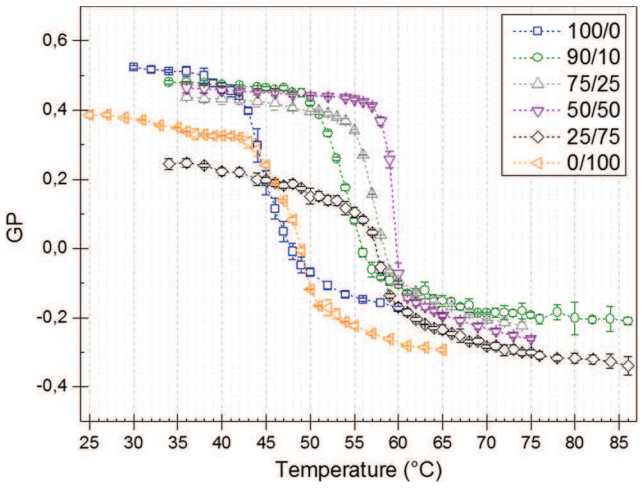

Fig. 2 Laurdan generalized polarization (GP) as a function of temperature in DPPC/DPTAP vesicles

decrease in GP in the first stage, followed by sharp GP decline, and then a further slight decrease in GP at the end. We quantified the differences between the location and slope of the intermediate area, which are both summarized and compared with results obtained by microcalorimetry in Fig. 3. The small deviation between the obtained results can be explained on the basis of the different principles of these two techniques. The phase transition temperature was higher for all studied mixtures compared to that for pure lipids, this increase being the highest for the equimolar DPPC/DPTAP mixture.

It is worth noting the low values of GP at low temperatures for mixtures with DPPC/DPTAP ratios of 25:75 and 0:100. According to the literature, GP ranges from −0.3 to 0.3 for the liquid phase of lipid bilayers and from 0.5 to 0.6 for the gel phase [12, 14]. According to these values, mixtures consisting mainly of DPTAP should not be in the gel state. However, if we consider the essence of GP, the decrease in GP is caused by an increase in the laurdan emission band located at around 490 nm, resulting from an increased polar head group area and the presence of some water molecules in the vicinity of laurdan naphthalene moiety, this indicating a larger head group area per molecule as a consequence of repulsion due to the presence of the positive charge located at the trimethylammonium group.

Another point of interest is the slope of the rapidly decreasing part in the dependences of GP on temperature. Figures 2 and 3 clearly show that all dependences have nearly the same slope for the intermediate part, except for the mixture with a DPPC/DPTAP ratio of 50:50, where the slope is doubled. This high slope could indicate the fastest transition from gel to liquid crystalline phase, as observed in microcalorimetry experiments.

This observation suggests tightly packed membranes, as was observed in equimolar dimyristoylphosphatidylcholine (DMPC)/dimyristoyltrimethylammonium propane (DMTAP) mixtures [31].

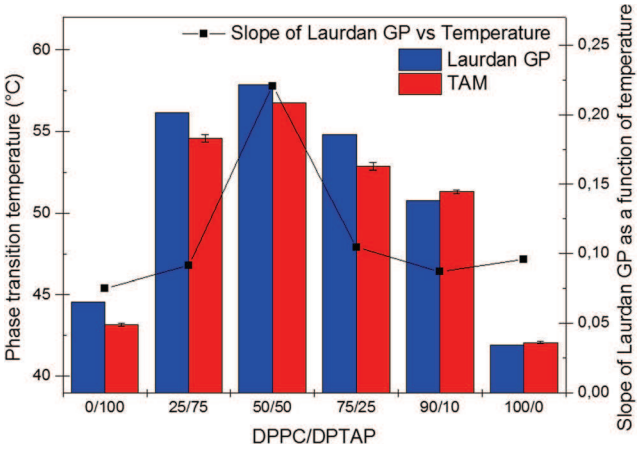

Fig. 3 Phase transition temperature in DPPC/DPTAP vesicles obtained using laurdan generalized polarization and microcalorimetry and the slope (absolute value) of the dependence of laurdan GP on temperature

Lipid order parameter

The change in the order of the lipid membrane was expressed by the effective lipid order parameter (S_{eff}), determined from the anisotropy of DPH fluorescence measurements. All measured values (Fig. 4) were higher than those reported in literature for different membrane constructs formed by 16:0–18:1 PC and cholesterol [28]. The reason for the high measured values probably lies in the presence of only one acyl chain type in each lipid, forming a relatively ordered membrane. The S_{eff} values increased slightly with the increasing proportion of DPPC in the DPPC/DPTAP mixture. This gentle fluidization of membranes at low DPPC portions may be caused by repulsive forces between positively charged DPTAP head groups, which are suppressed by an increasing amount of DPPC in the mixture. This would be in good agreement with the low values of laurdan GP obtained with high proportions of DPTAP.

These results are in agreement with literature, where the increase of hydration of the lipid headgroup region was observed with increasing DMTAP portion in DMPC/DMTAP system, because pure TAP membranes are less packed [32].

Aggregation of DPTAP with Hya

To study the influence of Hya on DPTAP aggregation, we used Hya of different concentrations and molecular weights (137, 458, 1697 kDa). On systems containing pyrene as a fluorescence probe, we measured steady-state fluorescence excitation and emission spectra and obtained EmPI (and ExPI) as described earlier.

The dependencies of pyrene EmPI on DPTAP concentration for pure DPTAP and its mixtures with Hya of different concentrations (5, 15, 50, 100, and 1000 mg dm^{-3}) and a molecular weight of 458 kDa are shown in Fig. 5. The

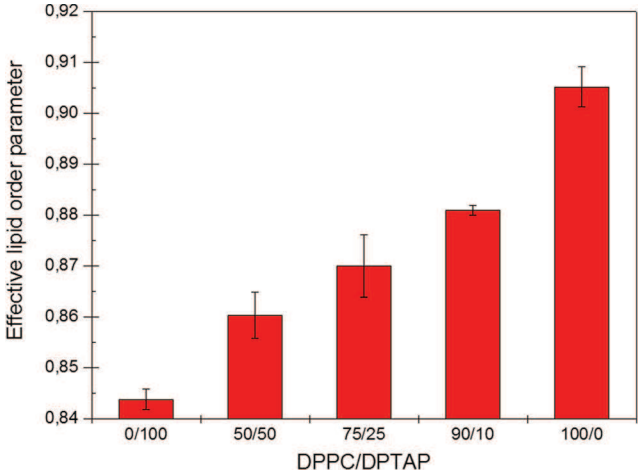

Fig. 4 Detail of the effective lipid order parameter of DPPC/DPTAP vesicles with different DPPC/DPTAP ratios

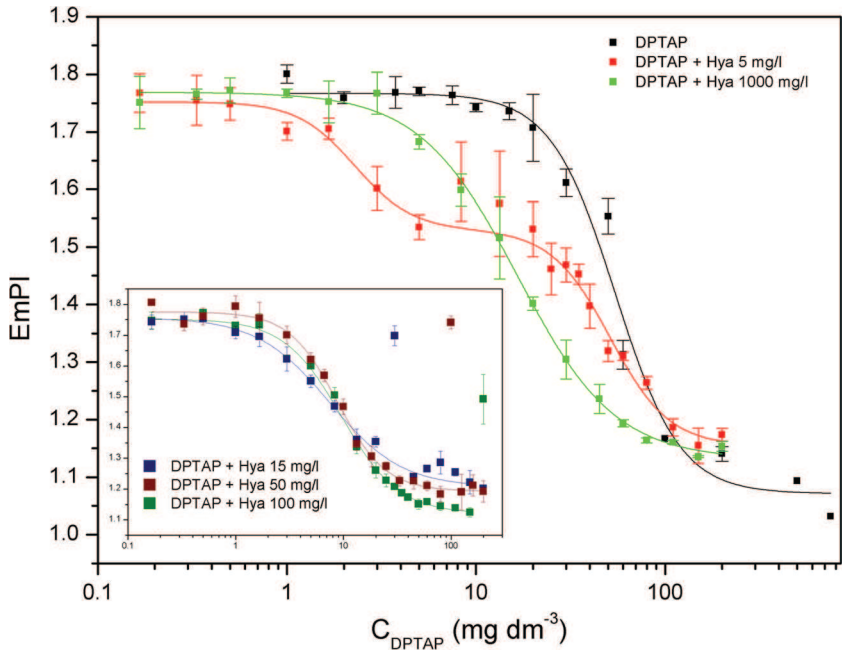

Fig. 5 Dependence of pyrene EmPI on DPTAP concentration for DPTAP and its mixtures with Hya of different concentrations and the same molecular weight of 458 kDa

dependence corresponding to DPTAP has a sigmoid character, with high EmPI values at low DPTAP concentrations indicating fluorescence from a polar (water) environment. At high DPTAP concentrations, EmPI values are low, because fluorescence occurs from the hydrophobic region.

In the presence of Hya, a reincrease in pyrene EmPI was observed at a DPTAP concentration dependent on the concentration of Hya, not only a smooth decrease in pyrene EmPI as observed in the case of pure DPTAP. This pyrene EmPI reincrease was accompanied by the formation of precipitate. From this behavior, we can suggest that almost all lipids in the sample are consumed for precipitate formation. Thus, a small amount of lipids remains in the solution, and high values of EmPI are found. The measured values of CAC for systems containing DPTAP and Hya are listed in Table 1. The parameters of pyrene EmPI reincrease are also shown. Values of the C_{DPTAP}/C_{Hya} ratio were 1.67 or 2.00. It can be said, with regard to the number of samples and the concentration step, that the C_{DPTAP}/C_{Hya} ratio of the EmPI increase is always the same (approaching a value of 2). No reincrease in EmPI was observed at the Hya concentration of 1000 mg dm^{-3}, because this concentration of Hya was too high to achieve a C_{DPTAP}/C_{Hya} ratio of "2." In contrast, a double Boltzmann sigmoid was used to fit the data obtained at the Hya concentration of 5 mg dm^{-3}. The concentration of the first point of inflection was lower than that at the Hya concentration of 15 mg dm^{-3}, and the concentration of the second point of inflection was nearly the same as CAC in the case of pure DPTAP. This may be a result of the mixture separating into two different systems, one of which contains a

Table 1 Measured values of CAC of DPTAP mixtures with Hya of different concentrations and molecular weights and parameters of pyrene EmPI reincrease

Hya		CAC (mg dm^{-3})	Pyrene EmPI reincrease	
M_w (kDa)	c (mg dm^{-3})	EmPI	C_{DPTAP} (mg dm^{-3})	C_{DPTAP}/C_{Hya} (mg dm^{-3})
–	–	52.7 ± 3.1	–	–
137	15	5.2 ± 0.2	25	1.67
458	5	4.5 ± 0.2	8.33	1.67
		55.9 ± 2.5[a]		
	15	7.8 ± 1.4	30	2.00
	50	8.9 ± 0.1	100	2.00
	100	9.6 ± 0.7	200	2.00
	1000	18.3 ± 0.1	–	–
1697	15	6.0 ± 0.7	25	1.67

[a] Parameter of the point of inflection of the second Boltzmann sigmoid

predominant amount of Hya, while the other behaves rather like pure DPTAP. A second explanation could be that the DPTAP concentration (for a C_{DPTAP}/C_{Hya} ratio of 2 and the Hya concentration of 5 mg dm^{-3}) is too low to form vesicles which should interact with Hya and form a precipitate.

The aggregation was also observed in the case of cationic liposomes (EPC/DOPE/DOTAP) and low molecular weight Hya. The increase of size of aggregates occurs in the concentration range of Hya 3 to 20% [33].

The values of CAC for DPTAP mixtures with Hya of different concentrations and a molecular weight of 458 kDa obtained using EmPI are also graphically depicted in Fig. 6. As can be clearly seen, a slight increase in CAC was observed with increasing Hya concentration but was not as pronounced as that obtained in the case of pure DPTAP. For the mixture of DPTAP with Hya of concentration 5 mg dm^{-3}, two values of CAC are shown, as described earlier.

The reincrease in EmPI (and also ExPI) was accompanied visually by the formation of precipitate on the wall of the vial (Fig. S1). Only in the case of samples with the Hya concentration of 50 mg dm^{-3} was the precipitate formed at a three times lower concentration than the concentration at which an increase in EmPI occurred. In this case, the appearance of the formed precipitate was different. Then, samples with higher DPTAP and Hya concentrations were prepared, the C_{DPTAP}/C_{Hya} ratio remaining at 2 (Fig. S2).

The dependencies of pyrene ExPI on DPTAP concentration (not shown) had a similar character to those of EmPI on DPTAP concentration; only slightly lower CACs values were obtained.

In addition, the influence of the molecular weight of Hya on precipitate formation with DPTAP was studied. Three

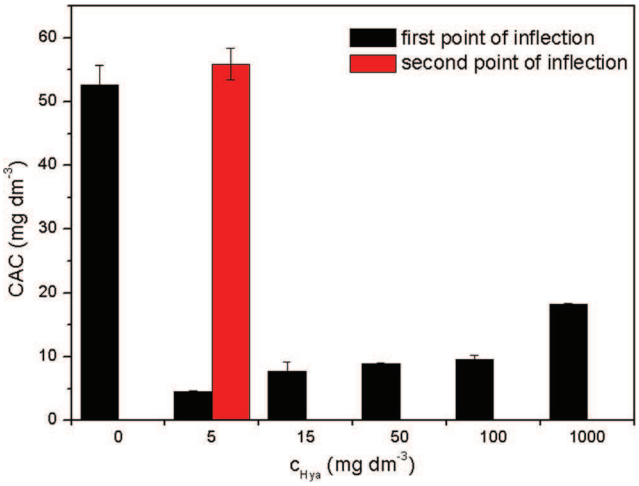

Fig. 6 CAC of DPTAP and Hya mixtures with different Hya concentrations determined by pyrene EmPI. In the case of a Hya concentration of 5 mg dm^{-3}, a double Boltzmann curve was used to fit the dependence of pyrene EmPI on DPTAP concentration, and two points of inflection were obtained

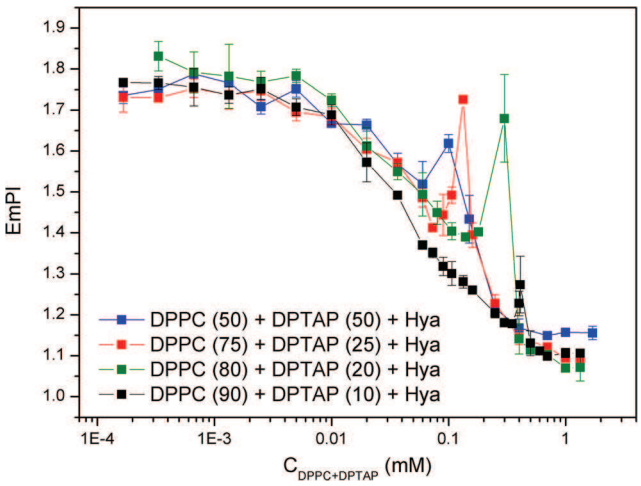

Fig. 7 Dependence of pyrene EmPI on DPPC and DPTAP concentration for different DPPC/DPTAP ratios in the presence of Hya (15 mg dm^{-3}, 458 kDa)

molecular weights of Hya were used (137, 458, and 1697 kDa), and its concentration was 15 mg dm^{-3} in all cases. No influence of Hya molecular weight was observed (see Fig. S3), and the measured values of CAC were nearly the same (Table 1). An abrupt increase in pyrene EmPI (and also ExPI) was observed in all cases at the same concentrations, and the formed precipitate had the same appearance.

Aggregation of DPPC/DPTAP mixture in the presence of Hya

Four mixtures with different DPPC/DPTAP molar ratios (50:50, 75:25, 80:20, and 90:10) were prepared to study the effect of Hya on DPPC/DPTAP aggregation. In the case of the DPPC/DPTAP mixture with a molar ratio of 50:50, the results

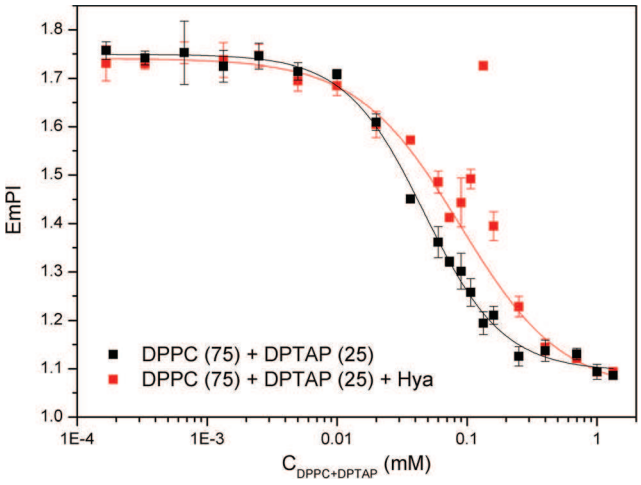

Fig. 8 Dependence of pyrene EmPI on DPPC and DPTAP concentration for a DPPC/DPTAP ratio of 75:25 in the presence and absence of Hya (15 mg dm^{-3}, 458 kDa)

Table 2 Measured values of the CAC of DPPC/DPTAP mixtures with Hya (15 mg dm^{-3}, 458 kDa) and the parameters of breaks in the Boltzmann curve of DPPC/DPTAP mixtures with Hya

DPPC/DPTAP	CAC (μM)			Break					
	DPPC + DPTAP	DPPC	DPTAP	C_{DPPC} (μM)	C_{DPPC} (mg dm^{-3})	C_{DPPC}/C_{Hya} (mg dm^{-3})	C_{DPTAP} (μM)	C_{DPTAP} (mg dm^{-3})	C_{DPTAP}/C_{Hya} (mg dm^{-3})
50:50	57 ± 2	28.65	28.65	–	–	–	–	–	–
50:50 Hya	85 ± 14	42.4	42.4	50	36.70	2.45	50	32.32	2.15
75:25	47 ± 4	35.2	11.8		–	–	–	–	–
75:25 Hya	86 ± 3	64.6	21.5	100	73.22	4.88	33	21.50	1.43
80:20	53 ± 2	42.3	10.5	–	–	–	–	–	–
80:20 Hya	134 ± 28	107.0	26.8	240	176.17	11.74	60	38.79	2.59
90:10	31 ± 2	27.6	3.1	–	–	–	–	–	–
90:10 Hya	52 ± 1	46.6	5.2	369	270.86	18.06	41	26.51	1.77

show that the molecular weight of Hya had no influence on either the dependence of EmPI on DPPC/DPTAP concentration (not shown) or CAC values (see Table S1). Therefore, further experiments were focused only on Hya of middle molecular weight (458 kDa).

Figure 7 compares the dependencies of EmPI on DPPC/DPTAP concentration as a function of different DPPC/DPTAP ratios. It is obvious that with a decreasing DPTAP ratio in the mixture, the reincrease in pyrene EmPI is localized at higher DPPC/DPTAP concentrations. Figure 8 shows an example of the dependences of EmPI on DPPC and DPTAP concentration (for a DPPC/DPTAP molar ratio 75:25) with and without Hya (of concentration 15 mg dm^{-3} and molecular weight 458 kDa). After the addition of Hya, a reincrease in EmPI was observed (similarly as in the case of DPTAP and Hya mixtures); however, CAC values increased for all DPPC and DPTAP mixtures (Table 2, Fig. 9), which was in contrast to the addition of Hya to DPTAP, when CAC values decreased by approximately ten times.

Even here, we monitored the parameters when the reincrease in pyrene EmPI was observed. Similarly as in the case of DPTAP mixtures with Hya, we monitored the concentration ratio, C_{DPTAP}/C_{Hya}, and, moreover, C_{DPPC}/C_{Hya} (Table 2).

C_{DPPC}/C_{Hya} ratio increases with decreasing portion of DPPC in DPPC/DPTAP mixture with Hya; therefore, the dependence of C_{DPPC}/C_{Hya} ratio on DPPC/DPTAP ratio is rather inconclusive.

Vice versa, the C_{DPTAP}/C_{Hya} ratio approached a value of 2 for all DPTAP and DPPC mixtures with Hya. It should be noted that the C_{DPTAP}/C_{Hya} ratio was also equal to 2 in the case of DPTAP/Hya mixtures (Table 1). Thus, aggregation is evidently controlled by the DPTAP concentration and C_{DPTAP}/C_{Hya} concentration ratios. It seems that the presence

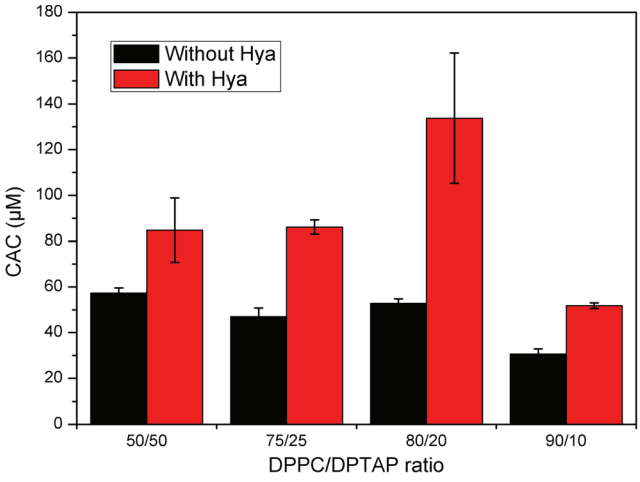

Fig. 9 Concentration of DPTAP and DPPC at the CAC (determined by pyrene EmPI) of various DPPC and DPTAP mixtures with Hya (15 mg dm^{-3}, 458 kDa)

of DPPC does not affect the aggregation behavior of these systems, although the concentration of DPTAP at the CAC value of the DPPC/DPTAP/Hya mixture decreases with a decreasing amount of DPTAP in these mixtures (Fig. 9). The concentration of DPPC at the CAC of these mixtures shows no dependence on DPPC/DPTAP ratio (Fig. 9). Therefore, we can say that DPPC participates in the formation of DPPC/DPTAP/Hya aggregates but does not affect this formation directly.

After the addition of higher concentration of Hya (1000 mg dm^{-3}), no reincrease in EmPI was observed and the influence on CAC values was insignificant.

Conclusion

In this work, we studied the influence of Hya on vesicles formed by DPTAP and DPPC/DPTAP mixtures. The formation of vesicles and their interactions with Hya was confirmed by fluorescence spectroscopy. In case of DPTAP, the presence of Hya caused the significant decrease of CAC of the system. On the other hand, in DPPC/DPTAP mixed system, addition of Hya resulted in only slight decrease of CAC of the studied system independently on DPPC/DPTAP ratio. In addition, the interaction between studied lipid systems caused the formation of precipitate, which was controlled only by the DPTAP concentration, even in the case of DPPC/DPTAP mixtures with Hya. The precipitate was formed after reaching a specific DPTAP/Hya ratio, not only in the case of DPTAP and Hya mixtures, but also in the case of DPPC, DPTAP and Hya mixtures. Thus, the formation of precipitate is managed by DPTAP. We also focused on the study of DPPC/DPTAP membrane properties. Membrane fluidity was studied by means of the fluorescence anisotropy of DPH. It was shown that with an increasing proportion of DPPC, the DPPC/DPTAP membrane was more rigid. Phase transition was studied by laurdan steady-state fluorescence and microcalorimetry. The phase transition temperature was shown to increase for mixtures of DPPC/DPTAP, this increase being particularly pronounced for an equimolar mixture of DPPC and DPTAP.

CAC, critical concentration of aggregation; DOTAP, 1,2-dioleyl-3-trimetylammonium-propan; DPH, 1,6-diphenyl-1,3,5-hexatriene; DPPC, 1,2-dipalmitoyl-sn-glycero-3-phosphatidylcholine; DPTAP, 1,2-dipalmitoyl-3-trimetylammonium-propan; EmPI, emission polarity index; ExPI, excitation polarity index; GP, generalized polarization; Hya, hyaluronan; PC, phosphatidylcholine; S, lipid order parameter; Seff, effective lipid order parameter.

Acknowledgements This work was supported by Project No. LO1211, Materials Research Centre at FCH BUT-Sustainability and Development (National Programme for Sustainability I, Ministry of Education, Youth and Sports of the Czech Republic).

Compliance with ethical standards

Conflict of interest The authors declare that they have no conflict of interest.

References

1. Gu L, Faig A, Abdelhamid D, Uhrich K (2014) Sugar-based amphiphilic polymers for biomedical applications: from nanocarriers to therapeutics. Acc Chem Res 47:2867–2877. doi:10.1021/ar4003009
2. Sapsford KE, Algar WR, Berti L, Gemmill KB, Casey BJ, Oh E, Stewart MH, Medintz IL (2013) Functionalizing nanoparticles with biological molecules: developing chemistries that facilitate nanotechnology. Chem Rev 113:1904–2074. doi:10.1021/cr300143v
3. Bode C, Trojan L, Weiss C, Kraenzlin B, Michaelis U, Teifel M, Alken P, Michel MS (2009) Paclitaxel encapsulated in cationic liposomes: a new option for neovascular targeting for the treatment of prostate cancer. Oncol Rep 22:321–326. doi:10.3892/or_00000440
4. Campbell RB, Balasubramanian SV, Straubinger RM (2001) Phospholipid-cationic lipid interactions: influences on membrane and vesicle properties. Biochim Biophys Acta Biomembr 1512:27–39. doi:10.1016/S0005-2736(01)00290-5
5. Thevenot J, Troutier AL, David L, Delair T, Ladavière C (2007) Steric stabilization of lipid/polymer particle assemblies by poly(ethylene glycol)-lipids. Biomacromolecules 11:3651–3660. doi:10.1021/bm700753q
6. Thevenot J, Troutier AL, Putaux JL, Delair T, Ladavière C (2008) Effect of the polymer nature on the structural organization of lipid/polymer particle assemblies. J Phys Chem B 112:13812–13822. doi:10.1021/jp805865r
7. Chen Y, Bothun GD (2011) Cationic gel-phase liposomes with "decorated" anionic SPIO nanoparticles: morphology, colloidal, and bilayer properties. Langmuir 27:8645–8652. doi:10.1021/la2011138
8. Troutier AL, Delair T, Pichot C, Ladavière C (2005) Physicochemical and interfacial investigation of lipid/polymer particle assemblies. Langmuir 21:1305–1313. doi:10.1021/la047659t
9. Troutier AL, Véron L, Delair T, Pichot C, Ladavière C (2005) New insights into self-organization of a model lipid mixture and quantification of its adsorption on spherical polymer particles †. Langmuir 21:9901–9910. doi:10.1021/la0507961
10. Parasassi T, De Stasio G, D'Ubaldo A, Gratton E (1990) Phase fluctuation in phospholipid membranes revealed by Laurdan fluorescence. Biophys J 57:1179–1186. doi:10.1016/S0006-3495(90)82637-0
11. Chong PL, Wong PT (1993) Interactions of Laurdan with phosphatidylcholine liposomes: a high pressure FTIR study. Biochim Biophys Acta 1149:260–266. doi:10.1016/0005-2736(93)90209-I
12. Parasassi T, Krasnowska EK, Bagatolli L, Gratton E (1998) Laurdan and Prodan as polarity-sensitive fluorescent membrane probes. J Fluoresc 8:365–373. doi:10.1023/A:1020528716621
13. Bondar OP, Rowe ES (1999) Preferential interactions of fluorescent probe Prodan with cholesterol. Biophys J 76:956–962. doi:10.1016/S0006-3495(99)77259-0
14. Sanchez SA, Tricerri MA, Gunther G, Gratton E (2007) Laurdan generalized polarization: from cuvette to microscope. In: Méndez-Vilas A, Diaz J (eds) Modern research and educational topics in microscopy. Formatex, Madrid, pp. 1007–1014
15. Muller JM, Ginkel G, Faassen EE (1996) Effect of lipid molecular structure and gramicidin a on the Core of lipid vesicle bilayers. A

time-resolved fluorescence depolarization study †. Biochemistry 35:488–497. doi:10.1021/bi951409h
16. Ghosh YK, Indi SS, Bhattacharya S (2001) Thermal lipid order −disorder transitions in mixtures of cationic cholesteryl lipid analogues and dipalmitoyl phosphatidylcholine membranes. J Phys Chem B 105:10257–10265. doi:10.1021/jp003940e
17. Repáková J, Čapková P, Holopainen JM, Vattulainen I (2004) Distribution, orientation, and dynamics of DPH probes in DPPC bilayer. J Phys Chem B 108:13438–13448. doi:10.1021/jp048381g
18. Kaiser RD, London E (1998) Location of diphenylhexatriene (DPH) and its derivatives within membranes: comparison of different fluorescence quenching analyses of membrane depth †. Biochemistry 37:8180–8190. doi:10.1021/bi980064a
19. Fraňová M, Repáková J, Čapková P, Holopainen JM, Vattulainen I (2010) Effects of DPH on DPPC−cholesterol membranes with varying concentrations of cholesterol: from local perturbations to limitations in fluorescence anisotropy experiments. J Phys Chem B 114:2704–2711. doi:10.1021/jp908533x
20. Kakehi K, Kinoshita M, Yasueda S (2003) Hyaluronic acid: separation and biological implications. J Chromatogr B 797:347–355. doi:10.1016/S1570-0232(03)00479-3
21. Velema J, Kaplan D (2006) Biopolymer-based biomaterials as scaffolds for tissue engineering. Adv Biochem Eng Biotechnol 102: 187–238. doi:10.1007/10_013
22. Kablik J, Monheit GD, Yu L, Chang G, Gershkovich J (2009) Comparative physical properties of hyaluronic acid dermal fillers. Dermatol Surg 35:302–312. doi:10.1111/j.1524-4725.2008.01046.x
23. Huang SL, Ling PX, Zhang TM (2007) Oral absorption of hyaluronic acid and phospholipids complexes in rats. World J Gastroenterol 13:945–949. doi:10.3748/WJG.v13.i6.945
24. Pasquali-Ronchetti I, Quaglino D, Mori G, Bacchelli B, Ghosh P (1997) Hyaluronan–phospholipid interactions. J Struct Biol 120:1–10. doi:10.1006/jsbi.1997.3908
25. Heatley F, Scott JE (1988) A water molecule participates in the secondary structure of hyaluronan. Biochem J 254:489–493. doi:10.1042/bj2540489
26. Crescenzi V, Taglienti A, Pasquali-Ronchetti I (2004) Supramolecular structures prevailing in aqueous hyaluronic acid and phospholipid vesicles mixtures: an electron microscopy and rheometric study. Colloid Surf A 245:133–135. doi:10.1016/j.colsurfa.2004.06.030
27. Harris FM, Best KB, Bell JD (2002) Use of laurdan fluorescence intensity and polarization to distinguish between changes in membrane fluidity and phospholipid order. Biochim Biophys Acta 1565: 123–128. doi:10.1016/S0005-2736(02)00514-X
28. Troup GM, Wrenn SP, Apel-Paz M, Doncel GF, Vanderlick TK (2006) A time-resolved fluorescence diphenylhexatriene (DPH) anisotropy characterization of a series of model lipid constructs for the sperm plasma membrane. Industrial 45:6939–6945. doi:10.1021/ie058084d
29. Heyn MP (1979) Determination of lipid order parameters and rotational correlation times from fluorescence depolarization experiments. FEBS Lett 108:81–87. doi:10.1016/0014-5793(79)80564-5
30. Lakowicz JR (2006) Principles of fluorescence spectroscopy, 3rd edn. Springer, New York
31. Gurtovenko AA, Patra M, Karttunen M, Vattalainen I (2004) Cationic DMPC/DMTAP lipid bilayers: molecular dynamics study. Biophys J 86:3461–3472. doi:10.1529/biophysj.103.038760
32. Olżyńska A, Jurkiewicz P, Hof M (2008) Properties of mixed cationic membranes studied by fluorescence solvent relaxation. J Fluoresc 12:925–928. doi:10.1007/s10895-008-0321-6
33. Gasperini AAM, Puentes-Martinez XE, Balbino TA, et al (2015) Association between cationic liposomes and low molecular weight hyaluronic acid. Langmuir 31:3308–3317. doi:10.1021/la5045865

THE JOURNAL OF PHYSICAL CHEMISTRY C

Article

pubs.acs.org/JPCC

Magnetical and Optical Properties of Nanodiamonds Can Be Tuned by Particles Surface Chemistry: Theoretical and Experimental Study

Irena Kratochvílová,*[,†,§] Jakub Šebera,[†] Petr Ashcheulov,[†,§] Martin Golan,[†,‡] Miroslav Ledvina,[∥] Julia Míčová,[∥] Filip Mravec,[⊥] Alexander Kovalenko,[⊥] Dmitry Zverev,[#] Boris Yavkin,[#] Sergei Orlinskii,[#] Stanislav Záliš,*[,△] Anna Fišerová,[◊] Jan Richter,[◊,▼] Luděk Šefc,[¶] and Jaroslav Turánek[+]

[†]Institute of Physics, Academy of Sciences Czech Republic v.v.i, Na Slovance 2, CZ-182 21 Prague 8, Czech Republic

[‡]Faculty of Mathematics and Physics, Charles University in Prague, Ke Karlovu 3, CZ-121 16 Prague 2, Czech Republic

[§]Faculty of Nuclear Science and Physical Engineering, Czech Technical University in Prague, Brehova 7, CZ-115 19 Prague 1, Czech Republic

[∥]Institute of Organic Chemistry and Biochemistry, Academy of Sciences Czech Republic, v.v.i., Flemingovo náměstí 2, CZ-166 10 Prague 6, Czech Republic

[⊥]Faculty of Chemistry, Materials Research Centre, Brno University of Technology, Purkyňova 118, CZ-612 00 Brno, Czech Republic

[#]Institute of Physics, Kazan Federal University, Kremlevskaya 18, 420008 Kazan, Russia

[△]J. Heyrovsky Institute of Physical Chemistry, Academy of Sciences Czech Republic v.v.i, Dolejškova 2155/3, CZ-182 23 Prague 8, Czech Republic

[◊]Institute of Microbiology, Academy of Sciences Czech Republic, v.v.i., Vídeňská 1083, CZ-142 20 Prague 4, Czech Republic

[¶]Institute of Pathological Physiology, First Faculty of Medicine, Charles University in Prague, Kateřinská 32, CZ-121 08 Prague 2, Czech Republic

[+]Department of Pharmacology and Immunotherapy, Veterinary Research Institute, CZ-621 00 Brno, Czech Republic

[▼]Faculty of Biomedical Engineering, Czech Technical University in Prague, Nam. Sítná 3105, 272 01 Kladno, Czech Republic

ABSTRACT: In this paper, new steps toward a better understanding and utilization of high-pressure high-temperature nanodiamonds (NDs) containing nitrogen-vacancy (NV) centers have been taken. NV^--related long-term luminescence of oxygenated particles increased in comparison to plasma hydrogenated NDs' NV^- luminescence. The optically detected NV^- electron spin resonance process can be also significantly affected by ND termination. For H-terminated ND particles the NV^- to NV^0 conversion energy is lower than the NV^- excitation energy, so that the delocalized triplet electrons can be more easily released from the original positions and drawn to the electron-attracting localities in the material. The final result of this study was application of luminescent NDs in cells, showing the detectability of luminescent NDs in a standard confocal microscope and ND subcellular distribution in the cells by TEM.

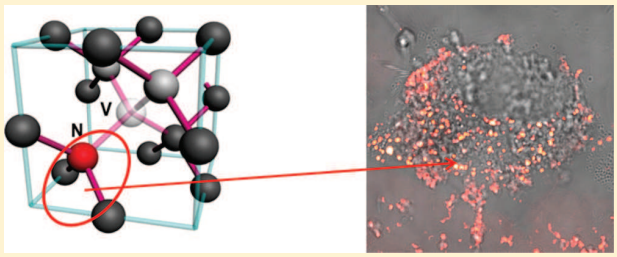

1. INTRODUCTION

Nanodiamond (ND) particles belong to a broad family of nanocarbon-based materials with a structural diversity given by specific synthesis conditions, postsynthesis processes, and modifications.[1−11] ND particles with sizes up to several tens of nanometers currently find broad applications.[12−18] Recently, controlled doping of NDs and on-demand production of defects has caused a major breakthrough that can open a new area of quantum information processing and quantum computing, nanoscale imaging magnetometry, and photoluminescent probes for biomedical imaging.[1−5,10]

A defect of particular importance in NDs is the nitrogen-vacancy (NV) center. NV centers can be created by irradiating diamonds with high-energy particles (electrons, protons, helium ions), followed by vacuum annealing. Two types of NV centers with different emission spectra are formed in the diamond−neutral (NV^0) and negatively charged (NV^-), with different zero phonon line emission wavelength properties, i.e., 575 nm for NV^0 and 638 nm for NV^-.

The luminescence from NV centers is stable without any photobleaching or photoblinking, and compared to better known quantum dots, ND brings additional advantages such as high biocompatibility and simple C-surface chemistry. This allows grafting of biomolecules that are interesting for the

Received: July 28, 2014
Revised: September 22, 2014
Published: September 30, 2014

cellular targeting or biomolecular drug delivery.[1,3,18] The NV^- center ground state consists of two unpaired electrons in a triplet configuration leading to a zero-field splitting. It is possible to selectively address transitions between the $m_s = 0$ and $m_s = 1$ (or $m_s = -1$) states with microwave radiation and manipulate a two-level spin triplet. Laser-assisted detection of the NV spin state makes use of differences in the absorption and emission properties of the spin states (Figure 1). A sensor capable of detecting such magnetic fields with nanometer spatial resolution would enable detection of magnetic signals in biological molecules or nuclear spin memory.[11−14]

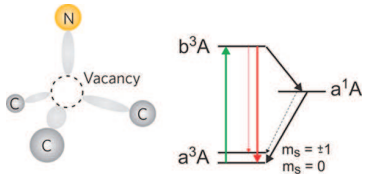

Figure 1. Nitrogen-vacancy (NV^-) center in a diamond (left) and its energy levels and transitions (right). The ground state is an orbital singlet and spin triplet.[12,13] Optical pumping initializes the center into the $m_s = 0$ spin state via specific spin-selective transition into the metastable singlet state, ^1A. A green arrow represents an excitation of a nitrogen-vacancy center. The mechanism responsible for optical pumping also provides a means for spin-sensitive detection, as the rate of fluorescence differs for the $m_s = 0$ and $m_s = \pm 1$ states.

In this paper, new steps toward a better understanding and utilization of high-pressure high-temperature NDs 20−50 nm in size containing NV centers have been taken.[19−27] Great effort was devoted to proper chemical termination of these particles. Most importantly, we studied NDs terminated by oxygen-containing groups and NDs hydrogenated in microwave-excited H plasma—NDs were functionalized by hydrogen, hydrogen/carbonyl or hydroxyl groups, and hydroxyl/carbonyl groups. The principle of surface functionalization driven luminescence, related to switching the occupation of NV-/NV0 states has been developed in works of Petrakova et al.[3,6]

In the scope of ND research we employed Raman spectroscopy, fluorescence lifetime measurements, electron paramagnetic resonance (EPR), transmission electron microscopy (TEM), and confocal microscopy. Using density functional theory (DFT), time-dependent density functional theory (TD-DFT), and density functional-based tight-binding (DFTB) methods[2,6,18−20] we acquired parameters that influence the NDs' optical and magnetic properties. A. S. Zyubin et al.[8] used TD-DFT for the analysis of optical properties of approximately 100 atoms containing ND particles with neutral and negatively charged vacancy-related point defects (N_2V^0 and N_2V^-). DFT methods have also been used for calculations of the optical gap, absorption spectrum, and luminescence of small Si nanocrystals, with hydrogen and oxygen at the surface.[22−24] In this work we were able to describe the impact of nanodiamond defects and surface states on the optical and magnetic properties of the whole nanoparticle, both qualitatively and quantitatively. Finally, we showed that luminescent oxygen-terminated NDs are visible in cells under a confocal microscope. The results and models reported in this work show a way toward surface-sensitive and stable nanodevices based on nanodiamonds.

2. EXPERIMENTAL SECTION

2.1. Sample Preparation. Monocrystalline diamond powder of HPHT NDs with particle sizes ranging from 20 to 50 nm (Qty 100 carats) was purchased from the Microdiamant AG. A commercial solution of HPHT NDs was lyophilized and heated in a slow stream of air at 510 °C for 6 h to remove any sp^2 carbon from the ND surfaces. After that, NDs were oxidized in a mixture of concentrated H_2SO_4−HNO_3 (9:1, v/v) at 80 °C for 3 days and proton irradiated (3−20 MeV). Irradiated NDs were thermally annealed in vacuo at 900 °C for 1 h forming either neutral (NV^0) or negatively charged (NV^-).

The NDs were then air-oxidized at 510 °C for 6 h (oxidized ND). Part of the oxidized NDs were annealed in vacuum at 750 °C for 2 h (sp^2 termination surface NDs/oxidized 750 °C annealed). The quartz plate with part of NDs was exposed to microwave-excited hydrogen plasma for 30 min at a temperature of 500 °C and at 1 mbar pressure to produce a H-terminated surface (hydrogenated).

2.2. Photoluminescence of NV^0/NV^- Centers. The presence of NV^0 and NV^- centers in our ND samples was confirmed by a Renishaw InVia Raman Microscope at 300 K, 514 nm excitation wavelength. The centers acted as an ion embedded in an inert solid matrix with long-term observation of a single diamond nanocrystal.

2.3. Electron Paramagnetic Resonance Spectroscopy. Continuous wave (CW) and ESE-detected EPR experiments were performed with a W-band (94 GHz) EPR spectrometer (Bruker ElexSYS E680, equipped with an Oxford Instruments CF-1200 cryostat) at $T = 50$ K. For CW-EPR experiments, a high frequency (100 kHz) field modulation at amplitudes of 0.5 mT and microwave power of 7×10^{-3} mW was applied. For ESE-detected EPR experiments the two-pulse Hahn echo sequence $\pi/2$-τ−π−τ-echo was applied where $\pi/2 = 24$ ns and $\tau = 300$ ns. The simulations of ESE-detected EPR spectra were performed using the EasySpin package for Matlab.[28]

2.4. Fluorescence Lifetime Measurements. Determination of fluorescence lifetime was performed at 20 ± 0.5 °C in a fluorescence microscopy system MicroTime 200 (Picoquant GmbH). Samples were excited at 375 and 510 nm by pulsed laser diodes with 20 MHz repetition frequency. For ultraviolet excitation, two simultaneous detection channels were used with different long-pass cutoff filters (ThorLabs) at 405 and 519 nm, respectively. Diode pulse width (fwhm) was below 70 ps for the 375 nm diode and below 80 ps for the 510 nm diode. Timing resolution of used detectors was better than 150 ps. For lifetime measurements, data were collected to reach 10 000 counts in the maximum peak channel. Fluorescence lifetime data were obtained within the FLIM technique, and in this case just multiexponential decay analysis can be used (software SymphoTime). The number of curves followed the current statistical accuracy by comparing the model with the data, typically containing 2−3 exponentials. IRF was deconvoluted. Also, Lim et al.[29] applied multiexponential analysis for ND particle fluorescence lifetime interpretation.

The number of lifetimes is related to the number of the used model parameters (number of exponential decays). Parameters were set according to the chi-square values; chi square was kept between 1.10 and 0.95 and the shape of residual analysis.

2.5. Computer Experiments. Modeling was performed using DFT/TD-DFT and density-functional-based tight-binding methods (DFTB)s—Gaussian 09[19] and Turbomole 6.3[20] program packages in clusters having from 82 to 695 carbon

dx.doi.org/10.1021/jp507581c | J. Phys. Chem. C 2014, 118, 25245−25252

atom defects free or containing one NV center either neutrally or negatively charged. The ND particle surfaces were terminated by hydrogen, hydrogen/carbonyl, or hydroxyl groups and hydroxyl/carbonyl groups. Clusters with positions of the NV defect either in the center or close to the particle surface were modeled. The lowest-lying excited states were calculated by a TD-DFT method, which is an extension of DFT determined to investigate the excited states and nonequilibrium properties of many-body systems in the presence of time-dependent potentials. This method enables analysis of the character and localization of individual excited states. In this work we modeled bigger clusters (containing even more than 1000 atoms,2.3 nm) than was presented in refs 8 and 22−24.

Geometries were optimized by two DFT functionals, B3LYP and BLYP. The calculations with BLYP were done with the Multipole Accelerated Resolution of Identity method, which enables us to speed up calculation of the Coulomb terms. Geometries of large nanodiamonds (no. of C atoms >200) were optimized by the DFTB method giving reasonably proper geometry of nanodiamonds with respect to the experimental data and B3LYP results.

The electron affinity, conversion energy (energy to convert the NV^- into NV^0), electronic transitions, and change in electron density were calculated by the B3LYP method with the use of 6-31G(d) basis set at optimized ground state geometry of the nanodiamonds. Vertical electron affinities (EAs) were calculated as an energy difference between the matter system and the system with one electron added.[24] From calculated Mulliken charges for full hydrogenated and oxygen groups containing NDs we obtained electron density per atom inside the ND (the surface was defined as consisting of noncarbon and non-nitrogen atoms).

2.6. Microscopic Techniques. *2.6.1. Cultivation of Cells.* A549 (adenocarcinomic human alveolar basal epithelial cells; ATCC CCL-185) were cultivated according to ATCC protocol in F-12 K medium suplemeted by 10% fetal bovine serum. HeLa cells (epithelial cells from human cervical adenocarcinoma; HeLa (ATCC CCL2) were cultivated according to ATCC protocol in E-MEM +10% fetal bovine serum + Pen/Strep. Culture Conditions: **Atmosphere**: air, 95%; carbon dioxide (CO_2), 5%; **Temperature**: 37 °C; CO_2 incubator: HERA Cell 150i (Thermoscientific).

2.6.2. Confocal Microscopy. HeLa cells were seeded to a glass-bottom petri dish at a concentration of 2×10^4 cells/mL and incubated in E-MEM medium supplemented with 10% FBS (IMG,CAS,CZ) and incubated for 24 h. NDs were well dispersed in an ultrasound bath. The quality of the dispersion was checked by dynamic light scattering using Zetasizer ZS (Malvern, UK). The dispersed NDs were added to the cells (final concentration 25 μg/mL), and the cells were incubated for 24 h in a serum-free H-MEMd medium (37 °C, 5% CO_2 HERA Cell 150i incubator (Thermoscientific)). Before microscopic observation, the cells were rinsed two times with PBS to remove nonendocytosed NDs. In vivo laser-scanning confocal microscopy (Olympus FV-1000 instrument) was performed to observe the localisation of the ND particles within the cells. 100× magnification with was used for image acquisition (e.g., 561 nm, emmission window: 630−730 nm).

2.6.3. Transmission Electron Microscopy (TEM): Ultrathin Section Method. Glutaraldehyde-fixed cells (3%) exposed to fluorescent nanodiamonds were centrifuged, and the pellet was rinsed in Milonig buffer, postfixed in 1% OsO_4 solution in Milonig buffer, dehydrated in 50, 70, 90, and 100% ethanol, embedded in an Epon-Durcupan mixture (Epon 812 Serva, Germany; Durcupan, ACM Fluka, Switzerland), and polymerized at 60 °C for 72 h. Ultrathin sections (the thickness of 60 nm) were cut with glass knives in a UC 7 ultramicrotome (UC 7, Leica, Austria). Afterward, they were directly observed without being previously contrasted (uranyl acetate and lead citrate) to prevent objectionable artifacts. The sections were examined under a Philips EM 208 S Morgagni transmission electron microscope (FEI, Czech Republic).

3. RESULTS AND DISCUSSION

3.1. Photoluminescence of NV^0/NV^- Centers. Photoluminescence spectra were taken from proton-irradiated NDs with oxidized and hydrogenated surfaces. NV^0- and NV^--related luminescence was observed at 575 and 637 nm, respectively, for oxidized ND particles. It should be noted that both before proton beam irradiation and after irradiation without annealing, no luminescence was observed.[3,6] Proton irradiation enhances number of vacancies and following annealing finally increases number of nitrogen-vacancy pairs. All spectra were normalized to the diamond Raman peak. From the zero-phonon luminescence line (dotted gray line in Figure 2) we found that the NV^-/NV^0 ratio is higher for oxidized NDs

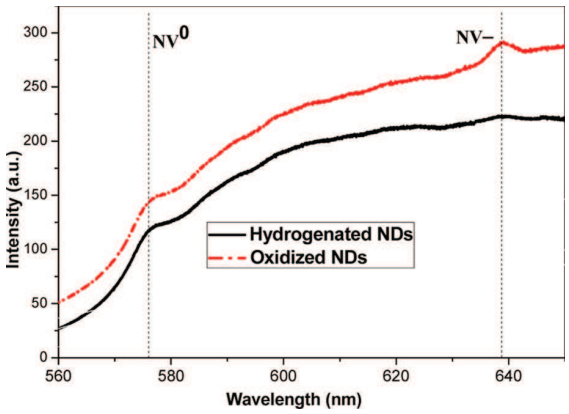

Figure 2. Photoluminescence spectra taken from proton-irradiated NDs with oxidized and hydrogenated surfaces. NV^0- and NV^--related luminescence was observed at 575 and 637 nm, respectively, for oxidized ND particles.[3,6] Zero-phonon luminescence lines are marked by dotted gray lines. All spectra were normalized to the diamond Raman peak, room temperature. Spectra were measured using a Renishaw InVia Raman Microscope at 300 K, 514 nm excitation wavelength, on solid state NDs.

compared to hydrogenated NDs, as also found in the work of Petrakova et al.[3,6] Relatively strong luminescence background originates from the complex surface of ND particles: variously terminated mixture of sp^2- and sp^3-hybridized carbon.

Changes in the photoluminescence spectra of oxidized NDs when interacting with charged polymers were also measured.[3] The luminescence of the NV^- centers decreased when interacting with positively charged molecules, while after adding negatively charged polymers the luminescence was restored to the original level.

3.2. Electron Paramagnetic Resonance Spectroscopy. Figure 3 shows the W-band CW EPR (a) and the first derivative of ESE-detected EPR (b) spectra measured in O- and H-terminated nanodiamond samples at T = 50 K. From the simulation of ESE-detected EPR spectra (Figure 3), it was

dx.doi.org/10.1021/jp507581c | J. Phys. Chem. C 2014, 118, 25245−25252

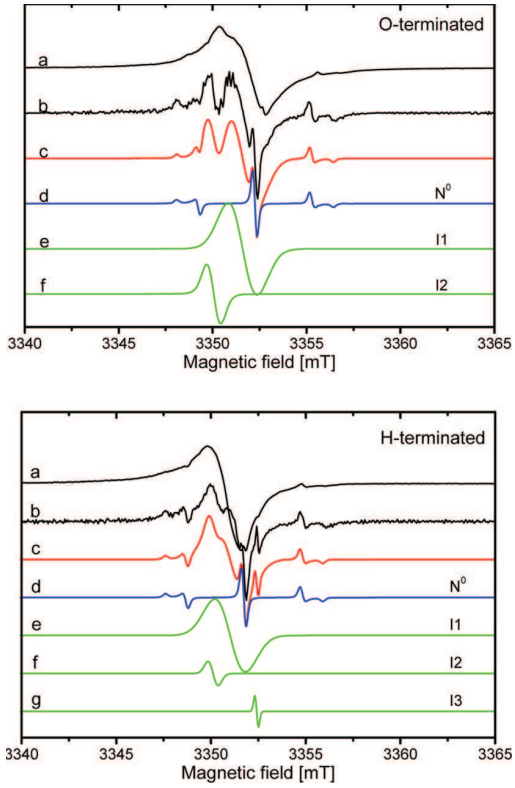

Figure 3. Experiment/simulation of two differently terminated ND samples: (top) O-terminated and (bottom) H-terminated: CW EPR (a) and the first derivative ESE-detected EPR (b) spectra, sum of simulated EPR spectra components (c), simulated N^0 center (d), and I1–I3 simulated components (Voigtian line shape) of EPR spectra (e–g); W-band, T = 50 K.

found that in O-terminated ND the ESE-detected EPR spectrum consists of three components (N^0, I1, I2), while the ESE-detected EPR spectrum of H-terminated samples could be described using four spectral components (N^0, I1, I2, I3). The zero-charged nitrogen atom (N^0) representing a triplet that could be described by effective spin Hamiltonian with spin S = 1/2 and nuclear spin I = 1[23,24] was observed in two samples. The corresponding g-tensor obtained in ref 26 and recently updated for ND[25] is found to be isotropic with g = 2.0024, A_x = A_y = 84 MHz, and A_z = 117 MHz. This uncharged nitrogen is the most common impurity in natural and synthetic diamonds as well as in the nanodiamonds of differing nature.

The I1–I3 paramagnetic centers are mainly not observed in the diamonds of macroscopic size and could be attributed to the radicals generated by breaking down the C–O and C–H bonds and formation of the condensed carbon (C) ring structure during the termination processes. In this case, the unpaired electron can be located on a C atom or oxygen (O) atoms and form two types of C radicals, namely: C-centered radicals and C-centered radicals with an adjacent O atom. The observation of a strong I1 signal (g = 2.0030 ± 0.0002, width ~2 ± 0.5 mT) of relatively similar intensity in all three types of samples could be explained either by a C-centered radical[26] or by sp^3 C–C dangling bonds. The parameters of the surface defects normalized to the intensity of the N^0 center are presented in Table 1. ^{1}H nuclei used in the termination possess nuclear spins and could be detected in the electron–nuclear double resonance experiment (ENDOR). The results obtained from the ENDOR spectra of the surface defects are promising in the interpretation of the differences for differently terminated samples.[28,30]

EPR spectra of ND particles consisted only of several signals with S = 1/2. Three of them are surface defects (I1–I3), and we did not observe any hyperfine interaction (HFI) from these defects. This is because centers themselves do not have HFI, and ligand HFI (superhyperfine interaction) is small in comparison with EPR line width (we observe HFI with distant fluorine and hydrogen nuclei in ENDOR spectra of these centers and can assign these defects to the surface of the ND particles without ambuguities). The only line with observable HFI in EPR spectra is N^0 (neutral nitrogen, not NV) defect S = 1/2 with normal HFI with its own nucleus (I = 1). The N^0 defect has triplet line structure, and we clearly observe it in EPR spectra (Figure 3). This defect is observable at lower temperatures also. The NV defect is also observable at EPR; however, it has strong orientation dependence, and its EPR spectrum is quite broad (it is averaged out in the powder spectra for more than 200 mT). We did not observe the signals from NV centers.

3.3. Fluorescence Lifetime Measurements. Fluorescence lifetimes measured at 20 ± 0.5 °C for NDs with different terminations are listed in Table 2. For green excitation the fraction of lifetimes above 15 ns increases with oxygen content. For ultraviolet excitation the fraction of long lifetimes increases in the surface modification series hydrogenated–oxygenated–oxygenated after 750 °C annealing.

For all ND terminations, at longer wavelength excitation (510 nm) the relative amount of longer lifetime processes is higher than for shorter wavelength excitations (375 nm). For high-energy excitation, a higher amount of electrons is also excited from the deep defects. Then, the triplet electrons in NV^- defects are strongly affected not only by phonons and material defects but also by a huge amount of other excited electrons—all these interactions shorten the lifetime of the luminescence. Moreover, our previous theoretical approach[2] has shown that surface termination can affect the interlaying singlet state, which also plays a significant role in the NV^- luminescence properties.

As far as differences between various terminations are concerned, mainly oxygen on the ND sp^2-terminated surface increases the fraction of longer lifetime states—e.g., O terminations on the C sp^2 surface (oxygenated, 750 °C annealed) keep settings of the original defects in basic and

Table 1. Summary of the EPR Fitting Results

termination		N^0	I1	I2	I3
O-terminated	intensity	1	13.6(4)	2.4(2)	—
	g	2.00245(5)	2.0028(5)	2.0037(3)	—
H-terminated	intensity	1	11.6(4)	0.42(5)	0.06(1)
	g	2.00245(7)	2.0029(5)	2.0034(3)	2.0020(2)

dx.doi.org/10.1021/jp507581c | J. Phys. Chem. C 2014, 118, 25245–25252

Table 2. Various Terminations of NDs' Fluorescence Lifetimes

	excitation 375 nm				excitation 510 nm	
	cut off 405 nm		cut off 519 nm		cut off 519 nm	
	lifetimes	amplitudes	lifetimes	amplitudes	lifetimes	amplitudes
termination	ns	-	ns	-	ns	-
oxygen	16.81	3%	18.40	3%	20.00	27%
	3.51	21%	3.68	20%	4.00	25%
	1.07	32%	1.15	31%	0.81	48%
	0.32	44%	0.33	46%		
hydrogen	15.40	3%	15.01	4%	14.93	10%
	2.36	10%	2.03	20%	2.64	29%
	0.76	28%	0.53	76%	0.61	61%
	0.25	59%				
oxygen, 750 °C annealed	17.12	12%	20.07	15%	21.5	38%
	1.61	27%	2.94	19%	3.57	34%
	0.27	61%	0.64	66%	0.73	28%

excited states and do not allow (NV^-) excited electrons to be so much drawn by the electron-attracting localities in the diamond. Oxygen-terminated negative surface potential plays an important role in this case. Specific shortening of the fluorescence lifetimes in the case of hydrogenated NDs may be caused by a number of processes—e.g. different spin/orbital settings and triplet electrons delocalized in the NV^- defect area.[30]

As a whole, ND luminescence parameters may be changed by the surrounding particles. A specific ND environmental state can lead to quenching, changes of luminescence lifetimes, or a spectral shift of emission.

3.4. Computer Modeling. New experimental findings bring the need for theoretical analysis. Here, we extend our previous theoretical results[2] and present a qualitatively new model/interpretation of NV centers containing ND particles' optical properties. It should be noticed that the calculated parameters such as excitation energies, electron affinities of particles, and geometry of NV centers are in a good correspondence with the experimental findings[26,27] and change with the calculated particles' dimensions. Particularly, the values of electron affinities calculated for defect-free O/H-terminated nanodiamond particles were: $C_{165}H_{88}O_{94}$, calculated electron affinity +1.7 eV, experimental +1.7 eV; $C_{165}H_{100}$, calculated electron affinity −2.2 eV, experimental −1.3 eV.[24] Due to the substitution of hydrogen- or oxygen-containing functional groups, the values of electron affinities increased.

In the case of hydrogen-terminated ND $C_{695}H_{302}N^-$ the surface is positively charged, and after replacement of part of the hydrogen atoms by O groups the surface potential is strongly modified. For $C_{695}H_{160}O_{150}N^-$ the electrostatic surface potential is negative in the place of substitution and its neighborhood—see Figure 4 (corresponding to experimental results[28−31]). Surface groups including oxygen are electron acceptors, which causes the change of Mulliken charges and electron density in NDs. Redistribution of electrons in NDs influences behavior of NV^- triplet electrons. On the basis of our calculations, we have proposed that in the case of O-containing group-terminated ND surfaces the excited electron will be kept (surface potential) in NV^- centers, so that standard luminescence conditions can be preserved. It should be noted that if we want to change the positive surface potential of H-terminated ND to a negative surface potential it is sufficient to replace just 9% of the CH_2 groups by carbonyl groups.[2]

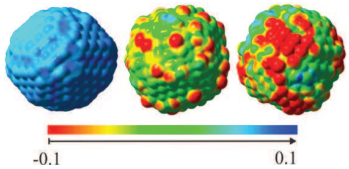

Figure 4. Mapping of the electrostatic potential onto the ground-state isodensity surface of the NV^--containing clusters $C_{695}H_{302}N^-$ (left), $C_{695}H_{260}O_{50}N^-$ (middle), and $C_{695}H_{160}O_{150}N^-$ (right). The NV^- center is located in the second layer in the left top part of both pictures.

Figure 5 indicates that for ND particle-containing NV^- centers with H-surface termination the unpaired/triplet

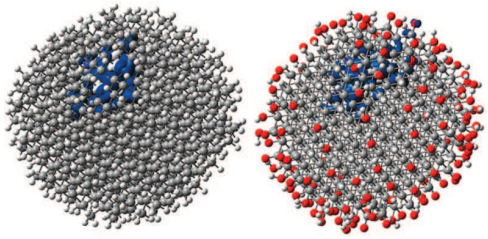

Figure 5. Plots of spin densities in the NV^--containing clusters $C_{695}H_{302}N^-$ (left) and $C_{695}H_{160}O_{150}N^-$ (right).

electrons from the NV^- center affect electron spin density on the positively charged surface very moderately—the spin density is located in the vicinity of the NV^- center. Similar results are obtained in the case of ND with oxidized surface, $C_{695}H_{160}O_{150}N^-$, where the spin density is slightly spread out to the O centers. In agreement with EPR results we concluded that the unpaired electron can be located on C or O atoms and form two types of C radicals, namely, C-centered radicals and C-centered radicals with an adjacent O atom.

The TD-DFT calculated lowest allowed triplet excitation energy for $C_{182}H_{120}N^-$ is 2.063 eV (close to experimental data). The oxidation of the surface slightly shifts the excitation energy to a lower value of 1.971 eV for $C_{182}H_{120}O_{28}N^-$. All lowest-lying excitation transitions are between β (spin down) orbitals.

Another important parameter is the energy necessary to convert the NV^- to NV^0 centers. The DFTB calculated NV^- to NV^0 conversion energy is 1.47, 2.58, and 4.65 eV for clusters

dx.doi.org/10.1021/jp507581c | J. Phys. Chem. C 2014, 118, 25245−25252

$C_{695}H_{302}N^-$, $C_{695}H_{160}O_{50}N^-$, and $C_{695}H_{160}O_{150}N^-$, respectively. For H-terminated ND particles the conversion energy is lower than the NV^- excitation energy, so that the delocalized triplet electrons can be more easily released from the original positions and drawn to the electron-attracting localities in the material. For a mix of oxygen group-terminated NV^- centers containing NDs, the conversion energies are higher than NV^- center excitation energy—in these types of particles it is easier to excite electrons in the NV^- center than to convert the NV^- centers into NV^0.[31]

Moreover, it follows from our calculations that electrons excited from the triplet ground state to the triplet excited state and relaxed to the triplet state b^3A can drop to triplet ground state a^3A (standard emission) or to singlet ground state a^1A, lying below the triplet excited state (different NV^- luminescence conditions). Since in oxidized NDs containing NV^- centers the singlet state a^1A energy level has higher energy than the excited triplet state b^3A energy level, the conditions for transition between the excited triplet and singlet ground state a^1A are changed. For neutrally charged NV centers singlet electrons are kept in the area of NV^0 centers, and standard luminescence conditions are preserved.

3.5. Imaging of ND Particles in Living Cells. By using confocal microscopy we investigated the ability of luminiscent ND particles to enter living cells (Figure 6). Oxygen-terminated

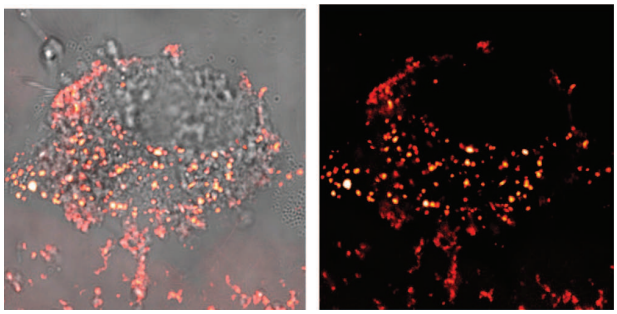

Figure 6. Confocal microscopy analyses of localization of fluorescence nanodiamonds in HeLa cells. Left: confocal image of fluorescent NDs in the cell, right: HeLa cell in transition light with incorporated fluorescent nanodiamond particles. The image shows numerous clusters of ND particles within the cytoplasm clearly showing the absence of any particles within the nucleus.

NDs were clearly visible within the cytoplasm of human epithelial cells and at the same time we could see numerous clusters of ND particles within the cytoplasm, clearly showing the absence of any fluorescent particles within the nucleus. Namely, Figure 6 shows a representation of the confocal image of HeLa cells with incorporated fluorescent ND particles. This interesting finding has been verified by electron microscopy using other cell lines (e.g., A549). In general, NDs tend to accumulate around some vesicles in the cytoplasm.

Our study shows that NDs are able to penetrate through the cell membrane in a targeted manner and probe changes in the inner cellular space—subcellular localization of nanodiamonds was clearly viewed by transmission electron microscopy (Figure 7). Combined with the exquisite molecular recognition of antibody ligands, ND-derived sensors could thus serve as powerful tools capable of exploring multiprotein molecular machineries in a living cell. Specific types of surface-sensitive ND-derived sensors could also be developed as multifunctional

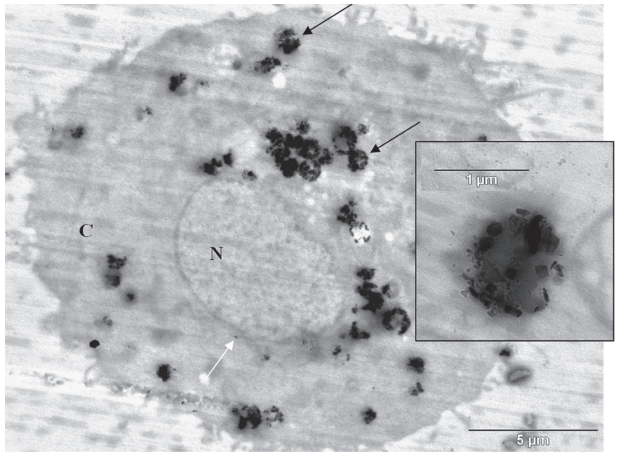

Figure 7. Subcellular localization of NDs in the A 549 cell viewed by TEM. NDs (black points) are localized in the cytoplasm outside the nucleus. Clusters of NDs are formed around vesicles (black arrows); several isolated NDs are recognized in the cytoplasm (white arrow). Inset: detail of cytoplasmic vesicle covered by NDs. Individual NDs are well visualized. N: nucleus, C: cytoplasm.

probes (antibody as well as DNA) that could measure, structure, or even alter biological components in single cells.[18]

NDs could serve not as only as probes but also as delivery systems for various agents effecting processes in the cell. In vitro studies were designed and are running to answer some questions on the effect of NDs on some cellular functions (e.g., induction of apoptosis, inhibition of intercellular communication, mitochondrial respiration, stability of microsomes, etc.)

4. CONCLUSIONS

In this article we show how surface chemistry influences ND magnetic and optical properties for modern devices. NV^--related long-term luminescence of oxygenated particles increased in comparison to plasma hydrogenated NDs' NV^- luminescence. Due to the ND small size, the charge at the ND surface can penetrate into the bulk of the ND and intermingles with the electronic NV^- states.

Attaching oxygen to a graphitized ND surface increased the share of states with longer lifetime and preserved ground and excited states (fluorescence lifetime measurements). Plasma hydrogenation of ND particles gave rise to characteristic defects with short lifetimes. Oxygen on the ND sp^2-terminated surface increases the fraction of longer lifetime states—e.g., O terminations on the C sp^2 surface keeps settings of the original (NV) defects in basic and excited states.

EPR spectroscopy confirmed the presence of paramagnetic centers that are not observed in the diamonds of macroscopic size. These centers could be attributed to radicals generated by the breakage of the C−O and C−H bonds as well as to formation of a condensed carbon ring structure during the termination processes.

Our theoretical models demonstrated that for H-terminated ND particles the NV^- to NV^0 conversion energy is lower than the NV^- excitation energy, so that the delocalized triplet electrons can be more easily released from the original positions and drawn to the electron-attracting localities in the material. For a mix of oxygen-group-terminated NV^- centers containing NDs, the NV^- to NV^0 conversion energy is higher than the NV^- center excitation energy. We also showed that the

dx.doi.org/10.1021/jp507581c | J. Phys. Chem. C 2014, 118, 25245−25252

surface termination affects the singlet metastable state ^{1}A. Optical pumping initializes the center into the $m_s = 0$ spin state via spin-selective transition into the metastable singlet state, ^{1}A (Figure 1). The mechanism responsible for optical pumping also provides a means for spin-sensitive detection, as the rate of fluorescence differs for the $m_s = 0$ and $m_s = \pm 1$ states. This optically detected NV^- electron spin resonance process can be significantly affected by ND termination. In oxidized ND NV^- centers the ^{1}A level is shifted to a higher energy in comparison with the hydrogenated ND NV^- singlet level. For small NDs the influence of surface chemistry is more significant—the singlet level shift to higher energies for small oxygenated NDs is more relevant. In agreement with EPR results we concluded that the unpaired electron can be located on C or O atoms and form two types of the C radicals, namely, C-centered radicals and C-centered radicals with an adjacent O atom.

The final part of our study concerned application of NDs in cells. Luminescent ND particles are able to penetrate through the cell membrane and accumulate in the cytoplasm (confocal microscopy and TEM), where they form clusters surrounding cytoplasmic vesicles. Luminescent ND particles are precisely detectable by confocal microscopy, and their subcellular distribution is easy to follow by this technique, making ND particles perfect luminescence probes.

AUTHOR INFORMATION

Corresponding Authors

*Tel.: +420 26605 2524. E-mail: krat@fzu.cz

*E-mail: zalis@jh-inst.cas.cz.

Notes

The authors declare no competing financial interest.

ACKNOWLEDGMENTS

We gratefully acknowledge the support by grants Nos. TA01011165, TA04020156, 14-10279S; Project Centre of Excellence at VRI for nanotoxicology CENATOX GAP503/12/G147; CZ.1.07/2.3.00/20.0164, DINAMO FP7 KBBE 245122 (Anna Fišerová); Formatted: Not Highlight NANO-INTEGRATION CZ.1.07/2.3.00/20.0306 CTU FBME, KladnoMaterials Research Centre at FCH BUT- Sustainability and Development, REG LO1211, with financial support GAP14-10279S from the National Programme for Sustainability I (Ministry of Education, Youth and Sports), CZ.1.07/2.3.00/30.0039 of Brno University of Technology. This work was also partially funded by the subsidy allocated to Kazan Federal University for the state assignment in the sphere of scientific activities and by the Russian Foundation for Basic Research, project no. 14_02_31881 mol a. We would like to acknowledge Jan Štursa for sample preparation.

REFERENCES

(1) Koizumi, S.; Nebel, C.; Nesladek, M. *Physics and Applications of CVD Diamond*; Wiley-VCH Verlag GmbH & Co.KGaA: Weinheim, 2008.

(2) Kratochvílová, I.; Kovalenko, A.; Fendrych, F.; Petráková, V.; Záliš, S.; Nesládek, M. Tuning of Nanodiamond Particles' Optical Properties by Structural Defects and Surface Modifications: DFT Modelling. *J. Mater. Chem.* **2011**, *21*, 18248−18255.

(3) Petráková, V.; Taylor, A. J.; Kratochvílová, I.; Fendrych, F.; Vacík, J.; Kučka, J.; Štursa, J.; Cígler, P.; Ledvina, M.; Fišerová, A.; Kneppo, P.; Nesládek, M. Luminescence of Nanodiamond Driven by Atomic Functionalization: Towards Novel Biomolecular Detection Principles. *Adv. Funct. Mater.* **2012**, *22*, 812−819.

(4) Domhan, M.; Wittmann, C.; Popa, I.; Jelezko, F.; Rabeau, J.; Greentree, A.; Prawer, S.; Trajkov, E.; Hemmer, P. R.; Wrachtrup, J. Photochromism in Single Nitrogen-Vacancy Defect in Diamond. *Appl. Phys. B: Lasers Opt.* **2006**, *82*, 243−246.

(5) Dantelle, G.; Slablab, A.; Rondin, L.; Laine, F.; Carrel, F.; Bergonzo, P.; Perruchas, S.; Gacoin, T.; Treussart, F.; Roch, J.-F. Efficient Production of NV Colour Centres in Nanodiamonds Using High-Energy Electron Irradiation. *J. Lumin.* **2009**, 1655−1658.

(6) Petráková, V.; Nesládek, M.; Taylor, A.; Fendrych, F.; Cigler, P.; Ledvina, M.; Vacik, J.; Stursa, J.; Kucka, J. Luminescence properties of engineered nitrogen vacancy centers in a close surface proximity. *Phys. Status Solidi A* **2011**, *9*, 2051−2056.

(7) Yu, S.-J.; Kang, M.-W.; Chang, H.-C.; Chen, K.-M.; Yu, Y.-C. Bright Fluorescent Nanodiamonds: No Photobleaching and Low Cytotoxicity. *J. Am. Chem. Soc.* **2005**, *127*, 17604−17605.

(8) Zyubin, A. S.; Mebel, A. M.; Hayashi, M.; Chang, H. C.; Lin, S. H. Quantum Chemical Modeling of Photoabsorption Properties of Two- and Three-Nitrogen Vacancy Point Defects in Diamond. *J. Phys. Chem. C* **2009**, *113*, 10432−10440.

(9) Mochalin, V. N.; Shenderova, O.; Ho, D.; Gogotsi, Y. The Properties and Applications of Nanodiamonds. *Nat. Nanotechnol.* **2012**, *7*, 11−23.

(10) Maze, J. R.; Stanwix, P. L.; Hodges, J. S.; Hong, S.; Taylor, J. M.; Cappellaro, P.; Jiang, L.; Dutt, M. V. G.; Togan, E.; Zibrov, A. S.; Yacoby, A.; Walsworth, R. L.; Lukin, M. D. Nanoscale Magnetic Sensing with an Individual Electronic Spin in Diamond. *Nature* **2008**, *455*, 644−647.

(11) Kratochvílová, I.; Zambova, A.; Mbindyo, J.; Razavi, B.; Holakovský, J. Current-Voltage Characterization of Alkanethiol Self-Assembled Monolayers in Metal Nanowire. *Mod. Phys. Lett. B* **2002**, *16*, 161−169.

(12) Budker, D. Diamond Nanosensors: The Sense of Colour Centres. *Nat. Phys.* **2011**, *7*, 453−454.

(13) Dolde, F.; Fedder, H.; Doherty, M. W.; Nöbauer, T.; Rempp, F.; Balasubramanian, G.; Wolf, T.; Reinhard, F.; Hollenberg, L. C. L.; Jelezko, F.; Wrachtrup, J. Electric-Field Sensing Using Single Diamond Spins. *Nat. Phys.* **2011**, *7*, 459−463.

(14) Balasubramanian, G.; Chan, I. Y.; Kolesov, R.; Al-Hmoud, M.; Tisler, J.; Shin, C.; Kim, C.; Wojcik, A.; Hemmer, P. R.; Krueger, A.; Hanke, T.; Leitenstorfer, A.; Bratschitsch, R.; Jelezko, F.; Wrachtrup, J. Nanoscale Imaging Magnetometry with Diamond Spins under Ambient Conditions. *Nature* **288**, *455*, 648−651.

(15) Aharonovich, I.; Greentree, A. D.; Prawer, S. Two-Level Ultrabright Single Photon Emission from Diamond Nanocrystals. *Nano Lett.* **2009**, *9*, 3191−3195.

(16) Bradac, C.; Gaebel, T.; Naidoo, N.; Sellars, M. J.; Twamley, J.; Brown, L. J.; Barnard, A. S.; Plakhotnik, T.; Zvyagin, A. V.; Rabeau, J. R. Observation and Control of Blinking Nitrogen-Vacancy Centres in Discrete Nanodiamonds. *Nat. Nanotechnol.* **2010**, *5*, 345−349.

(17) Fendrych, F.; Taylor, A.; Peksa, L.; Kratochvilova, I.; Vlcek, J.; Rezacova, V.; Petrak, V.; Kluiber, Z.; Fekete, L.; Liehr, M.; Nesladek, M. Growth and Characterization of Nanodiamond Layers Prepared Using the Plasma-Enhanced Linear Antennas Microwave CVD System. *J. Phys. D: Appl. Phys.* **2010**, *43*, 374018.

(18) Mašek, J.; Bartheldyová, E.; Turánek-Knotigová, P.; Škrabalová, M.; Korvasová, Z.; Plocková, J.; Koudelka, Š.; Škodová, P.; Kulich, P.; Křupka, J.; et al. Metallochelating Liposomes with Associated Lipophilised Norabumdp as Biocompatible Platform for Construction of Vaccines with Recombinant His-Tagged Antigens: Preparation, Structural Study and Immune Response Towards Rhsp90. *J. Controlled Release* **2011**, *12*, 193−201.

(19) Frisch, M. J.; Trucks, G. W.; Schlegel, H. B.; Scuseria, G. E.; Robb, M. A.; Cheeseman, J. R.; Scalmani, G.; Barone, V.; Mennucci, B.; Petersson, G. A. et al. *Gaussian 09*, Revision D.01; Gaussian Inc.: Wallingford, CT, 2009.

(20) Ahlrichs, R. et al., Turbomole 6.3, www.turbomole.com.

(21) Kratochvílová, I.; Golan, M.; Vala, M.; Špérová, M.; Weiter, M.; Páv, O.; Šebera, J.; Rosenberg, I.; Sychrovský, V.; Tanaka, Y.; Bickelhaupt, F. M. Theoretical and Experimental Study of Charge

Transfer Through DNA: Impact of Mercury Mediated T-Hg-T Base Pair. *J. Phys. Chem. B* **2014**, *118*, 5374−5381.
(22) Tiwari, A. K.; Goss, J. P.; Briddon, P. R.; Wright, N. G.; Horsfall, A. B.; Jones, R.; Pinto, H.; Rayson, M. J. Calculated Electron Affinity and Stability of Halogen-Terminated Diamond. *Phys. Rev. B* **2011**, *84*, 245305.
(23) Hauf, M. V.; Grotz, B.; Naydenov, B.; Dankerl, M.; Pezzagna, S.; Meijer, J.; Jelezko, F.; Wrachtrup, J.; Reinhard, F.; Garrido, J. A.; Stutzmann, M. Chemical Control of the Charge State of Nitrogen-Vacancy Centers in Diamond. *Phys. Rev. B* **2011**, *83*, 081304(R).
(24) Maier, F.; Ristein, J.; Ley, L. Electron Affinity of Plasma-Hydrogenated and Chemically Oxidized Diamond 100 Surfaces. *Phys. Rev. B* **2001**, *64*, 165411.
(25) Baranov, P. G.; et al. Enormously high concentrations of fluorescent nitrogen-vacancy centers fabricated by sintering of detonation nanodiamonds. *Small* **2011**, *7* (11), 1533−1537.
(26) Smith, W. V.; et al. Electron-Spin Resonance of Nitrogen Donors in Diamond. *Phys. Rev.* **1959**, *115* (6), 1546−1552.
(27) Baranov, P. G.; et al. Electron Spin Resonance Detection and Identification of Nitrogen Centers in Nanodiamonds. *JETP Lett.* **2009**, *89* (8), 409−413.
(28) Yavkin, B. V.; Mamin, G. V.; Orlinskii, S. B.; Kidalov, S. V.; Shakhov, F. M.; Vul', A. Y.; Soltamova, A. A.; Soltamov, V. A.; Baranov, P. G. Room Temperature High-Field Spin Dynamics of NV Defects in Sintered Diamonds. *Appl. Magn. Reson.* **2013**, *44* (10), 1235−1244.
(29) Lim, T. S.; Fu, C. C.; Lee, K. C.; Lee, H. Y.; Chen, K.; Cheng, W. F.; Pai, W. W.; Chang, H. C.; Fann, W. Fluorescence Enhancement and Lifetime Modification of Single Nanodiamonds Near a Nanocrystalline Silver Surface. *Phys. Chem. Chem. Phys.* **2009**, *11* (10), 1508−14.
(30) Stoll, S.; Schweiger, A. Easyspin, a Comprehensive Software Package for Spectral Simulation and Analysis in EPR. *J. Magn. Reson.* **2006**, *178* (1), 42−55.
(31) Liaugaudas, G.; Davies, G.; Suhling, K.; Khan, R. U.; Evans, D. J. Luminescence Lifetimes of Neutral Nitrogen-Vacancy Centres in Synthetic Diamond Containing Nitrogen. *J. Phys.: Condens. Matter* **2012**, *24* (43), 435503−435507.

Microchim Acta (2017) 184:1489–1497
DOI 10.1007/s00604-017-2149-8

ORIGINAL PAPER

Real-time monitoring of the UV-induced formation of quantum dots on a milliliter, microliter, and nanoliter scale

Lukas Nejdl[1,2] · **Jan Zitka**[1,2] · **Filip Mravec**[3] · **Vedran Milosavljevic**[1,2] · **Ondrej Zitka**[1,2] · **Pavel Kopel**[1,2] · **Vojtech Adam**[1,2] · **Marketa Vaculovicova**[1,2]

Received: 28 November 2016 / Accepted: 19 February 2017 / Published online: 3 March 2017

Abstract The authors report on a systematic study on the low-cost, low-temperature, and fast synthesis of water soluble quantum dots (QDs) stabilized by mercaptosuccinic acid by UV irradiation. The effects of UV irradiation (at 254 nm and 250 nm) and temperature on the precursors (Cd:Se, Cd:Te, Cd, Zn:S, Zn:Se and Zn) are described. Best results are achieved with a mixture of precursors containing cadmium, selenium and MSA where a 10-min irradiation with 254-nm light gives CdSe QDs with a quantum yield of 13.5%. The authors also describe the preparation and monitoring of the formation of QDs in sub-mg, sub-μg and sub-ng quantities, the smallest concentration being 258 pg in volume of 4 nL. The growth of the QDs can be monitored in real time by absorption, fluorescence and dynamic light scattering. The solutions of the particles also are characterized by fluorescence correlation spectroscopy and detected by LED-induced fluorescence. The preparation of such QDs by UV radiation is simple, easily controllable, and inexpensive. Conceivably, it can be integrated with lab-on-chip, micro total analysis systems or other instrumentation.

Keywords Nanocrystal · Capillary electrophoresis · Irradiation · Fluorescence

Introduction

Fluorescent nanoparticles with a size range of units or tens of nanometers, better known as quantum dots (QDs), possess unique properties [1]. Their optical and semiconductor properties are tunable by changing the size, shape, spatial arrangement, conductivity, and surface modification (i.e. conjugation with ligands) [2] QDs have been applied in (bio)sensors, in biosciences such as in vivo imaging, drug delivery and diagnostic, or in vitro labeling of molecules, cells and tissues [3, 4]. Due to their small size they not only retain properties of the material from which they originate, but also adopt new features related to their size [5]. For biological applications, nanocrystals of CdSe, CdSe/ZnS, CdTe, CdTe/CdS are the most widely used [6]. However, potential toxicity of heavy metals attracted a great attention to safety concerns for health and environment [7]. For this reason, QDs made from less toxic materials, such as zinc [8] and carbon [9] were developed. The photo-physical properties, which make QDs interesting compared to classic organic dyes include very narrow emission spectra, broad absorption spectra, long fluorescence lifetime, high quantum yield, high molar extinction coefficient, large effective Stokes shift, and high stability against photobleaching [10]. Generally, the techniques for synthesis of different nanoparticle types are categorized either as a top-down or bottom-up approach [11, 12]. Top-down (physical) methods includes different types of lithographic techniques (laser, ion and X-ray) or etching and grinding [13–18]. Among the more popular methods belongs bottom-up (chemical) approach. Usually it is a synthesis of the nanoparticles in non-aqueous solvents (organometallic synthesis)

Electronic supplementary material The online version of this article (doi:10.1007/s00604-017-2149-8) contains supplementary material, which is available to authorized users.

✉ Marketa Vaculovicova
marketa.vaculovicova@mendelu.cz

[1] Department of Chemistry and Biochemistry, Mendel University in Brno, Zemedelska 1, 613 00 Brno, CZ, Czech Republic

[2] Central European Institute of Technology, Brno University of Technology, Purkynova 123 3058/10, -612 00 Brno, CZ, Czech Republic

[3] Materials Research Centre, Faculty of Chemistry, Brno University of Technology, Purkynova 118, 612 00 Brno, Czech Republic

along with toxic instable precursors at high temperatures [19, 20]. Due to the complexity of these procedures, alternative method using aqueous solvents were developed [21, 22]. Both variants (non-aqueous or aqueous solvents) lead to formation of nanocrystals in the presence of stabilizing ligands, which prevent aggregation of QDs in the reaction medium. The bottom-up processes include a variety of methods such as microwave-assisted technique, ultrasonic-assisted technique [23], photochemicals-assisted technique [24], high temperature technique and biosynthesis (in microorganisms [25], animals [26], plant [27], fungi and actinomycete [28, 29]). Another option is the interaction with UV light. Earlier, number of nanoparticles able to interact with UV radiation was described including TiO_2 nanorods [30], ZnO nanoparticles [31] and others [32]. The processes of photoactivation, photoenhancement or photobrightening ware intensively studied, e.g. Guo-Yu Lan et al. in his work described a photo-assisted synthesis of highly fluorescent ZnSe QDs in aqueous solution stabilized with mercaptosuccinic acid (MSA) [33]. Uematsu et al. dealt with photoetching of CdTe nanocrystals [34], Shang Yazhuo et al. synthesized gold nanoparticles by reduction of $HAuCl_4$ under UV irradiation [35], Kao Mahalieo et al. presented the synthesis of indium nitride nano- and microstructures by UV-assisted procedure [36].

The study is focused primarily on investigation of low cost, low temperature, and fast synthesis of water soluble QDs stabilized by MSA by UV irradiation, where the optimal conditions are found. Moreover, the use three methods for synthesis of QDs were compared and their pros and cons are discussed.

Experimental section

Chemicals

Working solutions (buffers and standard solutions) were prepared daily by diluting the stock solutions. Standards and other chemicals were purchased from Sigma-Aldrich (St. Louis, MO, USA) in ACS purity unless noted otherwise.

Synthesis of quantum dots by UV

3 mL of prepared solution (precursors) was taken in a 4 mL quartz cuvette (Hellma GmbH & Co. KG, Müllheim, Germany) and irradiated by UV (λ_{em} = 254 nm) transilluminator (Vilber Lourmat, Marne-la-Vallee Cedex, France). The sample area of 20 × 20 cm was illuminated by 6 UV emitting tubes with power of 15 W each. The intensity of UV radiation incoming to the quartz cuvette was recorded by optical power meter (PM100D, sensor SV120VC, Thorlabs Inc., Newton, NJ, USA). Based on these measurements the intensity of incoming UV energy into the sample was determined as E = 0.14 mW·mm^{-2}.

Fluorescence and absorbance analysis

Fluorescence was acquired by multifunctional microplate reader Tecan Infinite 200 M PRO (TECAN, Switzerland). Wavelength of 250 nm was used for excitation and the fluorescence scan was measured within the range from 300 to 700 nm using 2-nm steps. The detector gain was set to 80. The samples (50 μL) were placed in UV-transparent 96 well microplate with flat bottom by CoStar (Corning, USA). Absorption spectra were recorded under the same conditions in the range 240–600 nm. All measurements were performed at 25 °C controlled by Tecan Infinite 200 PRO (TECAN, Switzerland).

Particle size and zeta-potential analysis

Zetasizer MALVERN, Malvern Instruments Ltd. Worcestershire WR14 1XZ, United Kingdom was used.

Particle size assessment (dynamic light scattering)

The particle size measurements were performed considering a refraction index of the dispersive phase of 3.00 and 1.33 for the dispersive environment. The absorption coefficient in both cases was 10^{-3}. The measuring temperature was set at a constant value of 25 °C, while the viscosity was 0.8872 cP. For each measurement, disposable cuvettes type ZEN 0040, were used, containing 40 μL of sample. The equilibration time was 120 s, at a measurement angle of 173° backscatter and pH of solution was 9. All measurements were triplicate and the data was expressed as the average value.

Zeta potential assessment

The particle size measurements were performed considering the same refraction index, pH and absorption coefficient as described in particle size measurements. Furthermore, the parameters such as, temperature and viscosity were the same as in particle size measurements. Calculations considered the diminishing of particles concentration based Smoluchowsky model, with a F(κa) of 1.50 and an equilibrating time of 120 s. For the measurements, a disposable cell DTS1070 was employed. In each case, the number of runs varied between 20 and 40. The measurements were carried out in triplicates and were performed under the automatic setting of attenuation and voltage selection.

Determination of quantum yields (QY)

The quantum yields were determined by analysis of emission maxima with the excitation at 250 (ZnS, ZnSe and Zn) or 380 nm (CdSe, CdTe and Cd). The absorbance was analyzed using the same excitation wavelength. The quantum yields

were calculated on the basis of integration of absorption and emission value. Absolute values were calculated using the standard samples (quinine sulfate), with known fluorescence QY value, according to the following Eq. [37]:

$$Ø_X = Ø_{ST}\left(\frac{Grad_x}{Grad_{ST}}\right)\left(\frac{\eta_x^2}{\eta_{ST}^2}\right) \quad (1)$$

where the subscripts *ST* and *X* denote standard and test, respectively, *Ø* is the fluorescence quantum yield (*Ø* ST = 0.54), *Grad* the gradient from the plot of integrated fluorescence intensity vs. absorbance (*GradST = 80,000,000*, and η the refractive index of the solvent (1.33).

Capillary electrophoresis with LED-induced fluorescence (CE-LED-IF) detection

CdSe QDs were analyzed by CE (PACE MDQ, Beckman Coulter, USA) with blue LED (λ_{em} = 380 nm) as an excitation source. Unmodified fused silica capillary with internal diameter of 75 μm and with the total length of 64.5 cm (14 cm to a special window for optical fiber and 54 cm to detector window) was used. Optical fiber (diameter 910 μm Core Multimode, High-OH for 250–1200 nm, Thorlabs Inc., USA) was focused to a capillary in the special window and connected with the UV LED with ball lens, λ_{em} = 250 nm, 1 mW (Thorlabs Inc., USA). Hydrodynamic injection by 5 psi for 5 s was employed. As pretreatment the separation voltage 20 kV and waiting time of 0, 5, 10, 15, 20, 25 and 30 min (for synthesis of QDs in special window) was used and after that 30 kV separation voltage was applied. 20 mM sodium borate buffer pH 9 was used as a separation electrolyte.

Results and discussion

Temperature testing of precursors

For biological applications, nanocrystals of CdSe, CdTe, ZnS, ZnSe are usually used [6, 38, 39]. For these reasons these common precursors (Cd:Se, Cd:Te, Zn:S, Zn:Se, Zn, Cd in combination with and without reducing agent, Note: utilization of the reduction agent is noticed by a label "red") with MSA as a capping agent were tested. First, the temperature dependent behavior was monitored (25, 35, 45, 55, 65, 75, 85 and 95 °C, samples were incubated at each temperature for 30 min). In this experiment, twelve aliquots of precursors were prepared. These aliquots contained various combinations of precursors, as described in Supplementary material. Samples (1 mL) were heated and afterwards cooled to the temperature of 25 °C, the samples were immediately analyzed. Absorption spectra in range 230–600 nm and emission spectra (λ_{ex} = 250 nm and λ_{em} = 380 to 800 nm) were recorded (data not shown). If the fluorescence was observed, the QY was calculated (Table S1). For most studied precursors, QY below 1% was observed. An exception was the sample labelled as CdTe red, which exhibited a significant increase in QY, increasing with temperature. Increasing the temperature caused a bathochromic shift of the emission spectrum (λ_{em} max = 494 nm (35 °C), 498 nm (45 °C), 506 nm (55 °C), 516 nm (65 °C), 520 nm (75 °C), 528 nm (85 °C), and 534 nm (95 °C)). The highest QY was achieved at 95 °C (λ_{em} max = 534 nm, QY = 20.1%).

UV (λ_{em} = 254 nm) synthesis of QDs from precursors by transilluminator

In the next step, the influence of UV irradiation (λ = 254 nm) on formation of QDs from precursors was tested. The samples (3 mL) were pipetted in to the quartz cuvette and placed to the canter of the illumination area of the UV transilluminator and irradiated in time (0, 10, 20 and 30 min). The temperature inside transilluminator increased from 25 to 35 °C (depending on the time of irradiation). For all investigated samples, interaction with UV light was observed. The values of λ_{em} maxima and QY are summarized in Table S2. The lowest QY (≤ 1) was recorded after 10-min irradiation in case of ZnS, ZnS red (Note: utilization of the reduction agent is noticed by a label "red") and ZnSe. Longer intervals of irradiation (20 and 30 min) caused a fluorescence loss in ZnS and ZnS red. For ZnSe, QY ≤ 1% was observed for all times of irradiation. On the other hand, the best result was achieved in case of CdSe. At all times of irradiation, QY of 13.4% was observed. For all investigated samples, a bathochromic shift of the emission maxima was observed depending on the duration of illumination.

Formation of CdSe - QDs from precursors monitored by spectroscopic techniques

Based on previous experiments, precursor solution composed of Cd and Se was chosen for fluorescence and spectrophotometric analysis. Precursors (3 mL) were pipetted into the quartz cuvette and placed in the center of UV transilluminator (emission spectrum of UV lamps, Fig. 1a) and irradiated for 0–60 min. In five-minute intervals, 50 μL aliquots were taken and absorption spectra were measured (240–600 nm), Fig. 1b. It is shown that increasing the illumination time caused an increase in the intensity and a shift of the absorption maximum of CdSe QDs, Fig. 1c**.** Absorption maximum of CdSe QDs after 5 min irradiation was λ_{max} = 324 nm. After another 55 min was shifted for about 54 nm (λ_{max} = 378 nm).

Subsequently, the emission maxima of these samples were measured (λ_{ex} = 250 nm a λ_{em} = 330–700 nm), Fig. 1d. An increase in the emission intensity was

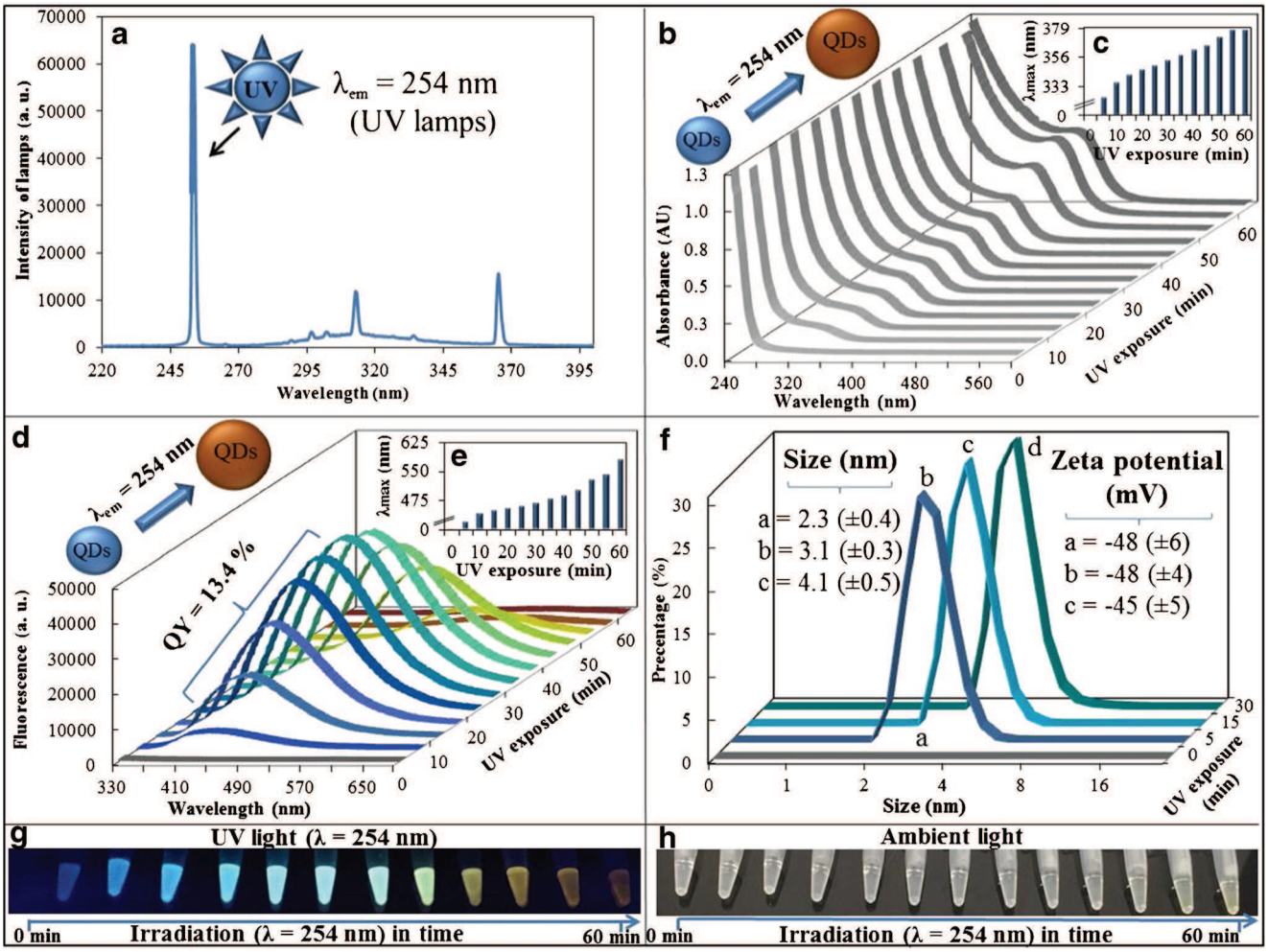

Fig. 1 Spectral analysis of UV-formed QDs **a** Emission spectrum of UV tubes in the transilluminator, **b** Absorption spectra of CdSe QDs (240–600 nm) obtained after illumination of precursors (0–60 min) by UV light (spectrum shown in 1a), **c** Absorbance maximum shift dependent on illumination time, **d** Fluorescence emission spectra (330–700 nm) dependent on illumination time (0–60 min), **e** Emission maximum shift dependent on illumination time, **f** Particle size distribution and zeta potentials of the UV-formed QDs, **g** Photographs of the UV-formed QDs under UV illumination, **h** Photographs of the UV-formed QDs under ambient light

observed during first 30 min of illumination, however in the time interval 35–60 min of illumination, the fluorescence intensity decreased. In addition, the emission spectrum exhibited a bathochromic shift as shown in Fig. 1e**.** After 5 min of illumination, the emission maximum was λ_{em} max = 420 nm, but after 60 min, the maximum increased for 158 nm to 578 nm. The presented results confirm that the UV illumination causes formation of the fluorescent nanocrystals ($[Cd(CH_3CO_2)_2 + Na_2Se \rightarrow CdSe\downarrow + 2Na(CH_3CO_2)]$), stabilized by the MSA via the thiol group, demonstrated by the red shift of the absorption and emission spectra. The chemical principle of this observation was explained elsewhere [40], stating that the thiol groups are photo-oxidized by the application of the UV light forming disulfide bridges in the molecules of the capping agents. These molecules are afterwards dissolved by the surrounding aqueous solution and released from the particle surface. The exposed hydrophobic surface of the particle causes subsequent aggregation of the crystals resulting in the increased particle size and therefore the red shift in the spectra.

Using the dynamic light scattering technique the increasing particle size dependent on the time of illumination was confirmed (Fig. 1f**).** It was observed that after 5-min illumination, QDs with the size of 2.3 (±0.4) nm and zeta potential of −48 (±6) mV were formed and after 15-min illumination, the size and increased to 3.1 (±0.3) nm. Finally, the illumination for 30 min caused the formation of nanoparticles with the size of 4.1 (±0.4) nm and zeta potential of −45 (±5) mV. From the values of zeta potential, the stability of the colloidal solution is commonly evaluated. The results suggested that the solution resulting by the UV light illumination was stable, because the solution with zeta potential of value above 30 mV or −30 mV is generally considered non-aggregating and stable [41]. The photographs of the QD solutions in UV and ambient light are shown in Fig. 1g, h, respectively**.**

Fluorescence lifetime and concentration of CdTe – QDs as a function of the duration of UV exposure

In this experiment, conventional fluorescence correlation spectroscopy (fluorescence correlation spectroscopy measurement is described in Supplementary material.) was modified as shown in Fig. 2a**.** The solution of Cd:Se precursors (15 μL) was pipetted on quartz glass (Fig. 2a – *a*) and on the top of this sample UV LED (λ_{em} = 250 nm, 1 mW), Fig. 2a – *b* was placed. After turning on the UV LED, the QDs started to be formed and observed in the confocal volume (Fig. 2a - *c*) as schematically shown in Fig. 2a – *d*. This process was recorded in real time by microscope objective with water immersion (Fig. 2a – *e*) and excitation laser (λ_{em} = 367 nm and 1 MHz repetition). Finally, beam continued through the optical elements (50 μm pinhole and longpass emission filter, Fig. 2a – *f*, *g*) in to the detector, Fig. 2a – *h*.

FCS is based on monitoring of the variations in the intensity of fluorescence of substances diffusing through a very small volume (1 fL) observed. Temporal fluctuations of the intensity of fluorescence are recorded and analyzed using the autocorrelation function G (τ). The correlation curves were fitted to the equation, see in supplementary material. In this manner, CdSe QDs synthesis from precursors was recorded in real time, as evidenced in Fig. 2b. According to the time of occurrence of individual CdSe - QDs the genesis of QDs may be subdivided into five parts QDs 1–5. Each part is characterized by the length of interval (QDs 1 = 270 s, QDs 2 = 269 s, QDs 3 = 207 s, QDs 4 = 101 s a QDs 5 = 39 s). Thanks to the deconvolution of the temporal waveform can be the intervals studied in separately. The measured decay curves are found best represented by a tetraexponential diffusion analysis function of the form $I(t) = a_1 \exp.(-x/\tau_1) + a_2 \exp.(-x/\tau_2) + a_3 \exp.(-x/\tau_3) + a_4 \exp.(-x/\tau_4)$, where τ_1, τ_2, τ_3 and τ_4 are the lifetime components and a_1, a_2, a_3 and a_4 are the corresponding amplitudes. The lifetime components τ_1 - τ_4, average lifetime of components τ, average amplitudes a and approximated concentration c, estimated using $\tau = (\tau_1 + \tau_2 + \tau_3 + \tau_4)/4$, $a = (a_1 + a_2 + a_3 + a_4)/4$ and approx. $c = \frac{N}{V_{eff} N_{av}}$ are in detail collected in Table S3. From the values in the table is clear that the longer the time of UV irradiation the new quantum dots are detected, which resulted in increasing average length lifetime τ. From the initial 40 ns (interval QDs 1) the time decay was growing up to 112.2 ns (2.8 times), interval

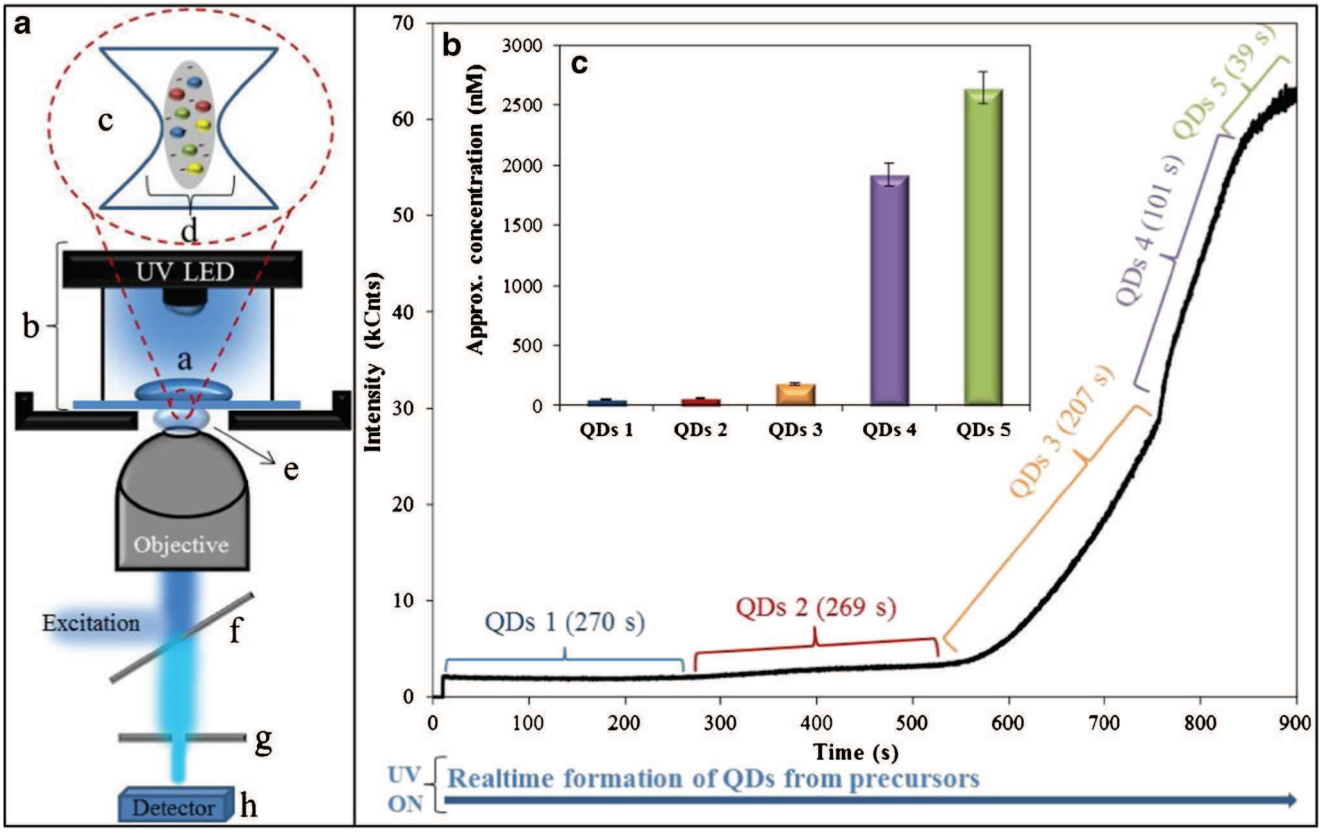

Fig. 2 **a** Schematic representation of the UV LED modified FCS a) 15 μL drop of precursors (Cd:Se) on quartz glass, b) UV LED (λ_{em} = 250 nm), c) idealized confocal volume, d) schematic representation of the QDs formation in a confocal volume, e) lens with water immersion, f, g) laser (λ_{em} = 367 nm, 1 MHz repetition), optical elements (50 μm pinhole and longpass emission filter) and h) detector. **b** Formation of CdSe QDs from precursors (Cd:Se) recorded in real time (0–15 min). **c** Approximated concentration of CdSe QDs generated during the UV irradiation

QDs 5. With increasing time, decay is directly proportional to increasing average lifetime amplitude a . Besides increasing τ and a there were also noted increasing concentrations of CdSe QDs, Fig. 2c. The sharp increase in the concentration of CdSe QDs was mainly reflected in the tenth minute after UV irradiation. The fluorescent intensity depends on the concentration of the fluorophore; however, the lifetime of the fluorophore is independent of concentration.

In-capillary formation of CdSe QDs

Finally, the work was focused on the direct synthesis of CdSe QDs in nanoliter scale (in capillary). For these purposes, the standard CE instrument was used with a little modification as shown in the schematic drawing, Fig. 3a. For the synthesis of CdSe QDs, the UV LED was used. It was connected to the capillary by optical fiber, Fig. 3a – *a*. The capillary pathway was partially modified by its local direction out of the cooling tube, Fig. 3a – *b*. An optical fiber was focused into the exposed capillary, where a special window was made (Fig. 3a – *c*). The QDs precursors were hydrodynamically injected (5 psi for 5 s) into the capillary and the procedure was stopped for 0, 5, 10, 15, 20, 25 and 30 min (to ensure the formation of QDs in special window, Fig. 3a – *d*). Subsequently, separation voltage of 30 kV was applied and formed CdSe QDs (Fig. 3a - *e*) migrated to the detection window, Fig. 3a – *f*.

First, CdSe QDs prepared by UV synthesis in a milliliter scale (using the transilluminator) were analyzed by CE-LIF. As shown in the electropherograms in Fig. 3b, Bright fluorescent signals were observed and their intensity was increasing with increasing time of UV illumination. Moreover, this effective separation technique showed that the solution was a mixture of different nanoparticles (various particle sizes) formed during the illumination process. For demonstration, four most distinct signals were labelled (QDs1 – QDs 4). There were probably more components present in the mixture; however, it was not the aim of the study to separate the mixture completely. The dependence of the peak heights on the illumination time is summarized in Fig. 3c and it is shown that the peak with migration time of 7 min is exhibiting the highest fluorescence intensity, reaching even fluorescence intensity over the detector range. However, it is shown that with increasing the illumination time, also other fluorescent signal started to be observed, which, as it is believed, belong to the QDs with higher particle sizes or to the QD aggregates.

Finally, the in-capillary formation of QDs by UV light was tested, which can be applied in microfluidic devices to significantly decrease the amount of chemicals used and meeting the requirements of green chemistry/analysis.

As describe above, the optical fiber guiding the UV light from the UV LED was focused into the special window made at the injection end of the capillary (14 cm from the start).

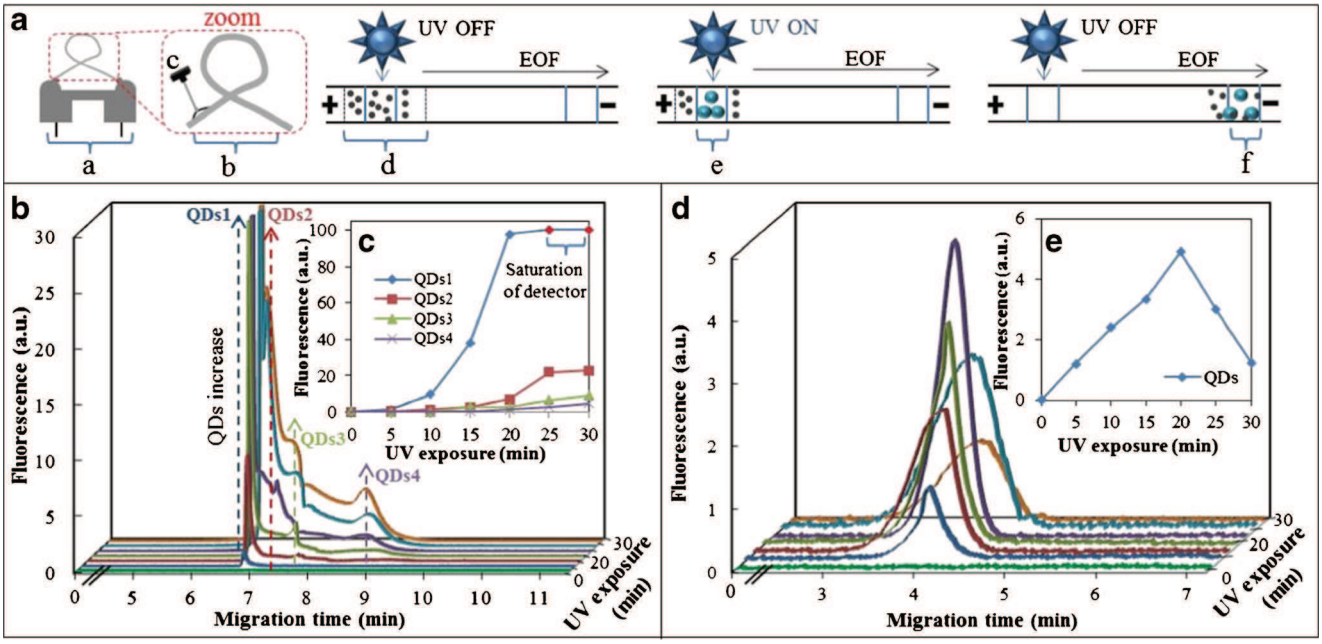

Fig. 3 **a** Scheme of modified capillary pathway and special window position, a) conventional capillary cartridge with the capillary inside the cooling tube, b) capillary directed out of the cooling tube, c) UV LED (λ_{em} = 250 nm) connected to the optical fiber focusing the light into the capillary, d) zone of QD precursors injected into the capillary UV LED off, e) formation of QDs using UV LED on, f) CE separation of formed QDs and LED-IF detection by 380 nm LED excitation. **b** Electropherograms of CdSe QDs formed by UV illumination in transilluminator (0–30 min) **c** Dependence of UV light illumination time on peak heights of four main fluorescent signals (QDs1– QDs4). **d** Electropherograms of CdSe QDs formed after in-capillary UV LED illumination (0–30 min). **e** Dependence of UV light illumination time on peak heights – in-capillary QD formation

Subsequently, the solution of precursors was hydrodynamically injected into the capillary and illuminated for 5, 10, 15 or 20 min. After the illumination time, the CE separation started and the formed QDs were conventionally detected. The electropherograms are shown in Fig. 3d. The fluorescent signals were observed with maximum in migration time of 4.3 min. The lower migration time compared to Fig. 3b is given by the shortened effective capillary length. In addition, the fluorescence intensity was lower due to the lower optical power of the UV LED. However, the signal-to-noise ratio was satisfactory. It has to be noted that the maximum fluorescence intensity in this arrangement was reached after 20 min of illumination and with increasing time, the intensity decreased significantly. On the other hand, only one signal is observed suggesting lower polydispersity of the QDs prepared by this technique.

In general, it can be stated that in situ (or flow through) synthesis of QDs by elevated temperature [42, 43] is convenient and effective; however for some, mostly biological, applications, the excessive heating may interfere the process in the fluidic device (e.g. protein denaturation, cell damage etc.). For these purposes, the in-line formation of QDs for automated, low-volume synthesis by UV light irradiation is advantageous. The UV light may be focused in the extremely low volume and the powerful lasers may be used, which increases the effectivity of the proposed method. Afterwards, the in-capillary interactions may take place without the need of interaction by the operator.

Quantification of CdSe QDs formed by UV light

Using three different optical arrangements, QDs formed by UV light illumination in three different volumes (3 mL, 15 μL, 4 nL) were observed and the amount of QDs formed was investigated. To quantify this amount, a sufficient amount of QDs powder was prepared by UV illumination (irradiation of the 21 mL of precursor's solution (CdSe)). The solution was filtered through Amicons Ultra 0.5 mL 3 K Centrifugal Filters and dried overnight at 50 °C. The powder was resuspended in 5 mM borate buffer pH 9 to create the calibration curve.

The concentration of QDs formed during large-volume (3 mL), middle-volume (15 μL) and low-volume (4 nL) synthesis was determined as 88 $\mu g.mL^{-1}$, 31.6 $\mu g \cdot mL^{-1}$ and 64.5 $\mu g \cdot mL^{-1}$, respectively. The higher concentration of QDs formed in capillary format (4 nL) was caused by higher radiation power because maximum of the light from the UV LED was focused into the capillary volume by optical fiber while in case of 15 μL drop, the light was distributed in a much larger area.

The absolute amount in the given volume (Fig. 4) calculated for each method demonstrates the possibility of the capillary-based methods to monitor the formation of very low amounts of QDs, which can be further transferred by electric field.

Conclusion

Even though the quantum dots will not probably replace conventional fluorescent labels based on organic fluorophores, they have several significant benefits (e.g. tuneability of optical properties and simplicity of synthesis compared to organic dyes) and therefore they will find their place in the family of fluorescent tracers.

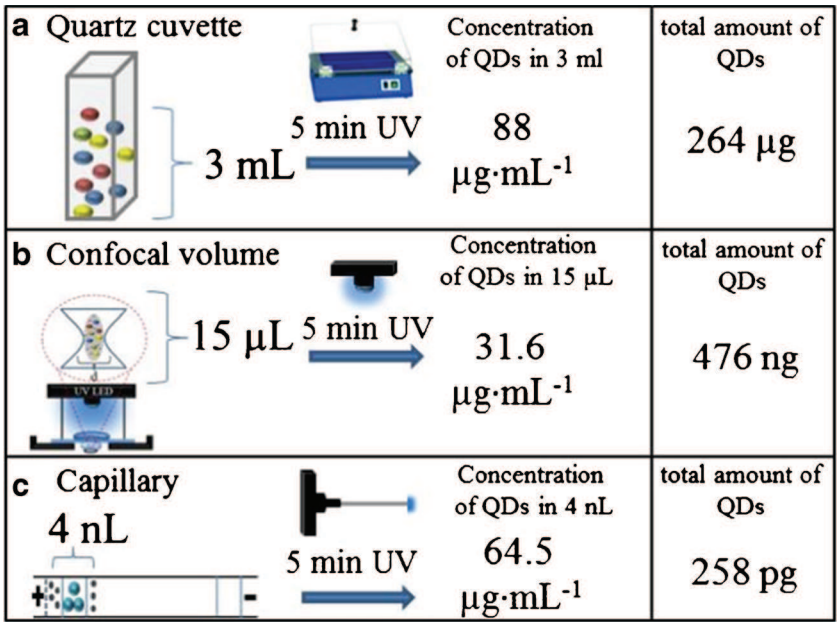

Fig. 4 Schematic representation of UV synthesis of CdSe QDs by **a** large-volume (3 mL) **b** middle-volume (15 μL), **c** low-volume (4 nL)

Based on a systematic study formation of QDs by UV light illumination from the most commonly used precursors, CdSe nanoparticles exhibited the best optical properties such as QY (13.4%). The formation of QDs was observed in milliliter (quartz cuvette), microliter (solution drop), and nanoliter (in-capillary) scale by spectrophotometry, fluorescence correlation spectroscopy and capillary electrophoresis with LED-IF detection, respectively.

The biggest advantage of formation of QDs by UV light is in the possibility of synthesis of QDs in very small volumes (nanoliters), which meets not only the requirements on green chemistry (low consumption of chemicals) but also can be easily integrated into the lab-on-chip, micro-total-analysis microfluidic devices or other methods.

For some applications, the QY of the UV-synthesized QDs may be insufficient. However, the flow-through method of synthesis requiring extremely low amount of precursors in combination with sensitive detection (i.e. laser-induced fluorescence or electrochemical detection) may be beneficial for certain analytical purposes.

Acknowledgements Financial support was provided by Grant agency of Czech Republic (GACR 16-23647Y) and project CEITEC 2020 (LQ1601) with financial support from the Ministry of Education, Youth and Sports of the Czech Republic under the National Sustainability Programme II.

Compliance with ethical standards The author(s) declare that they have no competing interests.

References

1. Kilina SV, Tamukong PK, Kilin DS (2016) Surface chemistry of semiconducting quantum dots: theoretical perspectives. Accounts Chem Res 49:2127–2135
2. Singh G, Fisch M, Kumar S (2016) Emissivity and electrooptical properties of semiconducting quantum dots/rods and liquid crystal composites: a review. Rep Prog Phys 79
3. Zhou J, Yang Y, Zhang CY (2015) Toward biocompatible semiconductor quantum dots: from biosynthesis and Bioconjugation to biomedical application. Chem Rev 115:11669–11717
4. Lim SY, Shen W, Gao ZQ (2015) Carbon quantum dots and their applications. Chem Soc Rev 44:362–381
5. Alivisatos AP (1996) Semiconductor clusters, nanocrystals, and quantum dots. Science 271:933–937
6. Reimann SM, Manninen M (2002) Electronic structure of quantum dots. Rev Mod Phys 74:1283–1342
7. Lin P, Chen JW, Chang LW, Wu JP, Redding L, Chang H, Yeh TK, Yang CS, Tsai MH, Wang HJ, Kuo YC, Yang RSH (2008) Computational and ultrastructural toxicology of a nanoparticle, quantum dot 705, in mice. Environ Sci Technol 42:6264–6270
8. Tan L, Rang CC, Xu SY, Tang YW (2013) Selective room temperature phosphorescence sensing of target protein using Mn-doped ZnS QDs-embedded molecularly imprinted polymer. Biosens Bioelectron 48:216–223
9. LeCroy GE, Yang ST, Yang F, Liu YM, Fernando KAS, Bunker CE, Hu Y, Luo PG, Sun YP (2016) Functionalized carbon nanoparticles: syntheses and applications in optical bioimaging and energy conversion. Coord Chem Rev 320:66–81
10. Galian RE, de la Guardia M (2009) The use of quantum dots in organic chemistry. Trac-Trends Anal Chem 28:279–291
11. Wang YL, Xia YN (2004) Bottom-up and top-down approaches to the synthesis of monodispersed spherical colloids of low melting-point metals. Nano Lett 4:2047–2050
12. Ghosh B, Shirahata N (2014) Colloidal silicon quantum dots: synthesis and luminescence tuning from the near-UV to the near-IR range. Sci Technol Adv Mater 15(1):014207
13. Erdem T, Soran-Erdem Z, Hernandez-Martinez PL, Sharma VK, Akcali H, Akcali I, Gaponik N, Eychmuller A, Demir HV (2015) Sweet plasmonics: sucrose macrocrystals of metal nanoparticles. Nano Res 8:860–869
14. Koch CC (2003) Top-down synthesis of nanostructured materials: mechanical and thermal processing methods. Rev Adv Mater Sci 5:91–99
15. Amendola V, Meneghetti M, Granozzi G, Agnoli S, Polizzi S, Riello P, Boscaini A, Anselmi C, Fracasso G, Colombatti M, Innocenti C, Gatteschi D, Sangregorio C (2011) Top-down synthesis of multifunctional iron oxide nanoparticles for macrophage labelling and manipulation. J Mater Chem 21:3803–3813
16. Bertino MF, Gadipalli RR, Martin LA, Heckman B, Leventis N, Guha S, Katsoudas J, Divan R, Mancini DC (2008) 236th National Meeting of the American-Chemical-Society, Philadelphia, PA, Aug 17-21, 2008. Published in: Abstracts of papers of the American Chemical Society, Vol. 236
17. Wu JZ, Ho PC (2006) Evaluation of the in vitro activity and in vivo bioavailability of realgar nanoparticles prepared by cryo-grinding. Eur J Pharm Sci 29:35–44
18. Zeng HB, Cai WP, Liu PS, Xu XX, Zhou HJ, Klingshirn C, Kalt H (2008) ZnO-based hollow nanoparticles by selective etching: elimination and reconstruction of metal-semiconductor interface, improvement of blue emission and photocatalysis. ACS Nano 2:1661–1670
19. Murray CB, Norris DJ, Bawendi MG (1993) Synthesis and characterization of nearly monodisperse CdA (E = S, Se, Te) semiconductor nanocrystallites. J Am Chem Soc 115:8706–8715
20. Peng ZA, Peng XG (2001) Formation of high-quality CdTe, CdSe, and CdS nanocrystals using CdO as precursor. J Am Chem Soc 123:183–184
21. Rogach AL, Katsikas L, Kornowski A, Su DS, Eychmuller A, Weller H (1996) Synthesis and characterization of thiol-stabilized CdTe nanocrystals. Ber Bunsen-Ges Phys Chem Chem Phys 100: 1772–1778
22. Talapin DV, Rogach AL, Shevchenko EV, Kornowski A, Haase M, Weller H (2002) Dynamic distribution of growth rates within the ensembles of colloidal II-VI and III-V semiconductor nanocrystals as a factor governing their photoluminescence efficiency. J Am Chem Soc 124:5782–5790
23. Zhu YL, Li CS, Xu Y, Wang DF (2014) Ultrasonic-assisted synthesis of aqueous CdTe/CdS QDs in salt water bath heating. J Alloy Compd 608:141–147
24. Lin YW, Hsieh MM, Liu CP, Chang HT (2005) Photoassisted synthesis of CdSe and core-shell CdSe/CdS quantum dots. Langmuir 21:728–734
25. Li XQ, Xu HZ, Chen ZS, Chen GF (2011) Biosynthesis of nanoparticles by microorganisms and their applications. J Nanomater. doi:10.1155/2011/270974
26. Kominkova M, Michalek P, Moulick A, Nemcova B, Zitka O, Kopel P, Beklova M, Adam V, Kizek R (2014) Biosynthesis of quantum dots (CdTe) and its effect on Eisenia fetida and *Escherichia coli*. Chromatographia 77:1441–1449
27. Borovaya MN, Naumenko AP, Matvieieva NA, Blume YB, Yemets AI (2014) Biosynthesis of luminescent CdS quantum dots using plant hairy root culture. Nanoscale Res Lett 9. doi:10.1186/1556-276X-9-686
28. Ahmad A, Mukherjee P, Senapati S, Mandal D, Khan MI, Kumar R, Sastry M (2003) Extracellular biosynthesis of silver

nanoparticles using the fungus Fusarium oxysporum. Colloid Surf B-Biointerfaces 28:313–318
29. Sastry M, Ahmad A, Khan MI, Kumar R (2003) Biosynthesis of metal nanoparticles using fungi and actinomycete. Curr Sci 85:162–170
30. Kandiel TA, Dillert R, Feldhoff A, Bahnemann DW (2010) Direct synthesis of Photocatalytically active rutile TiO2 nanorods partly decorated with Anatase nanoparticles. J Phys Chem C 114:4909–4915
31. Liu XJ, Pan LK, Zhao QF, Lv T, Zhu G, Chen TQ, Lu T, Sun Z, Sun CQ (2012) UV-assisted photocatalytic synthesis of ZnO-reduced graphene oxide composites with enhanced photocatalytic activity in reduction of Cr(VI). Chem Eng J 183:238–243
32. Adegboyega NF, Sharma VK, Cizmas L, Sayes CM (2016) UV light induces Ag nanoparticle formation: roles of natural organic matter, iron, and oxygen. Environ Chem Lett 14:353–357
33. Lan GY, Lin YW, Huang YF, Chang HT (2007) Photo-assisted synthesis of highly fluorescent ZnSe(S) quantum dots in aqueous solution. J Mater Chem 17:2661–2666
34. Uematsu T, Kitajima H, Kohma T, Torimoto T, Tachibana Y, Kuwabata S (2009) Tuning of the fluorescence wavelength of CdTe quantum dots with 2 nm resolution by size-selective photoetching. Nanotechnology 20(21):215302
35. Shang YZ, Min CZ, Hu J, Wang TM, Liu HL, Hu Y (2013) Synthesis of gold nanoparticles by reduction of HAuCl4 under UV irradiation. Solid State Sci 15:17–23
36. Kao M, Erasmus RM, Moloto N, Coville NJ, Mhlanga SD (2015) UV-assisted synthesis of indium nitride nano and microstructures. J Mater Chem A 3:5962–5970
37. Krizkova S, Dostalova S, Michalek P, Nejdl L, Kominkova M, Milosavljevic V, Moulick A, Vaculovicova M, Kopel P, Adam V, Kizek R (2015) SDS-PAGE as a tool for hydrodynamic diameter-dependent separation of quantum dots. Chromatographia 78:785–793
38. Samanta A, Deng ZT, Liu Y (2012) Aqueous synthesis of glutathione-capped CdTe/CdS/ZnS and CdTe/CdSe/ZnS Core/Shell/Shell nanocrystal Heterostructures. Langmuir 28:8205–8215
39. Chan WCW, Maxwell DJ, Gao XH, Bailey RE, Han MY, Nie SM (2002) Luminescent quantum dots for multiplexed biological detection and imaging. Curr Opin Biotechnol 13:40–46
40. Carrillo-Carrion C, Cardenas S, Simonet BM, Valcarcel M (2009) Quantum dots luminescence enhancement due to illumination with UV/Vis light. Chem Commun 45(35):5214–5226
41. Kirby BJ, Hasselbrink EF (2004) Zeta potential of microfluidic substrates: 1. Theory, experimental techniques, and effects on separations. Electrophoresis 25:187–202
42. Chakrabarty A, Marre S, Landis RF, Rotello VM, Maitra U, Del Guerzo A, Aymonier C (2015) Continuous synthesis of high quality CdSe quantum dots in supercritical fluids. J Mater Chem C 3:7561–7566
43. Nightingale AM, Krishnadasan SH, Berhanu D, Niu X, Drury C, McIntyre R, Valsami-Jones E, deMello JC (2011) A stable droplet reactor for high temperature nanocrystal synthesis. Lab Chip 11:1221–1227

FEMS Microbiology Letters, 363, 2016, fnw094

doi: 10.1093/femsle/fnw094
Advance Access Publication Date: 15 April 2016
Research Letter

RESEARCH LETTER – Physiology & Biochemistry

Accumulation of PHA granules in *Cupriavidus necator* as seen by confocal fluorescence microscopy

Filip Mravec[1,†], Stanislav Obruca[1,*,†], Vladislav Krzyzanek[2], Petr Sedlacek[1], Kamila Hrubanova[2], Ota Samek[2], Dan Kucera[1], Pavla Benesova[1] and Jana Nebesarova[3]

[1]Materials Research Centre, Brno University of Technology, Purkynova 118, 612 00 Brno, Czech Republic, [2]Institute of Scientific Instruments, The Czech Academy of Sciences, v.v.i., Kralovopolska 147, 612 64 Brno, Czech Republic and [3]Biology Centre, The Czech Academy of Sciences, v.v.i., Branisovska 31, 370 05 Ceske Budejovice, Czech Republic

*Corresponding author: Materials Research Centre, Brno University of Technology, Purkynova 118, 612 00 Brno, Czech Republic. Tel: +420-541-149-486; Fax: +420-541-211-697; E-mail: Stana.O@seznam.cz
†Authors contributed equally.
One sentence summary: Cells of *Cupriavidus necator* increase their length during PHA accumulation in order to maintain an intracellular PHA granule volume content of no more than 40%.
Editor: Alexander Steinbüchel

ABSTRACT

Many bacteria are capable of accumulating intracellular granules of polyhydroxyalkanoates (PHA). In this work, we developed confocal microscopy analysis of bacterial cells to study changes in the diameters of cells as well as PHA granules during growth and PHA accumulation in the bacterium *Cupriavidus necator* H16 (formerly *Ralstonia eutropha*). The cell envelope was stained by DiD® fluorescent probe and PHA granules by Nile Red. Signals from both probes were separated based on their spectral and fluorescence life-time properties. During growth and PHA accumulation, bacterial cells increased their length but the width of the cells remained constant. The volume fraction of PHA granules in cells increased during PHA accumulation, nevertheless, its value did not exceed 40 vol. % regardless of the PHA weight content. It seems that bacterial cultures lengthen the cells in order to control the PHA volume portion. However, since similar changes in cell length were also observed in a PHA non-accumulating mutant, it seems that there is no direct control mechanism, which regulates the prolongation of the cells with respect to PHA granules volume. It is more likely that PHA biosynthesis and the length of cells are influenced by the same external stimuli such as nutrient limitation.

Keywords: Polyhydroxyalkanoates; intracellular granules; confocal fluorescence microscopy; bacterial cell diameters

INTRODUCTION

Polyhydroxyalkanoates (PHA) are linear polyesters accumulated by a wide variety of taxonomically different groups of microorganisms under nutrient-limited conditions when a carbon source is readily available. It is generally proposed that PHA serve primarily as a carbon- and energy-storage material; however, there is also evidence that the capacity to accumulate PHAs enhances the resistance of bacterial cells to various stress conditions (Kadouri, Jurkevitch and Okon 2005; Obruca *et al.* 2016).

PHA are accumulated in bacterial cytoplasm in the form of inclusions called granules in varying numbers and sizes depending on culture conditions (Volova *et al.* 2013). PHA granules can represent a large fraction of cellular dry matter—under

Received: 4 March 2016; **Accepted:** 9 April 2016

extreme conditions, up to 90% (Obruca *et al.* 2014a). The PHA granules harbor a considerable number of proteins on their polymer surface, suggesting that they represent supramolecular complexes with specific functions rather than only simple sacks rich in carbon and energy. Therefore, the designation 'carbonosome' was suggested to indicate the multifunctionality and complex role of PHA granules (Jendrossek 2009). A detailed description of PHA granule-associated proteins has recently been provided in an excellent review by Jendrossek and Pfeiffer (2014).

Generally, the most studied bacterium in the context of PHA accumulation, granule formation and mobilization is the Gram-negative bacterium *Cupriavidus necator* H16 (formerly *Ralstonia eutropha*, *Wautersia eutropha* and *Alcaligenes eutrophus*), which represents the model organism for PHA metabolism (Reinecke and Steinbuchel 2009).

To our knowledge, only little attention has been paid to PHA granules with respect to bacterial cell morphology and even less to the effects of their presence in bacterial cells on the properties of such cells. For instance, such fundamental information as the volume fraction of PHA granules in cells is missing. The morphology of PHA accumulating cells as well as the numbers, sizes and localizations of PHA granules in bacterial cells is usually observed by Transmission Electron Microscopy (TEM) (Tian, Sinskey and Stubbe 2005; Wahl *et al.* 2012; Rodríguez-Contreras *et al.* 2013). In order to overcome the problems associated with TEM analysis and to shed light on the basic features of the morphology of PHA accumulating bacterial cells, we developed the analysis of bacterial cells and PHA granules in their cytoplasm by means of dual-staining time-resolved confocal fluorescence microscopy. This analytical protocol was used to study cells of *C. necator* during their growth in a medium supporting PHA accumulation.

MATERIALS AND METHODS

Materials and microorganisms

The fluorescent probes Nile Red and DiD (1,1′-Dioctadecyl-3,3,3′,3′-Tetramethylindodicarbocyanine, 4-Chlorobenzenesulfonate Salt) were purchased from Sigma Aldrich (Munich, Germany) and Molecular Probes (Thermo Fisher Scientific, Waltham, MA USA), respectively. *Cupriavidus necator* H16 (CCM 3726) was obtained from the Czech Collection of Microorganisms, Brno, Czech Republic. The PHA non-producing strain *C. necator* PHB-4 (DSM-541) was purchased from the Leibnitz Institute DSMZ-German Collection of Microorganism and Cell Cultures, Braunschweig, Germany.

Cultivations and determination of intracellular PHA

Erlenmeyer flasks (volume 250 mL) containing 100 mL of Mineral Salt medium described elsewhere (Obruca *et al.* 2014a) with fructose (20 g/l) as the sole carbon source were inoculated by 5 mL of the overnight culture of a particular strain of *C. necator* grown in Nutrient Broth medium. Subsequently, samples were taken in regular intervals during 80 h of cultivation, and the cells were harvested (centrifugation, 8000×g, 5 min) and subjected to fluorescent microscopy analysis. In the same cell samples, the content of biomass and PHA were determined as described previously (Obruca *et al.* 2014b).

Fluorescent microscopy analysis of bacterial cells

To determine the relative content and geometrical parameters of granules and cells, fluorescence lifetime imaging microscopy was employed. Cells were stained with two different fluorescence probes—amphiphilic DiD and hydrophobic Nile Red. DiD serves as a membrane probe since its dominant fraction can be found in the outer part of the bacterial cells. Nile red has a low quantum yield in an aqueous microenvironment and high quantum yield in a non-polar environment. Different fractions of Nile red can be found localized in granules (the dominant fraction), inside membranes, or on proteins.

The determination of cell dimensions and particular granules requires the gathering of all necessary information from one scan. This approach suppresses the possibility of photobleaching or misalignment. To resolve these two probes, Pulsed-Interleaved Excitation with spectral and temporal resolutions of detection was used. As a result, we obtained two different images from one scan, an NR-based granules image and a DiD-based whole cell image. For detailed information on the method, see Supporting Information.

Prior to staining, bacterial cells were washed twice by PBS buffer, permeabilized by ice-cold 20% ethanol for 10 min and washed by PBS buffer again. The staining of 1 mL of cell suspension (cell density $\sim 10^8$ cells per mL) was performed by the addition of 1 μl of Nile Red (0.01 mg/ml) in DMSO and 1 μL of DiD (0.01 mg/ml) in acetone. The cells were left to stain in the dark for 30 min at laboratory temperature. Afterwards, about 10 μL of the bacterial suspension was placed on the cleaned and dust-free surface of a coverslip (20 × 20 μm, 150 μm thick) and then superimposed by 200 μL of 2% agarose aqueous solution with temperature of about 45°C.

From each sample, at least 20 different cells were selected for precise scanning. The scanning method was designed with respect to random orientation and the elongate shape of bacterial cells. For details of the procedure, see Supporting Information.

Calculation of cell and PHA granule volumes

For every cell from the precise scan, two different images were obtained. From the red channel, information about the overall dimensions of the cell was extracted from the intensity profile. The total volume of the cell was calculated with the cell shape approximated to a cylinder. To determine the volume of a cylinder, it is necessary to know its diameter and length. The shape of *C. necator* is slightly different from an ideal cylinder; therefore, a correction was necessary. The width, i.e. the cylindrical diameter, of the cells was taken as the average of at least 10 width measurements at different locations along the cell. The length was taken as the average of three measurements. PHA granules were approximated to spheres and analyzed individually. The volume of each granule was determined using the average of three diameter measurements taken from different sides.

TEM analysis of bacterial cells

Bacterial cells must be prepared to a thickness which allows electrons to transmit through the sample. The specimen preparation protocol began with the addition of a cryoprotectant (20% BSA (Fluka)) to cell suspensions. Then, the sample (~0, 2 μl) placed in special carrier was frozen in a high pressure freezer (Leica EM Pact) and transferred under liquid nitrogen into a freeze substitution unit (Leica EM AFS). Two percent osmium tetroxide in acetone was used as a substitution solution. The substitution protocol began at a temperature of –90°C and finished at 4°C after 160 h of slow temperature increase. At room temperature, the sample was infiltrated and embedded in Polybed (SPI, acetone:resin ratios of 2:1, 1:1 and 1:2, for 1 h

of each and overnight in pure embedding media under vacuum using a desiccator). Polymerization was conducted for 48 h at 62°C. Ultrathin sections were cut on an Ultracut UCT ultramicrotome (Leica) using a diamond knife (Diatome) with a cutting angle of 45°. Sections were transferred on 300Mesh copper grids and stained with uranyl acetate and lead citrate solutions.

The ultrastructure of PHA accumulating cells was examined using a JEOL 1010 transmission electron microscope operating at an accelerating voltage of 80 kV. Images were recorded digitally using a Megaview III CCD camera (Olympus).

Image analysis of TEM microphotographs

From the TEM micrographs, the average volume fractions of PHA granules in the cells were determined. For this purpose, image processing and analysis were performed using the HarFA software application developed at the Faculty of Chemistry, Brno University of Technology. Using this software, the TEM micrographs (10 micrographs in total) were subjected to a black/white thresholding process followed by two-dimensional wavelet analysis. According to this analysis, for each individual micrograph, appropriate threshold levels were chosen in order to separately visualize PHA granules and the remaining intracellular space. Respective area fractions of PHA granules in the cells were then determined by simple B/W pixel counting (for more details on image analysis, see Supporting Information). Estimation of the respective volume fractions was based on the stereology formula stating that, in systems with random morphology, the volume fraction and the area fraction in a random section through the system are approximately equal (Slouf *et al.* 2015).

RESULTS AND DISCUSSION

The morphology and diameters of bacterial cells are crucial factors influencing the fate of the cells, because changes in cell volume or surface area can have profound effects on metabolic flux, biosynthetic capacity and nutrient exchange (Young 2007; Marsahll *et al.* 2012). Therefore, bacteria precisely control their sizes and shapes in order to import nutrients most efficiently, meet the requirements imposed by cell division, attach themselves to external surfaces, take advantage of passive dispersal mechanisms, move purposefully to pursue nutrients or avoid inhibitors and avoid predation by other organisms (Marsahll *et al.* 2012). Since little is known about the impact of PHA accumulation on the diameters and morphology of bacterial cells, we decided to investigate this phenomenon in *C. necator*.

At first, we performed TEM analysis of the PHA accumulating bacterial culture *C. necator* H16 (the weight content of PHA in the cell dry weight was 78%) and its mutant strain *C. necator* PHB^{-4}, which is not capable of PHA accumulation (Raberg *et al.* 2014). The results of TEM analysis are shown in Fig. 1a and b. Generally, TEM provides impressive pictures of PHA granules in bacterial cells; nevertheless, the method lacks the potential to provide morphological details on the level of single cells. The preparation of samples requires the very thin slicing (e.g. 70 nm) of bacterial suspensions in which the bacterial cells are randomly oriented and the overall picture can be influenced by various spherical effects (Fig. 1c). In fact, the reliability of the results of TEM depends on the positions of cells at the point where the thin section was performed. Only in the case of bacterial cells and granules which were cut exactly through the middle can determine diameters accurately. Hence, without statistical analysis, microphotographs acquired by TEM are not ideal for estimation of the sizes and shapes of bacterial cells and PHA granules. Further, during sample preparation for TEM analysis, the infiltration of the specimen by epoxy resin, embedding and polymerization can lead to the shrinkage of cells, which may influence the size of PHA granules (Mollenhauer 1993). In addition, the cutting process is connected with section compression, which is directly proportional to the value of the cutting angle (Studer and Gnaegi 2000). This phenomenon affects the shape of PHA granules (Fig. 1), causing them to be oval rather than circular.

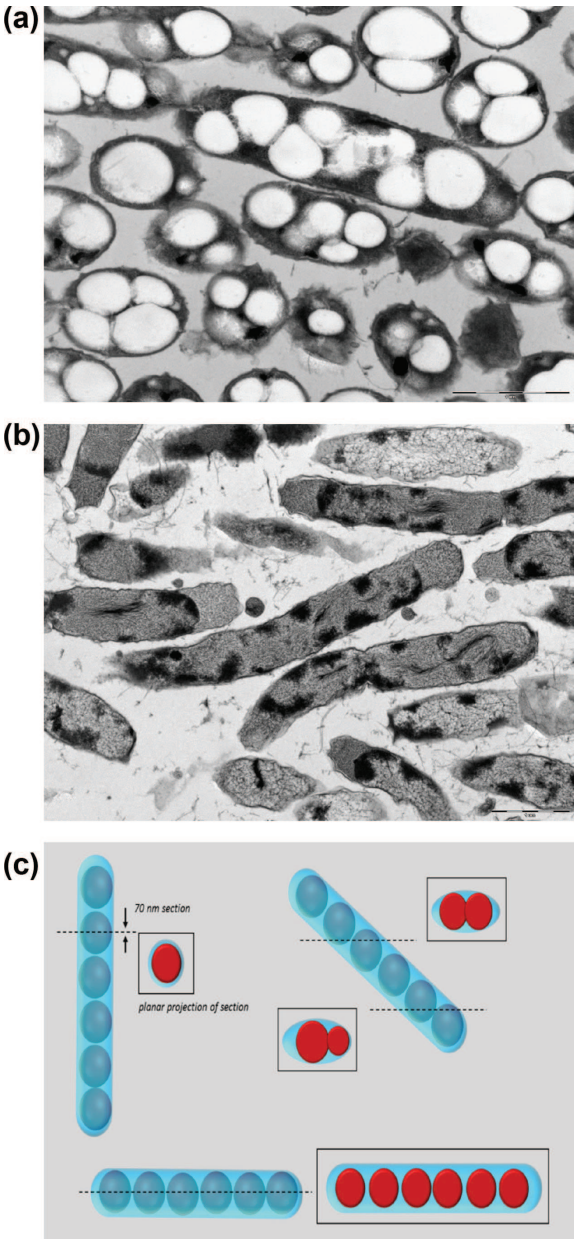

Figure 1. Cells of (**a**) PHA accumulating *Cupriavidus necator* H16 and (**b**) PHA non-accumulating *C. necator* PHB^{-4} observed by TEM and (**c**) the effect of the preparation of thin-slices for TEM on observed morphologies and diameters of PHA accumulating cells and granules.

On the other hand, TEM can be used to estimate the volume content of PHA granules in bacterial cells, since we can perform the image analysis of TEM microphotographs described above. Hence, we calculated the volume content of PHA granules in cells of *C. necator* H16 to be 35 ± 3%.

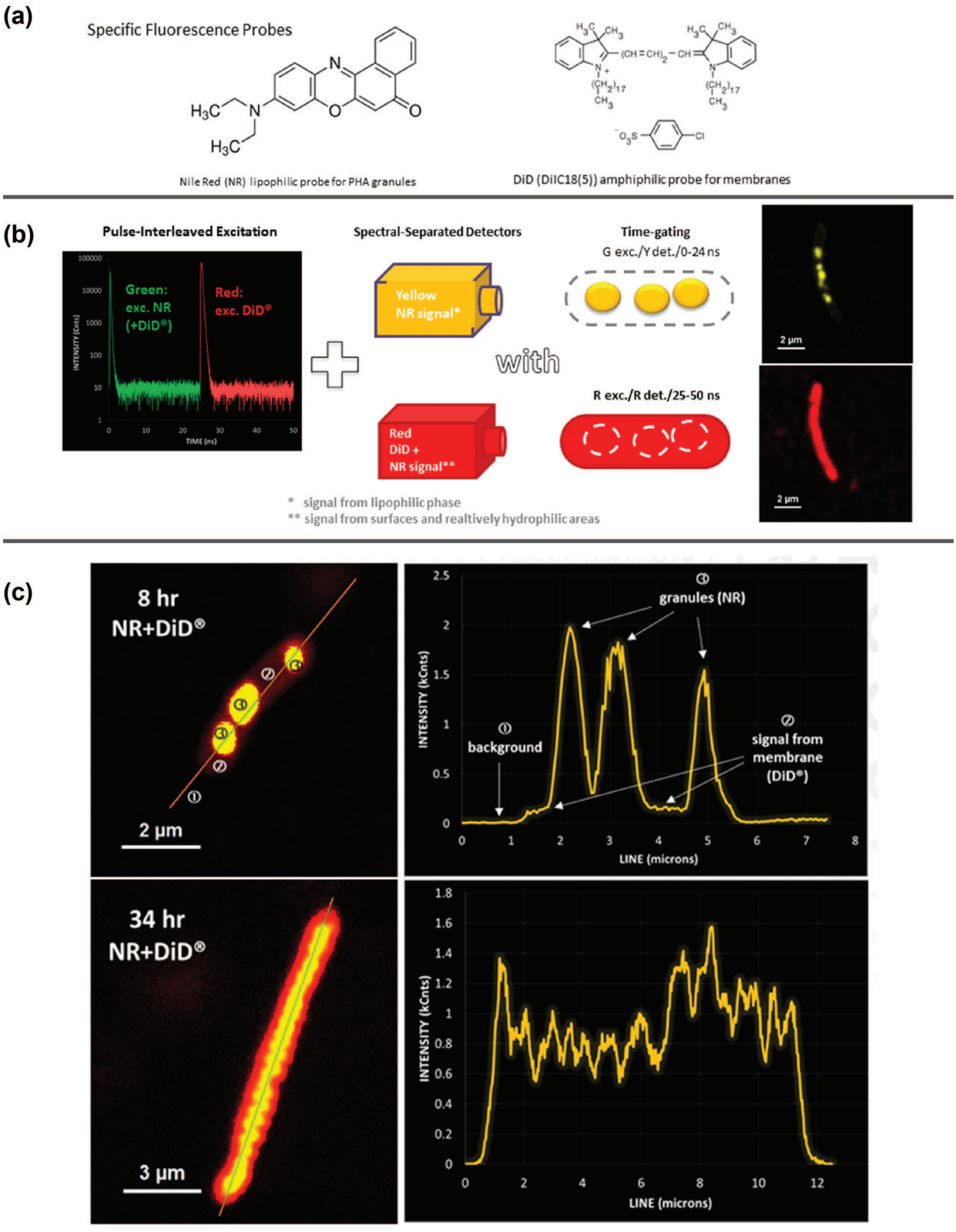

Figure 2. (a) Chemical formulas of individual fluorescent probes used in dual-staining confocal fluorescence microscopy analysis, (b) principle of separation of fluorescence signals from both probes (c) and the basic principle of data analysis.

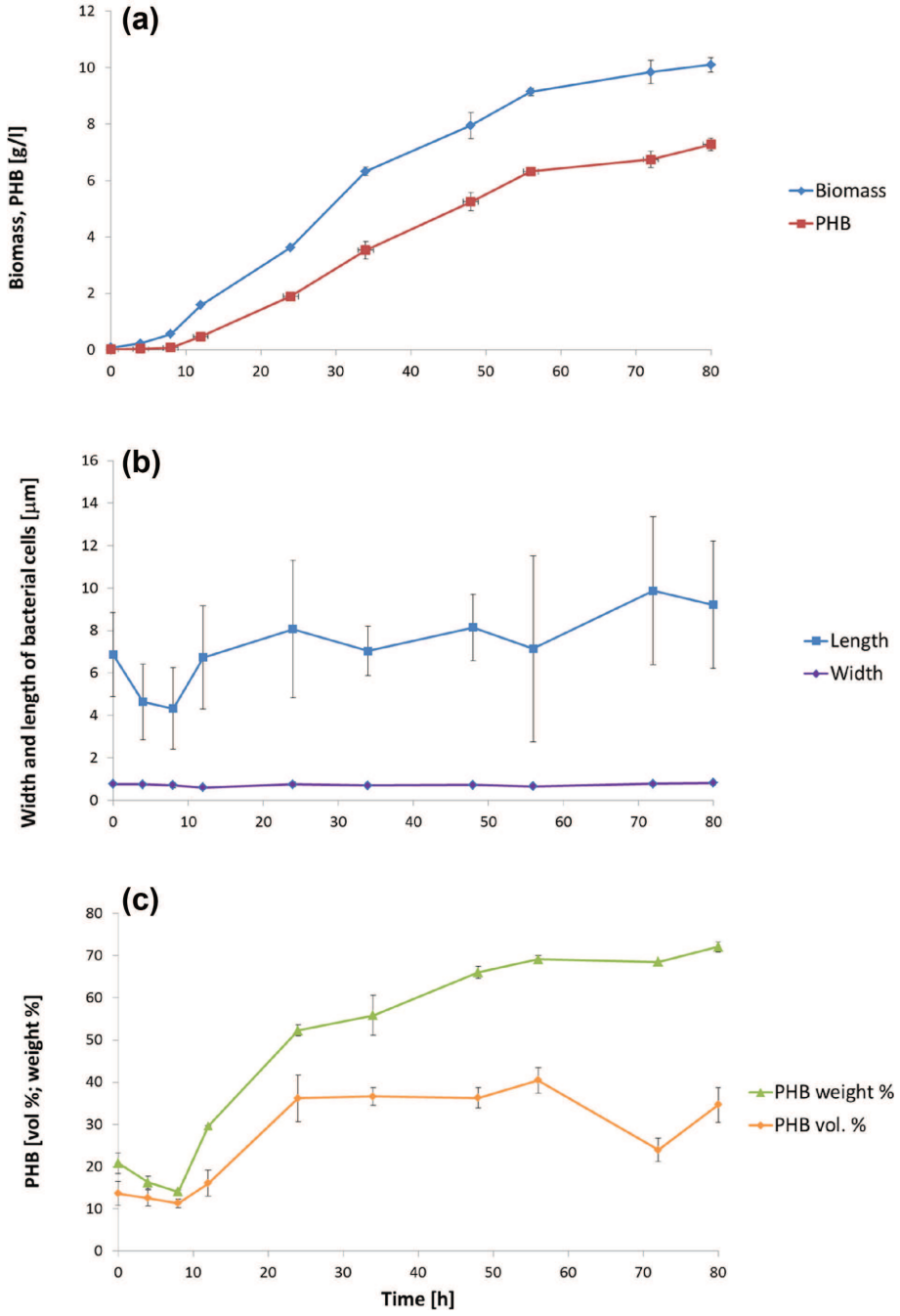

Figure 3. Development of following parameters during cultivation of *Cupriavidus necator* H16 in mineral medium with fructose as the sole carbon source (**a**) biomass and PHA concentration (**b**) length and width of bacterial cells (**c**) volume content of PHA granules in cells and weight content of PHA per cell dry weight.

To overcome the above-mentioned problems with TEM analysis, we developed an advanced confocal fluorescence microscopy technique (the principles of staining and data evaluation are described in the Materials and Methods and also shown in Fig. 2), which was used to study the morphology of cells and PHA granules during the growth of *C. necator* H16. In general, this technique allows the analysis of bacterial cultures to be performed at the single-cell level, which means that each parameter can be estimated individually for each cell, which, in turn, allows the degree of cellular heterogeneity to be described.

The time courses of the biomass and PHA concentrations during cultivation are shown in Fig 3a; the weight content of PHA in the cell dry weight (CDW) is shown in Fig. 3c. During the lag-phase of the growth curve (the initial eight hours of cultivation), the bacterial culture did not grow and, further, we observed a decrease in PHA content from 20.8% of CDW to 14.1% of CDW, which indicates that the cells slowly utilized their intracellular storage of PHA. It seems that the polymer might represent a carbon substrate which the bacteria use to cover energy demands during adaptation from one medium (the inoculum was prepared in complex NB medium) to another (a fructose and mineral medium).

Further, the data describing cell diameters during growth are shown in Fig. 3b and the volume content of PHA granules in cells

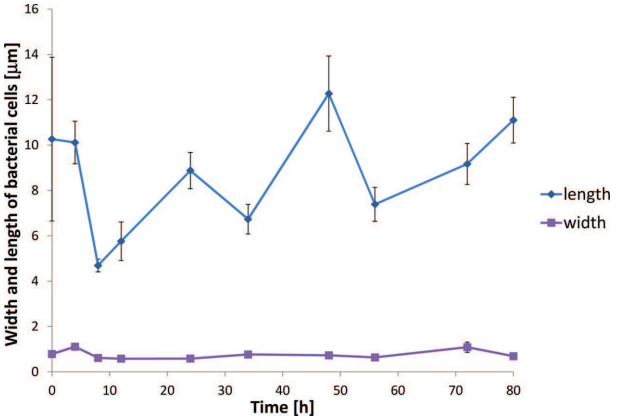

Figure 4. Length and width of the cells of PHA non-producing strain *Cupriavidus necator* PHB^{-4} during growth in mineral medium with fructose as the sole carbon source.

is presented in Fig. 3c. The utilization of PHA during the initial eight hours of cultivation was accompanied not only by a reduction in the weight content of PHA in biomass, but also by a reduction in the volume content of PHA granules in cells as well as a decrease in the length of the cells. In contrast, the width of the cells appeared to be independent of the stage of growth since it remained constant (about 0.7 μm) during the whole period of cultivation.

After the lag-phase, the bacterial culture started to grow and accumulate PHA, the weight content of PHA in bacterial cells reaching up to 75% of the CDW at the end of cultivation. Furthermore, despite the fact that the distributions of cell length in the samples were rather wide, after the lag-phase we also observed a considerable increase in cell length with increasing cultivation time.

The volume content of PHA granules in cell cytoplasm reached a maximum close to 40% (after 24 h of cultivation) and, thereafter, remained more or less constant (Fig. 3c). Therefore, the results obtained by confocal fluorescence microscopy for cells with high PHA content seem to be in agreement with TEM microscopy. It seems that bacterial cells compensate for the increase in the amount of PHA per cell by increasing their length in order to keep the PHA granule volume content per cell to a maximum of no more than ~40 vol. %.

The fact that cells of PHA accumulating bacteria possess a regulatory mechanism to maintain capacity for granule storage was suggested by Tian, Sinskey and Stubbe (2005). To investigate whether the elongation of *C. necator* cells is directly controlled by the presence of PHA granules in cells, we also performed confocal fluorescence microscopy analysis of the PHA non-producing mutant *C. necator* PHB^{-4}; data are shown in Fig. 4. Thus, we found that both the cell lengths and cell widths of the mutant strain are very similar to those of the wild type. It indicates that there is no direct control mechanism regulating the prolongation of cells in response to the presence of PHA granules. It seems more likely that the cell size is controlled by external factors. For instance, the bacterium *Caulobacter crescentus* increases its cell volume in phosphate-poor conditions in order to improve the uptake of this crucial nutrient (Young 2007). It is a well-known fact that PHA accumulation in *C. necator* H16 is induced by limitations on phosphate, nitrogen and other nutrients (Jendrossek and Pfeiffer 2014). Therefore, we can hypothesize that rather than by the existence of a direct control mechanism between PHA granules and cell length to maintain PHA volume content to below 40 vol. %, the regulation of maximum PHA volume content is enabled by the fact that both PHA biosynthesis and cell length are influenced by the same factors (e.g. nutrient limitation).

Table 1. Development of number of PHA granules per cell in *C. necator* H16 culture with respect to time of cultivation and PHA weight content.

Time of cultivation [h]	Weight PHA content [% of cell dry weight]	Number of PHA granules per cell
0	20.8 ± 2.4	6.6 ± 2.0
4	16.2 ± 1.5	3.0 ± 1.0
8	14.1 ± 0.4	3.6 ± 1.7
12	29.7 ± 0.1	6.2 ± 3.2
24	52.3 ± 1.3	13.7 ± 3.1
34	55.9 ± 4.7	13.8 ± 1.8
48	66.0 ± 1.4	15.3 ± 3.3
56	69.1 ± 1.0	10.2 ± 6.2
72	68.5 ± 0.1	13.1 ± 5.0
80	72.1 ± 1.2	10.9 ± 3.9

Apart from the volume of PHA granules, we were also able to determine the number of PHA granules per cell (Table 1). The number of PHA granules in cells correlated with the PHA weight and volume content, since the cells contained ~6.6 granules per cell at the beginning of cultivation, and the number of granules in cells further decreased during the lag-phase of growth but increased as the cells started to accumulate PHA. However, it should be pointed out that due to the limitations of optical microscopy we were probably unable to distinguish possible clusters of multiple small granules which can be expected during the initial phase of PHA accumulation, as suggested by Jendrossek and Pfeiffer (2014). The average number of granules per cell during the PHA accumulation phase varied between 10 and 15, which is in accordance with reports of Anderson and Dawes (1990) and Tian, Sinskey and Stubbe (2005).

CONCLUSION

The dual-staining confocal fluorescence microscopy method developed in this work seems to be a very promising technique for the simultaneous study of the fundamental diameters of bacterial cells and intracellular PHA granules at the single cell level. On the basis of our results, cells of *C. necator* H16, during PHA accumulation, appear to increase their length in order to maintain an intracellular PHA granule volume content of no more than 40%. However, rather than there being a direct control mechanism between PHA granule content and cell length, it is more likely that both parameters are dependent on the same external stimuli, such as nutrient limitation.

SUPPLEMENTARY DATA

Supplementary data are available at FEMSLE online.

FUNDING

This work was supported by the Ministry of Education, Youth and Sports of the Czech Republic [LO1211] and the Czech Science Foundation (GACR) [GA15-20645S].

Conflict of interest. None declared.

REFERENCES

Anderson AJ, Dawes EA. Occurrence, metabolism, metabolic role, and industrial uses of bacterial polyhydroxyalkanoates. *Microbiol Rev* 1990;**54**:450–72.

Jendrossek D. Polyhydroxyalkanoate granules are complex subcellular organelles (carbonosomes). *J Bacteriol* 2009;**191**:3195–202.

Jendrossek D, Pfeiffer D. New insights in the formation of polyhydroxyalkanoate granules (carbonosomes) and novel functions of poly(3-hydroxybuytrate). *Environ Microbiol* 2014;**16**:2357–73.

Kadouri D, Jurkevitch E, Okon Y. Ecological and agricultural significance of bacterial polyhydroxyalkanoates. *Crit Rev Microbiol* 2005;**31**:55–67.

Marshall WF, Young KD, Swaffer M *et al.* What determines cell size? *BMC Biol* 2012;**10**:101.

Mollenhauer H. Artifacts caused by dehydration and Epoxy embedding in transmission electron microscopy. *Microsc Res Techniq* 1993;**26**:496–512.

Obruca S, Benesova P, Oborna J *et al.* Application of protease-hydrolyzed whey as a complex nitrogen source to increase poly(3-hydroxybutyrate) production from oils by *Cupriavidus necator*. *Biotechnol Lett* 2014a;**36**:775–81.

Obruca S, Petrik S, Benesova P *et al.* Utilization of oil extracted from spent coffee grounds for sustainable production of polyhydroxyalkanoates. *Appl Microbiol Biot* 2014b;**98**:5883–90.

Obruca S, Sedlacek P, Mravec F *et al.* Evaluation of 3-hydroxybutyrate as an enzyme-protective agent against heating and oxidative damage and its potential role in stress response of poly(3-hydroxybutyrate) accumulating cells. *Appl Microbiol Biot* 2016;**100**:1365–76.

Raberg M, Voigt B, Hecker M *et al.* A closer look on the polyhydroxybutyrate-(PHB-) negative phenotype of *Ralstonia eutropha* PHB-4. *PLoS One* 2014;**9**:e95907.

Reinecke F, Steinbuchel A. *Ralstonia eutropha* strain H16 as model organism for PHA metabolism and for biotechnological production of technically interesting biopolymers. *J Mol Microb Biotech* 2009;**16**:91–108.

Rodríguez-Contreras A, Koller M, Miranda-de Sousa Dias M *et al.* High production of poly(3-hydroxybutyrate) from a wild *Bacillus megaterium* Bolivian strain. *J Appl Microbiol* 2013;**114**:1378–87.

Slouf M, Ostafinska A, Nevoralova M *et al.* Morphological analysis of polymer systems with broad particle size distribution. *Polym Test* 2015;**42**:8–16.

Studer D, Gnaegi H. Minimal compression of ultrathin sections with use of an oscillating diamond knife. *J Microsc* 2000;**197**:94–100.

Tian J, Sinskey AJ, Stubbe JA. Kinetic studies of polyhydroxybutyrate granule formation in *Wautersia eutropha* H16 by transmission electron microscopy. *J Bacteriol* 2005;**187**:3814–24.

Volova TG, Zhila NO, Kalacheva GS *et al.* Effect of intracellular poly(3-hydroxybutyrate) reserves on physiological-biochemical properties and growth of *Ralstonia eutropha*. *Res Microbiol* 2013;**164**:164–71.

Wahl A, Schuth N, Pfeiffer D *et al.* PHB granules are attached to the nucleoid via PhaM in *Ralstonia eutropha*. *BMC Microbiol* 2012;**12**:262–73.

Young KD. Bacterial morphology: Why have different shapes? *Curr Opin Microbiol*. 2007;**10**:596–600.

New Biotechnology 39 (2017) 68–80

Contents lists available at ScienceDirect

New Biotechnology

journal homepage: www.elsevier.com/locate/nbt

Full length Article

The presence of PHB granules in cytoplasm protects non-halophilic bacterial cells against the harmful impact of hypertonic environments

Stanislav Obruca[a,*], Petr Sedlacek[a], Filip Mravec[a], Vladislav Krzyzanek[b], Jana Nebesarova[c], Ota Samek[b], Dan Kucera[a], Pavla Benesova[a], Kamila Hrubanova[b], Miluse Milerova[a], Ivana Marova[a]

[a] Faculty of Chemistry, Brno University of Technology, Purkynova 112, 612 00 Brno, Czech Republic
[b] Institute of Scientific Instruments, Academy of Sciences of The Czech Republic, Vvi, Kralovopolska 147, 612 64 Brno, Czech Republic
[c] Biology Centre, The Czech Academy of Sciences, v.v.i., Branisovska 31, 37005 Ceske Budejovice, Czech Republic

ARTICLE INFO

Article history:
Received 17 January 2017
Received in revised form 3 June 2017
Accepted 16 July 2017
Available online 20 July 2017

Keywords:
Poly(3-hydroxybutyrate)
PHB
Cupriavidus necator
Hyperosmotic conditions
Plasmolysis
Stress conditions

ABSTRACT

Numerous prokaryotes accumulate polyhydroxybutyrate (PHB) intracellularly as a storage material. It has also been proposed that PHB accumulation improves bacterial stress resistance. *Cupriavidus necator* and its PHB non-accumulating mutant were employed to investigate the protective role of PHB under hypertonic conditions. The presence of PHB granules enhanced survival of the bacteria after exposure to hypertonic conditions. Surprisingly, when coping with such conditions, the bacteria did not utilize PHB to harvest carbon or energy, suggesting that, in the osmotic upshock of *C. necator*, the protective mechanism of PHB granules is not associated with their hydrolysis. The presence of PHB granules influenced the overall properties of the cells, since challenged PHB-free cells underwent massive plasmolysis accompanied by damage to the cell membrane and the leakage of cytoplasm content, while no such effects were observed in PHB containing bacteria. Moreover, PHB granules demonstrated "liquid-like" properties indicating that they can partially repair and stabilize cell membranes by plugging small gaps formed during plasmolysis. In addition, the level of dehydration and changes in intracellular pH in osmotically challenged cells were less pronounced for PHB-containing cultures, demonstrating the important role of PHB for bacterial survival under hyperosmotic conditions.

Introduction

The fluctuation of external osmolarity is one of the most frequently encountered types of environmental stress factor for numerous microorganisms. For example, soil bacteria are often exposed to rapid alterations in external osmolarity as the water activity of soil is dependent on quickly changing weather conditions [1]. Therefore, the ability to adapt to fluctuations in external osmolarity is fundamental to survival and bacteria (regardless of their salinity preference) have developed different strategies to cope with osmotic pressure and changes in extracellular osmolarity [2].

Driven by the difference of osmotic pressure inside and outside the cell, a rapid increase in external salt concentration is inevitably accompanied by water efflux, resulting in dehydration of the cytoplasm [1]. The cell envelope of Gram-negative bacteria consists of an outer membrane, murein wall and cytoplasmic membrane, which contract together forming a kind of composite material. When cells dehydrate as a consequence of exposure to osmotic upshock, the cytoplasmic membrane separates from the outer layers of the cell envelope in order to cover a smaller volume of cytoplasm. Such a process is called "plasmolysis" and is accompanied by the formation of a periplasmic space, which depending on the conditions can represent 5–70% of cell volume [3]. The ability to undergo plasmolysis indicates that a semipermeable membrane is functioning and able to maintain protoplast integrity [4]. However, plasmolysis may also be a problem because the cytoplasmic membrane is unable to shrink by more than 2–5%, so that massive plasmolysis might result in its damage and collapse [5].

Polyhydroxyalkanoates (PHAs) are storage polyesters accumulated in the form of intracellular granules by a wide range of prokaryotic microorganisms. Among PHAs, the polymer of 3-

* Corresponding author.
E-mail addresses: Stana.O@seznam.cz
(, sedlacek-p@fch.vut.cz (P. Sedlacek), mravec@fch.vut.cz (F. Mravec), krzyzanek@isibrno.cz (V. Krzyzanek), nebe@paru.cas.cz (J. Nebesarova), osamek@isibrno.cz (O. Samek), xckucerad@fch.vut.cz (D. Kucera), xcbenesova2@fch.vut.cz (P. Benesova), hrubanova@isibrno.cz (K. Hrubanova), xcmilerova@fch.vut.cz (M. Milerova), marova@fch.vut.cz (I. Marova).

http://dx.doi.org/10.1016/j.nbt.2017.07.008
1871-6784/

hydroxybutyrate, poly(3-hydroxybutyrate) (PHB) is commonest and best studied [6–8]. PHB granules can represent a large fraction of cellular dry matter – under extreme conditions, up to 90% [9]. However, bacterial cells control their size to restrict the volume content of PHB granules to a maximum of 40% [10]; hence, geometric factors are assumed to determine the upper limit of intracellular PHB content [11]. The biosynthesis and hydrolysis of intracellular PHB granules occur simultaneously; thus, PHB metabolism exhibits a cyclic mechanism. Biosynthesis prevails when an external carbon source is present in excess and, on the contrary, hydrolysis and utilization of PHB granules is dominant when an external carbon source is lacking [12]. Therefore, it is generally proposed that PHAs are primarily utilized as carbon and energy storage materials when exogenous carbon sources are exhausted.

Nevertheless, there are several reports indicating that the presence of PHA granules in the cytoplasm enhances the survival of bacteria under various stress conditions, including osmotic pressure. Zhao et al. observed that the disruption of the PHA synthase gene in *Aeromonas hydrophila* reduced its resistance against numerous environmental stress factors, including high osmotic pressure [13]. Breedveld et al. reported that *Rhizobium leguminosarum* TA-1 and *Rhizobium meliloti* SU-47 cultures responded to osmotic stress exposure by degrading the intracellular storage of PHB and simultaneously increasing trehalose content [14]. Wang et al. tested the stress durability of recombinant *Escherichia coli* strains. The first of these harbored only PHA synthetic genes, whereas the second recombinant strain harbored both PHB synthetic genes and intracellular PHB depolymerase. It was observed that both strains were more resistant against several stresses, including osmotic pressure, than the wild type which was incapable of PHB synthesis. However, the recombinant strain capable of synthesizing and degrading PHB was more resistant than the strain incapable of PHB degradation [15]. Further, it was reported that the application of mild osmotic pressure (about 10 g/L NaCl) supports PHB biosynthesis in *Cupriavidus necator* [16,17]. Moreover, the capacity to accumulate PHA was observed in many halotolerant and halophilic prokaryotes, while several Gram-negative halophiles such as *Haloferax mediterranei* or *Halomonas* sp. are considered as potential candidates for the industrial production of PHAs [18,19]. Recently, Gram-positive halotolerant strains have also been described as potential PHA producers under fluctuating salinities [20].

Therefore, we proposed to shed light on the effects of the presence of PHB granules in bacterial cells on the viability, morphology and other properties of osmo-mesophilic cells when exposed to a hypertonic environment. We employed the most studied organism in the context of PHA metabolism, namely the Gram-negative soil bacterium *Cupriavidus necator* H16 [21] and its mutant strain *Cupriavidus necator* PHB^{-4} which, due to the mutation in the gene encoding PHB synthase, is incapable of accumulating PHB [22].

Methods

Microorganisms

The PHB-producing strain *Cupriavidus necator* H16 (CCM 3726) was obtained from the Czech Collection of Microorganisms, Brno, Czech Republic, and its PHA non-producing mutant strain *Cupriavidus necator* PHB-4 (DSM-541) was purchased from the Leibnitz Institute DSMZ-German Collection of Microorganism and Cell Cultures, Braunschweig, Germany.

Cultivations and hyperosmotic challenge

Cultivations were performed in Erlenmeyer flasks (volume 250 mL) containing 100 mL of Mineral Salt (MS) medium. Composition of MS medium was: 20 g fructose, 3 g $(NH_4)_2SO_4$, 1 g KH_2PO_4, 11.1 g $Na_2HPO_4{\cdot}12\,H_2O$, 0.2 g $MgSO_4{\cdot}7\,H_2O$, 1 mL of microelement solution, and 1 L of distilled water; the microelement solution was composed of 9.7 g $FeCl_3$, 7.8 g $CaCl_2$, 0.156 g $CuSO_4{\cdot}5\,H_2O$, 0.119 g $CoCl_2$, and 0.118 g $NiCl_2$ in 1 L of 0.1 M HCl. The flasks were inoculated with 5 mL of the overnight culture of a particular strain of *C. necator* grown in Nutrient Broth medium consisting of 10 g peptone, 10 g beef extract, and 5 g NaCl in 1 L of distilled water. After 72 h of cultivation, the cells were harvested (centrifugation, 8000 × *g*, 5 min), washed with Na-phosphate buffer (pH 7.4; 50 mM), and exposed to various concentrations of NaCl (0, 50, 100 and 200 g per liter of Na-phosphate buffer) for 3 h at 30 °C. Afterwards, various analyses of the challenged bacterial cells were performed as described below.

Analysis of cell viability

First, cell viability was assayed by the analysis of colony forming units (CFU/mL). Cells of both *C. necator* strains (between 1×10^8 and 1×10^9 cells/mL) were exposed to various concentrations of NaCl for 3 h as described above. The numbers of viable cells (CFU/mL) were determined by dilution plating on Petri dishes with NB medium agar prior to and at the end of incubation (three replicates). NB medium agar consisted of 10 g peptone, 10 g beef extract, and 5 g NaCl and 20 g agar per 1 L of distilled water.

Secondly, the viability of challenged bacterial populations was assessed by flow cytometry, using a membrane integrity assay employing propidium iodide staining. The protocol described by Coder was employed [23]. From each sample, 100 μL aliquots were taken, washed with PBS buffer, and diluted to a cell count of approximately 1×10^6 cells/mL. Then, 1 mL of cell suspension was stained with 1 μL of 1 mg/mL propidium iodide in the dark for 5 min. Subsequently, cell viability was analysed by flow cytometry (Apogee A50, Apogee, GB) using a 488 nm laser for excitation and the red channel (FL3) for fluorescence detection.

Analysis of intracellular PHB content

To determine the biomass concentration and PHB content in cells after exposure to a hypertonic environment, samples (10 mL) were centrifuged and the cells washed twice with distilled water and dried at 80 °C until they achieved constant mass. The PHB content of the dried cells was analysed by gas chromatography (Trace GC Ultra, Thermo Scientific, USA), as reported previously [24].

Raman spectroscopy

Approximately 20 μL of cells from *C. necator* H16 cultures exposed for 3 h to various concentrations of NaCl were pipetted onto CaF_2 (Raman grade glass) and analysed using a Renishaw Invia system (Renishaw inVia Raman Spectrometer, Renishaw plc., Wotton-under-Edge, UK), with a 785 nm single-mode diode laser as excitation source. The laser beam was focused onto a sample by the microscope objective (Leica, Wetzlar, Germany, 50 ×, NA (Numerical aperture) 0.5), with a laser spot diameter of approximately 2 μm × 10 μm. Overview spectra were acquired in the range 700–1800 cm^{-1}. Spectra from different parts of the sample were measured for 15 s, to a total of 3 measurements per sample; the results were averaged.

Cryo-SEM

A thin layer of bacterial cultures of *C. necator* H16 and *C. necator* PHB-4 exposed to hypertonic environments induced by various NaCl concentrations on a TEM mesh grids were frozen quickly in liquid nitrogen and moved into a cryo-vacuum chamber (ACE600, Leica Microsystems), where they were sublimated at −95 °C for 5 min. Further, the samples were moved under high vacuum using a shuttle (VCT100, Leica Microsystems) into a Scanning Electron Microscope (Magellan 400/L, FEI) equipped with a cold stage, and the samples were observed in a 1 keV electron beam at 120 °C without metal coating.

Transmission electron microscopy analysis of bacterial cells

Bacterial cells of both *C. necator* strains exposed to osmotic upshock induced by various NaCl concentrations were analysed by Transmission Electron Microscopy (TEM). After exposure to stress conditions, 1 mL of the suspension was centrifuged (1000 rpm for 15 min) and the preparation protocol was initiated by the addition of a cryoprotectant (20% BSA (Fluka)) to cell suspensions. Then, each sample (approx. 0.2 μL) was placed in a special carrier, frozen in a high pressure freezer (Leica EM Pact), and transferred under liquid N_2 into a freeze substitution unit (Leica EM AFS). 2% osmium tetroxide in acetone was used as a substitution solution. The substitution protocol was initiated at a temperature of −90° C for 96 h, and subsequently the samples were warmed up at −20° C for 24 h (5 ° C per hour) and finally the temperature was increased at 4° C after 8 h (3° C per hour), at which the samples were kept for 18 h. The samples were washed at room temperature in anhydrous acetone (15 min, three times). Next, the samples were infiltrated and embedded with Polybed resin (SPI) using acetone:resin mixtures (2:1, 1:1 and 1:2, each set-up embedded for 1 h and then overnight in pure embedding media under vacuum using a desiccator). Polymerization was perfomed by heat treatment (48 h at 62° C). Ultrathin sections were cut on an Ultracut UCT ultramicrotome (Leica) using a diamond knife (Diatome) with a cutting angle of 45°. Sections were transferred onto 300Mesh copper grids and stained with uranyl acetate and lead citrate solutions.

The ultrastructure of PHA-accumulating cells was examined using a JEOL 1010 transmission electron microscope operating at an accelerating voltage of 80 kV. Images were recorded digitally using a Megaview III CCD camera (Olympus).

The volumes of the periplasmatic spaces of upshocked cells (the measure of plasmolysis) were determined by image analysis of TEM microphotographs using Harfa software, as described in Supplementary materials and our previous publication [10].

Time-resolved fluorescence microspectroscopy

This section covers two different measurement techniques. The first, Fluorescence Lifetime Imaging (FLIM), was used to resolve lifetime changes in differently localized fluorophores. A fluorescent probe (carboxyfluorescein) is formed *in situ* by enzymatic hydrolysis from BCECF-AM (Molecular Probes). The lifetime of the fluorescence of this probe is dependent on the local pH value of a cytosol (see Supplementary material for calibration of this dependence). The second method. fluorescence anisotropy imaging, is directly related to the free rotational motion of the fluorophore and so to the local viscosity. Carboxyfluorescein was excited with a pulsed laser at 467 nm and 40 MHz repetition (PicoQuant). Samples were scanned with the objective using a piezoelectric scanner (PhysikInstrumente, GmbH). Excitation and

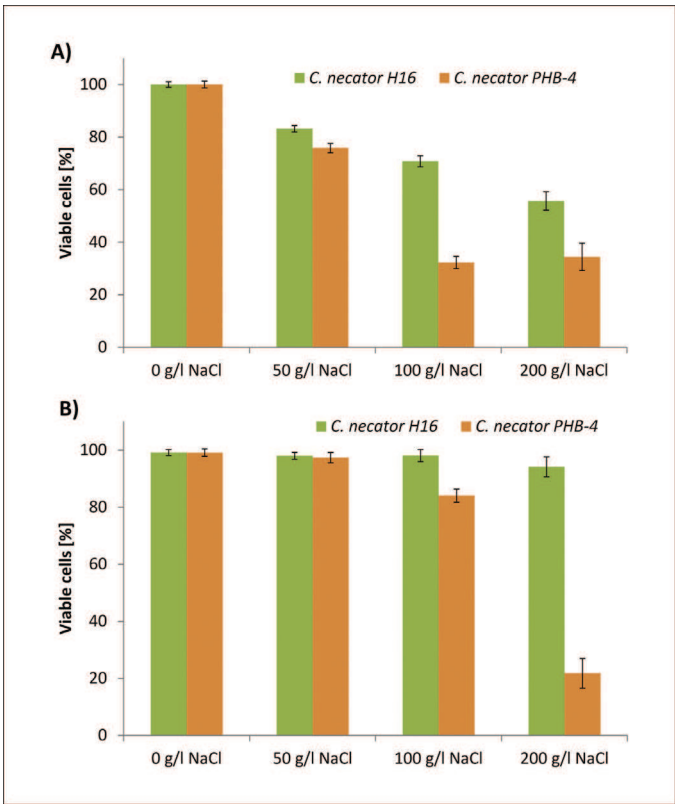

Fig 1. Viability of the PHB positive culture *C. necator* H16 and its PHB non-producing mutant *C. necator* PHB^{-4} exposed (3 h) to various NaCl concentrations assayed by (A) plating and (B) flow cytometry using propidium iodide staining.

emission light were collected via an UPlanSapo objective with 60× magnification, water immersion, Numerical Aperture 1.2 (Olympus, Inc.). Fluorescence signal was collected through a 50 μm pinhole, 520/35 emission filter (Semrock) and with a single photon avalanche-photodiode detector (MPD S.r.l.). Samples were fixed using a pre-heated 2% agarose solution in water and in a salt solution with a concentration of 200 g/L of NaCl. About 10 μL of cell suspension was placed onto a microscopy cover slide and superimposed with 2% agarose at ~40 °C. In the case of pH measurement, the dependency of carboxyfluorescein lifetimes from hydrolysed BCECF-AM on different pH values was studied. It was found that the average lifetime of a fluorophore exhibits a non-linear dependency on the pH of the environment. The calibration is presented in Supplementary materials.

Thermogravimetry of bacterial cells

A thermogravimetric analyzer (TGA, TA Instruments, Q5000IR) was used to quantitatively analyze the dehydration of osmotically challenged bacterial cultures. Prior to TGA analysis, a corresponding cell sample, cultivated and osmotically challenged by the procedures described above, was centrifuged and the supernatant was carefully decanted. About 15 mg of the remaining cell suspension were weighed into the aluminium TGA pan. In the TGA analyzer, the sample was heated instantaneously to 60 °C and subsequently kept at this temperature for 40 min. Then, the temperature was raised to 200 °C and maintained for further 20 min in order to determine the dry mass of the sample. Both bacterial cultures (*C. necator* H16 and *C. necator* PHB^{-4}) were analysed in unchallenged form as well as after exposure to 50, 100 and 200 g/L NaCl, respectively. Every experiment was performed in four replicates; for each replicate, a fresh bacterial culture was prepared. All the thermograms were analysed according to Uribelarrea et al. [25] in order to determine critical water contents (i.e. the points in the drying curves corresponding to a sudden change in the drying rate) as a quantitative measure of the respective intracellular water content.

Results

Influence of PHB accumulation on survival of osmotic stress

In the first experiment, both bacterial cultures were exposed to osmotic shock induced by 50, 100, and 200 g/L of NaCl for 3 h; control exposure to buffer without the addition of NaCl was also performed. First, cell viability was assayed by comparing the numbers of cultivable cells (CFU/mL) in samples prior to and after incubation; data are shown in Fig. 1A. The results demonstrated that the application of NaCl decreased the number of cultivable cells in both cultures and this adverse effect increased with increasing concentration of NaCl. Importantly, the culture of *C. necator* H16 exhibited a higher survival rate than its PHB non-accumulating mutant.

Secondly, the viability of the cultures was further assessed by flow cytometry using propidium iodide as the viability probe. In principle, staining easily penetrates cells with damaged membranes, which consequently reveal high fluorescence and can be discriminated from intact cells. Therefore, propidium iodide is considered to be a membrane integrity probe [23]. The results are presented in Fig. 1B. Also in this case, the PHB accumulating culture demonstrated higher resistance to osmotic shock, its viability decreasing only slightly with increasing NaCl concentration, while the viability of the PHB non-accumulating mutant strain dropped dramatically when exposed to 100 and 200 g/L NaCl. These results suggest that the presence of PHB granules in bacterial cytoplasm provides protection for cell membranes against the effects of osmotic stress. Nevertheless, due to substantial differences in the results obtained by plating assay and flow cytometry (especially in *C. necator* H16), it appears that membrane damage caused by plasmolysis is not the only factor causing a reduction in the number of cultivable cells during osmotic challenge. The cultivability of PHB containing cells may be reduced by other mechanisms, despite the fact that they cells are able to maintain membrane integrity even at very high salt concentrations.

Change in PHB content and the state of the polymer in cells during hyperosmotic challenge

Since some authors have reported that the increased stress resistance of PHA accumulating bacteria against osmotic pressure is associated with the degradation of intracellular polymer granules [14,15], we determined the PHB content in bacterial cells before and after exposure of *C. necator* H16 to hyperosmotic challenge (Table 1). It was observed that a substantial decrease in polymer content occurred only in cells which were incubated in the absence of additional NaCl. In this case, prior to incubation, PHB content amounted to 85.0% of cell dry mass (CDM); after 3 h of incubation the polymer represented 80.7% of CDM. Thus, it seems that the absence of an external carbon source shifted the PHB metabolism from accumulation to degradation, which is in agreement with previous reports for this organism [21]. Conversely, when the cells were exposed to hyperosmotic shock, no PHB degradation occurred and, in contrast, a slight increase in PHB content was observed in the cell material with increasing NaCl concentration in the buffer. It is unlikely that the exposure of bacterial cells to such a high concentration of NaCl induced PHB biosynthesis in the absence of an external carbon substrate. The slight increase in PHB content was probably caused by the partial hypotonic lysis of upshocked cells, which were subsequently washed during the preparation of samples for GC analysis. Hence, the results suggest that the involvement of PHB granules in the response to suddenly induced high osmotic stress in *C. necator* is rather metabolically passive and most likely not connected with their degradation, in contrast to findings of Breedveld et al., who observed that osmotic upshock is associated with mobilization of PHA storage [14].

The state of PHB in upshocked cells was determined by Raman spectroscopy. Under normal conditions, intracellular PHB granules consist of amorphous polymer which is also the substrate for intracellular PHB depolymerases [26]. However, we observed that in some cases the amorphous state changed such that crystallization was clearly identifiable from Raman spectra. The process of crystallization is associated with enhancement of the intensity/shift of particular PHB Raman peaks. Thus, it was possible to estimate the state of the polymer in samples which were exposed to 100 and 200 g/L NaCl, and to enable the start of the crystallization process within the cells to be visualized. Here, qualitative differences between crystalline and amorphous

Table 1
The PHA content of intracellular polymer in cells of *C. necator* H16 exposed to hypertonic conditions induced by various NaCl concentrations.

	PHA content in biomass [w%]
Prior to exposition	85.0 ± 3.2
0 g/L NaCl	80.7 ± 2.1
50 g/L NaCl	87.2 ± 0.9
100 g/L NaCl	90.9 ± 2.0
200 g/L NaCl	90.7 ± 0.8

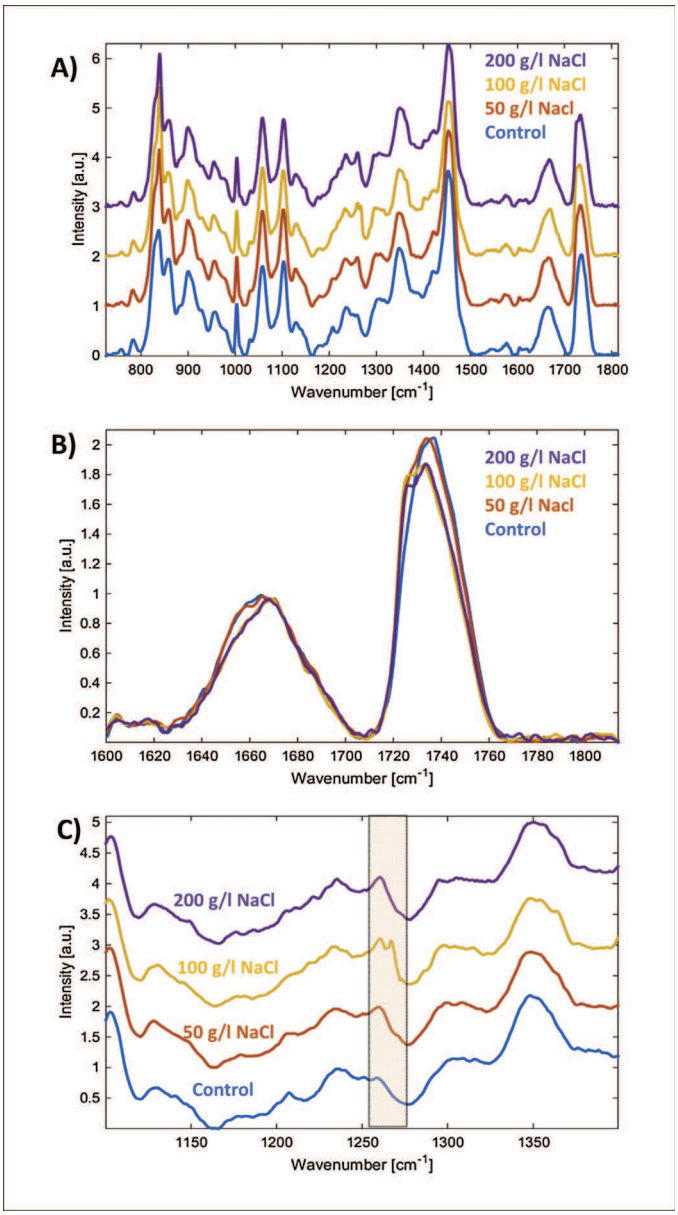

Fig. 2. Crystallization of PHB granules of upshocked cells of *C. necator* H16 recorded by Raman spectroscopy. (A) Whole Raman spectrum in the range 800–1800 cm^{-1}; (B) detail of crystallization indicating shift of PHB peak at 1736 cm^{-1} for samples exposed to 100 and 200 g/l NaCl; (C) formation of peak at 1260 cm^{-1} also indicating partial PHB granule crystallization.

polymer states can readily be evaluated by the naked eye using a set of 3 Raman emission lines which show quite significant changes (Fig. 2). The most significant changes in the line intensities of PHB during the process of crystallization were at 1260 and 841 cm^{-1}. The line shift related to the process of crystallization can also be observed for the PHB band from 1736 cm^{-1} (the amorphous state) to about 1725 cm^{-1} (the crystalline state), as reported previously [27–29]. Hence, it seems that the exposure of PHB containing bacterial cells to hyperosmotic shock causes the partial crystallization of PHB granules, which in turn might complicate its further mobilization by PHB depolymerases.

Observation of the morphology of challenged cells by Cryo-SEM

Cryo-SEM was used to analyze the surface morphologies of bacterial cells of both bacterial cultures exposed to hyperosmotic shock. This technique, in general, should reveal changes in the shapes or sizes of challenged cells. The results are shown in Fig. 3. In fact, no substantial differences in the shapes of PHB accumulating and non-accumulating cells were recorded during their exposure to osmotic stress, which indicates that the outer layers of the cell envelope are not drastically damaged by hyperosmotic treatment. Nevertheless, cryo-SEM analysis revealed another interesting phenomenon. Surprising “string-like” structures were observed in the areas where the cells were ripped during sample preparation (see the structures indicated by red arrows in Fig. 3). These structures were observed only in PHB accumulating culture, which indicates that they were formed by plastically deformed PHB granules. Plastic deformation of freeze-fractured PHB granules investigated by Cryo-SEM has also been observed by other authors [30,31]. It is interesting that “string-like” structures were absent in bacterial culture incubated in buffer

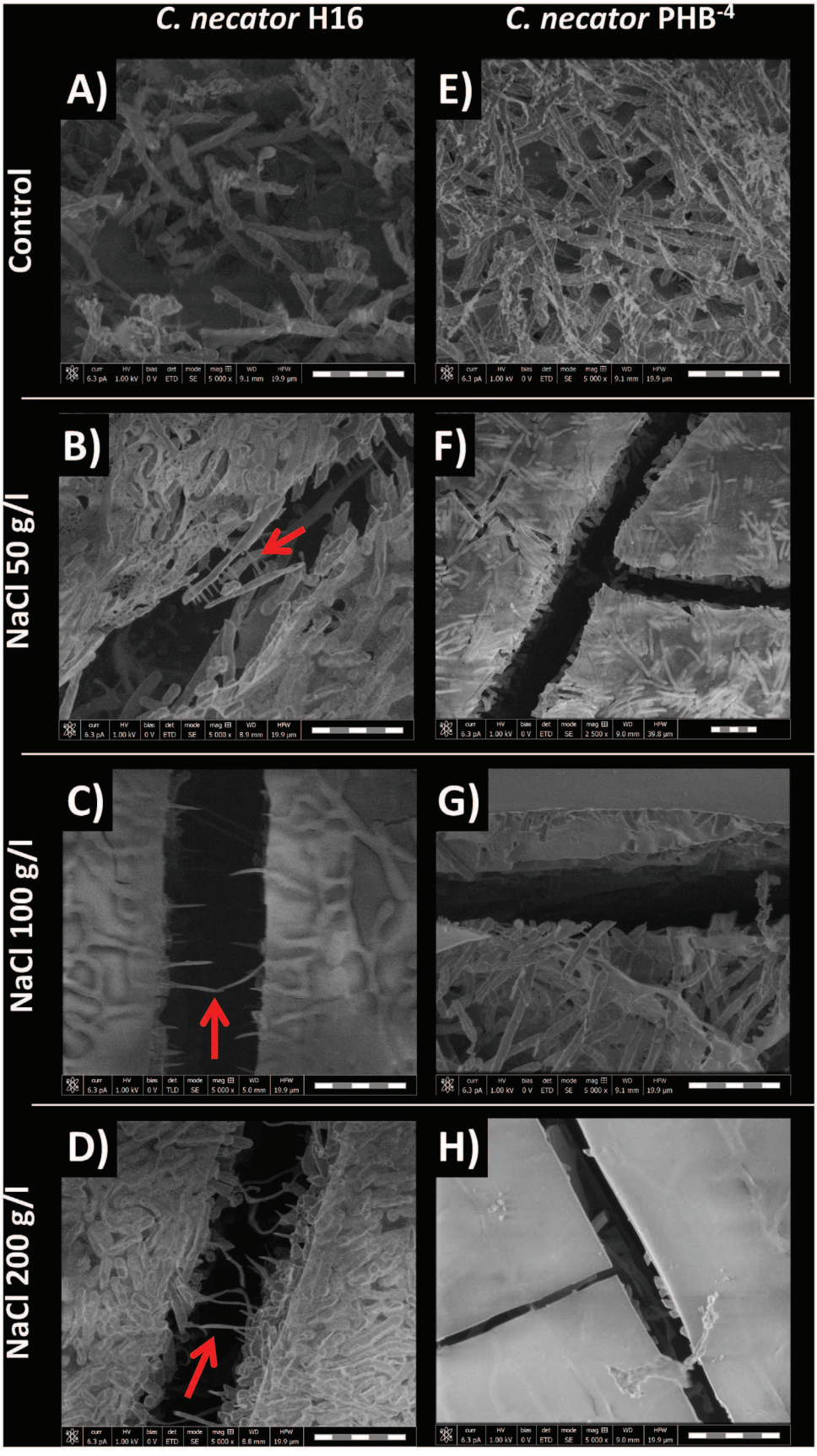

Fig. 3. Cryo-SEM analysis of PHB-accumulating *C. necator* H16 exposed to 0 (A), 50 g/L (B), 100 g/L (C), and 200 g/L NaCl (D); morphology of PHB non-accumulating strain *C. necator* PHB^{-4} exposed to 0 (E), 50 g/L (F), 100 g/L (G), and 200 g/L NaCl (H). Red arrows indicate "string-like" structures present in up-shocked PHB positive cells. Scale bar = 5 μm. (For interpretation of the references to colour in this figure legend, the reader is referred to the web version of this article.)

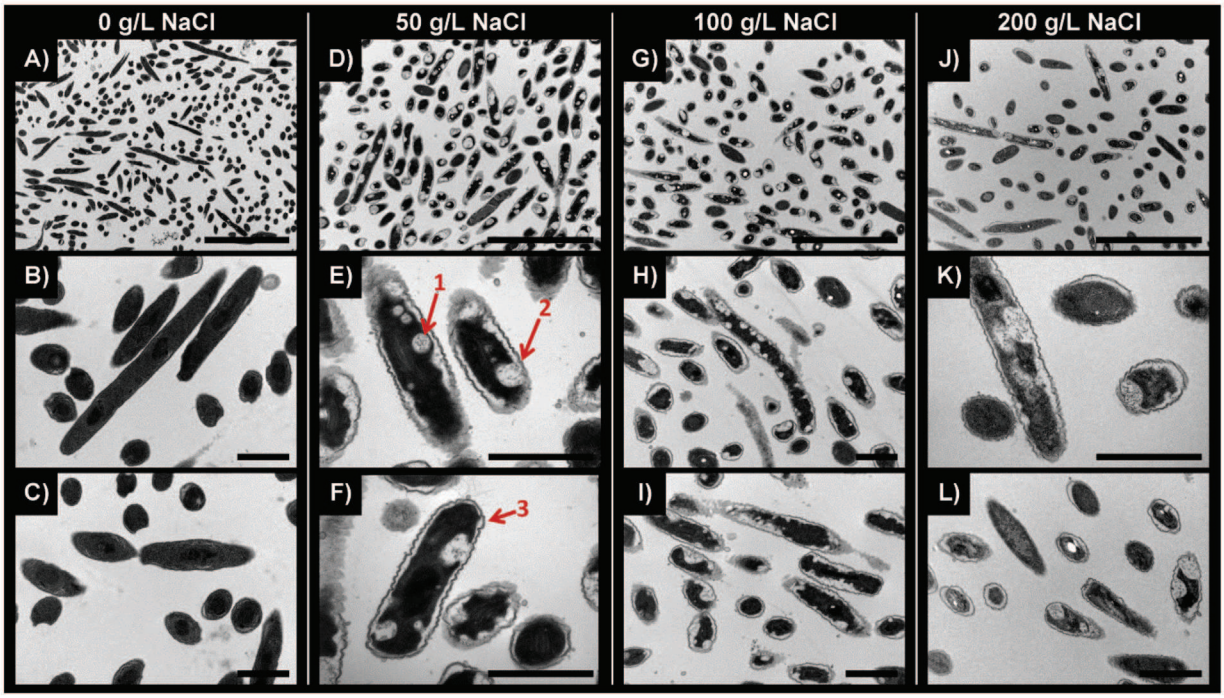

Fig. 4. TEM analysis of cells of the PHB non-accumulating strain *C. necator* PHB^{-4} exposed to 0 (A–C), 50 g/L (D–F), 100 g/L (G–I), and 200 g/L NaCl (J–L). Red arrows indicate the following observations: 1 – endocytotic vesicles; 2 – unsymmetrical plasmolysis of bacterial cells resulting in the formation of "hole-like" structures accompanied by the release of cytoplasm content into the periplasmatic space; 3–the wrinkling of the outer layers of the cell envelope – the outer membrane and murein layers. (A,D,G,J: scale bar = 5 μm, others: scale bar = 2 μm). (For interpretation of the references to colour in this figure legend, the reader is referred to the web version of this article.)

without NaCl and that their number as well as width seem to increase with increasing NaCl concentration. Evidently, the exposure of bacterial culture to osmotic upshock alters the properties of intracellular PHB granules, resulting in the more intensive formation of string-like structures. It is unlikely that the crystallization observed by Raman spectroscopy would support the formation of string-like structures requiring considerable plastic deformation of the polymer granules. Hence, it can be expected that hypertonic conditions induce further change(s) in the properties of PHB granules.

Transmission electron microscopy analysis of upshocked cells

Changes in the morphologies of the challenged cells of both bacterial cultures were also observed by TEM. Microphotographs of upshocked cells of the PHB non-accumulating mutant are shown in Fig. 4. Generally, the exposure of bacterial cells to hyperosmotic conditions induced massive plasmolysis in bacterial cells (the periplasmatic space represented about 44–49 vol% of the cells) and wrinkling of the outer layer of the cell envelope. The intensity of plasmolysis only changed slightly with increasing NaCl concentration and was accompanied by the formation of endocytotic vesicles in some bacterial cells and the formation of tubular structures and Scheie structures as described by Koch [3]. Surprisingly, the formation of the periplasmic space of upshocked PHB non-accumulating cells was not symmetrical or situated at the poles of the cells, as reported by others [3,5,32]; in numerous cases, "hole-like" structures (reminiscent of incompletely formed endocytotic vesicles) randomly distributed in the outer volume of bacterial cell cytoplasm were observed. It is very likely that such asymmetrical plasmolysis causes damage to the cytoplasmic membrane. In these "holes" it is possible to observe darker areas, which may be attributed to the leakage of cytoplasmic content through the damaged membrane.

Fig. 5 shows the morphology of the PHB accumulating bacterial strain of *C. necator* exposed to various NaCl concentrations. In this case, osmotic challenge also resulted in wrinkling of the outer layer of the cell envelope and plasmolysis; however, the plasmolysis was considerably less intense since the periplasmatic space represented only about 20–24% of cell volume and no tubular or Scheie structures were observed. Furthermore, unlike in the PHB-non-accumulating mutant, plasmolysis in *C. necator* H16 did not result in the formation of hole-like structures accompanied by the leakage of cytoplasm content. On the contrary, when plasmolysis occurred in the close vicinity of PHB granules, the polymer granules exhibited unexpected "liquid-like" behavior associated with their influx into the periplasmic space. Thus, it seems that PHB granules are able to decrease the degree of plasmolysis and change its nature; it is also likely that, due to their liquid-like properties, they might partially protect membranes from damage and decrease the leakage of cytoplasm content.

In addition, when PHB-positive bacterial cells were exposed to 100 and 200 g/L of NaCl, the aggregation of PHB granules was clearly obsered, usually resulting in the formation of one or several non-spherical PHB granule(s) per cell.

Time-resolved fluorescence microscopy analysis of upshocked bacterial cells

The fluorescence properties of labelled cytosol determined by a BCECF-AM fluorogenic probe were studied using two different

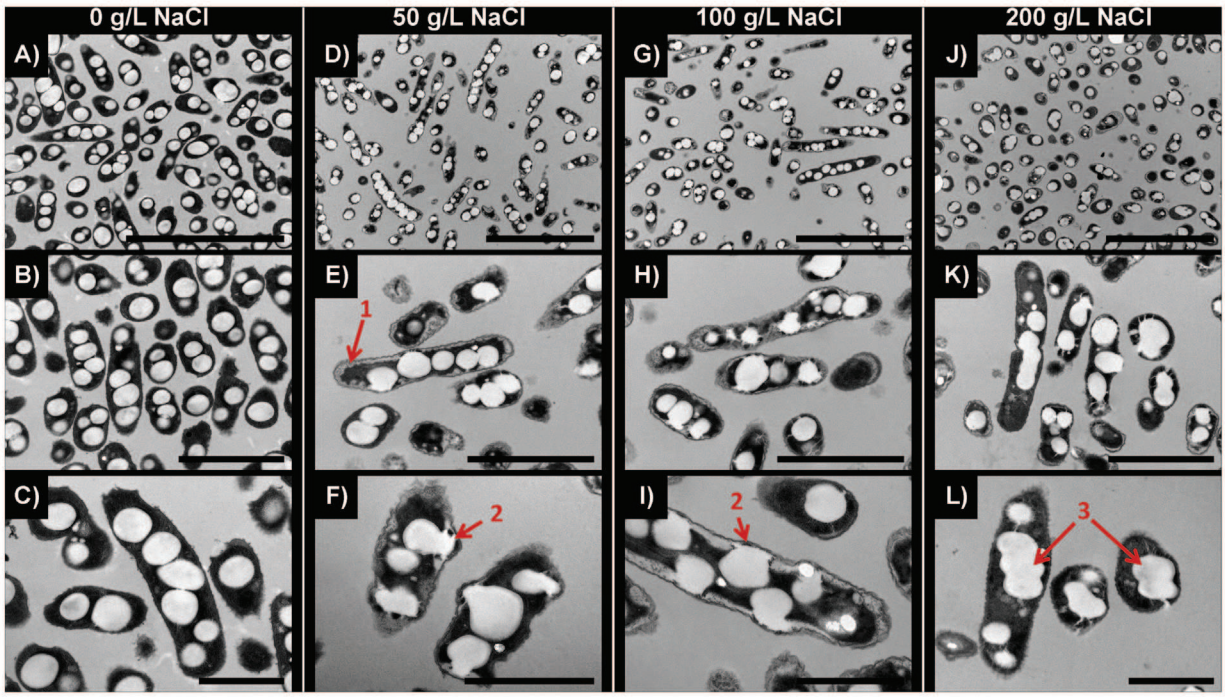

Fig. 5. TEM analysis of cells of the PHB-accumulating strain *C. necator* H16 exposed to 0 (A–C), 50 g/L (D–F), 100 g/L (G–I), and 200 g/L NaCl (J–L). Red arrows indicate the following observations: 1–the wrinkling of the outer layers of the cell envelope and symmetrical plasmolysis; 2–the influx of PHB granules into the periplasmatic space; 3–the massive aggregation of PHB granules. (A,D,G,J: scale bar = 5 μm; B,E,H, K: scale bar = 2 μm; C,F,I,L: scale bar = 1 μm). (For interpretation of the references to colour in this figure legend, the reader is referred to the web version of this article.)

approaches. Fluorescence lifetimes, dependent on the pH of the environment (see Supplementary material), were comparable in the case of standard environments. In both cell types, intracellular pH was in the range 7.4–7.5, with a homogenous distribution inside the cells. However, osmotic upshock shifted the intracellular pH value differently in each tested bacterial culture. For *C. necator*, the pH decreased to a value of 7.0 ± 0.1. In contrast, as can be seen from the fluorescence probe lifetimes, intracellular pH in cells of the PHB non-containing mutant decreased more substantially to values around 6.5 ± 0.3 when exposed to hypertonic conditions. A further important effect of salt addition can be seen in Fig. 6a, which displays images with time-resolved information. Cells under standard conditions are very well defined; however, after exposure to osmotic stress, some cells, especially in PHB non-containing culture, reveal hazy edges, which can imply the partial leakage of the fluorescence probe into the external space.

Another fluorescence parameter which can uncover changes in properties of bacterial cells is steady-state fluorescence anisotropy. This describes the possibility of the free-rotation of the fluorescent probe and therefore is usually associated with the "viscosity" of the environment; its mapping can be used to study the rheology of bacterial cell cytoplasm [33]. Generally, anisotropy directly correlates with the viscosity of the environment – the higher the anisotropy, the higher the viscosity. In the PHB non-accumulating mutant, the fluorophore exhibited a relatively high value of anisotropy, 0.214 ± 0.005. The addition of salt caused a decrease in anisotropy (0.176 ± 0.008), which can be related to the decrease in viscosity of the intracellular matrix due to its partial leakage through the damaged membrane. Thus, the results of fluorescence anisotropy imaging confirm our observation of the leakage of cytoplasm content in upshocked PHB non-containing cells obtained by TEM (see Fig. 5, arrow number 2). In contrast, anisotropy increased in *C. necator* H16 when the cells were exposed to osmotic upshock, indicating an increase in the viscosity of cytoplasm content associated with cell dehydration and plasmolysis. It seems that, unlike in the PHB negative strain, no substantial leakage of cytoplasm content occurred, implying that membranes were not heavily damaged by osmotic upshock (in agreement with the results of flow cytometry and TEM). Typical results are displayed as anisotropy-resolved images in Fig. 6b. The anisotropy values are scaled using a rainbow scale, with green dedicated to the free rotation of molecules and the low viscosity region. Red relates to the hindered rotation of fluorophores and high viscosity. Moreover, taking into account the homogeneity of the distribution of anisotropy values inside the cells, a further effect of salt addition can be seen. Both cell-types exhibit a homogenous distribution of anisotropy values before salt addition, whileafter exposure to the hypertonic environment, the anisotropy values are distributed more randomly inside the cells.

Quantitative analysis of the cell dehydration of up-shocked bacterial cells by TGA

Thermogravimetry (TGA) was employed to provide a quantitative estimate of the degree of osmotically-induced cell dehydration in PHB positive and negative bacterial cells. Centrifuged cell samples were continuously dried at 60 °C while corresponding changes in sample mass were recorded. Total water content in the sample was subsequently calculated from the residual mass content after further drying at 200 °C [34]. The results on both

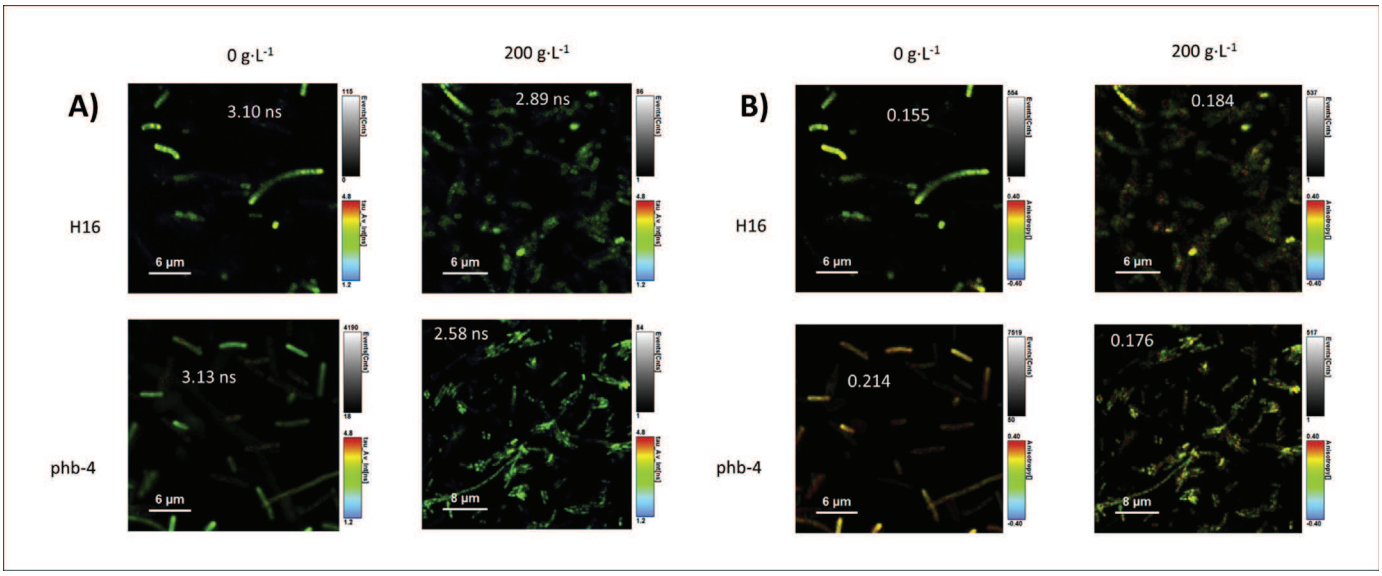

Fig. 6. The Influence of salt addition on cells stained with carboxyfluorescein. A) Fluorescence lifetimes, averaged by intensity, are displayed as rainbow scales. Inserted values are average values of lifetimes found for each sample. Corresponding pH values are for nonchallenged cells (7.4–7.5), which decrease with salt addition to 7.0 ± 0.1 in *C. necator* H16 and to 6.5 ± 0.3 in *C. necator* PHB^{-4}. B) Anisotropy of carboxy fluorescein inside the studied cells. Steady-state anisotropy values are displayed as rainbow scales in which green relates to low viscosity regions (an anisotropy value of approx. 0) and red to high viscosity regions (an anisotropy value close to 0.4). Inserted values are average values of anisotropy found for each sample. (For interpretation of the references to colour in this figure legend, the reader is referred to the web version of this article.)

tested bacterial cultures are shown in the form of drying curves in Fig. 7A, C.

It has been proposed that changes in the rate of water elimination from cell samples can be used as indicators of the quantitative content of various forms of water in cell samples [25,35,36]. For instance, Uribelarrea et al. interpret the critical point in the drying curve of a cell sample (i.e. the point where the evolution of sample mass versus time suddenly changes its course) simply as a boundary point where the drying of extracellular water ends and the elimination of intracellular water starts [25].

To obtain such critical points from the results of our TGA experiments, derivation of the water loss over time is given as a

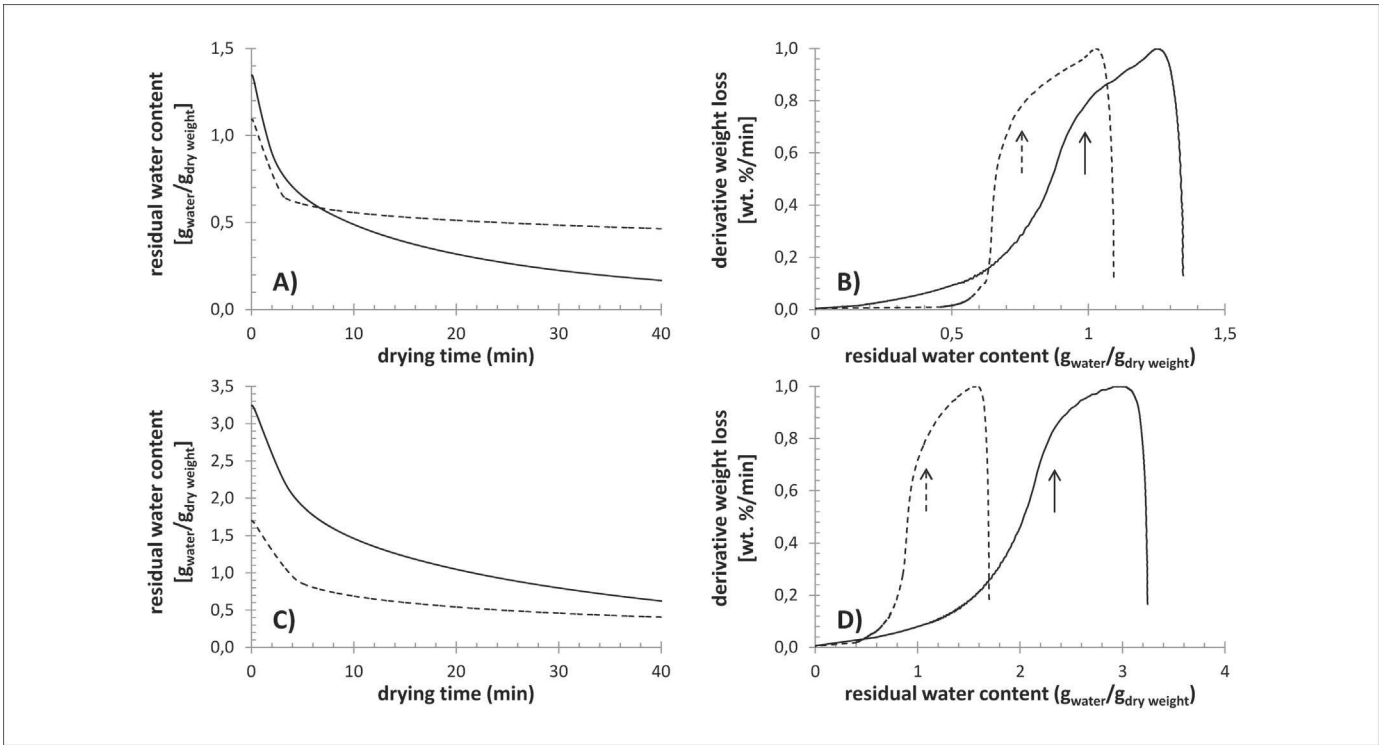

Fig. 7. The effect of osmotic challenge on drying curves determined by isothermal TGA experiments at 60 °C on *C. necator* H16 (A, B) and *C. necator* PHB-4 (C, D). Solid lines represent unchallenged bacterial samples, dashed lines represent samples exposed to 200 g/L NaCl. The heights of the derivative weight loss curves (B, D) were normalized for clarity. Arrows indicate respective critical water contents.

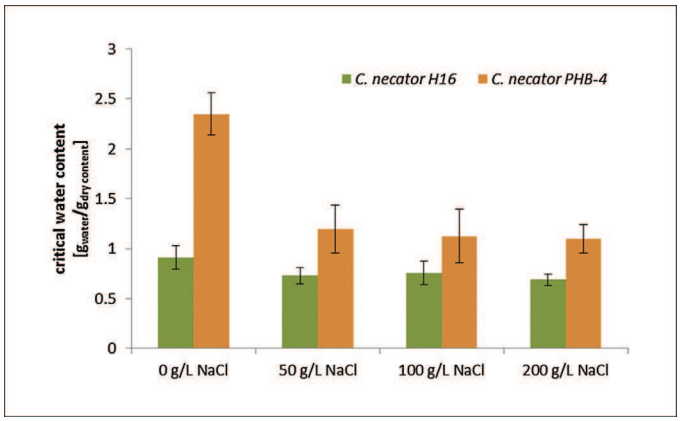

Fig. 8. Critical water content of the PHB-positive culture *C. necator* H16 and its PHB non-producing mutant *C. necator* PHB^{-4} exposed (3 h) to various NaCl concentrations determined by TGA (isothermal drying at 60 °C).

function of residual water content in the sample (see Fig. 7B, D). The drying rate curves of all the bacterial cells included in this study revealed a single critical point, corresponding to two distinguishable water contents in the samples. Because this critical point always represents the moment when the rate of sample drying begins to fall rapidly, a significant change in the drying process evidently occurs at this point. In Fig. 8, the relative water content at this critical point is shown for both tested bacterial cultures exposed to different concentrations of NaCl. It is evident from the comparison of unchallenged bacterial cultures that lower critical water content (i.e. water content at the critical point, given in $g_{water}/g_{dryweight}$) was found for *C. necator* H16 bacterial cultures, in which the dry mass of the cell samples was significantly increased by the presence of PHB granules.

A more interesting finding arises, however, from the comparison of unchallenged and osmotically upshocked cell samples. It was found that the critical water content was significantly decreased for osmotically challenged PHB negative cells. This decrease corresponds to about 50% of the original water content, determined for the unperturbed culture regardless of the concentration of NaCl in the medium. However, for PHB positive cells, the osmotically induced decrease in the critical water content, which can also be found in Fig. 8, was less pronounced at all NaCl concentrations (the average critical water content decreased by about 20% regardless of the concentration of NaCl).

Discussion

Since PHA is one of the most widespread storage materials in bacteria, it can be assumed that the ability to accumulate PHA represents a significant advantage in natural environments. The most obvious advantage is probably the possibility to utilize PHAs when external carbon sources are depleted. Nevertheless, PHAs play a much more complex role in stress survival and the adaptation of bacteria to various environments. There are reports that the capacity for PHA accumulation and degradation enhances the resistance of bacterial cells to stress conditions such as high temperature [37,38], low temperature and freezing [34,39], and oxidative stress [37,40]. However, the mechanisms by which PHA enables stress alleviation are not yet fully understood. It is likely that PHA granules offer physical protection under various stress conditions and it is also possible that their presence influences the overall properties of bacterial cells supporting their survival. Nonetheless, normally functioning PHA anabolic and catabolic pathways are considered to be essential in providing increased stress protection [12].

Although the ability to adapt to fluctuations in external osmolarity is fundamental to the survival of microorganisms and despite the fact that there are reports showing that the accumulation of PHA helps bacterial cells to survive osmotic challenge [13–15,41], we are not aware of any study investigating the possible protective mechanisms of PHA against hypertonic and/or hypotonic environments. To fill this gap, we have studied the possible protective mechanisms offered by the presence of PHB granules during hypertonic conditions by employing the common soil non-halophilic Gram-negative bacterium *Cupriavidus necator*, which is often in use as a model organism for PHB metabolism [21].

According to the results (Fig. 1), the presence of PHB in cell cytoplasm clearly supports the survival of *C. necator* cells exposed to osmotic challenge. Nevertheless, the mechanism of its protective action is unclear. Generally, the accumulation of a wide spectrum of so-called compatible solutes is the major strategy adopted by most bacteria under conditions of hyperosmotic stress. Along with balancing the external osmotic pressure, compatible solutes possess chemical chaperone activity providing protection for biomacromolecules, particularly proteins, against denaturation induced by various stressors [1,42]. It was recently reported that the monomer of PHB, 3HB, serves as a potent chemical chaperone protecting enzymes against various stress factors [43]. Alternatively, the hydrolysis of PHB can be used as a source of carbon and energy for the biosynthesis of other compatible solutes, as reported by Breedveld et al. [14]. Therefore, it was expected that upshocked PHB-containing cells hydrolyse PHB granules with the help of 3HB and/or other compatible solute(s) in order to cope with exposure to hypertonic environments. Nevertheless, no mobilization of PHB granules during the exposure of bacterial culture to hypertonic challenge was observed (Table 1).

Intracellular polymer in *C. necator* is hydrolysed by a battery of PHB depolymerases which are specific to the amorphous state of PHB [26]. Using Raman spectroscopy (Fig. 2), it was observed that the exposure of bacterial cells to hypertonic conditions initiated partial crystallization of the polymer, which, as a consequence, probably inhibited the mobilization of PHB granules by specific enzymes. According to Barnard and Sanders, a small amount of water is an integral component of PHB granules, acting as a plasticizer of the polymer [44]. Therefore, it seems likely that the partial dehydration of PHB granules during hypertonic challenge results in partial crystallization of the polymer and the inhibition of its hydrolysis. The results demonstrated that PHB hydrolysis yielding compatible solutes is not the mechanism by which PHB increases the survival of osmotically upshocked cells of *C. necator*.

The fact that the enhancement of stress tolerance in PHA producers can be achieved without mobilization of the previously accumulated granules was also reported by Goh et al., who observed that *E. coli* cells harboring PHA biosynthetic genes, but which were incapable of PHA mobilization, exhibited higher resistance to oxidative stress [40].

The results of viability analysis by means of flow cytometry using propidium iodide (Fig. 1B), TEM microphotographs (Figs. 4 and 5), and the results of the time-resolved fluorescence microscopy analysis (Fig. 6) indicated that the presence of PHB in bacterial cell cytoplasm stabilized cytoplasmic membranes against damage by hypertonic environments and the leakage of cytoplasm content. Generally, osmotic upshock leads to the dehydration and plasmolysis of bacterial cells. Due to the fact that the cell membrane is not able to shrink by more than 2–5%, intensive plasmolysis might be harmful, leading to cell membrane damage and even collapse [5]. The results of TEM analysis show that plasmolysis in PHB negative cells is much more intensive (Fig. 4) than in PHB-containing cells (Fig. 5). In addition, TEM demonstrated that while in PHB non-accumulating bacterial cells exposure to hypertonic environments resulted in the formation of "hole-like" structures and the leakage of cytoplasmic content into the periplasmatic space, no such fatal consequences were observed in PHB-containing cells. It seems that intracellular PHB granules serve as a scaffold protecting bacterial cells from adverse massive and unsymmetrical plasmolysis.

In addition, Bonthrone et al. reported that native intracellular PHB granules are formed by highly mobile amorphous elastomer, which is reminiscent of a supercooled liquid in terms of its properties [45]. When bacterial cells were exposed to hypertonic conditions, PHB granules revealed surprising liquid-like properties accompanying their efflux into the periplasmatic space when plasmolysis occurred in their close vicinity (see Fig. 5, red arrows number 2). Cryo-SEM observation also revealed PHB granules to have unusual plastic-like properties in challenged bacterial cells, as demonstrated by string-like structures in cells ripped during sample sublimation (Fig. 3). It should be pointed out that these deformations were formed at extremely low temperatures (-95 °C), demonstrating intracellular PHB granules to have very flexible liquid-like properties even at temperatures at which all the other components of bacterial cells are unambiguously crystalline and brittle. Taking into account their extraordinary liquid properties, it seems likely that PHB granules can partially repair and stabilize cell membranes by plugging small gaps in their structure which are formed during plasmolysis (see, for instance, Figs. 5F, I and L demonstrating a possible mechanism for this protective action).

Furthermore, when bacterial cells were exposed to higher NaCl concentrations (100 and 200 g/L), TEM microphotographs (Fig. 5, red arrow number 3) demonstrated another interesting phenomenon – the aggregation of PHB granules leading to the formation of one or several non-spherical granules per cell. Such behavior can explain the creation of the "string-like" structures observed by cryo-SEM (Fig. 3). As bacterial cells were exposed to increasing concentrations of NaCl, the PHB granules aggregated, and wider and more numerous string-like structures were formed when the cells were torn open during sample preparation for cryo-SEM analysis.

PHB granules, also designated "carbosomes" [46], are supramolecular structures consisting of a hydrophobic PHB polymer core and a proteinaceous surface layer preventing polymer granules from aggregating and coming into direct contact with the aqueous environment of the cell's cytosol [47]. The aggregation of PHB granules in upshocked cells was, therefore, probably induced by the dehydration-mediated partial injury of the protein layer, which allowed hydrophobic polymer to aggregate into larger particles. Regardless of the mechanism of granule aggregation, it is likely that this process damages the cell's ability to divide, since in numerous cases granular aggregates were situated in the central parts of cells (see Fig. 5), where cell division is usually initiated and takes place [48]. This could explain the differences between the viabilities of the PHB-containing cultures determined by plating or by flow cytometry (Fig. 1A,B). Generally, plating underestimates the number of viable cells in cultures when the fraction of the original culture loses the capacity to grow [32]. Therefore, a considerable fraction of PHB-containing bacterial culture might retain non-damaged membranes and functional metabolism even when exposed to very high concentrations of NaCl but is not capable of division and growth.

Nonetheless, the numbers of viable cells determined by plating and flow cytometry in the PHB non-accumulating mutant strain of *C. necator* are also disproportionate (although to a much lesser degree). Therefore, membrane damage is obviously not the only mechanism reducing the cultivability of bacterial cells exposed to a hypertonic environment. Another harmful consequence of osmotic upshock is cell dehydration, which can cause denaturation of proteins and other macromolecules, leading to irreversible loss of their biological activity. Therefore, it was also investigated how the presence of PHB granules in bacterial cells influences the critical water content (the water content at the moment of a sudden change in the drying mechanism) in bacterial cells exposed to hyperosmotic conditions (Fig. 7). In agreement with previous reports [34], it was observed that the critical water content is considerably lower in PHB-containing bacterial strains of *C. necator* than in PHB non-containing cells prior to their exposure to osmotic challenge (Fig. 7A). Nevertheless, when cells were exposed to hyperosmotic conditions, the PHB-non containing culture underwent more pronounced elimination of this more strongly-bound water than the PHB-containing strain (Fig. 7B).

In general, it is difficult to interpret the exact origin of the critical water content without further empirical justification, because the bacteria studied represent a complex combination of diverse aqueous structures. This is especially true for osmotically challenged plasmolysed cultures with a growing periplasmatic volume. The simplified interpretation by Uribelarrea et al. [25] and others that the critical water content equals the total content of water in the cell seems inappropriate in the case of plasmolysed cell samples, because such a massive decrease in total intracellular (i.e. cytoplasmic plus periplasmatic) water would inevitably be accompanied by a significant decrease in the total cell volume. In fact, no such decrease in the volume delimited by the outer membrane of the cell was found in the TEM microphotographs of the PHB negative cells.

On the other hand, the value of the observed decrease in the critical water content for both PHB positive and negative cells is in striking accord with the relative volume of the periplasmatic space, estimated from the image analysis of TEM microphotographs. This indicates that the critical volume content could be closely linked to the water content in the cell cytoplasm. In fact, the quantity of cytoplasmic water, calculated from the TGA experiment, may be underestimated for PHB negative cells as a result of leakage from the damaged cytoplasmic membrane, indicated by the results of electron and fluorescence microscopy analyses. Nevertheless, it seems that the presence of PHB granules protects cells against the intensive loss of water from the cytoplasm. Our results are in agreement with those of Kadouri et al., who observed that the mutant strain of *Azospirillum brasilense* incapable of intracellular PHB hydrolysis is more resistant to desiccation than its parental strain, suggesting that the presence of intracellular polyester itself may be needed to protect the cell against the harmful effects of desiccation and dehydration [41].

Conclusions

Using *Cupriavidus necator* H16 and its PHB non-accumulating mutant strain it was demonstrated that presence of PHB granules in cytoplasm of bacterial cells substantially improves stress resistance of the bacterial culture against osmotic up-shock. Surprisingly, bacterial cells did not utilize PHB to harvest carbon or energy in order to cope with osmotic stress, which can be attributed to partial crystallization of PHB granules in challenged cells. The results show that the effect of PHB is rather indirect since the presence of PHB granules influences overall properties of the bacterial cells reducing membrane damage caused by plasmolysis and, moreover, it seems that PHB granules themselves are able to partially repair and stabilize membranes of challenged cells. Nevertheless, PHB granules in bacterial cells exposed to osmotic upshock aggregate, which probably complicates further division and reproduction of the bacterial cells.

Since *C. necator* PHB-4 is a chemically induced mutant, it would be useful to include a complementation control (reintroduction of a wild type PHB synthase gene copy into PHB^{-4}) or to perform the study with a chromosomal PHB synthase and/or PHB depolymerase gene deletion mutant of the wild type. A follow-up study focused on the osmotic down-shock would be welcome in order to complete the overall concept of the role of PHB granules in the response of bacteria to osmotic stress.

Conflict of interest

The authors declare no conflicts of interest.

Funding

This study was funded by the project "Materials Research Centre at FCH BUT – Sustainability and Development" No. LO1211 of the Ministry of Education, Youth and Sports of the Czech Republic and by the project GP15-20645S of the Czech Science Foundation (GACR).

Acknowledgment

Authors kindly thank to Leona Kubikova for all the help with TGA measurement.

Appendix A. Supplementary data

Supplementary data associated with this article can be found, in the online version, at http://dx.doi.org/10.1016/j.nbt.2017.07.008.

References

[1] Morbach S, Kramer R. Body shaping under water stress: osmosensing and osmoregulation of solute transport in bacteria. Chembiochem 2002;3:384–97.
[2] Wood JM. Bacterial responses to osmotic challenges. J Gen Physiol 2015;145:381–8.
[3] Koch AL. The geometry and osmotic relations of plasmolysis spaces in bacteria and the role of endocytosis, tubular structures and Scheie structures in their formation. J Theor Biol 1995;176:471–92.
[4] Korber DR, Choi A, Wolfaardt GM, Caldwell DE. Bacterial plasmolysis as a physical indicator of viability. Appl Environ Microbiol 1996;62:3939–47.
[5] Schwarz H, Koch AL. Phase and electron microscopic observation of osmotically induced wrinkling and the role of endocytotic vesicles in the plasmolysis of the gram-negative bacteria. Microbiology 1995;141:3161–70.
[6] Khosravi-Darani K, Mokhtari ZB, Amai T, Tanaka K. Microbial production of poly(hydroxybutyrate) from C1 carbon sources. Appl Microbiol Biotechnol 2013;97:1407–24.
[7] Tan GYA, Chen CL, Li L, Ge L, Wang L, et al. Start a research on biopolymer polyhydroxyalkanoate (PHA): a review. Polymers 2014;6:706–54.
[8] Chen GQ, Hajnal I. The'PHAome'. Trends Biotechnol 2015;33:559–64.
[9] Johnson K, Jiang Y, Kleerebezem R, Muyzer G, van Loosdrecht MCM. Enrichment of a mixed bacterial culture with a high polyhydroxyalkanoate storage capacity. Biomacromolecules 2009;10:670–6.
[10] Mravec F, Obruca S, Krzyzanek V, Sedlacek P, Hrubanova K, et al. Accumulation of PHA granules in *Cupriavidus necator* as seen by confocal fluorescence microscopy. FEMS Microbiol Lett 2016363: 0.1093/femsle/fnw094.
[11] Vadlja D, Koller M, Novak M, Brauneg G, Horvat P. Footprint area analysis of binary imaged *Cupriavidus necator* cells to study PHB production at balanced, transient, and limited growth conditions in a cascade process. Appl Microbiol Biotechnol 2016;100:10065–80.
[12] Kadouri D, Jurkevitch E, Okon Y. Ecological and agricultural significance of bacterial polyhydroxyalkanoates. Crit Rev Microbiol 2005;31:55–67.
[13] Zhao YH, Li HM, Qin LF, Wang HH, Chen GQ. Disruption of the polyhydroxyalkanoate synthase gene in *Aeromonas hydrophila* reduces its survival ability under stress conditions. FEMS Microbiol Lett 2007;276:34–41.
[14] Breedveld MW, Dijkema C, Zevenhuizen LPTM, Zehner AJB. Response of intracellular carbohydrates to NaCl shock in *Rhizobium leguminosarum* biovar triforii TA-1 and *Rhizobium meliloti* SU-47. J Gen Microbiol 1993;139:3157–63.
[15] Wang Q, Yu H, Xia Y, Kang Z, Qi Q. Complete PHB mobilization in *Escherichia coli* enhances the stress tolerance: a potential biotechnological application. Microb Cell Fact 20098(47), doi:http://dx.doi.org/10.1186/1475-2859-8-47.
[16] Obruca S, Marova I, Svoboda Z, Mikulikova R. Use of controlled exogenous stress for improvement of poly(3-hydroxybutyrate) production in *Cupriavidus necator*. Folia Microbiol 2010;55:17–22.
[17] Passanha P, Kedia G, Dinsdale RM, Guwy AJ, Esteves SR. The use of NaCl addition for the improvement of polyhydroxyalkanoate production by *Cupriavidus necator*. Bioresource Technol 2014;163:287–94.
[18] Hermann-Krauss C, Koller M, Muhr A, Fasl H, Stelzer F, Braunegg G. Archaeal production of polyhydroxyalkanoate (PHA) co- and terpolyesters from biodiesel industry-derived by-products. Archaea 2013 art. no. 129268.
[19] Yin J, Chen JC, Wu Q, Chen GQ. Halophiles, coming stars for industrial biotechnology. Biotechnol Adv 2015;33:1433–42.
[20] Rodríguez-Contreras A, Koller M, Braunegg G, Marqués-Calvo MS. Poly [(*R*)-3-hydroxybutyrate] production under different salinity conditions by a novel *Bacillus megaterium* strain. New Biotechnol 2016;33:73–7.
[21] Reinecke F, Steinbuchel A. *Ralstonia eutropha* Strain H16 as model organism for PHA metabolism and for biotechnological production of technically interesting biopolymers. J Mol Microbiol Biotechnol 2009;16:91–108.
[22] Raberg M, Voigt B, Hecker M, Steinbuchel A. A closer look on the polyhydroxybutyrate- (PHB-) negative phenotype of *Ralstonia eutropha* PHB-4. PLoS One 2014;9:e95907, doi:http://dx.doi.org/10.1371/journal.pone.0095907.
[23] Coder DM. Assessment of cell viability. Curr Protocols Cytometry 1997 9.2. 1-9.2.14.
[24] Obruca S, Benesova P, Oborna J, Marova I. Application of protease-hydrolyzed whey as a complex nitrogen source to increase poly(3-hydroxybutyrate) production from oils by *Cupriavidus necator*. Biotech Lett 2014;36:775–81.
[25] Uribelarrea JL, Pacaud S, Goma G. New method for measuring the cell water-content by thermogravimetry. Biotechnol Lett 1985;7:75–80.
[26] Jendrossek D. Peculiarities of PHA granules preparation and PHA depolymerase activity determination. Appl Microbiol Biotechnol 2007;74:1186–96.
[27] Furukawa T, Sato H, Murakami R, Zhang J, Noda I, Ochiain S, et al. Raman microspectroscopy study of structure, dispersibility, and crystallinity of poly (hydroxybutyrate)/poly(L-lactic acid) blends. Polymer 2006;47:3132–40.
[28] Izumi CMS, Temperini MLA. FT-Raman investigation of biodegradable polymers: poly(3-hydroxybutyrate) and poly(3-hydroxybutyrate-co-3-hydroxyvalerate). Vibr Spectrosc 2010;54:127–32.
[29] Samek O, Obruča S, Šiler M, Sedláček P, Benešová P, et al. Quantitative Raman spectroscopy analysis of polyhydroxyalkanoates produced by *Cupriavidus necator* H16. Sensors 201616:, doi:http://dx.doi.org/10.3390/s16111808.
[30] Dunlop WF, Robards AW. Ultrastructural study of poly-β-hydroxybutyrate granules from *Bacillus cereus*. J Bacteriol 1973;114:1271–80.
[31] Sudesh K, Fukui T, Iwata T, Doi Y. Factors affecting the freeze-fracture morphology of in vivo polyhydroxyalkanoate granules. Can J Microbiol 2000;45:304–11.
[32] Dvorak P, Chrast L, Nikel PI, Fedr R, Soucek K, et al. Exacerbation of substrate toxicity by IPTG in *Escherichia coli* BL21(DE3) carrying a synthetic metabolic pathway. Microb Cell Fact 201514(201), doi:http://dx.doi.org/10.1186/s12934-015-0393-3.
[33] Swaminathan R, Hoang CP, Verkman AS. Photobleaching recovery and anisotropy decay of green fluorescent protein GFP-S65T in solution and cells: cytoplasmic viscosity probed by green fluorescent protein translational and rotational diffusion. Biophys J 1997;72:1900–7.
[34] Obruca S, Sedlacek P, Krzyzanek V, Mravec F, Hrubanova K, et al. Accumulation of poly(3-hydroxybutyrate) helps bacterial cells to survive freezing. PLoS One 2016;11:e0157778, doi:http://dx.doi.org/10.1371/journal.pone.0157778.
[35] Alcazar EB, Rocha-Leao MHM, Dweck J. Yeast intracellular water determination by thermogravimetry. J Therm Anal Calorim 2000;59:643–8.
[36] Ilmer P, Erlebach C, Schinner F. A practicable and accurate method to differentiate between intra- and extracellular water of microbial cells. FEMS Microbiol Lett 1999;178:135–9.
[37] Wu D, He J, Gong Y, Chen D, Zhu X, et al. Proteomic analysis reveals the strategies of *Bacillus thuringiensis* YBT-1520 for survival under long-term heat stress. Proteomics 2011;11:2580–91.
[38] Iustman LJR, Tribelli PM, Ibarra JG, Catone MV, Venero ECS, Lopez NI. Genome sequence analysis of *Pseudomonas extremaustralis* provides new insights into environmental adaptability and extreme conditions resistance. Extremophiles 2015;19:207–20.

[39] Pavez P, Castillo JL, Gonzales C, Martinez M. Poly-β-hydroxyalkanoate exert protective effect against carbon starvation and frozen conditions in *Sphingopyxis chilensis*. Curr Microbiol 2009;59:636–40.
[40] Goh L-K, Purama RK, Sudesh K. Enhancement of stress tolerance in polyhydroxyalkanoate producers without mobilization of the accumulated granules. Appl Biochem Biotechnol 2014;172:1585–98.
[41] Kadouri D, Jurkevitch E, Okon Y. Poly-β-hydroxybutyrate depolymerase (PhaZ) in *Azospirillum brasilense* and characterization of a *phaZ* mutant. Arch Microbiol 2005;180:309–18.
[42] Roberts MF. Organic compatible solutes of halotolerant and halophilic microorganisms. Saline Systems 20051(5), doi:http://dx.doi.org/10.1186/1746-1448-1-5.
[43] Obruca S, Sedlacek P, Mravec F, Samek O, Marova I. Evaluation of 3-hydroxybutyrate as an enzyme-protective agent against heating and oxidative damage and its potential role in stress response of poly(3-hydroxybutyrate) accumulating cells. Appl Microbiol Biotechnol 2016;100:1365–76.
[44] Barnard GN, Sanders JKM. The poly-β-hydroxybutyrate granule in vivo: a new insight based on NMR spectroscopy of whole cells. J Biol Chem 1989;264:3286–91.
[45] Bonthrone KM, Clauss J, Horowitz DM, Hunter BK, Sanders JKM. The biological and physical chemistry of polyhydroxyalkanoates as seen by NMR spectroscopy. FEMS Microbiol Lett 1992;103:269–77.
[46] Jendrossek D, Pfeiffer D. New insights in the formation of polyhydroxyalkanoate granules (carbonosomes) and novel functions of poly (3-hydroxybutyrate). Environ Microbiol 2014;16:2357–73.
[47] Bresan S, Sznajder A, Hauf W, Forchhammer K, Pfeiffer D, Jendossek D. Polyhydroxyalkanoate (PHA) granules have no phospholipids. Sci Rep 2016;6:26612, doi:http://dx.doi.org/10.1038/srep26612.
[48] Harry E, Monahan L, Thompson L. Bacterial cell division: the mechanism and its precison. Int Rev Cytol 2006;253:27–94.

Applied Microbiology and Biotechnology (2018) 102:1923–1931
https://doi.org/10.1007/s00253-018-8760-8

APPLIED MICROBIAL AND CELL PHYSIOLOGY

Light scattering on PHA granules protects bacterial cells against the harmful effects of UV radiation

Eva Slaninova[1] · Petr Sedlacek[1] · Filip Mravec[1] · Lucie Mullerova[1] · Ota Samek[2] · Martin Koller[3,4] · Ondrej Hesko[1] · Dan Kucera[1] · Ivana Marova[1] · Stanislav Obruca[1]

Received: 12 September 2017 / Revised: 3 January 2018 / Accepted: 4 January 2018 / Published online: 19 January 2018

Abstract
Numerous prokaryotes accumulate polyhydroxyalkanoates (PHA) in the form of intracellular granules. The primary function of PHA is the storage of carbon and energy. Nevertheless, there are numerous reports that the presence of PHA granules in microbial cells enhances their stress resistance and fitness when exposed to various stress factors. In this work, we studied the protective mechanism of PHA granules against UV irradiation employing *Cupriavidus necator* as a model bacterial strain. The PHA-accumulating wild type strain showed substantially higher UV radiation resistance than the PHA non-accumulating mutant. Furthermore, the differences in UV-Vis radiation interactions with both cell types were studied using various spectroscopic approaches (turbidimetry, absorption spectroscopy, and nephelometry). Our results clearly demonstrate that intracellular PHA granules efficiently scatter UV radiation, which provides a substantial UV-protective effect for bacterial cells and, moreover, decreases the intracellular level of reactive oxygen species in UV-challenged cells. The protective properties of the PHA granules are enhanced by the fact that granules specifically bind to DNA, which in turn provides shield-like protection of DNA as the most UV-sensitive molecule. To conclude, the UV-protective action of PHA granules adds considerable value to their primary storage function, which can be beneficial in numerous environments.

Keywords Polyhydroxyalkanoates · *Cupriavidus necator* · UV radiation · Turbidity · Integrating sphere · Nephelometry

Introduction

Bacteria are fascinating organisms due to their capability to cope with widely fluctuating environmental conditions such as changes in nutrient availability, temperature, pH value, or osmolarity. In addition, also radiation, which can be defined as energy manifested in the form of electromagnetic waves, can be considered an important stress factor and occurs in numerous ecological niches. UV radiation in sunlight is among the most common stressors and has many harmful impacts on living cells such as induction of oxidative pressure or the inducing of fatal changes to the molecular structure mainly of DNA, but also of RNA, lipids, and proteins (Gabani and Singh 2013). Generally, UV radiation is considered to be one of the most detrimental abiotic factors influencing microorganisms at both the community and single-cell level, thus severely affecting the diversity and dynamics of microbial communities. Moreover, it is expected that by the end of the twenty-first century, the intensity of UV radiation at the Earth's surface will increase by approximately 5–10% in temperate latitudes and by about 20% in high latitudes (Pérez et al. 2017). It can therefore be expected that the evolutionary significance of UV radiation and ability to face this stressor may even increase.

To cope with UV radiation, bacteria—and among them especially extremophiles inhabiting harsh environments exposed to harmful solar radiation—have evolved various strategies mainly based on efficient DNA repair mechanisms and active defense against UV-induced oxidative stress. Moreover,

✉ Stanislav Obruca
Stana.O@seznam.cz

[1] Faculty of Chemistry, Brno University of Technology, Purkynova 118, 612 00 Brno, Czech Republic

[2] Institute of Scientific Instruments, Academy of Sciences of The Czech Republic, Vvi, Kralovopolska 147, 612 64 Brno, Czech Republic

[3] Institute of Chemistry, NAWI Graz, University of Graz, Heinrichstrasse 28/III, 8010 Graz, Austria

[4] ARENA Arbeitsgemeinschaft für Ressourcenschonende and Nachhaltige Technologien, Inffeldgasse 21b, 8010 Graz, Austria

many pro- and eukaryotic microorganisms also rely on production of UV-protective metabolites such as pigments, mycosporine-like amino acids, scytonemin, ectoines, bacterioruberin, sphaerophorin, pannarin, or melanin (Koller et al. 2014; Singh and Gabani 2011).

Polyhydroxyalkanoates (PHAs) are polyesters accumulated by numerous prokaryotes in the form of intracellular granules (Tan et al. 2014). The number of granules can reach up to 10–15 granules per cell and their average diameter is about 200–400 nm, though individual values particularly depend upon the specific microorganism and the physiological state of the bacterial culture (Vadlja et al. 2016). The weight content of PHA in bacterial cells can reach up to 90% of cell dry weight, though bacteria regulate their diameters to confine the volumetric content of PHA granules at a level below 40 vol% (Mravec et al. 2016). The PHA polymer itself represents the hydrophobic core of the granules which is covered by numerous specific proteins with various functions. These proteins include PHA synthase, PHA depolymerases, regulatory proteins, and various PHA granule structural proteins which create a functional interface between the hydrophobic polymer and water-containing cytoplasm. These proteins are also responsible for intracellular localization of granules within bacterial cells. To emphasize their complexity and multifunctionality as de facto organelles, these granules are also referred to as "carbonosomes" (Jendrossek 2009).

The primary function of PHAs is the storage of carbon and energy. However, recent research has shown that the biological function of PHAs is much more complex and that the capability to accumulate PHA has many biochemical and biophysical consequences, enhancing the survival and fitness of bacterial cells when exposed to numerous stress factors including but not limited to high temperature (Pham 2004; Wu et al. 2011), low temperature (Tribelli and Lopez 2011), freezing (Obruca et al. 2016a; Pavez et al. 2009), or osmotic upshock (Obruca et al. 2017).

Moreover, there are reports stating that the presence of PHA granules in microbial cells also protects bacteria against UV radiation. For instance, a protective effect of PHA granules in bacterial cells against UV irradiation was observed in *Azospirillum brasilense* when PHA-rich (about 40 wt.% of PHA in cell dry weight) and PHA-poor cells (about 5 wt.% of PHA in cell dry weight) were compared (Tal and Okon 1985). The importance of PHA for the UV-radiation survival of *A. brasilence* was confirmed in following studies by Kadouri et al., who observed that the wild type was more resistant to numerous stressors, including UV radiation, than the PHA synthase deletion mutant incapable of accumulating PHA (Kadouri et al. 2003a). It was also more resistant than the PHA depolymerase deletion mutant, which was not capable of PHA hydrolysis (Kadouri et al. 2003b). Similarly, Zhao et al. (2007) compared the stress resistance of the wild type of *Aeromonas hydrophila* and its PHA synthase negative mutant incapable of PHA synthesis. As the major outcome, the wild type was substantially more resistant to several stress factors, including UV irradiation. Furthermore, the UV-radiation protective capacity of PHA granules was also confirmed with genetically modified *Escherichia coli* which harbored genes enabling either PHA biosynthesis or both PHA biosynthesis and hydrolysis. Both transgenic strains were more resistant to UV radiation and other stress factors than the PHA non-producing wild type (Wang et al. 2009).

Nevertheless, despite the fact that numerous studies have reported that the presence of PHA granules in microbial cells provides protection against UV radiation; to our best knowledge, there are no studies exploring the potential mechanism of the protective action. Therefore, we experimentally confirmed the UV-protecting effect of PHA granules for *Cupriavidus necator*, a soil bacterium which is considered the most important model strain for PHA metabolism. Subsequently, various spectroscopic approaches were employed to shed light on the interaction of PHA granules in bacterial cells with UV radiation and to provide an explanation for their UV-protective mechanism.

Materials and methods

Microorganisms and cultivation

The PHA-producing strain *Cupriavidus necator* H16 (CCM 3726) was obtained from the Czech Collection of Microorganisms, Brno, Czech Republic, and its PHA non-producing mutant strain *Cupriavidus necator* PHB^{-4} (DSM-541) was purchased from the Leibnitz Institute DSMZ-German Collection of Microorganism and Cell Cultures, Braunschweig, Germany.

Cultivations were performed in Erlenmeyer flasks (volume 250 mL) containing 100 mL of mineral salt (MS) medium. The composition of the MS medium was 20 g fructose, 1 g $(NH_4)_2SO_4$, 1 g KH_2PO_4, 11.1 g $Na_2HPO_4 \cdot 12\ H_2O$, 0.2 g $MgSO_4 \cdot 7\ H_2O$, 1 mL of microelement solution, and 1 L of distilled water; the microelement solution in turn was composed of 9.7 g $FeCl_3$, 7.8 g $CaCl_2$, 0.156 g $CuSO_4 \cdot 5\ H_2O$, 0.119 g $CoCl_2$, and 0.118 g $NiCl_2$ in 1 L of 0.1 M HCl. The flasks were inoculated with 5 mL of an overnight culture of a particular strain of *C. necator* grown in Nutrient Broth medium consisting of 10 g peptone, 10 g beef extract, and 5 g NaCl in 1 L of distilled water. The cells were cultivated for 72 h. The PHA content in microbial cells was determined by gas chromatography as described previously (Obruca et al. 2014).

UV challenge of bacterial strains C. necator H16 and C. necator PHB^{-4}

The suspension of bacterial cells cultivated for 72 h as described above was first diluted 30 times. Thereafter, the suspension of bacterial cells of *Cupriavidus necator* H16 was diluted to reach the cell density of the suspension of its mutant strain *Cupriavidus necator* PHB^{-4}. The solutions thus prepared were further diluted into approx. 10^8 CFU and 3 mL of the cell suspension was placed on a sterile Petri dish to form a thin layer (approx. 1 mm). After this, cells were exposed to UV radiation emitted by an UVA lamp (400–320 nm, height 25 cm) and samples were taken at regular intervals (15, 30, 45 min). From these samples, the number of viable cells was determined as CFU by plating of appropriately diluted cell suspensions on NB agars.

UV-Vis spectroscopy and nephelometry of bacterial cells

For UV-Vis spectroscopy characterization, the same cultivation suspension as described above was used. Firstly, both the suspension of bacterial cells of *C. necator* H16 and the suspension of its mutant bacterial strain were diluted step by step five times. The dilution process was repeated until the final solutions were diluted by a factor of 100. All solutions prepared this way were analyzed by UV-Vis absorption spectrophotometry (in a U-3900H, Hitachi) both in a regular transmission measurement mode and also in a spatially integrating mode (integration sphere attachment 60mmDIA for Hitachi U-3900H spectrophotometer). Simultaneously with the preparation of samples for UV-Vis spectroscopy, the number of viable cells was determined as described above.

Similarly, diluted bacterial suspensions of defined cell concentration were also investigated by means of nephelometry. As a simple nephelometer, we used a fluorometer (AMINCO-Bowman Series 2 luminescence spectrometer, Thermo Inc.) which was employed to detect scattered light at a fixed scattering angle of 90° to the incidental beam. Furthermore, this device offers the advantageous possibility of using different wavelengths ranging from 250 nm (ozone-free xenon lamps lowest wavelength) to approximately 850 nm (highest range of PMT detectors). To suppress detection of fluorescence or phosphorescence, which is common for biological samples at different excitation wavelengths (~340 nm for NADH, ~470 nm for flavonoids, etc.) a synchronous scan method was applied, where excitation and emission monochromators were set to the zero wavelength difference during scanning. In order to obtain more accurate results and also to protect the detector, slits were set to the minimum (1 nm bandpass). To compensate for the non-flat intensity profile of the excitation source (a 150-W xenon lamp), intensity was detected relative to the diode. The scan rate was set to 5 nm·s^{-1} and spectra were collected with a 1-nm resolution in the range 250–700 nm.

Analysis of intracellular ROS by flow cytometry

Determination of the intracellular level of reactive oxygen species (ROS) in bacterial cells of *C. necator* H16 and *C. necator* PHB^{-4} before and after 15 min exposition to UV irradiation (in details described above) was performed by flow cytometry employing CM-H2CFDA (Thermo Fisher Scientific), a fluorescent stain used as general oxidative stress indicator. Suspensions of cells with cell density of approx. 10^6 cells per mL were washed twice with PBS buffer; after that, 5 μL of CM-H2CFDA dissolved in HPLC-grade DMSO (the final concentration of the stain in 1 mL of the sample was 5 μM) was added to the suspensions, and the cells were then left to incubate in the dark at laboratory temperature for 10 min. After that, the fluorescence of stained as well as non-stained cells was immediately measured at single-cell level using the green fluorescence collecting channel (535 ± 35 nm) of the used flow cytometer (Apogee A50, ApogeeFlow Systems).

Results

UV exposure of C. necator cells

In the first experiment, cells of the PHA-accumulating strain *C. necator* H16 (the PHA content in microbial cells was 74% of cell dry weight as determined by gas chromatography) and its mutant strain which is not capable of accumulating PHA due to a mutation of the PHA synthase (Raberg et al. 2014) were exposed to a UV challenge. The viability of both bacterial strains was assessed during their exposition to UV irradiation in regular intervals; the results, expressed as the percentage of viable cells, are shown in Fig. 1. Generally, the PHA-containing culture demonstrated substantially higher resistance to UV radiation during the entire period of UV exposure, thus confirming the UV-protective effect of PHA granules which has been reported also for other microbial strains (Kadouri et al. 2003a, b; Tal and Okon 1985; Wang et al. 2009; Zhao et al. 2007). The decrease in viability of reference samples of both cultures, which were exposed to the same conditions but without being UV irradiated, was negligible (< 5%). Therefore, it can be stated that accumulation of PHA granules in cytoplasm represents a potent and generally observed strategy which protects bacterial cells from the harmful effects of UV irradiation.

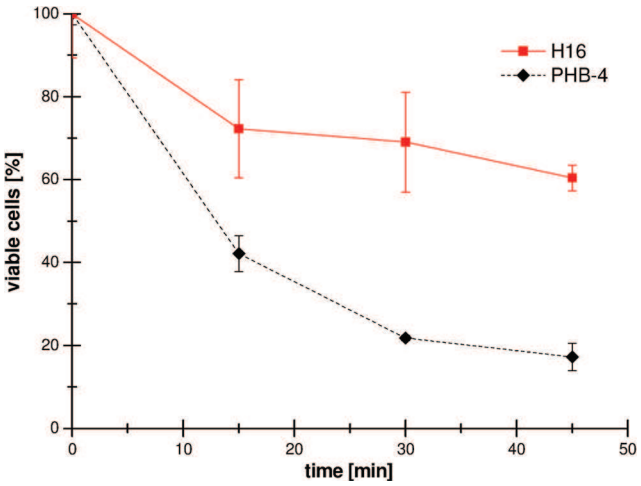

Fig. 1 Survival of both strains of *C. necator* during their exposition to UV irradiation

UV-Vis spectroscopy of bacterial cells

In order to understand how intracellular PHA granules interact with light, complex spectroscopic characterizations of the cell dispersions in the ultraviolet and the visible region were performed both for the PHA-accumulating strain (*C. necator* H16) and the non-accumulating mutant (*C. necator* PHB^{-4}). Three different optical arrangements were used for this purpose.

Firstly, turbidity measurements were performed using a standard UV-Vis spectrometer, where the intensity of the transmitted light is measured and optical density is calculated for the particular wavelength of the incident light. As the wavelengths are altered to cover the whole UV-Vis region, spectra such as those shown in Fig. 2a are collected. It is evident that except for the shortest measured wavelengths (close to 200 nm), the PHA-accumulating strain shows a significantly higher optical density of the cell dispersion with comparable cell density compared to the non-accumulating strain. It should be emphasized that the optical density measured this way comprises two individual contributions. On the one hand, the intensity of the transmitted light is decreased via absorption of the specific wavelengths by the photoactive cell components. Absorption of the radiant energy then initiates diverse photophysical (e.g., light emission in the form of fluorescence) or photochemical processes, where the latter ones may often (mainly in the case of light in the UV spectral region) have harmful or even fatal effects on the cell fitness. The other contribution to the optical density is represented by the light scattered away from the direction of the incident beam. Unlike the light absorption, light scattering is rarely damaging. On the contrary, it can even have a protective "shielding" effect on the photo-labile cell components caused by attenuation of the local intensity of the incident light in the cell, which might reduce the level of cell damage (Paunescu

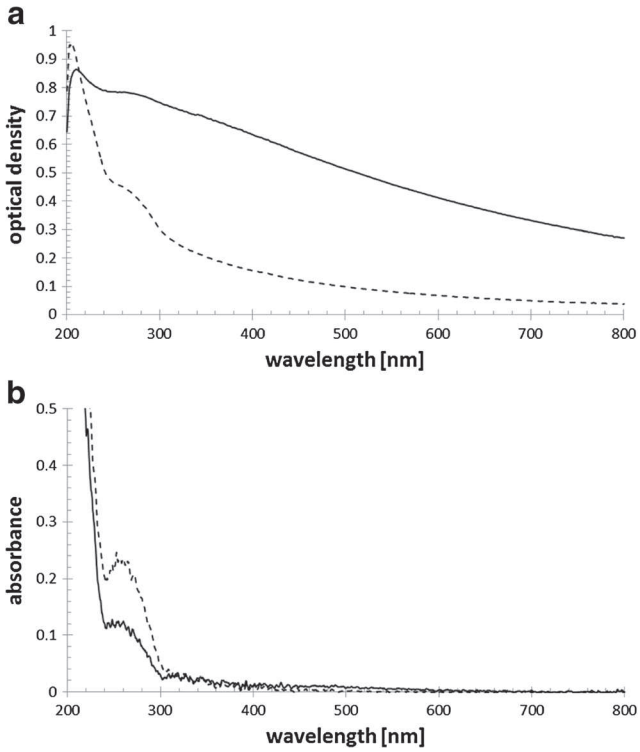

Fig. 2 Example of typical UV-Vis spectra of *C. necator* H16 (full line) and *C. necator* PHB^{-4} (dashed line). **a** Turbidity measurement of dispersions with cell density 1×10^6 CFU. **b** Absorbance measurement of dispersions with cell density 1×10^6 CFU

et al. 2014). Therefore, turbidity measurements such as those described above do not provide a relevant explanation of a harmful effect of light on the cells with light because they provide no direct information about the relative involvement of the light absorption and light scattering, respectively, in the interaction of the cells and their constituent with light.

With respect to this, we further measured the spectra of cell dispersions using the same UV-Vis spectrometer equipped with an integrating sphere accessory, specially designed for the absorbance measurement of turbid samples. Examples of the collected spectra are shown in Fig. 2b. In these spectra, effective suppression of the light-scattering artifacts can be clearly seen. No significant light absorption was found in the Vis region, which confirms the assumption that in this wavelength region, the optical density of the sample can be interpreted solely as a consequence of light scattering. With respect to this finding, additional interesting outcomes can further be deduced from the previously described differences in the turbidity spectra of dispersions of PHA-accumulating and non-accumulating strains with the same cell density. Generally, a significant increase in light scattering in the case of the PHA-accumulating cells of the *C. necator* H16 strain is evidently caused by light scattering on the cell ultrastructure, namely on the PHA granules present in the cell cytoplasm.

Figure 3 presents results from both types of spectroscopic assays in a more quantitative way. Fig. 3a shows very good

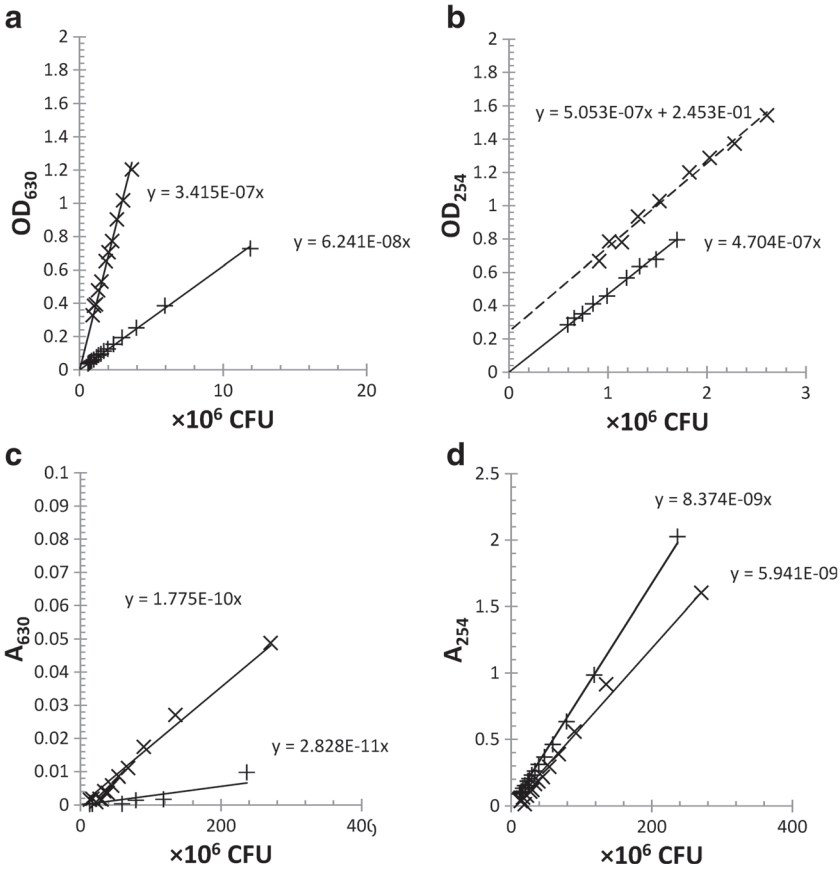

Fig. 3 Summarized results from UV-Vis turbidimetry and absorbance assays of cell suspensions of PHA-accumulating *C. necator* H16 strain (×) and PHA non-accumulating *C. necator* PHB^{-4} strain (+), respectively. **a**, **b** Dependency of optical density at 630 and 254 nm on cell density. **c**, **d** Dependency of absorbance at 630 and 254 nm on cell density

linearity of the dependency of optical density at 630 nm on the cell density for both strains. Evidently, light-scattering effects are cumulative regardless of a contribution of the light scattered by PHA granules. OD_{630} appears to represent a robust parameter suitable for quantification of cell density. Nevertheless, careful calibration is needed wherever intracellular light scatters occur, as is the case when PHA granules or other cell inclusions occur. However, it is evident from Fig. 3b that in the case of *C. necator* H16 strain, contributions of light scattering and light absorption in UV wavelength region are no longer cumulative (the dashed fitting line does not cross the origin of coordinates). Nevertheless, in this region, the crucial results are shown in Fig. 3d where a relative decrease of around 30% in the single cell absorption coefficient at 254 nm can be deduced. Finally, Fig. 3c is shown in order to illustrate the negligible residual apparent absorbance of the cell suspensions in the VIS region. This apparent absorbance represents an experimental artifact coming from the scattered light which does not reach the aperture of the integrating sphere.

In order to provide an experimental verification of the assumption that the difference between the optical density and absorbance of the cell suspensions is correctly assigned to the intensity of scattered light, we performed also a basic nephelometry assay of the same samples. Measurement was done with the synchronous scan method as was described above. We focused on monitoring the changes in scattered light intensity between the PHA-accumulating and non-accumulating strain suspension of the same cell density, where a high sensitivity of the fluorimeter photomultiplier and its strong light source provide an undisputed instrumental advantage. Figure 4 shows the ratio of the intensities of scattered light normalized per unit CFU for *C. necator* H16 and *C. necator* PHB^{-4}, respectively, vs. the wavelength. We use this means of data demonstration in order to suppress experimental artifacts coming from uneven light intensity emitted from the xenon lamp of the fluorimeter at different wavelengths (we assume that the results for both strains will be affected equally).

From the spectrum, it is evident that the nephelometry experiments confirmed the higher intensity of scattered light for the PHA-accumulating strain in the whole tested optical region. Furthermore, the relative efficiency of light scattering by the PHA producer as compared to the mutant strain increases significantly in the UV-region, where the light absorbance measurement revealed the most profound differences in intensity in the light absorption of the two strains. This finding was reproducible as far as similar results were found regardless of the particular suspension cell density. Therefore, it can be summarized that nephelometry confirmed the conclusions of the previous two spectroscopic assays.

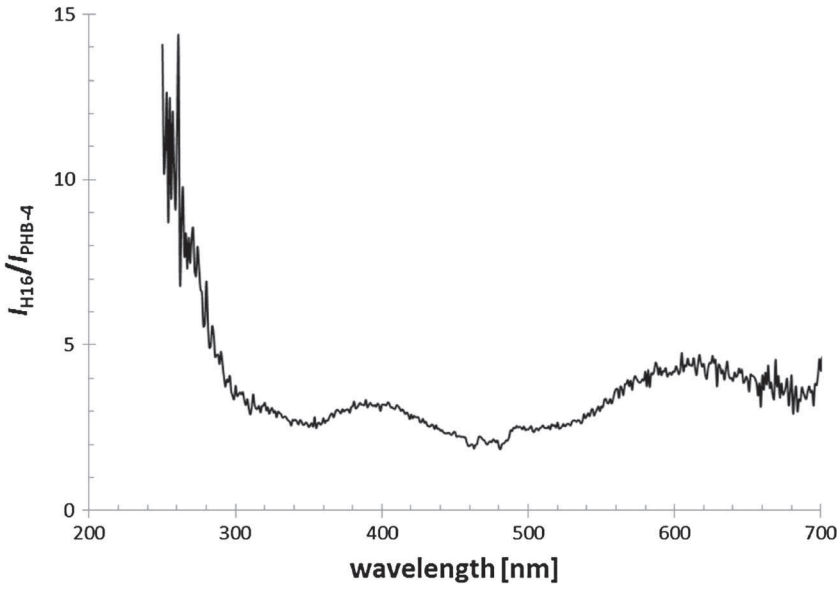

Fig. 4 Ratio of the intensities of single-cell scattered light for *C. necator* H16 strain and PHA non-accumulating *C. necator* PHB^{-4} strain at 90° as determined by nephelometry

ROS analysis by flow cytometry

To investigate whether scattering of UV irradiation on PHA granules influences the intracellular level of ROS in UV-challenged cells, the amount of ROS before and after UV exposition was analyzed by flow cytometry employing fluorescent stress indicator CM-H2CFDA. Green fluorescence of this stain is activated by its reaction with ROS (Dong et al. 2015). Hence, at single-cell level, we analyzed intensity of green fluorescence of both bacterial cultures prior and after their exposition to UV irradiation in stained as well as non-stained bacterial cells; the results are demonstrated in Fig. 5. The mean value of intensity of green fluorescence of PHA granules containing bacterial was only slightly (approx. 10%) increased after exposition of the cells to UV irradiation. On the contrary, when the culture of cells not containing PHA granules was exposed to UV irradiation, green autofluorescence of non-stained cells increased about 1.8-fold and, moreover, green fluorescence of CM-H2CFDA stained cells raised 3.6-fold. This clearly indicates that UV irradiation induces formation of substantially higher amount of ROS in PHA negative cells than in PHA-rich cells.

Discussion

Solar UV radiation on Earth can be considered an important stress factor which influences numerous living systems. Therefore, the influence of UV radiation on whole ecosystems has been studied for various aquatic environments (Häder et al. 2007), or high-altitude regions (Farías et al. 2009; Pérez et al. 2017). Moreover, UV-radiation resistance is also an important topic for astrobiology (Khodadad et al. 2017). The harmful effect of UV radiation is complex and it includes

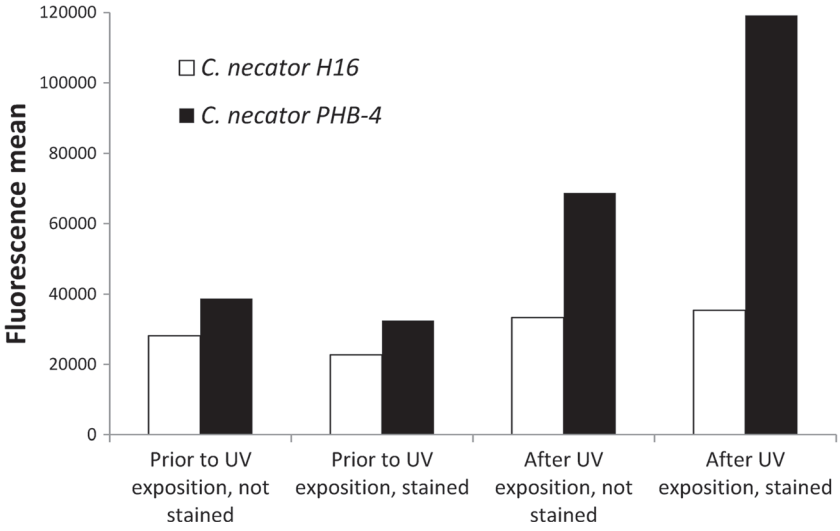

Fig. 5 Mean intensity of green fluorescence of stained and non-stained cells of *C. necator* H16 and *C. necator* PHB^{-4} prior and after UV exposition as determined by flow cytometry

numerous cell-damaging mechanisms. First and foremost, UV radiation is known for its mutagenic potential because DNA directly absorbs UVB radiation and this radiation induces numerous grave changes in DNA structure, among which the formation of dimeric pyrimidines, photo-adducts, and DNA–protein cross-links are considered the most important (Ravanat et al. 2001). Furthermore, despite the fact that DNA does not absorb UVA radiation, UVA can be absorbed by endogenous photosensitizers which may damage DNA throughout subsequent reactions (Ravanat et al. 2001). Apart from DNA, also other photosensitive biomolecules such as RNA, proteins, or lipids can be damaged by direct or indirect absorption of UV radiation, though changes in these molecules' structure do not have such fatal consequences as is the case for DNA due to their quick turnover. In addition, UV radiation induces the formation of reactive oxygen species (ROS) which may further damage crucial cell components such as DNA, RNA, proteins, and lipids (Kim et al. 2015).

There are numerous reports that the capability to accumulate PHA enhances the stress resistance of bacteria against various stressors (Ayub et al. 2009; Kadouri et al. 2003a, b; Obruca et al. 2016a, b, 2017; Tal and Okon 1985; Wang et al. 2009; Zhao et al. 2007). This can be considered an important "added value" to their primary biological function—storage of carbon, energy, and also reduction power. Generally, it has been observed that the presence of PHA granules influences the overall biophysical properties of bacterial cells, which further increases stress survival when they are exposed to various stress factors. For instance, the presence of PHA granules enhanced the rate of water transport out of the cells during freezing, which subsequently protected bacterial cells from formation of intracellular ice; this substantially contributes to PHA's cryo-protective effect (Obruca et al. 2016a). Moreover, PHA polymers in native intracellular granules represent a unique amorphous form of matter which resembles "supercooled" liquid in its properties (Bonthrone et al. 1992). The liquid-like properties of PHA granules seem to play a crucial role in the protective mechanism of PHA against osmotic upshock, since the presence of PHA granules turned out to reduce the level of plasmolysis in challenged cells and, moreover, according to the results of transmission electron microscopy analysis, PHA granules were even capable of stabilizing membranes of bacterial cells by closing the holes in the cytoplasmic membrane (Obruca et al. 2017). Therefore, even the simple presence of PHA granules in cytoplasm can be beneficial for bacterial cells when exposed to stress conditions.

Moreover, the enhancement of the UV resistance of PHA-accumulating bacteria which was reported in this work (Fig. 1), as well as by other authors (Kadouri et al. 2003a; Tal and Okon 1985; Wang et al. 2009; Zhao et al. 2007), is most likely primarily based on the biophysical consequence of the presence of PHA granules in cells. According to our results, PHA granules do not considerably absorb UV radiation but they are capable of efficient scattering of UV radiation as was indicated in the present study by the comparison of turbidity (Fig. 2a) and absorbance measurement (Fig. 2b) of the cells of PHA-accumulating *C. necator* and its PHA negative mutant. Furthermore, the fact that PHA granules efficiently scatter UV radiation was also confirmed by nephelometry measurement (Fig. 4). Because no considerable changes in cell dimensions were found for both strains in our previous work (Mravec et al. 2016), the significant increase in the light scattering of the *C. necator* H16 strain can be ascribed to the fraction of light scattered on the cell ultrastructure, namely on the PHA granules in the cell cytoplasm. This finding is in fact not surprising; a similar observation of an increase of the single cell light turbidity as a result of light scattering on inclusion bodies has previously been reported, e.g., for *E. coli* W3110 (Hwang and Feldberg 1990). Nevertheless, to the best of our knowledge, our results represent the first convincing experimental confirmation that intracellular PHA granules serve as effective in situ light-scatterers. Furthermore, according to the results presented in Fig. 2b, it is evident that UV radiation is absorbed by the bacterial cells quite effectively. The absorption band centered around 254 nm can be assigned to nucleic acid, especially to DNA. Nevertheless, from the comparison of the absorption spectra of cell suspensions with the same cell density, it can be seen that UV-radiation absorption in this wavelength region is considerably suppressed in the case of the PHA-accumulating strain. Bearing in mind that there is no significant difference in the cellular content of DNA for the two strains, this result supports the assumption of "shielding" effects of PHA granules resulting from their great light-scattering ability. Moreover, it can be stated that, apart from protecting DNA as the most sensitive molecule, scattering of UV irradiation on PHA granules also reduces level of intracellular ROS (see Fig. 5) generated by UV radiation. This new finding very likely substantially contributes to complex UV-protective function of PHA granules.

It should be pointed out that in natural producers, PHA granules are not randomly distributed in bacterial cells, but they are specifically attached to DNA. In *C. necator*, the attachment is performed via the protein PhaM which simultaneously binds to DNA and the PHA associated-protein PhaP5 (Wahl et al. 2012). Similarly, in *Pseudomonas putida*, the binding of PHA granules to DNA is enabled by the protein PhaF. This protein serves as a transcriptional regulator of PHA metabolism but it is also responsible for proper segregation of granules during cell division and ensures, under balanced conditions, equal distribution of granules between daughter cells. PhaF directs the PHA granules to the center of the cells, forming a characteristic needle array in the close vicinity of DNA (Galan et al. 2011). This might substantially contribute to a UV-protective effect since PHA granules represent a "shield" attached to the nucleoid which scatters UVB radiation away from the most sensitive molecule–DNA. Here, it

has to be emphasized that very recent findings by Karmann et al. (2017) show that, under carbon-limited conditions, the distribution of granules to daughter cells in statu nascendi occurs in an asymmetric way; the culture segregates into a PHA-rich and a PHA-poor subculture, thus displaying a "bistable behavior." Future investigations might provide insights if the PHA-rich subculture is definitely better protected when challenged by UV irradiation.

PHA metabolism reveals a cyclic nature, the so called PHA cycle, since in microbial cells the polymer is simultaneously synthesized and degraded (Kadouri et al. 2005). According to the results of Kadouri et al. (2003b), also the capability of intracellular PHA degradation is an important factor enhancing the UV-protective effect of PHA, since a PHA depolymerase deletion mutant strain of *Azospirillum brasilense* incapable of PHA degradation was shown to be more sensitive to UV irradiation than the wild type strain. The explanation can be that, due to the cyclic nature of PHA metabolism and activity of PHA depolymerase, a substantial amount of PHA monomers is present in bacterial cells. For instance, the intracellular concentration of 3-hydroxybutyrate (3HB) in the wild type strain of *C. necator* is 16.5-fold higher than in its PHA non-accumulating mutant. This is important since 3HB constitutes a potent chemical chaperone capable of preventing a model enzyme, lipase, against denaturation caused by high temperature or oxidative damage (Obruca et al. 2016b). Therefore, it is likely that the complete PHA cycle might in this way also prevent bacterial cells against oxidative pressure generated by UV radiation. Moreover, Ayub et al. (2009) suggested that PHA metabolism is essential for the maintenance of the redox state in *Pseudomonas* sp. 14-3 during oxidative pressure induced by exposure of bacterial cells to low temperatures.

In summary, the presence of PHA granules in bacterial cells has numerous biophysical and metabolic consequences, which alter the stress survival capacity of bacterial cells during their exposition to various stress factors. Their UV-protective action might be explained by their efficient UV-radiation scattering properties with high scattering efficiency in the wavelengths close to the DNA absorption maxima. Furthermore, presence of PHA granules in bacterial cells also protects them from ROS generated by UV irradiation since scattering of UV radiation on granules decreases levels of generated ROS and, moreover, PHA metabolism also provides efficient protection against oxidative stress induced by UV irradiation.

Funding This study was funded by the project "Materials Research Centre at FCH BUT-Sustainability and Development" No. LO1211 of the Ministry of Education, Youth and Sports of the Czech Republic and by the project GP15-20645S of the Czech Science Foundation (GACR).

Compliance with ethical standards

Conflict of interest The authors declare that they have no conflict of interest.

Ethical approval This article does not contain any studies with human participants or animals performed by any of the authors.

References

Ayub ND, Tribelli PM, López NI (2009) Polyhydroxyalkanoates are essential for maintenance of redox state in the Antarctic bacterium *Pseudomonas* sp. 14-3 during low temperature adaptation. Extremophiles 13(1):59–66. https://doi.org/10.1007/s00792-008-0197-z

Bonthrone KM, Clauss J, Horowitz DM, Hunter BK, Sanders JKM (1992) The biological and physical chemistry of polyhydroxyalkanoates as seen by NMR spectroscopy. FEMS Microbiol Lett 103(2–4):269–277. https://doi.org/10.1111/j.1574-6968.1992.tb05848.x

Dong TG, Dong S, Catalano C, Moore R, Liang X, Mekalanos JJ (2015) Generation of reactive oxygen species by lethal attacks from competing microbes. Proc Natl Acad Sci USA 112(7):2181–2186. https://doi.org/10.1073/pnas.1425007112

Farías ME, Fernández-Zenoff V, Flores R, Ordóñez O, Estévez C (2009) Impact of solar radiation on bacterioplankton in Laguna Vilama, a hypersaline Andean lake (4650 m). J Geophys Res Biogeosci 114: G00D04

Gabani P, Singh OV (2013) Radiation-resistant extremophiles and their potential in biotechnology and therapeutics. Appl Microbiol Biotechnol 97(3):993–1004. https://doi.org/10.1007/s00253-012-4642-7

Galan B, Dinjaski N, Maestro B, de Eugenio LI, Escapa IF, Sanz JM, Garcia JL and Prieto MA (2011) Nucleoid-associated PhaF phasin drives intracellular location and segregation of polyhydroxyalkanoate granules in *Pseudomonas putida* KT2442. Mol Microbiol 79:402–418. https://doi.org/10.1111/j.1365-2958.2010.07450.x

Häder DP, Kumar HD, Smith RC, Worrest RC (2007) Effects of solar UV radiation on aquatic ecosystems and interactions with climate change. Photochem Photobiol Sci 6(3):267–285. https://doi.org/10.1039/B700020K

Hwang SO, Feldberg R (1990) Effect of inclusion body production on culture turbidity and cell dry-weight in growing bacterial cultures. Biotechnol Prog 6(1):48–50. https://doi.org/10.1021/bp00001a007

Jendrossek D (2009) Polyhydroxyalkanoate granules are complex subcellular organelles (Carbonosomes). J Bacteriol 191(10):3195–3202. https://doi.org/10.1128/JB.01723-08

Kadouri D, Jurkevitch E, Okon Y (2003a) Involvement of the reserve material poly- beta-hydroxybutyrate in *Azospirillum brasilense* stress endurance and root colonization. Appl Environ Microbiol 69(6):3244–3250. https://doi.org/10.1128/AEM.69.6.3244-3250.2003

Kadouri D, Jurkevitch E, Okon Y (2003b) Poly beta-hydroxybutyrate depolymerase (PhaZ) in *Azospirillum brasilense* and characterization of a *phaZ* mutant. Arch Microbiol 180(5):309–318. https://doi.org/10.1007/s00203-003-0590-z

Kadouri D, Jurkevitch E, Okon Y, Castro-Sowinski S (2005) Ecological and agricultural significance of bacterial polyhydroxyalkanoates. Crit Rev Microbiol 31(2):55–67. https://doi.org/10.1080/10408410590899228

Karmann S, Panke S, Zinn M (2017) The bistable behaviour of *Pseudomonas putida* KT2440 during PHA depolymerization under carbon limitation. Bioengineering 4(2):58. https://doi.org/10.3390/bioengineering4020058

Khodadad CL, Wong GM, James LM, Thakrar PJ, Lane MA, Catechis JA, Smith DJ (2017) Stratosphere conditions inactivate bacterial endospores from a Mars spacecraft assembly facility. Astrobiology 17(4):337–350. https://doi.org/10.1089/ast.2016.1549

Kim BM, Rhee JS, Lee KW, Kim MJ, Shin KH, Lee SJ, Lee YM, Lee JS (2015) UV-B radiation-induced oxidative stress and p38 signaling pathway involvement in the benthic copepod *Tigriopus japonicus*. Comp Biochem Physiol C 167:15–23

Koller M, Muhr A, Braunegg G (2014) Microalgae as versatile cellular factories for valued products. Algal Res 6:52–63. https://doi.org/10.1016/j.algal.2014.09.002

Mravec F, Obruca S, Krzyzanek V, Sedlacek P, Hrubanova K, Samek O, Kucera D, Benesova P, Nebesarova J (2016) Accumulation of PHA granules in *Cupriavidus necator* as seen by confocal fluorescence microscopy. FEMS Microbiol Lett 363:fnw094

Obruca S, Benesova P, Oborna J, Marova I (2014) Application of protease-hydrolyzed whey as a complex nitrogen source to increase poly(3-hydroxybutyrate) production from oils by *Cupriavidus necator*. Biotechnol Lett 36(4):775–781. https://doi.org/10.1007/s10529-013-1407-z

Obruca S, Sedlacek P, Krzyzanek V, Mravec F, Hrubanova K, Samek O, Kucera D, Benesova P, Marova I (2016a) Accumulation of poly(3-hydroxybutyrate) helps bacterial cells to survive freezing. PLoS One 11(6):e0157778. https://doi.org/10.1371/journal.pone.0157778

Obruca S, Sedlacek P, Mravec F, Samek O, Marova I (2016b) Evaluation of 3-hydroxybutyrate as an enzyme-protective agent against heating and oxidative damage and its potential role in stress response of poly(3-hydroxybutyrate) accumulating cells. Appl Microbiol Biotechnol 100(3):1365–1376. https://doi.org/10.1007/s00253-015-7162-4

Obruca S, Sedlacek P, Mravec F, Krzyzanek V, Nebesarova J, Samek O, Kucera D, Benesova P, Hrubanova K, Milerova M, Marova I (2017) The presence of PHB granules in cytoplasm protects non-halophilic bacterial cells against the harmful impact of hypertonic environments. New Biotechnol 39(Pt A):68–80. https://doi.org/10.1016/j.nbt.2017.07.008

Paunescu D, Mora CA, Puddu M, Krumeich F, Grass RN (2014) DNA protection against ultraviolet irradiation by encapsulation in a multilayered SiO2/TiO2 assembly. J Mater Chem B 2(48):8504–8509. https://doi.org/10.1039/C4TB01552E

Pavez P, Castillo JL, González C, Martínez M (2009) Poly-β-hydroxyalkanoate exert a protective effect against carbon starvation and frozen conditions in *Sphingopyxis chilensis*. Curr Microbiol 59(6):636–640. https://doi.org/10.1007/s00284-009-9485-9

Pérez V, Hengst M, Kurte L, Dorador C, Jeffrey WH, Wattiez R, Molina V, Matallana-Surget S (2017) Bacterial survival under extreme UV radiation: a comparative proteomics study of *Rhodobacter* sp., isolated from high altitude wetlands in Chile. Front Microbiol 8:1173. https://doi.org/10.3389/fmicb.2017.01173

Pham TH (2004) The role of polyhydroxyalkanoate biosynthesis by *Pseudomonas aeruginosa* in rhamnolipid and alginate production as well as stress tolerance and biofilm formation. Microbiology 150(10):3405–3413. https://doi.org/10.1099/mic.0.27357-0

Raberg M, Voigt B, Hecker M, Steinbuchel A (2014) A closer look on the polyhydroxybutyrate- (PHB-) negative phenotype of *Ralstonia eutropha* PHB-4. PLoS One 9(5):e95907. https://doi.org/10.1371/journal.pone.0095907

Ravanat JL, Douki T, Cadet J (2001) Direct and indirect effects of UV radiation on DNA and its component. J Photochem Photobiol B 63(1-3):88–102. https://doi.org/10.1016/S1011-1344(01)00206-8

Singh OV, Gabani P (2011) Extremophiles: radiation resistance microbial reserves and therapeutic implications. J Appl Microbiol 110(4):851–861. https://doi.org/10.1111/j.1365-2672.2011.04971.x

Tal S, Okon Y (1985) Production of the reserve material poly-β-hydroxybutyrate and its function in *Azospirillum brasilense* cd. Can J Microbiol 31(7):608–613. https://doi.org/10.1139/m85-115

Tan GYA, Chen CL, Li L, Ge L, Wang L, Razaad IMN, Li Y, Zhao L, Wang JY (2014) Start a research on biopolymer polyhydroxyalkanoate (PHA): a review. Polymers 6(3):706–754. https://doi.org/10.3390/polym6030706

Tribelli PM, López NI (2011) Poly(3-hydroxybutyrate) influences biofilm formation and motility in the novel Antarctic species *Pseudomonas extremaustralis* under cold conditions. Extremophiles 15(5):541–547. https://doi.org/10.1007/s00792-011-0384-1

Vadlja D, Koller M, Novak M, Braunegg G, Horvat P (2016) Footprint area analysis of binary imaged *Cupriavidus necator* cells to study PHB production at balanced, transient, and limited growth conditions in a cascade process. Appl Microbiol Biotechnol 100(23):10065–10080. https://doi.org/10.1007/s00253-016-7844-6

Wahl A, Schuth N, Pfeiffer D, Nussberger S, Jendrossek D (2012) PHB granules are attached to the nucleoid via PhaM in *Ralstonia eutropha*. BMC Microbiol 12(1):262. https://doi.org/10.1186/1471-2180-12-262

Wang Q, Yu H, Xia Y, Kang Z, Qi Q (2009) Complete PHB mobilization in *Escherichia coli* enhances the stress tolerance: a potential biotechnological application. Microb Cell Factories 8(1):47. https://doi.org/10.1186/1475-2859-8-47

Wu D, He J, Gong Y, Chen D, Zhu X, Qiu N, Sun M, Li M, Yu Z (2011) Proteomic analysis reveals the strategies of *Bacillus thuringiensis* YBT-1520 for survival under long-term heat stress. Proteomics 11(13):2580–2591. https://doi.org/10.1002/pmic.201000392

Zhao YH, Li HM, Qin LF, Wang HH, Chen GQ (2007) Disruption of the polyhydroxyalkanoate synthase gene in *Aeromonas hydrophila* reduces its survival ability under stress conditions. FEMS Microbiol Lett 276(1):34–41. https://doi.org/10.1111/j.1574-6968.2007.00904.x